MICROWAVE/RF APPLICATORS AND PROBES

FOR MATERIAL HEATING, SENSING AND PLASMA GENERATION

A DESIGN GUIDE

MEHRDAD MEHDIZADEH

William Andrew is an imprint of Elsevier
The Boulevard, Langford Lane, Kidlington, Oxford OX5 1GB, UK
84 Theobald's Road, London WC1X 8RR, UK
Radarweg 29, PO Box 211, 1000 AE Amsterdam, The Netherlands
30 Corporate Drive, Suite 400, Burlington, MA 01803, USA
525 B Street, Suite 1900, San Diego, CA 92101 4495 USA

First edition 2010

British Library Cataloguing in Publication Data
A Catalogue record for this book is available from the British Library

Library of Congress Cataloging-in-Publication Data
A Catalog record for this book is available from the Library of Congress

ISBN–13: 978-0-8155-1592-0

Printed and bound in USA

10 11 12 13 14 10 9 8 7 6 5 4 3 2 1

Dedication

To Marcy for all her encouragement, understanding, patience 92.6% of the time

Preface

Interactions of electromagnetic fields with materials at high frequencies have given rise to a vast array of practical applications in industry, science, medicine, and consumer markets. Applicators or probes, which are the front end of these systems, provide the field that interacts with the material. Devices as diverse as the domestic microwave oven, medical therapeutic applicators, industrial microwave sensors, RF/microwave plasma applicators, and numerous others fall in the general category of near field applicators or probes.

While these devices are diverse in configuration, size, and applications, principally they share much in common; and to properly categorize them one must look beyond the specific application for which they are designed for. Much of the existing literature in this area, however, is written by the experts in specific application areas; and there have been few attempts at bringing that knowledge together. Due to the fragmented nature of work in this area, practitioners report new findings in publications within their own fields. Furthermore, in classical electrical engineering curricula, components such as resonant cavities are treated for their external frequency selective properties, and little is covered for cases where they are used for the interaction of fields with materials.

This book is written with three goals in mind. First, to bring together the overall area of high frequency applicators and probes for material interactions as an integrated science. Second, and even more importantly, it aims to be a useful reference to those who design these devices, and finally to provide an update on the most recent trends and findings in this area.

Above all, my ultimate goal has been to make this volume a comprehensive and useful source where the reader can find design rules and principles of high frequency applicators and probes for material processing and sensing applications. The reader will find that the key design principles of applicators and probes for diverse applications are often quite similar, and once understood can be applied readily, and a great deal of design trial and error can be avoided.

Application areas where these applicators and probes are used are growing, and they have plenty of room for further expansion. More innovation

is needed to foster this growth, which requires intuitive and phenomenological understanding on the part of the researchers and designers. Complex mathematical derivations, as well as modern numerical analysis techniques are useful in their own right, and tend to produce accurate results. In this book, however, the emphasis has been placed on producing an intuitive grasp of the subject matter using phenomenological explanations and well annotated figures. Mathematical expressions are provided as design tools, and are often simplified using curve-fitting techniques so that a practicing designer can rely on handheld calculators when possible. In cases where such simplification does not apply, Mathematica™ software by Wolfram Research is used, and the codes (notebooks) are included as Appendices.

The text is written to be useful for both expert and non-expert. For the expert, useful equations and worked out examples, using situations encountered in practice, are offered. For the non-expert, explanations of the phenomena involved are made without the usage of hard-to-follow mathematical derivations. In order to keep the book less cluttered, when rigorous derivations are needed, they are included as appendices.

As for the organization of the book, after covering the basics on field-material interactions in chapter 1, a unique overview and categorization of probes and applicators is made in Chapter 2. In the chapters to follow, applicators and probes are categorized, first by useful field type, electric field or magnetic field, and second by how the field is applied for specific geometric applications.

Finally, I am particularly interested in establishing contact with the users of this book, in order to improve and correct it for future editions and revisions; and to answer any questions. Please feel free to contact me with any comments or questions via email at: mehrdad@ieee.org.

Mehrdad Mehdizadeh, PhD
Wilmington, Delaware
February 18, 2009

Acknowledgements

I would like to express my debt of gratitude to Dr. Ronald J. Riegert who in many ways, directly, or indirectly contributed to this volume. Through many discussions over the years, his depth of knowledge in electromagnetic theory and modeling techniques has been instrumental in sharpening my understanding of many topics covered here. In addition, Dr. Riegert has written or contributed effectively writing of the Mathematica™ codes that are included in the appendices in this volume.

I would also like to thank Dr. Sina Ebnesajjaad for encouraging me to write the manuscript, and for his guidance as an experienced author of several excellent technical books.

CHAPTER 1

The Impact of Fields on Materials at RF/Microwave Frequencies

CHAPTER CONTENTS

INTRODUCTION

Field interaction with materials is a vast area of science, and a large body of literature is devoted to it. High-frequency applicators and probes operate in a relatively small, but important, part of the electromagnetic spectrum. This chapter serves as a brief background on electromagnetic and material topics related to the scope of this book. Furthermore, a number of definitions, concepts, and equations are reviewed that are referred to in other chapters. For a more extensive treatment of electromagnetic principles and material properties, the interested reader can consult many excellent sources, both in print and online [1–4], in this area.

Knowledge of field–material interactions is critical to the design of the high-frequency applicators, because the electrical properties of the material of interest will become a part of the device's functioning. This fact is a unique feature of these devices, which sets them apart. For example, in the design of a conventional furnace, it is of little importance what material is to be heated, but the dielectric properties of a material being processed by a microwave applicator are of great importance in the design of the device.

Microwave/RF Applicators and Probes for Material Heating, Sensing, and Plasma Generation

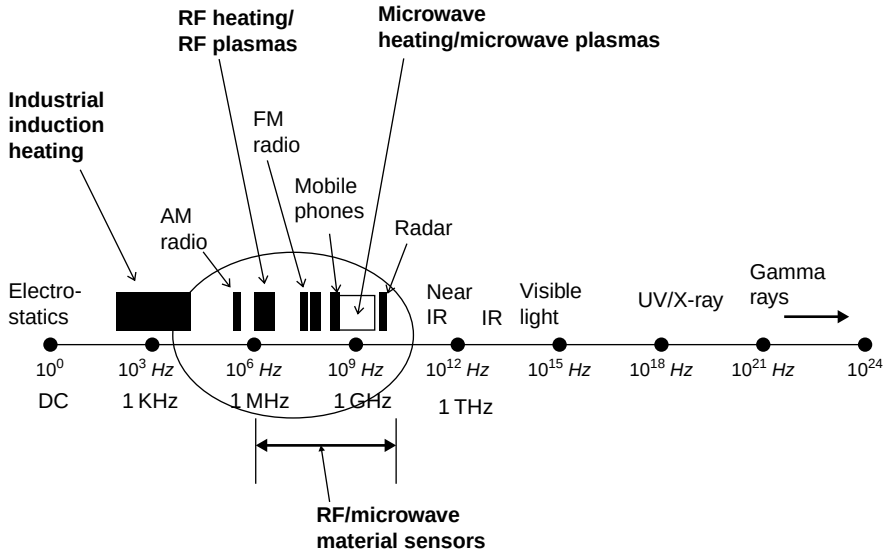

FIGURE 1.1
The electromagnetic spectrum and its usage at various frequencies.

The electromagnetic spectrum is shown in Figure 1.1, and the frequency bands of interest in this book are highlighted. This is a region in the spectrum covering a frequency range typically known as RF, through microwave and into millimeter wave (a few megahertz to tens of gigahertz). This general part of the electromagnetic spectrum happens to be where most wireless telecommunication devices are also housed. The major categories of applications covered in this book, together with their frequency ranges, are noted in Figure 1.1.

1.1 HIGH-FREQUENCY FIELDS IMPOSED ON UNIFORM MATERIALS

1.1.1 The wave equations and materials

The essential role of material properties in electromagnetics is readily evident in two of the four Maxwell equations that govern the relationships between electric field vector $\overline{E}$ and magnetic field vector $\overline{H}$:

$$\overline{\nabla} \times \overline{H} = \sigma \overline{E} + \varepsilon \frac{\partial \overline{E}}{\partial t} \tag{1.1}$$

$$\overline{\nabla} \times \overline{E} = -\mu \frac{\partial \overline{H}}{\partial t} \tag{1.2}$$

The three basic material properties σ, ε, and μ are called conductivity, permittivity, and permeability respectively. The above two equations, which are called Ampere's law and Faraday's law, relate time variations of one field to spatial variations of the other. In other words, they state that time-varying electric fields induce magnetic fields, and time-varying magnetic fields induce electric fields. The only exception to time-varying requirement is the term in Eq. (1.1), which means in the presence of mobile electric charges (free electrons in conductors), even a non-time-varying electric field can give rise to a magnetic field. This principle is the basis of all direct current (DC) electricity. The converse, however, is not true. Since there are no known magnetic charges, a time-varying electric field cannot exist without an accompanying magnetic field.

Further examination of Ampere's and Faraday's laws suggests that the ratio between the intensities of electric magnetic fields in time and space are set by surrounding material properties. Even a vacuum has permittivity and permeability, but not conductivity, since there are no free charges in a vacuum.

The subject of applicators and probes covered in this book is considered using steady-state time-varying systems throughout, which means the time variations of fields as shown in the right-hand sides of Eqs (1.1) and (1.2) are sinusoidal. This fact greatly simplifies relationships between electric and magnetic fields in steady-state systems. Instead of instantaneous values of fields, only the amplitudes of the fields along with the operating frequency need to be considered. In steady state, Eqs (1.1) and (1.2) become:

$$\overline{\nabla} \times \overline{H} = \sigma \overline{E} + j\omega\varepsilon \overline{E} \tag{1.3}$$

$$\overline{\nabla} \times \overline{E} = -j\omega\mu \overline{H} \tag{1.4}$$

where at the operating frequency f (in Hz), $\omega = 2\pi f$ is the angular frequency and $j = \sqrt{-1}$ is the complex operator. For the rest of this book, unless stated otherwise, the electric field and magnetic fields mentioned are either magnitudes of the steady-state values, or the root mean square (RMS) value, which is a time average of a sine wave.

For solving practical problems involving boundary conditions, combining Eqs (1.3) and (1.4) yields the wave equations in phasor form [5]:

$$\nabla^2 E + k^2 E = 0 \tag{1.5}$$

$$\nabla^2 H + k^2 H = 0 \tag{1.6}$$

where the operator is called Laplacian, and k is the wave number where:

$$k = \omega\sqrt{\mu\varepsilon} \tag{1.7}$$

The angular frequency is $\omega = 2\pi f$ in radians/second (rad/s) and f is the operating frequency in Hz. Note that permittivity, ε in farads/meter (F/m), and magnetic permeability, μ in henries/meter (H/m), in general, are complex quantities, as we will examine later. Their values in free space, however, are $\varepsilon_0 = 8.85 \times 10^{-12}$ F/m and $\mu_0 = 4\pi \times 10^{-7}$ H/m.

The wave equations (1.5) and (1.6) are better suited for solving practical boundary value problems such as those in applicators and probes, because each is a differential equation involving only one of the field types as a function of spatial dimensions. There are a number of analytical and numerical methods for solving such differential equations.

1.1.2 High-frequency electric fields and materials

We use Eq. (1.3) and the fact that current density J (in A/m^2) is related to the magnetic field by:

$$\bar{J} = (\sigma + j\omega\varepsilon)\bar{E} \tag{1.8}$$

This equation shows that the imposition of an electric field into a material will produce electrical currents, the amplitude and direction of which are proportional to the electric field intensity. These currents also have two components; one is conductivity, which produces conduction current that is basically frequency independent. Conductivity, σ in S/m (siemens per meter), represents that part of the electrical current responsible for movement of any free charges the material may possess, and is not dependent of frequency.

The second type of currents that are generated by the imposition of an electric field into a material are due to permittivity, represented by ε in Eq. (1.8). But permittivity itself is composed of real and imaginary components, and is represented in complex algebraic format as:

$$\varepsilon = \varepsilon' - j\varepsilon'' \tag{1.9}$$

The real part of the complex permittivity ε' is responsible for phase shift of the electric field, and the imaginary part ε'' is responsible for energy losses into the material. The permittivity of dielectric materials can be normalized to that of free space as follows:

$$\varepsilon' = \varepsilon_0\,\varepsilon'_{\mathrm{r}} \tag{1.10}$$

and

$$\varepsilon'' = \varepsilon_0 \varepsilon_r'' \tag{1.11}$$

where ε_r' and ε_r'' are called relative permittivity and loss factor respectively, and are dimensionless. Relative permittivity ε_r' is also called the dielectric constant (sometimes other designations such as D_k and K are used). The complex relative permittivity ε_r is then:

$$\varepsilon_r = \varepsilon_r' - j\varepsilon_r'' \tag{1.12}$$

The loss factor ε_r'' is also called the dissipation factor, and has other designations in different industries, such as D_f. The loss properties of dielectric are sometimes characterized by the loss tangent (sometimes called the "power factor") as:

$$\tan\delta = \frac{\varepsilon_r''}{\varepsilon_r'} \tag{1.13}$$

A full discussion of the polarization and phenomenon and dielectric relaxation is presented in many excellent sources [1,4].

Inserting Eq. (1.12) into Eq. (1.8) yields:

$$\bar{J} = (\sigma + \varepsilon_0 \varepsilon_r'' \omega)\bar{E} + j\varepsilon_0 \varepsilon_r' \omega \bar{E} \tag{1.14}$$

The first term on the right-hand side of Eq. (1.14) represent currents that lead to dissipation of power into the material.

It should be noted that the concepts of conductivity and dielectric loss include a number of material loss mechanisms as described extensively in the literature [1,4,6–12]. The major component of dielectric loss in RF/microwave frequencies comes from "orientational polarization", which occurs in materials consisting of molecules or particles with a permanent dipole moment. The electric field causes the reorientation of the dipoles, at the frequency of operation, toward the direction of the field [4]. The rotation meets the resistance due to thermal agitation, but also that due to the inertia resistance of the surrounding molecules, giving rise to mechanical friction. This friction would generate heat from the energy stored in the electric field, which is the basis for RF/microwave heating.

Rotational polarization is not the only mechanism for losses due to high-frequency fields. For example, there are a number of different loss mechanisms in a solid composed of conductive particle inclusions mixed in polymeric solids [13–15]. These are a combination of dielectric, interfacial,

and electronic losses, but from the vantage point of an external field, they can be summed up to fit within the first term on the right-hand side of Eq. (1.14).

The second term is the reactive component of the current that has a phase lag with respect to the imposed field, and is sometimes called the displacement current. This current does not take any part in power dissipation into the material.

1.1.3 Joule's loss effect in conductive materials with free charges

Joule's effect is the result of the imposing of an electric field on materials with free charges and finite conductivity. Looking at the loss part of Eq. (1.7), the first loss term is the Joule effect that can only occur in conductive materials with free charges, where the electric field vector $\bar{E}$ (in volts/meter) interacts with free electrons of a material with conductivity σ (siemens/meter) to produce a current density vector $\bar{J}$ (in amperes per square meter):

$$\bar{J} = \sigma \bar{E} \tag{1.15}$$

The power deposition into the material is expressed as:

$$P = \sigma E^2 \tag{1.16}$$

where P is power density in watts per cubic meter of material, E is the average electric field intensity, and σ is the material conductivity in S/m. Note that Eq. (1.15) is not frequency dependent as long as the conductivity is constant with frequency.

To reduce these ideas to a numerical example for a practical situation, consider the example of a 12 AWG copper wire (2 mm OD) with conductivity of $\sigma = 5.8 \times 10^7$ S/m that carries 20 A of DC. Dividing the current by the cross-sectional area of the wire, the current density is calculated as $J = 3.82 \times 10^6$ A/m^2, and using Eq. (1.15) the electric field intensity inside the wire would be $E = 0.065$ V/m. Using Eq. (1.15), the power deposition density would be $E = 2.45 \times 10^5$ W/m^3. Multiplying this by the volume of the wire means 1 meter of such wire dissipates 0.77 W.

1.1.4 Energy deposition into materials with the dielectric loss effect

Dielectric loss is another bulk energy deposition phenomenon that occurs due to imposition of an alternating electric field in media with dielectric

loss properties. Considering the second loss term in Eq. (1.14), the dielectric loss current component is defined as:

$$\bar{J} = \varepsilon_0 \varepsilon_r'' \omega \bar{E} \tag{1.17}$$

Note that, unlike the Joule current, the dielectric loss current is frequency dependent and cannot exist with static fields. The power dissipation per unit volume from the dielectric loss effect is [2]:

$$P_v = \varepsilon_0 \varepsilon_r'' \omega E_{rms}^2 \tag{1.18}$$

where P_v is the power deposition density in W/m^3 from dielectric losses and E_{rms} is the root mean square value of the electric field intensity, which is the average value for a sine wave.

Equation (1.18) is the basic equation for Industrial, Scientific, and Medical (ISM) applications of RF/microwave heating. While useful for explanation of the volumetric heating principle, its practical usage is somewhat limited by the fact that the value of the electric field amplitude is difficult to determine as a parameter in the design of an applicator. A further difficulty is that the presence of the material changes in an electric field within it; furthermore, the electric field intensity itself may not be spatially uniform within the material. This is often true even if the original electric field prior to the material insertion is uniform. One of the goals of this book is to study these issues for various types of applicators in use; as a part of this effort, Eq. (1.18) will be referred to on many occasions.

One useful way to utilize Eq. (1.18) in practical situations is for basic feasibility studies for dielectric heating methods. The example below will clarify this.

Example

Suppose that RF/microwave heating is being considered for heating of a material with the dielectric properties of $\varepsilon_r' = 4.2$ and $\varepsilon_r'' = 0.11$ at 1 GHz. A heat balance study concluded that a power deposition of 180,000 W/m^3 of the material is needed for the process to complete. Furthermore, due to safety regulations in the area, no electric fields above 20,000 V/m are allowed. We will determine the basic feasibility of such a process at two frequencies, 433 and 2450 MHz.

Solution

Let us first make a reasonable approximation that the dielectric properties at 433 and 2450 MHz are at the same level as that of 1 GHz. Applying Eq. (1.18) and rearranging we get:

For 433 MHz:

$$E = \sqrt{\frac{P}{2\pi f \varepsilon_0 \varepsilon_r''}} = \sqrt{\frac{180{,}000}{2 \times \pi \times 433 \times 10^6 \times 8.85 \times 10^{-12} \times 0.12}} = 7892 \text{ V/m}$$

The same computation for 2450 MHz yields $E = 3319$ V/m.

Note that the calculations above are the electric field requirements inside the material. For this study we must consider fields outside the material, which according to Eq. (3.45), may be higher by the factor of the dielectric constant. Therefore the actual maximum field in the case of 433 MHz is $7982 \times \varepsilon_r'' = 33{,}146$ V/m, and in the case of 2450 MHz $3319 \times \varepsilon_r'' = 13{,}939$ V/m. Therefore the 433 MHz frequency does not meet the maximum electric field of 20,000 V/m, but the 2450 MHz frequency does; microwave heating at 2450 MHz thus appears feasible, at least from the standpoint of the maximum electric field allowed.

1.1.5 High-frequency magnetic fields and materials

The impact of the imposition of high-frequency magnetic fields into a material can be divided into two categories: induction eddy current effect and ferromagnetic effect.

The establishment of eddy currents into a material requires sufficient electrical conductivity. A detailed description of the eddy current effect is made in Chapter 7. In essence, the alternating magnetic field in turn induces an electric field in the conductive material. Depending on the material conductivity, this electric field induces an eddy current in the material.

The second type of magnetic field impact on materials would require the material to be ferromagnetic. The ferromagnetic properties of materials at high frequencies can be mathematically modeled by the use of the complex permeability μ (in H/m):

$$\mu = \mu' - j\mu'' \tag{1.19}$$

where $\mu' = \mu_0 \mu_r'$ is the magnetic permeability in H/m, with $\mu_0 = 4\pi \times 10^{-7}$ H/m the permeability of free space, and μ_r' the relative permeability of the material. The complex part of the permeability is $\mu'' = \mu_0 \mu_r''$ in

which μ_r'' is the magnetic loss factor. Overall, the dimensionless relative magnetic permeability μ_r will become:

$$\mu_r = \mu_r' - j\mu_r'' \tag{1.20}$$

For free space, as well as most materials, $\mu_r = 1$. For ferrous metals $\mu_r' \geq 1$ and μ_r'' is very close to zero.

Only in ferromagnetic materials, with hysteresis properties, would the value of μ_r'' be significantly above zero. This phenomenon is due to losses associated with the magnetization/demagnetization cycle in the magnetic domains [1].

The power deposition due to the hysteresis effect P_{hyst} for a material with the relative magnetic loss μ_r'' can be formulated as:

$$P_{hyst} = \mu_0 \mu_r'' H^2 \tag{1.21}$$

where H is the root mean square (RMS) or average intensity of the high-frequency magnetic field intensity.

1.2 FIELDS AT MATERIAL BOUNDARIES IN RF/MICROWAVE FREQUENCIES

1.2.1 Fields at boundaries between two real materials

One of the main themes in the study of applicators for field–material interactions is the field configuration at the interface boundary between two materials with relative intensities as shown in Figure 1.2. Electric and magnetic fields at a material boundary can have components in parallel or vertical to the boundary, which can produce four conditions I–IV as shown with the relationships in the figure. In condition I in Figure 1.2, the electric field components are perpendicular to the boundary. The relation between electric field intensities across the boundary is proportional to permittivities as formulated by $\varepsilon_1 E_1 = \varepsilon_2 E_2$. Condition II shows that parallel electric fields across the boundary are equal.

In condition III the vertical magnetic fields are proportional to their permeabilities as $\mu_1 H_1 = \mu_2 H_2$ only in the static (DC) case. For high-frequency conditions the relationship between vertical H components is complicated by the possibility of current induction. One extreme is when both materials are good dielectrics; there is then no possibility of induced currents, the magnetic fields across the boundary remain totally undisturbed, and H fields are the same for both vertical and parallel components. Another extreme is

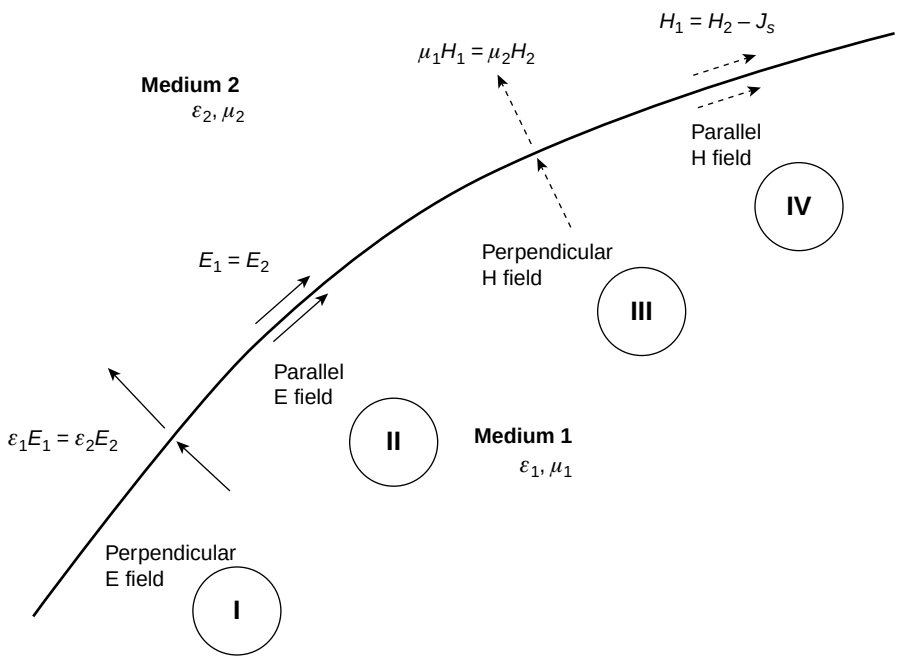

FIGURE 1.2
Electric and magnetic components at the boundary of two generic materials. Parallel field components are equal, but the relative intensities of perpendicular components are dependent on material properties.

when one of the two materials is a perfect conductor. In that case the vertical H field at the boundary vanishes. For a parallel H field as shown in condition IV, the relationship depends on surface currents J_s, as shown in Figure 1.2.

1.2.2 Wave impedance in various environments

In this section we will describe the crucial role that wave impedance plays in wave–material interactions. Furthermore, we will show how understanding of wave impedance will help in understanding the function of applicators.

Let us first examine fields in unbounded space, in the absence of any materials, where the solution of the wave equations (1.5) and (1.6) [3] reveals that the presence of a time-varying electric field gives rise to a perpendicular magnetic field, and vice versa. This field pair travels in a direction perpendicular to both fields, which is called the poynting vector. The ratio of electric to magnetic field in unbounded space is called the impedance of free space, $\eta = \sqrt{\mu_0/\varepsilon_0} = 377\ \Omega$, which is one of the constants of nature.

The presence of any materials would disturb the ratio of electric and magnetic fields, and the wave impedance in a medium with electrical

properties ε, σ, and μ as defined in Section 1.1.1 can be described by the following equation [16]:

$$\eta = \frac{E}{H} = \sqrt{\frac{\mu}{\varepsilon\left(1 + \frac{j\sigma}{\omega\varepsilon}\right)}} \tag{1.22}$$

Waves propagating inside a uniform dielectric medium with a dielectric constant of ε_r' and $\sigma \approx 0$ would reduce the wave impedance of Eq. (1.22) from its free space value, η, by:

$$\eta_e = \frac{\eta}{\sqrt{\varepsilon_r'}} \tag{1.23}$$

where η_e is the wave impedance in the dielectric medium. Therefore the presence of typical dielectrics would modify the impedance by a limited amount. For example, wave propagation in glass with dielectric constant of 4 reduces the wave impedance as follows:

For a conductive medium, where $\sigma/\omega\varepsilon >> 1$, Eq. (1.22) reduces to:

$$\eta = \frac{E}{H} = \sqrt{\frac{\mu_0\,\omega}{\sigma}} \tag{1.24}$$

For example, the wave impedance in a copper wire with the conductivity of $\sigma = 5.8 \times 10^7$ S/m at $f = 1$ GHz from Eq. (1.24) would be $\eta = 0.011\ \Omega$. This is a large deviation from the free space value of wave impedance. Figure 1.3b shows the case of a current-carrying wire. The current in the wire gives rise to a magnetic field that surrounds the wire in a circular loop. There is a weak electric field parallel to the wire. In essence, metals can be utilized to shape and guide electromagnetic fields, hence their wide usage in all electrotechnology, including field applicators that are the subject of this book. The wire example is the basis for magnetic field applicators such as solenoids, and will be covered in detail in Chapter 7.

On another extreme in wave impedance, when an electric field is established between two parallel plates, as shown in Figure 1.3b, a magnetic field is also present, but the wave impedance is typically higher than 377 Ω. In relative terms compared with waves in unbounded space, the electric field can be called strong at the expense of a "weak" magnetic field. The parallel-plate applicator will be covered in more detail in Chapters 2 and 3, where electric field applicators, which are characterized as "high-impedance" type, are considered.

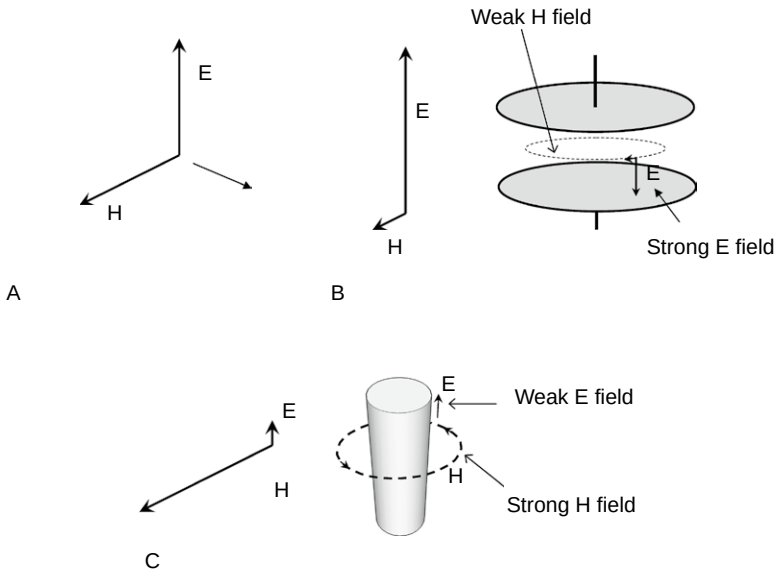

FIGURE 1.3 *Relations between electric and magnetic fields in three conditions. (A) Unbounded space traveling wave impedance ($\eta = 377\Omega$). (B) Strong electric field, weak magnetic field (parallel-plate capacitor example), where $\eta >> 377\Omega$. (C) Weak electric field, strong magnetic fields (wire example), where $\eta << 377\Omega$.*

The two examples of a parallel-plate capacitor and current-carrying wire show that high-conductivity metals can be used to shape fields and create wave impedances that deviate from that of the free space. Generally, a high-impedance structure, such as a pair of parallel plates, is appropriate for interfacing with dielectrics, and low-impedance structures such as coiled wires are better for interacting with fields with high-conductivity objects.

1.2.3 Lumped field approximations in electrically small systems

In the previous section we discussed how high-conductivity metals can be used as high- and low-impedance structures. When their dimensions are small compared with the operating wavelength, the system is said to be "electrically small". In electrically small systems, an assumption can be made that the dominant field type can be treated as the only field present. Such an assumption, which has excellent validity in many practical situations in applicator/probe design, can simplify the design in solving a wide variety of problems. This is called the static or quasi-static approximation because in electrostatic or magneto-static fields, one field can exist without the other.

In order to analyze an electrically small applicator/probe system, the second term on the left-hand sides of Eqs (1.5) and (1.6), which contains the frequency, can be ignored. The remaining terms containing the Laplacian are far easier to solve analytically. Another equation that can be used for solving certain quasi-static problems is the Laplace equation, which is discussed in detail in Chapter 3.

1.2.4 Fields at conductor boundaries, skin depth, and surface resistance

The boundary between perfect and real conductors and dielectrics is considered here. Figure 1.4 shows the fields at the boundary between a perfect conductor and a dielectric. At the surface of the conductor the component of the electric field parallel to the interface vanishes, therefore only the vertical component can exist.

As for real conductors, the normal electric field at the interface does not completely vanish, but a weak parallel E exists to support the surface currents. This surface electric field will decay further into the bulk of the conductor. The depth where the electric field is 1/e of the surface is called the skin depth and is shown as follows.

Applying metal–dielectric conditions for boundary III:

$$E_{\mathrm{P}} = -(1+j)\sqrt{\frac{\omega\mu_0}{2\sigma}}\,H_{\mathrm{P}} \tag{1.25}$$

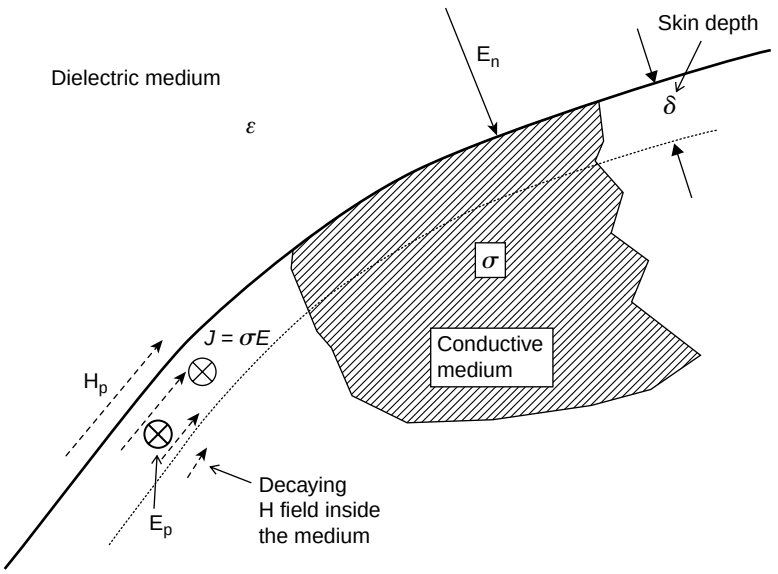

FIGURE 1.4 *Fields at conductive–dielectric boundary and decay of H field into the metal.*

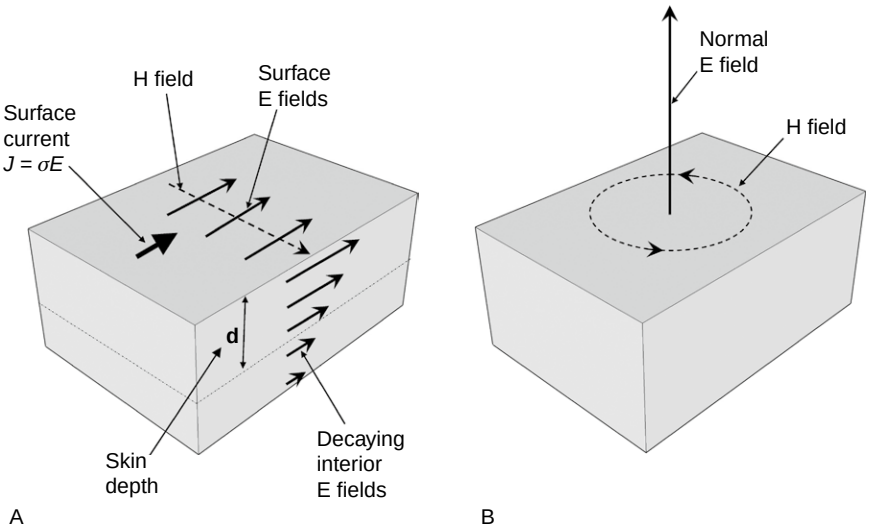

FIGURE 1.5
Fields at conductor–dielectric boundary and decay of E fields into the material. (A) Details of E field decay. (B) 3-D view of normal E field and curved H field on the surface of conductor.

Surface resistivity of metals is the ratio of E to H fields, found from Eq. (1.25) as:

$$R_s = \sqrt{\frac{\pi f \mu}{\sigma}} \tag{1.26}$$

The unit of surface resistivity is ohms per square (Ω/sq).

The depth of penetration or skin depth is:

$$\delta = \sqrt{\frac{1}{\pi f \mu \sigma}} \tag{1.27}$$

Therefore the surface resistivity is related to the skin depth and conductivity as:

$$R_s = \frac{1}{\delta \sigma} \tag{1.28}$$

Figure 1.5 shows a 3-D view of details of electric field decay into the conductive material.

1.2.5 Standing waves in cavity and transmission-line applicators

The existence of standing waves is the main principle behind microwave cavity applicators and many types of transmission-line applicators as described in Chapters 2, 4, 5, and 6. A standing wave, in essence, is

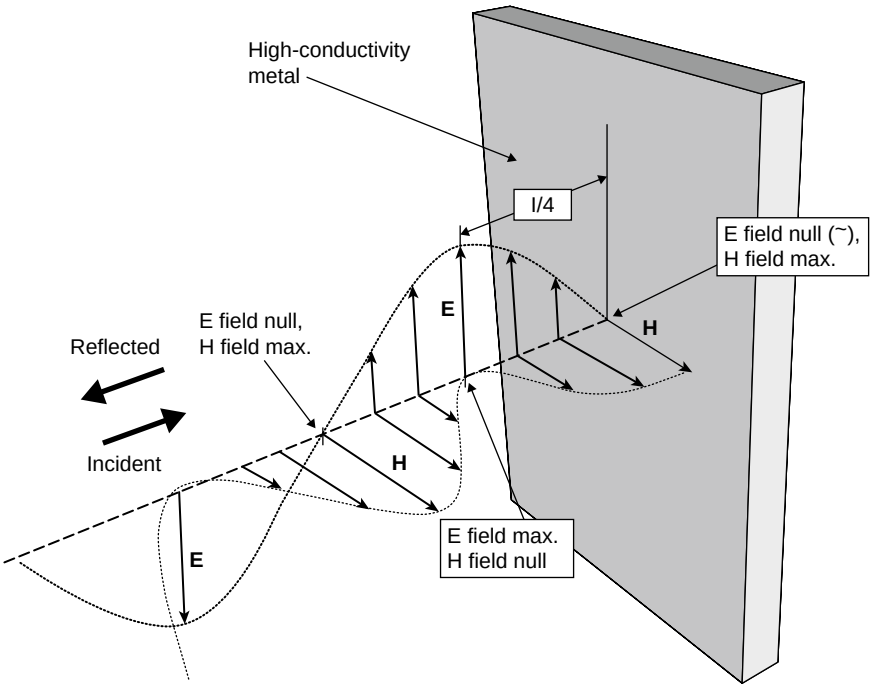

FIGURE 1.6
Representation of standing waves in the vicinity of a high-conductivity metal.

a superimposition of a forward and reflected wave from the surface of a highly conductive plane, as shown in Figure 1.6.

The most prominent feature of a standing wave is the stationary location of maxima (nodes) and minima (nulls) of fields. The magnetic field is at a node on the surface of the conductive plane, and at the distance of a quarter of a wavelength hits a null. The electric field is at a null on the conductive plane surface, but comes to a node at a quarter of a wavelength. The node–null patterns repeat every half wavelength.

1.2.6 Penetration and reflection of waves into lossy dielectrics

The real part of the propagation constant is considered. The unit N/m means for every meter of propagation into the material the amplitude of the field is reduced by a factor of 1/e = 0.368.

The solution of the wave equation (1.5) for electric fields in a lossy dielectric yields the following for the attenuation and phase constants [17]:

$$\alpha = \frac{2\pi\sqrt{\varepsilon_r'}}{\lambda}\sqrt{\frac{1}{2}\left(\sqrt{1+\left(\frac{\varepsilon_r''}{\varepsilon_r'}\right)^2}-1\right)} \tag{1.29}$$

The attenuation constant, α, given in nepers per meter (N/m), is the measure of diminishing field amplitude as it penetrates the lossy dielectric. It is often needed to express the attenuation in terms of dB/meter in practical systems. In that case the results of Eq. (1.29) need to be multiplied by the factor 8.686 to obtain the attenuation constant in dB/m.

The imaginary part of the propagation constant, β in radians per meter (rad/m), is called the phase constant and is the measure of shift of phase as the wave propagates through the material, as follows:

$$\beta = \frac{2\pi\sqrt{\varepsilon_r'}}{\lambda}\sqrt{\frac{1}{2}\left(\sqrt{1+\left(\frac{\varepsilon_r''}{\varepsilon_r'}\right)^2}+1\right)} \tag{1.30}$$

The phase shift through a dielectric as described by Eq. (1.30) is used often in dielectric sensing because the phase shift, which can be measured electrically, can be a gauge for dielectric properties.

As for attenuation, shown in Eq. (1.29), in most practical situations, which involve either a dielectric or highly conductive materials, the above two equations can be simplified as follows.

For most low-loss as well as many lossy dielectrics, the assumption that $(\varepsilon_r''/\varepsilon_r')^2 << 1$ is easily justifiable. Therefore, given the mathematical approximation of $\sqrt{1+x} \approx 1 + x/2$ for $x << 1$, and $\lambda = C/f$, the attenuation constant for dielectrics is reduced to:

$$\alpha = \frac{f\varepsilon_r''}{C\sqrt{\varepsilon_r'}} \tag{1.31}$$

The penetration depth is defined as the distance from the dielectric surface at which the power drops to 1/e from its value at the surface ($D_p = 1/2\alpha$):

$$D_p = \frac{C\sqrt{\varepsilon_r'}}{2\pi f\varepsilon_r''} \tag{1.32}$$

Note that the penetration depth (in meters) obtained in this equation is only valid when a normal plane wave hits the boundary between a vacuum and a dielectric, and is not necessarily valid when plane waves are not involved. As an example, Eq. (1.32) does not apply to a slab of dielectric located between two parallel plates as described in Chapter 3. In multimode microwave cavities, as covered in Chapter 5, Eq. (1.32) is only an acceptable

approximation, but in single-mode cavities (Chapter 4) it would be unacceptable to use Eq. (1.32) since a plane wave model cannot be justified.

For conductive or highly lossy materials, where $\varepsilon_r'' >> \varepsilon_r'$, Eq. (1.29) is reduced to:

$$\alpha = \sqrt{\frac{\omega^2 \mu \varepsilon_r'' \varepsilon_0}{2}} \tag{1.33}$$

where $\omega = 2\pi f$ is the angular frequency and μ is the magnetic permeability. The depth of penetration ($D_p = 1/2\alpha$), which is also called the skin depth, δ, becomes:

$$D_p = \delta = \sqrt{\frac{2}{\omega \mu \sigma}} \tag{1.34}$$

1.2.7 Wave reflection and transmission at boundaries between free space and materials

Aside from the penetration depth into lossy material, it is often useful to know how incident waves reflect or transmit. The ratio of power reflected from an air–dielectric interface, P_r, to the incident power, P_i, is given by the Fresnel reflection formula for a good dielectric [18]:

$$\frac{P_r}{P_i} = \left(\frac{\sqrt{\varepsilon_r} - 1}{\sqrt{\varepsilon_r} + 1}\right)^2 \quad \text{(good dielectric: } \sigma << \omega \varepsilon_r'' \varepsilon_0\text{)} \tag{1.35}$$

For a good conductor, the ratio is:

$$\frac{P_r}{P_i} = 1 - 4\sqrt{\frac{\omega \varepsilon_r \varepsilon_0}{2\sigma}} \quad \text{(good conductor: } \sigma >> \omega \varepsilon_r'' \varepsilon_0\text{)} \tag{1.36}$$

The two above equations show that the reflection is essentially 100% for both good conductors and high-dielectric materials.

1.3 MATERIAL/FIELD ISSUES OF INTEREST IN APPLICATOR/PROBE DESIGN

1.3.1 Distinction between dielectric loss and conductivity

So far we have learned that loss mechanism in insulators is accounted for by relative dielectric loss factor ε_r'', while the loss mechanism in conductors is

accounted for by conductivity σ. Imposing or inducing an electric field into the material would cause a current to flow, the density of which is expressed by Eq. (1.15). In many cases, to unify the representation of lossy dielectrics and conductors, the following equivalence is very commonly used:

$$\sigma = \omega\varepsilon'' = \omega\varepsilon_0\varepsilon_r'' \tag{1.37}$$

In many practical cases involving insulating or semiconductive materials, the above equation holds without any difficulty. However, the validity of Eq. (1.35) comes into question for highly conductive materials, because good conductors do not have dielectric polarization properties.

Another occasion where Eq. (1.37) is inaccurate is where electrical properties are used as complex variables. In such cases the following equivalence between conductivity and dielectric properties is more appropriate to use than Eq. (1.37):

$$\sigma = j\varepsilon' + \omega\varepsilon'' \tag{1.38}$$

An example of how Eq. (1.38) becomes useful is given here: when variable amounts of conductive particles are added [15] to an insulating base material with a dielectric constant of ε_r'. The dielectric property items on the right-hand side of Eq. (1.38) are controlled by the amount of conductive additive. If the idea is to represent the material in electromagnetic computation, then Eq. (1.38) would properly account for the case where the conductive additives are near zero by representing the material as a dielectric. When the amount of conductive additive is large, we have $\omega\varepsilon'' >> \varepsilon'$, which reduces Eq. (1.38) to Eq. (1.37). When the electrical conductivity is high enough that dielectric polarization is meaningless, then in Eq. (1.38) the quantity of $\varepsilon_r' = 1$ is used.

1.3.2 Temperature rise and thermal issues in electromagnetic heating

The most important attribute of electromagnetic methods of heating (microwave, RF, or induction) is the direct nature of energy deposition. There is no heat transfer in the conventional sense and, from a thermodynamic point of view, the material itself is the source of heat. While the energy is being deposited via electromagnetic methods, energy is also being lost to the environment via conventional methods of heat transfer, such as conduction, convection, or radiation. That is how an equilibrium temperature can be reached. In many cases involving low temperatures and rapid heating, exemplified by heating of food by a microwave oven, the energy losses during the process are minimal and can be neglected.

Temperature rise and energy losses

In high-temperature microwave heating [19], such as microwave sintering of ceramics, the energy losses are very important and are responsible for setting a temperature limit. For example, without a serious effort in thermal insulation, reaching a temperature beyond 1200°C is very difficult in a microwave heating situation. At such high temperatures equilibrium is reached where increasing the power input to the material does little to compensate for radiation losses. The Stefan–Boltzmann law relates the total amount of radiation emitted by an object to its temperature:

$$E_r = \sigma_r T^4 \tag{1.39}$$

where E_r is the total amount of radiation emitted by an object per square meter (W/m^2), $\sigma_r = 5.67 \times 10^{-8}$ W/m^2-K^4 is the Stefan–Boltzmann constant, and T is the temperature of the object in degrees kelvin. This means that the radiation increases quite rapidly with the object's temperature (the usual character for this constant is σ, but in the interest of not confusing it with electrical conductivity, σ_r is used here).

Here, we will examine volumetric temperature rise, neglecting the heat losses. The power required to raise the temperature of a mass M_a kg by an increment of ΔT°C in t seconds is given by (SI system):

$$P = \frac{M_a c_p \Delta T}{t} \tag{1.40}$$

where c_p is the specific heat in kJ/kg-°C. In cases where the specific heat is given with the older unit, cal/g-°C, that value must be multiplied by a factor of 4.18 before inserting in Eq. (1.40). Lists of specific heats of common materials can be found in many print or online sources [20,21].

Using the example of dielectric heating, which encompasses both RF and microwave methods, combining Eqs (1.18) and (1.40) [17] and replacing some of the constants with numerical values gives:

$$\frac{\Delta T}{t} = \frac{5.56 \times 10^{-11} \varepsilon_r'' f E_{rms}^2}{\rho c_p} \tag{1.41}$$

where ρ is the specific weight (density) in kg/m^3 and f is the frequency in Hz.

Electromagnetic heating provides both opportunities and challenges for practical usage. On the advantage side, the elimination of the need for conventional heat transfer means there is an opportunity for more rapid temperature rise over a larger volume of the subject material. Furthermore,

achieving very high temperatures becomes easier by, for example, insulating the subject material with a thermal insulator that is non-susceptible to the fields. In this method, the insulating material is placed between the source of the electromagnetic field and the subject material; therefore, energy loss from the heated material to the environment is reduced.

An important challenge in electromagnetic heating is reduced control over the maximum temperature, and heating uniformity profile. In conventional heat transfer, the maximum temperature over the volume is always at or below the maximum temperature of the heat source. Electromagnetic heating methods, however, do not have such a limitation. The highest temperature in the subject volume is determined by a balance between electromagnetic energy deposition at each location on one hand, and thermal losses to the environment on the other.

Thermometry challenge

The measurement of the temperature is often another challenge in electromagnetic heating. The most common type of temperature probe in industry is the thermocouple, which contains metals. In microwave or RF heating the metal probe distorts the fields and could cause arcing. In addition, the fields could interfere with the thermocouple's signal, and the thermocouple wires could act as an antenna that transmits interference to other instruments. To avoid these problems, alternate methods, such as fluoro-optic [22] or fiber-optic [23] or infrared thermometry methods are devised.

The second challenge with thermometry in electromagnetic heating is that measuring the temperature in one location does not necessarily guarantee the temperatures in other locations do not exceed this temperature, unless care is taken to know the temperature profile in advance. For assessment of temperature in non-uniform heating situations methods such as infrared thermal imaging or other methods of thermography are utilized.

1.3.3 Special and non-thermal electromagnetic effects on materials

The conventional wisdom about RF/microwave energy is that heating is the only expected effect. The reason is that microwave frequencies are too low to have quantum energies necessary to break chemical bonds similar to ionizing radiation such as X-rays or gamma rays. There are, however, claims of non-thermal effects from various quarters, some that can have plausible justification and some that are still questionable.

Some non-thermal effects, such as improved speed of chemical reactions [24], or quality and speed improvement in sintering of ceramics [25],

can be explained by the thermodynamic differences between conventional and volumetric methods of heating. A major challenge in investigating non-thermal effects is the difficulties associated with accurate temperature measurements in microwave heating, as described above. Therefore, making a fair comparison between the temperatures of conventional and microwave experiments would be difficult.

There have been a few research efforts showing that microwaves can improve diffusion and mass transport through solids [26–29]. An application of this effect is microwave ceramic sintering, where the densification, reactions, and bonding can occur at lower temperatures than those expected using conventional heating. This is significant for many reasons, especially the opportunity to use less expensive, lower temperature-rated refractories.

The cases of microwave-enhanced organic chemistry [24], as well as microwave-assisted heterogeneous catalysis [30] have been successfully applied in chemistry. Spectacular accelerations, higher yields under milder reaction conditions, and higher product purities have all been reported. Indeed, a number of authors have described success in reactions that do not occur by conventional heating and even modifications of selectivity (chemo-, regional stereoselectivity). The effect of microwave irradiation in organic synthesis is a combination of thermal effects, arising from the heating rate and superheating.

1.3.4 Nonlinearity issues and thermal runaway in electromagnetic heating

A linear material, from the standpoint of electromagnetic heating, is a material whose electrical properties remain constant with various parameters such as temperature, pressure, applied field intensity, frequency, etc. A linear material would greatly simplify applicators, probes or other hardware for interactions of fields with materials. Such material, in reality, does not exist, but in many cases the changes in properties are gentle enough that the material can be approximated as linear.

While most solids see an increase in their dielectric loss with temperature, some have a much stronger increase than others. As an example, Figure 1.7 shows an example of increase in dielectric loss, as well as the dielectric constant, for Mullite. The sharp increase in microwave absorption with temperature can cause a thermal instability, which is commonly known as a temperature runaway [31,32]. An increase in the local temperature is accompanied by an enhancement of microwave energy absorption, which results in the local acceleration of heating and further growth of temperature. The unstable nature of thermal runaway causes sharp increases of

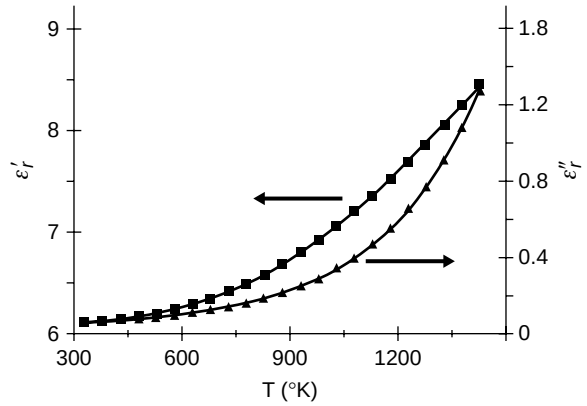

FIGURE 1.7 *Increase in dielectric constant and dielectric loss for Mullite (a ceramic) with temperature.*

temperature known as "hot spots", which could cause catastrophic degradation of the process material. A method of avoiding thermal runaway using field modifications in the applicator is worked out in detail in Chapter 9.

1.4 CLASSIFICATION OF MATERIALS AT HIGH FREQUENCIES

1.4.1 Solid dielectrics: ceramics and polymers

Ceramics and glasses

There are numerous areas in industry, scientific research, and medical technology where ceramics and glasses are subject to interactions with high-frequency fields. In most cases a combination of electrical, mechanical, or thermal properties of these materials makes them the ideal choice for use in hardware where high-frequency fields are present. There are also situations where ceramics are processed with high-frequency fields – for example, microwave sintering of ceramics. In all these cases a knowledge and understanding of electromagnetic properties at high frequencies is necessary to choose the right material when needed, or to find the appropriate processing parameters.

The most common requirement for ceramics and glasses used in high-frequency applications is having a low dielectric loss. The goal in these situations is to avoid signal or energy loss, while taking advantage of the desirable mechanical or thermal properties of ceramics. For example, in microwave plasma chambers used for semiconductor processing there is a

Table 1.1 Examples of Several Insulating Ceramic and Glass Materials

Material	Dielectric Constant (ε_r') @ 1 MHz	Dielectric Loss Factor (ε_r'') @ 1 MHz	Dielectric Strength (kV/mm)
Silicon nitride (Si_3N_4)	6.1	0.0006	20
Aluminum nitride (AlN)	8.8–8.9	0.001	15
Quartz (SiO_2)	3.8–5.4	0.0015	15–25
Boron nitride (BN)	4.2	0.004	35.6–55.4
Alumina (Al_2O_3)	8.8–10.1	0.003–0.02	10
Glass ($Na_2O•CaO•SiO_2$)	4.0–8.0	0.0005–0.01	7.8–13.2
Mullite	6.2–6.8	0.03–0.034	7.8
Zirconia (ZrO_2)	12.0	0.12	~5.0

need for a window that allows the fields into the chamber without being directly heated by microwaves. At the same time this window must withstand high temperatures and a corrosive plasma environment. Low-loss ceramics like boron nitride or glasses like quartz are ideal for such a window.

Microwave sintering of ceramics, due to the many advantages it provides, has become the subject of a new wave of recent interest and commercialization in recent times [25,33,34]. The sintering time for microwave sintering is a small fraction of that needed for conventional furnaces, and average grain size is much smaller with better bonding strengths.

Table 1.1, partially drawn from Buchanan [35], shows examples of several insulating ceramic and glass materials listed in order of low to high dielectric loss. While the frequency of interest in this book is higher than 1 MHz, the dielectric property trends remain the same at higher frequencies when a comparison needs to be made between these materials.

Polymers and plastics

At high frequencies, the dielectric loss response of polymers depends on the molecular polarity. In polar plastics, dipoles are created by an imbalance in the distribution of electrons and in the presence of an electric field the dipoles will attempt to move to align with the field [1]. This will create dipole polarization of the material. Examples of polar plastics are polymethyl methacrylate (PMMA) and polyvinyl chloride (PVC). These polymers, due to high dielectric loss, are suitable for RF welding applications, as covered in detail in Chapter 7.

The nonpolar plastics are truly covalent and generally have symmetrical molecules. In these materials there are no polar dipoles present and the

application of an electric field does not try to align any dipoles. The electric field does, however, move the electrons slightly in the direction of the electric field to create "electron polarization"; in this case the only movement is that of electrons and this is effectively instantaneous. Examples of nonpolar plastics are polytetrafluoroethylene (PTFE; and many other fluoropolymers); nonpolar molecules such as PTFE or polyethylene terephthalate (PET) have low losses, which make them suitable for use as insulating support structures in high-frequency applications, including applicator and sensor structures.

There has been a growth in applications of polymers that are filled with conductive particles, such as metals [13–15] or carbon [36]. Filled polymers have an entirely new set of electrical and mechanical properties that can serve the needs of the industry in meeting tough material requirements.

1.4.2 Conductive materials: metals and carbon-based conductors

Electrical conductivity, as a material property, can take a wide range of values, spanning more than 21 orders of magnitude in ambient conditions, as shown in Figure 1.8. The purpose of this section is to discuss the higher conductivity range (about $\sigma > 100$ S/m) at high frequencies.

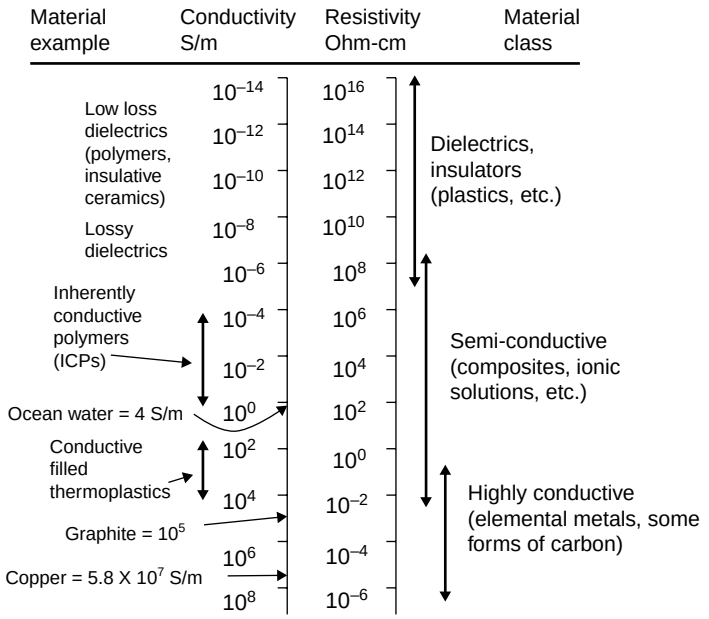

FIGURE 1.8 *Conductivity/resistivity spectrum.*

Conductive materials have a very strong impact on shaping and guiding of fields. However, the geometrical features of the conductive matter would also influence how the conductive matter and the fields would interact. For example, a thick solid sheet of aluminum can be approximated as a perfect conductor at microwave/RF frequencies, and will reflect all the incident waves, as shown in Figure 1.6. But aluminum is an excellent absorber of microwaves when it is deposited as a thin sheet of a few nanometers. Such a configuration is used extensively as a microwave susceptor for food applications, as described in more detail in Chapter 5.

Another important area of field interactions with highly conductive materials is the special effects related to sharp edges, which is the arcing effect observed with aluminum foil placed in a domestic microwave oven. Applying a high-frequency electric field to a metal with corners, there is a buildup of electric fields in the vicinity [3]. This phenomenon is quantified by the variation principle [37].

Carbon, in its more conductive forms, such as graphite ($\sigma = 10^5$ S/m) has similar interactions with fields as metals. Both metals and carbon, as fine powders, can be used as fillers for dielectric materials such as polymers to obtain desirable electrical or mechanical properties for various applications [14–16,38,39].

1.4.3 Water and water-rich organic materials

Water, with its highly polar molecule, has a high permittivity and loss factor compared with most substances. As such, its impact on fields is substantial in high-frequency applicator/probes. On the other hand, water's ubiquitous presence in life-based organic substances, such as food, biological tissues, etc., makes it extremely important in all areas related to field interactions with these materials. Furthermore, water absorbed in most matter, in the form of moisture, has great impact in the dielectric properties of the host medium.

Water content in solids can exist in two forms. The first is free water, which resides in small openings and capillaries within the microscopic structure of matter. Free water can move within the solid's matrix by diffusion processes. The second type is bound water, which is chemically attached to other molecules. For example, Ca_2CO_3, also known as "plaster of Paris", holds molecules of water as $Ca_2CO_3 \bullet 5H_2O$ to form gypsum.

The dielectric loss of water is directly linked with the relative energy absorption, which is shown across the frequency spectrum in Figure 1.9 [40]. The absorption increases gently with frequency, but there are absorption peaks at higher frequency ranges as shown. Among the frequencies

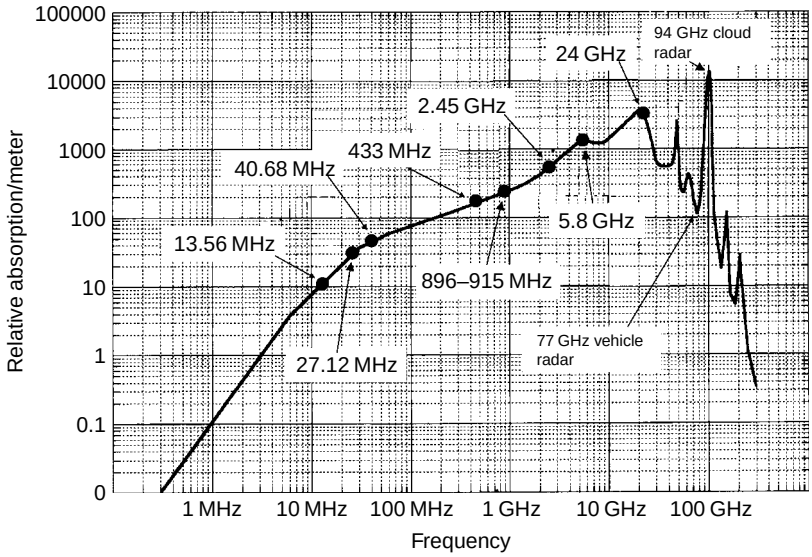

FIGURE 1.9 *Relative dissipation of electromagnetic energy by water over the frequency spectrum. There is a gentle increase in absorption with frequency. Above 20 GHz there are several absorption peaks. Certain frequencies of importance in industrial, scientific, and medical applications are noted. After Jordan [40].*

allowed by communications authorities for operation of industrial, scientific, and medical devices (ISM frequencies), 2450 MHz is most widespread in actual usage. The choice of this frequency for most microwave heating installation is not related to any water absorption peak, but its origins are related to early magnetron tubes developed for this purpose. However, two higher ISM frequencies, 5.8 and 24 GHz, are linked to water's increased absorption at these frequencies. At higher frequency ranges there are both peaks and valleys that have been chosen for various applications. For example, 77 GHz is chosen for automotive collision avoidance radar due to its low absorption by water, but 94 GHz is chosen for detection of clouds in meteorology due its higher response to the water molecule. Figure 1.10 shows the general variations of water's dielectric properties across the frequency spectrum from RF into millimeter waves on a logarithmic scale [41].

The addition of ionic substances, such as salt, to water tends to raise the dielectric loss at microwave frequencies appreciably, as shown in the graph of Figure 1.11. For example, adding 5% (by weight) salt to water has raised the dielectric loss factor (ε_r'') from 8 to 70, while the relative permittivity is changed little. The change in dielectric loss of water in microwave

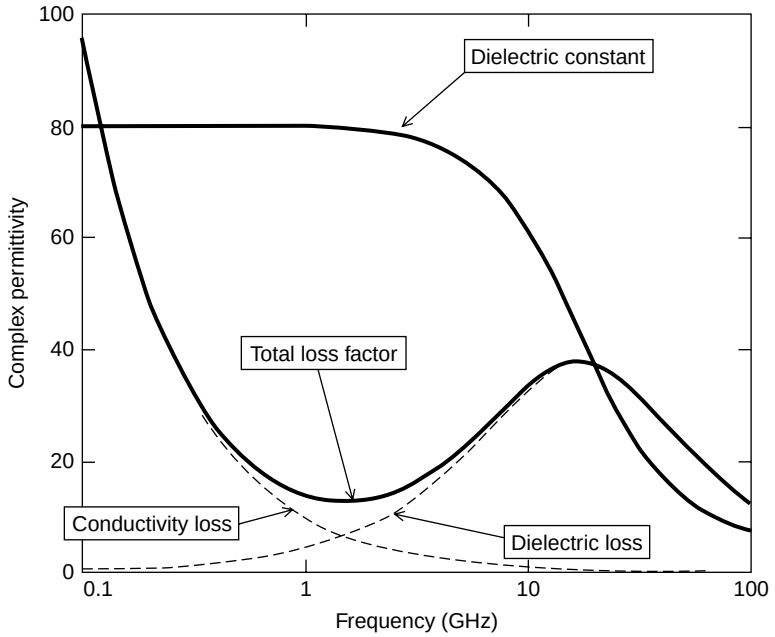

FIGURE 1.10 *Change in dielectric properties of water over the frequency spectrum. After Keam-Holdem [41].*

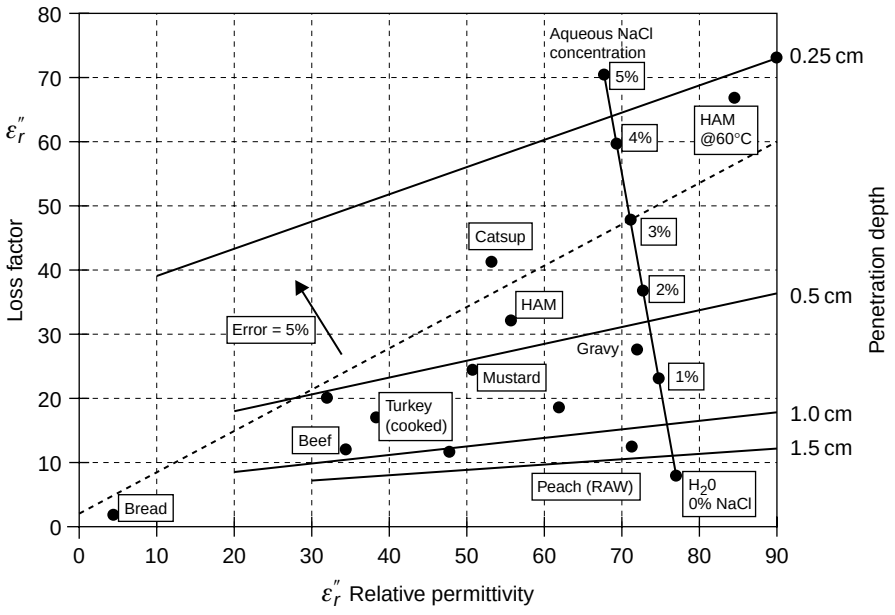

FIGURE 1.11
Dielectric properties of various food items at room temperature and 2450 MHz.
After C.R. Buffler, Microwave Cooking and Processing: Engineering Fundamentals for the Food Scientist, Van Nostrand Reinhold, New York, 1992.

frequencies is minuscule compared to that experienced at lower frequencies (1 MHz or below).

Food

Food items have a special place in dielectric studies due to the prevalence of domestic microwave ovens and industrial food processing [42,43]. Water, due to its dominant presence in most types of food, has a decisive role in setting the dielectric properties. Predicting the dielectric properties of foods, however, based on water content or other compositional information has proved to be unsuccessful for a large group of food materials [44]. This is due to the complex nature of interactions of the components. Salt ions can affect the dielectric properties of foods significantly, particularly the dielectric loss factor.

Most data on dielectric properties of food is generated and tabulated at the ISM microwave frequency of 2450 MHz. An example is the chart in Figure 1.11 [42] showing the dielectric properties of many common food items, where the permittivity and loss factors are on horizontal and vertical coordinates respectively. The chart also shows the penetration depth at 2450 MHz calculated using Eq. (1.32).

In addition to 2450 MHz, there are a few other frequencies where food is processed via electromagnetic methods. The ISM frequencies in the RF range, particularly of 27.1 and 40.68 MHz, are often used in the large-scale processing of foods [45]. For industrial microwave processing of foods, depending on location, ISM frequencies of 433, 896, and 915 MHz are also utilized.

High-frequency properties of biological and live tissues

The study of microwave and RF field interactions with biological and live tissues is important in the design systems for medical applications, such as microwave hyperthermia, RF ablation, and magnetic resonance imaging. Dielectric properties of live tissues have been studied extensively for this purpose. Empirical equations are a part of this work, one of which is presented as follows.

The relative permittivity ε'_r and the conductivity σ (in mS/cm) of a biological tissue at frequency f (in GHz) between 10 MHz and 17 GHz is given by the following empirical equations [46]:

$$\varepsilon'_r = 1.71 f^{-1.13} + \frac{\varepsilon_s^m - 4}{1 + (f/25)^2} + 4 \tag{1.42}$$

Table 1.2 Values of Parameters for a Few Tissue and Tumor Cases

Tissue Type	ε_s^m	$\sigma_{0.1}$ (mS/cm)	ε_r' @ 915 MHz	σ @ 915 MHz	ε_r' @ 2.45 GHz	σ @ 2.45 GHz
Fat	10	0.5	11.9	9.4	10.5	1.5
Muscle	47	7.0	48.8	10.1	47.2	16.3
Brain (gray matter)	44	7.0	45.8	10.1	44.2	15.9
Liver	43	6.7	44.8	9.7	43.2	15.3
Intestinal leiomyosarcoma	53	10.5	54.8	14.9	53.2	22.4

and

$$\sigma = 1.35\, f^{0.13}\, \sigma_{0.1} + \frac{0.022\,(\varepsilon_s^m - 4) f^2}{1 + (f/25)^2} \tag{1.43}$$

where ε_s^m and $\sigma_{0.1}$ (conductivity at 100 MHz) are tabulated parameters that depend on the type of tissue. The physical parameter that is the most responsible for determining ε_s^m and $\sigma_{0.1}$ is the water content of the tissue. Table 1.2 shows the values of these parameters for a few tissue and tumor cases, including the calculated ε_r' and σ for two selected ISM frequencies of 915 MHz and 2.45 GHz.

If it is desired to have the dielectric loss factor instead of conductivity, the equivalent loss factor from Eq. (1.37) can be used.

1.4.4 Gases/vapors

Gases, due to a lack of lattice structure and low specific weight, have very weak interactions with electromagnetic fields. For example, the relative dielectric constant of air at standard temperature and pressure is 1.0000004, which for most practical purposes is the same as that of a vacuum. Gases at higher pressures have somewhat higher dielectric properties, but still below the range of most practical concern.

Steam and vapors, due to their particulate consistency, can be detected by high quality factor microwave cavities, as described in Chapter 3. Microwave cavities have been used for humidity detection [47]. The cavity mode TE_{011} is used. In this mode of operation an open structure can be built without a reduction in sensitivity, where a high quality factor is maintained [48].

At frequencies above 20 GHz, certain gas molecules with dipole moments have an absorption spectrum. This phenomenon is used in

microwave and millimeter-wave spectroscopy [49], where gas species with rotational spectra are detected. The electric field at microwave or millimeter-wave frequency exerts a torque on these molecules. Diatomic molecules with symmetry, such as oxygen, do not have a dipole moment, but others such as carbon monoxide can be detected with microwave spectroscopy.

1.4.5 Plasmas

Plasma is a state of matter when the gas atoms have broken down into positive and negative charges. The ability of these charges to move somewhat independently makes the plasma electrically conductive so that it responds strongly to electromagnetic fields.

Viewed by a microwave or RF applicator, a plasma is seen as a lossy dielectric or conductive body. As such, the energy contained in the field is transferred to sustain the plasma. The conductivity of a Lorentzian plasma, which is the basis for most industrial plasmas of interest, is given (in S/m) by [50]:

$$\sigma = \frac{e^2 n_e}{m_e \nu_{ce}} \tag{1.44}$$

where $e = 1.602 \times 10^{-19}$ is the charge of an electron in coulumbs, n_e is the electron number density per m^3, $m_e = 9.109 \times 10^{-31}$ kg is the mass of the electron, and ν_{ce} is the electron collision frequency per second. Lower-pressure plasmas typically have smaller electron number density and therefore lower conductivities. As an example of typical industrial plasmas, an argon plasma torch has a conductivity range of 200–10,000 S/m.

Depending on the situation at hand, a plasma can be formed by either static fields (DC) or at RF or microwave frequencies. The advantage of RF/microwave power is that it interacts with plasma by displacement currents, rather than true currents. Therefore no contact between the electrodes and plasma is needed. The absence of electrodes will improve the reliability, reproducibility, and lifetime of plasma reactors and the products made in them.

As a load for an applicator, the main distinction between plasmas and normal material loads is the high nonlinear nature of plasmas. This means the loading conditions are radically different prior to the ignition and during the operation.

1.4.6 Metamaterials/periodic structures

A metamaterial is defined as an artificial composite that gains its electrical properties from its structure rather than inheriting them directly from the

materials it is composed of. This term is particularly used when the resulting material has properties not found in naturally formed substances [51]. Metamaterials, which in general can be made in microwave through optical wavelengths, are a subset of a larger group of heterogeneous structures consisting of a base solid material added with elements of a different material. The distinction of metamaterials is that they have special, sometimes anomalous, properties over a limited frequency band. In various applications, other terms have been used, such as periodic structures [52] or frequency-selective surfaces [53].

At microwave/RF frequencies, microwave frequency metamaterials are constructed as arrays of current-conducting elements (such as loops of wire) that have suitable inductive and capacitive characteristics. In order for the metamaterial to behave as a homogeneous material the feature sizes of the elements must be much smaller than the wavelength. For microwaves, at the frequency of 2450 MHz, for example, this is of the order of about a centimeter. Conventional printed circuit board construction can be used with specific shapes, sometimes resonant elements, etched.

In microwave heating, metamaterials have been investigated [54,55], where certain regularly spaced locations within a periodic structure can be utilized as a secondary source of localized intense electric fields. There is a potential of forming useful and special heating effects with this technology that is beyond the limitations placed by field patterns of conventional microwave applicators such as multimode cavities.

REFERENCES

[1] A. Von Hippel (Ed.), Dielectric Materials and Applications, second ed., Artech House, Boston, 1995.

[2] H.A. Haus, J.R. Melcher, Electromagnetic fields and energy, Hypermedia Teaching Facility, MIT, Available online at: <http://web.mit.edu/6.013_book/www/book.html>

[3] J.D. Jackson, Classical Electrodynamics, third ed., Wiley, Hoboken, NJ, 1998.

[4] KwanChi Kao, Dielectric Phenomena in Solids, Elsevier Academic Press, 2004.

[5] S. Ramo, J.R. Whinnery, T. Van Duzer, Fields and Waves in Communication Electronics, third ed., Wiley, Hoboken, NJ, 1994.

[6] W.R. Tinga, S.O. Nelson, J. Microw. Power 8 (1) (1973).

[7] A. Bur, J. Polym. 26 (1985) 963.

[8] M. Chen, et al., Polym. Eng. Sci. 33 (17) (1993).

[9] V.V. Daniel, Dielectric Relaxation, first ed.., Academic Press, San Diego, CA, 1967.

[10] N.G. McCrum, Anelastic and Dielectric Effects in Polymeric Solids, Dover Publications, New York, 1991.

[11] N.E. Hill, et al., Dielectric Properties and Molecular Behavior, first ed., Van Nostrand Reinhold, New York, 1969.

[12] G. Roussy, J.A. Pearce, Foundations and Industrial Applications of Microwave and Radio Frequency Fields, Wiley, New York, 1995.

[13] A.N. Lagarkov, et al., Dielectric properties of fiber filled composites, J. Appl. Phys. 84 (7) (1998) 3806–3814.

[14] A.K. Sarychev, et al., Giant high-order field moments in metal–dielectric composites, J. Phys. A 266 (1) (1999) 115–122.

[15] W.M. Merrill, et al., Effective medium theories for artificial materials composed of multiple sizes of spherical inclusions in a host continuum, IEEE Trans. Antennas and Propag. 47 (1) (1999) 142–148.

[16] C.A. Balanis, Advanced Engineering Electromagnetics, Wiley, New York, 1989.

[17] R.C. Metaxas, et al., Industrial Microwave Heating, Peter Peregrinus, London, 1983.

[18] M. Abraham, The Classical Theory of Electricity and Magnetism, Blackie, London, 1937.

[19] Y.V. Bykov, et al., High-temperature microwave processing of materials, J. Phys. D: Appl. Phys. 34 (2001) R55–R75.

[20] G. Van Wylen, et al., Fundamentals of Classical Thermodynamics, Wiley, New York, 1994.

[21] http://www.engineeringtoolbox.com.

[22] LumaSense Tehcnologies Inc. website: <http://www.lumasenseinc.com/>

[23] Neoptix Inc. website: <http://www.neoptix.com>

[24] A.D. Hoz, et al., Activation of organic reactions by microwaves, Adv. Org. Synth. 1 (1) (2005) 119–171.

[25] D. Agrawal, J. Cheng, Y. Fang, R. Roy, D.E. Clark (Ed.), et al., Microwave Processing of Ceramics, Composites and Metallic Materials, SpringerAmerican Ceramics Society Publishing, 2005, pp. 205–228.

[26] J. Jacob, et al., Thermal and non-thermal interaction of microwave radiation with materials, J. Mat. Sci. 30 (1995) 5321–5327.

[27] C. Gibson, I. Matthews, A. Samuel, Microwave enhanced diffusion in polymeric materials, J. Microw. Power. Electromagn. Energy 23 (1) (1988).

[28] V.E. Semenov, K.I. Rybakov, Enhanced mass and charge transfer in solids exposed to microwave fields, in: M. Willert-Porada (Ed.), Advances in Microwave and Radio Frequency Processing, Springer, 2006, pp. 472–481.

[29] Y. Nakai, et al., Enhanced gas permeability of cellulose acetate membranes under microwave irradiation, J. Memb. Sci. 256 (1–2) (2005) 72–77.

[30] J.K.S. Wan, et al., Microwaves and chemistry: the catalysis of an exciting marriage, Res. Chem. Intermed. 19 (2) (1993) 147–158.

[31] C.A. Vriezinga, S. Sanchez-Pedreno, J. Grasman, Thermal runaway in microwave heating: a mathematical analysis, Appl. Math. Model. 26 (11) (2002) 1029–1038.

[32] V.E. Semenov, N.A. Zharova, Thermal runaway and hot spots under controlled microwave heating, in: M. Willert-Porada (Ed.), Advances in Microwave and Radio Frequency Processing, Springer, 2006, pp. 482–490.

[33] R. Roy, et al., Decrystallizing solid crystalline titania, without melting, using microwave magnetic fields, J. Am. Ceram. Soc. 88 (6) (2005) 1640–1642.

[34] H.S. Shulman et al., Ceramic processing using microwave assist technology, Ceralink, Inc. website: <http://www.ceralink.com/publications/Bulletin-March-2008.pdf>, 2008.

[35] R.C. Buchanan, Ceramic Materials for Electronics, third ed., Marcel Dekker, 2004, pp. 1–86.

[36] A. Mdarhri, et al., Microwave dielectric properties of carbon black filled polymers under uniaxial tension, J. Appl. Phys. 101 (2007).

[37] G.B. Arfken, Mathematical Methods for Physicists, Academic Press, New York, 2005.

[38] K.I. Rybakov, et al., Microwave heating of conductive powder materials, J. Appl. Phys. 99 (2006).

[39] A.N. Lagarkov, A.K. Sarychev, Electromagnetic properties of composites containing elongated conductive inclusions, Phys. Rev. B 53 (10) (1996).

[40] E.C. Jordan (Ed.), Reference Data for Engineers: Radio, Electronics, Computer, and Communications, eighth ed., Howard W. Sams, Indianapolis, IN, 1993.

[41] Keam-Holdem Associates Inc. website: <http://www.kha.co.nz/>

[42] C.R. Buffler, Microwave Cooking and Processing, Van Nostrand Reinhold, New York, 1993.

[43] A.K. Datta, R.C. Anantheswaran (Eds.), Handbook of Microwave Technology for Food Applications, Marcel Dekker, New York, 2001.

[44] E. Sun, A.K. Datta, S. Lobo, Composition-based prediction of dielectric properties of foods, J. Microw. Power Electromagn. Energy 30 (4) (1995) 205–212.

[45] T. Koral, Radio frequency and bulk heating, Biscuit World 7 (4) (2004).

[46] J.L. Schepps, K.R. Foster, The UHF and microwave dielectric properties of normal and tumor tissues: variations in dielectric properties with tissue water content, Phys. Med. Biol. 25 (6) (1980) 1149–1159.

[47] E. Nyfors, P. Vainikainen, Industrial Microwave Sensors, Artech House, Norwood, MA, 1989.

[48] A.P. Toropainen et al., Microwave humidity sensor for difficult environmental conditions, Proceedings of 17th Microwave Conference, Rome, 1987.

[49] G.W. Ghantry, Modern Aspects of Microwave Spectroscopy, Academic Press, 1979.

[50] J.R. Roth, Industrial Plasma Engineering, Institute of Physics Publishing, Philadelphia, PA, 1995.

[51] N.P. Johnson, et al., A review of size and geometrical factors influencing resonant frequencies in metamaterials, Opto-Electronics Review 14 (3) (2006) 187–191. Available at http://eprints.gla.ac.uk/3715/.

[52] T. Itoh, Periodic structures for microwave engineering, MWE Conference, 2008. Available online at: <http://www.apmc-mwe.org/mwe2005/src/TL/TL06-02.pdf>

[53] B.A. Munk, Frequency Selective Surfaces: Theory and Design, Wiley, New York, 2000.

[54] Y. Nikawa, Microwave heating to artificial dielectric materials and metamaterials, 41st Annual International Microwave Power Symposium Proceedings, 2006, 61–63.

[55] Y. Nikawa, Apcom 2008 Conference, Kokushikan University. Available at: <http://apcom2008.kokushikan.ac.jp/dd/ABST-20080702135536-28.doc>

CHAPTER 2

Fundamentals of Field Applicators and Probes at RF and Microwave Frequencies

CHAPTER CONTENTS

INTRODUCTION

In Chapter 1 the first principles of field interactions with materials were discussed. Different effects of high-frequency electric fields and magnetic fields in various types of materials were established. The purspose of this chapter is to introduce the applicator and the probe head, which are devices for establishing those fields within the material. While the electromagnetic principles behind the two devices are the same, the functions are different.

The evolution and development of applicators and probes in RF/microwave frequencies have been fragmented due to their usage by a wide variety of disciplines and industries. Due to this fact, the terminology developed for these devices is often not standardized. We have made an attempt here to use the most frequently used terms, as long as they suggest accuracy and

Microwave/RF Applicators and Probes for Material Heating, Sensing, and Plasma Generation

are not too suggestive of specific applications. For example, some industries use the term material under test (MUT) or "sample" to refer to the material that is subjected to the electromagnetic fields. Here, such terminology is avoided because in many cases testing is not intended, and the idea is to heat or process the material. Instead we have used the term "material load" to describe the material subjected to the fields.

2.1 BASIC APPLICATOR/PROBE DEFINITIONS

2.1.1 Distinctions between applicators and probes

The term "field applicator" or simply "applicator" is used for a device that applies RF or microwave energy into a material volume at a level sufficient to create either a permanent or temporary change in a material parameter or property. The change could be a rise in temperature, driving out moisture, enhancing a chemical reaction, ablation of a biological tissue, breakdown of gases to form plasmas, etc. We use the term "energy deposition systems" to refer to this class of Industrial, Scientific, or Medical (ISM) systems.

The term "probe" or "sensor head" is typically used when the purpose of the field interaction is only to obtain information from the material. For example, in an industrial process, a probe system may be used to apply a field into the process material to obtain information about dielectric properties, which may indicate a material parameter such as moisture level. In that case, the field strength, and therefore the level of energy imparted into the material, is small and is enough for sufficient signal strength over the noise level. Typically, this signal level is far below the level needed to heat the material. There are cases, for example magnetic resonance (nuclear magnetic resonance, electron spin resonance), where the same device can act as both applicator and sensor.

While the fundamental physics are similar, there are practical differences between applicators and probes that make the design considerations quite different. These differences are mostly related to far higher levels of power, voltage, and current in the case of applicators versus signal levels in the case of probes. In addition to size differences, the choice of frequency for probes is far wider because of low power levels, which allow probes to work outside of allowed ISM frequency bands.

2.1.2 Far field and near field: antennas versus applicators/probes

Most applicators and probes discussed in this book are near field, which is generally defined as having the distances between the applicator and the

material small compared to the wavelength. In most cases of near-field systems, the material is actually enclosed within the applicator structure; an obvious example is the domestic microwave oven, where the food item is placed within the microwave cavity.

In far-field systems the distances between the antenna and the material can be large compared to the operating wavelength, and instead of applicator/probe terminology antenna terms are used. In far-field systems the field interacting with a material is in the form of traveling plane waves, with the ratio of electric field to magnetic field (wave impedance) at the free space level of 377 Ω, while in near-field systems the fields interacting with the material have impedances that typically deviate greatly from this value. The wave impedance issue was discussed in Chapter 1, and will be covered in the context of applicators and probes in this chapter as well.

Another distinctive feature of near-field applicator/probes is that the presence of the material load typically has a significant impact on the device's field configuration and some circuit variable such as impedance, voltage, and current. In essence, the subject material, through its electrical properties, becomes a part of the circuit. In far-field (antenna) systems, on the other hand, the effect of the material on the circuit variables is negligible. This book mainly deals with near-field systems. There are, however, excellent references for far-field material interaction systems that deal with microwave and millimeter-wave imaging, sensing, and tomography [1].

Applicators for field–material interactions are somewhat analogous to transmit antennas in communication systems, and probes are analogous to receive antennas. In the same manner as in communication systems, the reciprocity theorem [2] holds for applicators and probes.

2.1.3 Electrically small and electrically large applicators

High-frequency applicators can be categorized from the standpoint of electrical size, which is the relative size of an applicator compared to the operating wavelength. Obviously, in most cases the physical size of an applicator is mainly set by the size of the material load. The electrical size is a very important issue in applicator design, and determines the geometry, materials of construction, and method of analysis and design.

Electrically small applicators typically have dimensions of the order of one-eighth of the operating wavelength or smaller. As such there is insufficient room for significant field variations due to standing waves, and this would result in having inherently more uniform fields. While electrically small applicators can be used at any frequency range, they are traditionally used at lower frequencies (RF as opposed to microwaves). Two examples of

electrically small applicators are solenoid induction coils (Chapter 7) and parallel plates for RF heating (Chapter 3). There are, however, cases [3,4] where miniature applicators that can be classified as electrically small are used at microwave frequencies.

Electrically large applicators are those with dimensions of the order of, or larger than, the operating wavelength. Single-mode and multimode microwave cavities are examples (discussed in detail in Chapters 4 and 5), with the most familiar of these being the domestic microwave oven. This class of applicators suffers from inherent field non-uniformity borne out of standing waves, but there are several advantages including better sensitivity and efficiency. A typical feature of this class of applicator is self-resonance, i.e. both capacitive and reactive components needed for resonance are included in the applicator, as opposed to electrically small applicators, where an external resonating element must be added.

2.1.4 Applicator/probe categorization based on applicator/material load geometry

The material load that is to be processed or sensed by an applicator or probe can have one of the four geometrical relations with the probe/applicator as shown in Figure 2.1.

In the "volume" category shown in Figure 2.1a, the material load is placed substantially inside the applicator/probe. Examples of this type are microwave cavities or loads placed between the plates of a parallel-plate applicator, or inside a solenoid coil. This type of applicator typically applies the fields from all directions. The advantages are often better efficiency and field uniformity.

In the semi-volume case of Figure 2.1b, the probe surrounds the material load only in a partial manner. Such an arrangement is often used when access to the material load is limited. In the surface/fringing-field case of Figure 2.1c the applicator/probe is placed at the surface of a typically larger material load. The two arrangements of Figure 2.1b and c are often used in medical applications, such as magnetic resonance imaging [5], but the fringing-field applicator has much wider applications, particularly in open-ended transmission-line applicators, which are discussed in detail in Chapter 6.

Figure 2.1d shows the case where the applicator/probe is immersed in the material load, which is typically a fluid, even though that is not always the case, as in the example of medical applicator probes such as in RF ablation [6], which will be discussed in Chapter 3.

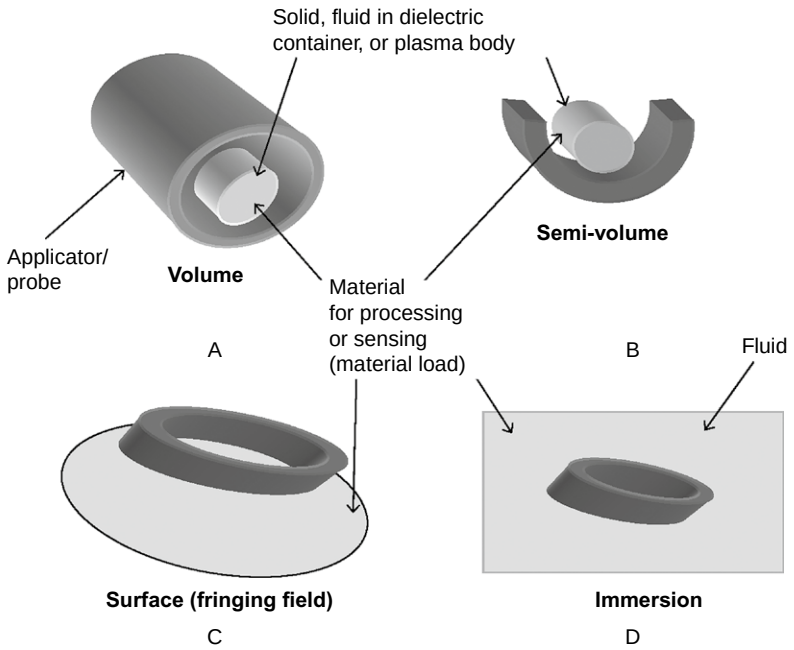

FIGURE 2.1 *Applicator/probe categories based on applicator/material load geometry. (A) Volume applicator/probe where the material load is surrounded by the applicator. (B) Semi-volume where the material is partially surrounded by the applicator. (C) Surface or fringing-field applicator, where the applicator/probe is placed on the surface of the material load. (D) Immersion applicator/probe is immersed in a material load which is in a fluid state.*

2.2 APPLICATOR/PROBE FIGURES OF MERIT

2.2.1 Applicator coupling, efficiency, and power management

Now, focusing on applicator figures of merit, a simplified and typical configuration of an electromagnetic energy deposition system is shown in Figure 2.2. A source of high-frequency energy, for example a microwave magnetron, is feeding power to an applicator through a coupling/matching subsystem. The utility power is supplying power P_u to the high-frequency power source. Utility power could mean DC or AC, depending on the situation. The high-frequency power source, in turn, supplies the power level P_s to the coupling subsystem, of which P_r is reflected due to mismatches. Power level P_a reaches the applicator. Therefore:

$$P_a = P_s - P_r \tag{2.1}$$

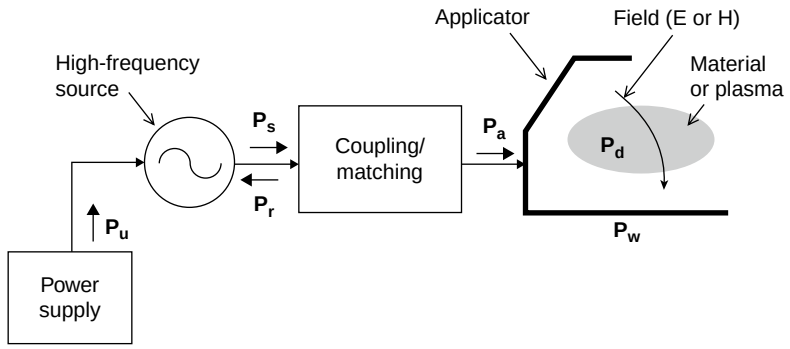

FIGURE 2.2 *Schematic diagram of a typical applicator system showing how the power from a power or signal supply is distributed.*

The applicator power P_a is split into P_d, which is power deposited into the material, and P_w, which is the wasted power:

$$P_a = P_d + P_w \tag{2.2}$$

In most applicators this wasted power is in the form of resistive heating in metal parts, while there could be other causes of waste such as radiation or heating of dielectric bodies that may be present for various purposes.

For the whole system, it is desirable to maximize the power deposited, P_d, versus the utility power P_u. Therefore the system efficiency, η_s, is defined as:

$$\eta_s = \frac{P_d}{P_u} \tag{2.3}$$

For the applicator and the coupling structure together, the total applicator efficiency, η_t, is defined as:

$$\eta_t = \frac{P_d}{P_s} \tag{2.4}$$

A figure of merit most useful in the design of an applicator is the applicator efficiency η_a, which is the ratio of power deposited into the material P_d to the power available to the applicator P_a:

$$\eta_a = \frac{P_d}{P_a} \tag{2.5}$$

which can also be expressed as:

$$\eta_a = 1 - \frac{P_w}{P_a} \tag{2.6}$$

For a perfectly matched coupling structure, $\eta_a = \eta_t$. The losses in the coupling/matching structure are usually quite minimal, but if they need to be accounted for, they could be added to P_w.

2.2.2 Effective field volume

The effective field volume (EFV) of an applicator or probe is the region over which the useful field is located. In the region outside of the EFV the fields are either zero or of insufficient amplitude for the intended function. As such, the definition of EFV for a given application is largely at the discretion of the designer, unless certain standardization is done in the industry.

In many simple applicator configurations, particularly those with largely uniform fields, defining the EFV is relatively simple, because it can be defined as the area where the field is substantially uniform. For example, in a parallel-plate applicator (studied in Chapter 3), the area between the plate is typically regarded as the EFV, and in a solenoid used for induction heating (Chapter 7), the cylindrical area within the solenoid is the EFV. In both of these cases there are fringing-field areas, but they are not counted as EFV because the fields diminish quickly.

There are cases where the fringing field is the only field available to the material. For example, in an open-ended coaxial line (studied in Chapter 6), the main fields are not accessible. Therefore the EFV is defined only in the area immediately next to the open end.

In some applicators with periodic-type field configurations, such as microwave resonant cavities (Chapters 4 and 5), the EFV is defined as the whole cavity volume, even though some areas may have very little useful field intensity.

In some application areas, industry-specific definitions are used to define EFV. For example, in magnetic resonance imaging (MRI), the term field of view (FOV) is often utilized [5].

2.2.3 Fill factor of applicators and probes

Fill factor, as its name implies, is a measure of extent to which the material load fills the applicator's effective field region (EFR). For example, in an induction heating work, if a metal rod is placed within a solenoid coil with uniform field, and the rod and the coil are assumed to have the same

height, the fill factor would be the ratio of the volumes, which is the square of the diameter ratios. To obtain higher applicator efficiencies, it is best to keep the fill factor as high as possible. In practice, the field is often non-uniform. A general expression for the fill factor ρ can then be defined as:

$$\phi = \frac{\iiint_{V_m} |\Psi| dv}{\iiint_{V_t} |\Psi| dv} \tag{2.7}$$

where Ψ is field intensity, which could be either electric or magnetic depending on which one would be useful for the given problem. The numerator is the field intensity magnitude integrated over the volume the material load would occupy, V_m, and the denominator is the integral of the field u over the whole effective field region (EFR), V_t. Note that in this definition the impact of the material load's presence on the electric field is not considered, and only the electric field intensity in its original form is integrated over the volume of the load.

According to Eq. (2.7), if the applicator has a non-uniform field, a material load will yield a larger fill factor when it is placed in a strong field area than when it is placed in a weak field area.

In an idealized case where the field is uniform over the volume of the applicator, Eq. (2.7) would be reduced to the ratio between the load volume and the total applicator volume:

$$\phi = \frac{V_m}{V_t} \tag{2.8}$$

In many practical instances such an approximation is valid. An example is the solenoid applicator (Chapter 7), where the magnetic field over the inside volume of the applicator is uniform for an adequately long coil compared to the material load. Another example is a parallel-plate applicator (Chapter 3), where the electric field is uniform between the plates if the load dimensions are sufficiently smaller than the area of the plates. In both cases the approximation shown in Eq. (2.8) becomes valid.

In the design of any applicator or sensor, it is desirable to maximize the fill factor, which means having the material volume in a location with highest field intensity, and filling as much of the field volume as possible. Doing so will increase the applicator efficiency in heating systems and improve the sensitivity in the sensing system. In practical applicators, however, there are many obstacles and tradeoffs, which will be discussed on a case-by-case basis; this is an issue frequently addressed in this book.

Both applicator efficiency and sensitivity, which is defined later in this chapter, are affected by the fill factor. In most situations both of these figures of merit are improved by a higher fill factor, but predicting them from the fill factor is not straightforward.

2.2.4 Field uniformity: definition and contributing factors

In most applications it is desired that the applicator perform its intended function in a spatially uniform manner. While the uniformity of field intensity is not the only factor in achieving that aim, it is certainly an important one. Field uniformity can be defined over the effective field volume as follows:

$$\rho = \frac{|\Psi_{max}| - |\Psi_{min}|}{|\Psi_{max}| + |\Psi_{min}|} \times 100\% \tag{2.9}$$

where $|\Psi_{max}|$ and $|\Psi_{min}|$ are the maximum and minimum amplitudes of either *E*- or *H*-field intensity (whichever is useful for the application at hand) within the EFV. In certain applications there are additional restrictions on this definition. For example, in magnetic resonance imaging (MRI) [5], only the *H* field perpendicular to the static magnetic field is useful. Therefore the field intensity used in Eq. (2.9) refers only to the magnetic fields in that direction.

The important question to answer is what factors cause the limitations of the field uniformity, and what can be done to reduce and eliminate them. Some of these factors that are specific to the applicator type or application will be covered in their proper context, but the most general are discussed here.

Standing waves are a main cause of non-uniformity. This phenomenon, which is often called the "wavelength effect", happens in electrically large applicators, or when the EFV is comparable in size, or significantly larger, than the operating wavelength. The second cause of field non-uniformity is the material itself, which changes the electromagnetic boundary conditions. Usually, the higher the dielectric loss or conductivity, the more non-uniform the fields become.

Even if the fields are perfectly uniform, there are several factors beyond electromagnetics that determine the outcome of process uniformity; for example, in RF drying [7] the variability of evaporation from the edges versus the center of the material may cause the final drying not to be uniform. In fact, in some cases the electromagnetic fields are intentionally modified to compensate for non-electromagnetic sources of non-uniform heating [8,9]. A full description of the design process is discussed in Chapter 4.

2.3 CATEGORIZATION OF APPLICATORS/PROBES BY USEFUL FIELD TYPE: *E* OR *H*

There is a vast array of high-frequency applicator and probe configurations for interaction of fields with materials. Arguably, a primary method to categorize them is by "useful" field type (electric or magnetic field). While any high-frequency applicator must contain both field types to satisfy the Maxwell equations, usually only one type of field is useful for the intended function. Efforts to maximize the useful field type and minimize the "unnecessary" field type are sometimes a part of the design process [5].

2.3.1 Rationale for making a distinction between useful field types

The energy deposited into a dielectric is proportional to the square of the electric field intensity as described by Eq. (1.18). Therefore the electric field must be maximized for best energy deposition. On the other hand, there are many situations, as will be described in Chapter 7, where the magnetic field must be maximized in order to have the desired field interactions. These include eddy current induction, magnetic hysteresis effect, and magnetic resonance.

Based on the discussion above, depending on the task at hand, either electric field or magnetic fields must be maximized [10]. But we know that at high frequencies one type of field cannot exist with the other. Hence there is no applicator with only electric or only magnetic field. From the discussion on wave impedance in Chapter 1, in high-impedance situations electric fields dominate, and with low impedances it is the magnetic field that is at the maximum. Furthermore, in cavity applicators, which are electrically large, there is a distribution of electric and magnetic fields that is in accordance with the established standing waves.

Figure 2.3 shows, in a schematic manner, the locations of the electric field, magnetic field, and cavity applicators in a standing-wave map. The electric field applicators (as represented by a pair of parallel plates) are at the electric field node and the magnetic field applicator (shown as a solenoid) is at the magnetic field node. The cavity resonator encompasses both electric field and magnetic fields in the form of standing waves.

2.3.2 Electric field applicator/probes

The simplest form of electric field applicator is the parallel plate, which is shown in Figure 2.4a. This applicator is mainly used for interfacing dielectrics and generally low-conductivity materials with electric fields. Electric field applicators are also used for exciting low-temperature plasmas, or

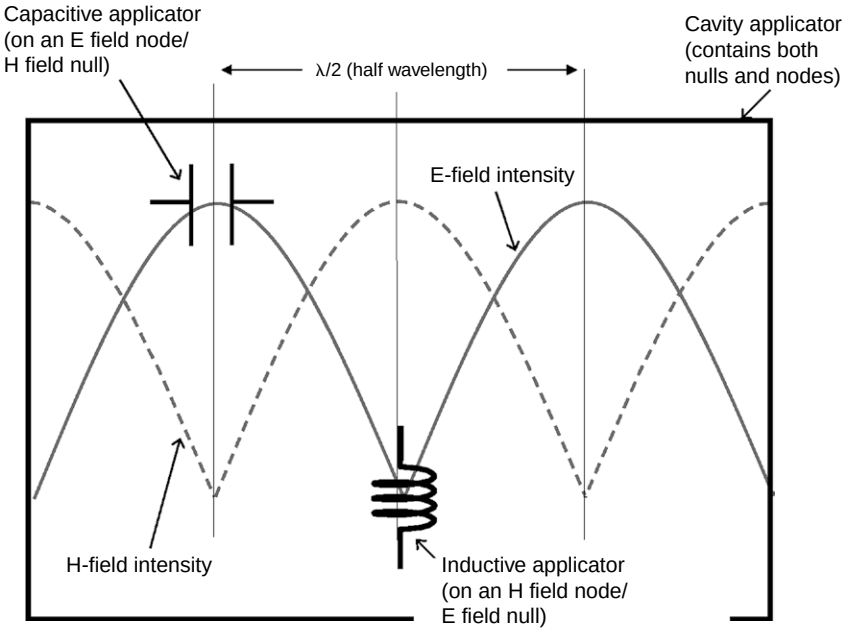

FIGURE 2.3 *Schematic of how electric field, magnetic field, and cavity applicators operate with respect to nodes and nulls of the electric and magnetic fields at high frequencies.*

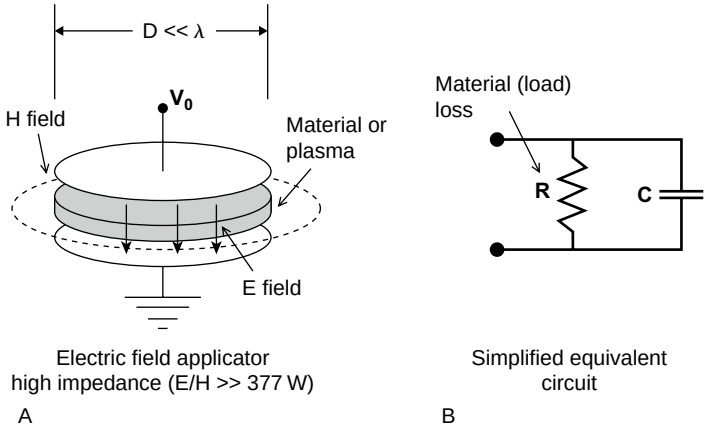

FIGURE 2.4 *Schematic of a simple form of electric field applicator, a parallel-plate applicator (A), and its equivalent circuit (B).*

plasmas with lower electrical conductivities. An equivalent circuit of the electric field applicator is shown in Figure 2.4b. A detailed study of electric field applicators, including a full explanation of this equivalent circuit, will be discussed in Chapter 3.

In parallel-plate applicators the *E* field is established generally perpendicular to the two plates. There is an *H* field with a circular pattern around the *E* fields as shown. The ratio of *E* field to *H* field intensity, also known as the wave impedance, is well over 377Ω, which is the natural ratio of electric field to magnetic field in an open space. Having a large ratio essentially means the electric field is dominant between two parallel plates as long as the dimensions remain significantly below the wavelength.

E-field applicators are "electrically small", which means they have dimensions that are typically a fraction of the operating wavelength. As such there is not enough space for multinodal standing waves. In practice, electrically small *E*-field applicators can be made at any frequency as long as they are made small enough to prevent multinodal standing waves. Chapter 3 is devoted entirely to electric field applicators.

2.3.3 Magnetic field (inductive coil) applicators/probes

The simplest form of magnetic field applicator/probe is a current loop, as shown in Figure 2.5a. In magnetic field applicators, which are often called coils, the main component is the magnetic field, where the wave impedance (the ratio of electric field to magnetic field) is far below the wave impedance in free space, 377Ω. The magnetic field is formed from the current that flows in the applicator according to the Biot–Savart law [11].

Magnetic field applicators are used in several classes of applications: induction heating of conductive materials, hysteresis heating of ferrous metals at low (kHz) level frequencies, magnetic heating of materials with magnetic loss, ignition and sustaining of higher temperature/pressure plasmas.

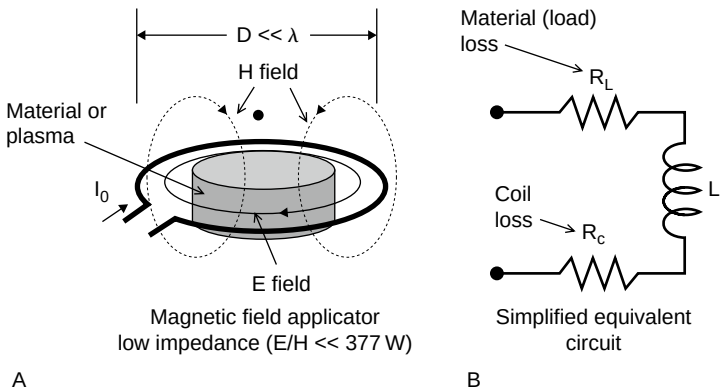

FIGURE 2.5 *Schematic of a simple form of magnetic field applicator, a single current loop (A), and its equivalent circuit (B).*

Magnetic field probes/sensors are also used in eddy current sensors, various modalities of magnetic resonance, nuclear magnetic resonance (NMR), magnetic resonance imaging (MRI), and electron spin/paramagnetic resonance (ESR/EPR).

A simplified equivalent circuit of the magnetic field applicators/probes is shown in Figure 2.5b. In addition to the inductance, which is varied slightly by the presence of the material load, there are two series resistance components, one representing the ohmic resistance of the applicator (coil) itself and another representing the material load's loss. Chapter 7 is devoted entirely to magnetic field applicators and probes.

2.4 RESONANCE IN APPLICATORS/PROBES

Resonance is a very useful technique that has broad applications in high-frequency engineering and science. There is a major difference between the use of resonance in an ISM microwave/RF system and its use in communication systems. In communication circuits, resonators are used because of their external behavior, i.e. their effect on neighboring circuits. For example, in a filter circuit resonance is utilized to suppress certain frequency bands, while allowing other frequency bands to transmit to the next circuit.

In field ISM applicators, however, resonance is used for impacting the intensity of field interaction with the material load. Therefore the discussion of resonance in ISM systems is oriented towards field configuration inside the applicator. In addition, resonance makes it possible to eliminate the reactive part of the input impedance, and have a purely resistive impedance, which would be easy to couple to transmission lines and external circuits.

Applicators and sensors come in both resonant and non-resonant types. The major role of resonance is to intensify the fields for a given power or signal level; therefore the material properties play an important role in determining if resonance is needed. For example, in a material with a very high dielectric loss, resonance may not be needed because even a low intensity of electric field can have sufficient effect according to Eq. (1.18).

2.4.1 Lumped resonance: fields and energy storage

In a mechanical resonator, such as a pendulum, there is an exchange of stored energy between potential energy and kinetic energy at every cycle. In electromagnetic resonance that exchange of energy happens between the energy stored in the electric field and magnetic field. A helpful model for resonance is a parallel L-C circuit, where the electric field is stored in the

capacitor and the magnetic energy is stored in the inductor. The wire in the two elements is the means by which the transfer of stored energy between them at each cycle takes place.

A fully lumped resonance, where magnetic and electric fields are completely separated in space, does not exist in reality. Figure 2.6 shows a somewhat more realistic case where the electric and magnetic fields are not fully separated, with a parallel-plate capacitor on the left and a solenoid inductor coil on the right connected via high-conductivity metal wires. The parallel plate stores most of the electric field energy, while the inductor stores most of the magnetic field energy.

At resonance, the total energy stored in the system alternates between the two components during every cycle via the conduction current. The conduction current in the wire turns into displacement current while in the parallel-plate capacitor, and creates an intense electric field between the plates. The parallel-plate capacitor also contains a small magnetic field component, in a circular pattern as shown in Figure 2.6. Typically, the ratio of electric field to magnetic field in a parallel plate is far larger than the open-space wave impedance of 377Ω.

Similarly, the conduction current in the coil windings creates a strong longitudinal magnetic field in the solenoid, while a relatively weak electric field also exists in the solenoid, as shown. The ratio of electric field to magnetic field is far smaller than the natural, open-space ratio of 377Ω.

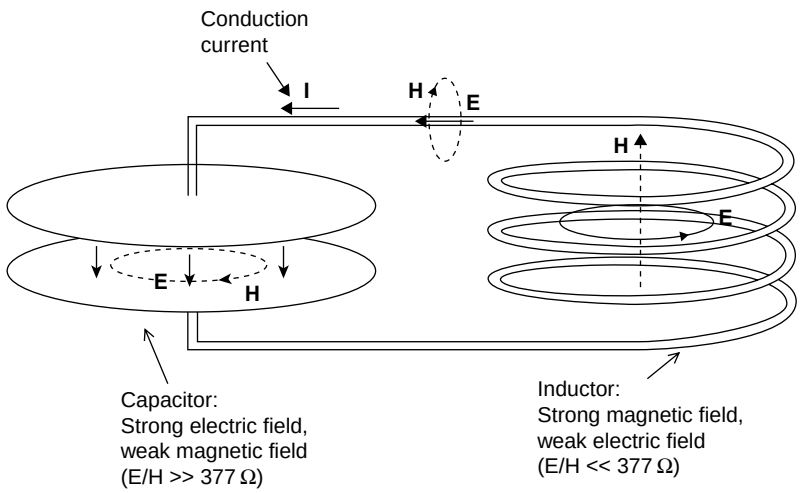

FIGURE 2.6 *An L-C resonant circuit composed of a parallel-plate capacitor and a solenoid-type inductor. This is a more realistic model than a fully lumped L-C circuit because of the presence of both* E *and* H *fields in each component.*

There are E and H components in and around the wire that carry the energy between the two main components. In the lumped resonant circuit, however, the magnitude of these fields is very small compared to the E-field maximum in the parallel plates and the H-field maximum in the solenoid.

2.4.2 Distributed resonance: field and energy storage

When the physical sizes of the resonant structure are comparable to the wavelength, the relative positions of the electric and magnetic fields become more intertwined, as opposed to lumped resonance where the energy stored in each field type is separated in space from the other. Figure 2.7 shows a half-wavelength transmission-line resonator, which is one of the simplest forms of distributed resonance [12].

The distribution of field intensity, also known as standing waves, is shown as a well, where the electric field has maxima at the two ends, where the

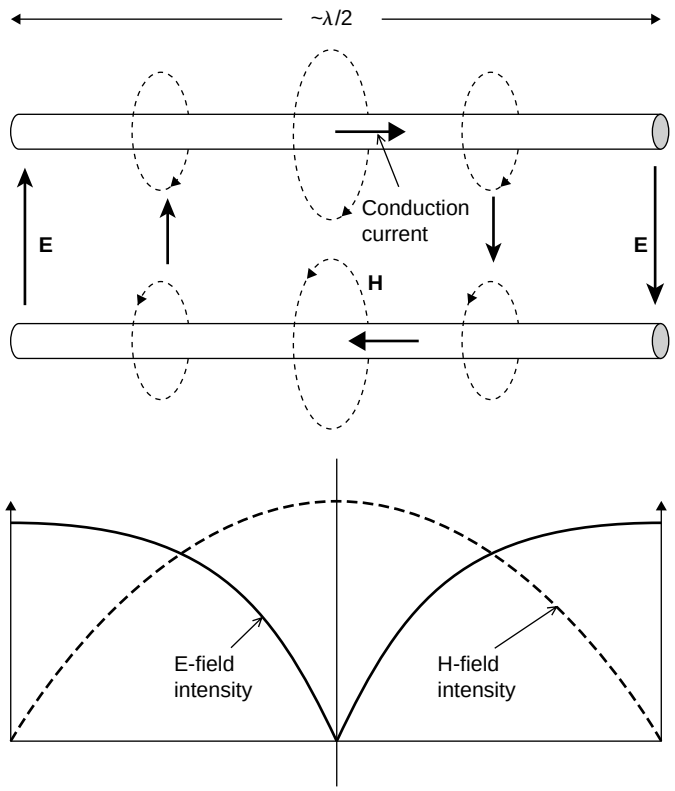

FIGURE 2.7 *Half-wavelength transmission-line resonator as an example of a simple distributed resonance.*

magnetic field nulls are located, and magnetic field energy maximum at the center, where the electric field is zero. In the areas between these two extremes the field intensities change gradually, ideally in a sinusoidal distribution. The conduction current distribution is similar to the magnetic field distribution, and the voltage potential distribution is similar to that of the electric fields.

A distributed resonator can act as either an electric field or magnetic field applicator, depending where the material load is located, but if the material load is large and extends through both the maxima and minima of the fields, the energy deposition into the material will be spatially non-uniform.

2.4.3 Resonant frequency

In a resonant system, the concept of frequency refers to two entirely different ideas. One is the stimulant frequency, which is an AC electrical signal, and then there is resonant frequency, which is the property of the resonant circuit (or applicator). In a properly operated resonant system either the stimulant frequency is adjusted to match the resonant frequency, or vice versa, where the resonant frequency is adjusted to match the stimulant frequency. In either case, the resonant properties of the system cannot be utilized unless this "tuning" is accomplished. The determination as to which of the two methods are used for matching of these two frequencies is dependent upon many factors specific to the problem at hand.

In applicators used for heating, for example, the frequency of operation is typically fixed for regulatory and economical reasons; therefore it is the applicator that needs to be designed or tuned to match the fixed stimulant frequency. In many other applications, such as those where resonant probes are used as sensors, the stimulant frequency can be adjusted to match the resonant frequency of the probe.

Understanding the relationship between the physical parameters of an applicator system and its resonant frequency is often quite important. The problem is posed either as finding the resonant frequency of a defined applicator or, more importantly, designing an applicator aimed at a given resonant frequency (typically a band allowed by regulation).

In some cases this can be done by experimental or trial-and-error methods, but in other cases it is necessary to determine the resonant frequency, or design for it in advance.

In such cases a challenge is that the resonant frequency shifts when the material load is introduced. In addition, changes in material geometry and consistency during the operation would result in variations as well.

This phenomenon happens to varying degrees, and is more severe in the case of electric field applicators than the magnetic field variety.

A general approach for finding resonant frequency is finding the eigenvalues, k_c, of the Helmholtz wave equation [12,13]:

$$\nabla^2 \psi + k_c^2 \psi = 0 \tag{2.10}$$

where ψ can be either an electric or magnetic field, chosen as appropriate for the problem at hand. In the simple case where losses are ignored and a uniform dielectric fills the space, then $k_c = \omega_0 \sqrt{\varepsilon \mu}$. In a realistic resonant applicator, which includes dissipative losses, and where the material load is only partly filling the field extent, the eigenvalues are complex numbers. Each eigenvalue corresponds to one resonant frequency, and is a function of material properties and the problem geometry.

The angular resonant frequency (or frequencies) ω_0 are embedded in the complex eigenvalues, which also contain the material properties of the load.

To solve Eq. (2.10) for a resonant applicator, the equation needs to be expanded in the proper coordinate system, and then the boundary conditions and material properties inserted. Even in cases with simple geometry, the presence of the material load would make the equation too difficult to solve without the use of numerical techniques.

In applicator designs dealing with the Helmholtz wave equation to solve for resonant frequencies, Eq. (2.10) is often used for electrically large applicators or resonant cavities. In these cases the problem is often stated in reverse, where the goal frequency, which is one of the ISM frequencies allowed by regulation, is known, and the applicator geometry and dimensions need to be synthesized so that the applicator's resonant frequency matches the ISM frequency.

In electrically small applicators, where the applicator can be approximated as a lumped element capacitor or inductor, designing for the goal resonant frequency is often simpler.

In these cases, the relationship between the angular resonant frequency ω_0 (in radians per second) and values of C (lumped capacitance in farads) and L (lumped inductance in henries) is given [12] as:

$$\omega_0^2 LC = 1 \tag{2.11}$$

where $\omega_0 = 2\pi f_0$, in which f_0 is the operating frequency in Hz. Equation (2.11), while not accounting for slight variations due to losses, is quite accurate for most practical situations.

2.4.4 Quality factor, bandwidth, and efficiency in resonant applicators

Quality factor (Q) is a measure of power dissipation in a general resonant circuit. In applicators Q is particularly important in defining the applicator's power efficiency. The most useful feature of the Q factor is that it can be measured readily using a frequency–amplitude method. The result of this measurement can be used to predict the applicator efficiency.

The Q factor is defined as [14]:

$$Q = \omega_0 \frac{W_m + W_e}{P_l} \tag{2.12}$$

where $\omega_0 = 2\pi f$ is the angular resonant frequency, W_m and W_e are the energies stored in the magnetic field and electric field respectively in joules, and P_l is the power lost per second in watts. In reality, since the stored energy changes between electric and magnetic energies at every cycle, it is more convenient to choose the instance when the electric energy is at its peak when we are considering an electric field applicator, and to choose the instance when the magnetic field is at its peak when magnetic field applicators are considered, i.e.:

$$Q = \omega_0 \frac{W_e}{P_l} \tag{2.13}$$

for electric field applicators, and:

$$Q = \omega_0 \frac{W_m}{P_l} \tag{2.14}$$

for magnetic field applicators.

The value of the quality factor for an applicator can be determined by geometrical data, operating frequency, and material loss data. Quality factor calculations for many important resonators of simple shapes have been calculated in many texts [11–14]. For some applicator types of interest here, Q calculations can be found in Chapters 3, 4, and 7. For empty applicators, without a material load, the only loss mechanism is the resistance of the metal that the applicator is made from. Therefore, to keep the efficiency high, very low resistivity metals such as copper or aluminum need to be used.

While several factors are involved in setting the value of the quality factor, most important is the dimensions of the device. Given the same metal of construction, the larger the resonant structure, the larger the quality factor

becomes. This is because of the nature of quality factor given in Eq. (2.12), where the stored energy is proportional to the volume, while the losses are proportional to the surface. Since larger volumes have higher volume-to-surface ratio, the quality factor follows suit. For example, a typical single-mode cavity, made of copper, at 1 GHz has a Q value of the order of 10,000 or more, but a miniature resonant loop for microwave circuits with the dimensions of a few millimeters has a Q value of the order of single digits.

On the other hand, the Q factor can be related to the bandwidth and resonant frequency as follows [13]:

$$Q = \frac{f_0}{\Delta f} \tag{2.15}$$

where Δf is the half-power (or 3 dB) bandwidth for the resonance curve. Both the resonant frequency and bandwidth can be measured using a scalar network analyzer.

The efficiency of a resonant applicator or probe, η_a, is then related to the Q factor and resonant frequency by [15]:

$$\eta_a = 1 - \sqrt{\frac{f_0}{f_m}}\frac{Q_m}{Q_0} \tag{2.16}$$

where f_0 and Q_0 are the resonant frequency and Q factor when the applicator is empty (without the material load), and f_m and Q_m are the corresponding values with the material load inserted. In most practical cases the shift in resonant frequency with insertion of the load is minimal, therefore f_0 and f_m are close, which will reduce Eq. (2.16) to:

$$\eta_a = 1 - \frac{Q_m}{Q_0} \tag{2.17}$$

We will see in Chapters 3 and 7 that applicator efficiency is often the starting point in the design process, and determines whether the design of the applicator as envisioned is possible. Therefore the determination of the efficiency using Q measurements, when possible, is quite important in the design of resonant applicators. In the design of heating applicators, the measurement of Q can be done at signal level, even though the actual efficiency is needed under power. The assumption here is that Q and resonant frequency do not change significantly with temperature. Such prediction of Q under load is not possible in the design of plasma applicators, since plasma cannot exist with signal level powers.

2.4.5 Parasitic energy storage in resonant applicators and probes

The concepts of effective field region (EFR) and fill factor were discussed in Section 2.2. In many situations involving resonance there are fields with significant energy storage that may occupy areas that cannot be recognized as the EFR. These field regions cause parasitic energy storage that may lead to serious reduction of efficiency for applicators, or reduction of sensitivity for probes/sensors.

The parasitic stored energy hurts the efficiency by reducing the impact of insertion of the load, thereby increasing Q_m (material-loaded quality factor). The reason for this increase is that when Eq. (1.17) or (2.17) is set up for the material-loaded condition, the parasitic stored energy is added to the numerator, while in the denominator the energy loss remains the same. An increase in Q_m would lead to a decrease in efficiency according to Eq. (2.17).

Figure 2.8 shows an example of parasitic energy storage involving an *E*-field parallel-plate applicator. In Figure 2.8a, while the main field below the active or "hot" electrode interacts with the material, the areas above and to the sides of the electrode store electric field energy, but do not contribute to the interaction. The result is a reduction of the fill factor and subsequent reduction of efficiency according to Eq. (2.13). The equivalent circuit is shown in Figure 2.8b, where the parasitic effects are shown as parallel capacitance C_p. Note that it is assumed a parallel inductance is utilized, but not shown, in Figure 2.8a. The solution to the parasitic field

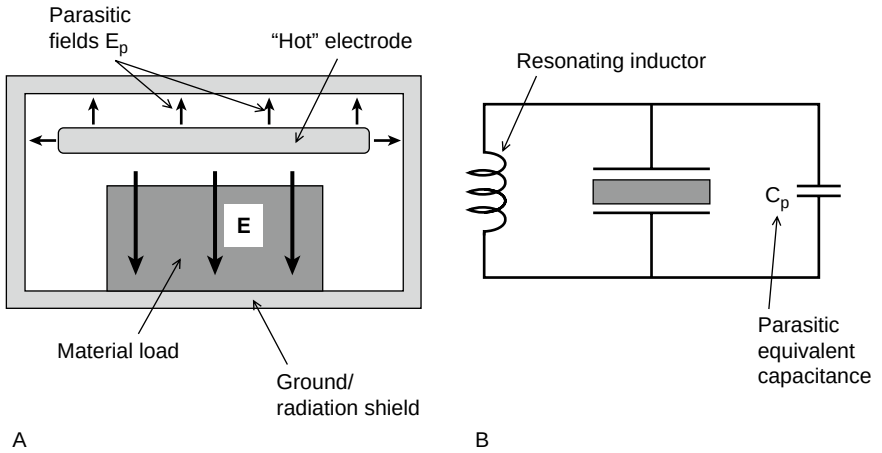

FIGURE 2.8 *Parasitic energy storage for an electric field applicator. (A) The applicator and load arrangement. (B) The equivalent circuit. The parasitic capacitance is added to the capacitance of the applicator.*

storage in this case is to reduce the parasitic capacitance by keeping the ground walls farther away from the active electrode.

Similarly, Figure 2.9a shows a resonated magnetic field applicator (induction coil), where there is a distance D_p between the working coil and the resonance capacitor. This distance and the circuit area allow room for a significant magnetic flux, so that a parasitic magnetic field H_p is formed. In the equivalent circuit of Figure 2.9b, the parasitic magnetic flux is shown as a series inductance L_p. This leads to a reduction of applicator efficiency. A solution that reduces the parasitic inductance is discussed in detail in Chapter 7 (Section 7.4.5).

2.4.6 Improving applicator efficiency and probe sensitivity

The importance of maximizing applicator efficiency goes well beyond energy savings. Low applicator efficiency often leads to difficulties in dealing with very high voltages (arcing) and high currents (removing dissipated heat from metal). In probes and sensors low efficiency could mean low signal-to-noise ratio and lack of adequate sensitivity. In essence, a lack of sufficient efficiency can make a well-sounding idea impossible to implement in practice.

In this section methods to improve efficiency are described in very general terms. In actual designs involving specific applicators/probes, some of the methods mentioned here may not apply at all; for example, the recommendation of higher material loss is irrelevant in most cases because the material is given, but there are cases involving susceptors where manipulating the dielectric loss or conductivity is part of the design.

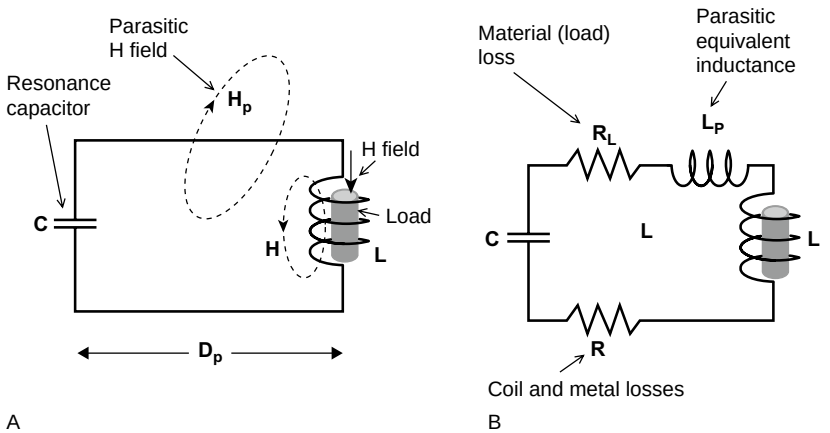

FIGURE 2.9 *Parasitic energy storage for a magnetic field applicator. (A) The applicator and load arrangement together with capacitance C to create resonance. (B) The equivalent circuit. The parasitic inductance is added to the inductance of the applicator.*

To maximize the efficiency Eq. (2.17) suggests maximizing Q_0 (the empty Q) and minimizing Q_m (Q with the material load). We will examine these separately below; the overall recommendations are shown in Figure 2.10.

To maximize Q_0, Eq. (2.13) suggests increasing the frequency and increasing the ratio of energy stored to metal losses, since in an empty applicator metal losses are often the only loss. To do this, the applicator should have a high volume (be physically larger). Fundamentally, physically larger applicators have a larger Q, because the stored energy (the numerator in Eq. (2.13)) follows the volume occupied by fields, and metal loss (the denominator) follows the metal surface area. Therefore quality factor follows the volume-to-surface ratio, which is higher when an object is larger.

To minimize the material-loaded quality factor, Q_m, the impact of the material's presence is to be maximized, which means a higher fill factor and higher loss factor material. There is also a need to reduce parasitic energy storage, as described in Section 2.4.5.

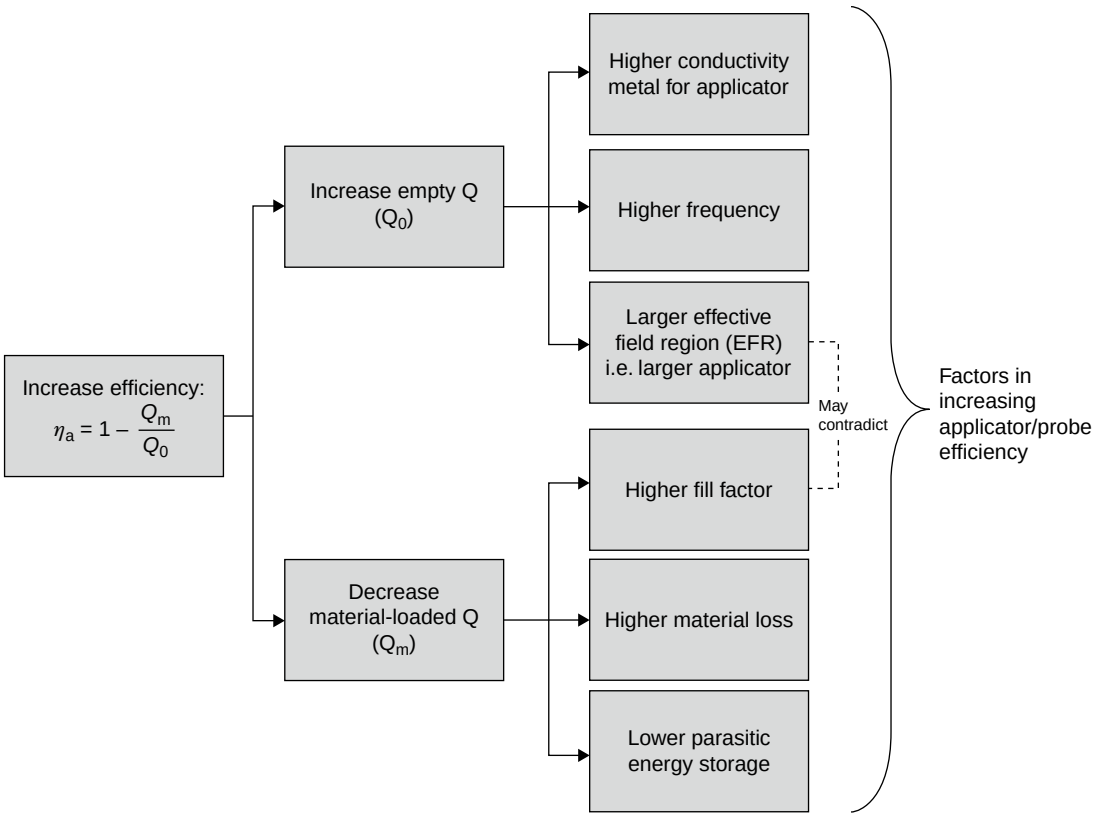

FIGURE 2.10 *Map of methods for increasing the efficiency of applicator/probes.*

2.4.7 Self-resonant and semi-lumped applicator/probes

In a lumped resonant circuit, like the one shown in Figure 2.6, the locations of the capacitor and the inductor are separate, but they are connected by a wire. In contrast, the loop–gap resonator, as shown in Figure 2.11, is an integrated semi-lumped resonant structure, where the capacitive and inductive elements are attached in the form of a hollow cylinder with a longitudinal slit (or gap). The electric fields reside mostly in the gap, while the magnetic fields surround the loop as shown. This type of structure was originally developed as a probe for Electron Spin Resonance (ESR) [16–18]. This modality of magnetic resonance requires a uniform magnetic field at microwave frequencies (1–10 GHz). The loop–gap resonator has the advantage of compactness. Cavities are approximately wavelength size, and ESR samples are very small quantities of chemicals, which lead to very low fill factor and low sensitivity when cavities are used. The dimensions of a loop–gap resonator are typically of the order of 5–10% of the wavelength, compared to 50–200% in the case of single-mode cavities. While many ESR spectroscopy experiments are performed at 8 GHz or above, where the cavities are compact, there was a need to develop probes for experiments at 1–2 GHz, where the cavities could be

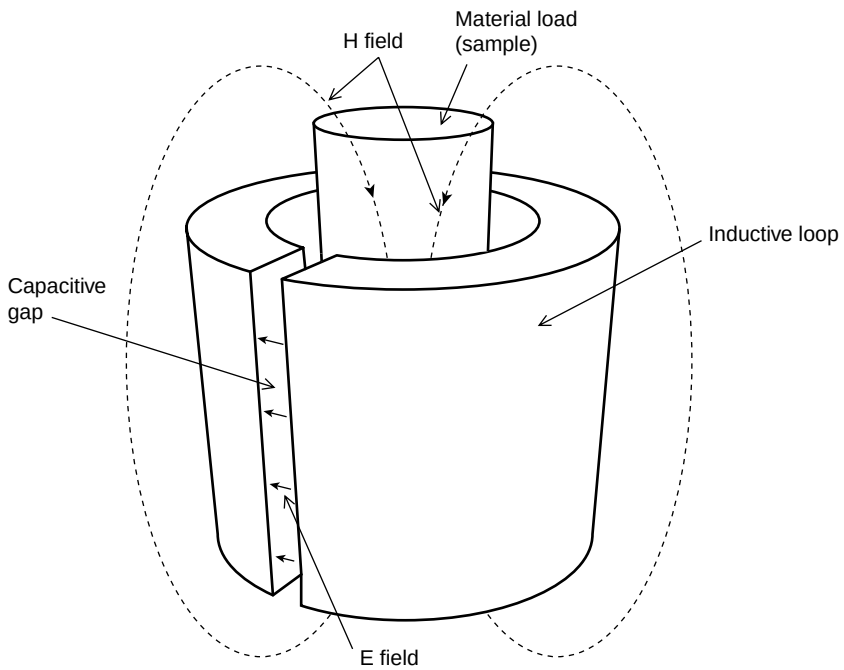

FIGURE 2.11 *The loop–gap resonator.*

very bulky (of the order of 30 cm). Loop–gap resonators have also been utilized as microwave frequency-selective components [19].

2.4.8 Cavity resonators as applicators or probes

Resonant cavities are metal-enclosed resonant structures [12–14], where the dimensions are comparable with, or larger than, the operating wavelength. As such, practical cavities are almost exclusively operated at microwave frequencies (300 MHz to 30 GHz), where wavelengths are of the order of 1 cm to 1 meter. The operating frequency of a cavity, when properly used, is the same as one of the resonant modes.

The resonance in cavities is of distributed nature, where the geometrical arrangement of electric and magnetic fields is based on standing waves. The half-wavelength transmission-line resonator of Figure 2.7, as well as the quarter-wave strip resonator of Figure 2.12, are simple forms of distributed resonance. The resonant cavities are fully enclosed versions of distributed resonators, and may have modes in two or three dimensions, as opposed to the single-dimensional mode structures of Figures 2.7 and 2.12. For simple cavity geometries in empty (without load) conditions, closed-form solutions of the wave equation (2.10) are available [12–14]. The mode chart of Appendix A2.1 shows the mode frequencies for empty cylindrical cavities. When cavities are used as applicators [15] or sensors [20], the material load modifies the fields.

Here, referring to Figure 2.13, we will attempt to clarify the concepts related to cavity modes and how they operate. Consider a generic cavity, shown schematically in Figure 2.13a, where there are four potential modes of operation with designations A, B, C, and D. Each of these modes has a distinct standing-wave field pattern as shown, and each has a resonant frequency, designated as f_a, f_b, f_c, and f_d, shown on a frequency domain spectrum. Figure 2.13b shows a frequency source that generates a stimulant frequency, f_s, which feeds the cavity through a coupling structure. When this stimulant frequency is set to equal the resonant frequency of mode B ($f_s = f_b$), the cavity will form a field pattern that matches that of mode B in Figure 2.13a. In this example case, among the four potential modes, mode B has become the only operating mode. If the frequency of the source does not match any of the mode resonant frequencies, there would be no operating cavity modes, and power emitted from the source would be reflected.

In the discussion above we used a simplistic model of a fictitious cavity to show how a cavity with several potential modes can be operated in a single mode. The whole of Chapter 4 is devoted to single-mode applicators and probes, and practical issues involved in using them for material interactions. Then, in Chapter 5, multimode cavity applicators are covered in detail.

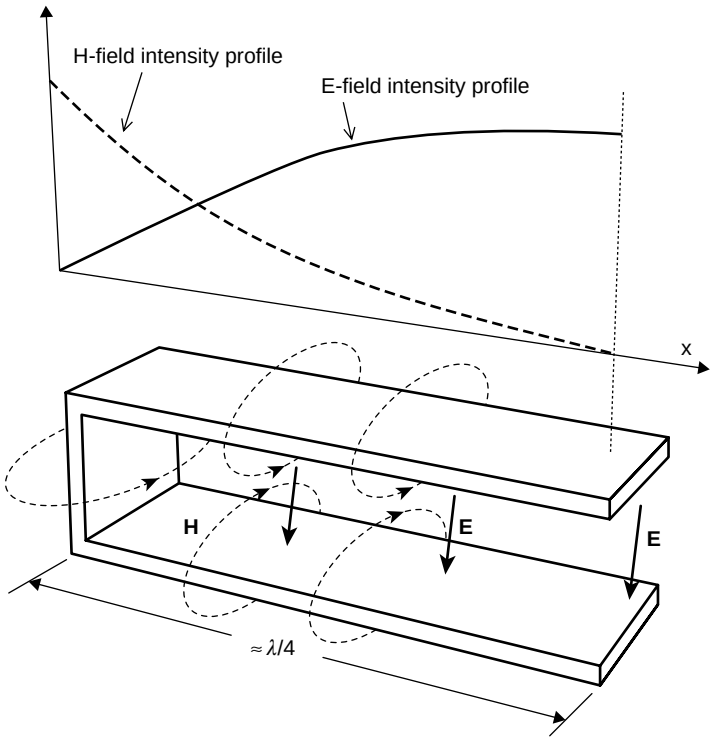

FIGURE 2.12 *Quarter-wavelength strip transmission-line resonator.*

2.5 COMMON PROPERTIES AND APPLICATIONS AS HEATING DEVICES AND SENSORS

2.5.1 Non-resonant and transmission-line applicators and probes

We discussed the advantages of resonant applicators in a previous section. Resonance, while advantageous, often brings hardware and operational complexities related to tuning, etc. Non-resonant applicators, when they are permissible to use, provide advantages such as lack of need for tuning (staying at resonance) and simplified structures. Therefore it is useful to avoid resonance when possible.

Lack of resonance typically means the electric field is not as strong; this is due to the fact that resonance tends to enhance the field strength. One of the situations where the resonance becomes unnecessary is heating of materials with very high loss. Referring to Eq. (1.18), if the loss factor is high, there is less need for a high electric field. We will describe two

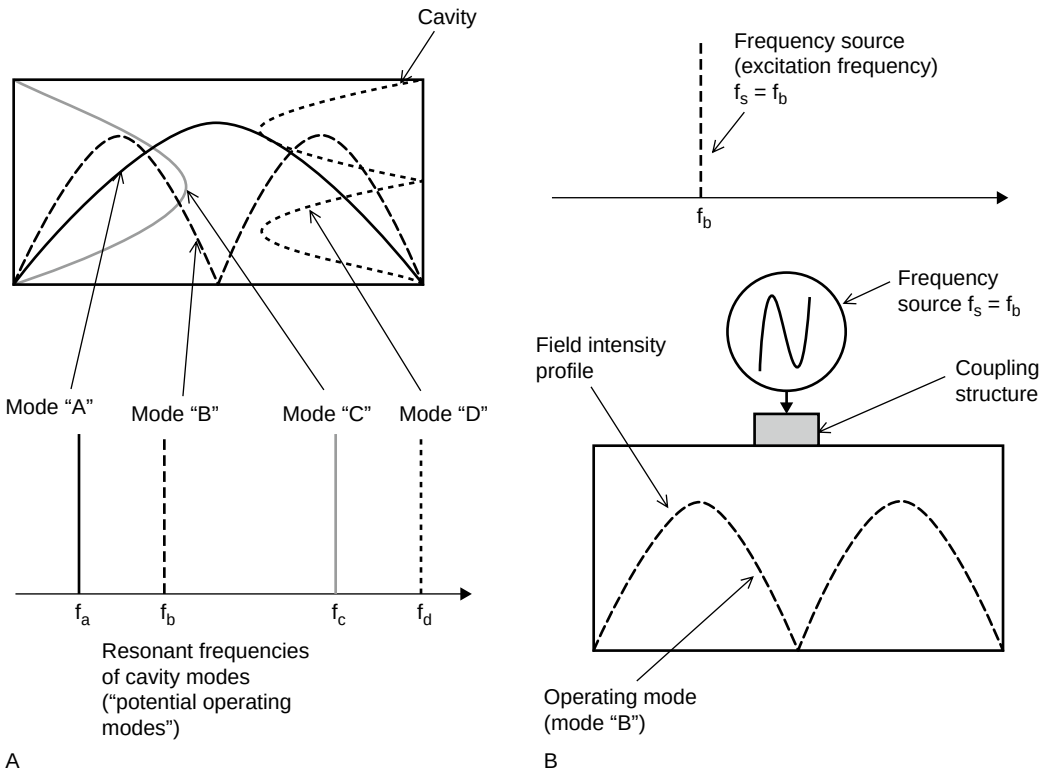

FIGURE 2.13 *Schematic description of cavity modes and operating mode in microwave cavities. (A) Cavity modes are "potential" operating modes. (B) Operating mode is the one that matches the excitation frequency.*

major types of non-resonant applicators here. More detailed analysis and applications of some of these configurations will be the subject of future chapters.

Transmission-line or traveling-wave applicator/probes are a class of devices where the effective field region (EFR) is the location where traveling energy flows. A schematic example is shown in Figure 2.14. In traveling-wave applicators the material load is placed in the path of traveling waves in a transmission medium. The fields established in the transmission medium interact with the material to provide the needed function. In Figure 2.14a and b the cross-sectional *E*-field configurations for a strip transmission line and a waveguide are shown. Figure 2.14c shows a schematic view of how a transmission-line applicator/probe operates. The *E* field that exists in the transmission line interacts with the material load. The details of this type of transmission-line applicator are covered in Chapter 9.

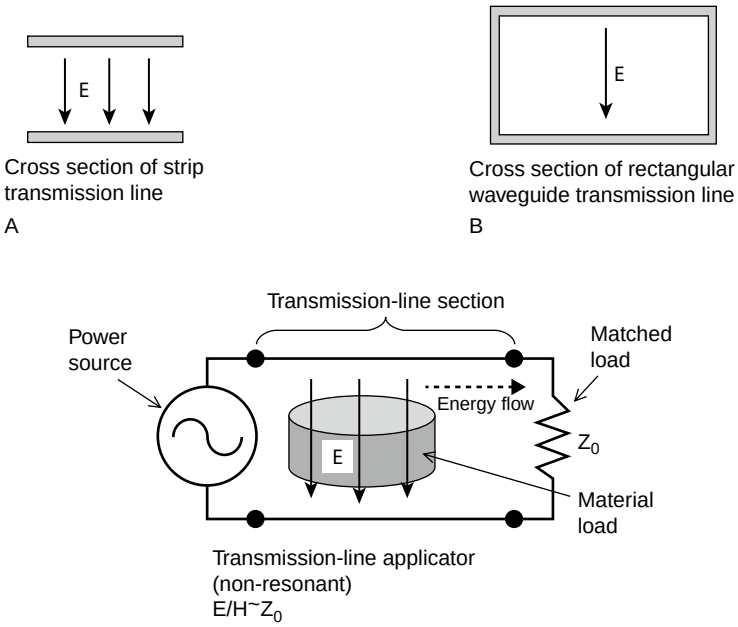

FIGURE 2.14 *The concept of transmission-line applicator/probe.*

In addition to applicators, there are transmission-line sensors that work on the same principle. An example is shown in Figure 2.15 [21], where the fringing fields from a microstrip transmission line interact with the contents of a low-loss cup for the purpose of fining the loss properties of the liquid. The operation of such sensors complies with the configuration shown in Figure 2.14c, where there is a signal flow from a source to a detector, which has an impedance matched with the characteristic impedance of the microstrip line.

2.5.2 Material loading effects

The introduction of a load (or a sample) to an applicator or probe has a typically large impact on its field configuration and port impedances. As such, the properties, geometry, and position of the load become a part of the electrical properties of the circuit. This fact becomes a particularly big challenge in designs where the load properties change with time, temperature, and other parameters.

The consideration of the load's impact has two distinct aspects: field configuration and circuit properties. In the study of field configuration, the

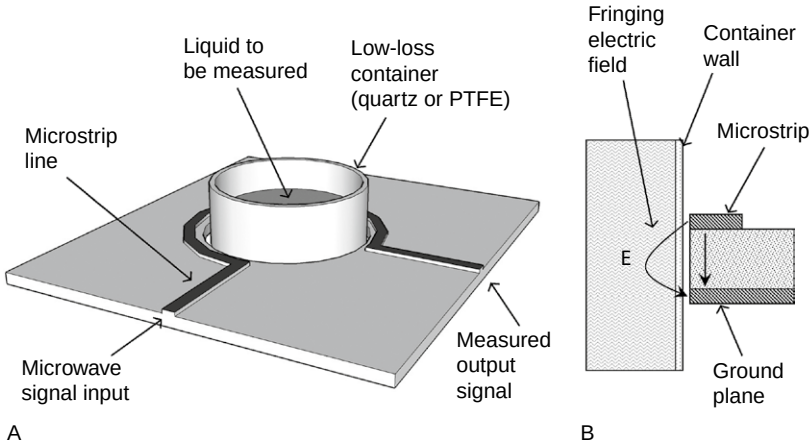

FIGURE 2.15 *A microstrip transmission-line sensor for detection of the dielectric loss properties of liquids. (A) General configuration (after Ref. [21]). (B) Close-up view of the fringing-field configuration.*

important issue is the change in the electromagnetic boundary conditions of the unloaded applicator, which typically takes the problem out of the realm of simple analytical solutions. In that case it is often necessary to resort to numerical techniques such as finite element analysis.

As for the impact of the material load on the circuit properties, use of equivalent circuit models is typically helpful. In distributed field applicators, equivalent circuits are only an approximation of the real situation because it is more difficult to separate the locations of electric and magnetic fields.

Another issue in material impact is nonlinearity. The root of the nonlinearity is the change in the material properties with the application of power. For example, in RF or microwave heating of materials, as the material is heated the dielectric properties change. With that change the electrical properties of the applicator, such as impedance, quality factor, and resonant frequency, also change. In some cases the changes in the material properties are small enough that the applicator's properties remain unchanged. This is a great simplifying fact that can be utilized in the applicator design. For example, an applicator can be tested with room temperature material to determine the loaded quality factor in advance using a network analyzer [22].

2.5.3 Reciprocity between applicators and probes: sensitivity

While applicators and probes are used for entirely different purposes, many figures of merit are common between them. One such figure of merit is sensitivity. Let us first examine the concept for an RF/microwave material sensor/probe. In such a device, a material property is related to, and is

quantified by, an electrical property. An example of a material property is the dielectric constant ε_r' and an example of the electrical property is the resonant frequency of a resonant cavity, f_0. In this particular example, the sensitivity can be defined as:

$$s = \frac{df_0}{d\varepsilon_r'} \tag{2.18}$$

In this example, a high-sensitivity probe is one where a small variation in the dielectric constant leads to a large change in the probe's resonant frequency. A high sensitivity would also lead to a high signal-to-noise ratio. In this example, noise is the natural tendency in the system to produce a shift in the measured quantity, which is the resonant frequency here.

The achieve a high sensitivity the design effort would point to designing the sensor so that the sample is placed at the highest field region of the sensor, and the fill factor must be high as well. For example, suppose that the sensor is a microwave cavity. A high fill factor means that the cavity needs to be made small, which would require a higher frequency and a low cavity mode. There are cases where the high sensitivity must be traded off for another figure of merit, such as field uniformity over a larger sample. In such an instance, sensitivity would become a geometrically defined property.

The same definition can be made for applicators. In an applicator, the absolute field strength $|\psi|$ at a location inside the load is the result of power input P. In that case the sensitivity can be defined as:

$$s = \frac{d|\psi|}{dP} \tag{2.19}$$

It has been proven [2] that the same design rules need to be followed for applicators and probes in order to have high sensitivity. Here again, a high fill factor and placing the load at the highest field area would lead to better sensitivity.

2.5.4 Applicators/probes for ISM applications across the frequency spectrum

The purpose of this section is to take a bird's eye view of how applicators and probes in RF/microwave frequencies are used in both frequency and material property domains. These devices are divided in type to *E*-field and *H*-field types. The applications are divided into applicators (for power deposition and processing) and probe/sensors (for sensing and characterization

of materials). The collection of applications for which these applicators and probes are utilized are commonly called Industrial, Scientific, and Medical (ISM) applications. Various "bubbles" in Figure 2.16 are discussed in detail in specific secions and chapters in this book. For example, *E*-field applicators (lower left bubble) are covered in Chapter 3, and *H*-field applicators (lower right bubble) are discussed in Chapter 7. Resonant cavities, though they are mostly used as *E*-field applicators, have found applications as *H*-field applicators as well, and have a separate bubble in the upper left of this figure.

Figure 2.16 shows an approximate map of operating frequency versus dielectric loss/conductivity for applicators. On the horizontal coordinate the material's dielectric loss and conductivity are put on the same scale, realizing that Eq. (1.37) ($\sigma = \omega\varepsilon'' = \omega\varepsilon_0\varepsilon_r''$) holds. The interchange of conductivity and dielectric loss should be made bearing the exceptions discussed in Section 1.3.1 in mind. The horizontal lines in Figure 2.16 depict the ISM frequencies allowed by regulatory agencies for power applications where stray emissions that may interfere with wireless communication may occur.

Figure 2.17 depicts the same ideas as those in Figure 2.16 for probe/sensor applications at RF/microwave frequencies. In most cases for sensors it is not necessary to be limited by the ISM frequencies, since most near-field sensors do not emit enough stray energy.

FIGURE 2.16

Approximate map of how RF/microwave applicators are used in the frequency versus conductivity/dielectric loss domain.

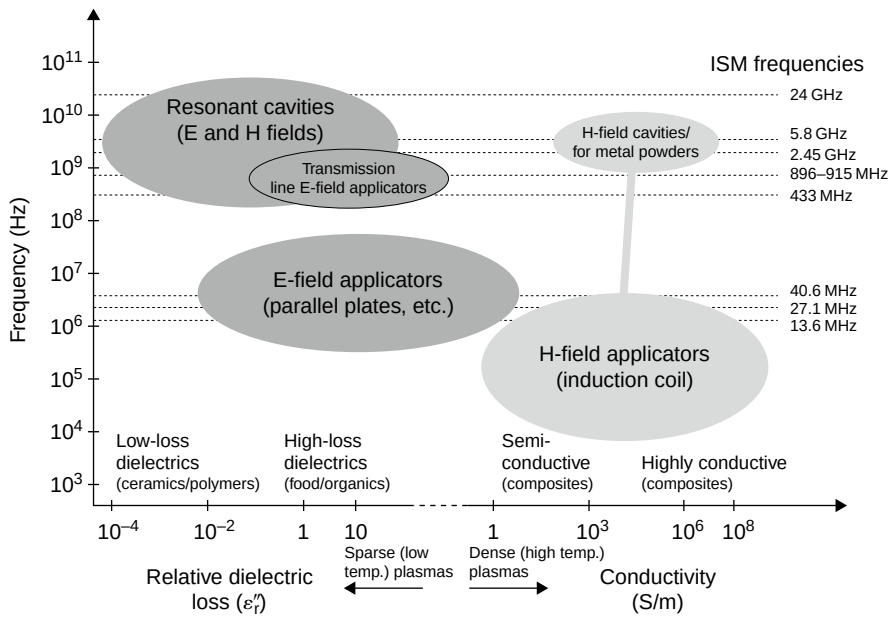

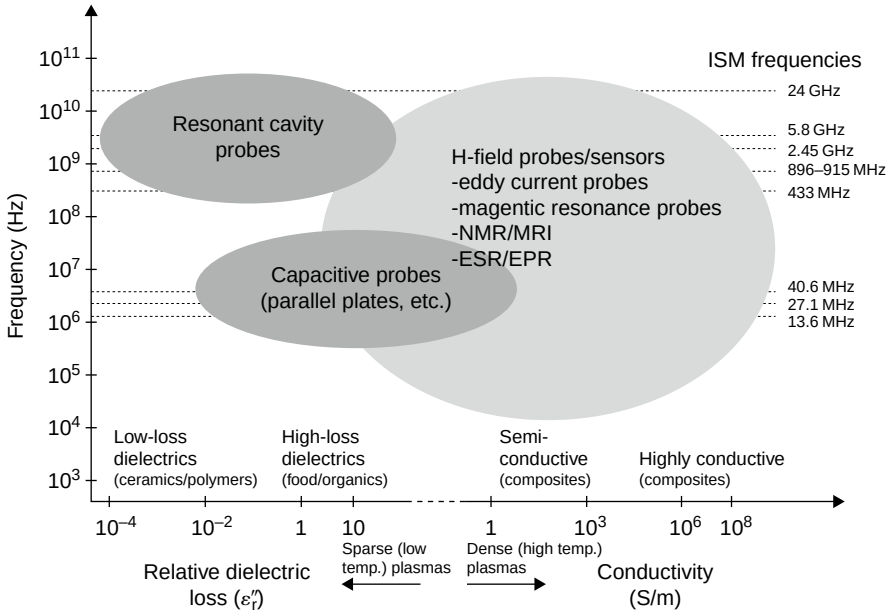

FIGURE 2.17 *Approximate map of how RF/microwave probe/sensors are used in the frequency versus conductivity/dielectric loss domain.*

REFERENCES

[1] B.D. Steinberg, Jin Au Kong (Ed.), et al., Microwave Imaging Techniques, Wiley Series in Remote Sensing, Wiley, New York, 1991.

[2] D.I. Hoult, The principle of reciprocity in signal strength calculations: a mathematical guide, Concepts Magn. Reson. 12 (4) (2000).

[3] M.S. Kim, et al., Tip–sample distance control for near-field scanning microwave microscopes, Rev. Sci. Instrum. 47 (9) (2003) 3675–3778.

[4] Kalkbrenner, et al., Optical microscopy via spectral modifications of a nanoantenna, Phys. Rev. Lett. 95 (2005) article 200801.

[5] J. Mispelter, et al., NMR Probeheads for Biophysical and Biomedical Experiments, Imperial College Press, London, 2006.

[6] M. Ahmed, et al., Radiofrequency thermal ablation sharply increases intratumoral liposomal doxorubicin accumulation and tumor coagulation, Cancer Res. 63 (2003) 6327–6333.

[7] G.A. Smith, Dielectric applications in textiles and auxiliary industries, in: Proceedings of Conference on Heating and Processing 1–3000 MHz, The British National Committee for Electroheat, Cambridge, 1986, Chaired by H. Barber, paper 2.2.

[8] D.J. Hill, C.D. Rudd, M.S. Johnson, Design and application of a cylindrical TM020 mode applicator for the in-line microwave preheating of liquid thermosets, J. Microw. Power Electromagn. Energy 33 (4) (1998).

[9] P.J. Goethel, R.W. Lewis, W.J. Teerlink, Process for preparing polymeric material with microwave, US Patent No. 5471037, 1998.

[10] H.A. Haus, J.R. Melcher, Electromagnetic Fields and Energy, Hypermedia Teaching Facility, MIT, available online at: <http://web.mit.edu/6.013_book/www/book.html>

[11] S. Ramo, et al., Fields and Waves in Communication Electronics, third ed., Wiley, New York, 1994.

[12] R.E. Collin, Foundations of Microwave Engineering, second ed., IEEE Press, 2001, p. 306.

[13] T.K. Ishii, Microwave Engineering, Harcourt Brace Jovanovich, San Diego, 1989.

[14] D.M. Pozar, Microwave Engineering, Wiley, New York, 2004.

[15] A.C. Metaxas, R.J. Meredith, Industrial Microwave Heating, Peter Peregrinus, 1983, p. 207.

[16] J.S. Hyde, W. Froncisz, A. Kusumi, Dispersion electron spin resonance with the loop–gap resonator, Rev. Sci. Instrum. 53 (1982) 1934–1937.

[17] W.N. Hardy, L.A. Whitehead, Split-ring resonator for use in magnetic resonance for 200 to 2000 MHz, Rev. Sci. Instrum. 52 (1982) 213–216.

[18] M. Mehdizadeh, T.K. Ishii, J.S. Hyde, W. Froncisz, Loop–gap resonator: a lumped-mode microwave resonant structure, IEEE Trans. Microw. Theory Tech. (December 1983) 1059–1064.

[19] M. Mehdizadeh, T.K. Ishii, Electromagnetic field analysis and calculation of the resonance characteristics of the loop–gap resonator, IEEE Trans. Microw. Theory Techn. (July 1989) 1113–1118.

[20] E. Nyfors, Industrical microwave sensors – a review, Subsurface Sens. Technol. Appl. 1 (1) (2000).

[21] F. Dachner, et al., Dielectric microwave sensor with multivariate calibration, Adv. Radio Sci. 1 (9) (2003) 9–13.

[22] R.I. Neophytou, A.C. Metaxas, Characterization of radio frequency heating systems in industry using a network analyzer, IEEE Proc. – Sci. Meas. Technol. 144 (5) (1997).

CHAPTER 3

Electric Field (Capacitive) Applicators/ Probes

CHAPTER CONTENTS

INTRODUCTION

Electric field probes/applicators were discussed briefly in Chapter 2 in the context of categorization of various high-frequency applicators and probes. In this chapter their various configurations, applications, analysis, and design methods are described in more detail. Electric field applicator/probes have found a wide range of application in industry, medicine, and scientific instruments and research. One goal of this chapter is to study the common themes among these applications and to create better understanding of the subject to aid designers in their specific applications.

We will start, in Section 3.1, with a general description of common characteristics, configuration, applications, and analysis methods. In Section 3.2, a detailed study of dielectric loaded parallel-plate applicator is made. The resonance characteristics and coupling circuits will be discussed in Section 3.3. We will then study the fringing-field and interdigital electrode systems in Section 3.4 and, finally, electrodes and systems used in RF heating will be discussed in Section 3.5.

3.1 CHARACTERISTICS AND APPLICATIONS OF CAPACITIVE APPLICATORS AND PROBES (SENSITIVITY, ETC.)

3.1.1 Description and definitions

Electric field applicators, as defined above, always have at least two distinct conductors, which are called electrodes, separated by an insulator, with a high-frequency potential between them as shown in Figure 3.1, a schematic and simplified view of a generic material-loaded *E*-field applicator/probe. The most common configuration has one of the electrodes at the zero or ground potential, as shown. The physical dimensions of capacitive applicators are a small fraction of the operating wavelength, as opposed to resonant cavities, which also apply electric fields but are physically larger than the operating wavelength. Considering the overall RF/microwave frequency spectrum as shown in Figure 1.1, electric field applicators/probes are typically used at its low end, but that is not necessarily a universal rule.

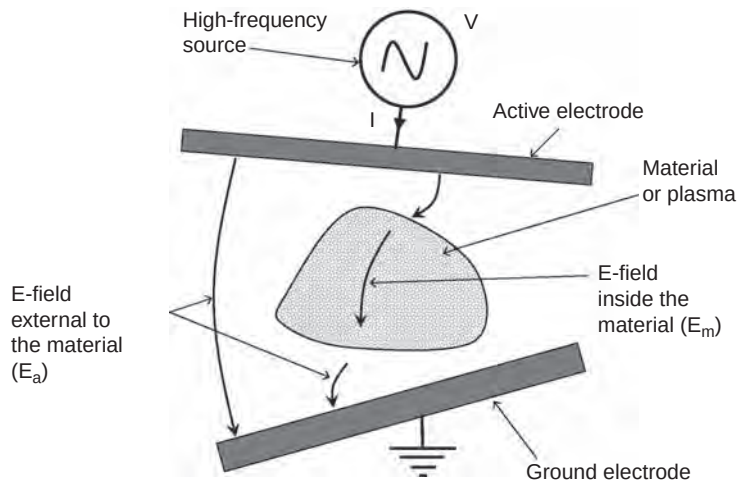

FIGURE 3.1 *A general representation of an electric field applicator/probe for definition of terms.*

When the objective is to provide a significant amount of power to heat the material, or sustain a plasma, the device is called an applicator. In this case the main concern is applicator efficiency, and whether the power can be delivered into the material without having to raise electric field, voltages, and currents to unacceptable levels.

When the objective is to use the device as a probe for material characterization or sensing, the high-frequency source provides only a small signal, sufficient in intensity for the purpose of measurement of impedance or another necessary electrical parameter. In this case the main concern is whether the probe has adequate sensitivity to reflect small changes in the material dimensions or dielectric properties. One of the most common electrical parameters used for material sensing is the impedance, which is the ratio of the voltage to current (V/I), as shown in Figure 3.1. Note that this impedance is a complex number that has both real and imaginary parts representing both amplitude and phase, which can be linked to the real and imaginary parts of the material's dielectric properties, as we will describe in detail later. We will discuss sensor applications in more detail in Sections 3.1.5 and 3.4.

3.1.2 Field configurations and methods of analysis

Electric field probes are utilized for their ability to impose a high-frequency electric field into a material. According to the Maxwell equation (1.1), however, no time-variable electric field can exist without the accompanying magnetic field. In E-field probes the magnetic fields are typically ignored because they are at their null according to Figure 2.3, while electric fields are at a node. This means that in every electric field applicator/probe, there is a point or an axis where the magnetic field is at zero, and moving away from that point, there is a rise in magnetic field intensity. The H-field intensity always remains weak in electric field devices, because E-field probes are defined as being electrically small, which means there is not enough space for the magnetic fields to reach a node. That is why the wave in E-field electrode systems possesses high impedance, which means at all locations the ratio of E field to H field is much higher than the impedance of free space at 377 Ω.

As described in Chapter 1, to analyze the field behavior of all near-field applicators, the wave equation shown in Eq. (1.5) can be used. Electric field applicators as we have defined them, however, can use a simpler approach for their field solution because of their small dimensions compared to the wavelength. For solving E-field applicator/probe problems the wave equation can be simplified by ignoring the frequency-dependent term and reducing it to the Laplace equation [1,2]:

$$\nabla^2 E = 0 \tag{3.1}$$

This approach of solving high-frequency problems is called the quasi-static method, in which the problem is approximated as a static-field case. In most *E*-field applicator problems, as long as the dimensions remain small compared to the wavelength, the quasi-static approach is a good approximation. In Section 3.5.4 we will discuss wavelength effects, which will correct certain errors that can be caused at high frequencies by using the quasi-static method.

In Section 3.3 and Appendix A3.1, the solution of Eq. (3.1) in one dimension is performed to study the material-loaded parallel-plate applicator. In addition, a solution to the one-dimensional coaxial solution in cylindrical coordinates is offered in Section 3.1.6 on asymmetrical electrodes. For solving the Laplace equation in two or three dimensions, several analytical methods have been used. One example is the method of separation of variables [2], another is conformal mapping [1].

Aside from the simplest of geometries, solving *E*-field electrode problems in two or three dimensions is often too complex for analytical solutions, particularly when a dielectric material is added. In such cases numerical techniques, such as the finite element method, are used. Figure 3.2 shows a problem of a uniform cylindrical lossy dielectric load in a pair of parallel plates using the COMSOL™ finite element package [3]. This solution shows that, even with perfect field uniformity prior to the introduction of the lossy load, the field uniformity is not preserved. Figure 3.3 shows the field intensity plot for the same problem of a cylinder in a parallel-plate applicator. The field intensity is higher in the gap areas between the cylindrical load and the electrodes.

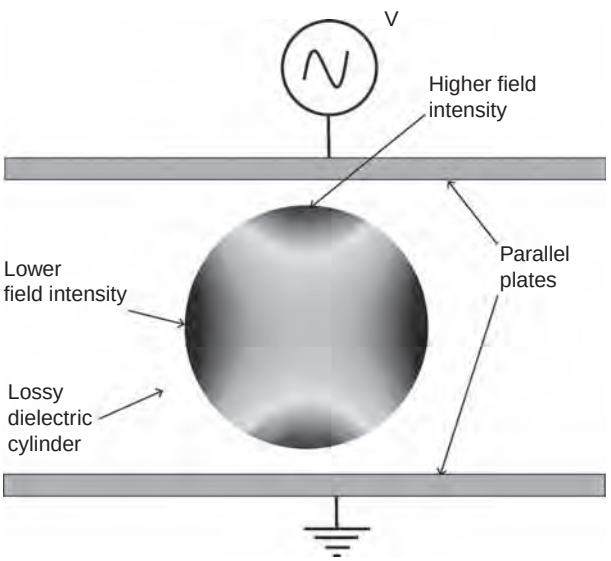

FIGURE 3.2 *Even though the field between two infinite parallel plates is uniform, the power deposition density for heating of a cylindrical object between the electrodes is not uniform. This is due to the distortion of the field in the presence of the load.*

In many practical cases involving the design of electrode systems for material applications, there is a need for the material to only partially fill the electrode's effective field region. In other words, non-contact heating, plasma activation, or sensing need to be treated and understood. Furthermore, many of these problems involve material shapes that are in sheet form or are oblong. In such cases, both theoretical field solutions and experiments have shown that designing an electrode system with the *E* field parallel to the sheet or oblong-shaped material, as

shown in Figure 3.4, provides better applicator efficiency and more sensitive sensor capability.

3.1.3 Field uniformity and methods of improvement

Consider an empty parallel-plate pair of electrodes with distance D and infinite area approximation. Such an electrode pair, with high-frequency voltage applied across them, can be considered to have perfect electric field

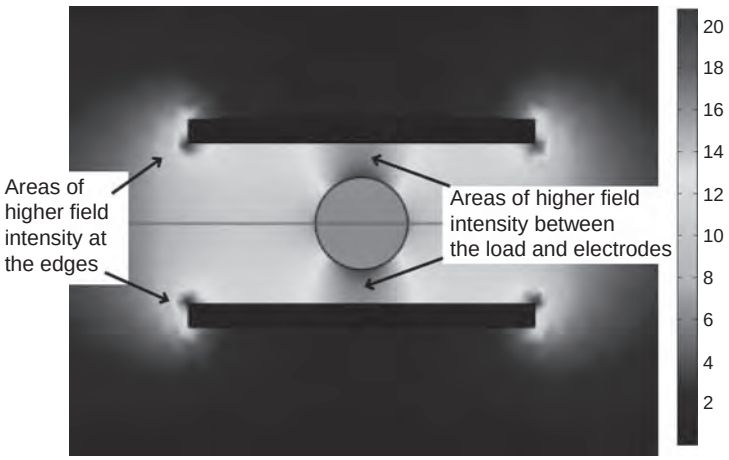

FIGURE 3.3 *The placement of a dielectric cylinder between parallel plates would alter the field intensity profile from a uniform to a non-uniform pattern, where the highest fields are in the gap area between the dielectric and the plates.*

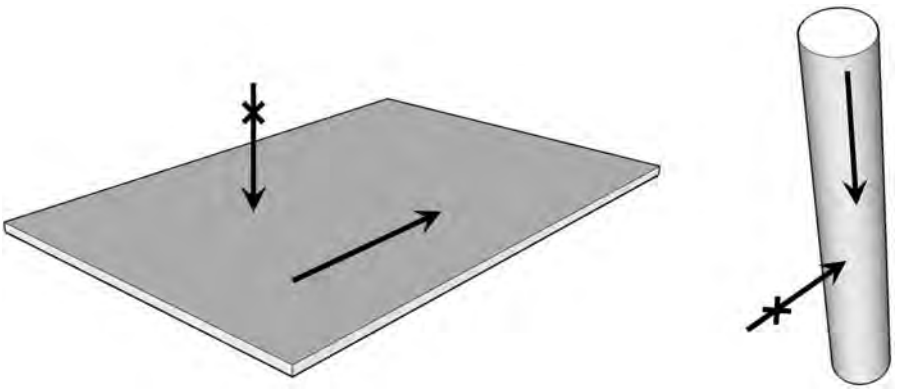

FIGURE 3.4 *In the design of E-field applicators and probes, the E-field configuration is more effective if it is in the longitudinal direction than the vertical direction in sheet-like or elongated dielectrics.*

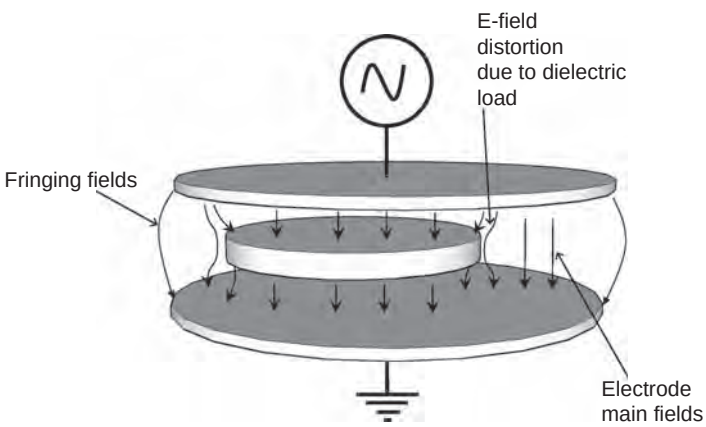

FIGURE 3.5
Main fields and fringing fields for the applicator, and the distortion of E-fields due to the dielectric load.

uniformity when the electrode dimensions are much larger than the distance between them. In such a case, the peak electric field intensity E (in V/m) between the plates, at all locations, will be:

$$E = \frac{V_0}{D} \tag{3.2}$$

where V_0 is the peak voltage of the source, while the instantaneous potential at time t will be $V(t) = V_0 \sin(\omega t)$, where $\omega = 2\pi f$ is the angular frequency in rad/sec and f is the operating frequency in Hz. Note that Eq. (3.2) is the solution to the Laplace equation (3.1) in rectangular coordinates in a single dimension; the details of this solution are given in Appendix A3.1.

Going beyond the simplest case described above, consider Figure 3.5, where a pill-shaped dielectric load is partially filling a more realistic parallel-plate applicator with limited plate area. There are fringing fields with curved field lines at the periphery of the electrode pair, as well as the periphery of the load. There are electric fields both inside and outside of the dielectric load, but due to the introduction of the material the original field uniformity is lost.

The solution of the Laplace equation (1.1) for a parallel-plate system where the electrode's lateral dimensions are comparable to the distance between electrodes reveals that there is an inherent field non-uniformity as shown in Figure 3.6a, where the electric field is maximal at the center and is reduced going toward the edges. A solution for such non-uniformity is given where "paddles" are added at the electrode ends to correct the uniformity, as shown in Figure 3.6b.

In high-frequency systems a second cause of field non-uniformity is the wavelength or standing-wave effect. This phenomenon happens when

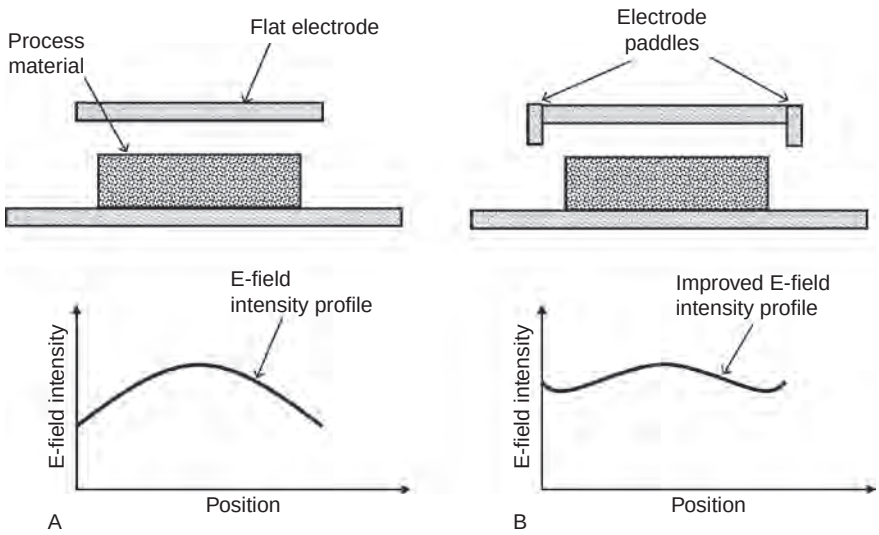

FIGURE 3.6
Addition of "paddles" can improve the field intensity profile in cases where the limited width of an electrode causes field non-uniformity. (A) Planar electrode. (B) Planar electrodes with paddles.

the lateral sizes of the parallel-plate system are a significant fraction of the wavelength; this effect, and the solutions for it, are discussed in more detail in Section 3.4.5 under RF heating. Note that the non-uniformity caused by the wavelength/standing-wave effects are of a different nature than those caused by inherent electrostatic effects mentioned above. In essence, these effects can be superimposed on one another in real systems. When electromagnetic modeling is done to solve higher frequency problems of this type, the best results are obtained if a full wave analysis is performed, instead of solving the Laplace equation (3.1), which does not account for wavelength or standing-wave effects.

Another source of applicator field non-uniformity is the sharp electrode edges, such as those shown from the modeling results in Figure 3.3. This effect can be mitigated by curving the electrode edges, and avoiding the proximity of the process material from these areas.

3.1.4 *E*-field applicators for material heating and plasma activation: principles

E-field applicators are used extensively for heating of lossy dielectrics and partially conducting materials, as well as activation of plasma bodies, particularly at radio-frequencies [4]. Applying Eq. (1.11) to the *E* field inside the material in Figure 3.1:

$$P_{\mathrm{v}} = \varepsilon_0 \varepsilon_{\mathrm{r}}'' \omega E_{\mathrm{m}}^2 \tag{3.3}$$

where E_m is the electric field amplitude inside the material, P_v is the power deposition density into the material in W/m^3, $\varepsilon_0 = 8.85 \times 10^{-12}$ is the permittivity of free space, ε_r'' is the dielectric loss factor of the material, $\omega = 2\pi f$ is the angular frequency, and f is the operating frequency. It should be noted that E_m itself is not generally constant over the volume of the material being heated, and its spatial value needs to be determined using analytical, numerical modeling, or experimental methods.

Another important point to emphasize is that the "depth of penetration" often discussed in microwave heating, and covered in Eq. (1.32), does not necessarily apply to materials being heated in an electrical-field applicator. The reason is "depth of penetration" assumes a plane wave incident upon a lossy dielectric, where the pointing vector is vertical to the interface plane, and therefore the *E*-field component of the wave is parallel to it. Such a calculation is more valid in multimode cavities where quasi-optical wave propagation can be used. In problems involving *E*-field applicators, such conditions are rarely found. For example, when a slab of the material is being heated in a parallel-plate applicator as shown in Figure 3.6, the electric field is vertical to the material interface; a condition that is not one of the assumptions of depth of penetration equation (1.32). Furthermore, the assumption of a traveling wave is not valid here. For calculations of depth of penetration, for *E*-field applicators, a study of field patterns inside the material is needed.

Various types of *E*-field applicators, including the parallel-plate and fringing-field types, are used for these heating applications [5–8]. Radio-frequency, being a volumetric method of material heating, provides the same fundamental advantages as microwave heating. But there are some distinctions, advantages [9], and disadvantages that will be discussed in Section 3.5. We will discuss a medical application of RF heating in Section 3.1.5, and industrial applications will be discussed in more detail in Section 3.5.

3.1.5 *E*-field probes as dielectic material sensors

Electric field probes are used extensively as dielectric sensors, at various scales, from miniature sensors [10–12] to large industrial scale [13]. In its simplest form, the high-frequency potential is applied to the electrodes, and the impedance across the electrodes is measured. In practical usage, the dielectric properties are linked to material parameters such as moisture, degree of cure, mass or dimensional variations, or contamination level.

To be more specific about the parameters involved, consider Figure 3.1, where the complex input impedance of the *E*-field applicator, $Z = V/I$, is a function of the frequency f, dielectric properties of the material $\varepsilon_r', \varepsilon_r''$, the

geometrical parameters of the material $\bar{\chi}_m$, geometrical parameters of the applicator $\bar{\chi}_a$, and electrical material properties of the applicator system $\bar{\xi}_a$:

$$Z = \Im(f, \varepsilon_r', \varepsilon_r'', \chi_m, \chi_a, \xi_a) \tag{3.4}$$

Note that the above expression assumes none of the parameters are dependent on the *E*-field intensity. Because of the very small *E*-field intensity in sensor systems, this condition is usually met in real systems.

In a typical sensor problem, one of the material-related parameters above, $\varepsilon_r', \varepsilon_r''$ or χ_m, is the variable under study. Therefore, if for example the relative dielectric constant is the variable under study, a good sensor is one where the following quantity is maximized:

$$s = \frac{d\Im}{d\varepsilon_r'} \tag{3.5}$$

In Eq. (3.5), the parameter s can be called the sensor's sensitivity. Quantitatively, a high sensitivity means a small variation in ε_r' would yield a large change in the impedance, which is the measurable variable. At the least, the sensitivity of Eq. (3.5) should be large enough to overcome the change in impedance due to other variables that are considered noise. In an *E*-field probe used as a sensor, a high sensitivity is typically gained by higher frequency and high fill factor. In essence, the signal-to-noise ratio of a sensor system is strongly linked to s in Eq. (3.5). In Section 3.2 the impedance of a partially loaded parallel-plate system is computed in terms of the electrode geometry and dielectric properties. Such analysis can be applied to Eq. (3.5) by using an algebraic derivative to find the sensitivity of such a sensor in real systems.

A powerful technique to enhance the capabilities of *E*-field probes/sensors is obtaining dielectric data from a wide spectrum of frequencies. The technique, which is called dielectric spectroscopy [14] or impedance spectroscopy [15], uses the dispersion properties of dielectrics [16], which encompass the dispersion curves of the dielectric spectrum.

A highly useful and practical technique related to dielectric spectroscopy is the dielectric biomass method for measurement of viable cells in fermentation vessels [17–19], which has been of great utility in a wide variety of biomass measurement applications. Using an *E*-field probe, the relative permittivity of the cell suspension is an indicator of the extent to which the localized charge distributions can be distorted by the applied electric field. The dispersive phenomenon of interest here is β-dispersion, which is due to charging up of the plasma-membrane capacitance by ions moving

due to the applied E field. The viable cells, due to intact membranes, show their presence by expressing a total permittivity, which is measured by the instrument as added capacitance.

3.1.6 Asymmetrical *E*-field electrode systems for localized heating: medical RF ablation

To illustrate the asymmetrical electrode concept, consider a coaxial electrode system as shown in Figure 3.7, where the annular region between the center conductor, with diameter a, and the ground conductor, with diameter b, is filled with a lossy dielectric with the relative loss factor of ε_r''. The electric field between the two electrodes is the solution of Eq. (3.1) in cylindrical coordinates, and is given as [1]:

$$\bar{E} = \frac{V_0}{\ln\left(\frac{b}{a}\right)}\frac{1}{r}\hat{a}_r \tag{3.6}$$

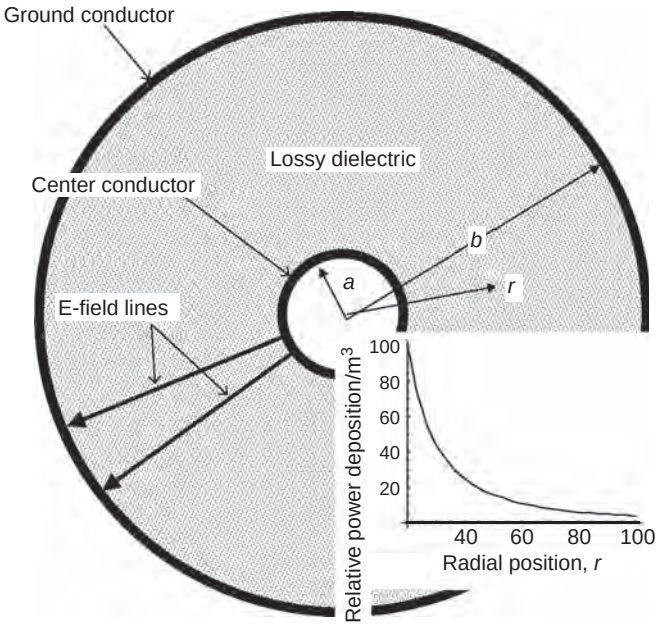

FIGURE 3.7 *A coaxial structure filled with lossy dielectric represents the concept of the asymmetrical E-field applicator. The plot is relative power deposition density versus diameter, which shows much higher deposition of power into areas closer to the smaller electrode.*

where V_0 is the RMS voltage at the center conductor and $\hat{a}_r$ is the vector operator in the radial direction. The power deposition density versus the radial position r from Eqs (3.3) and (3.6) becomes:

$$P_v = \omega \varepsilon_r'' \varepsilon_0 E^2 = \omega \varepsilon_r'' \varepsilon_0 \frac{V_0^2}{\left[\ln\left(\frac{b}{a}\right)\right]^2} \frac{1}{r^2} \tag{3.7}$$

where P_v is the power deposition density into the lossy dielectric in W/m^3 and $\omega = 2\pi f$ is the angular frequency, f being the operating frequency in Hz. The chart that is superimposed in Figure 3.7 shows the relative power density per Eq. (3.7). The conclusion that can be drawn is that in asymmetrical *E*-field applicators the power density in the vicinity of the smaller electrode is very high compared to that in the vicinity of the larger electrode. Another conclusion from Eq. (3.7) is that the ratio of power deposition density in the immediate vicinity of the center conductor to that at the outer conductor is equal to b^2/a^2. In cases where $b \gg a$, effectively all power deposition into the material happens in the vicinity of the small electrode. This phenomenon of asymmetrical electrodes can also be used to explain the reason for high electric field intensity in electrode areas with sharp edges as shown in Figure 3.3.

This property of asymmetrical electrode systems can be utilized in cases where intense heating is needed in a small area. A perfect example is medical RF ablation (RFA) [20–22]. This is a minimally invasive interventional technique that in recent years has been used in different medical fields, such as the elimination of cardiac arrhythmias or the destruction of tumors in various parts of the body. The idea with RFA is to create a lesion by generating localized heat at the location of interest.

Figure 3.8 shows a simplified diagram of the procedure; the smaller electrode, which is also known as the "active" electrode, is connected to the RF generator that typically provides a frequency between 100 kHz and 1 MHz at the power level of tens of watts. The heating occurs at a depth of penetration of a few millimeters around the electrode. The wire that carries the RF to the active electrode is

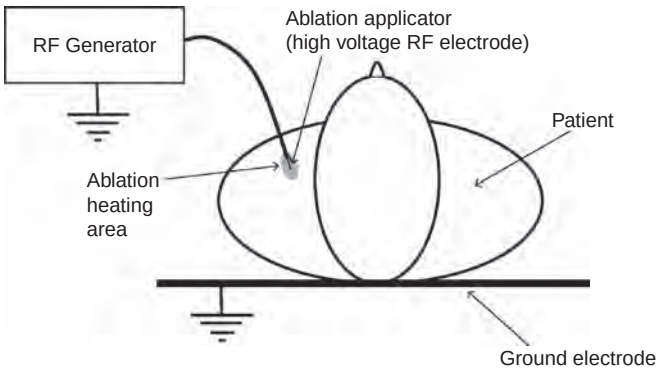

FIGURE 3.8 *Arrangement of a medical RF ablation procedure, which utilizes the concept of asymmetrical E-field electrodes to produce intense local heating around the small electrode.*

shielded by a low dielectric loss insulator to prevent heating of unintended areas. The larger ground electrode, which is often called the "dispersive electrode", is placed on the opposite side of the patient from the active electrode. Since the active electrode is far smaller than the ground electrode, according to Eq. (3.7), practically all the energy deposition happens in close vicinity to the active electrode, which causes the desired lesion to be formed. In some cases active electrodes of more complicated structures are made for various RFA applications. For example, a multipronged [22] active electrode is used in order to destroy large tumors.

3.2 PARALLEL-PLATE *E*-FIELD APPLICATOR WITH STRATIFIED DIELECTRIC LAYERS: EQUIVALENT CIRCUIT AND FIELD CALCULATIONS

In the design of *E*-field applicators, it is often important to know the relationships between two groups of variables. The first group is composed of the geometry/dimensions, the material electrical properties, field strengths, and signal/power density values. The second group is the electrical variables at the input/output ports of the applicator/probe, such as voltages, currents, frequency, and impedances. The device being studied is ultimately a circuit component of a larger electrical system; therefore, quantifying the relationships between the first and second groups of variables is critical in a proper understanding of the relationships between the electrical and material processing/sensing variables.

Such analysis of real applicator/probes often requires either rigorous analytical methods or numerical techniques such as finite element methods applied to the exact problem at hand. These methods are often powerful and valuable in solving specific cases. In this section, however, we will create a means for understanding the issues involved using a simple model, which is the parallel-plate applicator with two stratified layers of real dielectrics. This model can be analytically treated by solving the Laplace equation (3.1) in a single dimension provided that an infinite area approximation is used for the parallel plates. In this approximation a section with finite surface area is assumed as part of an infinite plane. Using this approximation the fringing fields are ignored.

In the following subsections, we will find closed-form equations for a parallel-plate applicator under various load scenarios.

As a result of this analysis, which is shown in Appendix A3.1, the equivalent circuit of the applicator/probe is calculated from the geometrical and material parameters. Furthermore, *E*-field strengths in the two layers are calculated from the material and induced voltages.

The benefits of this exercise are twofold: first, the results of the analysis are very useful in understanding and approximating more complex geometries; second, the parallel-plate electrode configuration is used in many systems, and the results of this analysis are directly applicable in those situations.

3.2.1 Equivalent circuit and fields for parallel-plate applicators with two lossy dielectric layers

Consider Figure 3.9a, where a pair of parallel plates with plate area A have two layers of dielectric materials with complex permittivities of $\varepsilon_1 = \varepsilon_0(\varepsilon'_{r1} - j\varepsilon''_{r1})$ and $\varepsilon_2 = \varepsilon_0(\varepsilon'_{r2} - j\varepsilon''_{r2})$ with thicknesses of d_1 and d_2 respectively. Here ε_0 is the permittivity of a vacuum. The derivation of the input admittance, impedance, and electric fields inside each layer is given in Appendix A3.1, using complex variable calculations with the Mathematica™ software package.

The simplified equivalent circuit is shown in Figure 3.9b. This equivalent circuit is composed of a capacitor with capacitance C, the value of which depends on the applicator geometry and the dielectric properties of the load. The second component is a parallel resistor, which represents the total amount of resistive losses. In a typical applicator, the metal losses are usually negligible compared to the load losses; therefore the resistancer R represents only the dielectric losses.

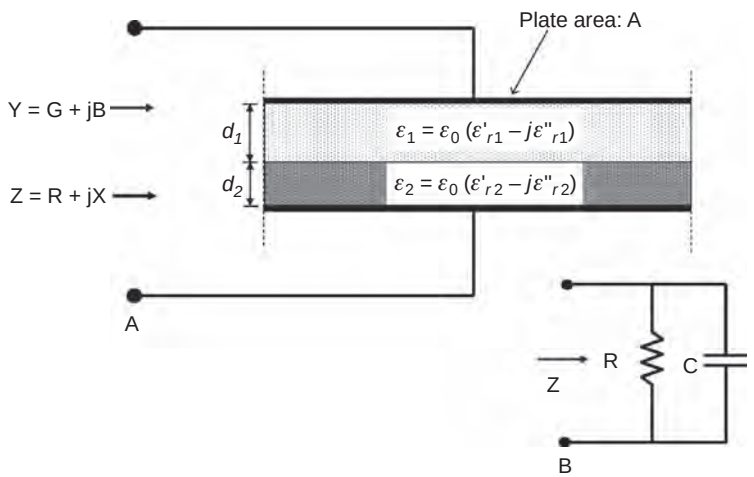

FIGURE 3.9 *The configuration of a parallel-plate E-field applicator filled with two stratified layers of real dielectrics. The infinite plate approximation is used, where the fringing fields are ignored. (A) Schematic applicator arrangement. (B) Equivalent circuit.*

From Appendix A3.1, the input impedance $Z = R + jX$ is derived as:

$$Z = \frac{1}{\omega\varepsilon_0 A}\left[\left(\frac{d_1\varepsilon''_{r1}}{\varepsilon'^2_{r1} + \varepsilon''^2_{r1}} + \frac{d_2\varepsilon''_{r2}}{\varepsilon'^2_{r2} + \varepsilon''^2_{r2}}\right) - j\left(\frac{d_1\varepsilon'_{r1}}{\varepsilon'^2_{r1} + \varepsilon''^2_{r1}} + \frac{d_2\varepsilon'_{r2}}{\varepsilon'^2_{r2} + \varepsilon''^2_{r2}}\right)\right] \quad (3.8)$$

Referring to the equivalent circuit of Figure 3.9b, Eq. (3.8) calculates the complex input impedance.

It is very common for many dielectrics to have a relative dielectric constant much larger than the relative dielectric loss ($\varepsilon'_r \gg \varepsilon''_r$). In such cases Eq. (3.8) simplifies to:

$$Z = \frac{1}{\omega\varepsilon_0 A}\left[\left(\frac{d_1\,\varepsilon''_{r1}}{\varepsilon'^2_{r1}} + \frac{d_2\,\varepsilon''_{r2}}{\varepsilon'^2_{r2}}\right) - j\left(\frac{d_1}{\varepsilon'_{r1}} + \frac{d_2}{\varepsilon'_{r2}}\right)\right] \quad (3.9)$$

We will use these results in the following sections, as well as in Chapter 8, for RF welding computations. In Appendix A3.1, in addition to the impedance and admittance, expressions for circuit components of the equivalent circuit of Figure 3.9, as well as electric fields in the two layers, are also derived.

3.2.2 Equivalent circuit of parallel plates partially filled with lossy dielectric

Many high-frequency *E*-field applicators or sensors operate in a non-contact (or partially filled) mode. In these cases, there is an "air" gap between the material and at least one of the electrodes. A full analysis of fields in cases involving complicated geometries requires either rigorous analytical or numerical methods. In this section, building on the single-dimensional analysis of Appendix A3.1, we will treat the problem of parallel plates partially filled with a real dielectric with the geometrical simplifications described previously.

Consider the applicator arrangement in Figure 3.10a, where a slab material with complex permittivity $\varepsilon = \varepsilon_0(\varepsilon'_r - j\varepsilon''_r)$ and thickness h is located between two parallel plates with a gap distance of $D \geq h$. The area of both parallel plates and the material is A, and fringing fields are neglected.

Using Eq. (A3.11) in Appendix A3.1, for one of the layers we use the relative complex permittivity $\varepsilon'_r - j\varepsilon''_r$, and for the other layer we use unity, which is the permittivity of free space. Then the real part of the admittance (conductance, G) is:

$$G = \frac{\varepsilon_0\,\varepsilon''_r\,\omega A\,h}{h^2 + 2h(D-h)\varepsilon'_r + (D-h)^2(\varepsilon'^2_r + \varepsilon''^2_r)} \quad (3.10)$$

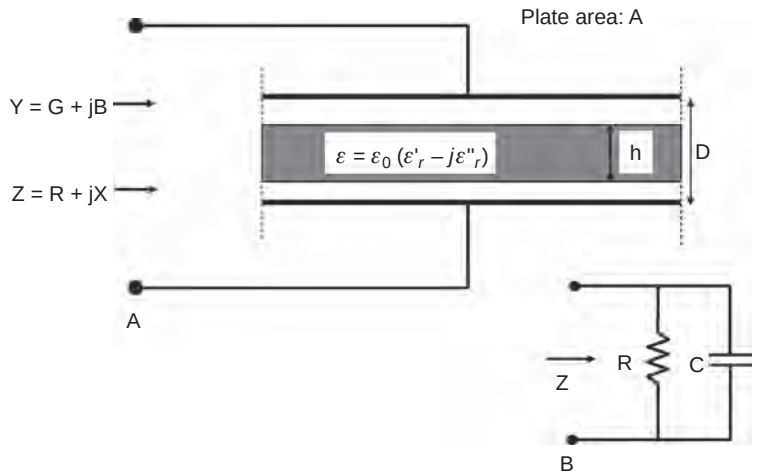

FIGURE 3.10 *Parallel-plate applicator with partially filled lossy dielectric. (A) Schematic applicator and load arrangement. (B) Equivalent circuit.*

The imaginary part of the admittance (susceptance, B) is:

$$B = \frac{A\varepsilon_0\omega[h\varepsilon'_r + (D-h)(\varepsilon'^2_r + \varepsilon''^2_r)]}{h^2 + 2h(D-h)\varepsilon'_r + (D-h)^2(\varepsilon'^2_r + \varepsilon''^2_r)} \tag{3.11}$$

where Y, the input complex admittance of the parallel plate with load, is:

$$Y = G + jB \tag{3.12}$$

Referring to the equivalent circuit of Figure 3.9b, the values of resistance R_a and capacitance C_a, using a convenient factor $\beta = h/D$, and considering the fact that $R = 1/G$ and $C = B/\omega$, become:

$$R = \frac{D}{\varepsilon_0\varepsilon''_r\omega A}\cdot\left[\beta + 2\varepsilon'_r(1-\beta) + \left(\varepsilon'^2_\rho + \varepsilon''^2_\rho\right)\frac{1}{\beta}(1-\beta)^2\right] \tag{3.13}$$

$$C = \frac{\varepsilon_0\varepsilon'_r A}{D}\cdot\frac{\beta + \dfrac{1}{\varepsilon'_r}(1-\beta)\left(\varepsilon'^2_r + \varepsilon''^2_r\right)}{\beta^2 + 2\varepsilon'_r\beta(1-\beta) + \left(\varepsilon'^2_r + \varepsilon''^2_r\right)(1-\beta)^2} \tag{3.14}$$

Let us consider the limiting case where the dielectric fills the parallel plate ($D = h$ or $\beta = 1$). The resistance and capacitance become:

$$R = \frac{D}{\varepsilon_0\varepsilon''_r\omega A} \tag{3.15}$$

and

$$C = \frac{\varepsilon_0 \varepsilon_r' A}{D} \tag{3.16}$$

At the other extreme, if the height of the dielectric becomes very thin, so that $h = 0$ or $\beta = 0$, then:

$$R = \infty \tag{3.17}$$

and:

$$C = \frac{\varepsilon_0 A}{D} \tag{3.18}$$

The last four equations are familiar cases of dielectric-filled and air-filled cases in well-known texts [1,2].

For most dielectrics we have $\varepsilon_r'^2 \gg \varepsilon_r''^2$. Then Eqs (3.14) and (3.15) are simplified as follows:

$$R = \frac{D}{\varepsilon_0 \varepsilon_r'' \omega A} \cdot \frac{\left[\beta + \varepsilon_r'(1-\beta)\right]^2}{\beta} \tag{3.19}$$

$$C = \frac{\varepsilon_0 \varepsilon_r' A}{D} \cdot \frac{1}{\beta + \varepsilon_r'(1-\beta)} \tag{3.20}$$

3.2.3 Quality factor of partially filled parallel plates with lossy dielectric

As discussed in Chapter 2, the quality factor Q is the primary measure of the efficiency of an applicator. Here we use what we have learned in Section 3.2.2 to derive an equation for the quality factor of a partially filled parallel-plate applicator.

Referring to the equivalent circuit of Figure 3.10b, the quality factor of a capacitor, in general, is defined as [2]:

$$Q = \omega RC \tag{3.21}$$

Inserting the expressions for R and C from Eqs (3.13) and (3.14) into Eq. (3.21), the quality factor, after some simplification, becomes:

$$Q = \frac{\varepsilon_r'}{\varepsilon_r''} + \left(\frac{1}{\beta} - 1\right)\left(\frac{\varepsilon_r'^2 + \varepsilon_r''^2}{\varepsilon_r''}\right) \tag{3.22}$$

Note that the quality factor of a fully filled capacitor is described in texts [16] as the first term of Eq. (3.22); therefore the second term of Eq. (3.22) represent the increase of quality factor due to the unfilled portion of the applicator (or the "air" gap). The second term is zero when $D = h$ or $\beta = 1$.

In almost all cases for practical dielectrics, $\varepsilon_r'^2 \gg \varepsilon_r''^2$; therefore:

$$Q = \frac{\varepsilon_r'}{\varepsilon_r''}\left[1 + \varepsilon_r'\left(\frac{1}{\beta} - 1\right)\right] \quad \text{or} \quad Q = \frac{\varepsilon_r'}{\varepsilon_r''}\left[1 + \varepsilon_r'\left(\frac{D}{h} - 1\right)\right] \tag{3.23}$$

3.2.4 Parallel-plate applicator partially filled with a conductive material

Electric field applicators are generally not considered effective for use with highly conductive materials such as elemental metals. This is because such materials tend to exclude *E* fields within, and build up large *E* fields at the exterior of the material. In such cases the usage of *H*-field (magnetic field) applicators (Chapter 7) is more common. Note that even magnetic field applicators ultimately induce an electric field, but that is done without the need to raise the *E* fields outside the material to high levels. There are, however, cases where semiconductive materials such as various forms of conductive-filled polymers, or carbons, including carbon nanotubes [12], are used in *E*-field devices at high frequencies. The goal of this section is to expand the derivations of the equivalent circuit of partially filled parallel plates to conductive material as well. When the material of interest is conductive, the dielectric polarization phenomenon becomes weak. In such instances the material is defined only by its electrical conductivity σ, which is generally a frequency-independent property.

For conducive materials inside partially filled parallel plates, in Eq. (A3.11) in Appendix A3.1, instead of the complex permittivity $\varepsilon = \varepsilon_0(\varepsilon_r' - j\varepsilon_r'')$, the following equation is used:

$$\varepsilon = \varepsilon_0\left(1 - j\frac{\sigma}{\omega\varepsilon_0}\right) \tag{3.24}$$

After similar manipulations as described in Appendices A3.1 and A3.2, the susceptance and conductance of the parallel plate with reference to Figure 3.9b become:

$$G = \frac{A\omega^2 \varepsilon_0^2 \sigma h}{(D-h)^2\sigma^2 + \omega^2\varepsilon_0^2 D^2} \tag{3.25}$$

$$B = \frac{A\omega\varepsilon_0[(D-h)\sigma^2 + \omega^2\varepsilon_0^2 D]}{(D-h)^2\sigma^2 + \omega^2\varepsilon_0^2 D^2} \tag{3.26}$$

Referring to the equivalent circuit of Figure 3.10b, the values of resistance R and capacitance C, using a convenient factor $\beta = h/D$, and considering the fact that $R = 1/G$ and $C = B/\omega$, become:

$$R = \frac{D}{\sigma A} \cdot \frac{\left(\frac{\sigma}{\omega\varepsilon_0}\right)^2 (1-\beta)^2 + 1}{\beta} \tag{3.27}$$

$$C = \frac{\varepsilon_0 A}{D} \cdot \frac{\left(\frac{\sigma}{\omega\varepsilon_0}\right)^2 (1-\beta) + 1}{\left(\frac{\sigma}{\omega\varepsilon_0}\right)^2 (1-\beta)^2 + 1} \tag{3.28}$$

3.2.5 Approximate equivalent circuit of a lossy dielectric pill in parallel plates

Another problem of interest is the equivalent circuit of a lossy dielectric object suspended within a parallel-plate applicator with lateral dimension smaller than that of the applicator. Figure 3.11 shows the geometry of a pill with area S, thickness h, and complex relative permittivity of $\varepsilon = \varepsilon_0(\varepsilon_r' - j\varepsilon_r'')$ suspended in a parallel-plate applicator of area $A \geq S$ and plate distance D.

The fringing fields, as shown in Figure 3.2, can be ignored if the conditions $\sqrt{A} \gg D$ and $\sqrt{S} \gg h$ are met. The problem can then be solved by dividing the whole area into a parallel plate with area S, and adding the admittance to the rest of the total parallel plate. Using a Mathematica™ program, and referring to the equivalent circuit of Figure 3.9,

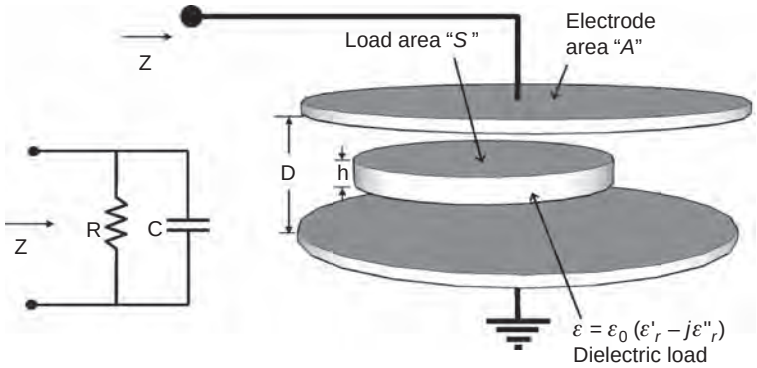

FIGURE 3.11 *A parallel-plate applicator with a dielectric pill and its equivalent circuit.*

the capacitance and resistance of the equivalent circuit can be found as follows:

For $\alpha = S/A$ and $\beta = h/D$, and $\varepsilon_r'^2 \gg \varepsilon_r''^2$:

$$C = \frac{\varepsilon_0 A\omega}{D}\left[\frac{\varepsilon_r' - \beta(1-\alpha)\left(\varepsilon_r' - 1\right)}{\beta + \varepsilon_r'(1-\beta)}\right] \tag{3.29}$$

$$R = \frac{D}{\varepsilon_0 \varepsilon_r'' S\omega}\left[\frac{\varepsilon_r'^2}{\beta} - 2\varepsilon_r'\left(\varepsilon_r' - 1\right) + \beta\left(\varepsilon_r' - 1\right)^2\right] \tag{3.30}$$

A note regarding the accuracy of Eqs (3.29) and (3.30) needs to be made. Since the fringing fields, particularly those at the periphery of the dielectric pill, are ignored, the shape of the pill becomes important in how accurate the results are. The aspect ratio of $\sqrt{S}/h$ must be high. While the pill does not have to have a circular shape, a very oblong shape will also affect the accuracy. Even when Eqs (3.29) and (3.30) are somewhat inaccurate, they would give useful guidance in many sensor or heating designs as to the choice of frequency or other major parameters.

3.3 RESONANCE, COUPLING, AND CIRCUIT ISSUES

3.3.1 Resonance and efficiency in *E*-field applicators

Most *E*-field applicator problems involve resonating of the applicator in order to optimize sensitivity. We have discussed the advantages of resonance in Chapter 2. As we discussed there, the resonance of an *E*-field applicator is accomplished by using an inductive element, as shown in Figure 3.12a. The

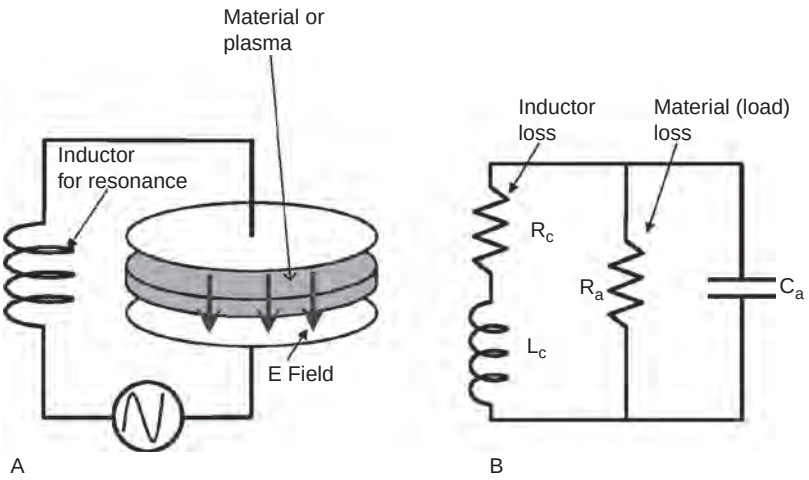

FIGURE 3.12 *An inductive element (coil) is used to create a resonant condition for an electric field applicator/probe. (A) Resonance arrangement. (B) Equivalent circuit.*

value of the inductance needed in order to bring an *E*-field applicator to resonance is found by:

$$L_r = \frac{1}{(2\pi f)^2 C_a} \tag{3.31}$$

where C_a is the capacitance of the applicator/probe (in farads) and L_r is the value of inductance (in henries) needed to create the resonance at frequency f (in Hz).

At radio-frequencies, it is quite important to pay attention to the inductor's stray *E* fields, which can cause large errors if they are not accounted for. A realistic inductor at high frequencies can be modeled as a pure inductance in parallel with a parasitic capacitance. In such a model, the stray capacitance C_s is added in parallel to the applicator's capacitance C_a, and the observed RF value of the inductor is higher than its real value at low frequencies. An empirical method can be used for finding the stray capacitance by first measuring the value of the inductor at much lower frequency (for example, if the frequency of interest is 27 MHz, use 100 kHz for this test). This would yield the true inductance value. Then extract the value of stray capacitance, C_s, using the following equation:

$$C_s = \frac{1}{(2\pi f)^2}\left(\frac{1}{L_{lf}} - \frac{1}{L_{rf}}\right) \tag{3.32}$$

where L_{rf} is the apparent inductance measured at frequency f (Hz), which is the RF frequency of interest, and L_{lf} is the more accurate inductance measured at a low frequency. In modeling the circuit, the value of C_s must be added as a parallel capacitor to C_a. The stored electric field energy in this stray capacitor would lower the fill factor of the applicator, which in turn may explain the reduced applicator efficiency.

Figure 3.12b shows the equivalent circuit of the resonant circuit, which includes the losses in the inductive element. To fully account for loss mechanisms and to find the applicator efficiency, it should be noted that aside from the dielectric losses in load, the losses in the coil are dominant. Even if the highest conductivity metals are used, and other precautions are taken such as building the coil from thick metal stock, the metal losses from inductors would still be quite significant. More details about coils, inductance calculations, loss and quality factor computation are given in Chapter 7. The total quality factor for the resonated applicator, Q_t, from Eq. (2.12) is:

$$Q_t = \frac{Q_a Q_c}{Q_a + Q_c} \tag{3.33}$$

where Q_a is the applicator quality factor and Q_c is the quality factor of the coil. For a partially filled parallel plate, Q_a is calculated from Eq. (3.22). For a solenoid coil the quality factor can be found from the method discussed in Chapter 7.

Assuming the only two loss mechanisms are from the load and the coil, from Eq. (2.16) the applicator efficiency becomes:

$$\eta = \frac{Q_c}{Q_a + Q_c} \tag{3.34}$$

Another method of determining the quality factors is the use of a network analyzer [23], assuming the electrical properties of the material load are the same in laboratory conditions. An example of a situation where a network analyzer cannot be used for this purpose is the design of applicators used for plasma activation, where the load has its electrical properties only under full power. In a typical network analyzer method, the quality factor is first measured with the empty applicator, then the load is added and the quality factor is measured again. The efficiency is then found by using Eq. (3.34).

Figure 3.13 shows a chart of E-field intensity for a typical situation for loaded and unloaded applicator at 40.68 MHz, where the E-field intensity is compared in the loaded and unloaded conditions. Starting with the unloaded Q of 500, which is a typical quality factor for an inductor in this frequency

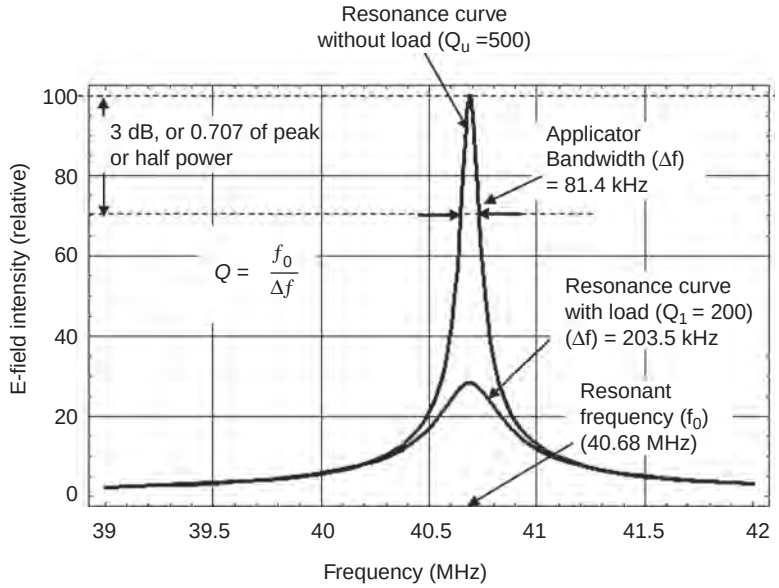

FIGURE 3.13 *The E-field intensity comparisons between loaded and unloaded conditions for a realistic RF heating applicator at 40.68 MHz.*

range, the bandwidth of 81.4 MHz is obtained. The electric field intensity is at a relative value of 100 in this unloaded condition. When a lossy dielectric load is added to the *E*-field applicator, *Q* drops to 200, with a 3-dB bandwidth of 203.6. The relative *E*-field intensity now drops to around 28.

3.3.2 Coupling to external circuits for *E*-field applicators

There are numerous methods for coupling of *E*-field applicators and probes to external circuits. In the case of probes and sensors there is far more flexibility than for applicators, where power losses are important, and even a small mismatch can mean large energy losses. In a typical applicator situation, the goal of coupling is to match the impedance of a resonant applicator system to the characteristic impedance of a transmission line, which is typically 50 Ω.

Figure 3.14a shows the flux linkage transformer method of coupling, where the mutual inductance *M* is the coupling variable. In RF systems, due to a sufficiently high frequency, there is no need for ferromagnetic-cored transformers and a flux linkage through air is typically used. The variability of coupling can either be provided by tapping, or a mechanical positioning system for adjusting the distance of the two coils can be employed.

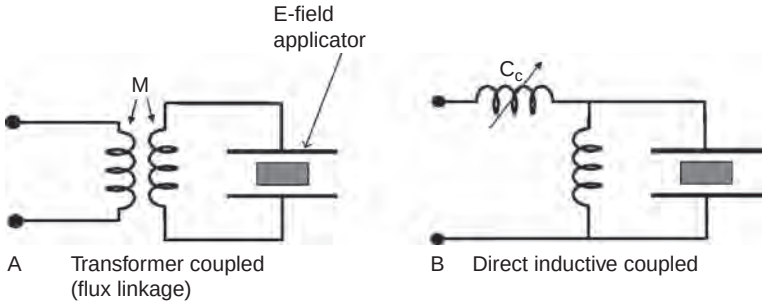

FIGURE 3.14 *Coupling methods that rely on mutual inductance/flux linkage and transformers. (A) Inductively coupled with flux linkage method, where variability is provided by mutual inductance. (B) The direct inductive method, where a variable inductor can be used.*

A second method of inductive coupling is shown in Figure 3.14b, where an inductor, possibly a variable type, is used. An advantage of this method over capacitive coupling approaches is that in high-power systems inductors are far less expensive and more reliable than high-voltage capacitors.

The capacitive methods of coupling *E*-field applicators are shown in Figure 3.15a and b. In the first one, a variable capacitor is used in series with the parallel resonant circuit. A second variable capacitor is added in Figure 3.15b, which provides both tuning and matching capability.

For the coupling circuit shown in Figure 3.15a, the circuit equations have been used in order to calculate the resonating and coupling components as follows.

In the previous section (Section 3.3.1), an equation for calculating the value of the resonating inductor L_r was presented in Eq. (3.31). The complicating issue is that a coupling circuit, such as that in Figure 3.15a, would alter the resonant frequency. The reason is that the coupling capacitor C_c, in series with the transmission-line characteristic impedance Z_0, would become parallel to the applicator capacitance C_a. This would tend to reduce the resonant frequency of the whole circuit. Therefore, in order to revert to the original resonant frequency, there needs to be change in the value of the inductor L_r. Using circuit theory, the value of L_r', which is the new value for the inductor, can be calculated as [24]:

$$L_r' = \frac{L_r}{1 + \frac{\sqrt{\frac{R}{Z_0} - 1}}{2\pi f R C_a}} \tag{3.35}$$

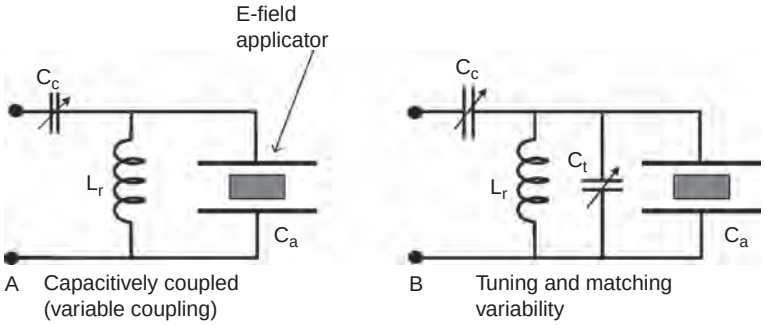

FIGURE 3.15 *Direct capacitive coupling methods in E-field applicators. (A) In the capacitor-coupled method, the coupling capacitor C_c provides variable coupling. (B) When matching and tuning variability is needed, both C_c and C_t are varied for optimization.*

where L_r is the inductance that is calculated by Eq. (3.31), Z_0 is the characteristic impedance of the transmission line, and R is the parallel resistance representing the material load losses.

The value of the coupling capacitor becomes:

$$C_c = \frac{1}{\omega\sqrt{(R - Z_0)Z_0}} \tag{3.36}$$

3.4 FRINGING-FIELD, INTERDIGITAL, AND STRAY-FIELD APPLICATORS AND PROBES

The electric field lines in parallel-plate applicators or the coaxial variety as shown in Figure 3.7 are typically straight lines, and are contained within the main applicator structure. Fringing-field lines, on the other hand, as shown in Figure 3.2, have typically curved shapes and protrude out of the main structure. As such, fringing fields are appropriate for interaction with materials that are outside the main electrode structure. Fringing field electrodes are a class of *E*-field applicator/probes that are specifically designed for interactions with materials in either a half space or in many situations involving planar or sheet-like materials.

Fringing-field structures have been used as both sensors and heating applicators. Most of this section is devoted to interdigital systems for sensing applications. Fringing-field heating applicators, used at a much larger scale for RF heating of planar or sheet-like dielectric materials, will be covered in Section 3.4.4.

FIGURE 3.16
Visualization of the evolution from parallel-plate to fringing-field interdigitated E-field applicator configuration. (A) Parallel plates with material in between (after Mamishev [11]). (B) A V-shaped probe. (C) A planar fringing-field probe sensor with a semi-infinite material body on one side.

3.4.1 Common characteristics and applications of fringing-field and interdigital electrode systems

Figure 3.16 shows the evolution [11] of a parallel-plate applicator into one type of fringing-field electrode system. In Figure 3.16a the material is sandwiched between the parallel plates, and in the second iteration of Figure 3.16b a V-shaped applicator is interacting with a material of similar shape. In Figure 3.16c, both electrodes are in the sample plane, the material fills a half space, and the *E*-field lines are curved between the two electrodes.

In the planar electrode shown in Figure 3.16c, the extent of penetration of the electric field into the half space of the material is limited, and quickly diminishes with distance away from the electrode plane. A non-uniform field pattern is one of the main characteristics of fringing-field electrode systems. In some cases this non-uniformity provides practical advantages, such as the ability to interact fields with large material bodies for non-destructive evaluation without regard for the depth of the object.

Fringing-field applicators or probes are often implemented by a repetitive pattern of alternate potential levels (or powered versus ground) in order to cover a larger surface area of the material, or to provide a larger total capacitance for better performance as a circuit element. Figure 3.17 shows a planar interdigital electrode system, typically used as a material sensor. An attractive feature of interdigital sensors is the ease of construction using thin film or other planar manufacturing techniques. The substrate is typically a low-loss dielectric film, such as a polyimide (Kapton™) [25,26].

Interdigital sensors are commonly used for measuring material properties that can be linked with dielectric properties, such as porosity, viscosity, and degree of cure in polymers. They are most appropriate for measuring fluids since they fill all the space without leaving air gaps that could cause measurement errors.

A different class of application for interdigital sensors is detection of gases, in which a coating of a selective gas-sensitive material is put on the electrodes [27]. The dielectric properties of the coating change with adsorption

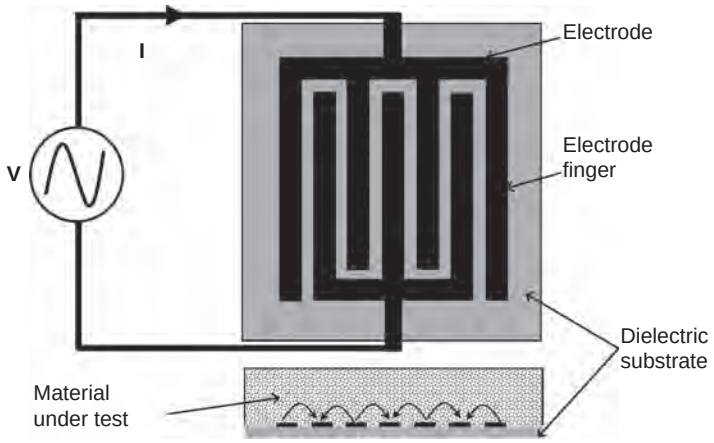

FIGURE 3.17 *A basic arrangement of an interdigital material sensor. The impedance between the electrode can be linked to the material's dielectric properties.*

of gases, and can be detected by changes in the impedance of the sensor. An example of a gas-sensitive coating is Parylene, which exhibits a very useful combination of electrical and physical properties plus a very low permeability to moisture and corrosive substances.

Carbon nanotubes coated on interdigital electrodes can be used as sensors for specific gases such as ammonia or carbon dioxide [28]. A thin layer of gas-sensitive multi-walled nanotube (MWNT)–SiO_2 composite is placed on the interdigital electrodes. Gas molecules of the right size, caught inside the tube-like molecular structure of carbon nanotubes, change the electrical properties significantly to be detectable by a set of miniature interdigital electrodes.

Interdigital sensors have been used over a wide range of frequencies from a fraction of a hertz [11] to many megahertz [10,28]. The choice of frequency depends on a number of factors, including the composition of the material to be sensed. While higher frequencies usually prove to have more sensitivity, particularly in materials with low complex permittivity, in some applications low frequencies are necessary due to the ionic nature of the material, that cannot be exploited for sensing at high frequencies due to large ions' lack of response to high frequencies.

3.4.2 Analysis methods and computation of electrode capacitance

Fringing-field electrode systems, due to their relatively complex field configurations, particularly in loaded conditions, generally do not yield themselves to analytical or closed-form solutions. There are three classes

of solutions that have been developed: finite element simulations [29], analytical methods, typically involving the solution to Laplace equation (3.1) [30], alternate analytical methods such as conformal mapping [31], and approximate/empirical equations sets derived from the above.

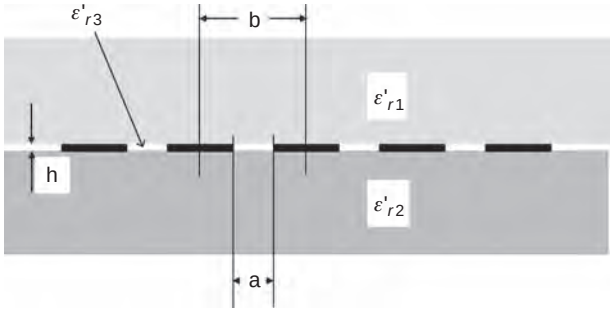

FIGURE 3.18 *The interdigital electrode structure for computation of capacitance.*

Prediction of the total capacitance between the two electrode sets in interdigital sensor applications is important because the value is needed for the design of the rest of the circuit, particularly the signal coupling front-end part. In addition, an equation for capacitance value can be used for sensitivity analysis of the sensor for dielectric property variations. A conformal mapping approach for one set of planar electrodes has been worked out [31]. Referring to the geometry shown in Figure 3.18, the results for the capacitance value between adjacent elements of an interdigital system is given by [11]:

$$C_1 + C_2 = \frac{\varepsilon_0\left(\varepsilon'_{r1} + \varepsilon'_{r2}\right)}{2} \frac{l \cdot K\left[\sqrt{\ell - \left(\frac{a}{b}\right)^2}\right]}{K\left[\frac{a}{b}\right]} \tag{3.37}$$

where C_1 and C_2 (in farads/m) are the capacitance per finger of half spaces below and above the electrode plane respectively, with ε'_{r1} and ε'_{r2} as their relative permittivities. The dimension a (in meters) is the edge-to-edge distance between adjacent electrodes as shown in Figure 3.18; b is the center-to-center distance between adjacent electrodes, and ℓ is the length of the electrode fingers. The function K is defined as elliptic integral of the first kind. This function is programmed in Mathematica™ as the "EllipticK" function. In cases where the thickness of the electrode h is significant, the additional capacitance C_3 for the relative permittivity of region 3 can be added to Eq. (3.27) as:

$$C_3 = \varepsilon_0\,\varepsilon'_{r3}\,\frac{h\ell}{a} \tag{3.38}$$

Curve fitting of Eq. (3.37) would yield the following polynomial form, which yields an accuracy of better than 2% for $0.1 \ll (a/b) \ll 0.9$:

$$C_1 + C_2 = \varepsilon_0\left(\varepsilon'_{r1} + \varepsilon'_{r2}\right)\ell\left(1.54 + 3.42\,x + 4.51\,x^2 - 2.48\,x^3\right) \tag{3.39}$$

where $x = a/b$. When either Eq. (3.37) or (3.39) is used, the total capacitance of the planar interdigital electrode system C_a becomes:

$$C_a = (N - 1)(C_1 + C_2 + C_3) \tag{3.40}$$

where N is the total number of electrode fingers. Note that in the above analysis the secondary capacitances, which are capacitances between nonadjacent electrode fingers, are ignored. For better accuracy, which would account for all effects, finite element software such as COMSOL™ [3] can be used.

3.4.3 Alternate configurations and applications of interdigital dielectric sensors

The basic concept of interdigital material sensor can be implemented by etching the pattern of metal electrode "fingers" on a low-loss dielectric substrate, as shown in Figure 3.17. The complex impedance between the two electrodes, plus a calibration procedure, would provide a means for analyzing a dielectric material that comes into close proximity of the electrodes. In addition to simplicity, an advantage of this configuration is two-sided exposure of electric fields to the material, which allows the sensor to be used for dipping into a fluid for highest sensitivity because all fringing fields on both sides of the sensor are interacting with the fluid for a high fill factor. Aside from this basic idea, there have been a number of variations and more advanced designs that we will attempt to cover in this section.

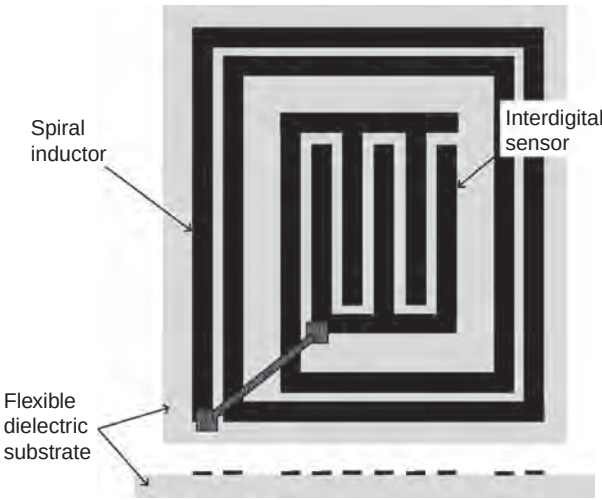

FIGURE 3.19 *An interdigital sensor made into a resonant L-C circuit using an integrated spiral inductor. This is an integrated L-C circuit.*

An alternate configuration [28] creates a resonant circuit by adding a multi-turn spiral inductor around the interdigital capacitor, as shown in Figure 3.19. The resonance, as well as a high frequency of 17–20 MHz, would yield a very-high-sensitivity gas sensor using carbon nanotubes. In addition, the high operating frequency provides a means for a remote and passive query of the sensor without the need for direct connection in a similar fashion as radio-frequency identification (RFID) tags.

Yet another alternate configuration is the addition of a ground plane below the dielectric substrate, providing a means for single-sided access to the material under study.

Using this approach, shown in Figure 3.20, makes the sensor unresponsive to the material below the ground plane, which is useful in packaging and support of the sensor without concerns for interference. The presence of the ground plane makes it feasible to use different methods of interfacing of the sensor to electronics, one of which is the sense-drive system shown in Figure 3.20. In this configuration, a signal source is connected to one electrode, called the "drive" electrode, while the second electrode, called the "sense" electrode, is connected to a receiver, which may include a low-noise figure preamplifier. Both the transmitter and receiver system have the ground plane as their voltage reference in common. The dielectric property of the material under test would alter the amplitude and phase of the received signal.

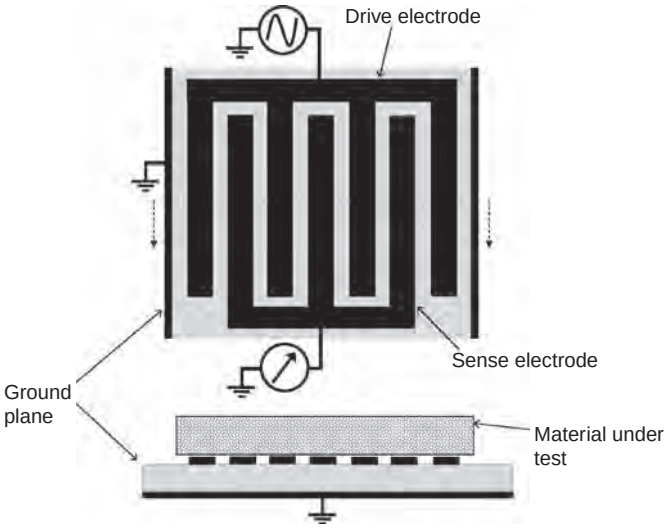

FIGURE 3.20 *An alternate arrangement of interdigital sensor with a ground plane, where separate signal source and detectors are connected to the two electrodes. The signal amplitude and phase arriving at the detector is the indicator of the material properties. After Mamishev [11].*

A design variable for interdigital sensors is the distance between the electrode fingers: the larger the distance, the larger the depth of penetration of electric fields into the material under test. This variability can be used [11] to make more than one interdigital sensor with various interdigital distances on the same substrate. Each sensor would be responsive to a different depth. Therefore the whole sensor system can be utilized to profile the material by depth. Using this method the properties of individual layers across the thickness of a stratified medium can be determined without direct access to each layer. A variation on this idea is capacitive sensor arrays, where by changing which electrode has the voltage and which has the ground, one can vary the field penetration to identify, and in essence "image", the various layers, as shown in Figure 3.21.

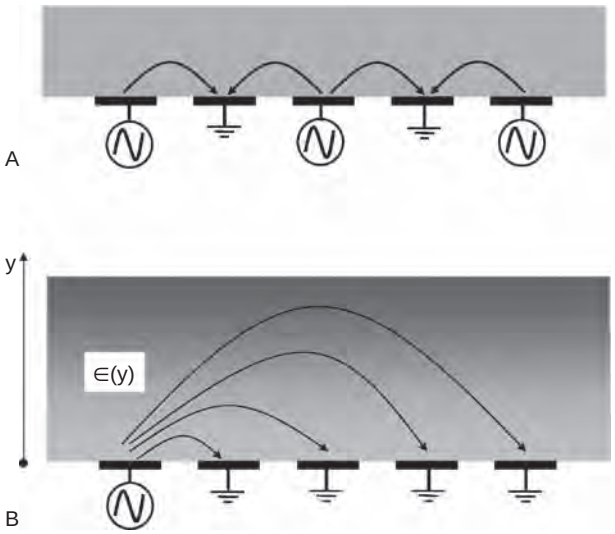

FIGURE 3.21 *In an interdigital electrode system the depth of detection can be adjusted based on how the electrodes are driven. (A) Every other electrode is active, shallow depth. (B) Electrodes with longer distances are more sensitive to deeper areas. After Mamishev [11].*

3.4.4 Stray-field and through-field applicators for RF heating of planar materials

When an *E*-field applicator is to be used for interactions with sheet-like materials, an effective method is to have the electric fields parallel to the sheet, as shown in Figure 3.4. Stray-field and through-field applicators, as shown in Figure 3.22, have been in use for this purpose for decades [6,7,32].

In this configuration of RF heating applicators, self-supporting rod electrodes are arranged so that they are fed with RF high voltage in an alternate fashion. This arrangement is used for continuous heating or drying of wide sheets in industrial settings. The *E* field has a strong component parallel to the sheet, which gives this method good applicator efficiency. The limit of the sheet material's width is set by the operating frequency based on wavelength effects. Large-scale applicators for dielectric sheets of up to 4 meters wide are marketed [6]. The thickness limitation of this applicator arrangement is set by how deep the electric field can penetrate.

The through-field applicator, as shown in Figure 3.22b, is more appropriate for thicker sheets due to vertically symmetrical application of the electric field.

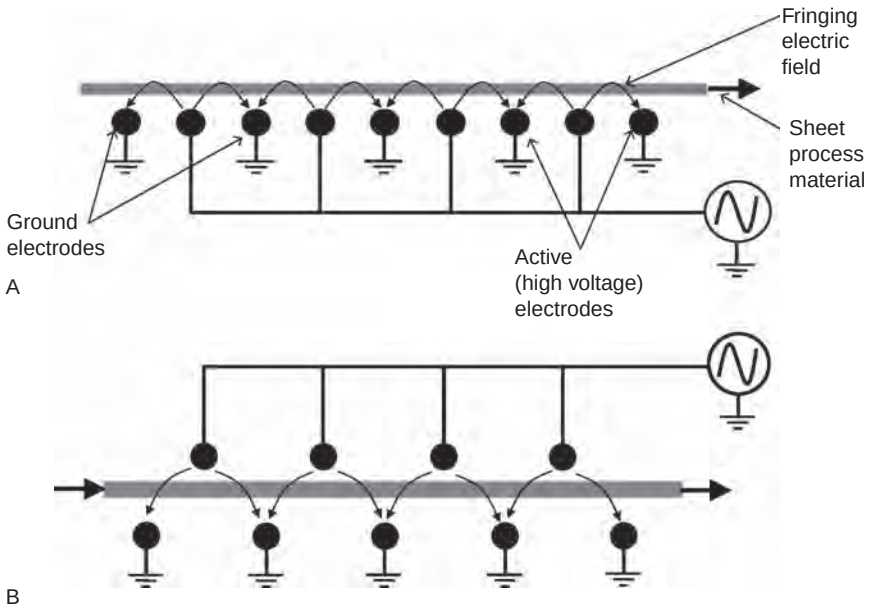

FIGURE 3.22 *Fringing (A) and through-field (B) electrode system for RF processing of sheet-like materials. In both configurations, there is a strong component of the electric field that is parallel to the material for effective coupling of RF power.*

The fringing-field RF method is very useful for moisture leveling applications for sheet materials. More moist areas tend to have higher dielectric loss, and absorb a higher power density per Eq. (3.3) than less moist areas. This will lead to a leveling of moisture.

3.5 ELECTRIC FIELD APPLICATORS AND SYSTEMS FOR MATERIAL HEATING (RF HEATING)

There is a large installed base of RF heating equipment that serves a wide variety of industries such as wood, cardboard, paper, plastic, and food [32–36]. Radio-frequency welding applications, due to special electrode arrangements, are treated separately in Chapter 8. The governing principles of RF heating, including key equation (3.3), were discussed in Section 3.1.4. In this part, we will describe the system and other engineering issues with RF industrial heating systems. Certain topics specifically related to continuous-flow RF systems are covered in Chapter 9.

3.5.1 Advantages and characteristics of RF heating

A key advantage of RF heating over conventional methods is that the heating is faster because of the volumetric energy deposition, which eliminates delays related to thermal heat transfer. In some drying applications where the initial moisture level is not uniform, RF drying tends to even out the moisture because RF preferentially heats the more moist areas due to their higher dielectric loss. In many applications, RF heating provides rapid on–off controls, which eliminate warmup time. There are also several advantages related to thermodynamics of the process. There would be no overheating of surfaces, which results in the ability to speed up the heating, and product deterioration due to high temperatures and long exposure time is reduced or eliminated.

Comparing RF heating with microwave heating, there are some distinctions, advantages, and disadvantages. Microwaves are more effective than RF in heating of certain lower-loss materials based on Eq. (3.3), which shows that power deposition density increases with frequency. Radio-frequencies also have a disadvantage when heating very high permittivity materials, such as water in liquid form, is attempted. The electric field inside the material is low, which reduces power deposition according to Eq. (3.3). The fields outside of the material, however, are very high, which increases the chances of air breakdown and arcing. One of the advantages of RF heating [9], because of the large wavelengths, is that it provides an inherently more uniform heating pattern. Furthermore the penetration

depth of RF heating into the material is larger. On a more practical level, RF heating systems can be acquired at much higher power levels than that at microwave frequencies. In addition, microwave is more effective in heating high-dielectric constant materials such as materials with very high water content. Water tends to exclude the E field and concentrate it outside the water-rich mass, which often leads to arcing in RF systems.

In certain applications such as biscuit heating [37], RF heating provides an advantage in the quality of the final product. The breakage and cracking of many conventionally dried biscuits are caused by a phenomenon called "checking", which arises due to the buildup of stresses during baking. These stresses are caused by differential moisture content between the outer surface and the center of the biscuit. RF heating, due to its volumetric energy deposition nature, prevents this phenomenon and yields a higher quality product.

There are three ISM frequencies allocated for RF power applications by communication authorities: 13.56, 27.12, and 40.68 MHz. Of these, the latter is not allowed in some countries.

3.5.2 Electric field strength inside and outside of material in RF heating

As mentioned above, one of the challenges faced in RF heating of high permittivity materials is high electric field outside the material that may result in arcing. Here the problem is studied using the partially filled parallel plates of Figure 3.10.

From Eq. (A3.13) in Appendix A3.1, if a dielectric layer and a free space layer are considered, the electric field in the free space (air) zone, E_a, is:

$$E_a = V_0 \sqrt{\frac{\varepsilon_r'^2 + \varepsilon_r''^2}{(\varepsilon_r'^2 + \varepsilon_r''^2)(D-h)^2 + 2\varepsilon_r'(D-h)h + h^2}} \tag{3.41}$$

The electric field inside the material is:

$$E_m = \frac{V_0}{\sqrt{(\varepsilon_r'^2 + \varepsilon_r''^2)(D-h)^2 + 2\varepsilon_r'(D-h)h + h^2}} \tag{3.42}$$

The ratio between the electric field intensity in air to that in the material is:

$$\frac{E_a}{E_m} = \sqrt{\varepsilon_r'^2 + \varepsilon_r''^2} \tag{3.43}$$

In most cases where $\varepsilon_r'^2 \gg \varepsilon_r''^2$, Eq. (3.42) is reduced to:

$$E_m = \frac{V_0}{h + \varepsilon_r'(D - h)} \tag{3.44}$$

and:

$$E_a = \varepsilon_r' E_m \tag{3.45}$$

which is better known as the boundary condition of electric fields perpendicular to a boundary layer [2].

In real-world systems the power dissipation in watts is known by the requirements of the process. It is very useful to know the field intensities that develop in the applicator in terms of these power requirements. Major system parameters, particularly the frequency of operation, can be determined to maintain a safe field intensity level, as we will explain later in this section.

Combining Eqs (3.3) and (3.43), the electric field in the gap E_a is given in terms of dissipated power P_d in the dielectric volume as:

$$E_a = \sqrt{\frac{(\varepsilon_r'^2 + \varepsilon_r''^2) P_d}{\varepsilon_0 \varepsilon_r'' \omega A h}} \tag{3.46}$$

And from Eq. (3.3), the electric field in the material, E_m, becomes:

$$E_m = \sqrt{\frac{P_d}{\varepsilon_0 \varepsilon_r'' \omega A h}} \tag{3.47}$$

It is interesting to note the absence of the plate distance D in the above equation. Given that the factor Ah is the volume of the dielectric, we can define the power per unit volume, P_v, as:

$$P_v = \frac{P_d}{A h} \tag{3.48}$$

Then Eq. (3.47) becomes:

$$E_m = \sqrt{\frac{P_v}{\varepsilon_0 \varepsilon_r'' \omega}} \tag{3.49}$$

In cases where $\varepsilon_r'^2 \gg \varepsilon_r''^2$, Eq. (3.46) is reduced to:

$$E_a = \varepsilon_r' \sqrt{\frac{P_d}{\varepsilon_0 \varepsilon_r'' \omega A h}} \tag{3.50}$$

A challenge encountered in dielectric heating is air ionization and breakdown, which is better known as arcing. This phenomenon happens when the electric field in the air surrounding the dielectric goes beyond the air breakdown threshold. This threshold is approximately 10 kV/cm. Given this fact, the above equation (3.50) is perhaps the most critical in judging whether a specific dielectric heating task is practical in a given frequency range, as examined in the following example.

Example

The job is to process a pelletized polymer flow under a set of RF parallel-plate electrodes. Bulk dielectric properties of the polymer are measured at $\varepsilon_r' = 2.3$ and $\varepsilon_r'' = 0.012$. Process requirements have demanded a power deposition of 20 kW in a product bed with the height $h = 5$ cm and electrode area $A = 0.25$ m^2. Determine the electric field in the air surrounding the product bed for the following ISM frequencies: 13.6, 27.12, and 40.68 MHz.

Solution

Using Eq. (3.50):

$$E_a = 2.3 \sqrt{\frac{20{,}000 \text{ W}}{8.8510 - 12 \times 0.012 \times 2\pi f \times 0.25 \text{ m}^2 \times 0.05 \text{ m}}} \text{ in V/m}$$

where f is the frequency of the operation in Hz. The results are as follows:

At 13.56 MHz, $E_a = 965{,}753$ V/m = 9.6 kV/cm
At 27.12 MHz, $E_a = 685{,}415$ V/m = 6.8 kV/m
At 40.68 MHz, $E_a = 558{,}400$ V/m = 5.6 kV/m

Of the three frequencies, 13.56 MHz is not appropriate to use because it is too close to air breakdown of 10 kV/cm.

3.5.3 Currents and voltages in RF heating systems

The ultimate goal of a dielectric heating system is to deliver a specific amount of real power into the bulk of the lossy dielectric volume. As such, other parameters need to be measured and judged against that goal. The power

deposition demand is set by the desired amount of temperature increase in a stationary (batch) system, or by additional factors such as flow in the case of continuous-flow systems, which are discussed in detail in Chapter 9.

Referring to the equivalent circuit of Figure 3.10b, the dissipated power into the dielectric P_d is equivalent to that deposited in the parallel resistor R, which can be written as:

$$P_d = \frac{V_0^2}{R} \tag{3.51}$$

Inserting Eq. (3.19) for R and arranging in terms of V_0:

$$V_0 = \sqrt{\frac{P_d\,[h^2 + 2h(D-h)\varepsilon_r' + (D-h)^2(\varepsilon_r'^2 + \varepsilon_r''^2)}{\varepsilon_0\,\varepsilon_r''\,\omega\,A\,h}} \tag{3.52}$$

In the case where $\varepsilon_r'^2 \gg \varepsilon_r''^2$, this equation is reduced to:

$$V_0 = [(D-h)\varepsilon_r' + h]\sqrt{\frac{P_d}{\varepsilon_0\,\varepsilon_r''\,\omega\,A\,h}} \tag{3.53}$$

Equations (3.52) and (3.53) are useful in the design of a dielectric heating applicator: first, because they determine how much electrode voltage is required for the necessary power dissipation, dielectric properties, frequency and geometry; second, they specify the voltage rating of any components that may be needed in parallel with the applicator. Examples for these components are a variable capacitor that may be put in parallel with the applicator for fine-tuning, or voltage rating of the resonating inductor. Generally, it is most advantageous to keep the electrode voltage as low as possible for the given task due to cost of higher voltage components, and possibility of arcing, as we will discuss in the next section. Most importantly, however, these equations are the simplest and the first test of whether a particular dielectric heating task at the given parameters is possible.

An important aspect of Eqs (3.52) and (3.53) is the effect of chosen frequency, which means that by using higher frequencies we can have more desirable lower voltages. On the other hand, higher frequency sources are more expensive and are only available at lower power levels. These tradeoffs should be considered carefully.

Figure 3.23 shows electrode voltage versus frequency curves for two dielectric material cases for a given geometrical configuration and power

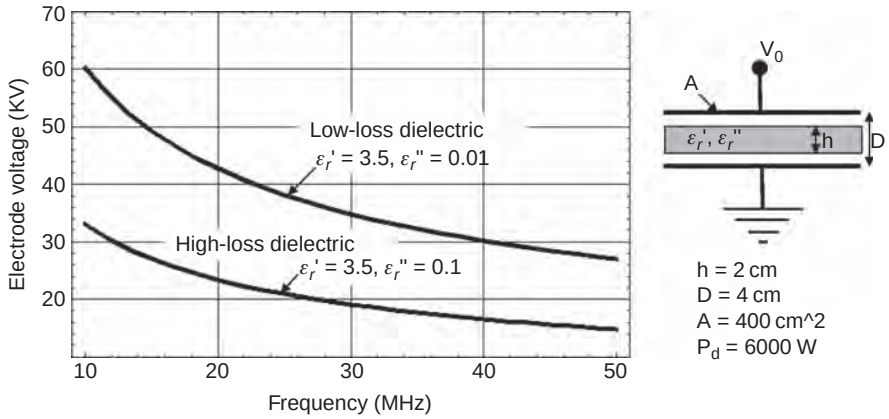

FIGURE 3.23 *The voltage required for dissipating a fixed amount of power into a load in an electric field applicator decreases with frequency. When the dielectric loss is lower the required voltage increases significantly.*

level. The designer can decide, for example, which one of the three ISM frequencies in the RF range can be used.

In addition to voltage, knowing the current is important in the determination of metal ohmic losses, the design of cooling systems, as well as determining the size of conductors. We know that the current and voltage in a capacitive load have a phase difference, which means if we assume the voltage is referenced at phase angle zero, then the current will lag that in phase. In reality all we need is the absolute value of the current. This value is given by:

$$|I| = V_0 \times |Y| \tag{3.54}$$

where $|Y|$ is the absolute value of the complex admittance and $|I|$ is the absolute value of current into the parallel-plate applicator. Then:

$$|Y| = \sqrt{G^2 + B^2} \tag{3.55}$$

After simplifications the current intensity becomes:

$$|I| = \sqrt{\frac{A\,\varepsilon_0\,\omega(\varepsilon_r'^2 + \varepsilon_r''^2)P_d}{h\,\varepsilon_r''}} \tag{3.56}$$

Note that in the above equation the parallel-plate distance D is not present, and unlike the electrode voltage, which decreased with higher

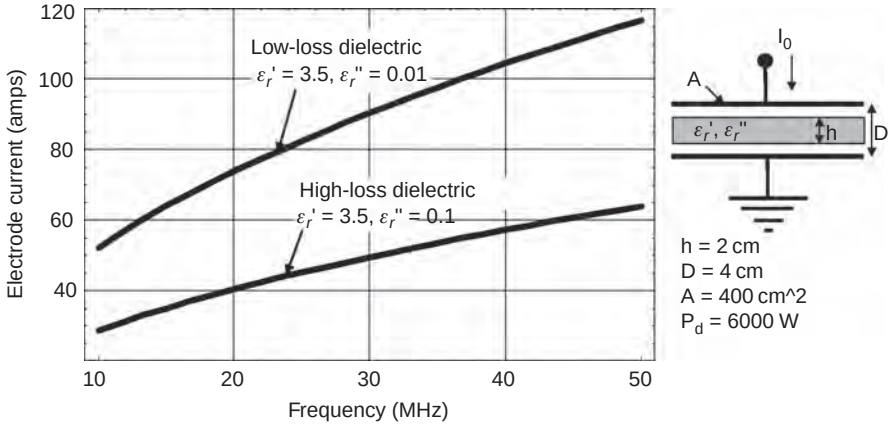

FIGURE 3.24 *The current required for dissipating a fixed amount of power into a load in an electric field applicator increases significantly with frequency. When the dielectric loss is lower the required current increases significantly.*

frequencies, the current increases with frequency and to heat lower dielectric loss materials more current is needed. Figure 3.24 shows two current curves for an example case. The figure shows that the lower loss material, in order to have the same amount of power deposition, would require much larger current. Such a condition may tax the limits of the system in some cases.

3.5.4 Modern RF heating system configurations

One of the challenges in system design for industrial RF systems is compliance with RF emissions regulations, which require no emissions outside of the ISM bands (13.56, 27.12, or 40.68 MHz). In a resonant system, with any variations in load conditions the resonant frequency of the tank circuit changes. Older RF systems designed prior to tightening of regulations were free-running oscillators, which means the operating frequency is the same as the tank circuit frequency. In this case the operating frequency does not necessarily stay within the ISM band. The second challenge is how to implement a power variability (also known as turndown) capability.

To deal with these challenges, two different electrode and system design schemes have emerged for industrial RF heating. Modern RF systems use either (or a combination) of these strategies. In the first one [38], shown in Figure 3.25, the triode tube oscillator is kept at a fixed ISM frequency using one of the frequency stabilization techniques, and the distance between the electrodes is used to provide the necessary variability in deposited power level. In Figure 3.25, the maximum power is delivered to the load when the system is in operating condition A, which means the electrode is at its

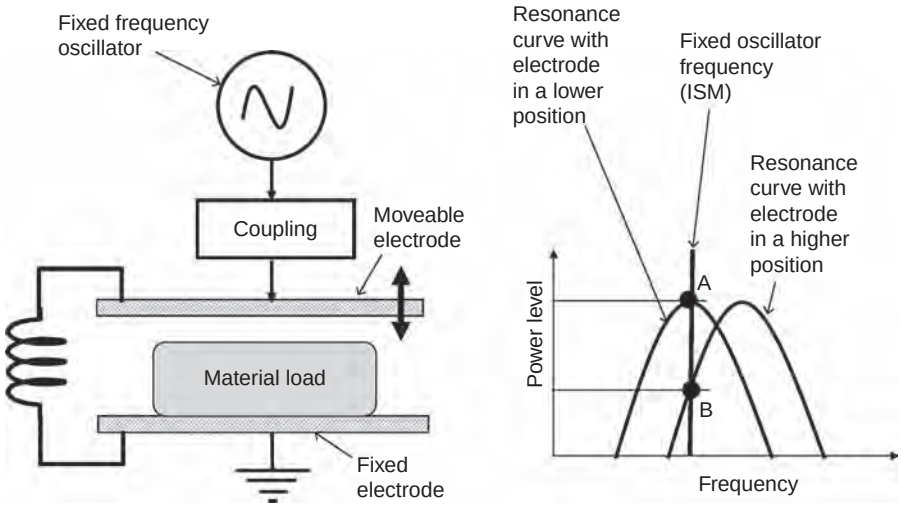

FIGURE 3.25 *Method of power control in RF heating systems using electrode height variations, while keeping the operating frequency constant. When the electrode is in the lower position (operating point A), power delivery to the load is maximal. When the electrode is in a higher position (operating point B), partial power is delivered to the load.*

lowest position. In this condition, the peak of the resonance curve matches the fixed oscillator frequency. When a power turndown is required, the electrode is moved higher, which reduces the applicator capacitance and raises the tank resonant frequency, which would take the system to the operating point B. At this operating point only a portion of the oscillators's power is delivered to the load because of the detuning. This scheme can also deal with load variations because the reductions in power delivery are sensed in the oscillator control system, and adjustments to the electrode height are made to compensate the variations.

In the second strategy, called the 50 ohm system [38,39], shown in Figure 3.26, the heart of the system is a digital controller that processes various inputs and provides controls for the system as follows. The fixed ISM frequency is provided by a low-power quartz-controlled oscillator at a standard 50 Ω transmission-line impedance, and adjustable power level. Then a power amplifier raises the power to what is needed for material processing. The electrode applicator system is fed through an electromechanically controlled tuning/matching box. A central digital controller receives a signal from a phase/magnitude discriminator that measures the input impedance to the tuning/matching box, and sends that information to the central digital controller, which in turn provides control signals to the tuning/matching box to keep the input impedance of the box at 50 Ω and zero phase angle.

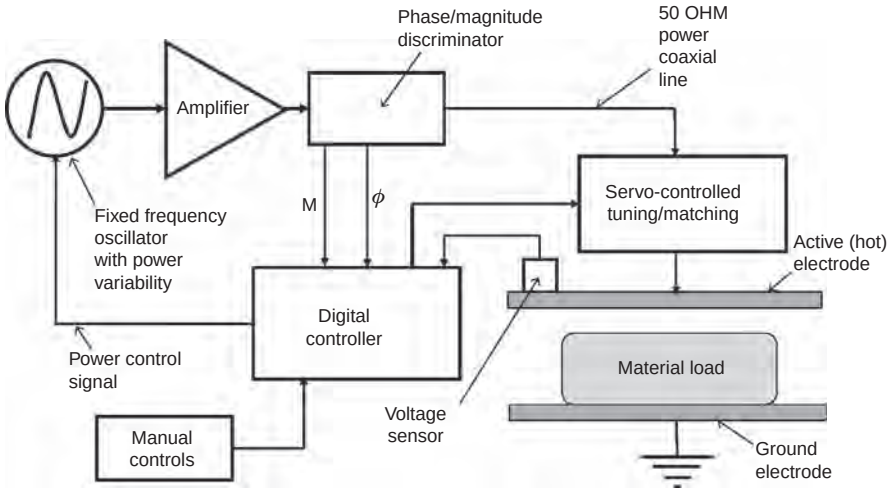

FIGURE 3.26 *Block diagram of a 50-ohm modern RF heating system. The operating system remains at a fixed ISM frequency, and changes in load conditions are compensated for by a controlled tuning/matching subsystem.*

3.5.5 Wavelength effects and standing waves in RF heating electrodes

In most *E*-field applicator problems the dimensions of the applicator are far smaller than the wavelength. In some large-scale RF heating applications, however, the applicator is large enough that standing waves are formed. This phenomenon causes the *E* fields to have geometrical variations along the electrodes. Provisions need to be made to enable prediction of the phenomenon and find ways to overcome it if necessary.

A practical example of a standing-wave problem in parallel-plate RF heating is worked through in Chapter 9, Section 9.3.3, in which an RF heating conveyor system at 27.12 MHz with an electrode length of 1.2 meters is fed at one end at about 5 kV, but the voltage at the other end of the electrode is about 7.2 kV, with proportional variations in the electric field. In that particular example the standing waves did not cause heating uniformity problems for the product, because the conveyor movement was at the same direction as the standing wave. Meanwhile the width of the electrode was too small to produce significant lateral variations in the electric field.

In the example mentioned above, the transmission-line theory was used for calculation of the standing waves, where the top and bottom electrodes were considered as the two conductors of a strip transmission line. In an electrode system with a material filling, the wavelength in the transmission

line is modified by the presence of the dielectric material. The effective wavelength λ_e would be:

$$\lambda_e = \frac{C}{f\sqrt{\varepsilon'_{reff}}} \tag{3.57}$$

where $C = 3 \times 10^8$ m/s is the speed of light, f is the frequency in Hz, and ε'_{reff} is the effective dielectric constant of material between the electrodes. In some applications, such as wood gluing, where the process material fills the whole space between the electrodes, the effective dielectric constant is the same as that of the material. But in cases where there is an air gap, a proportional estimation of the dielectric constant based on dielectric/air heights would be sufficient.

In cases where it is necessary to eliminate standing waves, the use of multiple inductive stubs placed periodically around the electrode [4,40] is proposed. The inductors, working together, are designed to resonate the electrode at the operating frequency.

REFERENCES

[1] L.C. Shen, J.A. Kong, Applied Electromagnetism, PWS Engineering, Boston, 1987, pp. 483–485.

[2] S. Ramo, J.R. Whinnery, T. Van Duzer, Fields and Waves in Communication Electronics, third ed., Wiley, Hoboken, NJ, 1994.

[3] COMSOL Inc. website: www.comsol.com

[4] A.C. Metaxas, Foundations of Electroheat: A Unified Approach, Wiley, Hoboken, NJ, 1996.

[5] Thermex-Thermotron Company website: <http://www.thermex-thermatron.com/thermex/rf-systems.html>

[6] Radio Frequency Company website: <http://www.radiofrequency.com>

[7] Strayfield Inc. website: <http://www.strayfield.co.uk/>

[8] PSC Company website: <http://www.pscrfheat.com/>

[9] M. Mehdizadeh, Engineering and scale-up considerations for microwave induced reactions, Res. Chem. Intermed. 20 (1) (1994) 79–84.

[10] T. Tsurumi, et al., Anamalous dielectric and optical properties in perovskite-type artificial superlattices, Sci. Tech. Adv. Mater. 5 (2004) 425–429.

[11] A.V. Mamishev, Interdigital sensors and transducers, Proc. IEEE 92 (5) (May 2004).

[12] K.G. Ong, K. Zeng, C.A. Grimes, A wireless, passive carbon nanotube-based gas sensor, IEEE Sensors J. 2 (2) (April 2002).

[13] E.D. Tsamis, et al., Design of planar capacitive type sensor for water content monitoring in a production line, Sens. Actuators A 118 (2005) 202–211.

[14] F. Kremer, A. Schönhals (Eds.), Dielectric Spectroscopy, Springer, 2003.

[15] E. Barsoukov, J.R. Macdonald, Impedance Spectroscopy: Theory, Experiment, and Applications, Wiley, Hoboken, NJ, 2005.

[16] A. Von Hippel (Ed.), Dielectric Materials and Applications, second ed., Artech House, Boston, 1995.

[17] C.L. Davey, G.H. Mark, D.B. Kell, Theory of dielectric biomass for viable cells, Pure Appl. Chem. 65 (9) (1993) 1921–1926.

[18] Aber Instruments Co. website: <http://www.aberinstruments.com/>

[19] Fogale Nanotech website: <http://www.fogalebiotech.com>

[20] E.J. Berjano et al., Theoretical modeling for radiofrequency ablation: state-of-the-art and challenges for the future, Biomedical Engineering Online 2006, 5:24 doi:10.1186/1475-925X-5-24. Available from: http://www.biomedical-engineering-online.com/content/5/1/24.

[21] M. Ahmed, et al., Radiofrequency thermal ablation sharply increases intratumoral liposomal doxorubicin accumulation and tumor coagulation, Cancer Res. 63 (2003) 6327–6333.

[22] S.A. Curley, F. Izzo, Radiofrequency ablation of primary and metastatic hepatic malignancies, Int. J. Clin. Oncol. 7 (2002) 72–81.

[23] R.I. Neophytou, A.C. Metaxas, Characterization of radio frequency heating systems in industry using a network analyzer, IEE Proc. – Sci. Meas. Technol. 144 (50) (September 1997).

[24] G. Matthaeei, L. Young, E.M.T. Jones, Microwave Filters, Impedance-Matching Networks, and Coupling Structures, originally McGraw-Hill, 1964, reprinted by Artech House, Dedham, MA, 1980.

[25] DuPont Co. website on Kapton™: <www.dupont.com/kapton>

[26] J.M. Fouke, et al., Sensor for measuring surface fluid conductivity in vivo, IEEE Trans. Biomed. Eng. 35 (1988) 877–881.

[27] H.E. Endres, et al., Dielectric gas sensors based on heteropolysiloxanes, Technol. Digest Eurosensors II (1988) 57–58.

[28] K. Ghee, K. Zeng, C.A. Grimes, A wireless, passive carbon nanotube-based gas sensor, IEEE Sens. J. 2 (2) (2002).

[29] M.C. Zaretsky, Parameter estimation using microdielectrometry with applications to transformer monitoring, Ph.D. Dissertation, EE Department, MIT, 1987.

[30] L. Zaretsky, et al., Continuum properties from interdigital electrode dielectrometery, IEEE Trans. Electr. Insul. 23 (1988) 897–917.

[31] E. Endres, S. Drost, Optimization of the geometry of gas-sensitive interdigital capacitors, Sens. Actuators B, Chem. 4 (1991) 95–98.

[32] D. Bialod, C. Marchand, A CAD package for radiofrequency strayfield applicators, Proceedings of Conference on Heating and Processing 1–3000 MHz, Cambridge, British National Committee for Electroheat, Chaired by H. Barber, paper 5.5, 1986.

[33] E.R. Cox, Developments in RF dielectric heating, Proceedings of Conference on Heating and Processing 1–3000 MHz, Cambridge, British National Committee for Electroheat, Chaired by H. Barber, paper 2.3, 1986.

[34] G. Swift, The ARFA (Air Radio Frequency Assisted) dryer, Proceedings of Conference on Heating and Processing 1–3000 MHz, Cambridge, British National Committee for Electroheat, Chaired by H. Barber, paper 3.1, 1986.

[35] G.A. Smith, Dielectric applications in textiles and auxiliary industries, Proceedings of Conference on Heating and Processing 1–3000 MHz, Cambridge, British National Committee for Electroheat, Chaired by H. Barber, paper 2.2, 1986.

[36] S. Wang, et al., Industrial-scale radio frequency treatments for insect control in walnuts: II: Insect mortality and product quality, Postharvest Biol. Technol. 45 (2) (2007) 247–253.

[37] T. Koral, Radio frequency and bulk heating, Biscuit World 7 (4) (November 2004).

[38] A.S. Mujumdar, Handbook of Industrial Drying, CRC Press, 2006.

[39] Sairem Co. website: <www.sairem.com>

[40] G.H. Brown, et al., Theory and Application of Radio-Frequency Heating, D. Van Nostrand, 1947.

CHAPTER 4

Single-mode Microwave Cavities for Material Processing and Sensing

CHAPTER CONTENTS

INTRODUCTION

We discussed the common themes of cavity applicators and their basis of operation in Chapter 2. The focus in this chapter is to provide more detail on the design and applications of applicator/probes that are based on single-mode microwave cavities.

The fundamentals of cavity field and mode analysis are covered in some excellent texts [1–4]. The focus here is on those aspects of the topic that are most relevant to material processing and sensing applications. It is noteworthy that most early work in the development of microwave cavities (from the 1940s to the 1960s) was focused on external behavior of empty cavities as components of communication circuits, as well as their utilization in particle accelerators. Single-mode cavities have been used as material processing applicators or sensors, and for plasma activation, over the past few decades [5–7], but their usage has been quite limited compared to the much wider and universal utilization of multimode oven cavities. In this chapter we will discuss the special features of single-mode cavities that make them uniquely useful for certain specialty applications. We will also cover updates of more recent applications and developments in this area.

After describing the basics and material applications of single-mode cavities, we will study the cylindrical TM_{0n0} cavity types, which are most commonly used in material interaction applications. We will then move on to other cavity types, and then cover the system issues of single-mode cavities. This chapter also covers some specialty and recent applications of these types of cavities.

4.1 GENERAL DESCRIPTION AND APPLICATIONS OF SINGLE-MODE CAVITY APPLICATORS/SENSORS

4.1.1 Configurations of field–material interactions: basics of single-mode cavities

Microwave cavities can be of many shapes and forms, and in essence they are voids that are mostly enclosed by high-conductivity metal walls. The stimulus frequency coupled into the cavity will set up standing waves only if the stimulus frequency matches one of the natural resonant frequencies of the cavity (Figure 2.13). Each natural resonant frequency represents a "mode", with its own field configuration. In a single-mode cavity, the material under processing or sensing is preferably placed in locations of highest field intensity node for the mode of interest. This is in contrast to multimode cavities, where the placement of the material load is typically random, and interacts with nodes of multitude of resonant modes.

The physical size of single-mode cavities is typically in the vicinity of the operating wavelength or slightly larger. This is as opposed to multimode cavities, which are electrically large, meaning that each dimension is at least a few times larger than the operating wavelength. As we will see in Chapter 5, the number of operating modes in the vicinity of the

operating frequency increases rapidly as the cavity size increases. While it is theoretically possible to operate an electrically large cavity in a single mode, doing so is practically daunting because of difficulties associated with singling out a specific mode among all the neighboring ones at the frequency of interest. In such a situation more than one mode will be excited by the frequency source.

A related issue is the presence of degenerate modes, i.e. multiple modes that operate at exactly the same frequency. If the goal is to excite only one mode so that the well-defined field pattern of that mode is exploited, the unintentional launching of other modes would prevent that aim, and undesired field patterns would emerge.

Cavities with simple geometrical shapes, such as rectangular or cylindrical types, when empty, have exact and closed-form analytical solutions for their field configurations [1–4]. Cavities used for material interactions, which are the topic of this chapter, are typically based on these simple shapes, and the analytical solutions for empty cavities serve as a good starting point for studying the field configuration in material-loaded conditions.

4.1.2 Description of material loading effects in single mode cavities

The addition of a material load to a cavity modifies the field configuration to varying degrees depending on the size and material properties of the load. Regardless of the exact geometrical shape or cavity type, there are typical field-line shapes for material interactions, shown in Figure 4.1. One of the most common field configurations for material interaction is that shown in Figure 4.1a, where the electric field line is formed between opposing parallel walls. This type of field configuration exists, for example, in cylindrical TM_{0n0} and rectangular TE_{101} modes, both of which will be discussed in more detail later in this chapter.

Another field configuration type is shown in Figure 4.1b, where the electric field forms a circular or oval shape and closes on itself. The material load in this case is typically a planar web or sheet parallel to the *E*-field plane. An example of this type is cylindrical TE_{011}, which will be discussed in more detail in Section 4.4.

An entirely different concept for the use of cavities for material interaction is applications where a magnetic field, instead of an electric field, is interfaced with the material, as shown in Figure 4.1c. Examples of such applications are magnetic resonance [8] and processing of metal powders [9,10]. More details on such applications and the cavities used for them is found in Chapter 7 on inductive applicators.

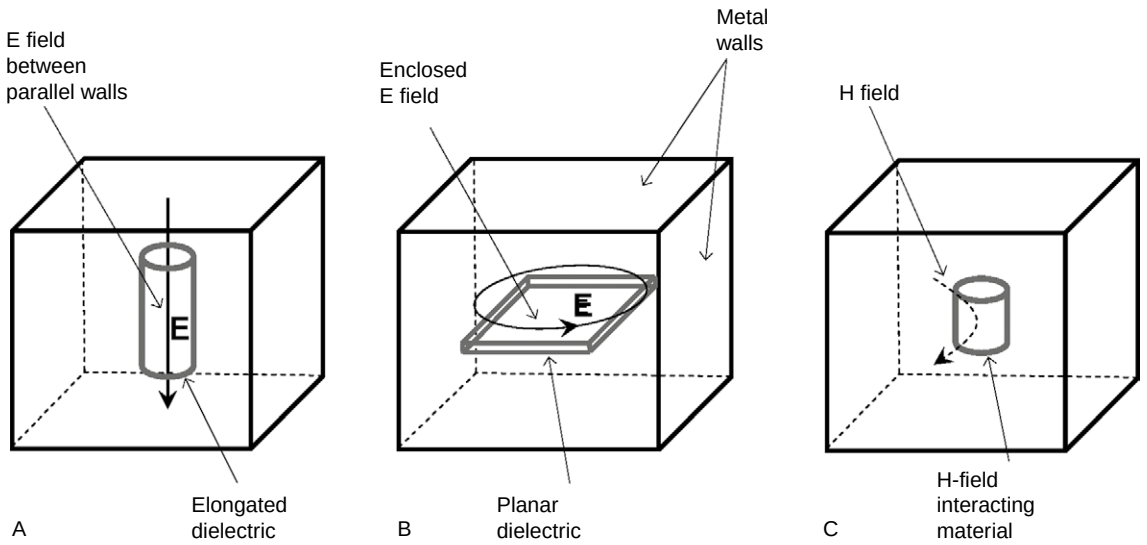

FIGURE 4.1 *Most common field configurations in single-mode cavities for interactions with materials. (A) Electric field between parallel walls is uniform longitudinally, and is used most often. (B) Enclosed E-field is often used for planar-shaped materials. (C) H-fields used for conductive materials, or in magnetic resonance.*

A note needs to be made here regarding cavity modes in loaded condition. In classical texts, cavity modes are defined exclusively for empty cavities. When the material load is inserted, we may consider the cavity as having the same mode only if the basic mode shapes remain intact, though modified. In many cases this cannot be guaranteed, especially when the load has high dielectric constant and losses, and/or the size of it is large. In those cases, the field configuration may change to an extent that the original mode shape is no longer recognizable.

4.1.3 Comparison of single-mode cavities with other applicator/probe types

Single-mode cavities are distributed self-resonant structures. As such, the storage of magnetic- and electric field energies are not as geometrically separable as that of electric field applicators (Chapter 3) or magnetic field applicators (Chapter 7).

In comparison with multimode applicators, the main distinguishing feature of single-mode cavities is that only a specific cavity mode of interest is excited to interact with the material. Conversely, in multimode applicators many cavity modes are excited simultaneously, and the interaction between the material and fields takes place in a largely random fashion among these modes.

Given the fact that a specific mode is used, the design process for single-mode cavities involves careful examination of physical dimensions, location, material properties, and the power/signal coupling structure to excite the correct mode of operation. Care must also be taken to suppress any unwanted modes from interacting with the material.

The above-mentioned features allow the designer to define a volume where the material of interest can be placed where a predictable, often uniform, electric field can be imposed on it. This is as opposed to multimode cavities where analysis and prediction of exact field configuration is of less interest, and obtaining a predictable and uniform field is more difficult.

Another advantage of single-mode cavities is their high sensitivity. When the cavity is used as an applicator, this high sensitivity leads to a more intense field in the area of interest for a given power input. This is why single-mode cavities are often said to provide more "focus" for microwave energy [11], which describes their highly sensitive nature in comparison to multimode cavities.

In comparison with multimode cavities, single-mode cavities provide the advantage that the locations of *E*-field and *H*-field maxima can be separated. This feature has been utilized recently by workers in the area of microwave metal sintering [12,13]. Microwave sintering of metals involves sintering of a "green" part, which is a powder compacted into a desired shape by applying pressure. Compared with a conventional furnace, where heating is due to convection, a microwave furnace provides a more rapid and efficient way of heating and sintering. Furthermore, such rapid heating limits grain growth during sintering and thus helps to improve the microstructure and mechanical properties of the sintered products. The use of single-mode cavities gives workers in that area the opportunity to place the part in either the *E*-field or *H*-field maximum to find the best sintering performance.

In the operation of single-mode cavities, the cavity must always stay tuned and impedance must be matched with the source. The variability of the load properties may take the cavity out of this tuned and matched condition. This is a particular challenge in the operation of single-mode cavities in some situations. Therefore single-mode cavities are usually used in situations where the load properties are stable during the process, such as heating of pumpable fluids [14].

4.1.4 Applications of single-mode cavities for material processing and sensing

Single-mode cavities, due to the specific advantages listed above, have found several different classes of applications as follows.

Material heating/processing

It is true that an overwhelming majority of microwave material processing cases are done with either multimode cavities or transmission-line applicators. The reason is simplicity and robust hardware and operation for these two modalities. There are specialty applications, however, that require the specific advantages that only single-mode cavities can provide. Single-mode cavities possess predictable field patterns and therefore a desirable heating profile can be devised. This feature is highly appropriate for industrial processing of chemicals, liquid, semi-liquid and pumpable or conveyed solid materials that are moving through a pipe [14]. A unique solution to problems associated with heating of viscous liquids, which uses a particular field pattern of a TM_{020} cavity, is described in detail in Section 4.3.3. Single-mode cavities, due to very low metal loss (typical Q of the order of tens of thousands), are highly efficient material heaters. This advantage makes single-mode cavities useful even in cases where the dielectric loss of the material is too low for other types of microwave/RF heating. For example, quartz is one of the lowest dielectric loss materials in existence, yet a high-Q cavity can be used for melting it [15].

Plasma activation

The high quality factor and high sensitivity of single-mode cavities make it possible to create very high electric fields at modest power levels prior to the ignition of the plasma.

Therefore single-mode cavities can ignite plasmas at higher pressures than other high-frequency methods [16,17].

Material sensors for Industrial/Scientific and Medical Applications

Single-mode cavities, due to their extremely high sensitivity, provide a great advantage when used as dielectric material sensors in difficult applications. Small variations in dielectric properties or mass can be measured with a high signal-to-noise ratio using either shifts in resonant frequency or signal loss. One of the uses is moisture measurement or aquametry [18–20].

The sensitivity of single-mode cavities is high enough that they have also been used in measuring small variations in the dielectric properties of gases [21] and air humidity [19]. In that application a TE_{011} single-mode cavity with proper ventilation can be used to detect small amounts of moisture in ambient air.

Dielectric measurements

Single-mode cavities are used for dielectric measurements [6,22,23] when a high degree of accuracy is required, as well as in situations where the

dielectric properties are needed at microwave frequencies. The advantage comes from the high sensitivity of single-mode cavities and the fact that they yield themselves to exact analytical or numerical solutions.

When analytical methods are used, extraction of dielectric properties from the cavity's physical and electrical parameters is called the inverse problem. This term comes from the fact that in other applications of cavities the dielectric properties are used as an input to find the electrical or physical parameters; this class of problems is called the "forward" problem.

To avoid major errors in dielectric measurements, care must be taken that the proper cavity mode is identified and that no degenerate modes are excited. A disadvantage of using single-mode cavities for dielectric measurement is that the solution is obtained for a single frequency. For most materials, however, the dielectric properties vary quite gently in the frequency spectrum up to about 10 GHz. Therefore a measurement at a single frequency is a good indicator of dielectric properties for a substantial range.

Magnetic resonance (ESR/EPR)

Electron spin resonance (ESR), also known as electron paramagnetic resonance (EPR), is a modality of magnetic resonance that requires microwave frequencies. Further explanation of this topic is given in Chapter 7.

4.2 METHODS FOR DETERMINATION OF FIELD DISTRIBUTION, MATERIAL EFFECTS, COUPLING, AND ELECTRICAL PARAMETERS OF SINGLE-MODE CAVITIES

In order to facilitate the description of analysis and design methods for single-mode cavity applicators/probes, in this section we will focus our attention on the cylindrical TM_{010} cavity as shown in Figures 4.2 and 4.3. This mode of operation is one of the most commonly used in material applications, which is due to its ease of construction and field of the type shown in Figure 4.1a. A useful feature of this type of field configuration, in which the E field is formed between two parallel walls, is the fact that the field is perfectly uniform along the length of the field line (z direction). This would yield itself to placing elongated objects, or a process fluid. In this section we will go through various issues that are encountered in completing the design of such cavities for material interaction applications.

FIGURE 4.2
Cavity and load arrangement and field configuration and intensity profiles for a cylindrical TM_{010} cavity applicator with material load.

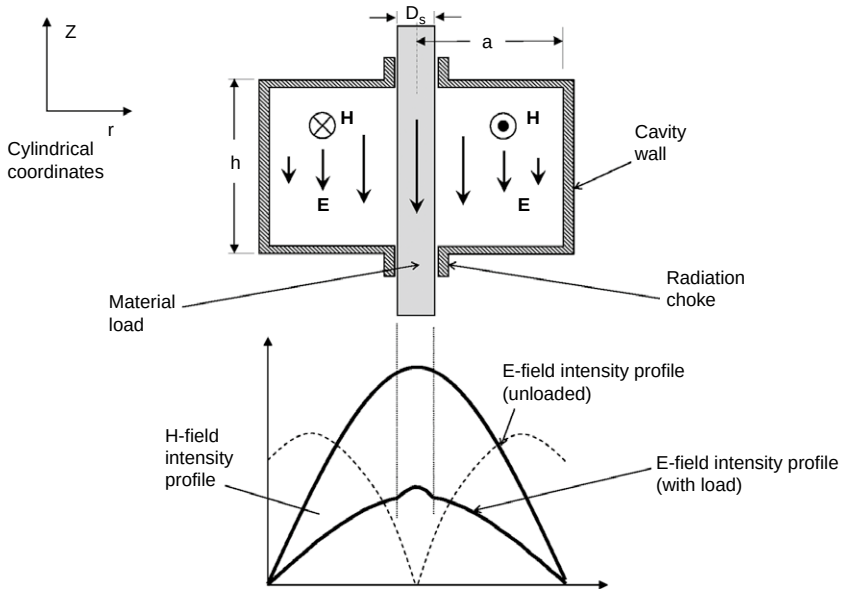

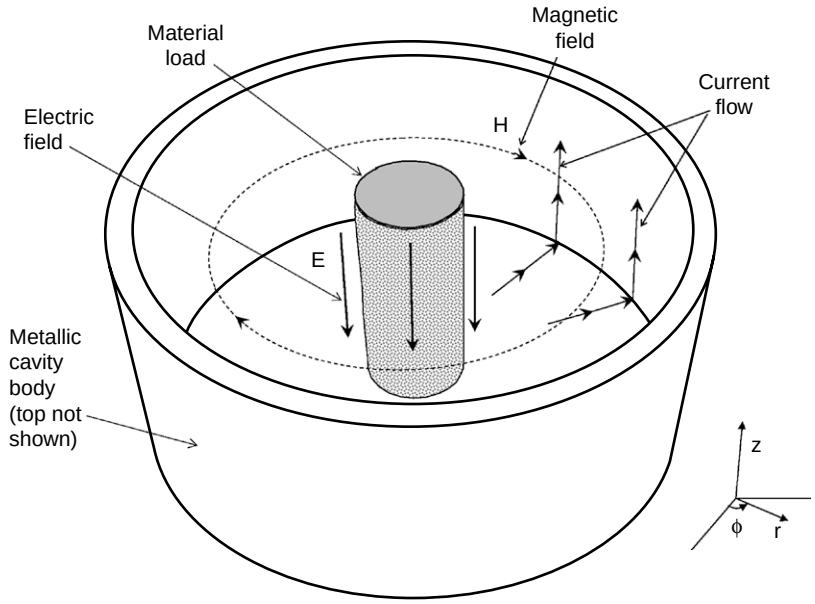

FIGURE 4.3 *Fields and load configuration in a TM_{0n0} cavity used for material interactions (the top plate is not shown).*

4.2.1 The design parameters for a cavity applicator/probe design

Depending on the type of application, the design process for a single-mode cavity is to predict the values of certain unknown parameters based on those that are known. These parameters can be grouped in three classes: geometrical parameters (physical dimensions), material properties (dielectric properties of the process material, supporting structures, and the cavity's material of construction), and electrical parameters (resonant frequency, quality factor, and coupling parameters). In every application a number of these variables are known, and the unknowns are to be determined to complete a design task.

As mentioned before, exact and closed-form solutions for empty cavities of simple geometries are available in many texts. The presence of the material load, however, would change these electrical parameters, often drastically, and simple closed-form solutions do not exist. In some cases where the material is of small size compared to the cavity's internal dimensions, the perturbation theory can be used for an approximate solution. We will use perturbation theory in Section 4.3. Otherwise a more rigorous method is needed.

In addition to analytical solution methods, finite element analysis methods can also be employed in solving cavity problems [24]. The finite element software packages such as COMSOL and CST [25,26], in addition to determining the field configuration in complex geometries, are capable of doing multi-physics analysis, which means they can provide simultaneous electromagnetic and thermodynamic solutions, so that issues such as temperature profile can be determined.

The modern CAD software packages are equipped with modules called "solvers", which tackle various problems useful in the design of microwave cavities. For example, the eigenmode solver in both COMSOL and CST is capable of finding the resonant frequency of a general cavity with a material load. Conversely, this feature can be utilized to determine the dimensions of a material-loaded cavity at a specific resonant frequency.

4.2.2 Field configuration and geometry of TM_{010} cavity

Figure 4.2 shows a side view of a cylindrical TM_{010} cavity that has a cylindrical dielectric load placed coaxially with the cavity. The electric field is at its maximum intensity at the axis of the cavity when empty. The placement of the dielectric load would typically reduce the intensity of the field, and some distortion of the original field intensity will occur as well, which is mostly due to the reduction of the wavelength inside the dielectric material. A detailed and exact analysis of the loading effect can be calculated by using the analytical method shown in Appendix A4.1.

While the field is uniform along the z-axis, in practice there is a small disturbance in the uniformity due to the openings at the top and bottom for loading of the material.

As for uniformity across a cylindrical column, Metaxas [5] shows that, for the case of water, which is a worst case due to its high dielectric constant, the field at the wall of a cylinder containing the water is only 4% lower than at the center.

Figure 4.3 shows more detail of the field configuration and the direction of surface currents on the interior surface of the cylindrical TM_{010} cavity. The field intensity profile can be found from the solution to the wave equation in cylindrical coordinates [2]. Then for the empty cavity with diameter a, the electric longitudinally directed electric field E_z and circumferentially directed magnetic field intensity H_ϕ as a function of radial distance r are:

$$E_z = E_0 J_0\left(\frac{p_{01}\, r}{a}\right) \quad \text{and} \quad H_\phi = \frac{j E_0}{\eta} J_1\left(\frac{p_{01}\, r}{a}\right) \tag{4.1}$$

where E_0 is the maximum electric field at the axis and $\eta = 377\ \Omega$ is the impedance of free space. The functions J_0 and J_1 are the Bessel functions of the first kind of zero and first order respectively, which are tabulated, but are standard functions in modern mathematics software such as Mathematica™ [27]. The constant p_{01} is equal to 2.405, and $j = \sqrt{-1}$ is the complex operator, which signifies the E and H fields are out of phase.

Figure 4.4 shows the relative electric and magnetic field intensity distribution, with the electric field having a maximum at the axis and the magnetic field having a maximum at the radius of $0.76a$.

When a cylindrical dielectric load is placed at the axis of the cavity, as shown in Figure 4.2, the general configuration of the fields remain somewhat similar to the unloaded case. We will examine the exact ramifications of cavity loading in the rigorous analysis of Appendix A4.1.

4.2.3 The resonant frequency, quality factor, and tuning issues

An early step in the design of single-mode cavities for material applications is to find the resonant frequency and quality factor in the empty case, which we will call the unloaded condition here. For example, the resonant frequency (in Hz) for a cylindrical TM_{010} cavity with internal radius a and height h (both in meters) is [2]:

$$f_0 = \frac{p_{01}}{2\pi a\sqrt{\mu_0 \varepsilon_0}} \tag{4.2}$$

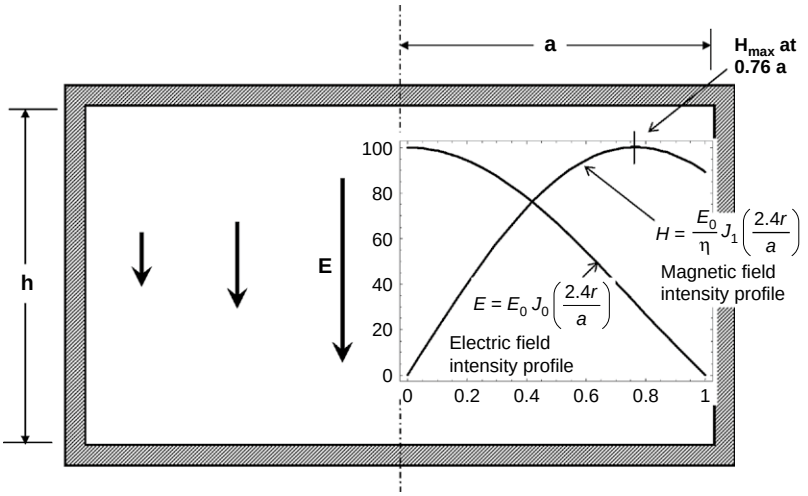

FIGURE 4.4 *Relative electric and magnetic field intensity profiles in an empty TM_{010} cylindrical cavity. The electric field peaks at the axis, but the magetic fields peak at 0.69 times the radius.*

where $\mu_0 = 4\pi \times 10^{-7}$ and $\varepsilon_0 = 8.85 \times 10^{-12}$ are the permeability and permittivity of free space respectively, and $p_{01} = 2.405$ is the first root of the Bessel function of first type and order zero. Replacing all the constants, the above equation can be converted into a more practical version for design as:

$$a\,(\text{in cm}) = \frac{11.5}{f_0\,(\text{in GHz})} \tag{4.3}$$

When a dielectric load is added to a given cavity, the resonant frequency is reduced. Conversely, for a given resonant frequency, with the addition of the load, the diameter must be reduced to maintain the same resonant frequency. Note that in a TM_{010} cavity the resonant frequency is independent of the cavity height.

The theoretical empty Q factor of a TM_{010} cavity with internal diameter a and height h is [2]:

$$Q_0 = \frac{\eta}{R_s} \frac{p_{01}}{2\left(\frac{a}{h} + 1\right)} \tag{4.4}$$

where $\eta = 377\ \Omega$ is the impedance of free space and R_s is the surface resistance of the metal of cavity construction. Using Eq. (1.26) for surface

resistance ($R_s = \sqrt{\pi f \mu_0/\sigma}$) and Eq. (4.2), and inserting all the constants, the empty cavity quality factor becomes:

$$Q_0 = \frac{21.29\sqrt{a\sigma}}{1 + \frac{a}{h}} \tag{4.5}$$

One of the most common aspect ratios used is when the diameter is equal to the height ($h = 2a$). In this case the quality factor is simplified to:

$$Q_0 = 14.2\sqrt{a\sigma} \qquad \text{if} \qquad h = 2a \tag{4.6}$$

or

$$Q_0 = 152{,}073\sqrt{\frac{\sigma}{f}} \qquad \text{if} \qquad h = 2a \tag{4.7}$$

For example, if a cylindrical TM_{010} cavity designed for resonance at 1 GHz has a diameter-to-height ratio of unity, and is made of aluminum ($\sigma = 3.9 \times 10^7$), the empty quality factor from Eq. (4.7) is 30,032, with radius $a = 11.48$ cm and height $h = 22.96$ cm. Unless the interior walls of the cavity are properly polished, the actual measured quality factor will be lower than this figure, typically by about 20%, due to surface roughness.

The insertion of the material load to the single-mode cavity reduces the quality factor to an extent that is dependent upon the size and dielectric properties of the load. For a typical lossy dielectric this reduction is very significant. Given the high Q of single-mode cavities, they are very efficient applicators based on Eq. (2.17) ($\eta_e = 1 - Q_l/Q_0$). The following practical measured example will clarify this point. A cylindrical TM_{010} cavity, which is made of aluminum with a conductivity of $\sigma = 3.9 \times 10^7$ S/m, has a radius of 11.26 cm and a height of 17 cm. From Eq. (4.5), the theoretical empty Q factor is found to be $Q_0 = 26{,}838$. Actual measurement with a network analyzer finds the empty Q to be 24,540. Inserting a quartz tube with ID 7.8 mm that is filled with water into the axis of the cavity reduces the quality factor to $Q_l = 37$. Therefore the applicator efficiency is at $1 - 37/24{,}540 = 99.84\%$. The insertion of the water column has also reduced the resonant frequency from 1021 to 827 MHz. Considering the fact that the diameter of the tube is only 3% of the cavity diameter, this example shows the high sensitivity of single-mode applicators.

4.2.4 Coupling methods and interface with external circuits

The design of a coupling structure to connect a transmission line to a single-mode cavity requires careful examination of the field configuration of both the cavity and the transmission line. Regardless of what type of cavity or transmission-line type is used, the designer can consider either of two methods, magnetic flux linkage or electric field antenna coupling.

Figure 4.5 shows the configuration of a waveguide iris coupling to a TM_{0n0} mode cylindrical cavity from a TE_{10} rectangular waveguide [7]. Waveguides are normally used for power applications where a lower loss transmission line is required to avoid energy losses. An iris is an opening at the physical junction between the end of the waveguide and the cavity, the shape of which comes in several varieties [3]. The inductive iris, being a vertical opening perpendicular to the broad wall of the waveguide, is the most appropriate for power applications due to its better high-field air breakdown capability.

In waveguide iris coupling, the magnetic flux lines of both the cavity and the waveguide must be parallel at the location of the iris. Such is the case with the TE_{10} waveguide and TM_{010} cylindrical cavity, where the broad wall is in parallel with the cavity's end plates. The width of the inductive iris determines the strength of the coupling. For heavier microwave loads, where Q is lower, critical coupling will occur with a wider iris. An

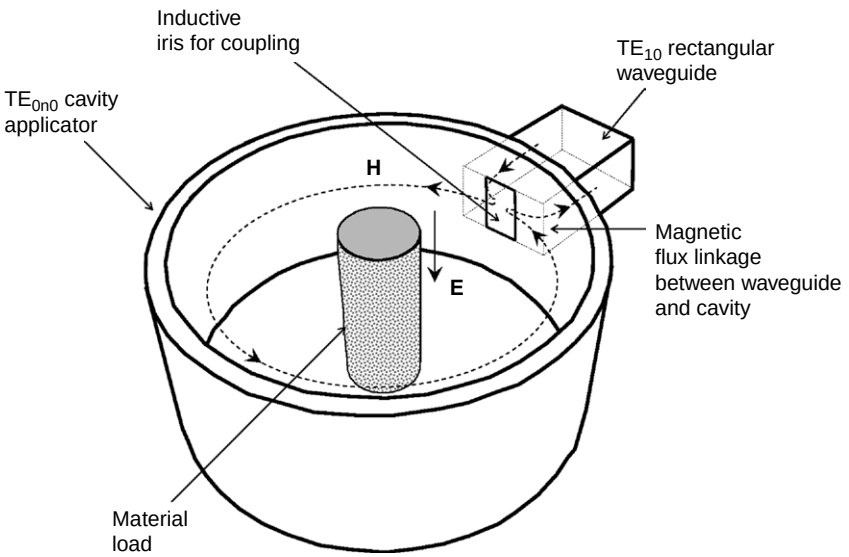

FIGURE 4.5 *Waveguide coupling to a cylindrical applicator.*

adjustable iris [28] provides the opportunity to accommodate variations in load, while keeping the cavity matched to the source.

When using iris coupling for microwave heating there may be excessive local heating in the process material areas closest to the coupling iris. This is particularly true in heating lossy dielectrics. This fact must be taken into account when choosing an operating frequency and cavity mode.

Figure 4.6a shows the loop coupling method [7,29], in which the surface area of the loop is placed perpendicular to the *H*-field line on the inner surface of the cavity. This arrangement would ensure a good flux linkage for effective coupling, and the area of the loop determines the strength of the coupling. Figure 4.6b shows the monopole antenna method of coupling [7] between a coaxial line and a cavity, where the center conductor of the coaxial line is extended into the cavity and the length of the monopole determines the strength of the coupling. The monopole antenna is placed in a location on the walls of the cavity where there is a perpendicular *E* field present.

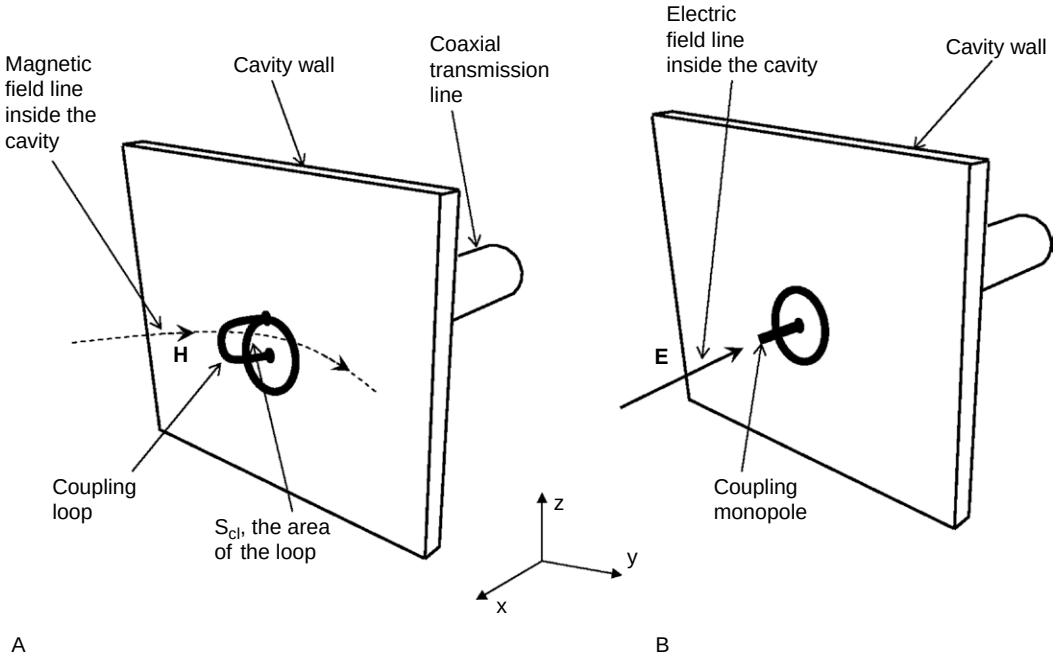

FIGURE 4.6 *Coaxial line coupling with a microwave cavity must be done in consideration of the location of and direction of electric and magnetic fields on the cavity's inside walls. (A) Magnetic field coupling loop is placed perpendicular to the direction of magnetic field line. (B) Electric field coupling monopole is placed in parallel with the electric field line.*

Figure 4.7 shows both loop coupling and monopole antenna coupling on a cylindrical TM_{010} cavity. The designer must first consider the *E*- and *H*-field configurations at the inner wall of the cavity and place the coupling elements properly according to those field directions. For the loop coupling method, which is more commonly used, an equation to calculate the area of the loop is presented in Section 4.3.

For best impedance match the coupling strength can be set by designing the area of the coupling loop or the length of the monopole antenna to an optimum size. This condition is called critical coupling. The variations in the dielectric properties of the load, for example by change in temperature, may change the coupling strength. Even though the change is often undesirable, there are conditions where it can be advantageous.

As an example, Huang [30] has developed a method to avoid thermal runaway in microwave heating of polymers, where the change in coupling due to the rise in temperature would weaken the energy transfer, thereby

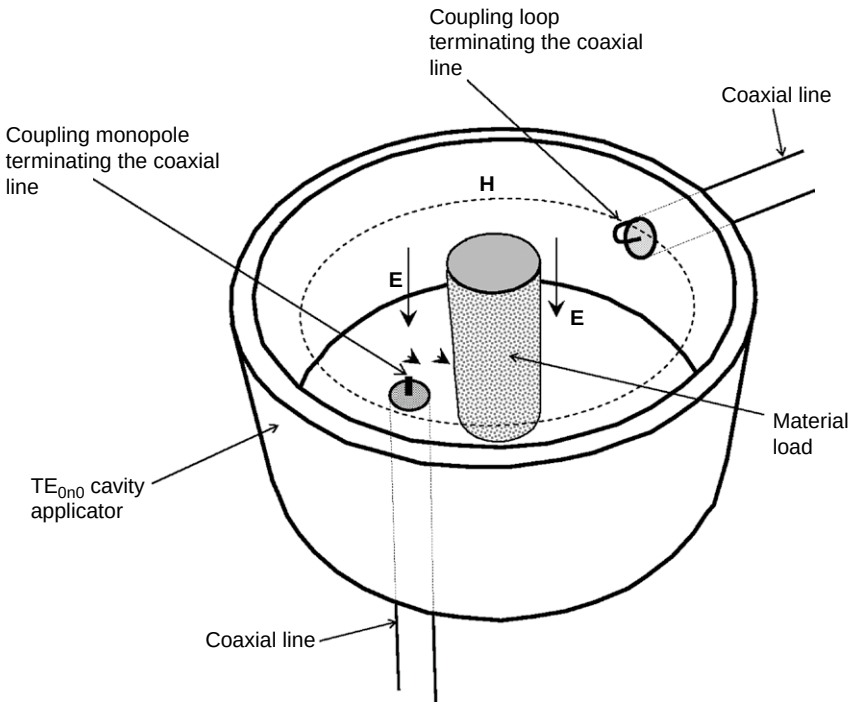

FIGURE 4.7 *Two methods for coupling a coaxial transmission line with a TM_{0n0} cavity. On the right, a coupling loop on the side wall of the cavity is placed perpendicular to the direction of the H-field line. On the left, a monopole antenna, made from extension of the center conductor of the coaxial line, is placed in parallel with the E-field line.*

automatically reducing the microwave energy absorption by the material to avoid a thermal runaway situation.

4.2.5 Dual-port cavities, insertion loss, and return loss

A dual-port, single-mode microwave cavity applicator is shown in Figure 4.8a. There are many reasons for having more than one coupling port in single-mode cavities. In sensor applications two ports are utilized in order to use the insertion loss as a measure of loss properties of the material under test. The dual port can also be used for swept measurements of resonant frequency. In heating applications the second port can be used as the sampling port for feedback loop operation of the cavity, as we will describe in Section 4.5.2.

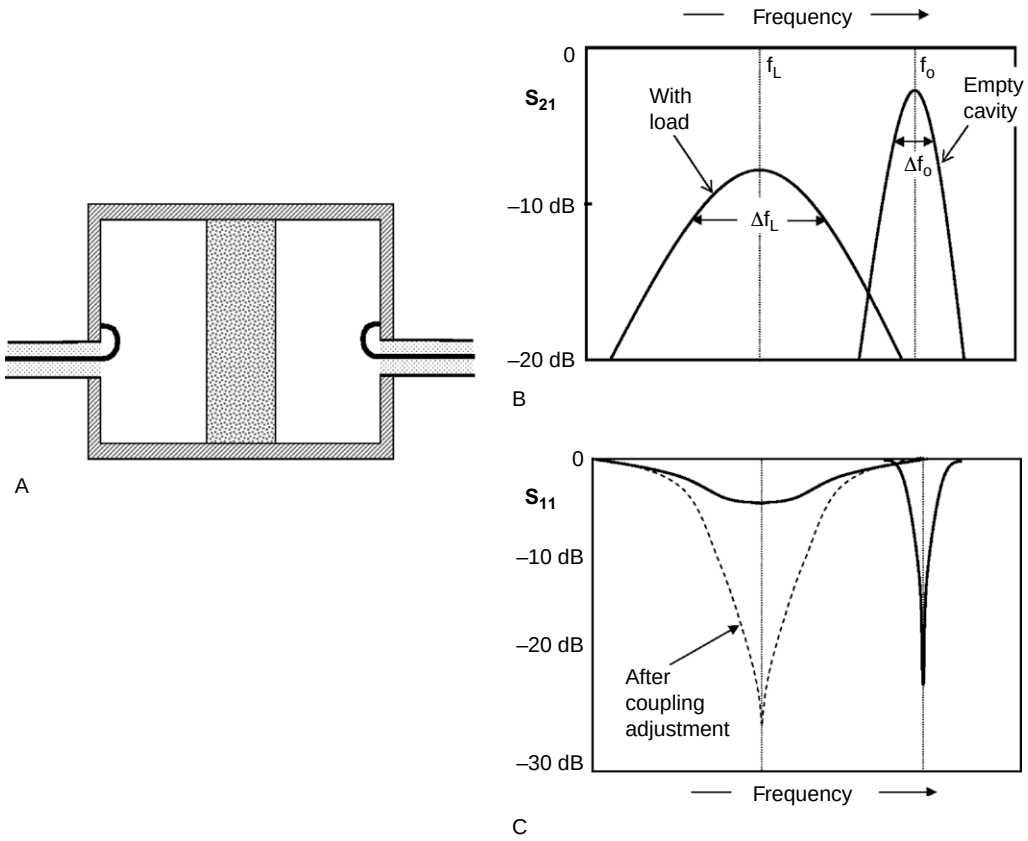

FIGURE 4.8 *Typical network analyzer displays for insertion loss and return loss of a dual-port single-mode cavity. (A) Cavity, load, and coupling ports. (B) Typical insertion loss curves. (C) Typical return loss curves.*

Figure 4.8b and c show typical scattering parameter curves as seen for insertion loss (S_{12} or S_{12}) or return loss (S_{11} or S_{22}) from a network analyzer. The empty cavity and loaded condition curves are shown together on each graph. The insertion of the material load would reduce the resonant frequency and increase the bandwidth (reduce the quality factor). On the insertion loss curve of Figure 4.8b, the insertion loss at the peak resonance is increased. In the return loss graph of Figure 4.8c, the return loss is over -20 dB at the resonant frequency when the cavity is empty, which means the cavity is critically coupled, so the cavity is impedance matched with the transmission line. The insertion of the load will change the return loss to below -5 dB in this example, which means the cavity is now under-coupled. In order to improve the impedance match, the designer can increase the coupling strength by increasing the area of the coupling loop at the measurement port. In the case of a waveguide iris coupling situation, the iris should be widened to achieve the same effect. The dashed curve shows the matched curve with the load after that process is performed.

4.2.6 Equivalent circuit of a cylindrical TM_{010} cavity

Single-mode cavities are distributed resonant structures, and as such they cannot be represented by a lumped element equivalent circuit that is accurate over a wide range of parameters. It is, however, possible to define an equivalent circuit that is only valid in the vicinity of the resonant frequency.

The approximate equivalent circuit of the TM_{010} cylindrical mode is shown in Figure 4.9 [1]. The critical component in this equivalent circuit is the capacitor, which is the component responsible for interacting with a dielectric cylinder, as shown in Figure 4.2. In order to find an expression for the equivalent capacitor, an analysis is used where the total stored electric field energy of the cavity is put equivalent to the energy stored in a parallel-plate ideal capacitor as shown in Figure 4.10, which has a diameter of $a' < a$ and a parallel plate distance of h. After doing the proper integration for the stored energies, the diameter of the equivalent capacitor is found to be

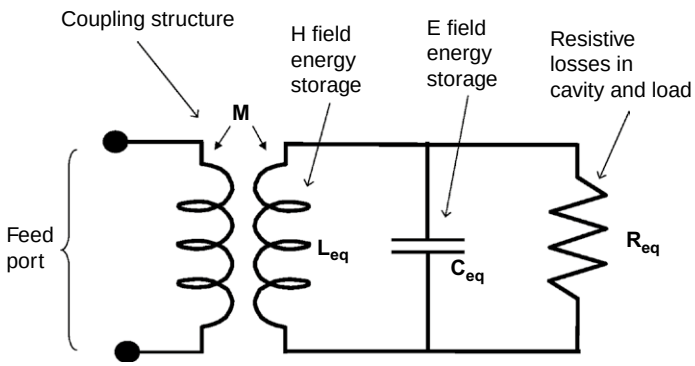

FIGURE 4.9 *The equivalent circuit of a TM_{010} cylindrical cavity.*

$a' = 0.52a$. The equivalent capacitance with the axial load with diameter a_l is found to be:

$$C_{eq} = \frac{\pi\varepsilon_0}{h}\left[a'^2 + a_l^2\left(\varepsilon_r' - 1\right)\right] = \frac{\pi\varepsilon_0}{h}\left[0.27a^2 + a_l^2\left(\varepsilon_r' - 1\right)\right] \tag{4.8}$$

and the relationship between the loaded resonant frequency f_l and the empty cavity resonant frequency becomes:

$$f_l = f_0\sqrt{\frac{0.27a^2}{0.27a^2 + a_l^2\left(\varepsilon_r' - 1\right)}} \tag{4.9}$$

In the equivalent circuit of Figure 4.9, the value of the resistor is:

$$R_{eq} = \frac{Q_l}{2\pi f_l C_{eq}} \tag{4.10}$$

and the value of the inductor can be found from:

$$L_{eq} = \frac{1}{4\pi^2 C_{eq} f_l^2} \tag{4.11}$$

Using the same methodology, for a loop coupled cylindrical TM_{010} cavity, the mutual inductance from the equivalent circuit becomes:

$$M = \frac{J_1(p_{01})\mu_0 S_{cl}}{2\pi^2\varepsilon_0\eta f_l\left[0.27a^2 + a_l^2\left(\varepsilon_r'' - 1\right)\right]} \tag{4.12}$$

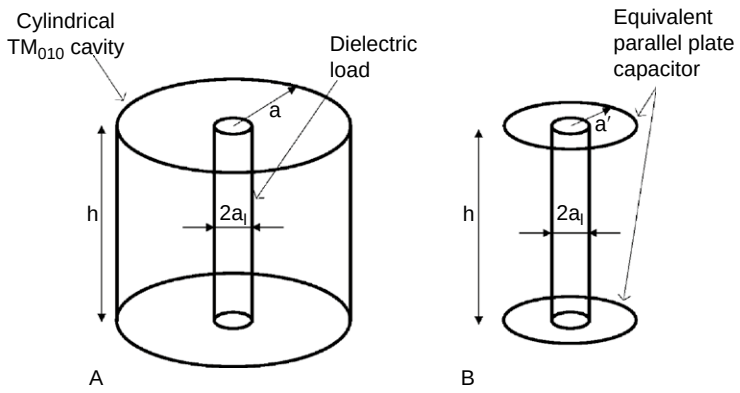

FIGURE 4.10
Method of finding the approximate equivalent capacitance of a cylindrical TM_{010} cavity. (A) The cavity configuration with an axial load. (B) The equivalent capacitor that holds the same amount of stored electric energy.

where $J_1(p_{01}) = 0.519$ and S_{cl} is the area of the coupling loop in m^2, provided that the loop is properly oriented with respect to the magnetic field at the inner surface of the cavity.

4.2.7 Wall surface current considerations in single-mode cavities

Every resonant mode, in addition to fields in the cavity volume, possesses a characteristic pattern of current flow on the interior surface of the cavity. The direction and distribution of the surface current can be exactly determined using the same methods by which field distributions are predicted. The knowledge of these current patterns, and in particular their directions, is quite useful and often critical in the design of single-mode cavities as applicators and sensors.

An elongated slit that is made for any purpose on a cavity must be made in parallel to the local current flow to preserve the integrity of the mode of interest. In a TM_{010} mode cavity, for example, any slit or cut made in the longitudinal direction on the curved wall, as well as in the radial direction on the end plates, will not disturb the operating mode, as shown in Figure 4.11a. This is useful in practice because the cavity can be made in two halves, or could have side slits for other purposes without any negative effects on its properties or utility.

Making slits perpendicular to the direction of current flow will tend to kill the mode. This concept is often used for suppressing unwanted or degenerate modes. For example, the cylindrical modes TE_{011} and TM_{111} are degenerate (see the cylindrical cavity mode chart of Appendix A2.1), which means they resonate at the same frequencies regardless of geometrical parameters. The currents associated with the TM_{111} mode flow longitudinally (z direction), while TE_{011} mode currents flow cicumferentially (ϕ direction). Therefore, making a circumferential slit will dispose of the TM_{111} mode, while keeping the TE_{011} mode intact.

4.3 MATERIAL LOADING IMPACT IN SINGLE-MODE CAVITIES: APPROXIMATE AND RIGOROUS METHODS

In most cases where single-mode cavities are used for material processing and sensing applications, it is important to examine and predict the impact of material loading on the electrical parameters of the cavity. For example, in heating applications, since only ISM frequencies are available, the cavity should be designed such that the final resonant frequency of the cavity, after the material to be processed is added, is at the ISM frequency of interest.

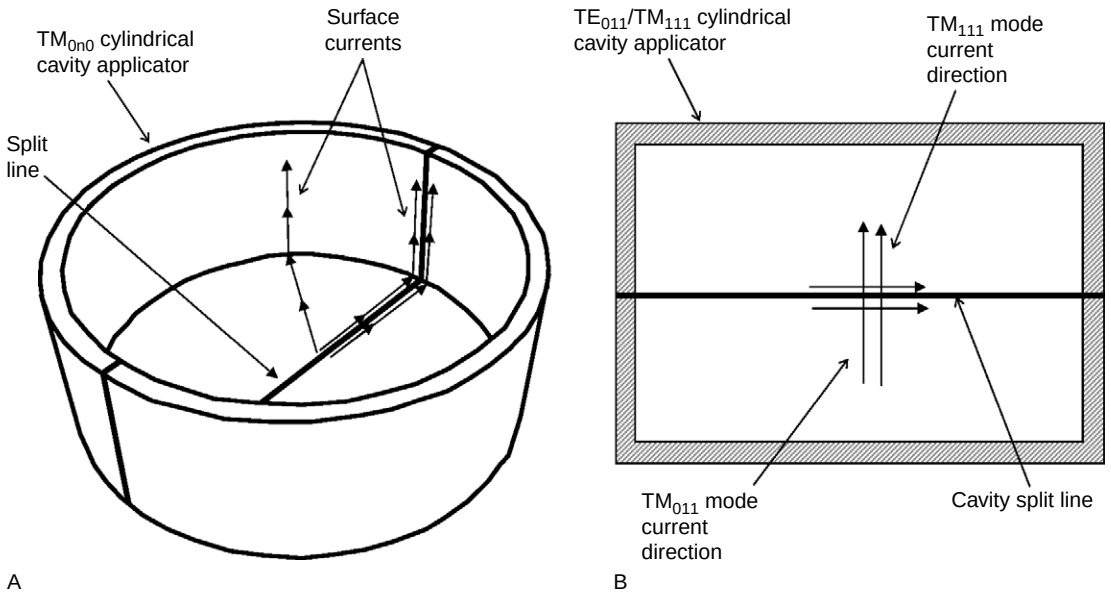

FIGURE 4.11 *The knowledge of surface current directions can aid in proper design of single-mode cavities. (A) A cylindrical TM_{0n0} cavity can be split in half without disturbing the currents. (B) Cylindrical cavity TM_{111} and TE_{011} modes are degenerate. A circumferential split will destroy the TM_{111} mode, but keeps the TE_{011} mode intact due to perpendicular current directions.*

When single-mode cavities are used as sensors, the impact of the variations of the material properties must be examined for effective design. There are various methods available, from simple approximate ones such as the cavity perturbation method, to highly rigorous analytical or numerical methods. In this section we will start with perturbation methods and proceed to a detailed analytical method that applies to cylindrical TM_{0n0} cavities.

4.3.1 The perturbation method for material loading studies

In using perturbation methods [31], the assumption is that the volume of the material that loads the cavity is small compared to the volume of the cavity, and therefore the basic field configuration of the cavity remains relatively intact.

For the cylindrical TM_{010} cavity the following approximate expression [32], which is derived from perturbation theory, calculates the shift in the resonant frequency, Δf, with the insertion of a small cylindrical dielectric load of at the axis:

$$\frac{\Delta f}{f_0} = \frac{\varepsilon_r' - 1}{2J_1(p_{01})} \cdot \frac{V_l}{V_c} \qquad \text{if} \qquad V_l << V_c \tag{4.13}$$

where V_l is the volume of the cylindrical load, V_c is the volume of the cavity, f_0 is the unloaded resonant frequency of the cavity before the insertion of the rod, ε_r' is the relative dielectric constant of the rod, and $J_1(p_{01}) = 0.52$ is the first-order Bessel function of the first type with the argument $p_{01} = 2.405$, which is the first root of the Bessel function of the first kind and zero order. In Eq. (4.13) it is assumed that the material is not highly lossy ($\varepsilon_r' << \varepsilon_r'$). If this criterion cannot be met, better accuracy can be obtained if instead of ε_r', the factor $\sqrt{\varepsilon_r'^2 + \varepsilon_r''^2}$ is used.

The quality factor change for a cavity with a dielectric rod is given as [32]:

$$\frac{1}{Q_l} - \frac{1}{Q_0} = \frac{\varepsilon_r''}{J_1^2(p_{01})} \cdot \frac{V_l}{V_c} \qquad \text{if} \qquad V_l << V_c \tag{4.14}$$

where ε_r'' is the relative dielectric loss factor of the dielectric rod.

Considering the fact that the applicator efficiency is defined by $\eta_e = 1 - Q_l/Q_0$, and the volumes are $V_l = \pi a_l^2 h$ and $V_c = \pi a^2 h$, the following equation will hold:

$$\eta_e = \frac{1}{1 + \dfrac{0.27}{\varepsilon_r'' Q_0}\left(\dfrac{a}{a_l}\right)^2} \qquad \text{if} \qquad a_l << a \tag{4.15}$$

where the numerical value of $J_1(p_{01}) = 0.52$ is used. Equations (4.14) and (4.15) provide a good approximation when the load diameter is much smaller than the cavity diameter. In more general situations, and when more exact results are needed, the analytical method described in Section 4.3.3 and Appendix A4.1 should be used.

4.3.2 Application example: use of perturbation method in the design of a sensor with a cylindrical TM_{010} mode cavity

The cylindrical TM_{010} single-mode cavity has been used extensively as a material sensor in many practical applications [20,33–35]. As an example, Figure 4.12 shows the results of a sensor for detecting the contamination of one liquid mixed with another. For proper design of such sensors, the following analysis and example is useful.

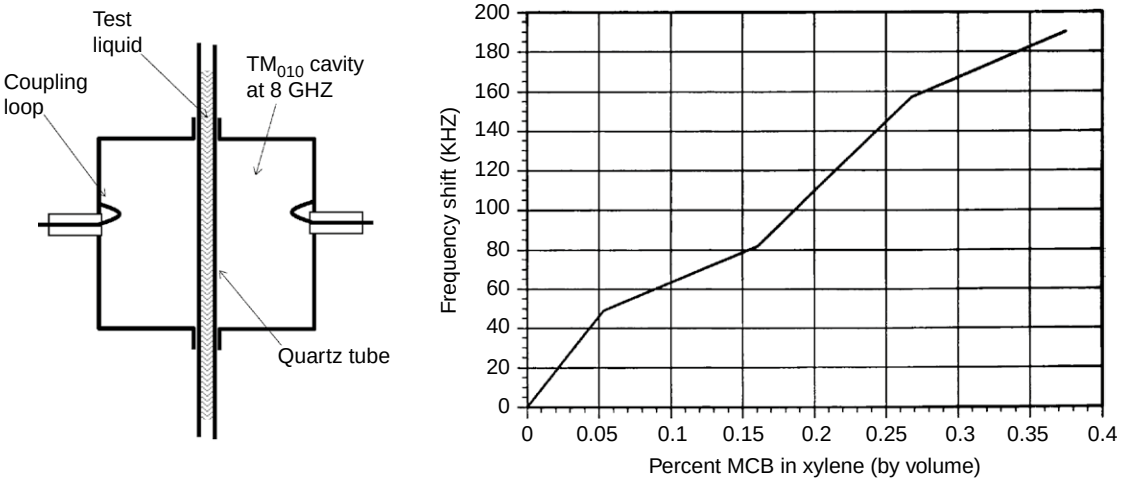

FIGURE 4.12 *Detection of small impurities in liquids using a TM_{010} cavity's shift in resonant frequency. In this case the resonant frequency indicates the concentration of MCB in xylene (both organic solvents).*

Placing a cylindrical rod with the diameter a_1 in a TM_{010} cylindrical cavity, as shown in Figure 4.2, Eq. (4.13) can be modified by using $\Delta f = f_0 - f_s$, $V_1 = \pi a_1^2 h$, and $V_c = \pi a^2 h$, to:

$$f_1 = f_0\left[1 - \frac{1}{2}\left(\frac{a_1}{a}\right)^2 \frac{\varepsilon_r' - 1}{J_1^2(p_{01})}\right] \tag{4.16}$$

But the cavity diameter a is related to the resonant frequency using Eq. (4.2), which turns Eq. (4.16) into:

$$f_1 = f_0\left[1 - \frac{2\pi^2 a_1^2 f_0^2}{J_1^2(p_{01})\, p_{01}^2 C^2}\left(\varepsilon_r' - 1\right)\right] \tag{4.17}$$

If the material variable of interest is the relative dielectric constant, and the electrical variable to be measured is the resonant frequency, the sensitivity of such sensor would be:

$$\frac{df_1}{d\varepsilon_r'} = -\frac{2\pi^2 a_1^2 f_0^3}{J_1^2(p_{01})\, p_{01}^2 C^2} \tag{4.18}$$

Example

In an industrial process, a rod-like dielectric material with diameter 1 mm and relative dielectric constant of 3.4 is produced. The goal is to use a

TM_{010} cavity to detect variations of the dielectric constant with an accuracy of 100 ppm. A separate study has shown that measurement of the resonant frequency is limited to a resolution of 10 kHz. Estimate the working frequency acceptable in such an application and the dimensions of the cavity.

Solution

Replacing all the constants, the right-hand side of Eq. (4.18) becomes $-1.4 \times 10^{-16} a_1^2 f_0^3$. Then using $df_1 = 10^4$ Hz and $d\varepsilon_r' = 3.4 \times 10^{-4}$ (100 ppm of 3.4), the solution of Eq. (4.18) yields $f_0 = 9.43 \times 10^9$ Hz = 9.43 GHz. Using Eq. (4.3), the internal diameter of the cavity needed for this sensor would be 24.35 mm. Theoretically, the length of such a cavity does not enter this calculation; therefore this parameter should be chosen for other practical considerations. Usually length is chosen to be approximately equal to the diameter. Since the volume of a cavity has turned out to be much larger than the volume of the sample, using the perturbation theory approximation is appropriate.

4.3.3 Analytical field solution for TM_{0n0} applicators

In Section 4.3.1 we described an approximate solution for material loading of a cylindrical TM_{010} cavity based on the perturbation theory, which assumes the load occupying only a small fraction of the cavity's volume. In this section a full rigorous solution [36,37] is described for the general case of a TM_{0n0} family of cylindrical cavities. This solution, which is described in detail in Appendix A4.1, uses a Mathematica™ worksheet (Riegert) to solve the wave equation. The solution allows for a load at the axis of the cavity to have two concentric layers of real dielectrics.

The following example shows one of the practical ways the Mathematica™ notebook of Appendix A4.1 can be used.

Example

Suppose that a pumpable liquid with the complex relative dielectric constant of $\varepsilon_r^* = 21.5 - j\ 3.5$ flows through a dielectric pipe with internal diameter 2.5 cm and wall thickness 4 mm. The complex relative dielectric constant of the pipe is $\varepsilon_r^* = 3.5 - j\ 0.0015$. The goal is to heat the liquid with microwaves using a single-mode cavity. There are three choices for the ISM frequency: 433, 915, and 2450 MHz. The idea is to simulate the problem using the Mathematica™ notebook of Appendix A4.1 to examine the feasibility of doing the heating with these frequencies and possible TM_{010} or TM_{020} modes.

Solution

Table 4.1 can be constructed from the results of the simulation. In the first two columns the ID of the empty cavities for the two possible modes are calculated for each ISM frequency of interest. In the next two columns

Table 4.1 Comparison of single cavity parameters for three ISM bands in TM_{010} and TM_{020} modes.

Frequency (MHz)	Unloaded Cavity ID (cm) to Resonate at Specified ISM Frequency		Resonant Frequency with Load Placed (MHz)		Loaded Cavity ID to Resonate at Specified ISM Frequency (cm)	
	TM_{010}	TM_{020}	TM_{010}	TM_{020}	TM_{010}	TM_{020}
433	53.06	115.70	391	431	46.60	115.14
915	25.10	54.75	638	780	12.0	44.19
2450	9.37	20.45	1054	1875	3.6	15.68

the new frequency for each case is calculated after the load is inserted. In the next two columns the ID of the loaded cavity is calculated for the ISM frequency of interest. A careful examination of this table shows that only some of the cases are practically possible. For example, using the TM_{010} mode at 2450 MHz is problematic because the ID of the cavity is very close to the OD of the pipe. Attempting to construct such a cavity may cause overheating at the location of the coupling port due to the proximity of the coupling iris.

4.3.4 Application example: industrial application of TM_{020} cavities for viscous liquid heating

Many problems are encountered when a heat-sensitive viscous liquid needs to be heated continuously in industrial settings. The flow is mainly laminar as viscous fluids pass along a pipe, and the lack of turbulence prevents mixing. Therefore a uniform temperature is not achieved when the pipe is being heated from outside by conventional means. High power densities at the outer surface of the pipe lead to excessive heating of boundary layers compared with higher flow rates along the axis of the pipe. This localized heating can cause degradation of the product at the pipe walls.

Microwave heating, with its volumetric nature, can possibly be of help in overcoming this problem if an electrically insulating pipe is used, and microwave is applied from outside of the pipe. However, in some instances the viscosity is so high that the differential speeds at the center versus the wall of the pipe are high enough that even uniform volumetric heating is not sufficient to prevent overheating at the walls.

The usage of a cylindrical TM_{020} mode cavity, as shown in Figure 4.13, has been shown to overcome this problem [37–39]. In this cavity mode the electric field intensity is dropped to zero at a point between the axis and the inside wall of the cavity. If the geometry of the insulating pipe and the

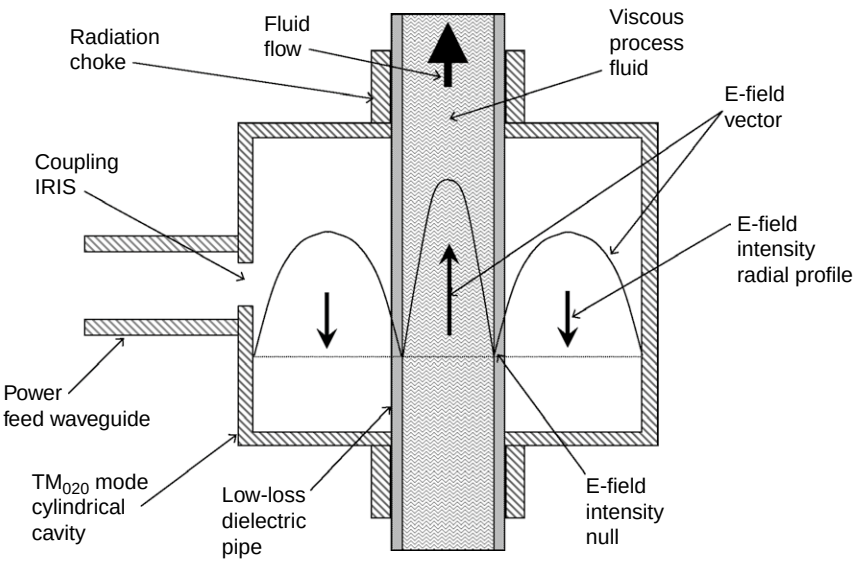

FIGURE 4.13

A TM_{020} cavity arrangement for gentle heating of a flowing viscous fluid. The design is such that the energy deposition null is designed to match the dielectric tube's inner wall. Therefore the energy deposition is zero at the wall and maximum at the axis of the tube.

cavity is designed such that the zero point of the *E*-field intensity is placed at the inner wall of the dielectric pipe, then the profile of the microwave heating matches that of the laminar flow. Therefore the part of the flowing material on the wall that lags behind would not be overheated due to zero microwave deposition at that location. Hill et al. [37] have used this method for heating of adhesives for automobile interior assembly.

There are several other examples of single-mode cavities being used for industrial applications [40–44]. A photograph of one of these applications [14] is shown in Figure 4.14.

4.4 OTHER (NON-TM_{0n0}) SINGLE-MODE CAVITY TYPES FOR MATERIALS INTERACTION

In addition to the cylindrical TM_{0n0} cavity applicators, which we have covered so far, there are a few other single-mode cavity types that are also of interest in material processing and sensing applications. TE modes, in both rectangular and cylindrical shapes, are also of interest due to specific advantages they provide, which will be covered in this section.

4.4.1 TE_{10n} waveguide-based single-mode cavities

Waveguide-based cavity applicators are important, particularly in microwave material heating laboratory research, because they are conveniently

FIGURE 4.14 *A two-stage single-mode cavity heating installation for microwave processing of fluids. (Courtesy of Industrial Microwave Systems (IMS).)*

manufactured from modifications to a TE_{10} mode waveguide. Figure 4.15 shows the side view of a waveguide that is shorted at one end using a shorting plunger, and is fed from the other side through a microwave iris. Figure 4.16 shows the vertical field intensity of a TE_{103} and how the specific designation of TE_{10n} is derived from the generic TE_{mnk} designation. There is one full variation of field intensity from one side wall to another, which accounts for $m = 1$, and no variation of E field in the y direction, which accounts for $n = 0$, and in the case of Figure 4.15 there are three variations of the field intensities in the z direction, which account for $k = n$, where in this case $n = 3$.

The only E-field component in the TE_{10n} cavity is the y-directed component, E_y. The solution of the wave equation [3] will yield the following for this field component for a cavity with width a, height h, and length z:

$$E_y = E_0 \sin\left(\frac{\pi x}{a}\right) \sin\left(\frac{n\pi z}{l}\right) \tag{4.19}$$

where E_0 is the maximum electric field intensity.

In order to examine the relationships between the resonant frequency f_0 and the dimensions of the cavity, starting from the general equation for

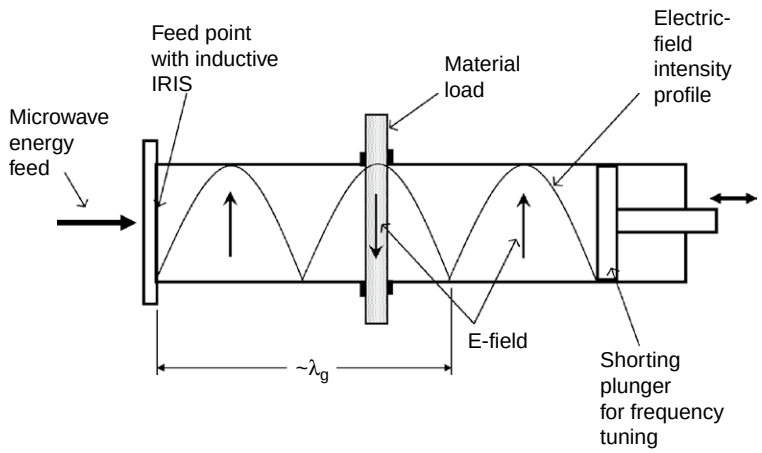

FIGURE 4.15 *A waveguide-based TE_{103} cavity arrangement with a shorting plunger for tuning.*

rectangular waveguides [1], the resonant frequency of a rectangular TE_{10n} cavity with width a, height h, and length ℓ, as shown in Figure 4.16, becomes:

$$f_0 = \frac{C}{2}\sqrt{\frac{1}{a^2} + \frac{n^2}{\ell^2}} \tag{4.20}$$

where $C = 3 \times 10^8$ m/s is the speed of light in free space. In most cases of design for material heating/sensing applications, the frequency of operation is a known ISM frequency, such as 2.45 GHz. Therefore the goal of the design is finding the dimensions so that the resonant frequency is equal to the source frequency. If the cavity width a is known, the length ℓ for the empty cavity becomes:

$$\ell = \frac{n}{\sqrt{\left(\frac{2f_0}{C}\right)^2 - \frac{1}{a^2}}} \tag{4.21}$$

The above equation is only valid when the width is above the "waveguide cutoff", which means $a > \lambda_0/2$, where $\lambda_0 = C/f_0$ is the operating wavelength. The waveguide width should be designed to be substantially

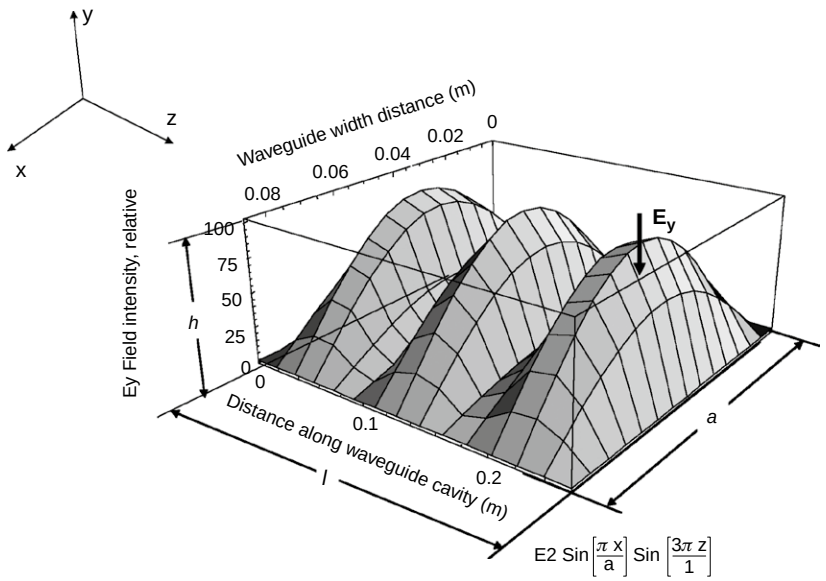

FIGURE 4.16 *Vertical (E_y) electric field intensity in a TE_{103} rectangular cavity.*

above this cutoff. A careful examination of Eq. (4.20) reveals that if a is chosen too close to the cutoff wavelength, then the length of the cavity would become unreasonably long. For best cavity efficiency, an optimization to find the lowest cavity volume would yield the following for the optimum dimensions of an empty cavity:

$$a_{\text{opt}} = \frac{\lambda_0}{\sqrt{2}} = \frac{C}{\sqrt{2}\, f_0} \qquad \text{and} \qquad \ell_{\text{opt}} = n\frac{\lambda_0}{\sqrt{2}} = n\frac{C}{\sqrt{2}\, f_0} \tag{4.22}$$

For example, for optimum operation, with a TM_{101} cavity ($n = 1$), the optimum dimensions for an empty cavity are $a = \ell = 86.6\,\text{mm}$.

The introduction of a material load to the cavity, as shown in Figure 4.15, will reduce the length, if the resonant frequency is to remain constant. As an example, for the arrangement shown in Figure 4.15, the maximum length set by the shoring plunger is what is calculated by Eq. (4.21) or (4.22), and for a loaded condition the shorting plunger is set to make the length shorter until the desired operating frequency is found using a network analyzer.

The quality factor of the empty TE_{10n} rectangular cavity is found by slight modification of an existing formula [2] as:

$$Q_0 = \frac{1}{2}\eta\sqrt{\frac{\pi\sigma}{\mu_0 f_0}}\,\frac{\sqrt{1+x^2}}{x\left(\frac{h}{a}\right) + 2\frac{1+x^3}{1+x^2}} \tag{4.23}$$

where:

$$x = \frac{n}{h\sqrt{\left(\frac{2f_0}{C}\right)^2 - \frac{1}{a^2}}} \tag{4.24}$$

For material applications, the most important mode in the family of TE_{10n} modes is the base mode, which is the rectangular TE_{101} cavity. This mode has a field configuration somewhat similar to that of the cylindrical TM_{010} mode, where the maximum field where the load should be placed is at the center of the cavity, as shown in Figure 4.17.

Perturbation theory can be used in order to find the loading effects of loads that are physically small compared with the volume of the cavity. For a rectangular TE_{101} cavity and a rod-like dielectric load inserted parallel to the main E field as shown in Figure 4.17, the perturbation model [32]

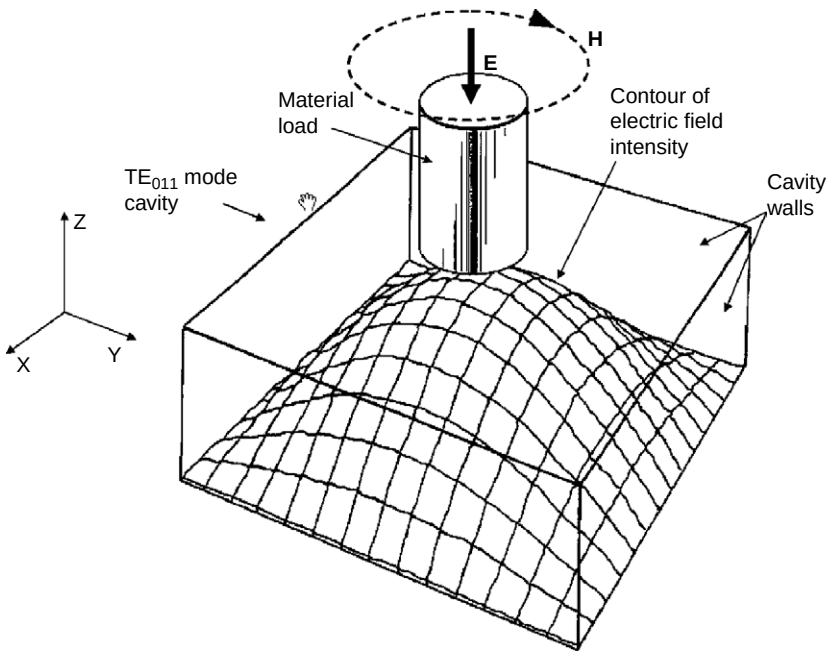

FIGURE 4.17 *The E-field intensity contour for a TE_{101} rectangular cavity applicator.*

can be modified to arrive at the following equations for the material-loaded resonant frequency and quality factor:

$$f_l = f_0\left[1 - 2\left(\sqrt{\varepsilon_r'^2 + \varepsilon_r''^2} - 1\right)\frac{V_l}{V_c}\right] \tag{4.25}$$

and

$$Q_l = \frac{1}{\dfrac{1}{Q_0} + 4\varepsilon_r''\dfrac{V_l}{V_c}} \tag{4.26}$$

4.4.2 Application example: rectangular TE_{101} cavity for gas-phase catalysis

Certain gas-phase endothermic chemical reactions require very high temperatures upwards of 1000°C at the surface of a catalyst, which is often a metal such as platinum or rhodium. This catalyst must have a high surface area for better yield. The catalyst is often a micron-sized metallic powder

that is impregnated on ceramic support beads. Microwave heating of such catalysts [45–47] provides the advantage of putting the energy exactly where it is needed without the need to confront the problems associated with heat transfer at high temperatures.

The metal content of such supported catalysts is quite small, which means the effective dielectric loss is somewhat low. To raise the catalyst to the required high temperatures a very high electric field is needed, which single-mode cavities can provide due to their high sensitivity.

A general view of the aluminum applicator, which is a rectangular TE_{101} cavity, is shown in Figure 4.18. The microwaves at a frequency of 2450 MHz are carried by a standard waveguide through a flared transition section. An inductive microwave iris is used to couple the energy into the cavity. The cavity wall across from the iris is movable, while maintaining electrical contact with the other wall through silver-plated spring-loaded finger stocks. The catalyst tube is placed vertically at the middle of the cavity. The replacement of the reactor tube is done by opening the cavity through the hinge at the rear of the assembly.

The process in this example is catalytic synthesis of hydrogen cyanide (HCN), which is a very useful compound as an intermediate for production of a wide range of chemicals, phamaceuticals, and polymers. A variety of alumina-supported platinum catalysts have been tested for susceptibility to microwaves. The support for these catalysts is composed of alumina spheres, ranging in size from 200 mesh to 4 mm. A fine platinum

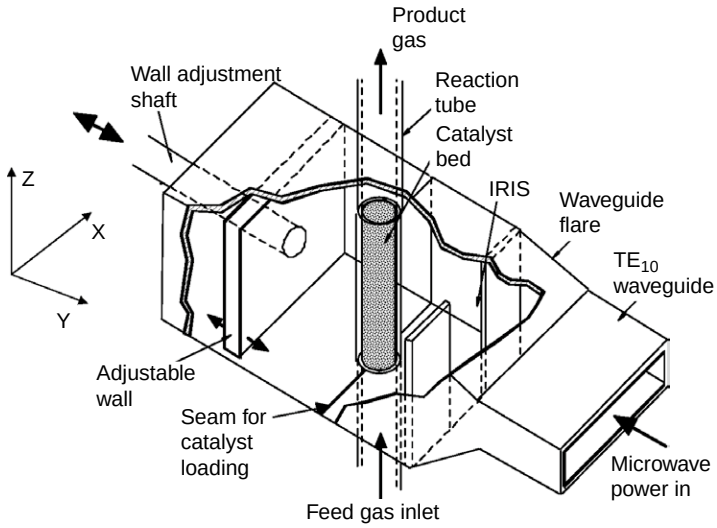

FIGURE 4.18 *A rectangular TE_{101} cavity for microwave-assisted gas-phase catalysis.*

powder coats this support. Since alumina itself has very low susceptibility to microwaves, the percentage of platinum content determines the overall susceptibility. Catalysts containing less than 2% platinum content were determined to have less than 20% applicator efficiency and not to be usable. The catalyst used in most of our experiments was 10% platinum catalyst with 200 mesh alumina support. This catalyst, when put in a quartz tube with 0.5 inch diameter, yields an applicator efficiency of 92%.

4.4.3 Application example: TE_{101} cavities for sintering of ceramics

Some materials such as many ceramics, due to their low loss, are difficult to heat to high temperatures with RF/microwave methods. The reason is that according to basic microwave heating equation (1.18), either the electric field or frequency must be very high. This excludes RF frequencies due to their low frequency, and excludes multimodal microwave ovens due to their low field strength. Very high microwave frequencies in the ISM band of 24 GHz are effective for this method, but the gyrotron power source is not economical for this purpose on an industrial scale.

Single-mode cavities, due to their exceptional efficiency and sensitivity, can be used for heating even low-loss materials [15]. Sintering of ceramics, which often have very low loss, can be accomplished with this method by raising the material to very high temperatures. The method [48] calls for using either a cylindrical TM_{010} or rectangular TE_{101} cavity in a manner similar to that shown in Figure 4.18 in the previous section. The ceramic material, in rod form, is fed via a motor control into the cavity, and a thick annular high-temperature insulator surrounds the ceramic for thermal insulation. A temperature of 1300°C was achieved and superior results have been reported for sintering of Ba_2TiO_4 ceramics.

4.4.4 Cylindrical TE_{011} and other cavities for interactions with sheet dielectrics

There are certain single-mode cavity configurations that are particularly suited for interactions with planar and sheet materials. A major criterion for such cavities is the capability to make slits or splits in the cavity for sheet material insertion. Figure 4.19 shows the field configuration of a cylindrical TE_{011} cavity. The main feature that makes this cavity type appropriate for sheet material insertion is the electric field line, which is maximum at the center of the height and forms a circle parallel to the inserted sheet as shown. The current flow on the side wall of the cavity is circumferentially directed, which makes it possible to split the cavity

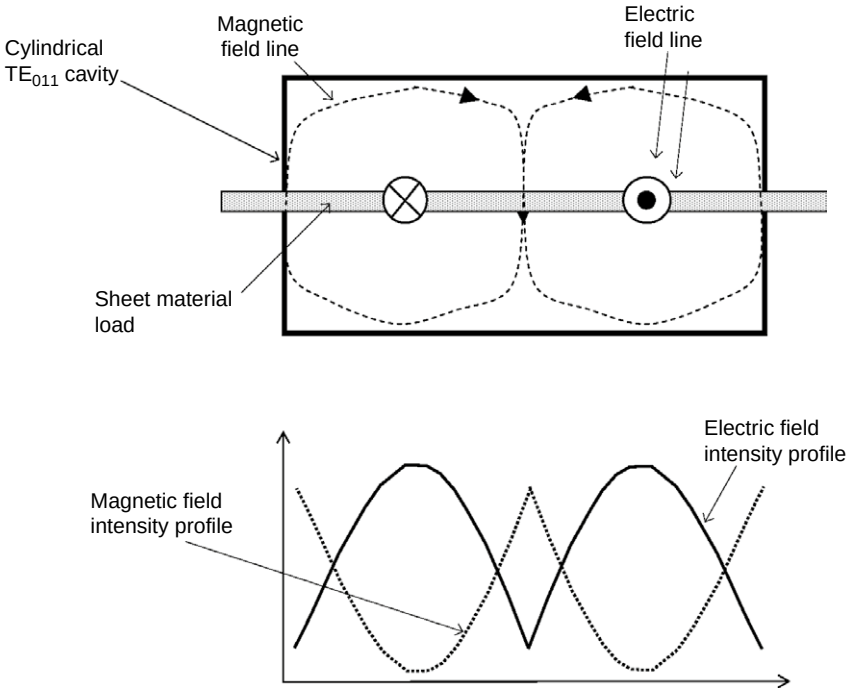

FIGURE 4.19 *Side view of a cylindrical TE_{011} cavity used for interaction with a sheet dielectric material.*

in half for convenient material loading. The split also serves as a mode suppressor for TM_{111}, which is degenerate with the desired TE_{011} mode at all frequencies. This type of configuration is used for dielectric measurements of planar materials [49–51].

Another cavity method of interest for planar material interactions is the cylindrical TM_{010}, as shown in Figure 4.20. In this configuration the same principle of current flow and splitting as shown in Figure 4.19 applies. The E field in this configuration is uniform along the z direction as shown, which makes it appropriate for continuous sheet material processing. A similar situation is fully described for a rectangular TE_{101} mode in Chapter 8 for industrial processing of sheet materials.

4.4.5 Some special and alternative applications of single-mode cavities

In this section we will describe certain methods and ideas for utilization of single-mode cavities that go beyond the conventional methods described earlier in the chapter.

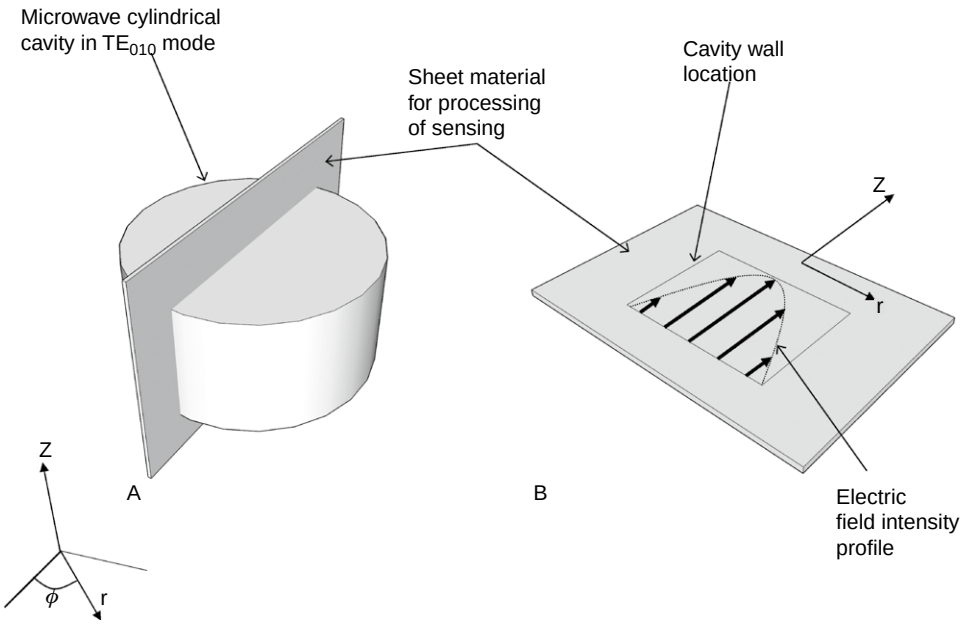

FIGURE 4.20 *A cylindrical TM_{010} cavity for interaction with sheet material. The split for feeding the sheet does not disturb the fields due to the parallel nature of surface current flow with the split. (A) 3-D perspective. (B) Field interaction with sheet.*

One such application is the use of a single-mode cavity for the measurement of the conductivity of metals at microwave frequencies [52]. In this method, one of the walls of the microwave cavity is replaced by the conductive material under test. The losses of the material will impact on the quality factor of the complete cavity. Using analytical or numerical methods the conductivity of the material can be evaluated.

Another application of this type is batch processing of dielectric ceramic rods [53] using a TM_{020} cylindrical cavity, as shown in Figure 4.21. The special field configuration of this cavity mode has a peak at the axis of the cavity and another annular peak at about half distance from the axis to the wall. The rods are placed in the annular peak in the longitudinal direction as shown. For tuning of the cavity to the frequency of the source, a low-loss dielectric rod is placed at the central peak of the cavity for tuning purposes.

One of the more recent developments in improving the field uniformity of single-mode cavities is the use of dielectric slabs [54] close to the walls for cavity modes such as cylindrical TM_{010} or rectangular TE_{101}, as shown in Figure 4.22. In this mode of operation, the wavelength inside the

FIGURE 4.21

Batch processing of rods in a TM_{020} mode cavity is an example of how the specific field configuration of certain single-mode cavities can be utilized (see Barmatz [53]).

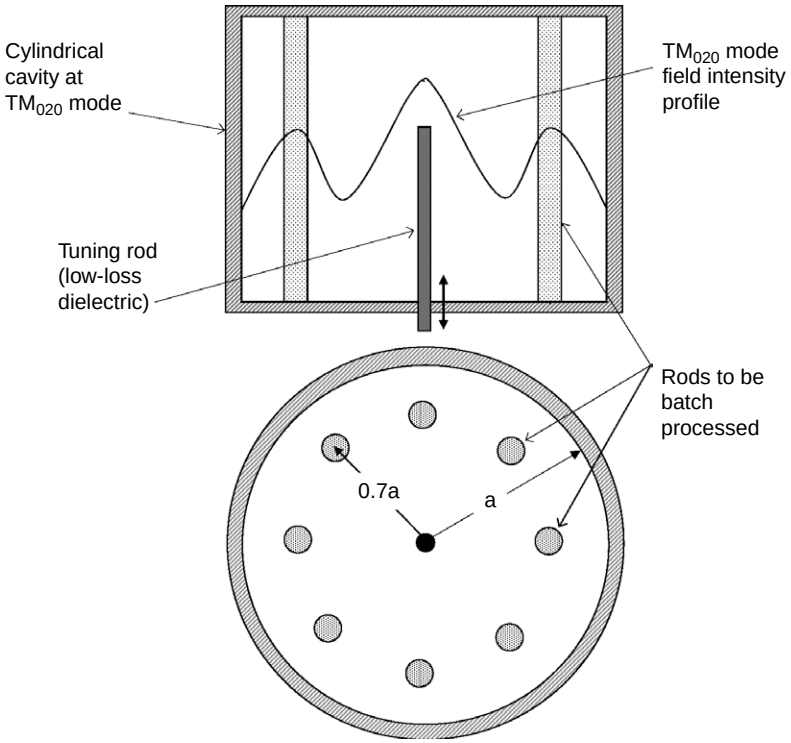

FIGURE 4.22

A cavity loaded with low-loss dielectric slabs on the walls has a more uniform E-field intensity profile (see Bernhard and Joines [54]).

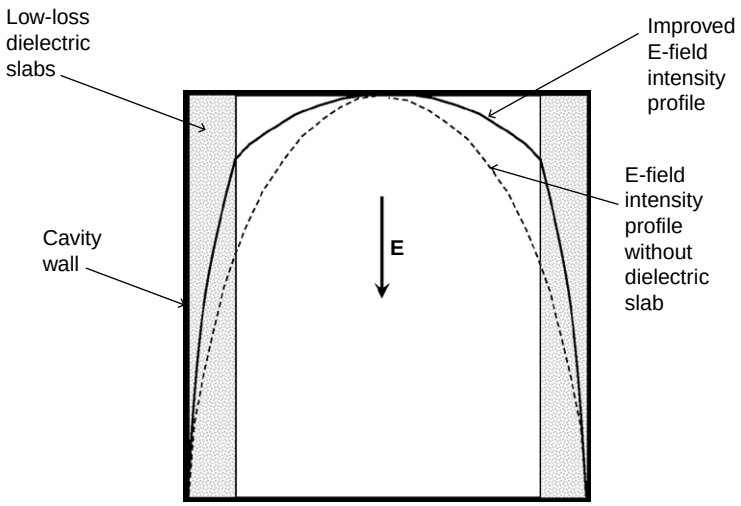

low-loss dielectric slab is shorter, and therefore most of the large variations occur inside the slab, which causes the area in the middle to have a more uniform electric field, as shown. An example of a low-loss dielectric for this purpose is boron nitride.

4.5 POWER/SIGNAL SOURCE AND SYSTEM DESIGN ISSUES IN SINGLE-MODE MICROWAVE CAVITIES

A challenging issue in successful operation of single-mode cavities for heating or plasma applications is stable and efficient power coupling into the applicator. This challenge stems from the fact that the desired cavity mode has a specific resonant frequency, which is often narrow in bandwidth. Furthermore, changes in the load properties due to mechanical, material, or temperature issues tend to affect the resonant frequency and coupling properties. The microwave power source needs to be fixed at the resonant frequency and follow its variations, if necessary. In this section we will describe methods developed to deal with source-cavity tuning and coupling issues.

4.5.1 Practical challenges related to control and signal coupling into single-mode cavities

The most convenient and inexpensive method of providing power for a single-mode cavity is to use a magnetron that is connected to the input coupling structure of the impedance matched cavity. Such an arrangement would work if certain criteria are met. One is that the material load must be stable enough so that the resonant frequency and input impedance of the cavity do not vary. In some cases, it is possible to use modern automated tune and match networks [55] to maintain an impedance match. The second criterion for direct feeding of a single-mode cavity with a magnetron power source is that the bandwidth of the cavity at its mode of operation must be greater than the output bandwidth of the magnetron. The output power of a magnetron is not spectrally pure and is distributed over several tens of megahertz. A single-mode cavity that has a light load has a bandwidth a fraction of this. Therefore other methods must be found to effectively feed a lightly loaded single-mode cavity.

4.5.2 The use of solid-state amplifiers for feeding of single-mode heating cavities

To resolve the issues related to bandwidth mismatch between the magnetron and the cavity, a spectrally pure signal source can be used to

feed a power amplifier, which in turn would provide power to the matched input impedance of the cavity via a transmission line. In the past, adequate solid-state technology has been difficult to find at reasonable costs. But due to the requirements of the mobile communication industry for higher power base stations, there has been a great deal of progress in practical power transistors that have enough power for small-scale microwave heating [56,57]. Wide band-gap devices are an entirely new type of solid-state power technology [58], which would make power in the multi-100 W range available for small-scale microwave heating. The wider band-gap allows a higher operating voltage due to the higher breakdown threshold and since they have a larger area for a given impedance, they allow larger RF currents and higher power.

In using solid-state devices to feed heating cavities using an oscillator and an amplifier, as shown in Figure 4.23a, a problem still remains in small-bandwidth (high-Q) situations. Even a small variation in the load conditions may change the resonant frequency away from the signal

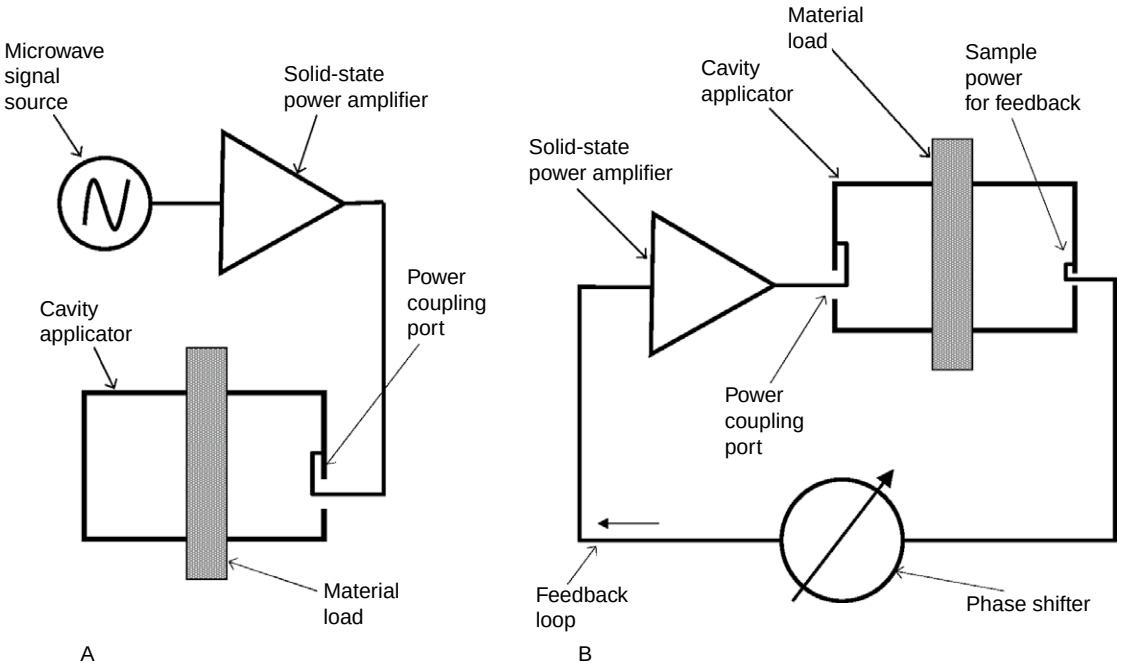

FIGURE 4.23 *A solid-state power amplifier can be used for transferring power to process a material. (A) Direct feed using a signal source and a power amplifier. (B) Feedback loop that eliminates the signal source and follows the variations in the load.*

source's frequency. To resolve this issue, using the cavity in a feedback loop to set the resonant conditions has been proposed [59]. This feedback arrangement is shown in Figure 4.23b, where the cavity has two coupling ports. The power feed port is impedance matched. The coupling strength of the sampling port must be at a level such that the total insertion loss between the two ports in decibels must be smaller than the power gain of the amplifier. Since a matched port would reduce the quality factor of the cavity by a factor of 2, it is better to use a higher gain amplifier in order to minimize the Q reduction, which in turn would reduce the field strength in the cavity. A means needs to be found to adjust the power level. Using the DC voltage to vary the power has been suggested and implemented. When such a technique is used, at least one of the stages of amplification must be run in saturation mode so that the variation of the DC voltage does not reduce the power gain of the amplifier to below the insertion loss of the cavity. Furthermore, a means is needed to adjust the overall phase shift of the feedback loop to maintain feedback criteria.

4.5.3 Magnetron injection locking for single-mode cavities used in material heating

To solve the problem of bandwidth mismatch between single-mode cavities and the magnetron source, a method of injection locking the magnetron for use as a reflection amplifier is required. The method of injection locking of the magnetron has been employed extensively for stabilizing the magnetron output spectrum for radar applications [59]. The method involves using a spectrally stable power source at a power level that is a fraction of the magnetron's output into the magnetron in the reverse direction of power flow from the magnetron to the load.

A version of injection locking can be used for microwave heating applications with single-mode cavities with an arrangement as shown in Figure 4.24 [60–62].

The injection-locked magnetron operates at precisely the same frequency as the locking signal. As a result, it is possible to control the frequency of oscillation to maximize the efficiency of microwave heating in a given application. For example, if the material being processed is heated in a high-Q cavity, the frequency of the source can be set to be precisely on resonance. As the material is processed, its dielectric properties may change. When this happens, it is possible with the injection-locked magnetron to be able to tune the source to compensate for the change in the resonant frequency of the cavity. This can be done provided that the frequencies are within the range of the power source bandwidth.

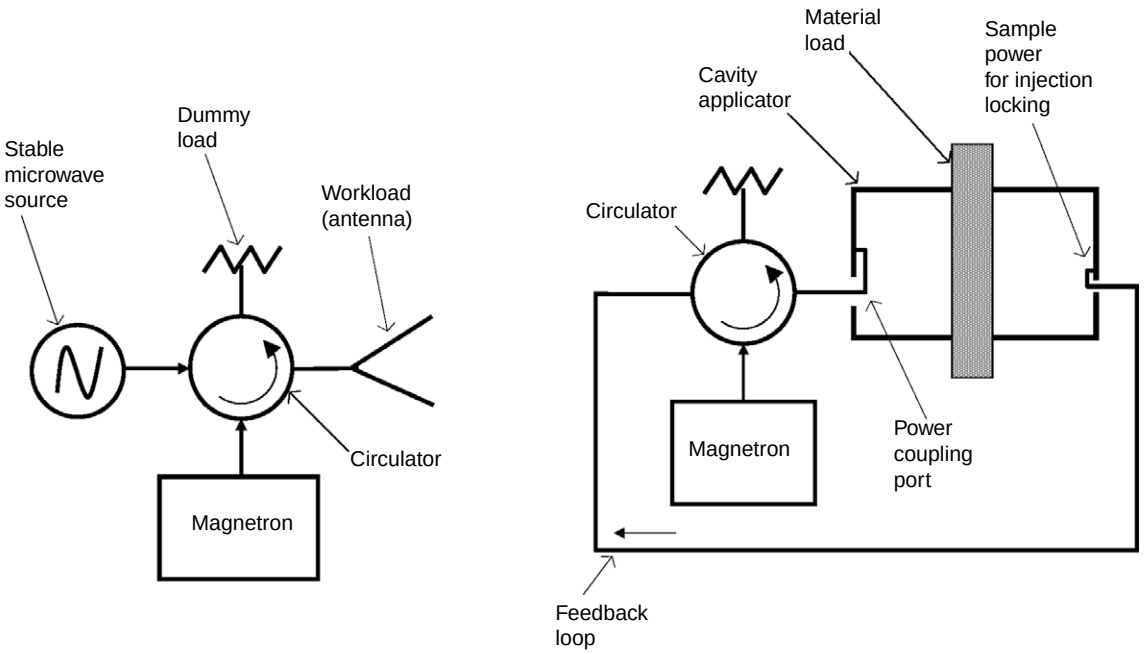

FIGURE 4.24 *Injection locking of magnetron for feeding a narrow-bandwidth microwave cavity applicator. (A) Conventional injection locking for radar applications. (B) Injection locking for coupling of a magnetron output to a narrow-bandwidth single-mode microwave cavity applicator.*

4.6 THE GENERAL PROCESS FOR THE DESIGN OF SINGLE-MODE CAVITIES FOR MATERIAL INTERACTIONS

- If possible, measure or estimate the dielectric properties of the material.
- Establish the necessity of using a single-mode cavity.
- Find the desired frequency of operation on the basis of Eq. (4.2) and interference regulations (if applicable) or sensitivity criteria shown in Section 4.3.2.
- Find the correct cavity mode for the job and how the material is placed within the field configuration of that mode.
- Calculate the dimensions of the cavity based on one of the following methods. Use simple perturbation theory if the load is very light. In this case the dimensions of the cavity are almost the same as that of

the empty cavity. If perturbation theory is not applicable, use either finite element analysis or analytical methods, such as in Appendix A4.1, to establish the correct cavity size for the frequency of interest.

- Find out what other modes operate in the vicinity of the operating frequency of interest and suppress them using one of the mode suppression techniques discussed in Section 4.2.7.
- Use a method similar to that used to make Table 4.1 to establish the practical possibility.
- Chose the power or signal coupling methods as discussed in Section 4.5.
- Use a network analyzer to test the cavity/material, if applicable.
- Adjust the coupling structure or other adjustments, if applicable.

REFERENCES

[1] R.E. Collin, Foundations of Microwave Engineering, second ed., IEEE Press, New York, 2001.

[2] S. Ramo, et al., Fields and Waves in Communication Electronics, third ed., Wiley, New York, 1994.

[3] T.K. Ishii, Microwave Engineering, Harcourt Brace Jovanovich, San Diego, 1989.

[4] D.M. Pozar, Microwave Engineering, Wiley, New York, 2004.

[5] R.C. Metaxas, et al., Industrial Microwave Heating, Peter Peregrinus, London, 1983.

[6] R. Meredith, Engineer's Handbook of Industrial Microwave Heating, The Institution of Electrical Engineers, London, 1998.

[7] T.V. Chan, H.C. Reader, Understanding Microwave Heating Cavities, Artech House, Boston, 2000.

[8] A. Carrington, Microwave Spectroscopy of Free Radicals, Academic Press, New York, 1974, pp. 50–53.

[9] D. Agrawal, et al., Effect of microwave electric and magnetic fields in single mode cavity on material processing, Proceedings of International Symposium on Microwave Science and its Application to Related Fields, 2002.

[10] J. Luo, et al., Theory and experiments of electromagnetic loss mechanism for microwave heating of powdered metals, Appl. Phys. Lett. 84(25) (2004) 21.

[11] http://www.cem.com/biosciences/disc_EnDig.asp

[12] M. Gupta, et al., Microwaves and Metals, Wiley (Asia), Singapore, 2007.

[13] J. Ma, et.al., Single mode microwave heating of copper powder metal compact, Proceedings of the COMSOL User's Conference, 2006.

[14] Industrial Microwave Systems Inc. website: http://www.industrialmicrowave.com

[15] Y. Hassler, et al., Microwave heating of fused quartz to high temperatures in the fabrication process of optical fibers, Proceedings of 18th European Microwave Conference, Madrid, Spain 1988, pp. 613–618.

[16] A. Ganguli, et al., Understanding plasma sources, Curr. Sci. 83 (3) (2002).

[17] D.L. Haas, et al., An internally tuned TM_{010} microwave resonant cavity for moderate power microwave-induced plasmas, Appl. Spectrosc. 37 (1) (1983) 1–87.

[18] A. Kraszewski, Microwave aquametry: an effective tool for nondestructive moisture sensing, Subsurface Sens. Technol. Appl. 2 (4) (2001).

[19] E. Nyfors, P. Vainikainen, Industrial Microwave Sensors, Artech House, Norwood, MA, 1989.

[20] E. Nyfors, Industrical microwave sensors – a review, Subsurface Sens. Technol. Appl. 1 (1) (2000).

[21] http://www.roxar.com/wetgas/

[22] J. Li, et.al., Complex dielectric measurement using TM010 cylindrical cavity, Progress in Electromagnetics Research Symposium Proceedings, pp. 588–591, 2007. Available at PIERS website: http://www.piers.org

[23] H. Kawabata, Analysis and experiments of a TM_{010} mode cylindrical cavity to measure accurate complex permittivity of liquid, IEICE Trans. Electron. E87-C (5) (2004) 694–699.

[24] X. Zhao, et al., Numerical analysis of a TM_{010} cavity for dielectric measurements, IEEE Trans. Microwave Theory Tech. 40 (10) (1992) 1951–1959.

[25] http://www.comsol.com

[26] http://www.cst.com

[27] http://www.wolfram.com

[28] H.S. Saadaldin, et al., Coupling with an adujustable compound Iris in a single mode applicator, Material Research Society Symposium Proceedings, 1992, pp. 91–96.

[29] V. Vyacheslav, et al., Coupling and power dissipation in a coaxially excited TM_{011} mode cylindrical applicator with a spherical load, Microwave Opt. Technol. Lett. 48 (6) (2006 June).

[30] H.F. Huang, Temperature control in a microwave resonant cavity system for rapid heating of nylon monofilament, J. Microw. Power 11 (4) (1976).

[31] J.L. Altman, Microwave Circuits, Van Nostrand, Princeton, NJ, 1964.

[32] M.R. Lakshminarayana, et al., Simple microwave technique for independent measurement of sample size and dielectric constant with results for gunn oscillator system, IEEE Trans. Microwave Theory Tech. 27 (7) (1979).

[33] M. Huang, Microwave sensor for measuring the properties of a liquid drop, Meas. Sci. Technol. 18 (2007) 1934–1938.

[34] J. Jow, et al., Microwave processing and diagnosis of chemically reacting materials in a single-mode cavity applicator, IEEE Trans. Microwave Theory Tech. 35 (12) (1987) 1435–1443.

[35] J.M. Catala-Civera, et al., Microwave non-destructive evaluation of moisture content in liquid composites in cylindrical cavity at a single frequency, in: M. Willert Porada (Ed.), Advances in Microwave and Radio Frequency Processing, Springer, Berlin, 2006, p. 138.

[36] R.J. Riegert, Private communication.

[37] D.J. Hill, et al., Design and application of a cylindrical TM020 mode applicator for the in-line microwave preheating of liquid thermosets, J. Microw. Power Electromagn. Energy 33 (4) (1998) 216–230.

[38] P.O. Risman, et al., Theory and experiments with a TM02n applicator, J. Microw. Power 10 (3) (1975).

[39] P.J. Goethel, R.W. Lewis, W.J. Teerlink, Process for Preparing Polymeric Material with Microwave, US Patent No. 5,471,037, 1995.

[40] D.E. Christiansen, Use of A TM010 microwave cavity at 2.45 GHz for aerosol and filament drying, Los Alamos National Laboratory Accession Report ADP007773, 1992, available at: http://www.ntis.gov

[41] Microwave Heating Applicator for Heating a Moving Fluid, European Patent EP1397939.

[42] H.W. Jackson, et al., Microwave power absorption profile in a cylindrical sample contained in a resonant cylindrical cavity, Jet Propulsion Laboratory, Available on: http://trs-new.jpl.nasa.gov/dspace/bitstream/2014/33825/1/94-0556.pdf

[43] J.R. Thomas, et al., Microwave sintering of ceramic rods: experiments and models, J. Microw. Power Electromagn. Energy 33 (2) (1998) 113–120.

[44] R.W. Lewis, US Patent 3,557,334, 1969.

[45] J.K.S. Wan, T.A. Koch, Application of microwave radiation for the synthesis of hydrogen cyanide, Res. Chem. Intermed. 20 (1) (1994) 29–37.

[46] M. Mehdizadeh, et al., Microwave assisted synthesis of HCN, International Microwave Power Symposium Proceedings, 1997.

[47] T.A. Koch, K.R. Krause, M. Mehdizadeh, US Patent 5,470,541.

[48] D.K. Agrawal, Microwave processing of ceramics, Curr. Opin. Solid State Mater. Sci. 3 (1998) 480–485.

[49] G. Kent, S.M. Bell, The gap correction for the resonant-mode dielectrometer, IEEE Trans. Instrum. Meas. 45 (1) (1996) 98–101.

[50] C. Wan, et al., Two new measurement methods for explicit determination of complex permittivity, IEEE Trans. Microwave Theory Tech. 46 (1998) 1614–1619.

[51] F. Peiiaranda-Foix, et al., A non-destructive method of measuring the dielectric and magnetic properties of laminate materials in open cavities, IEEE MTT-S Digest (2004).

[52] A. Hernandez, et al., Resonant cavities for measuring the surface resistance of metals at X-band frequencies, J. Phys. E: Sci. Instrum. 19 (1986).

[53] M. Barmatz, et al., Improved tuning of a microwave cavity for heating samples, Nasa Tech Briefs, 1998. Available at: http://www.nasatech.com/Briefs/Nov98/NPO20409.html

[54] J.T. Bernhard, W.T. Joines, Dielectric slab-loaded resonant cavity for applications requiring enhanced field uniformity, IEEE Trans. Microwave Theory Tech. 44 (3) (1996) 457–460.

[55] Gerling Laboratories website: www.2450mhz.com

[56] M. Bindra A., et al., Next-generation wireless propels GaN power transistors, CMOS RFICs and Passives, RF Design (January 2006) 16–21.

[57] F. Schwierz, J.J. Liou, Modern Microwave Transistors, Wiley, New York, 2003.

[58] R.J. Trew, SiC and GaN transistors – is there one winner for microwave power applications?, IEEE Proc. 90 (2002) 1032–1040.

[59] E. Schwartz, et al., Transistor-based miniature microwave heater, International Microwave Power Institute, 40th Annual Symposium Proceedings, pp. 246–249, 2006.

[60] P. Pengvanich, et al., Modeling and experimental studies of magnetron injection locking, J. Appl. Phys. 98 (2005) article 114903.

[61] C.M. Walker, The Use of Injection Locked Magnetron as a Source for Microwave Processing Applications, Mater. Res. Sympo. Proc. IV 347 (1994) 119–130.

[62] W.S. Best, Private communication.

CHAPTER 5

Microwave Multimode Cavities for Material Heating

CHAPTER CONTENTS

INTRODUCTION

Multimode resonant cavities are by far the most commonly used form of high-frequency applicator. Their enormous success in the form of the domestic microwave oven is due to the robustness and simplicity of the concept. In essence, any metal enclosure a few times larger than the wavelength can serve as a basic multimode microwave applicator. The microwave energy, carried by a waveguide or a transmission line into the cavity, is deposited into a lossy material placed within. Such devices, unlike many other high-frequency applicator systems, would not need a skilled operator or sophisticated tuning devices.

Microwave/RF Applicators and Probes for Material Heating, Sensing, and Plasma Generation

A simple multimode applicator as described above, though functional, may be far from optimal in performance. In this chapter we will cover the principles of operation, design, and optimization of multimode cavity applicators. Furthermore we will describe the latest developments in applicator design, and new applications that go beyond microwave heating of food.

Multimode cavities are almost exclusively used in power applications for material heating and plasma activation. This is as opposed to most other applicator modalities discussed in this book, where they can also be used as material sensors. Traditional applications of multimode cavities in heating of materials such as foods are covered in tutorial papers [1–3]. There are also newer applications, such as microwave-enhanced chemistry [4,5], which is utilized for enhancing chemical reactions. One of the newest applications is in the area of sintering of materials, particularly ceramics [6].

A main goal of this chapter is to discuss methods of optimization of multimode applicators. In Sections 5.1–5.3, basics of the multimode cavities and methods of optimization and power coupling are covered. In Section 5.4, susceptors and field modifiers are discussed, and finally in Section 5.5 some special and alternative configurations are covered.

5.1 FIELD PATTERNS, MODES, AND ENERGY DISTRIBUTION

The basic ideas about standing waves, cavities and their modes, and the relationships between them were discussed in Chapters 1, 2, and 4. The goal of this section is to discuss specifics about the mode structure, analysis method of multimode cavities, and how they are used in practice for material processing.

5.1.1 Description of fields and resonant modes in multimode cavities

Multimode microwave cavities can be made of any three-dimensional shape, as long as the dimensions are significantly larger (about 2× or more) than the operating wavelength. The rectangular cavity, however, is the most convenient shape to manufacture and mathematically analyze. The exact analytical solution for such as simple shape is available from many texts [7–10].

As a demonstration of a typical mode structure in a multimode cavity, we will concentrate on a particular mode, TE_{324}, in a rectangular cavity with the dimensions of 35 cm × 25 cm × 30 cm in the x, y, and z directions respectively, as shown in Figure 5.1a.

To clarify some definitions, mode type TE stands for 'transverse electric', which means there are electric field components in the x and y but

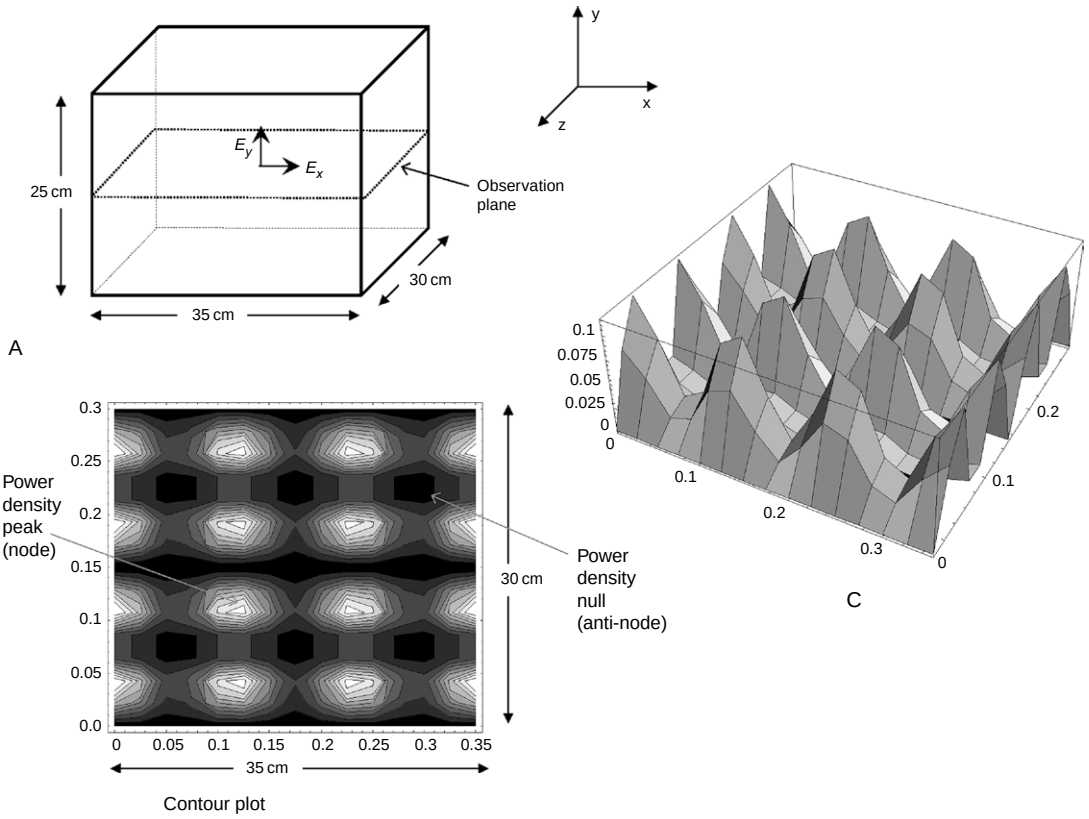

FIGURE 5.1 *Power density (E^2) distribution in a TE_{324} mode in a rectangular 35 cm × 30 cm × 25 cm cavity at 2452.12 MHz. The uniformity of the distribution is very poor due to the presence of true nulls. (A) Cavity and plane of observation in the middle of the height. (B) Contour plot. (C) 3-D plot.*

none in the z direction. The mode number $mnk = 324$ means there are 3, 2, and 4 variations in the x, y, and z directions respectively.

Since the focus here is on heating applications, the important parameter of interest here is energy density, which is proportional to the square of the electric field intensity. For the TE mode the energy density becomes proportional to $\left|E_x^{\,2} + E_y^{\,2}\right|$, where E_x and E_y are the electric field components in the x and y directions. The objective is to find a possible operating mode closest to 2450 MHz, which is the most common ISM microwave frequency. For this particular cavity one such frequency is found to be 2452.12 MHz, based on the analysis in the next section. Using a textbook analysis [9], and inserting all the proper values as shown in the Mathematica™ [11]

worksheet of Appendix A5.1, the normalized power density at the plane of observation, halfway in the y direction as shown in Figure 5.1a, becomes:

$$P_d \;;\; \left[\cos^2(12.56\,y)\sin^2(26.92\,x) + 0.214\cos^2(26.92\,x)\sin^2(12.56\,y)\right] \times \sin^2(41.89\,z) \tag{5.1}$$

Figure 5.1b and c show the contour plot and the 3-D plot of the above function respectively. The plots clearly show three variations along the x and four variations along the z direction, which signifies the mode indices along the x and z directions.

A striking conclusion from these plots is that the uniformity of the power density is very poor. In every few centimeters the power density goes from a maximum value to a minimum of zero. Using Eq. (2.9) for field uniformity, the figure turns out to be 100%, which is the worst uniformity figure possible over the effective field volume (EFV) of an applicator. While this analysis was done on an empty rectangular cavity, it is typical of other cavity shapes as well. One of the goals of this chapter is to explore various methods of either improving the field uniformity, or finding techniques to compensate for it in practical situations.

5.1.2 Resonant frequency and number of possible modes in multimode cavities

The goal here is to build an understanding of a multimode cavity's operation by finding a relationship between cavity dimensions, mode number, and the resonant frequency. For a cavity of generic geometry, in general, such a relationship must be found by a rigorous solution to the wave equation (1.5) and (1.6), to find its eigenvalues. An empty rectangular cavity, which yields itself to a relatively simple analytical solution, is usually used as a demonstration case. In the empty cavity shown in Figure 5.1a the following simple equation [9] governs the relationship:

$$f_0 = \frac{C}{2}\sqrt{\left(\frac{m}{a}\right)^2 + \left(\frac{n}{b}\right)^2 + \left(\frac{k}{l}\right)^2} \tag{5.2}$$

where f_0 (in Hz) is the resonant frequency of mode TE_{mnk} or TM_{mnk} for a rectangular cavity with dimensions a, b, and l (in meters), in the x, y, and z directions respectively, and $C = 3 \times 10^8$ m/s is the velocity of light. While the indices m, n, or k can be any integer including zero, there are a number of rules that eliminate some combinations [12]. The first rule is that there are no modes with two zero indices. Also, if one of the indices is zero, the mode can either be TM or TE but not both, but when none of the indices

is zero the modes are degenerate, which means both TE and TM modes are at the same resonant frequency.

Equation (5.2) shows that there are only certain distinct resonant frequencies that a cavity can have. This rule applies to all multimode cavities regardless of geometry or whether they are empty or loaded with a process material. In material processing applications the power source, which is most likely a magnetron tube, can only operate on a single ISM frequency, and has a bandwidth that is only a few percent of the intended frequency. For example, a magnetron that works at 2450 MHz typically has a 50 MHz bandwidth, which means the output energy is spread over that band.

Appendix A5.2 is a Mathematica™ [11] worksheet [13] that uses Eq. (5.2) to calculate the number of possible rectangular cavity modes over a given bandwidth. Figure 5.2 shows the result of this calculation for a cavity whose dimensions are proportional to the cavity in Figure 5.1a (25 cm × 30 cm × 35 cm), with a multiplication constant $\beta \geq 1$. The number of modes shown in the graph of Figure 5.2 is the possible modes for the bandwidth of 50 MHz around the resonant frequency of 2450 MHz. This calculation shows that the number of modes increases rapidly as the size of the cavity becomes larger. For example, when $\beta = 1$ (25 cm × 30 cm × 35 cm cavity) the number of possible modes in the 2450 ± 25 MHz band is only six, but for $\beta = 2$ (50 cm × 60 cm × 70 cm), the number of possible modes over the same frequency band is 40.

Earlier in this section we demonstrated the poor field uniformity of one particular mode in a multimode cavity. Appendix A5.2 and Figure 5.2 show that in reality the uniformity picture is better, because as more modes participate in

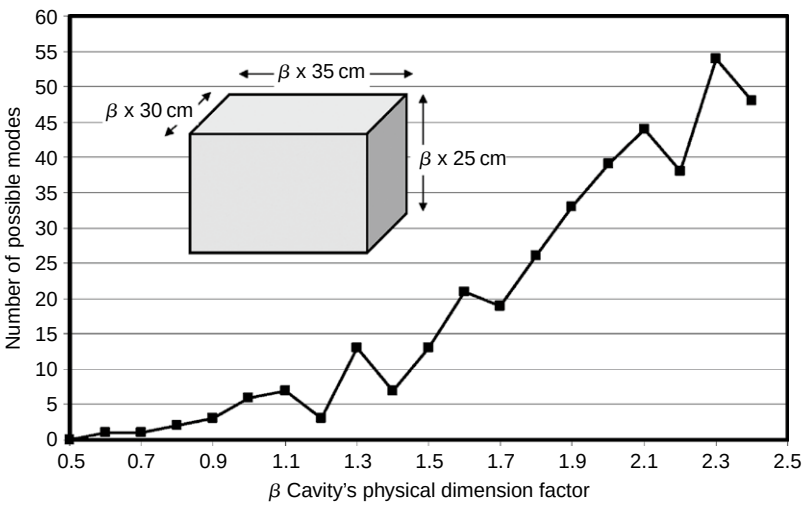

FIGURE 5.2

The number of possible resonant modes versus dimension factor β for a multimode rectangular cavity for the frequency band of 2450 ± 25 MHz. For $\beta = 1$, the dimensions of the cavity are 25 cm × 30 cm × 35 cm. This shows a rapid rise in the number of possible modes as the dimensions increase.

a microwave heating process, the fields from various modes are superimposed, which reduces the probability of true field nulls. Therefore the superimposition of modes would lead to improved uniformity [14] and the larger the number of possible modes, the better the uniformity would be. The graph of Figure 5.2 also indicates that the larger the cavity for a given operating frequency, the larger the number of possible modes. Therefore a large cavity is one important factor in improving energy deposition uniformity. While the above discussion centered around a rectangular cavity for the sake of ease of analysis, the same principles apply to other geometries as well.

5.1.3 Field polarization and field line types with respect to cavity walls

A careful study of field configurations of various multimode cavities reveal that the E fields, which are primarily responsible for interactions with materials, can take vertical or horizontal polarizations, depending on the coordinates of the reference chosen. In addition, the E-field lines can take a number of forms with respect to the cavity walls. Once again using the example of the rectangular cavity, Figures 5.3 and 5.4 show the variety in a generic manner for horizontally and vertically oriented field configurations respectively. Note that in a cavity with the geometry of a general shape, there are any number of polarization angles that are possible beyond the vertical and horizontal varieties.

The usefulness of this type of categorization is based on the fact that prediction and analysis of field configurations in multimode cavities are difficult, and can be considered somewhat random. Therefore it would be helpful to know the type of possible shapes. For example, if the objective is to heat planar objects in the x–z direction, it would be more efficient to launch horizontally polarized modes. In such a case using a launching structure that creates a preference for such polarization would be more advantageous.

5.1.4 The optical beam method of studying multimode cavity behavior

So far we have described the operation of a multimode cavity using mode analysis. An entirely different way of viewing the operation of such cavities is a quasi-optical approach, which says that the power source, through the coupling structure, would emit a wave front very similar to an optical beam with photons [15,16]. Such a model becomes ever more valid for cavities that

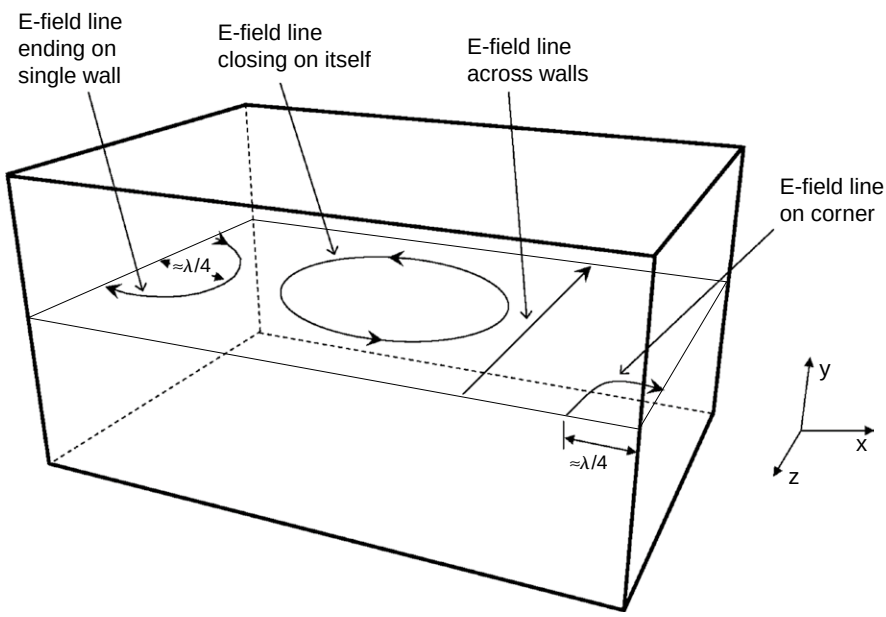

FIGURE 5.3
E-field line types for a horizontally polarized mode in a multimode cavity.

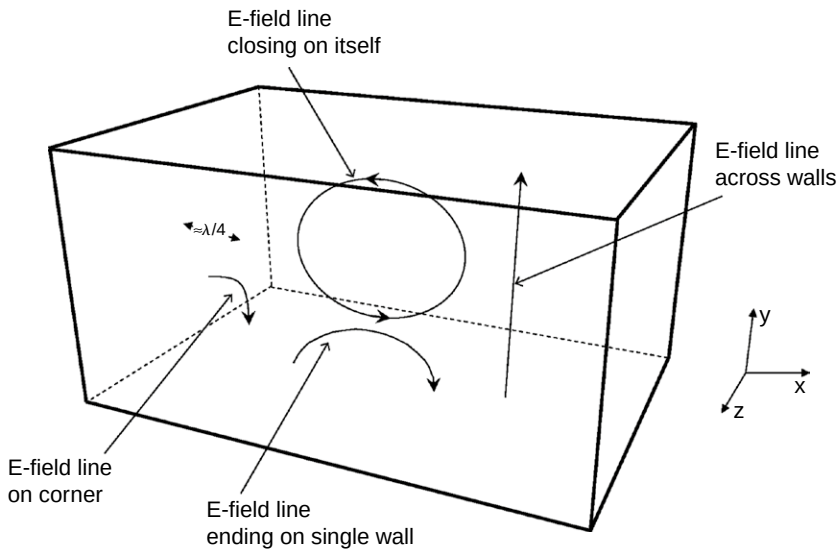

FIGURE 5.4
E-field line types for a vertically polarized mode in a multimode cavity.

are very large compared to the operating wavelength (large mode indices). A practical example is a large cavity that is used with a 24 GHz source for sintering of ceramics [17]. Even with that said, the optical model has been used to explain the operation of single-mode cavities as well [18].

Figure 5.5 shows a schematic of a multimode cavity that contains a material load, where a quasi-optical beam is shown emitting from the coupling port. The beam (or wave front), when it arrives at the material load's surface, can either be reflected, absorbed, or transmitted. In this case absorption means the dissipation into heat, which is the goal of microwave heating. Transmission means that part of the wave that goes through the material and comes out on the other side. Transmission through a material load can only happen if the material is very low loss, or it is thinner than the penetration depth as calculated by Eqs (1.30) and (1.34). A beam can also be reflected from the material load or a cavity wall.

The total picture of all reflections, as well as transmissions and absorptions, will create the standing wave that is the mode structure of the cavity. Therefore the quasi-optical and mode approaches are in essence equivalent. The usefulness of the quasi-optical approach is that it can be used to explain certain phenomena that are more difficult to explain with mode analysis only, as we will see later.

5.1.5 A phenomenological description of power source/multimode cavity interactions

In Chapter 2 the operational concepts of a generic resonant cavity and how a mode operates were described. In particular, in Section 2.4.8, using

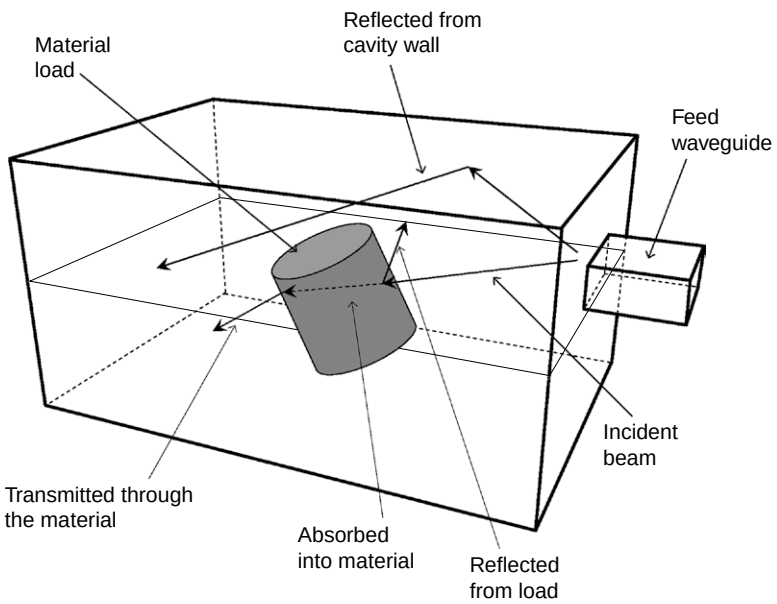

FIGURE 5.5
Schematic of an optical beam model for the operation of a multimode cavity.

Figure 2.13, we described how the stimulant frequency couples into a single potential mode and excites it. The goal here is to expand that phenomenological description to a multimode cavity with a material load. In the following discussion, with the aid of Figure 5.6, the basic operation of multimode cavities and why they are not in need of "tuning" are discussed.

Consider Figure 5.6a, where the resonant frequencies of modes A–P for an empty cavity are shown. In this designation, a mode designated by a letter could be an indexed mode of rectangular cavity (like TM_{321}), or a specific resonant mode of a cavity with more complex shape. The microwave source has a fixed center frequency and a finite bandwidth of Δf_s that happen to encompass modes D and E of the empty cavity. This means that modes D and E are now operating, or active, modes. Since there is no dielectric load, some of the power from the microwave source is dissipated

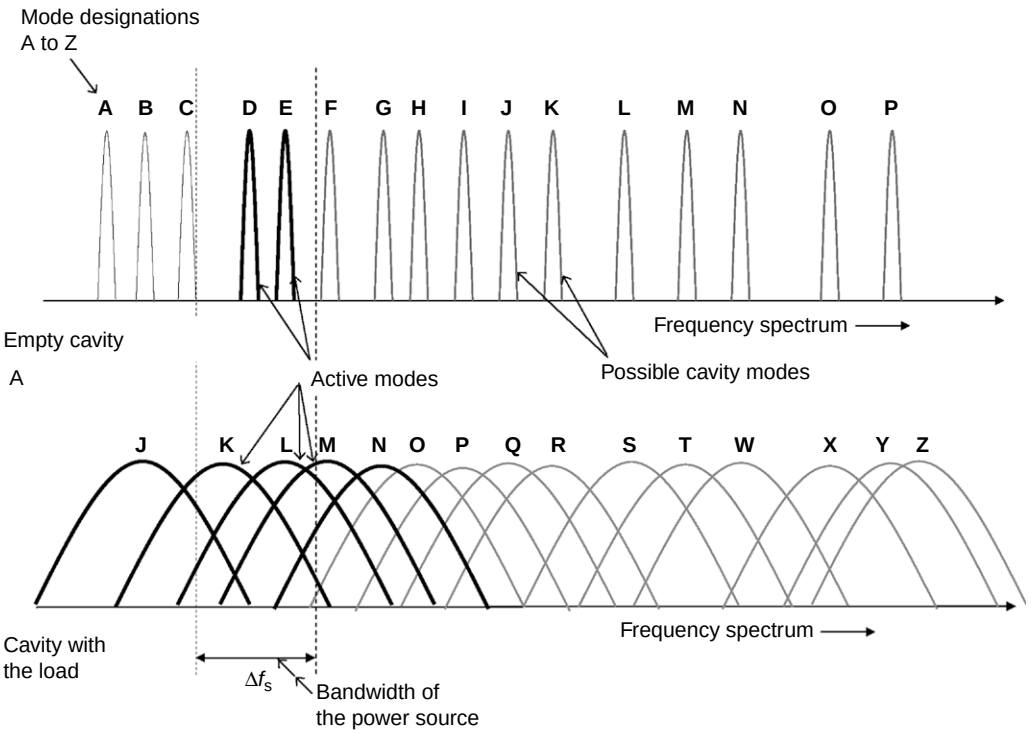

FIGURE 5.6 *A phenomenological explanation of multimode cavity operation. (A) The empty cavity has a large number of possible modes, some of which fall within the bandwidth of the power source, and are excited. (B) With the arrival of the dielectric load, all modes move down the frequency spectrum. Now there are several new modes within the bandwidth of the source, and these are excited to varying degrees of coupling strength. In this instance, modes K and L are strongly coupled, while J and N are weakly coupled.*

on the walls of the cavity in the form of surface currents, and the rest is reflected.

Now consider Figure 5.6b, where a lossy dielectric load is inserted into the cavity. The modes are now widened in the frequency band, reflecting a reduction of the Q factor for each mode due to the increase in cavity loss. The original modes D and E are no longer within the bandwidth of the microwave source, because the introduction of the dielectric load has pushed those modes down in frequency. Instead of modes D and E, we now have modes J, K, L, and M that are either fully or partially within the bandwidth of the source, and have become active. In this example, modes K and L are strongly coupled, while modes J and M are coupled weakly, which means their fields are not as strong.

This is the reason for the robustness of microwave heating with multimode cavities. In essence, even if the load changes, there is an abundance of other modes, a few of which are always within the bandwidth of the source. For a typical magnetron source that operates at 2450 MHz, the bandwidth is of the order of 40–100 MHz, depending on the construction and price. More expensive and industrial magnetrons have more pure spectrum and lower bandwidth.

The above phenomenological study only shows a typical situation involving a load that is small compared to the cavity. There are a number of load–cavity cases that vary from this typical explanation. For example, a large and lossy load may change the boundary condition of the cavity so heavily that none of the original modes can survive. In such a case, an entirely new mode structure is formed. In almost all cases, however, the abundance of modes would cause some modes to fall within the bandwidth of the source, which leads to versatile characteristics of the multimode ovens.

5.1.6 Comparison of multimode cavities with other RF/microwave applicators

In Chapter 4, the operation and application of single-mode cavities were discussed. One advantage of a single-mode cavity is that it is highly sensitive, which means a modest amount of deposited power can create very large E fields in the effective field volume of the cavity for processing of low-loss materials. The drawback of single-mode cavities, however, is that the resonant frequency of the cavity must match the frequency of the source, which causes potential problems with operational robustness. The multimode cavity, however, is highly robust because of the abundance of modes, which allows the microwave source to always couple into at least one or more of the available modes.

The dimensions of a multimode cavity must be significantly larger than the operating wavelength. For example, at 2450 MHz, with the wavelength of 12.2 cm, each dimension of the cavity must be a few times larger, which brings us to the size that most domestic microwave ovens are. This requirement for a minimum size reduces the fill factor and sensitivity. Fortunately, this is not a major issue for water-laden food items with their very high dielectric loss, but heating of lower loss materials is a challenge for multimode cavities.

A further issue with load dimensions is that if the size of a large load becomes too close to that of the cavity, two problems could arise, both related to heating uniformity. First, a large load is bound to have one of its sides in the proximity of the feed point. In that case there would be a hot spot in that location. Second, a large load in a multimode oven will have hot and cold spots. If the load size is small compared to the wavelength, then the fill factor will be small, which has very little efficiency associated with it. Generally, in order for heating to happen for a small load in a multimode oven, the dielectric loss has to be very high (food).

A classification system for microwave heating was developed by Bows [19] and can be used to predict the microwave heating of materials. At one extreme of this classification is a very light load, which means a combination of small size and low dielectric loss. The mode structure of the cavity is only slightly modified by the presence of such a material load, and the fields are usually transmitted through the material, and are largely uniform within it, except for the basic field pattern of the cavity itself. The other extreme is a large load with high dielectric loss. In such cases, the mode structure of the cavity is completely changed and the penetration depth into the material is small, according to Eqs (1.30) and (1.34).

At the extreme, a very large and lossy load may completely stop the operation of the multimode cavity, because the residual space left after the insertion of the load may not be enough to allow multimode operation. Note that a highly lossy load does not allow any waves on its interior beyond the penetration depth.

5.1.7 Methods for computation of energy distribution

The concept of mode designation with specific indices (such as TM_{321}) is only valid for empty cavities with simple geometries. In material-loaded cases, or when the cavity shape is complex, the cavity still has numerous specific modes with standing-wave patterns containing nodes and nulls, but the concept of specific indices can no longer be justified. In the early history of microwave device development, cavities were exclusively used

as empty structures for their frequency selectivity capabilities. Analytical modal analysis was very important in such applications. In the context of cavities as applicators, however, that type of analysis is useful only as an academic exercise to understand the operation of cavities.

Due to the immense complexity of multimode cavity problems, analytical solutions for the field problem, particularly in loaded conditions, are not available. Empirical methods involving field probing measurements [12] or numerical methods are more appropriate for studying cavities as applicators.

Modern finite element method (FEM) or finite difference time domain (FDTD) methods are now used for this purpose [20], and commercial packages such as COMSOL [21] have made the job of problem setup easier to accomplish. One of the latest developments in this area is the multi-physics capability, where the electromagnetic and thermodynamic aspects of the problem can be solved simultaneously. This is particularly useful in microwave heating applications, since the ultimate goal is to predict the thermal behavior of the material load [22,23]. While these methods have grown in capability and utility, there are still some limitations when both large and fine structures are elements of the same problem. For example, when a large multimode oven is being modeled, if the coupling structure or the load contain fine features, the modeling encounters difficulties due to mathematical convergence problems.

Among the capabilities of such FEM packaged programs is generating a concise 3-D view of the problem during the preprocessing stage. This involves an increasingly user-friendly graphical interface together with pull-down menus and preprogrammed material properties. An example of the graphical output of such modeling for heating of a potato in a microwave oven is shown in Figure 5.7 [21]. The intermediate step after preprocessing and building of the model is dividing the problem into a mesh structure, which is done automatically. In this process, the areas of the problem that have finer features are recognized by the program, and a finer mesh pattern is assigned to them. Once the solver completes solving the problem, the postprocessing includes features such as power reflection and scattering parameters, energy density, and power deposition density.

Figure 5.8 shows an example of the capability of FEM methods to predict the heating behavior of the microwave multimode cavities. A resistive sheet composed of a carbon-loaded polymer, which has a sheet resistivity of 400 Ω/sq is placed 5 cm above the bottom of a rectangular multimode cavity with the dimensions of 35 cm width, 30 cm length, and 25 cm height. The cavity is fed with a 2450 MHz magnetron that can be finely adjusted to a low power of 100 W using a continuously variable power supply. A layer of thermal fax paper is placed above the resistive sheet, and the structure is

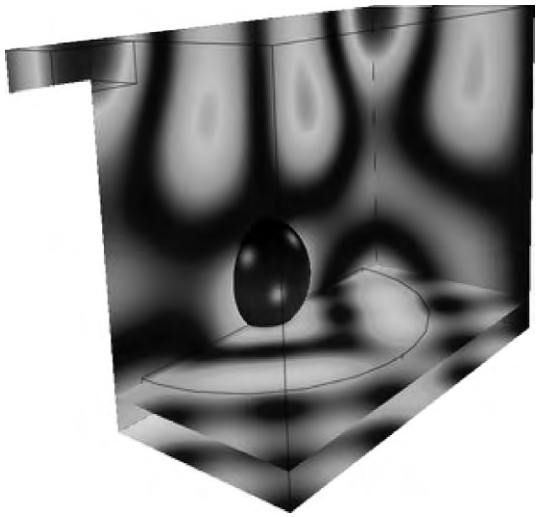

FIGURE 5.7
Field intensity and temperature distribution (boundary plot of potato) in a microwave oven. This is a model of the heating process in a microwave oven. The distributed heat source is computed in a stationary, frequency domain electromagnetic analysis. This is followed by a transient heat transfer simulation showing how the heat redistributes in the foodstuff. (Courtesy of COMSOL Inc.)

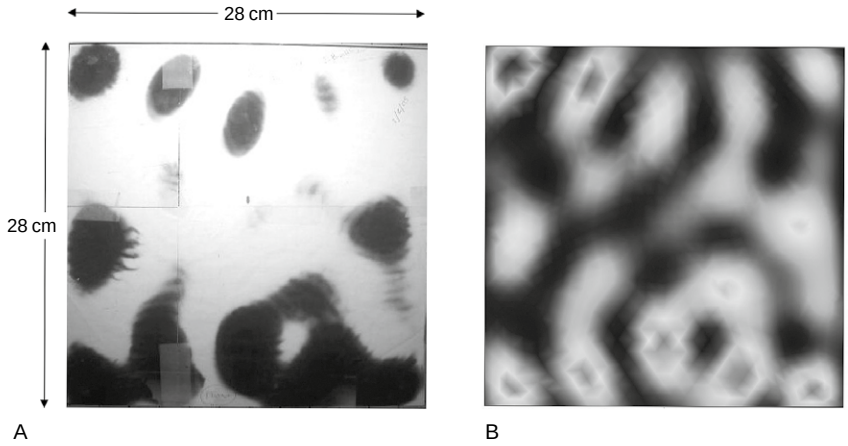

FIGURE 5.8 *Comparison of thermal paper pattern and a finite element model for a thin resistive sheet heated in a rectangular multimode cavity at 2450 MHz to verify the model's capability to predict the location of field nodes. (A) Pattern of field nodes appears on thermal paper placed in intimate proximity to the resistive sheet. (B) A finite element model of the same structure. (After Riegert [13].)*

sandwiched between two thin layers of glass to ensure intimate contact between the resistive sheet and the thermal paper. As the resistive sheet is heated, the pattern of electric field nodes is shown as dark areas in Figure 5.8a. The problem with all its features was solved [13] in 3-D with the COMSOL package and the results of the model, as shown in Figure 5.8b, are in very good agreement with the location of the electric field nodes (hot spots).

5.2 METHODS TO IMPROVE THE FIELD AND HEATING UNIFORMITY IN MULTIMODE CAVITY APPLICATORS

A well-known challenge in material processing with multimode cavities is poor heating uniformity. The goal of this section is to study various sources of non-uniformity, and solutions devised for improvement of uniformity.

5.2.1 Factors other than fields that contribute to non-uniform heating

The variations in field intensity borne from the modal field configuration contribute to temperature non-uniformity in multimode cavities. This factor, however, is not the only one, and there are a number of other issues that also contribute to the spatial temperature variations in the material load. These are as follows:

- **Dielectric depth of penetration.** Equation (1.32) define the depth of penetration of fields for plane waves into a lossy dielectric. Assuming a quasi-optical model for the operation of a multimode cavity oven, these equations apply. Regardless of field variations, the depth of penetration is a major contributor, particularly in highly lossy materials, such as most foods.
- **Geometry of the material load.** The incorporation of the material into the cavity sets a new boundary condition for the fields, and the shape of the material plays an important role in how the fields are configured inside the material. This is particularly true when the relative permittivity and losses are high. In an object of complex shape, edges and elongated ends receive more intense fields, and therefore reach higher temperatures. For example, in a triangular-shaped object like a fish fillet, the narrow end becomes hotter than the wider end [24]. In a disk-like object the edges typically receive more heat [25].
- **Proximity to the feed point.** In a typical multimode cavity the side of the material load that faces the feed point receives more energy, and becomes hotter, than the opposing side. This issue becomes more severe as the material is brought closer to the feed point. One method of reducing the feed point effect is to have multiple ports, which also provide the added advantage of exciting more modes for better uniformity. Rotation of the load, as done in domestic microwave ovens, also proves to be helpful.

5.2.2 Basic cavity design to improve the field uniformity

From the discussion in Section 5.1.5, it was concluded that exciting a larger number of potential modes would enhance the overall heating uniformity in multimode cavities. This desired increase in the number of modes can be achieved in various ways as follows. One of the methods of increasing the number of excited modes is to increase the dimensions of the cavity with respect to the wavelength. In the example depicted in Figure 5.2, the number of excited modes increased from 6 to 40 by doubling all the dimensions.

Fehrer et al. [26,27] have developed a microwave cavity with a hexagonal cross-section, as shown in Figure 5.9, where the dimensions are 180 cm $\times$ 155 cm $\times$ 330 cm, which operates at 2450 MHz.Using Appendix A5.2, it was calculated that a rectangular cavity with the same volume will have 962 excited modes at 2450 $\pm$ 25 MHz.Comparing this with the corresponding number for a domestic microwave oven, which is about 4–6, shows that the cavity of Figure 5.9 [27] can have a very uniform field.

Another method of improving the number of excited modes is to consider the optical beam method of studying the multimode cavity, as described in Section 5.1.4. The multiple reflections of a beam on a cavity with parallel walls, such as a rectangular cavity, will result in parallel beams [15], which tend to excite the same modes. Having a cavity that has angular or curved walls [28] would avoid these parallel beams, which will result in each reflection exciting a different mode. Another example is the hexagonal shape of multimode cavity shown in Figure 5.9 [25], which would also serve the same purpose.

5.2.3 Mechanical movement methods to improve heating uniformity

The turntable, which is universally available in domestic microwave ovens, is a simple and inexpensive device that provides a limited improvement in heating uniformity. The areas of the food item away from the center of the turntable move through the standing-wave pattern. An asymmetrical load, or a load that is placed off the center of the turntable, would also stir the fields by modifying the boundary conditions continuously. This is an additional function beyond the simple movement of the food within a static field pattern. The turntable improves the overall heating uniformity compared to a static case, but it creates a circularly symmetrical non-uniform heating pattern that is variable based on the field pattern of the multimode cavity after it is loaded. Figure 5.10 shows an example where the same disk-shaped load was heated in two different domestic ovens with turntables.

Aside from turntables, mode stirrers are moving metallic devices that are placed at a location away from the material load to continually perturb

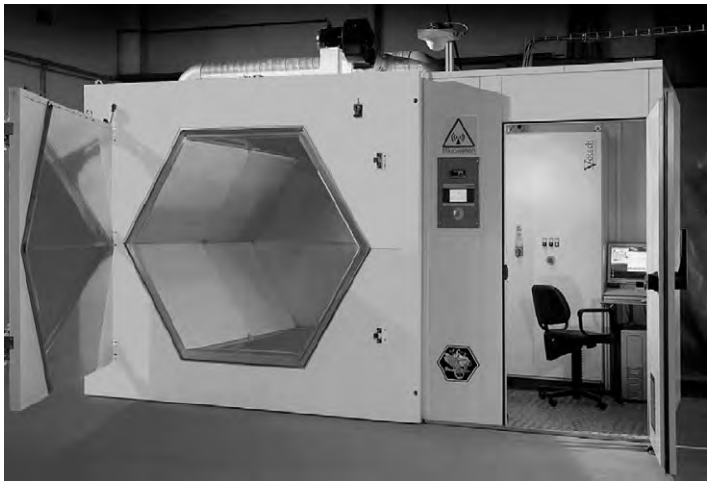

FIGURE 5.9 *A large microwave cavity for uniform heating in batch industrial applications. The large size compared to the wavelength at 2450 MHz ensures launching a large number of modes that contribute to heating uniformity. Multiple source, multiple feed points at total power level up to 30 kW also contribute to uniformity and high energy deposition intensity.*
(Courtesy of Vötsch Industrietechnik GmbH; the unit is commercially marketed as the Hephaistos System. After Ref. [26].)

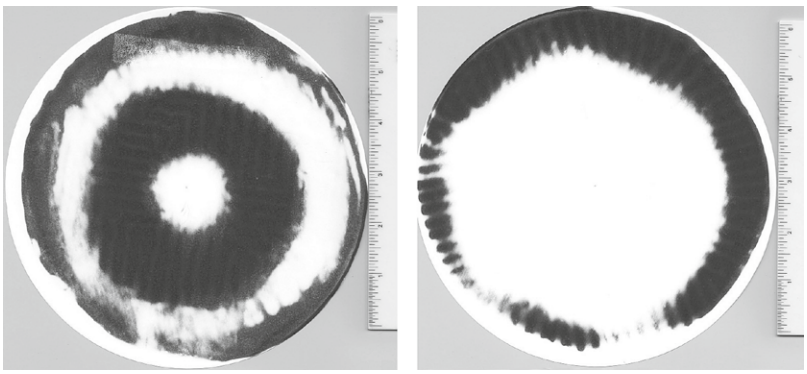

FIGURE 5.10 *The domestic microwave oven turntable helps to establish a more uniform field pattern, but creates a circularly symmetrical non-uniform heating pattern that is variable from oven to oven. (A) and (B) show two patterns generated in two domestic ovens of the same disk-shaped load using thermal paper.*

the fields. As a result of a periodic change in the boundary conditions, the field nodes and nulls move, and that action tends to spread the size of the field nodes averaged over time and therefore improves the heating uniformity. Depending on the design, location, and type of load, the mode stirrer's

impact on the overall heating uniformity is variable. A detailed study [29] involving finite element methods and experiments have shown that for thick and high-loss loads the impact of mode stirrers is minimal. In addition, for disk-like loads the edge overheating is not resolved by stirrers [25]. Mode stirrers have a large impact on uniform heating of small and low-loss loads.

A very effective method is to place the mode stirrers at a location close to the power feed [30,31]. Looking at the problem from a quasi-optical standpoint, deflecting a beam close to the source would make the reason for this step clearer. In some microwave oven designs the mode stirrer is a rotating blade, and the driving force for it is the forced cooling air that has cooled the magnetron.

In addition to improving the heating uniformity, mode stirrers provide a means for reducing possible leakage emissions from locations such as door seals by averaging out a field node at a particular location that may cause a larger portion of leakage than others [12]. Such action will reduce the need and expenses associated with improving the EMI seal over the whole system.

5.2.4 Frequency sweeping/multi-frequency methods to improve field uniformity

An advantageous way to improve the uniformity of a multimode cavity applicator of fixed dimensions is to use a higher frequency. The heating uniformity improvement happens by two entirely separate phenomena. First, the same cavity can now have a larger number of operating modes, because the same dimensions can fit a higher number of wavelengths for standing waves. Second, the nodes and antinodes become closer together. This promotes conventional heat transfer between adjacent nodes and nulls. In addition to conventional 2.45 GHz magnetrons, those with a higher ISM frequency of 5.8 GHz are becoming more readily available [32–35]. The next highest ISM frequency available for microwave heating is 24 GHz. Gyrotron sources at 24 GHz have been used for ceramic sintering [17].

The field uniformity can be improved if the number of excited modes within the bandwidth of the microwave source is increased. This means that the wider the bandwidth of the source, the larger number of modes are excited. But a truly wide bandwidth source at high power is difficult to achieve. Electronic frequency sweeping is an alternative method, and may be performed at high rate of speed, thereby creating a much more uniform time-averaged power density throughout the multimode cavity. The desired frequency sweeping may be accomplished through the use of a variety of microwave electron devices. A helix traveling wave tube (TWT), for example, allows the sweep to cover a broad bandwidth, for example 2–8 GHz, versus magnetrons that have essentially fixed frequencies [36,37].

Variable frequency microwave (VFM) ovens can average the fields very effectively [38]. The dielectric depth of field penetration, however, remains only as large as the lowest frequency in the sweeping range allows, per Eq (1.32). The high expense of the variable frequency power source is one disadvantage. In addition, since the frequency of operation goes outside the ISM bands, there is the added expense of shielding to bring them in compliance with communication regulations. These regulations, as far as emission limits are concerned, are far more stringent than the rules designed for safety concerns.

A simpler and less expensive way to improve uniformity by frequency methods is to use two magnetrons at two ISM frequencies to excite a larger number of modes and thereby improve the uniformity [39]. For ceramic sintering, the higher frequency can achieve faster heat-up while the ceramic is at lower temperatures and has a lower loss factor. At higher temperatures, when the ceramic has a higher loss factor, the two frequencies work together to compensate for the higher radiation losses.

5.3 ENERGY COUPLING AND SYSTEM ISSUES IN MULTIMODE HEATING SYSTEMS

5.3.1 Coupling structures for optimum transfer and uniformity

The power from the source, typically a magnetron, is transmitted to the multimode cavity via a low-loss transmission line. A waveguide, particularly a rectangular one with TE_{10} mode of propagation, is a typical choice, even though circular waveguides and even coaxial lines with air dielectric are also used.

The first design goal of a coupling structure for a multimode cavity is to have matched impedance so that, at least for the typical load, the reflections are minimal. The second design goal is to launch as many potential modes as possible, so that the maximum field uniformity is attained.

The simplest form of coupling structure is a rectangular waveguide that is connected directly, or through an inductive iris [9], to the cavity. Usually, the width of the iris, which determines the coupling strength, is designed for an impedance-matched condition for a typical load. This design can either be done experimentally with the aid of a network analyzer, or through modeling studies. The disadvantage of simple waveguide/iris coupling, however, is that the polarization of launching is linear and only in a single direction. Therefore only those modes that have polarization in the direction of the launching point are strongly coupled to. An important part of microwave oven design is a coupling structure that is capable of launching as many modes as possible.

An ideal coupler design, which is often implemented in commercial microwave ovens, is a relatively complex design that launches the waves

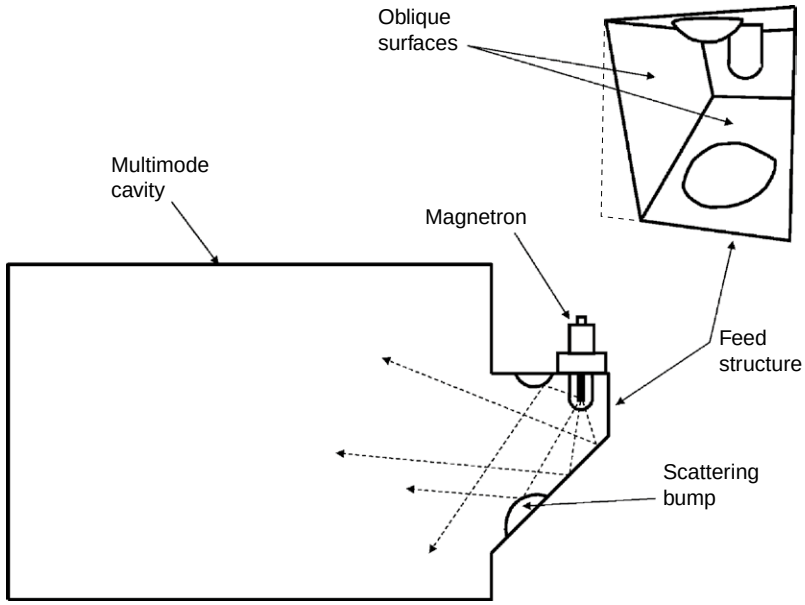

FIGURE 5.11
A coupling structure in a domestic microwave oven that uses oblique surfaces and scattering bumps to deflect microwave beams in an effort to launch as many cavity modes as possible.

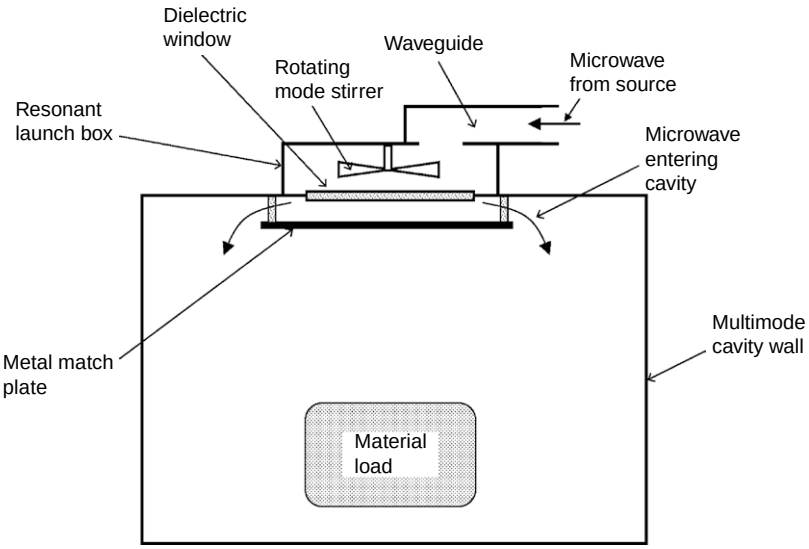

FIGURE 5.12
A microwave coupling structure for better uniformity (after Ref. [13]).

so that various polarizations [40] are covered with the goal of launching as many modes as possible. Figure 5.11 shows one such coupling structure from a Panasonic™ microwave oven that has oblique surfaces and scattering bumps, designed to use the optical beam model of multimode cavities so that the waves are scattered in as many directions as possible.

A more advance coupler design [31] for a multimode cavity, as shown in Figure 5.12, utilizes a secondary resonant cavity, which is the principal part of the coupling structure. The coupling cavity is formed as an extension to the main multimode cavity as shown in Figure 5.12, and a metal match plate is also considered as one of the walls of the coupling cavity, which has the dimensions 238 mm × 238 mm × 76 mm. Referring to Eq. (5.2), four modes – TE_{211}, TM_{211}, TE_{121}, and TM_{121} – are within the frequency range of 2435–2475 MHz.

The coupling cavity also contains a small mode stirrer. The mode stirrer tends to launch a combination of the four coupling resonant modes at various times during its rotation cycle. The entry of the waves into the multimode cavity is through an almost 1-meter-long opening around the periphery of the match plate. Such distributed coupling provides two main advantages. First, the largest number of potential cavity modes is launched. Second, the distributed coupling aperture reduces the uneven field distribution that favors areas close to the feed point being overheated.

5.3.2 Multiple port/multiple source coupling for improvement of uniformity and increase of total microwave power

Feeding microwave power at more than one location to a multimode cavity [12,41–43] provides several advantages, the most important of which is improvement of field uniformity. The main reason for this improvement is the fact that each feed point couples independently to a different set of modes provided that the coupling geometry and polarization are chosen correctly [12]. The second mechanism for enhancement of uniformity is that the distributed feeding reduces the "hot spot" that specifically arises in areas close to the feed point. This is particularly troublesome in cases where the load has large dimensions, and parts of it are in the proximity of the feed point.

Aside from improvement of uniformity, there are other reasons for feeding of microwave cavities at multiple points. Since magnetrons have limited lifetimes, in industrial applications it is often better to have more than one operating, so that if one fails the process would not shut down. An added advantage comes in very high power applications of more than tens of kilowatts, where single power sources are not available.

Even though single magnetrons of up to 30 kW at 2450 MHz are advertised as being available, their reliability is inadequate [44], and multiple magnetrons at 6 kW or maximum 15 kW are more appropriate for industrial use. Therefore the total load can be divided among multiple power sources.

One disadvantage of multiple power sources is that magnetrons are more efficient at higher power levels, therefore total power efficiency is higher when fewer sources are used [45]. Another challenge with multiple sources is the possibility of cross-coupling, which leads to system impedance

mismatches. It has been determined that cross-coupling occurs when the two feed points couple to the same set of modes [12]. This issue can be resolved by either empirical or modeling approaches.

Figure 5.13 shows a block diagram of a multimode cavity being fed by two sources. The job of a circulator [46] here is to divert the reflected power to a dummy load to prevent damage to the magnetron. Circulators are particularly important in multiple feed cavities because they prevent the power from one source from damaging the others.

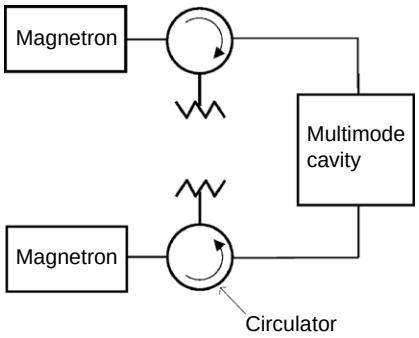

FIGURE 5.13 *System diagram of a multimode cavity being fed by two separate magnetrons.*

Another method of feeding a cavity at multiple points is to divide the power coming from the source first, and then feed the cavity at more than one point [31]. Figure 5.14 [12] shows another power division scheme where the power from a single magnetron is divided and fed to two different feed points on the cavity to improve the heating uniformity and avoid hot spots due to the feed points. The phase shifter provides an empirical means for optimization of field patterns.

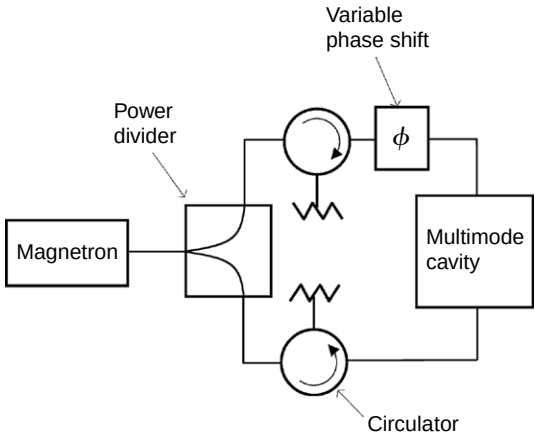

FIGURE 5.14 *System diagram of a single magnetron feeding a multimode cavity at two locations to improve field uniformity.*

5.4 MANIPULATION OF ENERGY DISTRIBUTION USING SUSCEPTORS AND FIELD MODIFICATION DEVICES

5.4.1 Principles of microwave susceptors

In microwave heating, susceptors are auxiliary lossy materials that are heated by the fields, and transfer that heat to the intended processed material via conventional heat transfer methods. As such, the susceptor's function is to manipulate and manage the energy available from the microwave source for an intended purpose.

Susceptors are used for a number of reasons – for example, in food applications their job is to direct a part of the energy to provide intense heat to the surface of the food to create a crisping and browning effect. In ceramic sintering they are used because ceramics have low microwave loss at low temperatures, therefore the susceptor first heats the workpiece to a temperature at which it becomes lossy enough to absorb microwaves.

As for choice of material, susceptors are typically made from conductive, resistive, or semiconductive materials. Referring to Figure 5.5, the energy from the microwave source can either be absorbed, reflected, or transmitted

(going through the material). In the case of a susceptor the idea is to maximize energy absorption and minimize the reflected or transmitted power.

5.4.2 Planar susceptors for food applications

Disposable food susceptors, which are surface heating elements, are used extensively in commercial food packaging. The idea is to generate a high temperature at the surface of the food to crisp, brown, or prevent sogginess [47–51]. To be commercially viable, a susceptor must be inexpensive and robust. Because of the high temperatures that must be reached, the susceptor must be safe, which means it should stop generating high temperatures if it is inadvertently left in a powered microwave oven.

Figure 5.15 shows the structure of a typical disposable susceptor, the active part of which is an ultra-thin (a few nanometers) layer of aluminum or other metal that is vacuum deposited on a thin polymeric sheet, and is supported by a cardboard sheet. The susceptor layer acts as a resistive sheet, and the thickness of the deposition is chosen so that the sheet resistivity is about 200 Ω/sq. This level of surface resistivity is arrived at using the quasi-optical model of a microwave oven (Figure 5.5), which suggests that maximum absorption is achieved at this level of resistivity for plane waves. For a perfectly smooth vacuum deposition surface, about 1 nm of aluminum deposition should suffice, but due to the surface roughness of the PET film, about 6–10 nm of deposition is actually used. The figure of merit that shows how much microwave power a susceptor turns into heat is called the "heat flux" in W/cm^2. Heat flux is measured by a calorimetric technique [52,53], which measures the temperature rise of a vial of a liquid with the susceptor wrapped around it. A typical figure for heat flux of a food susceptor is 2 W/cm^2, which means for a round pizza susceptor of 18 cm in diameter, the total power absorbed is about 500 W. This is a significant fraction of a microwave oven's power (typically 700–1100 W).

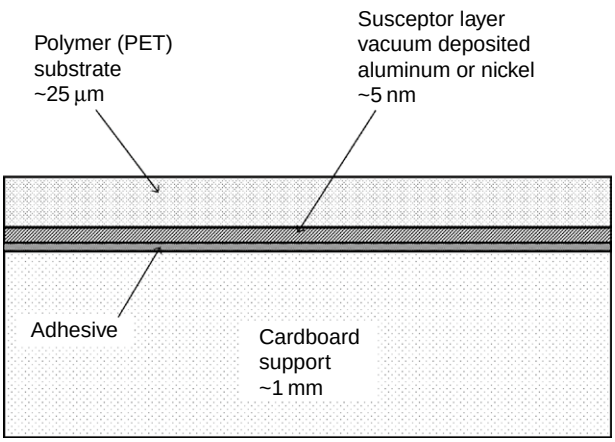

FIGURE 5.15 *Layer structure of a susceptor for food applications.*

The safety need, which requires the susceptor to "shut down" after a while, is satisfied by the fact that the PET substrate shrinks with heat and breaks up the aluminum susceptor into "islands", which disrupts the currents in the susceptor. Therefore the susceptor's terminal temperature, as shown

in Figure 5.16, is the result of an equilibrium reached when the breakup of the susceptor layer is complete. A comparison of the heating profile versus time between a non-shrinkable substrate and a commercial susceptor as shown in Figure 5.16 shows this "shutdown" effect.

In addition to disposable susceptors, there is a separate market for food susceptors as permanent appliances, which are also called browning dishes. The safety concern of overheating is addressed by ferrite technology [54], which takes advantage of the Currie point of ferrites to limit energy absorption beyond that temperature.

5.4.3 Refractory susceptors for high-temperature applications

In high-temperature applications, such as microwave sintering of ceramics [55], it is necessary to use refractory susceptors to heat up the material load when sufficient microwave loss is not available for certain parts of the process. Typically, silicon carbide or similar susceptors are used to initiate heating from room temperature, where many ceramics have low dielectric losses. The loss increases with temperature, and at some "kick-in" transition temperature, the ceramic load heats preferentially over the susceptors. In this work the effect of dopant type and crystal structure of zirconia on the "kick-in" temperature was observed using silicon carbide susceptors. Figure 5.17 shows the arrangement for this type of susceptor application.

5.4.4 Metallic field modification devices in multimode ovens

Properly designed metallic objects, within a multimode cavity, have the capability to shape and modify fields to create desired heating effects. We have already discussed mode stirrers, which are moving metallic objects, in Section 5.3. The goal here is to introduce field modification devices that are placed in the immediate vicinity of the material load.

One application of such field modification devices is for shielding the edges of a large food item, such as in defrosting a 1 kg lasagne in a microwave oven [50]. Without a field modification device, the edges and corners of such food items are overheated, while the middle of the item remains cold. Metallic shielding elements on the vertical sidewalls of

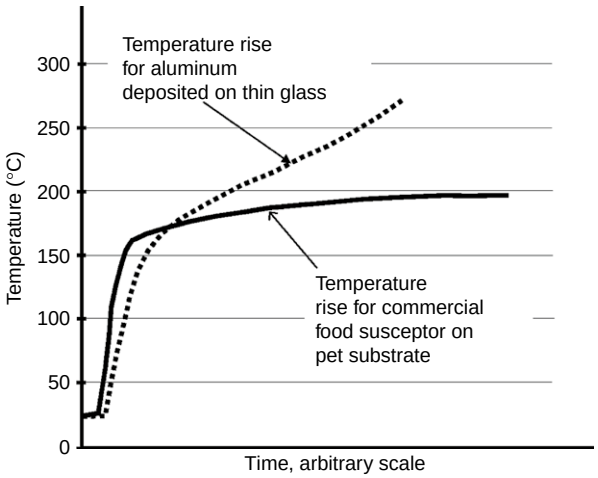

FIGURE 5.16 *The PET substrate in food susceptors shrinks due to temperature, which breaks the aluminum layer for self-limiting of temperature. The same aluminum layer on a non-shrinkable substrate like glass can rise to much higher temperatures.*

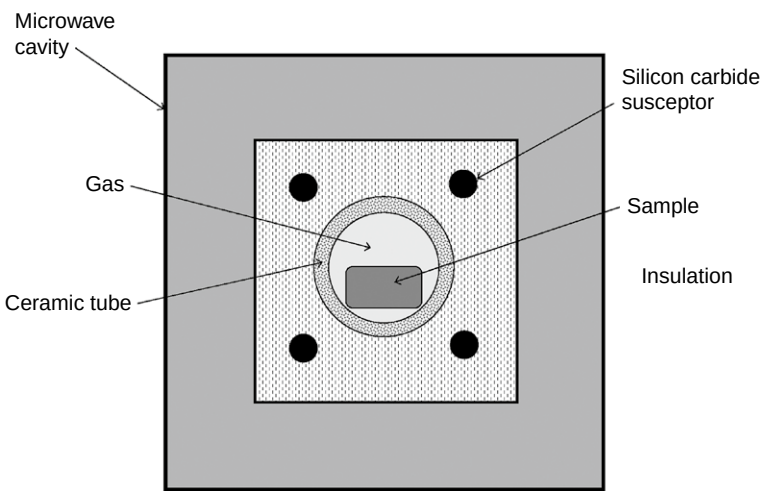

FIGURE 5.17
The use of refractory susceptors for high-temperature sintering of ceramics in a multimode applicator.

the tray containing the food item have been added to direct energy away from these edges. Then resonant loops were added to the bottom of the tray to overcome the tendency for low heating rates by increasing energy coupling at the bottom center of the product.

Metallic field modification devices can also be used for enhancing the uniformity of browning in conjunction with susceptors. A field director assembly using metallic foil vanes that are vertical to the plane of the susceptor has been used [56] that greatly improves the uniformity of browning of the pizza crust. The presence of multiple vanes under the susceptor would enhance the electric field that is parallel to the surface of the susceptor. This E-field component is responsible for heating the susceptor, and increasing it at the expense of E fields in other directions would contribute to a better browning uniformity.

In the design of metallic field modification devices care must be taken to avoid arcing at the edges and corners of the metal. Among the several techniques used [57], a simple approach is to provide a cellulose margin for the conductive pattern. An example is a conductive vane that is made of a rectangular-shaped aluminum foil with dimensions of 88.9 mm $\times$ 192 mm, adhered to a paperboard backing of 101.6 mm $\times$ 25.4 mm. A cardboard margin of about 6 mm around the metallic foil device is adequate to eliminate arcing even when the food item is not present, which is the worst case scenario in arcing probability. Such an arrangement works on the principle that the paperboard margin reduces the intense E field at the edges of the aluminum foil by dissipating the power from such fields into heat deposited into the paperboard.

5.5 SPECIAL AND ALTERNATIVE MULTIMODE APPLICATOR CONFIGURATIONS

5.5.1 Millimeter-wave (24 GHz) multimode applicators for ceramic sintering

Gyrotron tubes [17,58,59] are capable of generating significant microwave power of the order of 3–100 kW in the millimeter-wave range. In ceramic sintering applications [17], a gyrotron source equipped with a diode electron gun was used, which can provide 0.1–3.5 kW of power at 24 GHz by variations of the electron beam voltage. The output of the gyrotron is transported to the multimode applicator through oversized circular waveguide components. The efficiency of microwave power transport in the transmission line exceeds 95%.

There are four reasons why millimeter waves are desirable for sintering ceramics. First, many ceramics have very low dielectric loss, particularly at ambient temperatures, therefore higher frequencies are useful to raise the power deposition density based on Eq. (1.18). The second motivation for using millimeter waves lies in the heating uniformity gained by having close field nulls and nodes. The third advantage for using millimeter waves is that the cavity, being much larger than the wavelength, has a far greater number of active modes, which enhances field uniformity greatly. The fourth reason is that millimeter waves lend themselves to optical focusing. For example, in processes based on surface heating of materials using millimeter waves, if the radiation is focused into a spot of about λ^2, an intensity of 10^4–10^5 W/cm^2 is achievable with millimeter-wave sources. Therefore such high intensity makes the millimeter-wave beam processing somewhat similar to infrared laser processing.

Figure 5.18 shows the multimode applicator arrangement for bulk heating of the ceramic. The incoming beam first hits a metallic mirror, which deflects the beam unto a mode stirrer. The beam, in turn, is deflected from the mode stirrer to various directions, launching the maximal number of modes. Because of the high frequency and excellent field uniformity, ceramics such as alumina, which have very low loss factors at room temperatures, can be sintered without the use of a susceptor at temperatures close to 1600°C.

5.5.2 Modified domestic microwave ovens for continuous power adjustment and control

The domestic microwave oven is a highly available and inexpensive tool that has also been utilized in many laboratories for scientific experimentation, particularly microwave chemistry. The major driver in the design of

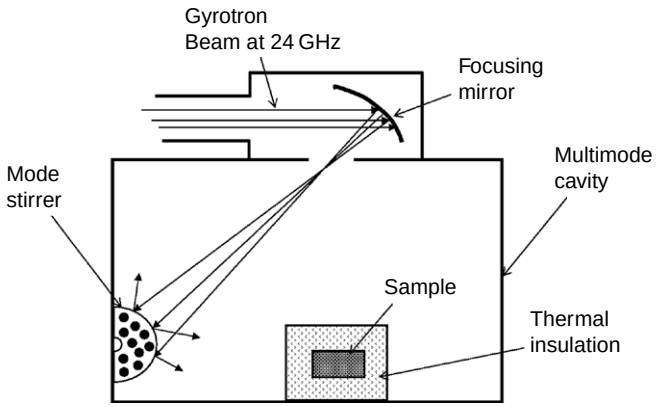

FIGURE 5.18
A 24 GHz gyrotron beam system for uniform processing of ceramics without a need for susceptors.(After Bykov et al. [17].)

the domestic oven is to bring down the cost of manufacturing. Therefore the power control scheme is very simple, as shown in Figure 5.19a, where a single high-voltage transformer is used and both the anode and filament voltages are tapped from the secondary. The power control is achieved by controlling the duty cycle, where the oven is turned on and off at regular intervals when power levels lower than full power are chosen.

Such a simple scheme is incompatible with the needs of scientific experiments where continuous power control is required. An industry for experimental microwave ovens for scientific purposes has been developed [60,61]. In addition, turnkey microwave sources with sophisticated controls are available from several manufacturers [32].

A different solution is the modification of a domestic microwave oven system [62,63], as shown in Figure 5.19b. The scheme involves the addition of two transformers, a small fixed one for feeding the filament, which only needs a few volts [24], and a second variable transformer (or Variac), which can vary the input voltage to the main transformer. This provides a variable anode voltage to the magnetron for power variability.

5.5.3 Multimode applicators for plasma generation

As described in Chapter 1, a plasma body with sufficient electron density acts as a highly lossy dielectric at high frequencies. Therefore the microwave energy in a multimode applicator can be absorbed into the plasma to sustain it. A multimode cavity, specifically a modified microwave oven, has been developed as a laboratory plasma generator [64] and has been commercialized [65].

Figure 5.20 shows the basic components of a multimode cavity laboratory plasma system. A Pyrex glass bell jar is placed in the oven, which

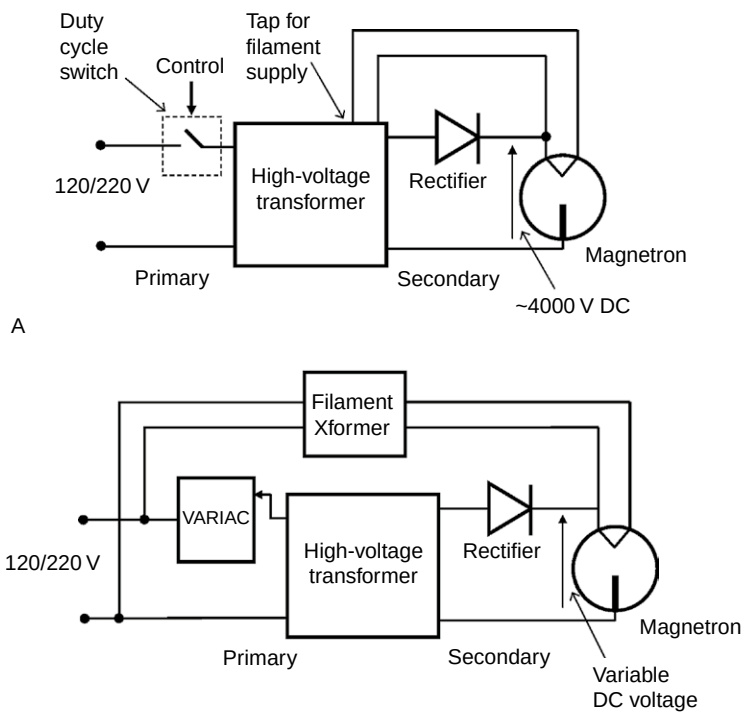

FIGURE 5.19

Modification of a domestic microwave oven for continuous power control. (A) Simplifield block diagram of domestic microwave oven power controls. (B) Modifications for continuous power control.

has an external gas controller. The substrate to be cleaned or otherwise processed is placed at the bottom of the cavity. In order to prevent the field interacting directly with the sample substrate, it is important to place it flat as close as possible to the cavity floor because the parallel *E* fields in that area are minimal. Note that the goal is to have the ionized species interact with the substrate and not the microwave fields.

The bell jar is filled with low-pressure gas to provide the proper species for the job at hand. For example, argon is suitable for applications that involve epoxy-bonded surfaces since it will not "sputter" epoxy. It is also the preferred medium for removing metal oxides. Oxygen, because it attacks epoxy, should be used selectively in the presence of epoxy bonding. It is, however, ideal for cleaning contaminants from ceramic or oxide parts. The plasma would easily ignite due to the proper gas pressure provided by the gas controller.

5.5.4 Microwave fluidized bed applicators

Fluidized bed reactors are widely used in material processing industries for processes that require very good heat and mass transfer between particles

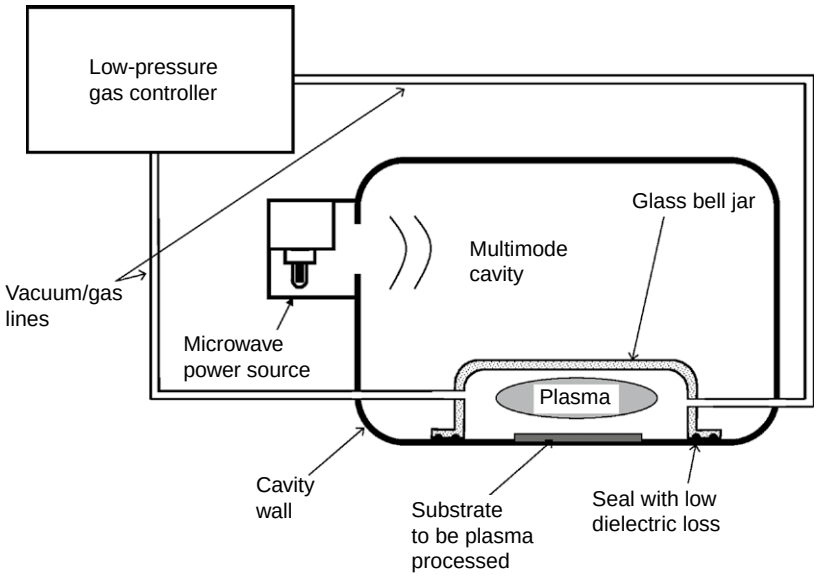

FIGURE 5.20 *Multimode oven used for plasma processing of substrates.*

and a gas. The energy provided to the fluidized bed typically comes from the warm gas that fluidizes the bed as well. In many cases an additional source of energy is required beyond what is stored in the gas. Providing that energy by conventional means is often difficult due to heat transfer limitations. Microwave is considered an attractive choice and several pilot studies have beeen performed in recent times [66,67].

Since the fluidized bed is made up of a large metal container, it can be considered as a multimode applicator. Because of constant agitation of the bed, the field non-uniformity is not a problem except for the possibility of overheating at the microwave feed point if the location is not chosen properly. Due to the dusty environment, the feed point needs to be isolated from the bed using very-low-loss materials such as certain ceramics or quartz. Due to separation of particles in a fluidized bed reactor, the bulk permittivity and loss of the bed is far lower than the base material, therefore there is deeper wave penetration into the material bed [68,69].

In every instance of microwave fluidized bed reactor design, after the conceptual process issues are studied there are microwave engineering issues that need to be resolved [70]. The issue of microwave emissions from various openings is one of them, where the chocking and suppression techniques discussed in Chapter 9 need to be applied.

REFERENCES

[1] J.M. Osepchuck, Microwave power applications, IEEE Trans. Microw. Theory Tech. 50 (3) (March 2002) 975–985.

[2] R.F. Schiffman, State of the art of microwave applications in the food industry in the USA, in: M. Willert Porada (Ed.), Advances in Microwave and Radio Frequency Processing, Springer-Verlag, Berlin, 2006.

[3] D.E. Clark, W.H. Sutton, Microwave processing of materials, Annu. Rev. Mater. Sci. 26 (1996) 299–331.

[4] H.M. Kingston, S.J. Haswell, Microwave Enhanced Chemistry, American Chemical Society, Washington, DC, 1995.

[5] M. Mehdizadeh, Engineering and scale-up considerations for microwave induced reactions, Res. Chem. Intermediat. 20 (1) (1994) 79–84.

[6] J.D. Katz, Microwave Sintering of Ceramics, Ann. Rev. Mater. Sci. 22 (1992) 153–170.

[7] R.E. Collin, Foundations of Microwave Engineering, Wiley-IEEE Press, 2000.

[8] S. Ramo, et al., Fields and Waves in Communication Electronics, third ed., Wiley, New York, 1994.

[9] T.K. Ishii, Microwave Engineering, second ed., Oxford University Press, 1995.

[10] D.M. Pozar, Microwave Engineering, Wiley, New York, 2004.

[11] Wolfram Reseach, website URL: www.wolfram.com

[12] T.V. Chan, H.C. Reader, Understanding Microwave Heating Cavities, Artech House, Boston, 2000.

[13] R.J. Riegert, Private communication.

[14] R. Meredith, Engineer's Handbook of Industrial Microwave Heating, The Institution of Electrical Engineers, London, 1998.

[15] G. Roussy, J.A. Pearce, Foundations and Industrial Applications of Microwave and Radio Frequency Fields, Wiley, New York, 1995.

[16] A.C. Metaxas, Foundations of Electroheat: A Unified Approach, Wiley, Chichester, UK, 1996.

[17] Y. Bykov, et al., 3.5 kW Compact gyrotron system for microwave processing of materials, in: M. Willert-Porada (Ed.), Advances in Microwave and Radio Frequency Processing, Springer-Verlag, Berlin, 2006, pp. 24–30.

[18] Y.V. Bykov, et al., High-temperature microwave processing of materials, J. Phys. D Appl. Phys. 34 (2001) R55–R75.

[19] J.R. Bows, A classification system for microwave heating of food, Int. J. Food Sci. Technol. 35 (2000) 417–430.

[20] V.V. Yakovlev, Examination of contemporary electromagnetic software capable of modeling problems of microwave heating, in: M. Willert Porada (Ed.), Advances in Microwave and Radio Frequency Processing, Springer-Verlag, Berlin, 2006.

[21] COMSOL Inc., website URL: www.comsol.com

[22] R. Akarapu, B.Q. Li, Y. Huo, J. Tang, F. Liu, Integrated modeling of microwave food processing and comparison with experimental results, J. Microw. Power Electromagn. Energy 39 (3/4) (2004).

[23] T.V. Chan, et al., 3-Dimensional Numerical Modeling of an Industrial Radio Frequency Heating System Using Finite Elements, J. Microw. Power Electromagn. Energy 39 (2) (2004) 87–105.

[24] C.R. Buffler, Microwave Cooking and Processing: Engineering Fundamentals for the Food Scientist, Van Nostrand Reinhold, New York, 1992.

[25] S.V. Egorov, et al., Edge effects in microwave heating of conductive plates, J. Phys. D Appl. Phys. 39 (2006) 3036–3041.

[26] L. Fehrer, et al., The industrial hephaisstos microwave system technology, 40th Annual Microwave Symposium Proceedings, IMPI, 2006.

[27] IHM-Forschungszentrum Karlsruhe GmbH, URL: http://vitw.cms.schunk-group.com/en/schunk01.c.17111.de/all_vitproductsarticle.

[28] Y.M. Lee, et al., Microwave Oven for Uniform Heating, US Patent 6,384,392 B1, May 2002.

[29] P. Plaza-Gonzalez, et al., Effect of mode-stirrer configurations on dielectric heating performance in multimode microwave applicators, IEEE Trans. Microw. Theory Tech. 53 (5) (May 2005) 1699–1706.

[30] A.C. Metaxas, R.J. Meredith, Industrial Microwave Heating, The Institution of Engineering and Technology, 1988.

[31] I.K. Eke, R. Schiffmann, US Patent 6,909,077 (B2), 2005.

[32] Gerling Applied Engineering Inc.: http://www.2450mhz.com.

[33] Linn High Therm GmbH, website at URL: http://www.linn-high-therm.de.

[34] J., Suhm, et al., New development for industrial microwave heating, International Scientific Colloquium on Modeling for Electromagnetic Processing, Hannover, Germany, 2003. Available online at URL: http://www.modlab.lv/publications/mep2003/pdf/141.pdf.

[35] W. Tang, et al., Study of 5.8 GHz Magnetron in Microwave De-Icing, J. Electromagn. Waves Appl. 22 (10) (2008) 1351–1360.

[36] A.C. Johnson, et al., Bandwidth and Uniformity of Multimode ovens, MRS Symposium Proceeding IV 347 (1994) 453.

[37] Lambda Technologies Inc., URL: http://www.microcure.com/lt_technology.html

[38] R.J. Lauf, et al., Method for Curing Polymers Using Variable-Frequency Microwave Heating, US Patent 5,721,286, February 1998.

[39] M. Moeller, H.S. Shulman, H. Giesche, A Novel Approach to Understanding Microwave Heating of Zirconia, Ceralink website, 2007. Available at URL: http://www.ceralink.com/publications/A_NOVEL_APPROACH.PDF.

[40] C.I. Sangdao, et al., An applicator for uniform heating using perpendicular slots on a concentric cylindrical cavity excited by perpendicular waveguides, Int. J. Electron. 93 (5) (2006) 313–334.

[41] V. Adegbite, et al., Uniform microwave heating of polymer matrix composites, Ceram. Trans. 59 (1995) Microwaves: Theory and Applications in Materials Processing III.

[42] J.E. Gerling, Microwave processing equipment – a modular approach, Food Technol. 22 (1968) 1968.

[43] G. Roussy, et al., Supply of microwave applicator with two magnetrons and a magic tee for obtaining an uniform electric field distribution, 35th International Microwave Power Symposium Proceedings, 2000, pp. 51–54.

[44] B. Krieger, (Cober Electronics), Private communication, January 2009.

[45] R.J. Meredith, Trends in high power generators for industrial microwave, 5th International Conference on Microwave and High Frequency Heating, University of Cambridge, 1995, pp. F1.1–F1.8.

[46] M.B. Steer, Passive microwave devices, in: M. Golio (Ed.), The RF and Microwave Handbook, CRC Press, Boca Raton, FL, 2001, pp. 613–621.

[47] H. Zuckerman, et al., Characterization of thin layer susceptors for the microwave oven, J. Food Process. Pres. 16 (1992) 193–204.

[48] H. Zuckerman, et al., Changes in thin-layer susceptors during microwave heating, Packag. Technol. Sci. 7 (1994) 21–26.

[49] H. Zuckerman, et al., Temperature profiles at susceptor/product interface during heating in the microwave oven, J. Food Process. Pres. 19 (1995) 385–398.

[50] T.H. Bohrer, R.K. Brown, Packaging techniques for microwaveable foods, in: A. K. Datta, R.C. Anantheswaran (Eds.), Handbook of Microwave Technology for Food Applications, Marcel Dekker, New York, 2001.

[51] J. Cesnek, et al., Properties of thin metallic films for microwave susceptors, Czech. J. Food Sci. 21 (1) (2003) 34–40. Available online at URL: http://www.cazv.cz/2003/CJFS1_03/5-Cesnek.pdf.

[52] H.F. Huang, Packaging for convenience foods: microwave food packaging – what to specify and how to measure, Proceedings of the 23rd Interanational Microwave Power Symposium, 1988.

[53] T. Labuza, et al., An Alternate Method for Measuring the Heating Potential of Microwave Suseptor Films, J. Microw. Power Electromagn. Energy 27 (4) (1992).

[54] D.A. Copson, US Patent 2,830,162, 1958.

[55] D. Agrawal, J. Cheng, Y. Fang, R. Roy, D.E. Clark (Ed.), et al., Microwave Processing of Ceramics, Composites, and Metallic Materials, American Ceramics Society Publishing, 2005, pp. 205–228.

[56] N.L. Blankenbeckler, H.C. Chi, M. Mehdizadeh, R.J. Riegert, Susceptor assembly and field director assembly for use in a microwave oven, US Patent Application 20070187399 A1, August 2007.

[57] N.L. Blankenbeckler, W.R. Corcoran, D.W. Kawka, M. Mehdizadeh, R.J. Riegert, Field director assembly having arc-resistant conductive vanes, US Patent Application 20070210078 A1, Septemper 2007.

[58] G.S. Nusinovich, et al., Modern Microwave and Millimeter-Wave Power Electronics, Wiley-IEEE Press, New York, 2005.

[59] R.J. Barker, E. Schamiloglu (Eds.), High Power Microwave Sources and Technologies, Wiley-IEEE Press, New York, 2001.

[60] CEM Corporation, website URL: www.cem.com.

[61] Biotage AB, website URL: www.biotage.com.

[62] C.H. Tong, et al., A Microwave oven with variable continuous power and a feedback temperature controller, Biotechnol. Prog. 9 (1993) 488–496.

[63] J.E. Gerling, Microwave oven power: a technical review, J. Microw. Power 222 (2) (1987) 199–211.

[64] A. Ribner, US Patent 4,804,431, February 1989.

[65] Plasma Preen Co., website URL: http://www.terrauniversal.com/cleaning_systems/plasma_preen_cleaners.php.

[66] J.M. Tranquilla, Treatment of Metal Ores in Microwave Fluidized Bed Reactor, US Patent 6074533, June 2000.

[67] T. Gerdes, R. Tap, P. Bahke, M. Willert-Porada, CVD-processes in microwave heated fluidized bed reactors, in: M. Willert Porada (Ed.), Advances in Microwave and Radio Frequency Processing, Springer-Verlag, Berlin, 2006.

[68] H.W. Zhao, et al., Theoretical Study of Fluidized-Bed Drying with Microwave Heating, Ind. Eng. Chem. Res. 39 (3) (2000) 775–782.

[69] S. Okamura, Y. Zhang, Thermal modeling of microwave heated packed and fluidized bed catalytic reactors, J. Microw. Power Electromagn. Energy 35 (3) (2000) 165–171.

[70] M.K. Doelling, Microwave assisted fluidized bed processor, US Patent 4,967,486, November 1990.

CHAPTER 6

Applicators and Probes Based on the Open End of Microwave Transmission Lines

CHAPTER CONTENTS

INTRODUCTION

In previous chapters we discussed conditions where the material under study or processing is placed within the applicator or probe, microwave cavities and parallel-plate applicators being examples. Those structures are only useful when the physical configuration of the material lends itself to being surrounded by the applicator or the sensor. There are many applications, however, where only a part of a physically large material can be, or needs to be, heated or sensed.

The focus of this chapter is applicator/probes where evanescent electric fields protrude from the open end of a transmission line or the open side of a cavity resonator, where the material under study or processing is placed.

Microwave/RF Applicators and Probes for Material Heating, Sensing, and Plasma Generation

There are numerous applications where the use of such structures is beneficial or necessary. One prominent example is microwave hyperthermia or diathermy, where a local area of the body needs to be thermally treated for killing a malignant tissue. An example of a sensing application where an open probe is used is the non-destructive study of a dielectric object. In general, open-ended transmission-line or cavity applicators are used where access to the material is limited, either because inducing fields into the whole object is not possible or not allowed.

Depending on the application, there are many factors that go into the basic structure and detailed design of open-ended applicators and probes that will be covered in this chapter. There are sections devoted to examples of the latest developments and applications in the area of open applicators such as microwave drills and microwave microscopes.

6.1 COMMON CHARACTERISTICS OF OPEN-ENDED TRANSMISSION-LINE STRUCTURES

6.1.1 Basic structure and equivalent circuit

Figure 6.1a shows a simple representation of an open-ended transmission-line probe or applicator, where the fringing fields from the open end interact with the material under study or processing. The transmission line can be any type for the purpose of this discussion, and the fringing field is a modified form of the field that usually exists in that type of line. When the structure is used as a probe, the purpose is to study the material's dielectric characteristics by examining the forward and reflected signals. On the other hand, when the structure is used as an applicator, the forward power input is utilized to impose an electric field to deposit energy into the material. In that case, the reflected power must be minimized for good power efficiency.

A simplified equivalent circuit is shown in Figure 6.1b, where the fringing field is represented by a capacitance C_{oe} and the added capacitance due to the material's dielectric polarization is shown as C_m. The resistance R_m represents the dissipative loss of the material. It should be noted that this simplified equivalent circuit is only valid under certain circumstances. In many cases, particularly when the electrical size of the structure is large, which happens at higher frequencies, the equivalent circuit of the open end will be far more complex than shown here due to the distributed nature of the fields.

This equivalent circuit is useful because it can be incorporated as a load for the transmission-line model in various design tasks. For example, in a material heating situation, the equivalent circuit can be utilized to design

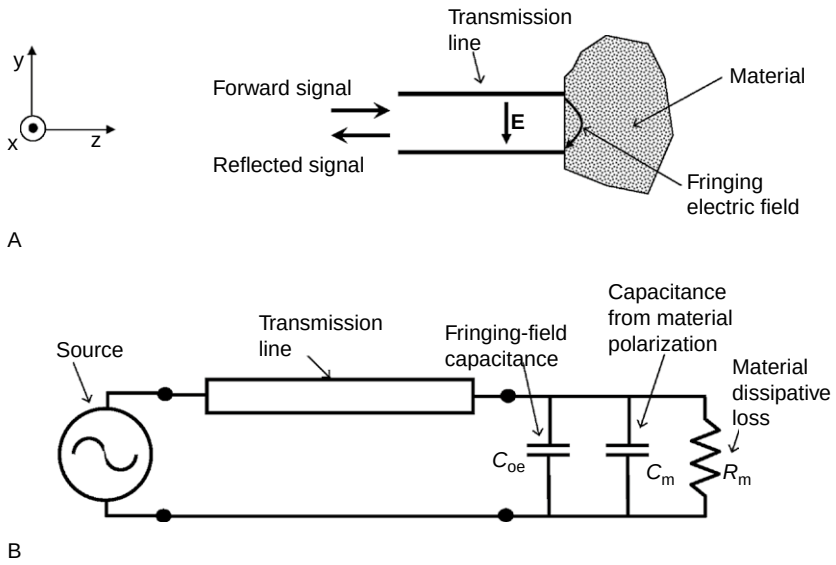

FIGURE 6.1 *Representations of open-ended transmission-line applicators/probes. (A) General configuration with the electric fields inside the transmission line and fringing fields that interact with the material. (B) Equivalent circuit, which includes the lumped element representation of fringing fields and those resulting from the interactions of the fringing fields with the material. The equivalent circuit, which consists of a parallel RC circuit, in which the resistance represents the material losses and the capacitance represents both open-ended capacitance and additional capacitive element representing the polarization of the material.*

a matching circuit for optimal transmission of power into the material. In probing or characterization problems the input impedance is measured and the values of the equivalent circuit components are found, which give information about the dielectric material. A part of the content of this chapter is to find the elements of this equivalent circuit for various open-ended transmission-line structures.

6.1.2 Field of view (field of coverage)

Open-ended applicator/probes have a limited volume of field coverage. On the interface surface between the applicator and the material (x–y plane in Figure 6.1) the coverage is limited to the aperture opening of the applicator/probe. In the z direction, which is the direction of field penetration into the material, the fields diminish quickly with distance.

A note of caution needs to be made here: the diminishing of the fields we discuss here is an entirely different phenomenon than the depth of wave penetration into the material as discussed in Chapter 1 (Section 1.2.6,

Eq. (1.34)). The fields at the end of an open-ended transmission line diminish even if no material is located at the open end. Obviously, both effects could be present at the same time as well.

The limited penetration, while it can be a disadvantage, in some cases is a useful feature. For example, in material test and evaluation, a material could be tested without regard for its thickness, as long as the thickness is significantly larger than the field penetration.

6.1.3 Categories of open-ended applicator/probes

The operating principles and analysis of open-ended applicator/probes is heavily determined by what type of transmission lines they are made of. Transmission lines, in general, are divided into two main categories [1,2]. The transverse electromagnetic (TEM) category is that in which both electric and magnetic fields are vertical to the cross-section of the transmission line. In this category there are at least two distinct conductors surrounded by dielectrics or open space. One example is the coaxial transmission line, which has a center conductor and a shield; a second example is the stripline or microstrip lines that have two parallel and planar conductors. An important characteristic of TEM transmission lines is that they operate over a very broad frequency band. There is no lower frequency limit for their operation. The upper frequency limit happens when the wavelength becomes comparable to the cross-sectional dimensions of the line, and the devices cease to operate at TEM mode. Clear examples of TEM open-ended probes are the open-ended coaxial line [3] and open-ended strip transmission line [4].

The second category is transverse electric (TE) and transverse magnetic (TM) modes [2], which do have an electric or magnetic field component in the direction of the signal flow, meaning that their field direction is not limited to the cross-section of the transmission line. One important attribute of TE/TM transmission lines is that they can operate with only one conductor, which is typically a hollow waveguide. Another characteristic of this category is that there is a lower limit to the frequency of operation, which is called the cutoff frequency.

The open-ended coaxial line is the most widely used in the TEM category, almost exclusively as a material evaluation and sensing device, even though there are exceptions that will be covered later. In the TE/TM category, the open-ended waveguide or waveguide horn, which is a flared version of the waveguide, is used as both a heating applicator and a probe. Open resonant cavities (or resonators) can be called the third category of open-ended applicator/probes.

6.2 TEM-MODE OPEN-ENDED TRANSMISSION-LINE APPLICATORS

The most important general category of open applicators/probes is the open-ended TEM-mode transmission line. In conventional applications of transmission lines, a frequency source delivers a signal to a load that has an ohmic contact to the transmission line. In an open-ended transmission-line probe, in contrast, the material is placed in proximity on this open end without the requirement of an ohmic contact.

6.2.1 Open-ended parallel strips

A very simple form of transmission line is parallel strips [5]. If a pair of parallel strips is butted against a solid material, the result is a simple form of open-ended transmission line, as shown in perspective in Figure 6.2. While this type of open-ended applicator is not often used in practice, it is a good instructional example to understand the properties of this type of applicators and probes. Note that in Figure 6.2 the parallel strips are suspended with no dielectric material in between. The presence of a dielectric substrate, which is needed for practical realization of this transmission line, does not make a major difference for the purpose of this discussion.

In Figure 6.2, a signal or power source feeds the parallel-strip transmission line at one end, and the material to be evaluated or processed is placed at the other end. The main electric field components are vertical to the parallel

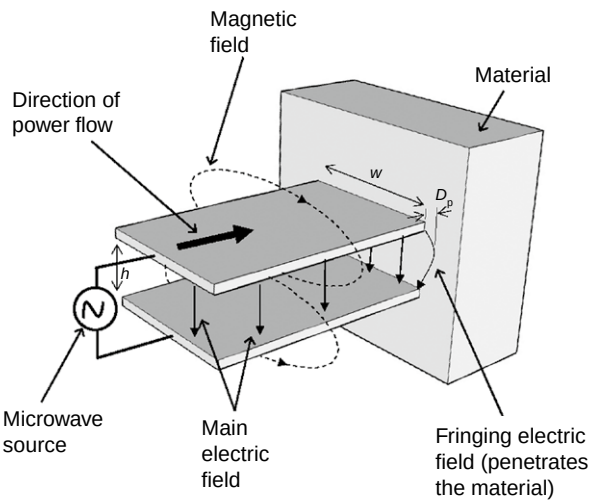

FIGURE 6.2
An open-ended parallel-strip transmission-line applicator/probe: the geometry and field configurations are shown.

strips and the magnetic fields are mostly directed parallel to the strip, as shown. The fringing electric fields at the open end of the transmission line penetrate into the material.

In most applications involving dielectric materials only the fringing electric fields are effective. In principle, however, if the material is sufficiently conductive or possesses significant magnetic permeability or magnetic loss properties, the fringing magnetic fields would also participate in interacting with the material. In the overwhelming majority of practical cases, however, electric field interactions predominate, which is the focus of this chapter.

6.2.2 Effective field interaction volume

In the open-ended strips transmission line of Figure 6.2, the volume of field interaction is essentially a rectangular cube with dimensions w (the width of the strips), h (the distance between the strips), and D_p (the depth of penetration of the field into the material). This depth is defined as the location where field strength is 1/e or 36% of the field at the end of the transmission line.

Note that in the above definition of depth of penetration we have not used the general designation of δ (Eq. (1.27)), which is the depth of penetration of plane waves. In the case of open-ended applicators the depth of penetration D_p is dependent upon the geometry of the open end, since the fields at that location are not plane waves in open space. For example, the depth of penetration in open-ended parallel-strip transmission lines is small when the distance between the plane h is small and large when the distance is large. In a parallel-strip transmission-line case, a penetration depth of $h/2$ is a reasonable estimate, as long as this figure does not exceed the basic penetration depth of plane waves, δ.

In various configurations of open-ended applicators, the effective field volume is dependent upon the geometry of that configuration. For example, in a coaxial open-ended probe, the effective volume would have a doughnut shape.

There are applications where the effective field volume must be modified for various reasons. For example, when the area of heat treatment must be increased, the open end of the parallel strips may be flared out as shown in Figure 6.3b [4], or when the field volume needs to be focused in a smaller area, the strips are brought together as shown in Figure 6.3c [6]. In all configurations of open-ended transmission-line applicators a similar approach can be used for modifying the effective field volume. For example, in the case of an open-ended waveguide, a horn applicator is used when there is a need for an increased area of study or processing.

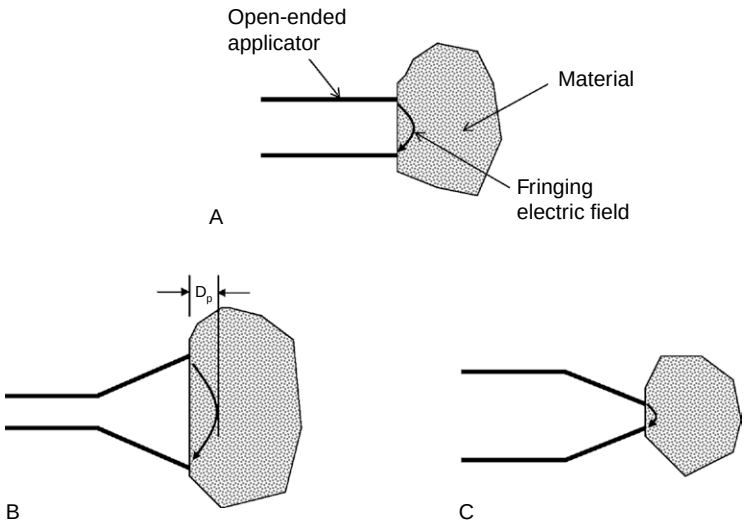

FIGURE 6.3

Three types of open-ended transmission-line applicator/probes. (A) Straight type, where the open end is the same size as the cross-section of the transmission line itself. (B) Flared (or horn) type, where the open end is larger than the transmission-line cross-section. (C) Focused type, where the open end is smaller than the transmission-line cross-section.

6.2.3 Impedance mismatch and signal/power transfer to the material

In most applications where TEM open-ended transmission lines are used, there is an inherent impedance mismatch between the open end and the material. This can be quantified by a comparison between the E fields inside the transmission line, if it was terminated by an impedance matched load, on the one hand, and E field required to deposit the same power into the material on the other. If the amplitudes of these two E fields are similar, then we can assume a significant amount of signal power can be transferred from the source into the material. In this section we will pursue this logic to explore the impedance match between the transmission line and the material.

To do this, consider the case of the open-ended parallel transmission line of Figure 6.2. Suppose, for a moment, that the parallel-strip line is connected to the source at one end and to a matched resistor (which must have a resistance equal to the characteristic impedance of the line) at the end where the material is supposed to be. The power transmitted from the source to the load can be shown as [2]:

$$P = \frac{V^2}{Z_0} \tag{6.1}$$

where V is the RMS voltage between the strips and Z_0 is the characteristic impedance of the transmission line. Given that $V = E/h$, where E is the

electric field intensity and h is the distance between the strips. The electric field at the open end becomes:

$$E = \frac{\sqrt{P Z_0}}{h} \tag{6.2}$$

On the other hand, let us calculate the electric field intensity necessary to dissipate the same power P into the material block shown in Figure 6.2:

From Eq. (1.18), the power deposited into a material with a dielectric loss ε_r'' at the frequency f is governed by:

$$P = 2\pi\varepsilon_0 \varepsilon_r'' f E^2 v \tag{6.3}$$

where ε_0 is the permittivity of a vacuum, E is the electric field intensity and v is the volume subjected to the field. Considering the parallel-strip width of w, distance h, and approximate field penetration $h/2$, the E field requirement becomes:

$$E = \frac{1}{h}\sqrt{\frac{P}{\pi\varepsilon_0 \varepsilon_r'' f w}} \tag{6.4}$$

If an open-ended parallel strip is butted against a material, according to the field configuration shown in Figure 6.2, at the interface between the open end and the material, the E fields are parallel to the material surface; therefore the E fields must be equal. Let us now use a practical example and compare the E fields in the impedance-matched case of Eq. (6.2) and the required field from Eq. (6.4).

Suppose that a parallel-strip transmission line has a characteristic impedance of about 50 Ω, a width of 1 cm, and the distance between the parallel strips is 0.3 cm. If a matched load is connected to the ends, using Eq. (6.2) the E field between the plates for 1 W of power delivery is $E = 2357$ V/m. If, instead of the matched load, the open end of the transmission line is butted against a lossy material block with dielectric loss factor of $\varepsilon_r'' = 0.8$, from Eq. (6.4) the required E field for the same 1 W of power delivery at the frequency of 1 GHz becomes $E = 22{,}351$ V/m, which is about an order of magnitude above the matched load case.

The great discrepancy of E fields between the matched case and the power absorption case proves that when open-ended TEM lines are used

for evaluation or processing of typical dielectrics, there would always be an impedance mismatch. Therefore, for efficient power or signal delivery to dielectric materials using open-ended TEM transmission lines there is a need for an external impedance matching technique. In the next section we will discuss one such method in the case of open-ended coaxial lines.

The above calculation raises a question: if interfacing of open-ended TEM lines to dielectrics results in a large mismatch, under what circumstances is an efficient power delivery to the material possible without impedance matching hardware? The answer is found by equating Eqs (6.2) and (6.4) to find the minimum dielectric loss required in order to obtain a good impedance match:

$$\varepsilon_r'' = \frac{1}{\pi \varepsilon_0 f w Z_0} \tag{6.5}$$

Using parameters for the previous example we find that the approximate required material dielectric loss for a good impedance match is $\varepsilon_r'' = 72$, which is above the range of known dielectrics. Using $\sigma = \varepsilon_0 \varepsilon_r'' \omega$, the conductivity of such a material would be $\sigma = 4\,\text{S/m}$, which is in the semiconductive range.

6.2.4 Equivalent circuit of open-ended transmission-line applicators

In general, the input admittance of an open-ended transmission line is a complex function of two complex variables [7]:

$$Y(s, \varepsilon_r) = G(s, \varepsilon_r) + j B(s, \varepsilon_r) \tag{6.6}$$

where functions G and B are the real and imaginary parts of the admittance function Y, j is the complex frequency variable, and $\varepsilon_r = \varepsilon_r' - j\varepsilon_r''$ is the complex relative permittivity.

In the case of a TEM applicator, where the cross-sectional size of the transmission line is far smaller than the operating wavelength, a simple parallel RC equivalent circuit can be defined to replace Eq. (6.6). This simplified equivalent circuit has a capacitive component that reflects the fringing fields, such as those shown in the open-ended transmission-line applicator of Figure 6.2. The presence of the material that needs to be evaluated or processed would increase this fringing capacitance. The loss

factor of the material would add a parallel resistance R to the capacitance C. Therefore Eq. (6.6) simplifies to:

$$Y = \frac{1}{R} + j\omega C \tag{6.7}$$

The capacitance C, in turn, is made up of two components:

$$C = C_{oe} + C_{m} \tag{6.8}$$

where C_{oe} is the capacitance in open space and C_{m} is the added capacitance due to the presence of the material. Figure 6.1b shows the equivalent circuit that depicts the transmission line as well. Modeling and computation of the complex admittance for open-ended transmission lines is often critical in the proper design of these applicators. We will show some of these methods for open-ended coaxial lines later.

The approximate analysis of the previous section proved that in most cases there is a large mismatch between practical transmission lines and the open end's circuit. In cases where open-ended transmission-line applicators are used for power delivery to a load for heating applications, an impedance matching technique is required. In addition to impedance matching techniques, resonant methods have also been used in order to resolve the impedance match issue [8,9].

6.3 OPEN-ENDED COAXIAL TRANSMISSION-LINE PROBES

Open-ended coaxial transmission-line probes are widely used as microwave sensors for industrial processes and quality control applications [10–17]. In addition, they are used for measurement of the dielectric properties of materials. They have the advantage of simple construction and most notably the commercial availability of numerous types of coaxial lines for a myriad of communication applications. Other advantages include capability of operation over a broad frequency range of kilohertz to tens of gigahertz due to the TEM nature of signal propagation. In comparison, the operating frequency of hollow waveguides is highly dependent upon their cross-sectional dimensions, which means the aperture formed by the open end of a conventional waveguide needs to be large to accommodate most practically useful frequencies. Another advantage of open-ended coaxial lines is the lack of any wave leakage and radiation from the sides, as opposed to configurations such as parallel planar strips.

If the frequency is high enough, higher order modes or non-TEM modes are possible in open-ended coaxial lines. But in practical applications the cross-sectional geometry is chosen to be much smaller than the wavelength; therefore the TEM mode is the only possibility. As such, the approximate analysis in Section 6.2 applies to coaxial open-ended probes and applicators as well.

The electric and magnetic field configuration of the open end of a coaxial line is shown in Figure 6.4. In practical applications involving dielectric materials only the *E* field is considered as useful. Due to the high-impedance nature of this geometry, the presence of the magnetic field can be ignored in most applications. Since open-ended coaxial lines are almost exclusively used in sensing and dielectric measurement applications, we use the designation "probe" as opposed to applicator for this configuration.

6.3.1 Analytical solutions for the admittance of the open-ended coaxial probe

In many applications of the open-ended coaxial probe, there is a need to find the mathematical relationship between the dielectric properties of the material under study and the electrical parameters at input to the transmission line. It is convenient to use admittance (reciprocal of impedance) for this purpose. In this case, the admittance of the open end needs to be calculated versus the applicator geometry and the dielectric parameters of the material. The geometry and notations for an open-ended coaxial line are shown in Figure 6.5 in the form of a longitudinal cutaway to show the

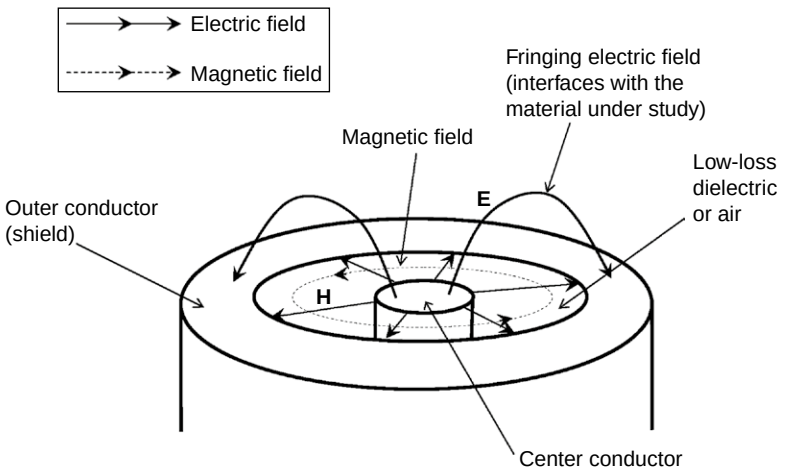

FIGURE 6.4
The geometry and field configuration of an open-ended coaxial line.

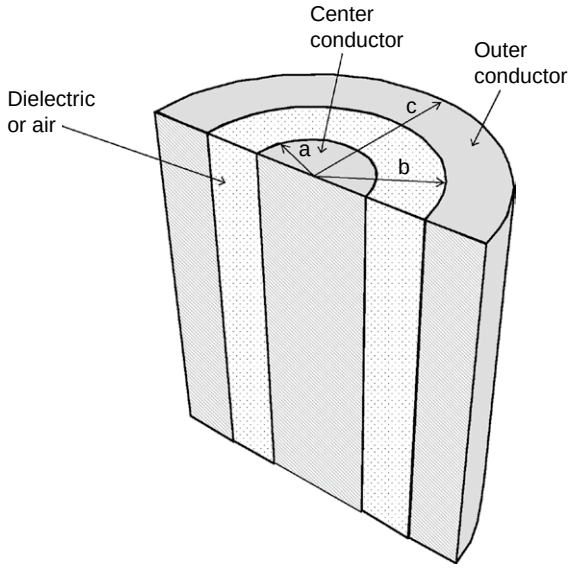

FIGURE 6.5
A longitudial cutaway to show the geometry and notations used in the analytical solution to the open-ended coaxial line.

details. Due to the relative complexity of the field configuration, no acceptable closed-form formula exists for calculation of the input admittance. There are several analytical methods for both simple and layered media [7,12,18], which involve numerical solution methods. According to these solutions the admittance depends upon the permittivity of the material under test, the radius of the probe, and the operating frequency.

Note that most analytical methods usually assume an infinite flange ($c = \infty$ in Figure 6.5), and it is conventionally presumed that a small flange would cause discrepancies between measurement and theory. However, McLaughlin et al. [13] have proved that flangeless cases provide adequate accuracy as long as the ratio of the outer conductor to the annular dielectric radius is at least 2 ($c > 2b$).

Among the analytical methods to find Y, the admittance of the open-ended coaxial line in contact with a material, three different integral equations were compared by Xu et al. [19]. Of these, the equation by Levine et al. [20] is deemed appropriate for lossy dielectrics, which is of most interest:

$$Y = \frac{jk\varepsilon Y_0}{\ln\left(b/a\right)\sqrt{\varepsilon_i}} \int_0^\infty \frac{d\xi}{\xi\sqrt{\xi^2 - k^2\varepsilon}} [J_0(\xi a) - J_0(\xi b)]^2 \tag{6.9}$$

where Y_0 is the characteristic impedance of the coaxial line, $\varepsilon = \varepsilon_r' - j\varepsilon_r''$ is the complex dielectric permittivity of the material, ε_i is the permittivity of

the coaxial line's filling material, ξ is the integral variable, and function J_0 is a first-type Bessel function of zero order. The integral equation (6.9) was formulated in Mathematica™ [21] by Riegert [22], as shown in Appendix A6.1, together with a numerical example.

6.3.2 Dielectric characterization of materials with open-ended coaxial line

Analytical solutions for the open-ended coaxial probes, such as Eq. (6.9), provide the impedance or admittance of the open end from geometrical data and the dielectric properties. These methods, which are called "forward" problems, are useful in many practical instances – for example, when the impedance results are needed to assess matching, and to possibly implement one of the available impedance matching methods.

When the open-ended coaxial line is used for dielectric characterization, the inverse problem must be solved, i.e. starting with a measured admittance using a vector network analyzer (VNA), there is a need to arrive at the dielectric properties of the material. Since the existing analytical solutions such as Eq. (6.9) are in integral form, the solution of the inverse problem is not as straightforward as inverting a closed-form function. A number of methods of solving the inverse problem have been developed [23]. The inverse problem can be turned into a polynomial for convenient use [24].

When open-ended probes are used as industrial sensors [9,10], custom circuits are normally used for impedance matching, signal detection, and data acquisition.

6.3.3 Advantages and limitations of material characterization with open-ended coaxial probes

Open-ended coaxial lines are one of the preferred methods for characterization of dielectric materials, because of several advantages they offer. Aside from their non-destructive nature, which they have in common with other RF/microwave techniques, they can be used over a wide frequency band of up to 50 GHz [11,13]. This is as opposed to resonant cavity and waveguide techniques, which are either single frequency or exclude a group of frequencies. Another advantage is that there is no necessity to prepare a sample of a specific size, as long as the sample meets the minimum size requirements.

The limitations of the open-ended coaxial method are mostly related to the requirement for sample shape, size, consistency, and placement. As for shape, the sample needs to be thick enough so that all the available fields in

the vicinity of the probe are located inside the material. For best accuracy, having the material thickness four times the aperture diameter is recommended [11]. As for measurement of sheets or films, there are methods available for analysis of stratified dielectrics [18], the inverse problem, for these analyses are problematic when measurement of thin sheets is attempted.

Air gaps between the sample and the probe, as well as any air pockets within the sample, are a source of problems in dielectric studies done with open-ended coaxial probes. This would exclude solids for accurate characterization, unless special care is taken to flatten the surface and fit it perfectly aligned with the probe. Powders and granules can be characterized with reasonable accuracy for their bulk dielectric properties with open-ended coaxial probes as long as the aperture size is at least two orders of magnitude larger than the average particle size. This would average out the impact of air pockets between the particles. Bianchi et al. [25] have been able to measure the moisture content of sand accurately using an open-ended coaxial probe.

Open-ended coaxial probes are not accurate for characterization of the dielectric loss factor (ε_r'') for very-low-loss dielectric samples. The reason for this limitation is metal losses of the coaxial line itself, which may be comparable to sample losses as viewed from the instrument. Though this limitation is variable based on the type and dimensions of the coaxial line used, a lower limit of 0.05 for the dielectric loss factor is recommended. This limitation, however, does not affect the capability to characterize the relative permittivity. Most low-loss liquids also have low permittivity, for example the solvent xylene has a complex relative complex permittivity of about 2.1 – j0.0001. Therefore, if the permittivity is low (below 3.0), then there is a good chance that the dielectric loss factor measured with an open-ended coaxial line is inaccurate.

For characterization of a low-loss dielectric, it is better to use high-*Q* resonant cavities, instead of the open-ended coaxial line. The cavity measurements rely on bandwidth to account for losses, and due to loose coupling between the cables and the cavity, cable losses do not affect the measurement.

6.3.4 Factors in performance optimization of open-ended coaxial lines

In the previous section it was mentioned that cable losses are one of the limitations of open-ended coaxial probes. An improvement in cable losses would result in better accuracy for the measurement of low-loss dielectrics,

and when the probe is used as an industrial sensor it would have more sensitivity for the process parameter being monitored. The influence of various variables on the final sensitivity of open-ended coaxial probes was studied [26] and the results obtained can be used as guidelines for the design of open-ended coaxial probes.

To study this issue further, we will start with Ramo et al. [27], who give a formula for total coaxial transmission line losses. After a slight modification the equation becomes:

$$\alpha = \frac{R_s\sqrt{\varepsilon_r'}}{2b\eta}\left[\frac{1+\frac{b}{a}}{\ln\left(\frac{b}{a}\right)}\right] + \frac{\pi f \varepsilon_r''}{C\sqrt{\varepsilon_r'}} \tag{6.10}$$

The first term on the right-hand side represents metal losses and the second term losses due to the cable dielectric filling the annular region between the center and outer conductors. In Eq. (6.10) α is the total cable losses in nepers/m, R_s is the surface resistivity of the cable metal, constant $\eta = 377\,\Omega$ is the impedance of free space, $C = 3 \times 10^8$ m/s is the speed of light in free space, $\varepsilon_r' - j\varepsilon_r''$ is the complex permittivity of the cable dielectric, and a and b are inner and outer radii of the cable according to geometry shown in Figure 6.5. To calculate losses in dB/m, the result of Eq. (6.10) should be multiplied by a factor of 8.686.

First, looking at metal losses, which are usually the dominant form of cable losses, the first obvious reduction of cable losses is made when the outer radius b is increased. This means that larger cable diameter improves the cable losses proportionally, which is an important point in dielectric characterization and monitoring; that availability of a larger sample size to accommodate a larger cable would result in a more accurate dielectric loss measurement.

Second, when a mathematical optimization is performed on the ratio b/a, it shows that $b/a = 3.6$ is where the metal losses are at a minimum. It turns out that if this ratio is used, for $\varepsilon_r' = 2.1$, which is the dielectric constant of polytetrafluoroethylene (PTFE), the characteristic impedance of the cable is close to 50 Ω, which is the reason for this figure being used historically for PTFE-filled coaxial cables.

The second term on the right-hand side of Eq. (6.10) relates to cable losses due to the dielectric. Obviously, to minimize cable losses it would be best to use no dielectric if at all possible. Bianchi et al. [25], for their industrial

sensor, have used air dielectric with a thin plastic sheet to prevent the sample from going into the annular region of the sensor to protect the interior of the sensor from the sample.

6.3.5 Application example: miniature open-ended coaxial probes for dielectric spectroscopy

McLaughlin et al. [13] have used open-ended coaxial probes for dielectric spectroscopy of human liver for the assessment of fatty liver disease and its relationship to transplant survivability outcomes. This medical application, due to its invasive nature, requires the use of very small submillimeter coaxial-line probes. This would allow the sensor to directly contact the tissue for precise sensing while causing minimal tissue damage. The probe system allows the use of a very wide spectrum of frequencies from 500 MHz to 40 GHz in order to obtain the optimum information from the tissue in a short invasive test. This feature shows the great advantages of the TEM mode in general, and the coaxial configuration in particular, for material investigations.

The idea is to use the dielectric properties measured by the open-ended coaxial probe to determine the type of tissue. A vector network analyzer is utilized to measure the impedance, and the dielectric properties were determined using inverse methods as discussed in Section 6.3.2. Referring to Figure 6.5 for the geometry, the inner conductor has a radius of $a = 0.065$ mm and a dielectric radius of $b = 0.203$ mm, and an outer conductor radius of $c = 0.355$ mm.

A cone-shaped probe tip [13] has been used, as shown in Figure 6.6. The advantage of cone-shaped and pencil-type probes [28] over conventional flat open-ended coaxial lines is that they reduce the possibility of gaps between the probe and the tissue, which could cause large errors in the dielectric characterization. A further advantage is that they make the penetration into the tissue less damaging. Since analytical solutions for the cone-shaped probe do not exist, McLaughlin et al. [13] have used a numerical method for analysis and extraction of dielectric parameters. Another example of the use of cone-shaped open-ended coaxial probes is shown in Figure 6.7 [28], which shows a comparison between analytical and calibrated microwave measurements of bovine fat liver.

6.3.6 Extended coaxial-line (monopole antenna) applicators

A monopole applicator or probe composed of a coaxial line with extended center conductor is shown in Figure 6.8. The structure of this type of applicator/probe is akin to the monopole antenna, but the application and analysis

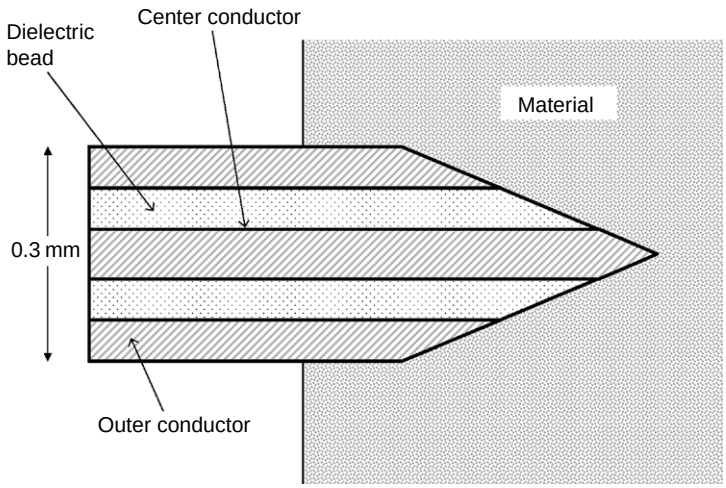

FIGURE 6.6
Cone-shaped open-ended coaxial probe allows for penetration into a soft body, such as the human liver, without air gaps. (After McLaughlin et al. [13].)

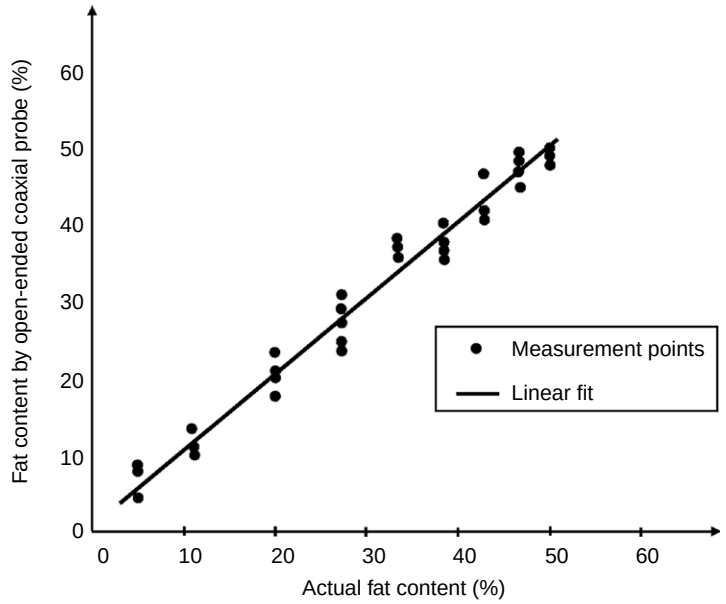

FIGURE 6.7
Measurement of fat content of bovine liver by conical coaxial line. (After Keam and Holdem [28].)

are radically different due to the near-field nature of field interaction with the material.

The extended coaxial applicator has a much larger field of view, but if the length is comparable to the operating wavelength it may be more susceptible to radiation. An exception is cases where the material under study

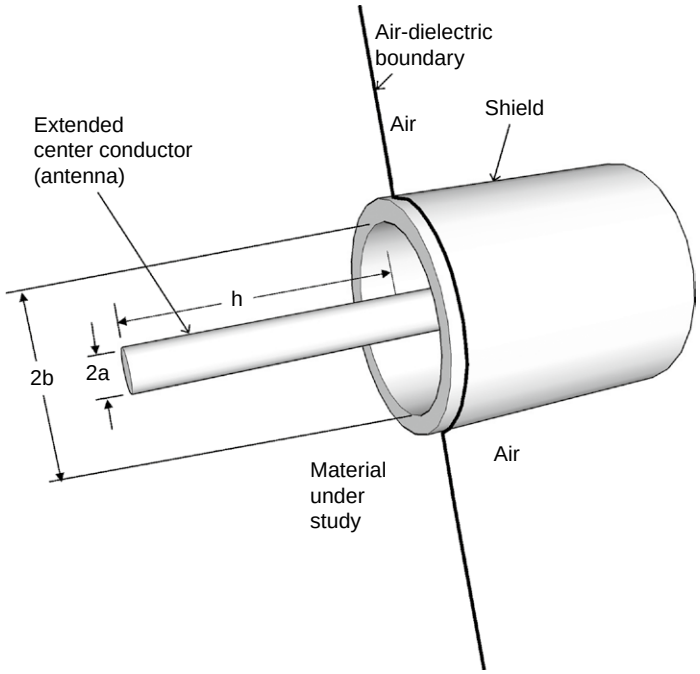

FIGURE 6.8
Coaxial probe/applicator with extended center conductor (monopole applicator) has a larger volume of field interactions with the material than flat open-ended coaxial probe.

or processing has a very high loss, where the dielectric losses dominate over radiation. In measurement applications the radiation causes reflections from nearby objects that cause error [9]; generally the length of the extension needs to be kept much below one-quarter of the wavelength.

There are several applications for this structure. Misra [29] has studied medical applications as a probe and Rhattoy et al. [30] as an applicator. Furthermore, Jerby et al. [31] have developed the structure as a microwave drill, which we will cover as an application example later. On a much larger physical scale, the monopole applicator is considered for in situ heating of shale for fuel exploration purposes [32,33].

The equivalent circuit of the extended coaxial probe/applicator is shown in Figure 6.9. There are two resistive components: R_{heat}, which is responsible for the electric field in the adjacent area to the probe, and R_{rad}, which is the component associated with radiation from the probe. Both these components are involved in deposition of energy to the medium. There is also a reactive component X_{D}, which is capacitive for electrically short center conductor extension, but can become inductive if the electrical length is significantly longer than a quarter wavelength in the medium under consideration.

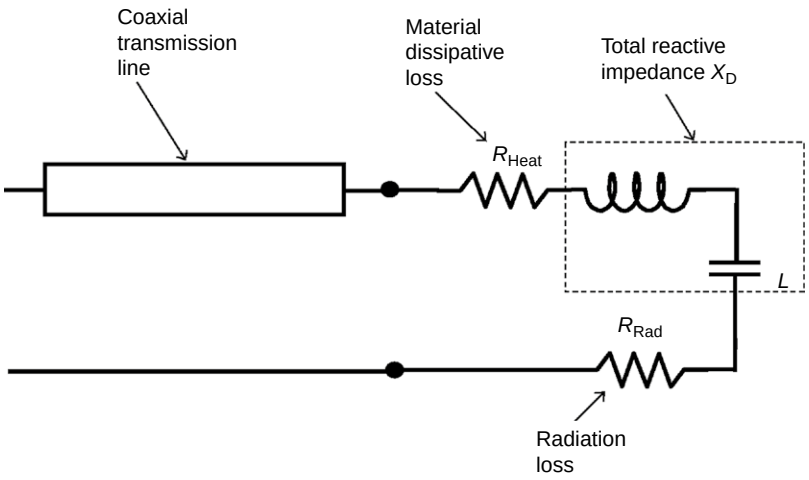

FIGURE 6.9
A simplified equivalent circuit for the extended coaxial line probe/applicator.

The following approximate formulae can be used to calculate each of these components [31]:

$$R_{rad} \approx 10\frac{k}{\beta}L_{eq}^2\left\{1 + 0.133\left[1 - \left(\frac{\alpha}{\beta}\right)^2\right]L_{eq}^2 + 0.02\left[1 - 6\left(\frac{\alpha}{\beta}\right)^2 + \left(\frac{\alpha}{\beta}\right)^4\right]L_{eq}^4\right\} \quad (6.11)$$

The resistive component due to absorption by the material (heating) is:

$$R_{heat} = \frac{k}{\beta}\frac{K_a}{1 + \left(\frac{\alpha}{\beta}\right)^2}\frac{A(1 + B^2) + \frac{\alpha}{\beta}B(1 - A^2)}{A^2 + B^2} \quad (6.12)$$

and the reactive component of the impedance is:

$$X_D = \frac{k}{\beta}\frac{K_a}{1 + \left(\frac{\alpha}{\beta}\right)^2}\frac{\frac{\alpha}{\beta}A(1 + B^2) - B(1 - A^2)}{A^2 + B^2} \quad (6.13)$$

assuming the probe is inserted in a medium with complex relative dielectric constant $\varepsilon_r' - j\varepsilon_r''$ at a free space wavelength of λ. In the above

equations α and β are the decay factor and the wave number in the medium, respectively:

$$\alpha = k\sqrt{(\sqrt{1+x^2}-1)\varepsilon_r'/2} \tag{6.14}$$

$$\beta = k\sqrt{(\sqrt{1+x^2}+1)\varepsilon_r'/2} \tag{6.15}$$

where $x = \tan\delta = \varepsilon_r''/\varepsilon_r'$ is the loss tangent of the medium and $k = 2\pi/\lambda$ is the free space wave number. The extended center conductor (the antenna's) equivalent length L_{eq} is approximately defined as:

$$L_{eq} \approx \beta h\{1 + 0.19/[\ln(h/a) - 0.81]\} \tag{6.16}$$

and $K_a = 60[\ln(h/a) - 1]$ is the "average" characteristic impedance of the extended center conductor antenna in free space. The other parameters are $A = \tan h[(\alpha/\beta)L_{eq}]$ and $B = \tan L_{eq}$. In this model the assumption is that $h/a \gg 10$ and the electrical length of the extended center conductor is smaller than half wavelength in free space ($\beta h \leq \pi/2$).

The above formulation is written as a Mathematica™ notebook in Appendix A6.2 together with a numerical example.

6.3.7 Application example: microwave drill

An example of the practical use for a coaxial applicator with extended center conductor is the microwave drill developed by Jerby et al. [31] shown in Figure 6.10. The microwave drill takes advantage of certain materials with thermal runaway properties. The applicator, which is powered by a small 700 W magnetron, will cause a "hot spot", which is an area of high E-field intensity, in the immediate vicinity of the extended center conductor. This will lead to a thermal runaway and a hole is developed due to melting at high temperatures. The advantage of this method for drilling a hole is that some materials with thermal runaway properties have very high melting points and, in addition, because of hardness are difficult to drill into using conventional mechanical methods. The capability of this method for drilling into various ceramics, glass, silicon [34], and bones for surgical applications has been demonstrated [35].

An example [31] has been worked out, where the inner conductor radius $a = 1$ mm, outer conductor radius $b = 5$ mm, and the length of the extended center conductor varies from 0 to 16 mm at a frequency

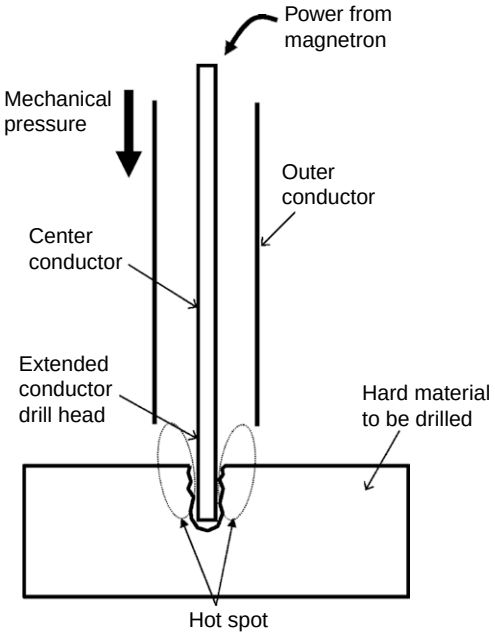

FIGURE 6.10
The arrangement of a microwave drill based on an extended open-ended coaxial line.

2450 MHz. The material to be drilled into is mullite, which has the complex dielectric properties of $6.1 - j0.08$ at room temperature. The numerical results of this example are shown in the Mathematica™ [36] notebook of Appendix A6.2.

In the silicon drilling example [34], in addition to the microwave drill, an optical technique based on the Fabry-Pérot effect illuminated by In–GaAs lasers is used for measuring the temperature. Silicon samples of $\sim 2 \times 2\,\text{cm}^2$ area were radiated in an air atmosphere by a microwave drill operating at 2.45 GHz in the range of 20–450 W. The experimental results indicate heating rates of ~ 150 K/s and a temperature range of 300–900 K across the silicon sample during the microwave heating process. Further operation of the microwave drill caused local melting of the silicon samples.

6.3.8 Industrial material measurements using resonant coaxial probe

In many industrial applications of dielectric sensors, such as instantaneous on-line moisture measurement, the open-ended coaxial probe can be quite advantageous [8]. The techniques for dielectric characterization as discussed in Section 6.3.2 can be employed for this purpose. The laboratory

method uses the vector network analyzer (VNA) to perform reflection measurements, but this method is not suited for industrial applications due to the expense and difficulties associated with adapting a network analyzer to an industrial setting. Moreover, such a method requires a very accurate characterization of the probe for calibration.

To resolve these issues, the resonant method shown in Figure 6.11a has been devised [8,9]. The structure is composed of a section of a coaxial transmission line that is open at one end for material interactions, and is shorted at the other end to form a quarter wavelength resonator. Bianchi et al. [8] used a resonator that, when empty, had the resonant frequency in the range of 600–680 MHz, with an unloaded quality factor of 500, and was used for moisture measurements of powder products. Figure 6.11b shows a typical swept frequency response, which has two measurable parameters, the resonant frequency and the quality factor (or insertion loss at the resonant frequency). Both these parameters can be measured without the need for the vector function of a network analyzer. A relatively simple circuitry can accomplish this task [8].

The sensor's dedicated circuitry allows the measurement of the moisture content in sand layers of up to 10 cm thickness in less than 1 second with accuracy up to 0.1%. Using a circuit model that is similar to Figure 6.1 for calibration, in situ calibration without a priori knowledge on the dry powder permittivity and with just three known moisture levels can be done. This type of calibration allows very practical and effective use of the sensor without the need for accurate and complex permittivity measurements. Figure 6.12 [25] shows swept frequency responses for three moisture levels for the powder.

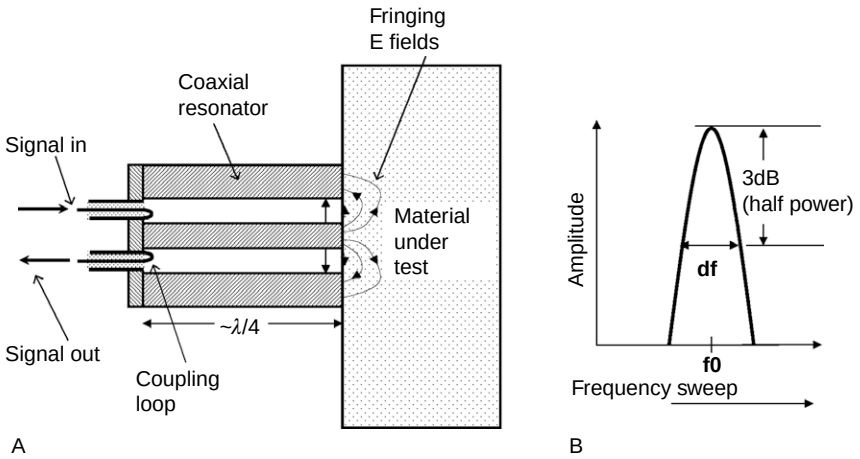

FIGURE 6.11

A resonant open-ended coaxial line is used as an industrial sensor. (A) The arrangement and field configuration. (B) The resonance curve from the insertion loss display on a network analyzer.

6.3.9 Application example: microwave microscopy with focused open-ended coaxial transmission lines

Microwave microscopy, which is based on a focused open-ended coaxial probe, is a method for mapping of planar samples where the variations in the dielectric properties in two dimensions are examined with high resolution [37–41]. The applications of microwave microscopy include mapping of small material property variations on a dielectric plane including flaw or crack detection.

While there are different designs, a microwave microscope is typically composed of a thin metallic probe that scans a planar object, and is connected to a microwave resonator. The probe, in effect, picks up small variations in dielectric properties of the object under examination and modifies the resonant properties of the resonator. These modifications are characterized by variations in the resonant parameters of the resonator, which can be measured with great precision. These resonant parameters are typically the resonant frequency and the quality factor.

A microwave coaxial microscopy probe, as shown in Figure 6.13, consists of a quarter wavelength resonant coaxial probe where the center conductors narrow to a sharp tip of 50–100 mm. A sapphire disk with a center hole of a size close to the diameter of the probe tip and a metal cover layer are used as radiation shield to keep the Q of the resonator high. The electric field at the probe tip interacts with the material in its immediate vicinity. This interaction changes the resonant frequency and Q factor of the resonator. A swept

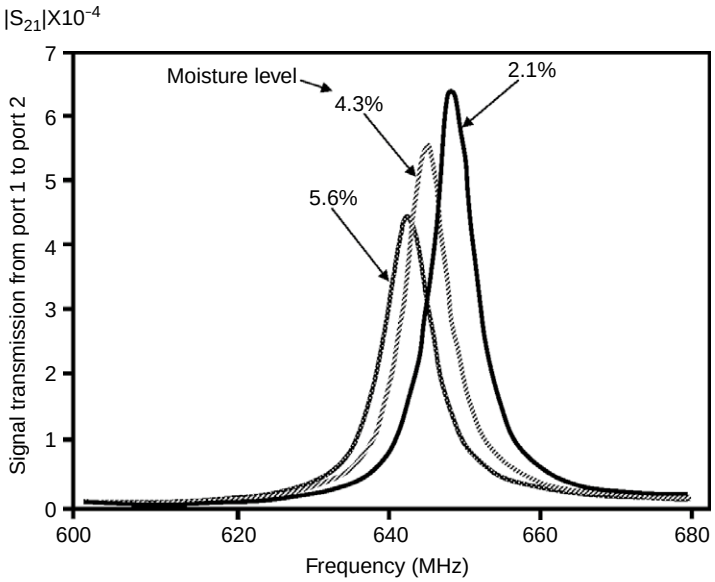

FIGURE 6.12
Insertion loss resonant curves from the open-ended coaxial resonator for three moisture levels. For higher values of moisture level both the quality factor and the resonant frequency of the resonator decrease, which can be used for measurement of moisture after proper calibration. (After Bianchi et al. [25].)

FIGURE 6.13
Arrangement of a coaxial microwave microscope.

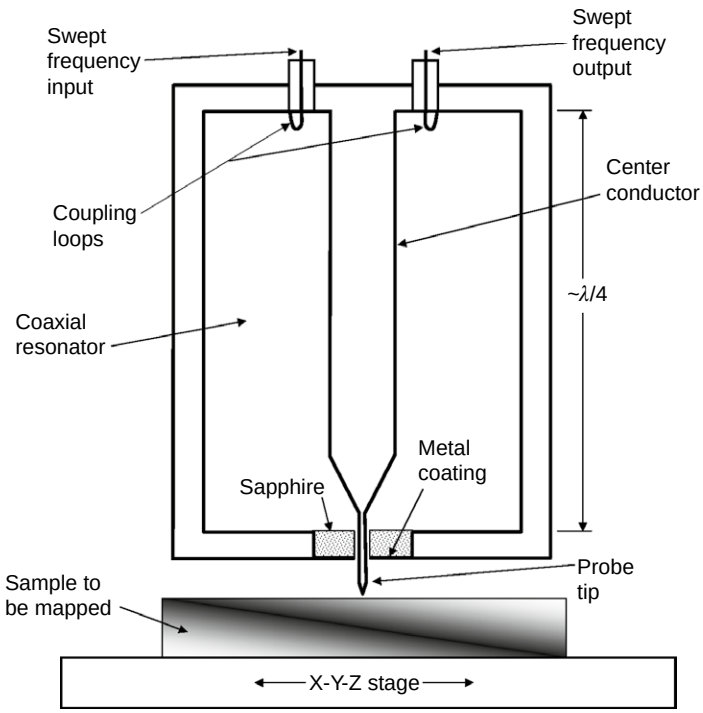

frequency system, such as a network analyzer, keeps track of the variations of the resonant properties.

6.4 OPEN-ENDED WAVEGUIDE, HORN, AND CAVITY APPLICATORS

So far in this chapter we have discussed open-ended probes and applicators that are based on TEM-mode transmission lines. These include strip transmission lines in Section 6.2 and coaxial transmission lines in Section 6.3. In this section we will cover open-ended applicators and probes that are based on non-TEM (TE or TM) transmission lines.

From a practical standpoint, the most important distinction between waveguide-type and coaxial-type open-ended applicators is the electrical size of the material under study or processing. In coaxial-type probes the dimensions of the coverage volume (field of view) are much smaller than the operating wavelength, while in waveguide and non-TEM types the material is comparable in size or larger than the operating wavelength.

We will start with the open-ended waveguides, and then will discuss horn applicators and finally dielectric-filled cavity applicators.

6.4.1 Open-ended waveguides as near-field applicators and probes

Open-ended waveguides [42–47], when used as near-field applicators or sensors for material interaction applications, have found a number of applications in thermography, medical diathermy and hyperthermia, and material measurements and characterizations. The advantage of open-ended waveguides over the coaxial types is larger cross-section for the same operating frequency. The larger cross-section treats a larger area, and often provides a deeper penetration depth. There is also less sensitivity to air gaps.

Figure 6.14 shows the arrangement of an open-ended rectangular waveguide used as a near-field applicator and sensor, together with the geometrical parameters and the coordinate system used here. While circular waveguides can also be used, most applications use a waveguide in the TE_{10} mode of operation. This is also the mode that is most often used in other applications of waveguides and most standard commercial waveguides are made for primary use in this mode.

Computation or measurement of the complex aperture admittance for open-ended waveguides is critical in their use as both an applicator and as a probe. As an applicator, the admittance can be used for predicting the refection performance of the system for impedance matching. As a probe, the admittance information can be used for characterization of material using numerical techniques [48].

Referring to the terminology shown in Figure 6.5, Lewin [49] has derived the following integral equation for a rectangular open-ended waveguide radiating into a half-space dielectric medium with the complex dielectric constant of $\varepsilon_r = \varepsilon_r' - j\varepsilon_r''$:

$$Y = G + jB = \frac{2j}{\pi a b k_1}\int_0^a\int_0^b (b - x)\left[K_2(a - y)\cos\frac{\pi y}{a} + \frac{a}{\pi}K_1\sin\frac{\pi y}{a}\right]G_e\,dy\,dx \tag{6.17}$$

where G and B are the conductance and the susceptance of the aperture, a and b are the broad and narrow dimensions of the waveguide cross-section respectively, and k_1 is the dominant mode wave number given by:

$$k_1 = \sqrt{k_0^2 - \left(\frac{\pi}{a}\right)^2} \tag{6.18}$$

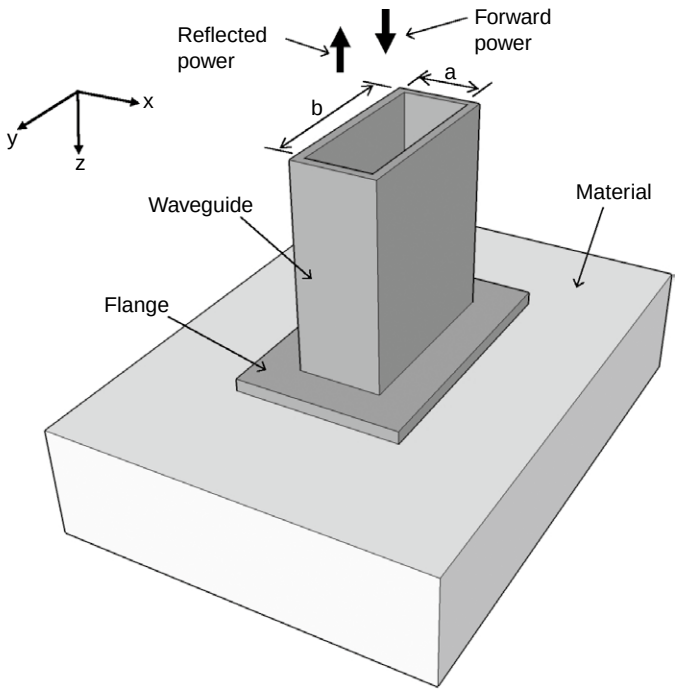

FIGURE 6.14
An open-ended waveguide is used for heating or characterization of materials. The flange is necessary when an analytical method is used for calibration in dielectric characterization. Analytical methods assume the presence of the flange.

with $k_0 = 2\pi/\lambda_0$ is the free space wave number. The parameters K_1 and K_2 are given by:

$$K_1 = k_r^2 + \left(\frac{\pi}{a}\right)^2 \quad \text{and} \quad K_2 = k_r^2 - \left(\frac{\pi}{a}\right)^2 \tag{6.19}$$

and

$$k_r = k_0\sqrt{\varepsilon_r} \quad \text{and} \quad G_e = \frac{1}{r}e^{-jk_r\sqrt{x^2+y^2}} \tag{6.20}$$

The solution to Eq. (6.17) is found with Mathematica™ software [21], and the code (Mathematica "notebook") with proper explanations is shown in Appendix A6.3. Figure 6.15 shows the field intensity distribution of an open-ended waveguide [47].

6.4.2 Horn applicators

Horn applicators [50–52] are, in essence, a variety of open-ended transmission-line applicators, where a section of the transmission line closest

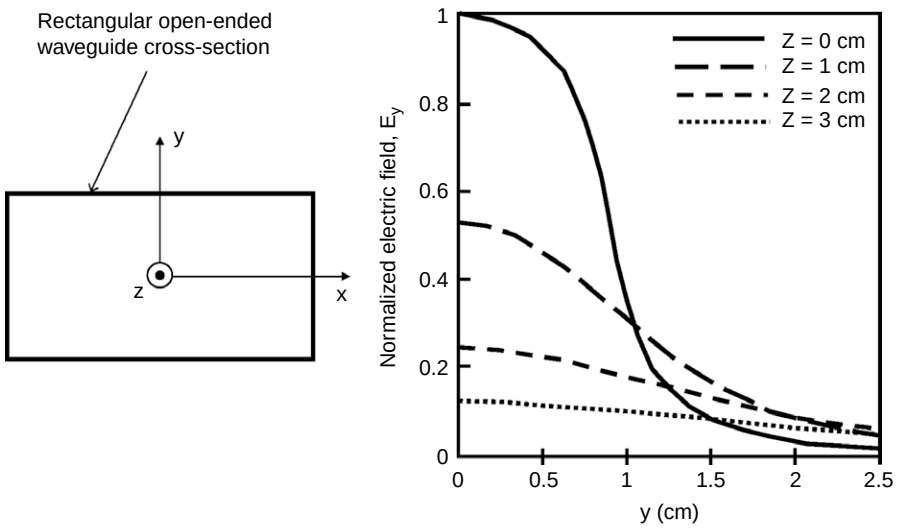

FIGURE 6.15
Electric field distribution from an open-ended waveguide along the y-axis. (After Habash [47].)

to the load is flared out so that the open end is larger in dimensions than the cross-section of the transmission line. Horn applicators offer specific advantages and are used in a variety of applications, both as sensor head devices and heating applicators. The rectangular waveguide horn, as shown in Figure 6.16, is the most frequently used type of horn applicator.

A major difference between simple open-ended applicators and horns is related to the penetration of fields into the material. In open-ended transmission lines the depth of penetration is often limited by the geometry of the open end, i.e. when the cross-section is small, the fringing-field penetration is limited. In horn applicators, however, a single-mode propagation inside the transmission line is often turned into a multimodal or plane wave propagation, and the depth of field penetration would only be limited by the material's D_p, as given by the penetration equation (Eq. (1.32)).

In addition to the "taper" advantage, there is another factor that enhances the signal or power transfer, which is inherent in a larger aperture of a horn applicator. This is realized by considering Eq. (6.4), where the E-field requirements for transfer of a certain amount of power into the material load are calculated. The two parameters w and h represent cross-sectional dimensions of the open end touching the material. They are both at the denominator, which means having them larger means smaller E-field requirements, and thereby a better match to the E field within the transmission line, which means a better impedance match. A lower E-field requirement also means a lower intensity of "feed point" hot spot, which is often a big problem in microwave heating applications when the material is close to the load.

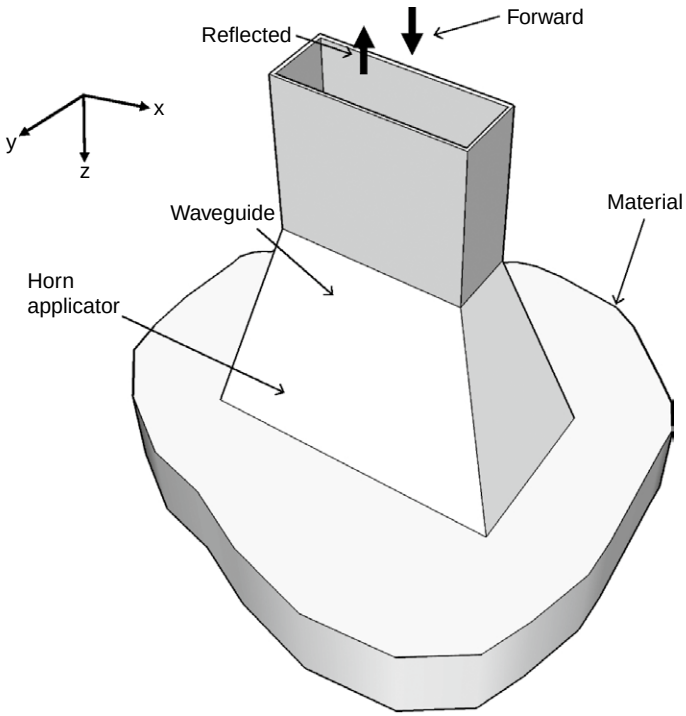

FIGURE 6.16
Arrangement of a horn applicator and the process material.

One of the most traditional applications of horn applicators is microwave moisture measurements [50], where the horn applicators are used for sending and receiving the electromagnetic signal through the wet dielectric load. In industrial heating applications at microwave frequencies horn applicators are often utilized to feed microwave power into a microwave multimode cavity with lossy loads [51], particularly when the load fills a substantial part of the cavity. The advantage of such an arrangement over waveguide-fed cavity methods is that the hot spot associated with the feed area is minimized. Such an arrangement would heat only one side of the load. In industrial settings a multi-feed arrangement with horn applicators is used, where alternate horn feeds heat the load on both sides.

An application example of horn applicators is for de-infestation of a wooden beam from woodworm [53], where a dual polarized circular horn applicator is developed. This makes the existence of two orthogonal modes of field application possible. Each mode can be fed independently from a microwave source, giving a 2 kW applicator using two low-cost 1 kW magnetrons.

6.4.3 Array and lens applicators

Simple open-ended waveguide applicators suffer a distinct disadvantage in certain medical heating applications because of the tendency to overheat the area closest to the applicator, and under-heat areas deep within the material. In microwave hyperthermia of malignant tissues, which are often deep below the skin, these need to be heated to a few degrees above the normal body temperature. Array and lens applicators are designed to overcome this problem by focusing the fields to locations away from the applicator head using phase shifting of multiple beams coming from several apertures [54–57].

One of the more successful methods is the water-loaded lens applicator shown in Figure 6.17. The applicator head, which is attached to the end of a waveguide, has several vertical metal plates as shown in Figure 6.17a. The phase of the waves guided between the metal plates is shifted based on the longitudinal length of each plate. With proper design of these plates, the beams coming out of each window are added constructively to create an "optical" focus at a desired distance from the open end.

A flow of water within the applicator head would serve two purposes: first, because water has high dielectric constant of about 80, it would create a medium where the wavelength is about nine times smaller than the free space wavelength. This would make the width between the metal plates adequate so that each one is a waveguide above cutoff frequency. The second utility of the water flow is cooling. It should be noted that because of the great attenuation of microwaves in water, the efficiency of such applicators is very small. In other words, most of the microwave energy is dissipated in the cooling water. On the other hand, the energy requirement for heating the tissue is very modest, since it has to be heated by only a few degrees in order to be effective for treatment. For example, of 1000 W provided by the magnetron, only a few watts are actually deposited in the tissue. Therefore in this method efficiency is sacrificed for a proper field pattern.

The results are shown in Figure 6.18, where the electric field intensity versus the distance from the applicator is plotted, and in Figure 6.19, where the temperature elevation versus the distance for another case is given. In both these figures the patterns are compared with simple open-ended waveguides. Note that in Figure 6.19 the temperature rise at very shallow depths is low because of water cooling, but the maximum temperature is sent deeper into the tissue with the lens applicator. There are several other methods to implement array and lens applicator principles. One prominent example is the use of dielectric blocks [56], which improves the heating pattern even further.

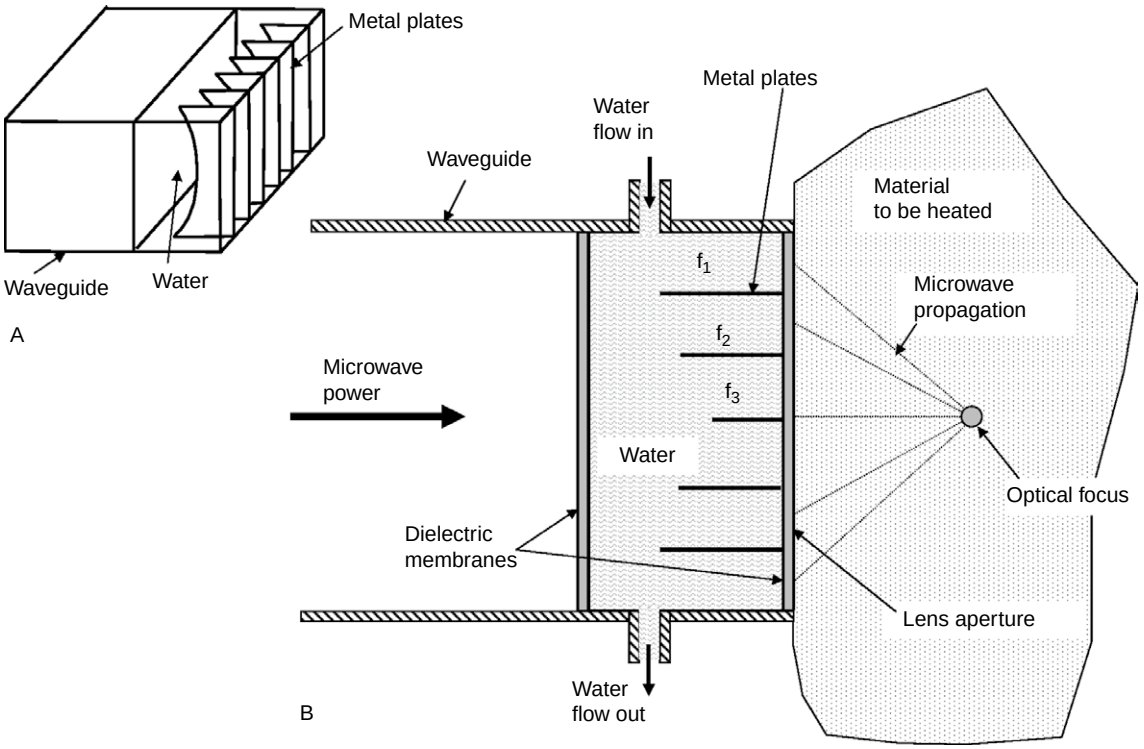

FIGURE 6.17 *(A) A general view of the water-loaded lens applicator. (B) The top view of the applicator where the metal plates divide the waveguide's open end into several apertures. The field from these apertures is combined to focus the microwave energy in an area away from the applicator head.*

6.4.4 Over-moded dielectric-filled open cavity applicators

In some instances it is useful to have a resonant microwave cavity where one of the walls is removed and replace it with a material for microwave heating. Such a method would be problematic in practice because the removal of one of the walls would disturb the surface currents and take the cavity out of its intended mode. In essence, the cavity stops operating as a cavity, and because of radiation to the environment will have a very low Q.

To overcome this limitation, Sinclair et al. [58,59] have devised a ceramic-loaded evanescent cavity shown in Figure 6.20. This is a rectangular cavity where one of the small walls has been removed. In turn, most of the cavity is filled with a ceramic piece that leaves a small portion of the length adjacent to the open wall unfilled. The ceramic has a high relative permittivity ε_r', which would decrease the effective wavelength within the

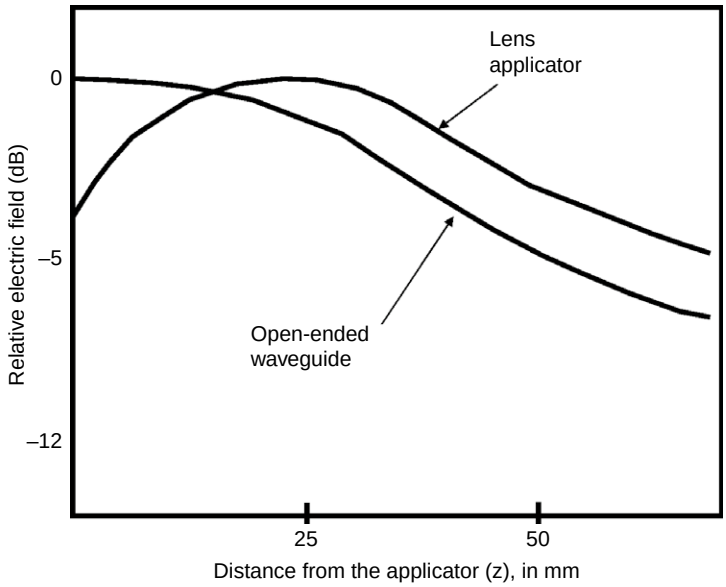

FIGURE 6.18
Electric field intensity versus distance for the lens applicator. Medium: muscle model. (After Nikawa et al. [55].)

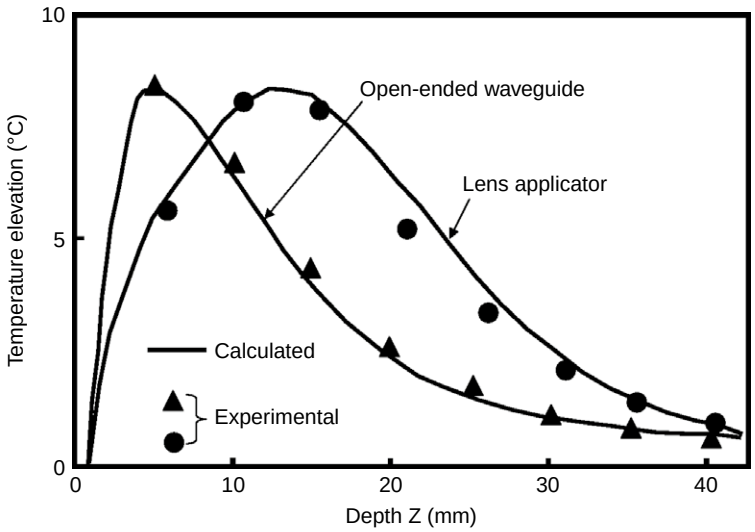

FIGURE 6.19
Temperature elevation versus depth at 2450 MHz by a lens applicator and a waveguide applicator. Surface temperature is kept at room temperature via water cooling. (After Nikawa et al. [56].)

ceramic-filled portion of the cavity by a factor of $\sqrt{\varepsilon_r''}$. A low-loss ceramic such as barium titanate is chosen to minimize any self-heating and to keep the quality factor (Q) of the cavity high.

As a result the cavity can have higher-order modes at a given frequency than prior to the insertion of the ceramic piece. At the interface between

the ceramic and air the fringing fields of the ceramic-filled portion penetrate the unfilled portion and create an evanescent field that cannot propagate far into the air, since the unfilled section is a waveguide below cutoff for the operating frequency. The unfilled portion therefore becomes a site where a small dielectric load can be heated while the cavity resonance maintains its high quality factor because radiation to the surrounding environment is minimal.

The intended application of the ceramic-filled open cavity is microelectronic manufacturing. A vast majority of adhesive materials currently used in that industry are cured using infrared, UV curing or convection heating. These conventional thermal processing steps (especially convection heating) can take up to several hours to perform and result in slow throughput and high cost of packaging. They are also inadequate for devices and materials that require a low thermal power budget like organic light-emitting polymer diodes (OLEDs). With the demand for lighter, faster, and smaller electronic devices, the ceramic-filled open cavity can answer these demands.

The operating mode is to place the unfilled portion of the open cavity directly above a flip-chip or wafer-scale bonder, as shown in Figure 6.20. The open cavity design therefore utilizes RF curing of adhesives used in microelectronics, MEMS, optoelectronics and medical devices packaging, especially for flip-chip, wafer-scale bonding and encapsulation. In addition, it would produce micron-alignment accuracy in bonding of the devices onto wafer or PCBs.

There are a few methods to improve the heating uniformity. One is to use a ceramic with the highest possible relative permittivity while maintaining a low loss. This would result in higher mode numbers in the filled section of the cavity, which results in a more uniform fringing field in the unfilled section that contains the heating part. The second method to improve the uniformity is by sweeping across a range of frequencies so that different modes are excited at each frequency, which would result in a uniform average heating into the load.

As an example, Sinclair et al. [58] have built a cavity with the following dimensions: 24 mm × 24 mm × 110 mm. The cavity is excited with the TM_{334} mode. A ceramic material with a relative permittivity of 6 is inserted into the cavity. A small air gap of 0.7 mm length is located 82.5 mm from the coupling probe in the base of the cavity. The gap position corresponds to the position of one of the longitudinal electric field maxima within the dielectric. Since the gap is small compared to the physical length of the field variation through the longitudinal axis, the normal field is relatively continuous through the gap, ensuring good field penetration into the upper part of the dielectric to be heated.

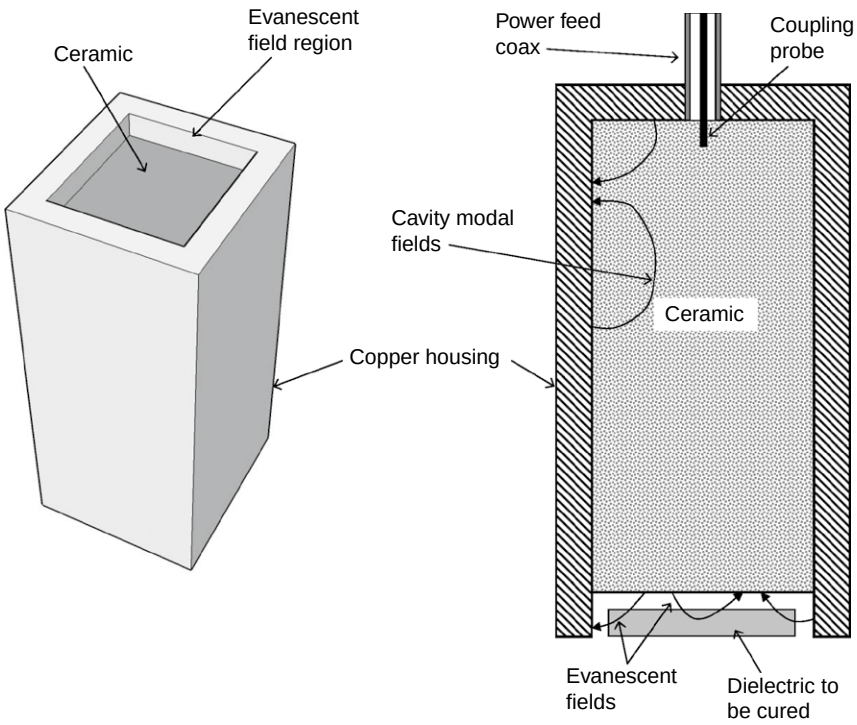

FIGURE 6.20
Over-moded ceramic-filled open-ended cavity for heating of small planar loads in electronic curing applications.

REFERENCES

[1] R.E. Collin, Foundations of Microwave Engineering, second ed., IEEE Press, New York, 2001.

[2] S. Ramo, et al., Fields and Waves in Communication Electronics, third ed., Wiley, New York, 1994.

[3] T.W. Athey, M.A. Stuchly, S. Stuchly, Measurement of radio-frequency permittivity of biological tissues with an open-ended coaxial line: I, IEEE Trans. Microwave Theory Tech. 30 (1982) 82–86.

[4] J. Herza, et al., TEM wave applicators with large effective aperture, 15th International Conference: Radioelektronica, Prague, Czech Republic, 2005. Available at: http://www.urel.feec.vutbr.cz/ra2008/index.php?page = archive05.

[5] S. Ramo, et al., Fields and Waves in Communication Electronics, third ed., Wiley, New York, 1994, pp. 216, 279.

[6] C. Gao, et al., Quantitative microwave near-field microscopy of dielectric properties, Rev. Sci. Instr. 69 (1) (1999) 3846–3851.

[7] S.S. Stuchly, et al., A new aperture admittance model for open-ended waveguides, IEEE Trans. Microwave Theory Tech. 42 (2) (1994).

[8] G. Bianchi, et al., A microwave system for moisture monitoring in wet powders for industrial applications, IEEE MTT-S Digest (1999) 1603–1606.

[9] E. Nyfors, P. Vainikainen, Industrial Microwave Sensors, Artech House, Norwood, MA, 1989.

[10] E. Nyfors, Industrical microwave sensors – a review, Subsurface Sens. Technol. Appl. 1 (1) (2000).

[11] Agilent Dielectric Probe Kit. http://www.home.agilent.com/agilent/product.jspx?pn = 85070E&NEWCCLC = USeng.

[12] C.L. Pournaropoulos, D.K. Misra, The Co-Axial aperture electromagnetic sensor and its application in material characterization, Meas. Sci. Technol. 8 (1997) 1191–1202.

[13] B.L. McLaughlin, et al., Miniature open-ended coaxial probes for dielectric spectroscopy applications, J. Phys. D Appl. Phys. 40 (2007) 45–53.

[14] D. Blackham, et al., An improved technique for permittivity measurements using a coaxial probe, IEEE Trans. Instrum. Meas. 44 (1997) 1023–1029.

[15] P. de Langhe, et al., Measurement of low-permittivity materials based on spectral-domain analysis for the open-ended coaxial probe, IEEE Trans. Instrum. Meas. 42 (1993) 879–886.

[16] A. Gregory, et al., RF and microwave dielectric measurements upon layered materials using a reflectrometric coaxial sensor, National Physical Laboratory Report, DES, Vol. 125, UK, 1993.

[17] L. Anderson, et al., Analysis of an open-ended coaxial line sensor in layered dielectrics, IEEE Trans. Instrum. Meas. 35 (1986) 13–18.

[18] S. Bakhtiari, et al., Analysis of radiation from an open-ended coaxial line into stratified dielectrics, IEEE Trans. Microwave Theory Tech. 42 (7) (July 1994).

[19] Y. Xu, et al., Some Calculation methods and universal diagrams for measurement of dielectric constants using open-ended coaxial probes, IEE Proc. H 138 (4) (1991).

[20] H.R. Levine, et al., Theory of the circular diffraction antenna, J. Appl. Phys. 22 (1951) 29–43.

[21] Wolfram Research website: www.wolframresearch.com.

[22] R.J. Riegert, Private communication.

[23] M.A. Stulchy, et al., Measurement of radio frequency permittivity of biological tissues with an open-ended coaxial line: Part II – experimental results, IEEE Trans. Microwave Theory Tech. 30 (1) (1982).

[24] S.I. Ganchev, et al., A novel numerical technique for dielectric measurement of generally lossy dielectrics, IEEE Trans. Instrum. Meas. 41 (3) (1992).

[25] G. Bianchi, et al., A microwave system for moisture monitoring in wet powders for industrial applications, IEEE MTT-S Digest (1999) 1603–1606.

[26] B. Garcia-Banos, et al., Design rules for the optimization of the sensitivity of open-ended coaxial microwave sensors for monitoring changes in dielectric materials, Meas. Sci. Technol. 16 (5) (2005) 1186–1192 Online at: stacks.iop.org/MST/16/1186.

[27] S. Ramo, et al., Fields and Waves in Communication Electronics, third ed., Wiley, New York, 1994, p. 250.

[28] R.B. Keam, J.R. Holdem, Permitivity measurements using a coaxial-line conical-tip probe, Electron. Lett. 33 (1997) 353–355.

[29] D.K. Misra, A study on coaxial line excited monopole probes for in situ permittivity measurements, IEEE Trans. Instrum. Meas. 36 (4) (1987) 154–159.

[30] A. Rhattoy, et al., Coaxial antenna for microwave hyperthermia, J. Electromagn. Waves Appl. 19 (14) (2005).

[31] E. Jerby, et al., Theoretical analysis of the microwave drill near-field localized heating effect, J. Appl. Phys. 97 (2004) article 034909, IMPI Proceedings 2007.

[32] J.A. Cogliandro, European Patent Application WO/2007/078350, 2007.

[33] US Department of Energy Report: Secure Fuel from Domestic Sources, 2007. Available at: http://www.nevtahoilsands.com/pdf/Profiles-of-Companies-Engaged-in-Domestic-Oil-Shale-Tar-Sands.pdf.

[34] R. Herskowits, et al., Silicon heating by a microwave-drill applicator with optical thermometry, Semicond. Sci. Technol. 22 (8) (August 2007) 863–869.

[35] Penn State, www.microwave-drill.com.

[36] www.wolfram.com.

[37] Y.G. Wang, et al., Simultaneous imaging of dielectric properties and topography in a $PbTiO_3$ crystal by near-field scanning microwave microscopy, Appl. Phys. Lett. 76 (22) (2000) 3295–3297.

[38] F. Duewer, et al., Tip-sample distance feedback control in a scanning evanescent microwave probe for nonlinear dielectric imaging, Rev. Sci. Instrum. 71 (6) (June 2000) 2414–2417.

[39] D.E. Steinhauer, et al., Imaging of microwave permitivity, tunability, and damage recovery in $(Ba,Sr)TiO_3$ thin films, Appl. Phys. Lett. 75 (20) (November 1999) 3180–3182.

[40] M.S. Kim, et al., Tip-sample distance control for near-field scanning microwave microscopes, Rev. Sci. Instrum. 74 (8) (August 2003) 3675–3678.

[41] M. Kim, et al., Nondestructive high spacial resolution imaging with a 60 GHz near-field scanning millimeter-wave microscope, Rev. Sci. Instrum. 75 (3) (March 2004) 684–688.

[42] Z. Shen, et al., Applications of anisotropic PML in mode-matching analysis of open-ended waveguides, IEEE Trans. Magn. 38 (2) (2002).

[43] V. Theodoridis, et al., The reflection from an open-ended rectangular waveguide terminated by a layered dielectric medium, IEEE Trans. Microwave Theory Tech. 33 (5) (1985) 359–366.

[44] J. Herza, et al., TEM wave applicators with large effective aperture, Radioelectronica 15th International Conference, 2005. http://www.urel.feec.vutbr.cz/ra2008/index.php?page = archive05.

[45] C. Fray, et al., Reflection analysis of flanged circular waveguide radiating through small aperture into absorbing medium, Electron. Lett. 17 (19) (1981) 718–720.

[46] J. Li, C. Liu, Noncontact detection of air voids under glass epoxy jackets using a microwave system, Subsurface Sens. Technol. Appl. 2 (4) (2001) 411–423.

[47] R.W.Y. HaBASH, Non-invasive microwave hyperthermia, Thesis, Indian Institute of Science, 1994. Available at: http://etd.ncsi.iisc.ernet.in/handle/2005/193?mode = full.

[48] S.I. Ganchev, et al., A novel numerical technique for dielectric measurement of generally lossy dielectrics, IEEE Trans. Instrum. Meas. 41 (3) (1992).

[49] L. Lewin, Advanced Theory of Waveguides, Iliffe, London, 1951.

[50] R.C. Metaxas, et al., Industrial Microwave Heating, Peter Peregrinus, London, 1983.

[51] A.C. Metaxas, Foundations of Electroheat, Wiley, New York, 1996.

[52] V.N. Tran, et al., Microwave heating and field distribution of an infinite cylinder of dielectric material, Mikrowellen HF Mag. 17 (3) (1991).

[53] P.J. Plaza, et al., Dual Polarized Horn Applicator for Open Microwave Systems, Italian Art Restoration Center Technology Center, 2007 www.ciart.it/Biblioteca/dual.pdf.

[54] J. Vrba, et al., Arrays of waveguide applicators for microwave thermotherapy, Progress in Electromagnetics Research Symposium, Hangshou, 2005.

[55] Y. Nikawa, et al., A direct-contact microwave lens applicator with a microcomputer-controlled heating system for local hyperthermia, IEEE Trans. Microwave Theory Tech. 34 (5) (May 1986).

[56] Y. Nikawa, et al., Dielectric-loaded lens applicator for microwave hyperthermia, IEEE Trans. Microwave Theory Tech. 39 (7) (July 1991).

[57] R.C. Gupta, et al., Analysis of the SAR distributions in three-layered biomedia in direct contact with a water-loaded modified box-horn applicator, IEEE Trans. Microwave Theory Tech. 53 (9) (September 2005).

[58] K.I. Sinclair, et al., A novel RF-curing technology for microelectronics and optoelectronics packaging, Electronics System Integration Technology Conference, Dresden, Germany, 2006.

[59] K.I. Sinclair, et al. Open ended microwave oven for flip-chip assembly, Microwave European Conference, 2007, Vol. 9, No. 12, 2007, 620–623, DOI 10.1109/EUMC.2007.4405268

CHAPTER 7

Magnetic Field and Inductive Applicators and Probes at High Frequencies

CHAPTER CONTENTS

INTRODUCTION

In Chapters 2 and 3 we discussed capacitive or *E*-field applicators and probes where the subject material interacts with the electric field nodes (or maxima). In those applicators the electric fields interact with lossy dielectric, since they require a larger electric field intensity to be of practical use. In this chapter, however, we will address *H*-field applicators where the material is placed in the magnetic field node (local maximum). This is the location where the electric field is at its minimum intensity. We discussed these principles of field maxima and minima in more detail in Chapters 1 and 2.

Microwave/RF Applicators and Probes for Material Heating, Sensing, and Plasma Generation

In magnetic field applicator/probes the subject materials may be a conductive material, a plasma body, a ferromagnetic material, or a material subject to the magnetic resonance effect. Regardless of differences in specific applications, the applicator design has many figures of merit in common, which will be considered in this chapter.

We will first discuss the categories of applications and applicator types and their differences in Section 7.1, then in Section 7.2 the fundamentals of magnetic/inductive probe design will be covered. Next, in Section 7.3 we will perform a more detailed study of the solenoid, which is the oldest and most commonly used inductive applicator. We will then cover induction heating, which is a modality of electromagnetic energy deposition into conducive materials, in Section 7.4. Circuit and coupling issues are discussed in Section 7.5 and, finally, in Section 7.6 we will cover some special and recent development in this area.

Due to the extensive range of applications for this type of applicator, a threefold approach is used in this chapter, first to introduce the principles involved, second to broadly describe various types briefly with the use of references, and third to maintain a proper level of detail by focusing on a few of the most common examples.

7.1 *H*-FIELD PROBES: CATEGORIZATION OF APPLICATIONS AND APPLICATOR/PROBE TYPES AT HIGH FREQUENCIES

There are a variety of magnetic/inductive probes covering a wide range of applications. To put these in proper context, we will first categorize them by physics of material–field interactions. Figure 7.1 shows these categories as being the eddy current effect, magnetic hysteresis, and magnetic resonance. Each of these broad categories is divided into more specific applications as shown. These categories are explained in more detail in the following sections.

While very different in construction, the applicator/probe designs for these applications have some figures of merit in common. For example, in all cases where delivery of energy to the material is needed, the energy loss to the applicator/probe must be minimized to obtain the best power efficiency. In cases where the device is used as a probe to obtain information from the material, reducing probe loss will lead to a better signal-to-noise ratio. Another figure of merit that is commonly desired in most applications is field uniformity over an area of interest. This topic will be further discussed later in this chapter.

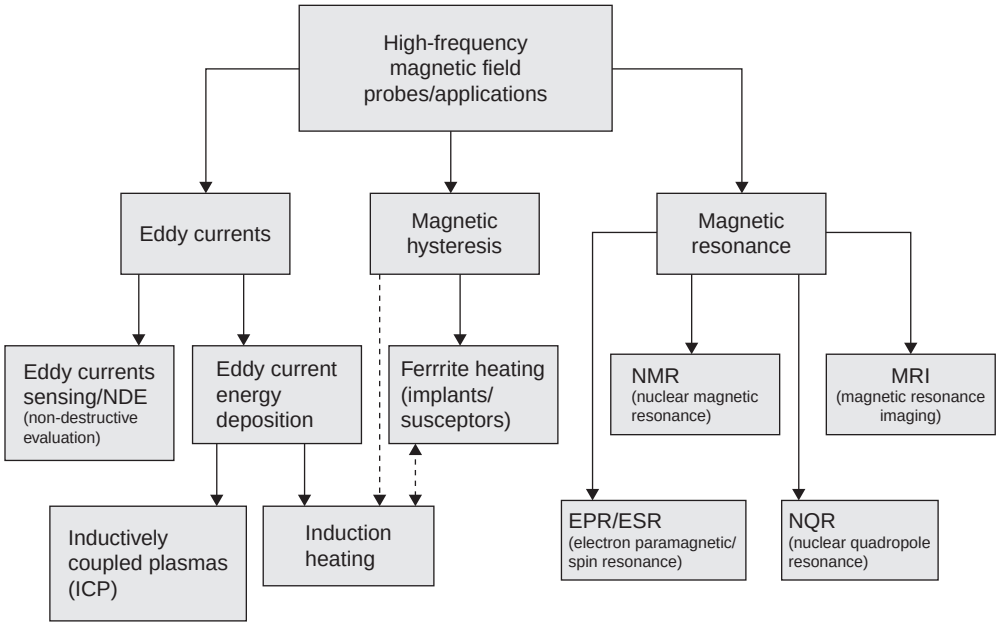

FIGURE 7.1 *Categorization of magnetic/inductive applicator/probes by physics.*

7.1.1 The eddy current effect and its formation

The idea of eddy current induction is the basis for the functioning of most applications of inductive applicators. A prerequisite for the establishment of eddy currents is sufficient electrical conductivity, but the threshold of conductivity depends on parameters such as operating frequency that we will quantify later. Figure 7.2 shows the basic idea, in which a high-frequency current that is established in the applicator creates a magnetic field that interacts with the material. This alternating magnetic field, in turn, induces an electric field in the material. Depending on the material conductivity, this electric field induces a current in the material.

The induction of eddy current is utilized in practice in two ways: energy deposition and material characterization. In energy deposition, which is called induction heating, the resistance of the material to the eddy current flow produces heat according to Ohm's law. In inductively induced plasmas the effect is similar; the plasma body is electrically conductive and an eddy current is formed in it. While in these applications eddy currents are useful, there are many other practical instances where the establishment of eddy currents is undesirable and methods are developed to suppress them. The simplest example is the core of electrical transformers, which are made of thin laminated metal sheets to avoid losses associated with eddy currents.

FIGURE 7.2
A schematic depiction of the eddy current effect.

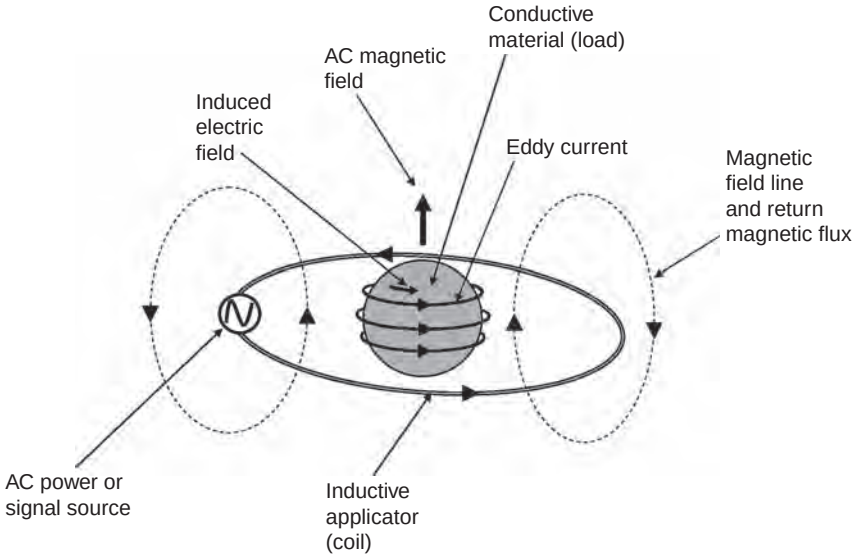

In the class of applications where the inductive effect is used for material evaluation or detection, the eddy current is induced into the material under test. The characteristics of the eddy current flow, such as the amplitude or the direction of the flow, impact on the input impedance of the driving circuit, which in turn provides information about the material's electrical conductivity, any defects, corrosion, etc. This general class of application is one of many methods that are sometimes called non-destructive evaluation (NDE).

In order to examine the impact of a high-frequency magnetic field in forming eddy currents, it is convenient to use the example of a thin cylindrical sheet, as shown in Figure 7.3, which is made of a material with conductivity σ and an alternating magnetic field H_0 that is parallel to the axis of the cylinder [1]. The imposed magnetic field creates an eddy current in J_ϕ, which creates a secondary magnetic field H_z. There is also an electric field E_ϕ established in the material:

$$H_z = J_\phi d = \sigma E_\phi d \tag{7.1}$$

The total magnetic field is the superposition of the original magnetic field and that created by the induced eddy current:

$$H = \widehat{a_z}(H_0 + \sigma E_\phi d) \tag{7.2}$$

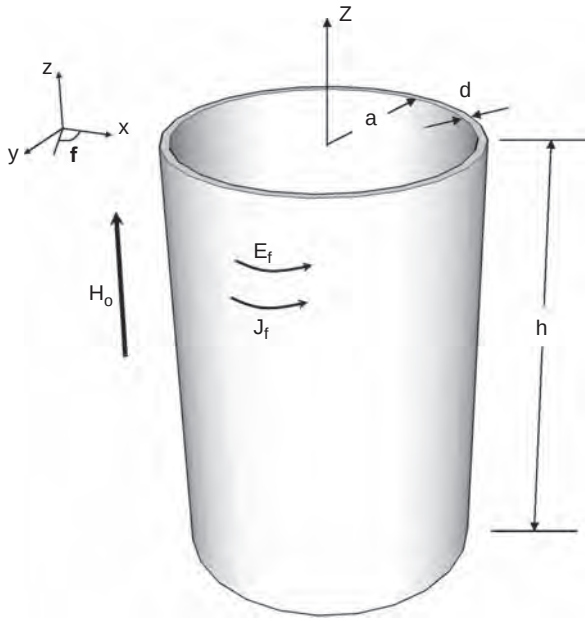

FIGURE 7.3
A thin cylindrical shell made of a conductive material is subject to an AC magnetic field parallel to its axis.

Applying the Faraday law to Eq. (7.2), we obtain:

$$2\pi a E_\phi = -j\omega\mu_0(H_0 + \sigma E_\phi d)\pi a^2 \tag{7.3}$$

Solving for E_ϕ:

$$E_\phi = \frac{-j\frac{\omega a}{2}\mu_0 H_0}{1 + j\frac{\omega\mu_0\sigma a d}{2}} \tag{7.4}$$

Then, from Eq. (7.1) the following governs the relationship between the imposed magnetic field and the resulting eddy current in the shell:

$$J_\phi = \frac{-jH_0 a/\delta^2}{1 + jad/\delta^2} \tag{7.5}$$

where the skin depth δ is:

$$\delta = \sqrt{\frac{2}{\omega\mu_0\sigma}} \tag{7.6}$$

Note that the current density in Eq. (7.5) is a complex quantity, which means there is a phase difference between the imposed magnetic field and the eddy current developed. Finding the absolute value of the complex expression (7.5), the amplitude of the eddy current density becomes:

$$J_\phi = \frac{H_0}{\sqrt{d^2 + \frac{\delta^4}{a^2}}} \tag{7.7}$$

In cases where $\delta >> \sqrt{a\,d}$, which happens in low-frequency, low-conductivity, or thin shells, Eq. (7.7), in combination with Eq. (7.6), simplifies to a linear function:

$$J_\phi = 2\,H_0\,\omega\,\mu\,\sigma \tag{7.8}$$

Under these conditions, the magnitude of eddy current density becomes proportional to field intensity, frequency, and conductivity. This linearity is not valid when the simplifying conditions of this analysis are not met, but the general trend of higher eddy currents for increasing of these parameters still holds.

7.1.2 High-frequency magnetic fields imposed on ferromagnetic materials

In addition to eddy currents established due to conductivity, materials with ferromagnetic properties create another set of phenomena when a high-frequency magnetic field is applied.

In an analogous way to dielectric properties, the ferromagnetic properties of materials at high frequencies can be mathematically modeled by the use of the complex relative permeability, μ_r^*:

$$\mu_r^* = \mu_r' - j\,\mu_r'' \tag{7.9}$$

where μ_r' is the relative permeability and μ_r'' is the magnetic loss factor, and each one is responsible for a different aspect of the interactions of high-frequency magnetic fields with ferromagnetic materials.

The first phenomenon, which is an extension of the eddy current effect, involves a reduction of the skin depth due to the presence of permeabilities

larger than that of free space. However, ferromagnetic materials, due to having a relative permeability greater than 1, have smaller skin depth:

$$\delta_f = \sqrt{\frac{2}{\omega \mu \sigma}} = \sqrt{\frac{2}{\omega \mu_r \mu_0 \sigma}} \tag{7.10}$$

where δ_f is the skin depth of a ferrous metal, and from Eq. (7.10), is related to the skin depth of a non-ferrous metal of the same conductivity δ as:

$$\delta_f = \frac{\delta}{\sqrt{\mu_r}} \tag{7.11}$$

The permeability of most ferrous metals is of the order of 100 to thousands, which according to Eq. (7.11), would make these materials have a lower cross-sectional area available for eddy current flow, and therefore a higher surface resistivity. This would result in an enhanced power dissipation compared to non-ferrous materials of the same conductivity. As an example, the induction stovetop, which is a relatively new product on the consumer and professional cooking market [2], works only with cookware made of ferrous metals, because of the reduced skin depth from their high permeability.

One of the difficulties in accounting for the enhanced eddy current effect with ferrous metal is the fact that the exact level of relative permeability is highly nonlinear and difficult to measure because it is a function of frequency, temperature, and field strength. For example, low-carbon steel has relative permeability in the range of 200–4000 depending on these parameters [3]. Another issue is that it is quite difficult to distinguish the eddy current that is purely from conductivity from the eddy current that is affected by permeability properties [4].

Magnetic hysteresis is an entirely different effect than eddy current and, referring to Eq. (7.9), it is related to the imaginary part of the relative magnetic permeability μ_r', also known as the magnetic loss factor. This phenomenon is due to losses associated with the magnetization/demagnetization cycle in the magnetic domains.

The power deposition due to the hysteresis effect P_{hyst} for a material with relative magnetic loss μ_r'' can be formulated as:

$$P_{hyst} = \mu_0 \mu_r'' H^2 \tag{7.12}$$

where H is the root mean square (RMS) or average intensity of the high-frequency magnetic field intensity.

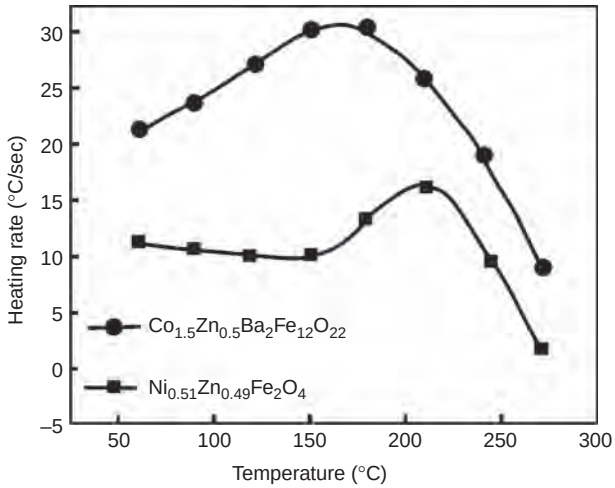

FIGURE 7.4
Magnetic field heating rate curves of two ferrite compounds, which show self-limiting behavior due to the Curie point at 5.85 MHz.

An interesting and often useful characteristic of this type of inductive heating is that the hysteresis effect has a temperature limit known as the Curie point, beyond which the hysteresis effect stops working. In conjunction with this, materials with hysteresis properties can be made from ferrous metal oxides (typically NiZn or cobalt ferrites) that have low electrical conductivities, particularly when they are made into powder or pressed powder forms. Therefore negligible amounts of eddy currents are formed in them. Therefore these materials can be used as temperature-controlled susceptors [5]. One application is welding of polymers, as described in Chapter 8 (welding/bonding). Because of the limit set by the Curie point, the temperature stays below that for the susceptor and prevents damage to the polymer in a welding process. Figure 7.4 [6] shows the heating rate curve and self-limiting behavior due to the Curie point for two ferrite materials heated in a 5.85 MHz magnetic field.

7.1.3 Magnetic resonance applications of *H*-field applicators

In magnetic resonance, a magnetic field applicator/probe interacts with the sample at frequencies that range from sub-MHz in the case of nuclear quadropole resonance (NQR) to above 10 GHz in the case of electron spin/paramagnetic resonance (ESR/EPR). In magnetic resonance the coil or probe is used in two ways: to send a powerful pulse into the sample and then to receive the magnetic resonance signal [7,8].

While the function here is very different from other applications of inductive applicators, many of the design goals remain similar. For example, in order to attain the best performance in both transmit and receive cycles, the highest unloaded quality factor is needed. A low-loss coil decreases the amount of power required during the transmit cycle and enhances the signal-to-noise ratio in the receive cycle.

A desire for high Q means the construction of the probe must be from the highest conductivity metals (at least at surfaces deep enough to accommodate the skin depth). Any dielectric support hardware, as well as resonating capacitors, also need to be of the low-loss variety. When using PTFE or a PET resin, as in other applications of inductive probes the electric field must be minimized. In magnetic resonance coils the subject of coil efficiency is not considered an important parameter because it is best for the loaded Q to remain high as well. When the material subject is conductive, such as in live tissue, eddy currents are formed, but their presence is undesirable because the lower quality factor diminishes the ability to excite the nuclei in the transmit mode and reduces the signal-to-noise ratio in the receive mode.

One specific requirement in the design of magnetic resonance coils and probes is the direction of the magnetic field. In some modalities of magnetic resonance, namely magnetic resonance imaging (MRI) and nuclear magnetic resonance (NMR), the direction of the magnetic field must be perpendicular to the direction of the DC magnetic field (only those components matter).

7.1.4 Frequencies and power levels for various applications of *H*-field applicators/probes

Various applications of magnetic/inductive applicators and probes cover a wide range of frequencies and operate over a range of power levels. To put these in perspective, the chart in Figure 7.5 shows a map of key applications and where they are located in the power versus frequency range. Power level and frequency range are very important parameters that determine most other aspects of applicator and probe design.

Among these applications, industrial induction heating is the oldest and most prevalent. In traditional applications, induction heating is implemented at low frequencies, but more recent requirements have increased the need to move to ever higher frequencies. As we will see later, the state of the art in induction heating has moved to microwave frequencies in the form of sintering of metal powders. Applicators for inductively coupled plasmas (ICPs) [9] operate at radio-frequencies, mainly the ISM band of 13.56 MHz.

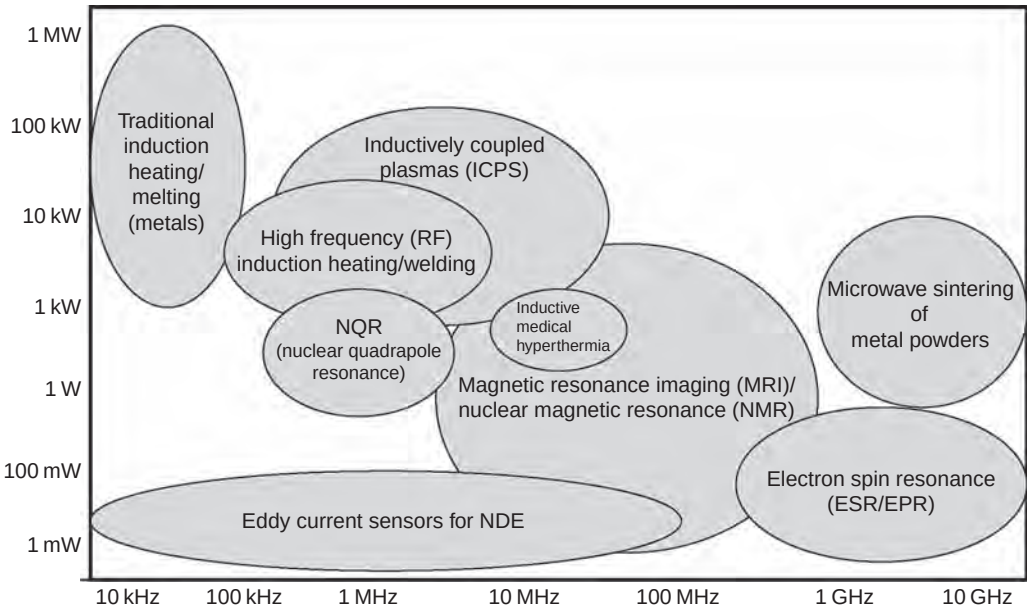

FIGURE 7.5 *An approximate map of various applications related to high-frequency magnetic field interactions with materials in the power level versus frequency domain.*

7.2 FUNDAMENTALS OF INDUCTIVE APPLICATOR DESIGN

7.2.1 Field patterns in inductive applicators

The field distribution is often an important figure of merit in magnetic and inductive applicators. In most cases it is desired for the magnetic field to be uniform over the area of interest where the material load is to be located. Note that the material load will certainly disturb the original (unloaded) field pattern, but that is not as important as having the unloaded field pattern meeting the uniformity criteria. As for the geometrical relationship between the applicator and the material load, magnetic field applicators are categorized by the same designation as used in Figure 2.1. Those configurations that enclose the material, such as a solenoid, tend to have more uniform field distributions, while those geometries where the applicator stays outside of a larger material load tend to have highly non-uniform magnetic field patterns.

Modern computational techniques, mostly based on finite element methods, are available to characterize the field distribution of an applicator, even in the presence of the load material. Finite element methods are available in commercial software such as COMSOL [10].

Analytical methods offer an attractive alternative to solving field distribution problems in simple geometry cases [11]. An example of a non-uniform applicator that analytical solutions are available for is the circular loop coil, which is used often for many applications, such as surface induction heating and as surface coils for MRI.

A simplifying factor in the analytical study of field patterns is that if the physical dimensions considered are a small fraction of the operating wavelength, then an electrostatic approximation can be used, where the variations of field due to wavelength effects can be ignored. Under this assumption, for determination of the unloaded magnetic field distribution, the Biot–Savart law [12] can be used as follows for $\mathrm{d}\vec{H}$, the magnetic field a point of observation as shown in Figure 7.6a:

$$\mathrm{d}\vec{H} = \frac{I\,\mathrm{d}\vec{L} \times \vec{r}}{4\pi r^3} \tag{7.13}$$

where I is the current in a filament, $\mathrm{d}\vec{L}$ is the infinitesimal length of current filament in vector form, carrying the current I, and r is the vector from the location of the wire to the observation point, and $\vec{r}$ is the length of vector r.

Equation (7.13) can then be integrated over the path of the current filament to yield the magnetic field at the point of observation. Using an

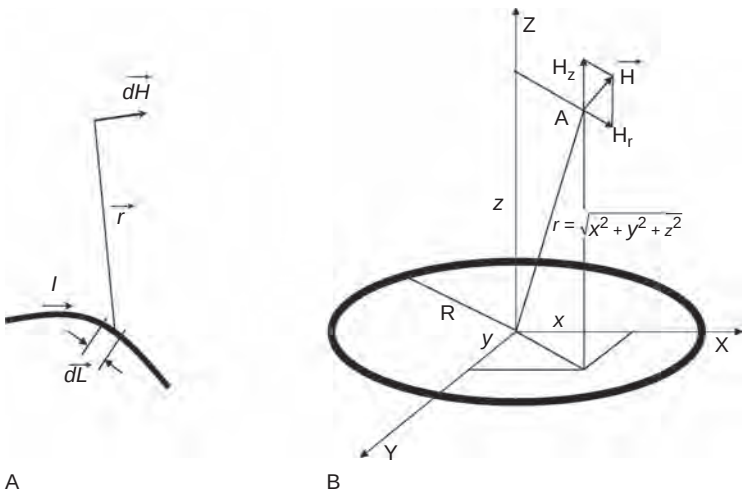

FIGURE 7.6 *(A) Magnetic field from an infinitesimal length of a current-carrying wire at a location defined by vector r. (B) Configuration and vectors related to the magnetic field from a circular current-carrying loop.*

example of a circular loop with diameter R, which carries a current I, as shown in Figure 7.6b, the magnetic field components H_z and H_r at point A are given [13] as:

$$H_r = \frac{I}{2\pi} \frac{z}{r\sqrt{(R+r)^2 + z^2)}} \left[\frac{R^2 + r^2 + z^2}{(R+r)^2 + z^2} E(k) - K(k) \right] \tag{7.14}$$

$$H_z = \frac{I}{2\pi} \frac{1}{\sqrt{(R+r)^2 + z^2)}} \left[\frac{R^2 - r^2 - z^2}{(R-r)^2 + z^2} E(k) + K(k) \right] \tag{7.15}$$

Where z is the elevation of the observation point from the plane of the loop, $r = \sqrt{x^2 + y^2 + z^2}$ is the distance of the point A to the center of the circle, and $E(k)$ and $K(k)$ are the complete elliptical integrals of the first and second type respectively.

The complete elliptical integrals are built-in functions in Mathematica™, and Eqs (7.14) and (7.15) can be formulated in Appendix A7.1 in Mathematica™ with some examples and plots of the field distribution.

As a special simplified case, the field on the axis of the circular loop is given as [14]:

$$H_{z0} = \frac{I R^2}{2(R^2 + z^2)^{3/2}} \tag{7.16}$$

To improve the uniformity of H-field applicators, several methods have been suggested, such as that by Carter et al. [15], which is based on a Chebychev ripple technique. A method based on proper division of current between parallel legs of the applicator [16] uses a combination of empirical data and synthesis to achieve optimum uniformity in H-field applicators.

There are applications where the magnetic field concentration needs to be modified away from or toward a certain direction. Magnetic flux concentrators [17,18] provide this capability. They are ferromagnetic materials placed next to an H-field applicator's conductors. By capturing part of the flux, in essence they act as a mirror for reflecting the magnetic field toward the area where a higher intensity is needed. At RF frequencies, field concentrators are composed of packed powder metallurgy ferromagnetic ceramics in the size range of 40 μm.

7.2.2 Inductive applicator definitions and circuit parameters

In most cases the *H*-field applicator can be approximated by the equivalent circuit representing a lumped inductor plus series resistive elements representing losses. Figure 7.7a shows this simplified equivalent circuit for the unloaded case (empty applicator) and Figure 7.7b for the case with a material load. In the unloaded case, the equivalent circuit is an inductor L_c and a resistor R_c, which represents the ohmic resistance of the applicator itself. The presence of the load, as shown in Figure 7.7b, impacts on the equivalent circuit. The loss associated with the load is represented by an additional series resistor R_{le}, commonly known as the equivalent load resistor.

The presence of the load also changes the inductance to L_c'. For nonferromagnetic loads $L_c' \leq L_c$, but in most practical cases the drop in the inductance is quite small.

In the case of ferromagnetic loads, whether the inductance increases or decreases depends on several factors.

The applicator efficiency then becomes:

$$\eta = \frac{R_{le}}{R_{le} + R_c} \tag{7.17}$$

which, neglecting the change in the inductance, becomes equivalent to Eq. (2.17) ($\eta = 1 - Q_l/Q_u$), given that $Q = \omega L/R$.

The values of coil and load equivalent resistance, and thereby the applicator efficiency, can be found using either computational or measurement methods. For simple structures analytical methods, as discussed in Section

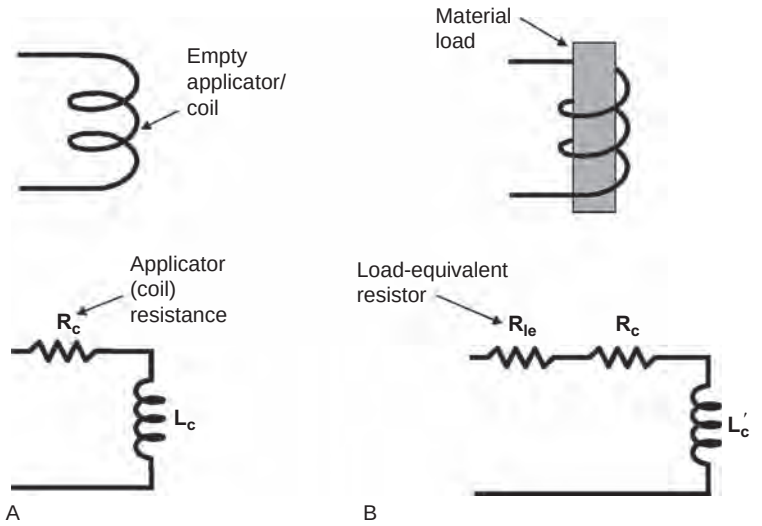

FIGURE 7.7
Simplified equivalent circuits of an H-field applicator have an inductor in series with a resistor representing the dissipative losses. (A) In the unloaded condition, the resistance R_c represents the ohmic losses of the applicator itself. (B) In the loaded condition, an additional load-equivalent resistor represents the losses associated with the load.

7.2.1, can be used. For more complex geometries numerical techniques [10] are useful. In most practical cases, however, Q values can be measured using bandwidth measurements with a network analyzer [19].

7.2.3 A simplified model of a conductive load in a uniform AC magnetic field

In the design of an H-field applicator or probe, knowing the field configuration inside the material load is very useful. That information will help in finding the applicator's circuit parameters, the depth of field penetration into the material, the effective field uniformity, and the signal or power absorption.

In order to examine the impact of the presence of conductive material on a high-frequency H field, it is instructive to use a simple case that can be readily analyzed. Consider a cylindrical load with diameter r_0 with its axis parallel to a uniform external magnetic field with intensity H_0, as shown in Figure 7.8. Assuming the infinite length approximation, as in the analysis by Riegert [20], from the Mathematica™ worksheet in Appendix A7.2, the magnetic field at the radius ρ is expressed as:

$$H_z(r) = H_0 \frac{J_0\left[(1+j)\frac{\rho}{\delta}\right]}{J_0\left[(1+j)\frac{r_0}{\delta}\right]} \tag{7.18}$$

Note that this is a complex function, which means the magnetic field inside the load has a phase difference with the externally imposed magnetic field H_0.

The electric field, which is in the ϕ direction, can be obtained by taking the derivative of Eq. (7.18) according to the Faraday law:

$$E_\phi(r) = -\frac{(1+j)H_0\ J_1\left[(1+j)\frac{r}{\delta}\right]}{\delta\sigma J_0\left[(1+j)\frac{r_0}{\delta}\right]} \tag{7.19}$$

Using the absolute (ABS) function in Mathematica™, Figures 7.9 and 7.10 show the variations of magnetic and electric fields within the load for three different cases of the ratio between the load radius and the skin depth. The magnetic field at the surface of the cylinder is the same as the constant field H_0, and it diminishes moving inwards. The abruptness of the reduction depends on the r_0/δ ratio. In the limiting case of very small

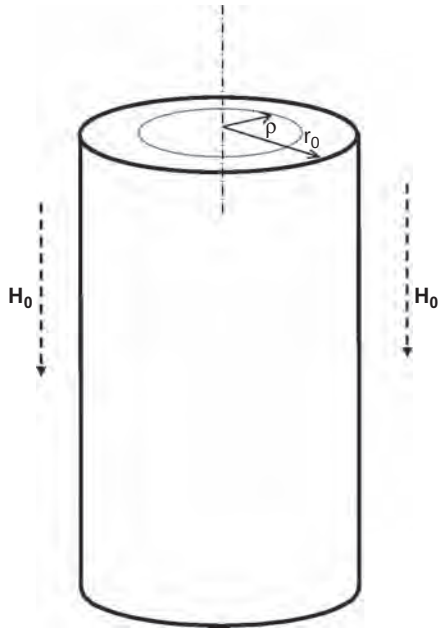

FIGURE 7.8 *An infinite conductive cylinder in a quasi-uniform AC magnetic field.*

skin depth (corresponding to very high frequency or very high conductivity) the penetration of the field is very small, and drops to zero. In the other limiting case, corresponding to low frequency or low conductivity, the load would be transparent to the magnetic field.

In the case of the electric field distribution shown in Figure 7.10, the field is always zero at the axis of the cylinder and increases as we move toward the surface. The value of the electric field at the surface of the cylinder is higher in the case of high r_0/δ ratio. At the limit of $r_0/\delta \rightarrow 0$ the electric field is zero everywhere. This means that the presence of the electric field goes hand in hand with the presence of eddy current, and one cannot exist without the other on the basis of $J = \sigma E$.

Note that the initial premise of a uniform magnetic field without a corresponding electric field by itself is an approximation. In reality, in every AC magnetic field applicator there is an electric field null, and the electric field value increases as one moves away from the axis until it reaches a maximum a quarter wavelength from the axis. In an electrically small (physically small compared to the wavelength) case, that electric field can be approximated as zero for most practical purposes until a conductive load is introduced, where eddy currents are formed.

FIGURE 7.9

The relative magnetic field intensity inside a conductive cylinder (0 at the axis and 1 at the surface) for three values of radius divided by skin depth. For large skin depth the H field is more uniform.

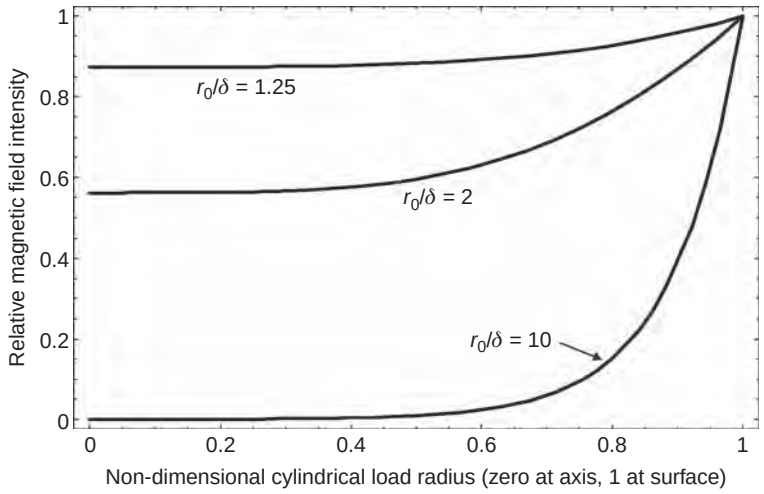

FIGURE 7.10

The relative electric field intensity inside a conductive cylinder (0 at the axis and 1 at the surface) for three values of radius divided by skin depth. The E field is always zero on the axis.

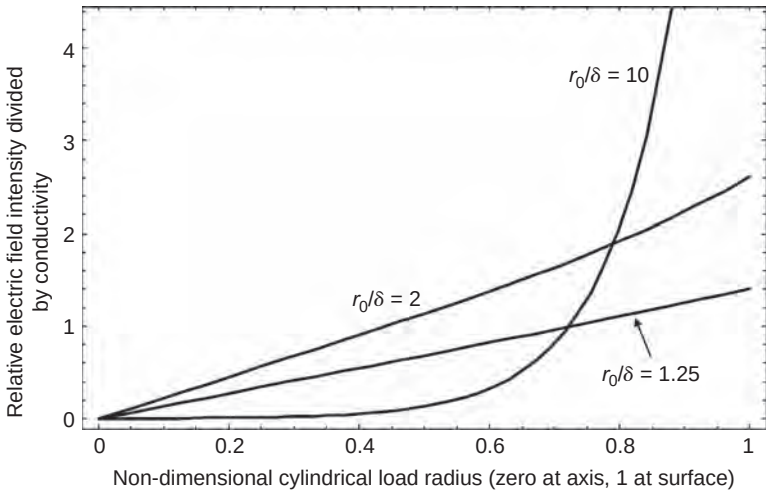

It can be shown that the main conclusions drawn from the above analysis are generally valid for more complex geometries as well. For loads where the infinite length approximation cannot be used there are field variations in the z direction. For example, in the case of a sphere, the H fields at the equator are higher than those of the poles.

7.2.4 Wire/filament magnetic/inductive applicators (coils)

The oldest and most prevalent types of magnetic field applicators, also known as coils, are metal wires shaped in various forms such as circular or rectangular loops, and solenoids and spirals. Major advantages of such

structures are simplicity of construction and the fact that the magnetic field distribution can be designed by correct placement of the wires.

As a first approximation the current is assumed to flow in an infinitesimally thin wire with negligible diameter. In practice, however, the wire will have significant diameter out of necessity that the resistance needs to be minimized to minimize power losses to the wire. When analytical methods are used, however, it is more convenient to start with the thin wire approximation and modify for wire thickness later as necessary.

The most common type of inductive applicator is where the source of the magnetic field is current-carrying distinct wires, which are frequently called coils. Figure 7.11 shows the general form of a coil, where the magnetic field generated at the point of interest is a superposition of those generated by each wire. A simple and most commonly used coil is a solenoid, which has the advantage of simplicity and good field uniformity, as will be discussed later.

As a first approximation the wires can be considered infinitesimally thin, which is often a good approximation for computations of magnetic field uniformity, at least in areas away from the location of the wires. This type of coil is universally used, particularly in lower frequency applications. A design advantage that wire-type coils provide is the flexibility to design the field pattern based on location and current intensity.

A typical feature in wire-type induction coils is that they are electrically small, which means the dimensions are far smaller than the operating wavelength. As such, based on the discussion in Section 2.3.3, the wave impedance, or the ratio of electric to magnetic field, is very small compared to the wave impedance in free space. In essence, at low frequencies the problems associated with electric field interactions with the intended material do not cause problems in inductive applicators. At higher frequencies, or more precisely when the dimensions of the inductive applicator become comparable to the wavelength, the electric field issues become important. To overcome problems associated with higher frequencies, while at the same time having better uniformity with multi-conductor coils, several methods involving the use of parallel turn coils have been suggested [16,21].

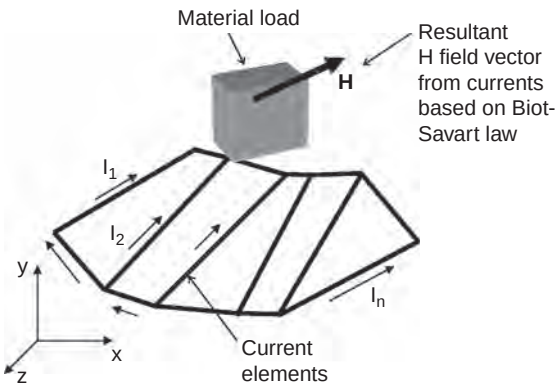

FIGURE 7.11 *General configuration of an H-field applicator.*

7.2.5 Current foil-type magnetic applicators

The second type of inductive applicator is the foil type, where the source of the magnetic field

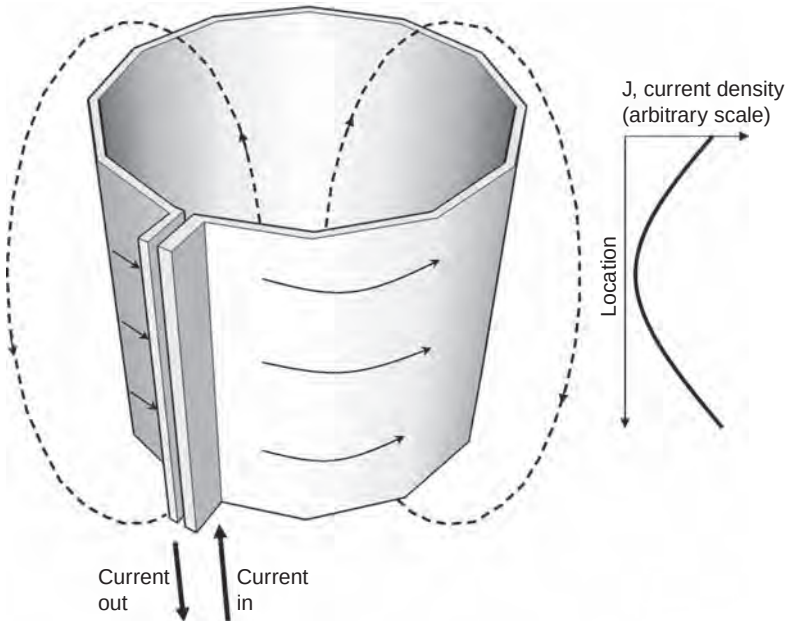

FIGURE 7.12 *A current sheet-type magnetic field applicator has a current distribution that is set by the electromagnetic boundary conditions. In a cylindrical applicator the currents tend to concentrate on the top and bottom edges.*

is a current-carrying metal sheet. Figure 7.12 shows a simple example of a folded foil [22]. A specific example is the Adelman–Grant resonator for NMR applications [23]. The loop–gap resonator [24–27] as described in Chapter 2 belongs to this group of *H*-field applicators.

Current foil-type coils provide advantages at high frequencies because of their high self-resonance and less intense stray *E* field. Foil-type coils can produce relatively large fields of view with low inductance, which makes them appropriate for higher frequency applications. One challenge is that there is less control of the field pattern generated because the current distribution on the foil is dictated by the wave equations and the boundary conditions. For example, in the cylindrical foil applicator in Figure 7.12, the currents tend to be more intense at the ends than in the middle [22], as shown in the figure.

7.2.6 Resonant cavity-type magnetic field applicators

At microwave frequencies the imposition of a magnetic field into materials can be accomplished by using the magnetic field nodes (peaks) of resonant cavities [28,29].

An example is the use of the TE_{011} cylindrical cavity, as shown in Figure 7.13. This modality of magnetic field interaction has been used in the field of electron spin resonance, also known as electron paramagnetic resonance spectroscopy [30–32]. In that mode of operation there is a magnetic field node in the axis of the cavity, as shown in Figure 7.13c. There is an electric field null at the axis, but the electric field intensity increases in the radial direction away from the axis, and reaches a peak at about half distance between the axis and the vertical wall of the cavity. Since electric fields often create undesirable effects such as excessive loading and detuning, the diameter of the material sample must be limited.

To design a TE_{011} mode cavity having resonant frequency f_0 (MHz), height h, and diameter D (both in cm), the following equation can be used, which is a numerical variation of a more fundamental equation given elsewhere [33]:

$$\left(\frac{f}{150}\right)^2 = \left(\frac{121.6}{D}\right)^2 + \left(\frac{100}{h}\right)^2 \tag{7.20}$$

For example, using the above equation, for operation at ISM frequency of 2450 MHz, $D = 20.54$ cm and $h = 98.9$ cm are found. Note that Eq. (7.20) assumes an empty cavity with no variations due to coupling, but it would

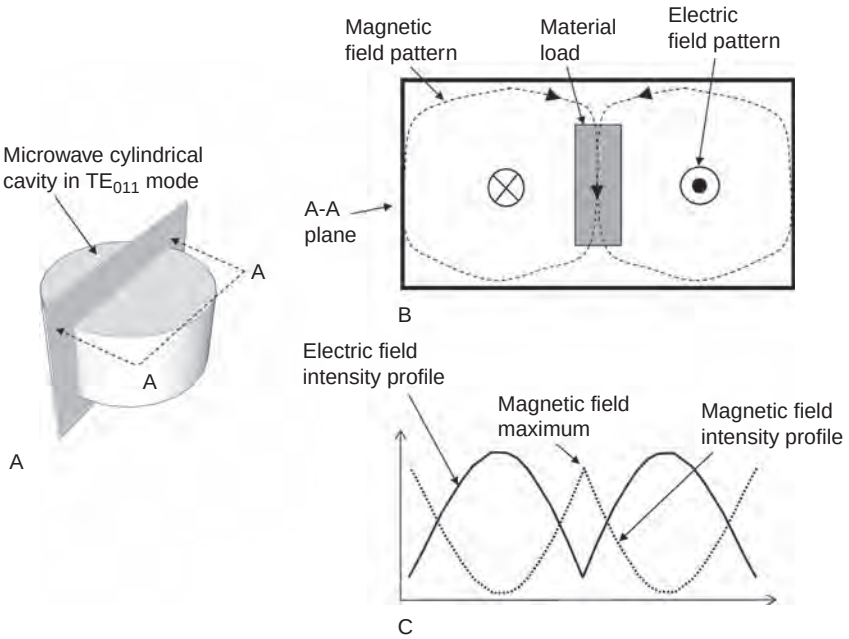

FIGURE 7.13
Field configuration of a TE_{011} resonant cavity used for magnetic field interactions with materials at microwave frequencies. (A) TE_{011} mode cavity. (B) Magnetic and electric field lines. (C) Field intensity profile showing the maximum of the magnetic field at the center of the cavity.

provide a good starting point for a proper design, particularly since experiments show that the detuning for small conductive loads in *H*-field maxima is very small.

Another example of the use of microwave cavities for magnetic field interactions with materials is the new area of microwave sintering of metal powders [34,35]. For this purpose the magnetic field node in a rectangular TE_{103} cavity is used. The conclusion reached is that a far faster and improved sintering of metal powders can be accomplished using the magnetic field nodes of microwave cavities rather than the electric field maxima, which are conventionally used for heating of lossy dielectrics [29,36].

7.2.7 Saddle coils and *H*-field applicators designed for specific field direction

The solenoid is used extensively for interaction of magnetic fields with substantially cylindrical-shaped conductive materials. There are, however, applications such as magnetic resonance, where the direction of the magnetic field must be perpendicular to the axis of the cylindrical subject load. Saddle-type coils, the simplest of which is shown in Figure 7.14, are used for this purpose. The electric current is split between the two sides of the "saddle", and a field that is vertical to the axis of the cylinder is formed.

A major figure of merit in the design of saddle coils is the uniformity of the magnetic field. Referring to Figure 7.14, and the designation of field uniformity in Chapter 2, the saddle coil's field uniformity is defined over the *X*–*Y* plane. It has been proven [37] that the optimum uniformity for a saddle coil is when the angle α in Figure 7.14 is 60°. Figure 7.15 shows the contour plot and 3-D plot of the magnetic field intensity over the *X*–*Y* plane when the saddle coil is optimized in this manner. This plot is obtained by the application of the Biot–Savart law over the cross-sectional (*X*–*Y*) plane.

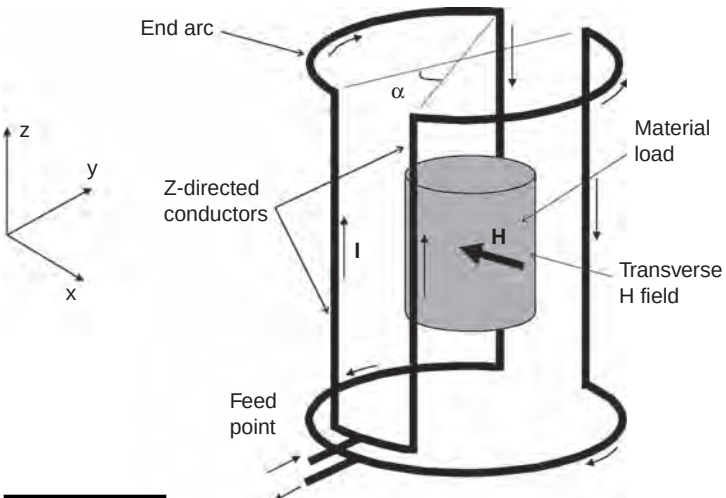

FIGURE 7.14 *A saddle coil for imposition of a transverse H field on a load in a cylindrical outline.*

Other coils of this type are the slotted tube resonator [13,38] and birdcage coil [39], which uses a larger number of conductors to improve the field uniformity of the saddle coil.

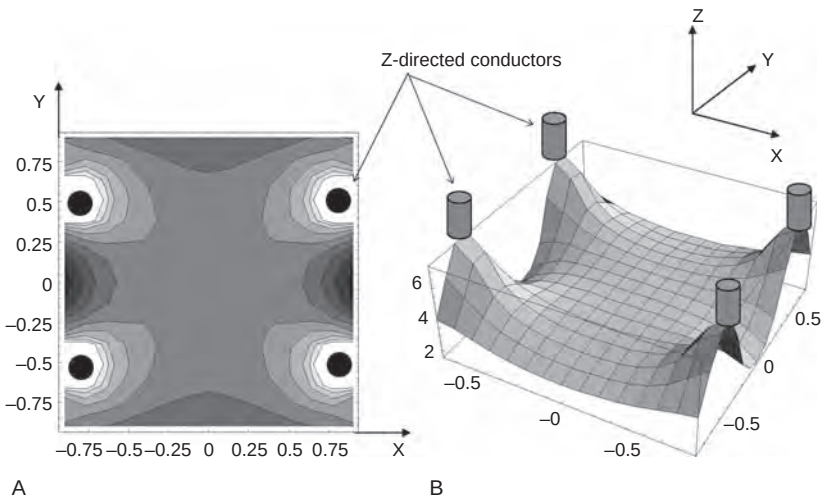

FIGURE 7.15

Relative magnetic field intensity in the X–Y plane of a saddle coil with a cross-sectional radius of 1. The cross-section is taken at the middle of the coil in the Z direction with the infinite length approximation. The computation is done using the Biot–Savart law. (A) The contour plot. (B) The 3-D plot.

7.3 SOLENOID/HELICAL AND SPIRAL COILS AT HIGH FREQUENCIES

As we described above, there are a wide variety of *H*-field applicators. In this section we will focus on solenoid and spiral coil designs, since they are utilized most extensively and in the widest range of applications. The methods used here in studying them can also be applied to other *H*-field applicator types. In addition, we will examine some practical issues in the use of such applicators.

7.3.1 Description and field distribution of solenoid-type applicators

There are many types of practical wire-type magnetic field applicator structures, the most widely used and important being a solenoid, which is shown in Figure 7.16 with its magnetic field configuration. A solenoid with a height-to-diameter ratio of above 2 has a substantially uniform internal field pattern. The infinite length approximation is often used. A solenoid of finite length has a *z*-directed field intensity H_z (in A/m) pattern that is at a maximum at the middle, as follows [40]:

$$H_z = \frac{N I}{2h}\left[\frac{x + h/2}{\sqrt{a^2 + (x + h/2)^2}} - \frac{x - h/2}{\sqrt{a^2 + (x - h/2)^2}}\right] \tag{7.21}$$

where a and h are the radius and height of the coil, N is the number of turns, I is the current in amperes, and x is the location on the axis where

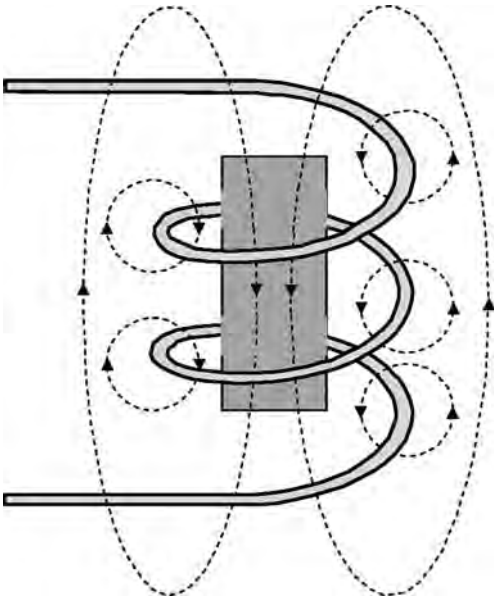

FIGURE 7.16 *Magnetic field pattern of a solenoid-type induction coil creates a generally uniform field within the coil, except for higher intensities in the immediate vicinity of the conductors.*

the field intensity is being considered, with the origin being at the middle of height.

7.3.2 Calculation of solenoid inductance and quality factor

Inductors, in general, have a wide variety of applications beyond material interactions, which are the subject of this book. Therefore there is a body of literature devoted to inductance calculations of various coil shapes and forms [41–43].

The solenoid, however, is the oldest and most prevalently used of all inductive applicators for material interactions. The reasons are field uniformity, simplicity, and ease of construction.

Inductance

An approximate formula for the inductance of a solenoid is [44]:

$$L = \frac{\pi \mu_0 D_c^2 N^2}{4(h + 0.45 D_c)} \tag{7.22}$$

This closed-form equation is accurate for solenoids with large height-to-diameter ratios, $h/D_c > 3$.

A more accurate method that holds over a wider range of geometries is given in the form of a nomogram by the SAMS reference manual [45]. This nomogram was curve fitted by Riegert [46] as follows.

The inductance of an N-turn circular coil with diameter D_c in meters:

$$L_c = 10^{\beta} N^2 D_c \tag{7.23}$$

In the above, the factor β is given as the following polynomial:

$$\beta = -6.17 + 0.67x - 0.19x^2 - 0.09x^3 + 0.12x^4 \tag{7.24}$$

and:

$$x = \log_{10}\left(\frac{D_c}{h}\right) \tag{7.25}$$

Quality factor of a solenoid

The simplest calculations based on uniform distribution of the current on the surface of the wire cross-sections yield higher Q values than found in practice. The reason is the proximity effect, where the currents are more concentrated in certain parts of the conductor cross-section [47].

Based on empirical data, for a solenoid the quality factor is given by [48]:

$$Q_u = A D_c \sqrt{f} \tag{7.26}$$

where the form factor A is fitted by Riegert [49] from a nomogram:

$$A = 3.95 + 2.9x - 0.62x^2 - 0.7x^3 \tag{7.27}$$

and:

$$x = \log_{10}(h/D_c) \tag{7.28}$$

where D_c and h (in meters) are the diameter and length of the coil respectively, and f is the frequency of operation (in Hz).

7.3.3 Spiral-type applicators

Spiral coils, also known as pancake coils in the induction heating industry, are appropriate for certain material heating, plasma excitation, or material sensing applications that require a planar applicator structure. Figure 7.17 shows the configuration of this coil and load arrangement. In situations where the workload is only on one side of the applicator, the fill factor becomes limited, which would reduce the efficiency of this type of applicator.

Referring to the geometry shown in Figure 7.17, the inductance of the spiral coil can be found using an empirical formula [50], which is modified for SI units as:

$$L_c = \frac{N^2(r_1 + r_2)^2}{1.5\, r_1 - 0.7\, r_2} \tag{7.29}$$

where L_c is the inductance (in μH), r_1 and r_2 are the inner and outer radii of the coil turns in meters, and N is the number of turns. This formula has been shown to be accurate within 3% for closely wound spirals. To gain accuracy when more open geometries are considered, rigorous and numerical methods are used [51].

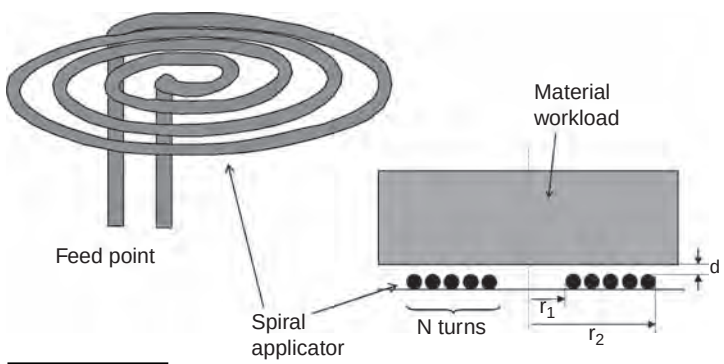

FIGURE 7.17 *Spiral coil as a planar inductive or magnetic field applicator.*

Table 7.1

Material	L @1 MHz (mH)	Q @1 MHz	h @1 MHz Efficiency (%)	L@10 MHz (mH)	Q @10 MHz	h @ 10 MHz Efficiency (%)
Air	3.08	41.5	0	3.17	127	0
Carbon steel	1.26	3.5	91	0.934	8.8	93
Titanium	0.887	5.7	86	0.760	15.1	88
Aluminum	0.793	19.3	53	0.768	61.7	51
Graphite	1.32	4.2	90	1.03	9.32	92
Ionic liquid @ $\sigma = 7.7$ S/m	3.08	38.2	7.9	3.06	25.8	80
Ferrite	4.09	32	23	4.12	85.5	32
Metal-filled polymer @ $\sigma = 95$ S/m	3.06	8.2	80	2.34	2.11	98

In loaded conditions, either numerical modeling methods or measurement should be used to account for the impact of the material load on coil parameters. In order to create a numerical sense of how common materials load a spiral coil, Table 7.1 shows measured results. The parameters of this spiral coil for this table are $r_1 = 6.5$ mm (0.0065 m), $r_2 = 32.5$ mm (0.0325 m), and $N = 10$. Table 7.1 shows the measured inductance, Q factor, and efficiency based on Eq. (2.17) for a number of different materials at two frequencies, 1 and 10 MHz.

7.3.4 High-frequency issues, stray electric field, and self-resonance

In most practical applications of H-field applicators as depicted in Figure 7.1, there is a motive for moving toward higher frequencies. In induction heating, for example, higher frequencies create the capability to heat smaller objects with low fill factors, as well as lower conductivity workloads. In magnetic resonance, higher frequencies increase the signal-to-noise ratio and in plasma activation higher frequencies yield higher temperature plasmas.

Higher frequencies, however, create major challenges in applicator design. These are mostly borne out of increased impact of electric fields at higher frequencies. One major issue is the fringing or stray E fields, as shown in Figure 7.18a. In the equivalent circuit of the applicator as in Figure 7.18b, these fringing E fields can be approximated by a lumped capacitor. While this equivalent circuit is not frequency dependent, there is a frequency, called the self-resonant frequency, at which the fringing capacitance causes resonance with the applicator's inductance. At frequencies approaching self-resonance, most basic assumptions about H-field applicators become

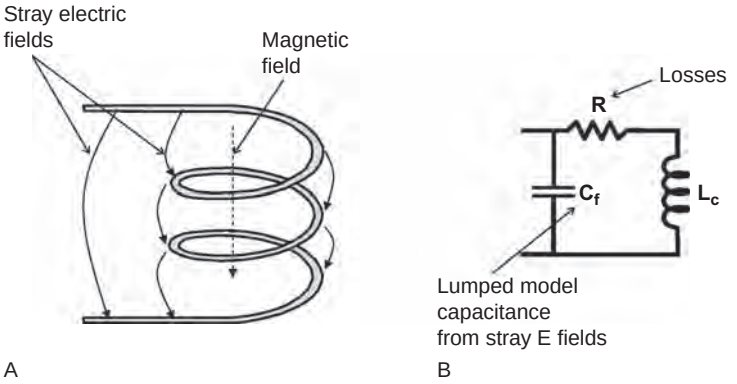

FIGURE 7.18 *Undesirable stray electric fields create various design issues, particularly at higher frequencies. (A) Stray-field lines in a solenoid. (B) Lumped element circuit model of the stray E fields.*

invalid, and control and tuning of the applicator becomes difficult. In reality there are numerous self-resonant frequencies [52], but for practical purposes the first and lowest self-resonance is the most important. Ideally, the operating frequency should remain well below the self-resonance, but as the operating frequency is increased practical problems start to appear, detuning as described above being just one of them.

To get a quantified idea about self-resonance, a practical example is given here. An eight-turn solenoid with a height of 60 mm and average diameter of 56 mm is made of copper wire with a diameter of 3.14 mm. Using a pickup loop method with a scalar network analyzer, the self-resonance is found to be 45.25 MHz. Note that at this frequency the dimensions of the coil are approximately 1% of the wavelength. The use of such a coil as an *H*-field applicator would be problematic at frequencies above the 27.12 MHz ISM band due to *E*-field and detuning problems. This particular coil has an inductance of 2.23 μH that is measured at 500 kHz, which is safely below the self-resonance frequency. As the frequency increases, the measurement of the inductance will show an apparent inductance that is higher. This is due to interference by the self-resonance capacitance, that can be determined to be 5.5 pF from the equivalent circuit of Figure 7.18a.

The above example shows that designing *H*-field applicators for physically larger workloads at higher frequencies is not straightforward. To overcome this design difficulty, an effective method is to design applicators with parallel, instead of series, current paths, as shown in Figure 7.19. The self-resonant frequency of such an applicator is several times higher than a simple solenoid with the same dimensions.

Aside from the fringing *E*-field problems, another issue is the basic *E* fields that exist in all *H*-field applicators even before the material load is inserted. According to Figure 2.3, there is a point or an axis in any *H*-field applicator where the electric field is zero, but there is a rising level of *E* fields moving away from that axis. At higher frequencies the dimensions of the workload become large enough that more electric field of the unloaded applicator interacts with the material. As a rule of thumb, concern about *E*-field problems starts when the largest dimension of the applicator approaches 0.3% of the operating wavelength.

Another issue with the presence of an *E* field is detuning of the applicator from its design resonant frequency. With sufficient *E*-field presence this detuning will happen with variations in the material load's size or electrical properties. In an ideal *H*-field applicator, the presence of the load typically makes a small impact on the value of the inductance. The presence of stray *E* fields in *H*-field applicators changes this, and detuning of the resonance will result, which will complicate the system design. To solve this problem, distributing the capacitance of the applicator system has been proposed as a solution [53]. Figure 7.20 shows this solution, which is typically applied in magnetic resonance applicators. Instead of one resonating capacitor, several capacitors of higher value are used, which keep the resonant frequency the same but keep most of the electric field energy storage within the capacitors and away from the material load.

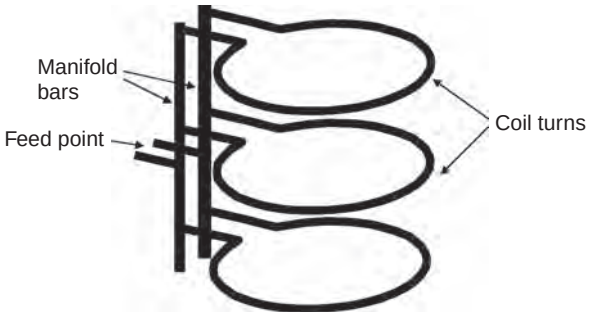

FIGURE 7.19 *Parallel-turn coils are often used in higher-frequency induction heating to avoid problems associated with excessive E field and self-resonance, while maintaining a large heating volume.*

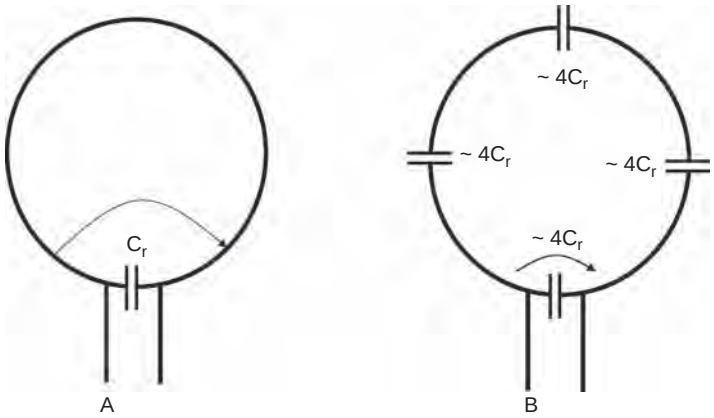

FIGURE 7.20
An effective method of reducing the effects of stray electric fields is distributing the resonating capacitance. (A) A single-turn coil is resonated by one capacitor. (B) By using four capacitors of quadruple the value, more electric field energy is stored inside each capacitor, thereby reducing the stray fields.

7.4 ENERGY DEPOSITION INTO MATERIALS AND HIGH-FREQUENCY INDUCTION HEATING

Induction heating [17,54–56] has been an established method of non-contact heat treatment of conductive materials for decades. Various modalities and applications of induction heating are used over a wide frequency band from a line frequency of 50–60 Hz to well into the tens of megahertz range. Most industrial and conventional applications of induction heating operate below 450 kHz. Frequencies in the megahertz range are used for certain specialty applications when either the conductivity of the material is low, such as in non-metals or composites [57], or in applications where the workload is far smaller than the coil (low fill factor). High frequencies, such as 13.56 or 27.12 MHz, are also used for inductive plasma processing [9].

7.4.1 General description of induction heating via eddy currents

In Section 7.1.1 we described and quantified how eddy currents are formed when a conductive body is subjected to a high-frequency magnetic field. Induction heating occurs when the eddy current is intense enough that the resistance of the material to it causes ohmic losses and therefore heat.

The advantages of induction heating over conventional methods of heating are somewhat similar to the advantages sought when microwave and RF heating of dielectrics are considered. These are related to the non-contact nature of electromagnetic methods that eliminate the limitations of thermodynamic heat transfer, which result in more intense heating per unit surface area when needed. Another major advantage of induction heating is when heating of a conductor through a non-conducting medium is needed. For example, induction heating is extensively used for heating of conductive components inside a sealed glass vacuum tube.

In order to solve and analyze induction heating problems, modern numerical methods are available [10]. In these methods, in addition to electromagnetic solutions, their multi-physics capability can be used to do thermal computations as well [58].

7.4.2 Induction heating of a hollow cylindrical shell

To quantify the induction heating effect, we refer to Figure 7.3 and the results of Section 7.1.1, where we described eddy currents. Using the notation from Figure 7.3, the total real power dissipated in the shell, $\langle P_{\mathrm{d}} \rangle$ is [1]:

$$\langle P_{\mathrm{d}} \rangle = \frac{1}{2}\mathrm{Re}\int \mathrm{d}V\, j_{\phi}^{*} E_{\phi} = \pi a h d \sigma |E_{\phi}|^2 \tag{7.30}$$

Then inserting the electric field from Eq. (7.4) into Eq. (7.30), we obtain:

$$\langle P_d \rangle = (\pi a h d \sigma) \frac{(\omega a \mu_0 H_0/2)^2}{1 + (\omega \mu_0 \sigma a d/2)^2} \tag{7.31}$$

This shows the inductive power deposition (in watts) into a hollow cylindrical shell with the radius a, height h and shell thickness d (all in meters), and conductivity σ (in S/m) when the magnetic field has an amplitude H_0 (in A/m) at radial frequency of $\omega = 2\pi f$.

A close examination of Eq. (7.31) derived for this simple geometry reveals several facts and trends about induction heating that would remain true for more complex geometries and conditions as well. One major issue is the impact of the hollow shell's conductivity on the magnitude of induction heating, all other parameters remaining constant. A quick look at Eq. (7.31) shows that the power deposition approaches zero when the electrical conductivity of the material is either zero or infinity. These two extremes correspond to insulators ($\sigma = 0$) in which eddy currents are not possible, and highly conductive materials ($\sigma \to \infty$) where the eddy current does not meet enough resistance to cause heat. Obviously, then, there has to be a value of material conductivity where the power deposition peaks.

Figure 7.21 shows a graph of relative power deposition versus conductivity in a case with numerical values of $a = 1\,\text{cm}$, $d = 1\,\text{mm}$, and frequency of 1 MHz. The trend shown in this graph, though based on a number of simplifying assumptions for a simple geometry, is still universally true for induction heating in general. This trend indicates that there is an optimum

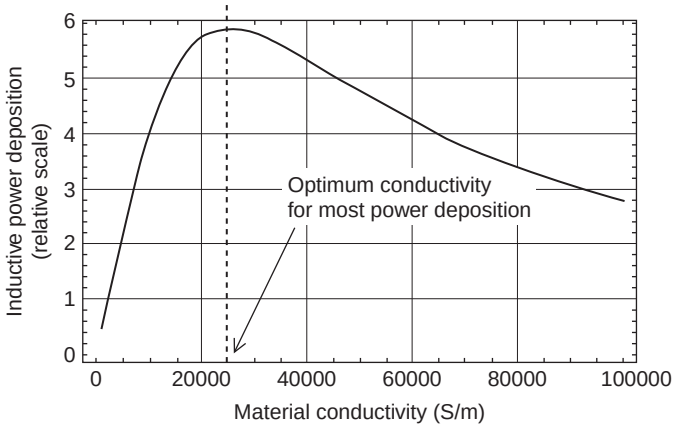

FIGURE 7.21 *Inductive power deposition (on a relative scale) into a cylindrical shell versus the conductivity of the shell (frequency of 1 MHz, shell radius of 1 cm, shell thickness of 1 mm).*

value for conductivity for a given set of other parameters. In this particular case the optimum conductivity turns out to be $\sigma = 25{,}330\,\text{S/m}$.

In reality, for the particular case of a hollow shell, a more general factor can be used for optimization. If we introduce a variable ψ as the product of the material conductivity and the shell thickness as:

$$\psi = \sigma d \tag{7.32}$$

and take the derivative of Eq. (7.31) with respect to ψ, we obtain:

$$\frac{dP_d}{d\psi} = \pi H_0^2 \mu^2 \omega^2 h a^3 \frac{4 - (a\psi\mu\omega)^2}{\left[4 + (a\psi\mu\omega)^2\right]^2} \tag{7.33}$$

The optimum value ψ_{opt} is found by equating the above to zero and solving for ψ:

$$\psi_{opt} = \frac{2}{a\mu\omega} \tag{7.34}$$

Combining Eqs (7.34) and (7.6) we get:

$$d = \frac{\delta^2}{a} \tag{7.35}$$

where δ is the skin depth. This means that in induction heating of a thin hollow shell, the power deposited is maximized if the thickness of the shell is chosen according to Eq. (7.35). Note that trying to perform this optimization based on other parameters, such as frequency and shell diameter, would not yield an optimum value because power deposition always increases with those parameters.

Example

A ceramic rod with diameter 2 cm is to be coated with a thin layer of copper and used as a susceptor for radiating heat at the induction frequency of 13.6 MHz. What thickness of copper would make this susceptor optimized for most energy absorption?

Solution

Using Eq. (7.6), the skin depth of copper with $\sigma = 5.8 \times 10^7$ at 13.6 MHz is $\delta = 17.9\,\mu\text{m}$. Considering $a = 0.01\,\text{m}$, and using Eq. (7.35), then $d = 32\,\text{nm}$. Such a thin layer of copper can be achieved using one of several

vapor deposition techniques. In this solution a perfectly smooth ceramic is assumed, otherwise the surface roughness will require a thicker layer of copper to compensate for the surface roughness [58].

7.4.3 Energy deposition into a cylindrical load from a uniform magnetic field

In Section 7.2.3 we examined distributions of H and E fields for a cylinder of radius r_0 with conductivity σ, which is placed in a uniform AC magnetic field parallel to its axis, as shown in Figure 7.8. The electric field, which flows in a circumferential direction within the conductive cylinder, will cause a circumferential eddy current ($J_\phi = \sigma E_\phi$) to flow in the cylinder. The goal in this section is to study the inductive heating of the cylinder by examining the real power dissipation due to this eddy current. The peak power dissipated energy P_{core} is given as [12]:

$$P_{\text{core}} = \int_v \bar{J} \bullet \bar{E}\, dv = \int_v \sigma \left|E_\phi\right|^2 dv \tag{7.36}$$

For our geometry and parameters, the total power real deposition P_l into the length ℓ of the cylindrical load is given by Riegert [20] in the Mathematica™ worksheet of Appendix A7.2 as:

$$P_l = \frac{2\pi r_0 \ell H_0{}^2 \Im(x)}{\delta \sigma} \tag{7.37}$$

where the parameter x is the ratio of the load radius to the skin depth:

$$x = \frac{r_0}{\delta} \tag{7.38}$$

and the function $\Im(x)$ is defined as:

$$\Im(x) = \frac{1}{2}(1+j)\left\{\frac{j J_1[(1-j)x]}{J_0[(1-j)x]} - \frac{J_1[(1+j)x]}{J_0[(1+j)x]}\right\} \tag{7.39}$$

Even though this function contains the complex operator $j = \sqrt{-1}$, the final result is always a real number. The complex Bessel functions in Eq. (7.39) are built in to Mathematica™, as shown in Appendix A7.2. A plot of the function $\Im(x)$ is shown in Figure 7.22 and can be used graphically for

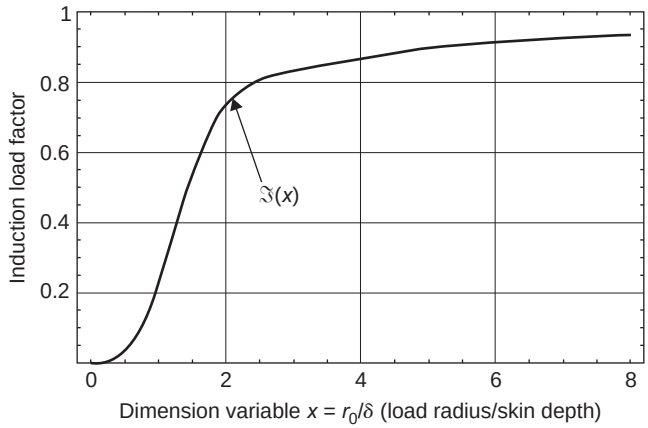

FIGURE 7.22 *The function for computation of inductive heat deposition into a cylinder.*

approximate computations. Alternatively, a polynomial curve-fit is shown below, which is only valid within ±5% in the important range of x between 1 and 8:

$$\Im(x) \approx -0.75 + 1.36x - 0.419x^2 + 0.05558x^3 - 0.002663x^4 \quad (1 \leq x \leq 8) \tag{7.40}$$

Note that the $\Im(x)$ function in a different form is given in older texts [54,59] using the ber/bei functions, which are the real parts of the complex Bessel function. The values of ber/bei functions were either tabulated or given in nomograms in the tradition of texts prior to the era of advanced computation.

7.4.4 Induction heating of a cylindrical load in a solenoid-type coil

In the previous section we examined the power dissipation for the case of a cylindrical load being placed in a uniform AC magnetic field. In this section the source of the magnetic field is identified as a solenoid that is external to, and coaxial with, the cylindrical load, as shown in Figure 7.23. The solenoid has N turns, with diameter D_c and length ℓ, which has a current flow I_c. The RMS value of the magnetic field H_0 in the annular area between the coil and the cylinder is related to the other parameters by [60]:

$$H_0 = \frac{N}{\ell \kappa} I_c \tag{7.41}$$

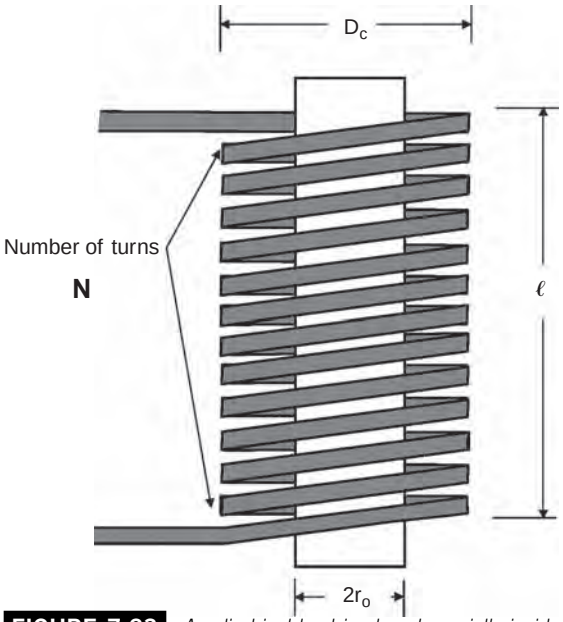

FIGURE 7.23 *A cylindrical load is placed coaxially inside a solenoid.*

where κ is a shape factor to account for the deviation from the infinite length approximation and is defined by [61]:

$$\kappa = \ell + 0.44\frac{D_c}{\ell} \tag{7.42}$$

In cases where $D_c \upsilon \ell$, then $\kappa = \ell$ and the infinite length approximation would apply.

The power into the load is related to the equivalent load resistance R_l by:

$$P_\ell = R_\ell I_c^2 \tag{7.43}$$

Using Eq. (7.35) the load's equivalent resistance becomes:

$$R_\ell = \frac{2\pi N^2 r_0}{\sigma \delta \ell \kappa^2} \Im(x) \tag{7.44}$$

where $x = r_0/\delta$ and function $\Im(x)$ is defined by Eq. (7.39). This equation is important in predicting the efficiency of loads.

In the special limiting condition where $\delta \gg r_0$, for example when either the load conductivity or the frequency are low, the load equivalent resistance from Eq. (7.44) will become [46]:

$$R_\ell(\delta / r_0 \rightarrow \infty) = \frac{\pi N^2}{2\sigma \ell \kappa^2}\left(\frac{r_0}{\delta}\right)^4 \tag{7.45}$$

Another limiting condition is when the skin depth is very small compared with the load radius ($\delta \gg r_0$), for example in a very-high-frequency or high-conductivity situation. Then the function $\Im(x)$ approaches unity, and the load's equivalent resistance becomes:

$$R_\ell(\delta/r_0 \rightarrow 0) = \frac{2\pi r_0 \ell N^2}{\delta \sigma} \tag{7.46}$$

Between these two extremes, the optimum power deposition, which corresponds to the highest level of load equivalent resistance, occurs when r_0/δ

is in the vicinity of 2. This optimum is not a sharp peak, and a wide range of parameters that provide this approximate ratio would produce good induction heating results.

7.4.5 Practical issues in high-frequency induction heating

It is often necessary, due to geometrical constraints, to place the tank capacitor at a distance away from the induction coil. This causes the problem of reduced fill factor and lowering of efficiency due to wasted magnetic energy storage. A method to overcome this is to use a low-impedance transmission line between the coil and the tank capacitor [17], as shown in Figure 7.24. A sheet of low-loss dielectric, such as PTFE, sandwiched between two copper parallel plates is often used for this purpose. This arrangement, which is often called the fishtail assembly, often has a significant capacitance value that must be accounted for in designing the tank capacitance. The thickness of the PTFE sheet must be designed to safely withstand the highest voltage.

Another practical issue is the cooling of the coil in induction heating. A large current flows through the coil; due to skin effect issues, the cross-sectional area of this current flow is quite small, which causes significant resistance and therefore heat. The amount of heat generated can easily be calculated by knowing the applicator efficiency as shown in Section 7.4.4. The cooling is performed by using hollow copper as the coil conductor and running water through it. Among the considerations is the minimum necessary flow of water needed to prevent the water from overheating. The standard practice is to make sure the water exiting the coil does not exceed 35°C. The flow can be too restricted if the passageway is too narrow, and this consideration often sets the minimum for conductor thickness [17].

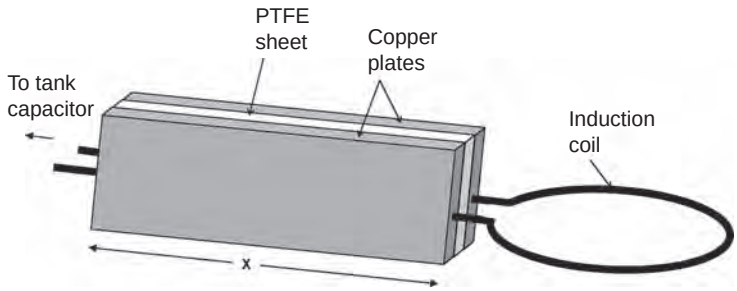

FIGURE 7.24 *A low-impedance transmission line, often called a "fishtail assembly" is used when there is a need to put distance between the induction coil and the tank capacitor (often called the "heat station"). This would reduce the excessive inductance that reduces the applicator efficiency.*

7.4.6 Uniformity of energy deposition in induction heating

We previously discussed the issue of magnetic field uniformity of the empty applicator, and how to improve it. When a conductive material is introduced into the applicator as a workload, the electric field distribution inside the material is always non-uniform, even if the applicator has a perfectly uniform magnetic field distribution.

Depending on several parameters, it is certainly true that, on the material load, the values of both magnetic and electric fields drop from their surface values, and the rate of this drop is dependent upon the skin depth. This fact may create the impression that, for a sufficiently large skin depth, uniform induction heating may be possible. The chart in Figure 7.25 proves that this is not true. Under the right circumstances, it may be possible to maintain a relatively uniform magnetic field inside a solid object, but the electric field, which is solely responsible for induction heating, is always zero at the core of the object. Therefore the energy deposition density is always highly non-uniform. In the example depicted in Figure 7.25, a cylinder is subjected to an externally uniform magnetic field parallel to its axis and the analytical solution in Section 7.4.4 is used.

Careful examination also challenges another assumption that the rate of field reduction from the surface of the workload to the interior is always at the rate of the skin depth, i.e. at the distance of skin depth from the surface the intensity of the electric field drops to 1/e, or 37% of the surface intensity. In reality, this is only true if the diameter of the workload is much larger than the skin depth, which holds in most practical cases of conventional induction heating, where high conductivity metals with small skin depths are heated. The chart in Figure 7.26 shows a more general view where the ratio of electric fields one skip depth below the surface is plotted

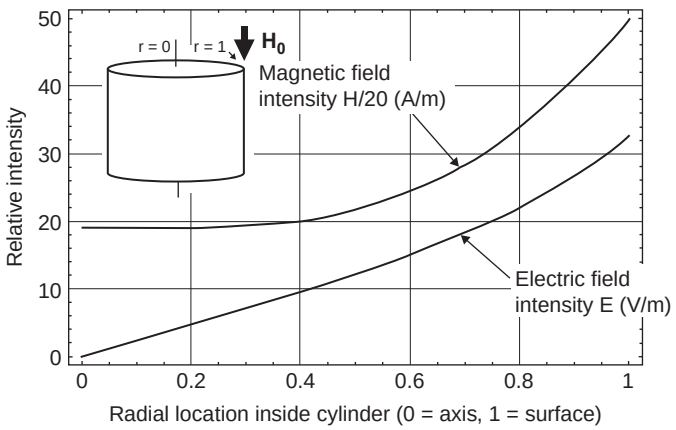

FIGURE 7.25

Relative intensities of electric field and magnetic fields inside a cylinder of radius 1 m, subject to uniform AC magnetic field of H_0 = 1000 A/m, skin depth of 0.4 m, and conductivity of 100 S/m. Inside the cylinder both the magnetic field and the electric fields are reduced from their surface values. While the magnetic field has a finite value at all locations, the electric field vanishes to zero at the axis.

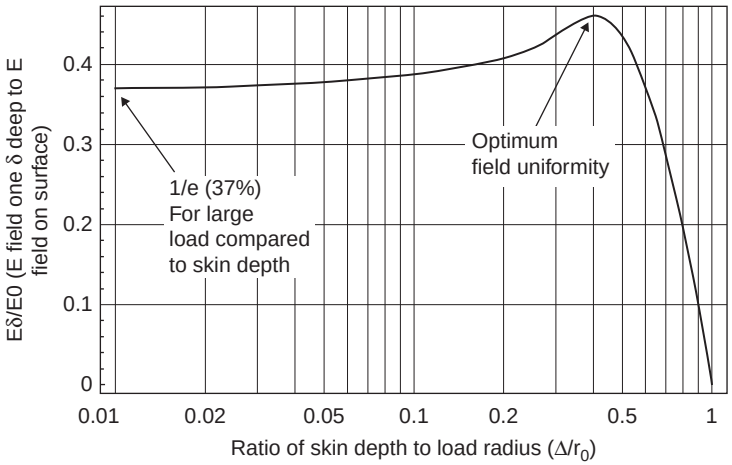

FIGURE 7.26

In induction heating, if the skin depth is small compared to the load radius, the E-field intensity at one skin depth into the cylinder is 1/e (37%) of the surface value. In a situation where the skin depth is comparable with the radius, the ratio deviates from 1/e as shown. In all cases the electric field, and therefore induction heating at the center of the load, vanishes to zero. The optimum uniformity is obtained when $\delta/r_0 = 0.4$.

versus the ratio of skin depth to the radius for a cylinder (δ/r_0) with the infinite length approximation. Starting from the small skin depth case toward a radius comparable to the skin depth, there is an optimum uniformity that occurs at about $\delta/r_0 = 0.4$, and then there is a rapid decline toward the condition where the radius is equal to the skin depth.

This highly non-uniform nature of induction heating, where the energy deposition vanishes to zero in all cases, is in contrast to heating at the node of electric fields, as covered in Chapter 3, where approximately uniform heating is possible under some conditions when dielectric materials are subjected to electric fields in capacitive applicators.

7.4.7 Application example: induction heating leading to silicon–silicon wafer bonding

Silicon–silicon bonding is used in the production of micro-fabricated structures and in components used in power electronics. In the conventional bonding process, the polished surfaces of silicon wafers are pressed together at moderate temperatures to form an initial pre-bond. To complete the bond and achieve full strength, the wafers require baking at temperatures greater than 900°C. Conventionally, this is done in large furnaces, which require long ramp times, consume large amounts of power, and have significant manufacturing footprints.

Thompson et al. [62,63] describe a method for effecting bonding of silicon wafers using induction heating. The arrangement for this work is shown in Figure 7.27. A spiral coil, operating at 13.56 MHz, will heat silicon above 1000°C in only a few seconds. Typical power requirements fall

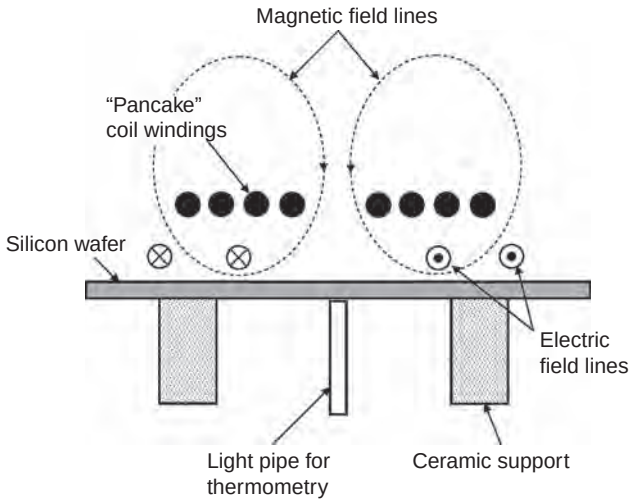

FIGURE 7.27 *Arrangement for induction joining of silicon wafer. After Thompson-Booske.*

between 900 and 1300 W for silicon wafers 75–100 mm in diameter. This technique has successfully produced direct silicon wafer-to-wafer bonds without the use of an intermediate glue layer. Infrared imaging is used to observe the quality and has indicated void-free bonds. In addition, four pairs of stacked wafers were bonded simultaneously in 5 minutes, demonstrating the potential for multi-wafer bonding.

7.5 CIRCUIT PARAMETERS AND DESIGN IN MAGNETIC FIELD APPLICATORS

7.5.1 Applicator current, voltage, and power efficiency

In this section we will see that coil efficiency is an exceptionally important attribute of induction heating. While higher efficiency contributes to electrical energy savings, its importance in the design of induction heating circuit goes well beyond that, and often can determine if a project can be done at all.

In the design of an inductive applicator, a proper approach is to determine applicator efficiency based on a typical load in advance; that is how a proper design with the right assumptions can be completed without the need for redesign in case of any failures. To determine the efficiency, depending on the type of the load and other practical or economical considerations, a choice between a few methods can be made. For some simple geometrical cases, such as a cylindrical load in a solenoid, an analytical solution may be found, such as that covered in Section 7.4. For more complicated geometries, numerical methods such as finite element analysis, sometimes offered by commercial entities such as COMSOL [10], can be used.

In situations where the load electrical properties change little with temperature, room temperature measurement of loaded and unloaded Q factors using a network analyzer [64], and the use of Eq. (2.17) ($\eta = 1 - Q_l/Q_u$) to find the efficiency may be the most practical approach. This method is not useful for workloads where the electrical properties change greatly between signal level and power levels, for example plasmas.

Regardless of how the applicator efficiency is determined, the following equations can be used to find coil currents and voltage from the efficiency figure.

For voltage across the coil V, by setting up the circuit equations we get:

$$V = \sqrt{P_{\text{in}} L\omega\left[Q_{\text{u}}(1-\eta) + \frac{1}{Q_{\text{u}}(1-\eta)}\right]} \tag{7.47}$$

where P_{in} is the power required in the load in watts, L is the inductance of the induction coil, $\omega = 2\pi f$ is the angular frequency, Q_{u} is the unloaded Q of the coil, and η is the applicator efficiency as determined by one of the above methods.

In most practical cases $Q_{\text{u}}(1-\eta) \gg 1/Q_{\text{u}}(1-\eta)$, which combined with Eq. (7.47) gives:

$$V = \sqrt{P_{\text{in}} L\omega Q_{\text{u}}(1-\eta)} \tag{7.48}$$

Using the same theory and approximation, the current through the coil and the resonating capacitor I_{c} becomes:

$$I_{\text{c}} = \sqrt{\frac{P_{\text{in}} Q_{\text{u}}(1-\eta)}{\omega L}} \frac{1}{\sqrt{1 + \frac{1}{\left[Q_{\text{u}}(1-\eta)\right]^2}}} \tag{7.49}$$

Again, using the approximation of $Q_{\text{u}}(1-\eta) \gg 1/Q_{\text{u}}(1-\eta)$, this simplifies to:

$$I_{\text{c}} = \sqrt{\frac{(1-\eta)P_{\text{in}} Q_u}{L\omega}} \tag{7.50}$$

Equations (7.48) and (7.50) show that both current in the induction coil and voltage across the coil are proportional to $\sqrt{1-\eta}$. This makes both current and voltage in a case with 50% efficiency 2.3 times larger than a case with 90% efficiency. In the design of a practical induction heating system, the levels of voltage and current are of prime economical practical importance. A low-efficiency system with a high current level would require larger investment in cooling equipment and copper mass for the coil and interconnections. Similarly, a high voltage rating would require physically larger and much more expensive tank capacitors, and larger distance between coil turns, which add to the system's mass and expense. In short, a low-efficiency situation could make a reasonable-sounding idea totally impractical.

Realizing the importance of having high applicator efficiency, there are several methods to increase efficiency using the parameters discussed previously. Using higher frequencies, better fill factors, and lower loss materials for coils, tank capacitors, and support structures helps the efficiency. Even though copper, with its high conductivity, is universally used for construction of the coil, the coil's ohmic losses usually dominate other types of loss.

7.5.2 Resonance and the tank capacitor

As discussed in Chapters 2 and 3, resonance is often a necessary condition for effective use of applicators. A capacitive applicator, as covered in Chapter 3, must be resonated using an inductor. Here, in the case of inductive applicators, the resonance is accomplished by using a capacitor, which is often called a tank capacitor.

The value of a capacitor C for resonating with a purely inductive applicator with an inductance value of L can be determined by setting up circuit equations:

$$\omega^2 LC = \frac{1}{\frac{1}{Q^2} + 1} \tag{7.51}$$

where Q is the total quality factor of the circuit involving all loss mechanisms combined. In most practical cases $Q \gg 1$, which simplifies Eq. (7.51) into $\omega^2 LC = 1$. Given $\omega = 2\pi f$, the value of the capacitor can be found as:

$$C = \frac{1}{(2\pi f)^2 L_c} \tag{7.52}$$

where f is the desired frequency of operation and L_c is the measured inductance of the coil frequency at that frequency. Note that in many cases involving high frequencies, the measured inductance of the coil at the desired frequency is higher than the reported inductance, which may have been measured at a lower frequency. The difference lies in the impact of the stray E fields that is represented by capacitor C_f in Figure 7.18.

Another issue that often modifies the value of the resonating capacitor calculated by Eq. (7.52) is the impact of the coupling circuit; therefore an allowance for variability of the resonating capacitor must be made. Various circuit computation methods, including the use of high-frequency circuit simulators, such as Agilent ADS [65], can be used to account for the coupling effects on the tank capacitance value.

In induction heating and inductively coupled plasma systems, the tank capacitor must bear large voltages and currents at the same time.

Capacitors made for this purpose are rated for a figure of merit named KVAR (kilo-volt-amp-reactive), which is the product of the maximum voltage and current they can tolerate in continuous use. This rating must be obeyed in addition to other ratings, such as maximum voltage. In some cases water or oil cooling increases the KVAR rating greatly. One way of achieving high KVAR ratings is using a very-low-loss dielectric medium for the capacitor. Vacuum capacitors are compact but very expensive, and in cases where enough space is available an air capacitor is another solution as long as a safe space between the plates is allocated to prevent breakdown.

7.5.3 Coupling circuits for *H*-field applicators and coils

The resonated circuit comprising of the induction coil and the tank capacitor typically has a high impedance that needs to be matched to the power source's lower impedance. This is accomplished through a coupling circuit. One class of coupling methods involves the use of a capacitive or inductive component to provide the impedance needed. Three types of direct coupling methods are shown in Figure 7.28.

Capacitive coupling is usually preferred, particularly in low-power systems, because variability of coupling is often needed and variable capacitors are more readily available. The capacitor-coupled method shown in Figure 7.28a is very similar in operation and design to that showed in Figure 3.15 for *E*-field applicators.

The inductor-coupled method shown in Figure 7.28b is used in situations where a fixed load provides the opportunity to use a fixed coupling

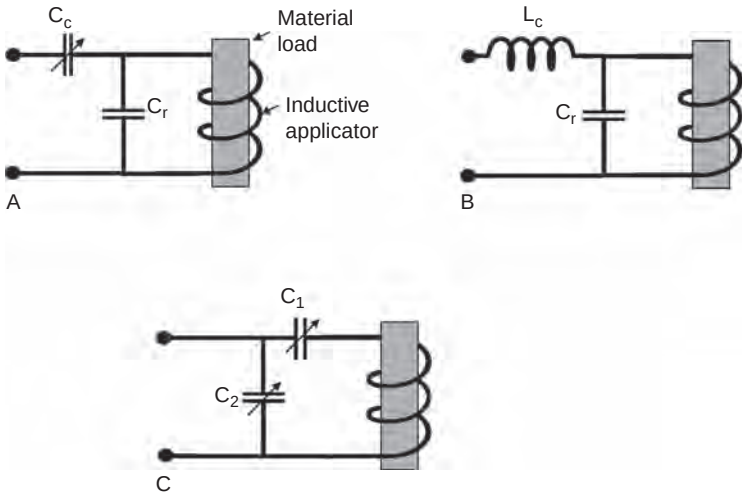

FIGURE 7.28
Direct coupling methods in H-field applicators. (A) In the capacitor-coupled method, the coupling capacitor C_c provides variable coupling. (B) In the inductor-coupled case, the coupling inductor is usually fixed for a specific load. (C) The dual variable capacitor case is normally used for automated tuning.

inductor to save the expense and maintenance of issues related to capacitors. In higher-power systems, inductors are less expensive and more reliable than capacitors. Therefore they are preferred if such an option is available.

The dual variable capacitor method shown in Figure 7.28c is usually used for systems with a highly variable load such as inductively coupled plasmas (ICPs), where the two capacitors are controlled by an automatic matching system. In the design of a dual capacitor system it is often necessary to know the values for typical load situations. The following equation can be used for computing the capacitance values:

$$C_1 = \frac{1}{\omega^2 L\left(1 - \dfrac{\sqrt{R_s Z_0}}{L\omega}\right)} \tag{7.53}$$

where $\omega = 2\pi f$ is the angular frequency of operation, L is the inductance of the coil, Z_0 is the characteristic impedance of the power source (such as $50\,\Omega$), and R_s is the equivalent total resistance of the induction coil, which includes the coil and load losses as described in Section 7.4.4. The capacitance C_2 can be calculated from:

$$C_2 = \frac{X}{\omega\left(X^2 + R_s^2\right)} \tag{7.54}$$

where:

$$X = L\omega - \frac{1}{C_1\,\omega} \tag{7.55}$$

The second method of coupling, which is transformer coupling, is shown in Figure 7.29. In this method, instead of a reactive component, flux linkage is utilized to provide the coupling impedance transformation.

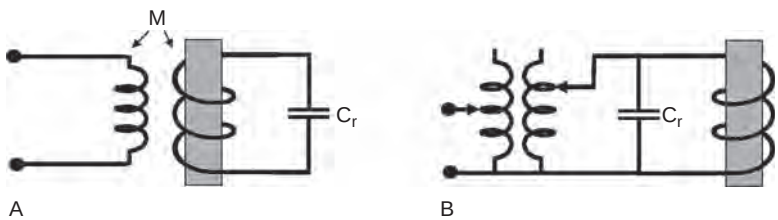

FIGURE 7.29 *Coupling methods that rely on mutual inductance/flux linkage and transformers. (A) Inductively coupled with flux linkage method is used at higher and RF frequencies. (B) The transformer method is normally used in conventional induction heating systems up to 450 kHz.*

7.5.4 Numerical example of an induction heating applicator

Here we will use an example of high-frequency induction heating design and use some of the equations introduced in this chapter.

The goal is to inductively induce 2.5 kW of power into a silicon carbide cylinder with a diameter of 25 mm ($r_0 = 17.5$ mm). The bulk conductivity of the cylinder at the operating temperature is determined to be 55 S/m. A solenoid with 13 turns of average diameter $D_c = 50$ mm and height $\ell = 55$ mm made of copper tubing with diameter $d_w = 3.2$ mm is used. Due to the low conductivity of the cylinder, it has been determined that conventional induction systems that work below 450 kHz are not usable in this application; therefore an RF generator with the ISM operating frequency of $f_0 = 13.6$ MHz is used. The silicon carbide cylinder is placed coaxially inside the coil. We need to find the applicator efficiency and voltage and current needed in order to find the rating and the value of the tank capacitor needed.

Answer

The inductance of the coil is calculated from Eq. (7.23) to be 5.28 μH and the unloaded quality factor is found from Eq. (7.26) to be $Q_u = 750$. The equivalent series resistance corresponding to this Q value is:

$$R_c = \frac{\omega L_c}{Q_u} = \frac{2\pi \times 13.6 \times 10^6 \times 5.28 \times 10^{-6}}{750} = 0.6\,\Omega \qquad (7.56)$$

The skin depth δ for the silicon carbide load based on conductivity $\sigma = 55$ S/m is:

$$\delta = \sqrt{\frac{2}{\omega\sigma\mu}} = \sqrt{\frac{2}{2 \times \pi \times 13.6 \times 10^6 \times 55 \times 4\pi \times 10^{-7}}} \qquad (7.57)$$
$$= 0.0184\,\text{m} \quad = 1.84\,\text{cm}$$

For $r_0 = 0.0125$ m, the parameter $x = r_0/\delta$ becomes $x = 0.68$. Using the Mathematica™ worksheet of Appendix A7.2 or the chart of Figure 7.22, the value of function $\Im(x) = \Im(0.68) = 0.076$.

Using Eq. (7.42), the value of the coil's shape factor κ is:

$$\kappa = \ell + 0.44\frac{D_c}{\ell} = 1.4 \qquad (7.58)$$

Then the value of the equivalent load resistance from Eq. (7.44) becomes:

$$R_{\ell e} = \frac{2\pi N^2 r_0}{\sigma \delta \ell \kappa^2} \Im(x) = \frac{2 \times 3.14 \times 13^2 \times 0.0125}{55 \times 0.0184 \times 0.055 \times 1.4^2} \times 0.076 = 9.24\ \Omega \tag{7.59}$$

The applicator efficiency from Eq. (7.17) is then:

$$\eta = \frac{R_{\ell e}}{R_{\ell e} + R_c} = \frac{9.24}{9.24 + 0.6} = 0.94 \tag{7.60}$$

The voltage from Eq. (7.48) becomes:

$$V = \sqrt{P_{in} L \omega Q_u (1 - \eta)} = \sqrt{3000 \times 5.28 \times 10^{-6} \times 2\pi \times 13.6 \times 10^6 \times 750 \times (1 - 0.94)} = 7802\ \text{V} \tag{7.61}$$

and the current from Eq. (7.50) is:

$$I_c = \sqrt{\frac{(1 - \eta) P_{in} Q_c}{L \omega}} = \sqrt{\frac{(1 - 0.94) \times 3000 \times 750}{5.28 \times 10^{-6} \times 2\pi \times 13.6 \times 10^6}} = 17.3\ \text{A} \tag{7.62}$$

The value of a capacitor to resonate this coil at 13.6 MHz can be calculated by using Eq. (7.52):

$$C_r = \frac{1}{[(2\pi f)^2 \times L_c]} = \frac{1}{[(2 \times 3.14 \times 13.6 \times 10^6)^2 \times 5.28 \times 10^{-6}]} = 2.59 \times 10^{-11}\ \text{F} = 25.9\ \text{pF} \tag{7.63}$$

7.6 SPECIAL TOPICS IN MAGNETIC/INDUCTIVE APPLICATORS

7.6.1 Applications of induction heating of packed beds

In our discussion on induction heating of singular and contiguous conductive workloads, we have proven that the energy deposition into such a load is highly non-uniform, and the center of the workload receives zero deposited power due to induction. When the workload within an induction applicator is composed of multiple pieces, eddy currents will be established in

each piece independently, as shown in Figure 7.30. If the magnetic field intensity is the same for multiple identical objects, then each would carry an identical amount of eddy current. This condition provides an opportunity to inductively heat a packed bed of conductive objects such that the bulk heating is essentially uniform [66]. While it is ideal for the objects to have spherical symmetry, in practical situations such a condition is not necessary. For the sake of convenience, however, we will refer to the components of the packed bed as "spheres".

To realize such bulk uniform heating, an important condition is that there should not be any significant current transfer between the adjacent spheres, otherwise large paths of eddy current are formed that would defy the advantage of independent eddy current paths. In practice such conditions are met [67] due to weak ohmic contact between these adjacent spheres. One should realize, however, that if the spheres fuse together due to overheating or other phenomena, the eddy current characteristics and the temperature profile may be altered.

A practical application of such an arrangement is the efficient, gentle, and uniform heat transfer into fluids, which occurs due to high surface area of the packed bed. In this application the conductive spheres are used as susceptors of induction heating. The high surface area of the packed bed would create an opportunity to use this approach for the gentle transfer of heat to a fluid, as shown in Figure 7.31. The method is effective and energy efficient since the surface of the spheres is exactly where both eddy current heat generation and transfer to the fluid takes place.

This application was further developed [61,68] with an analytical formula for the equivalent load resistance as follows. A packed bed with radius r_0 and length l containing spheres with diameter D_s is placed in a N-turn

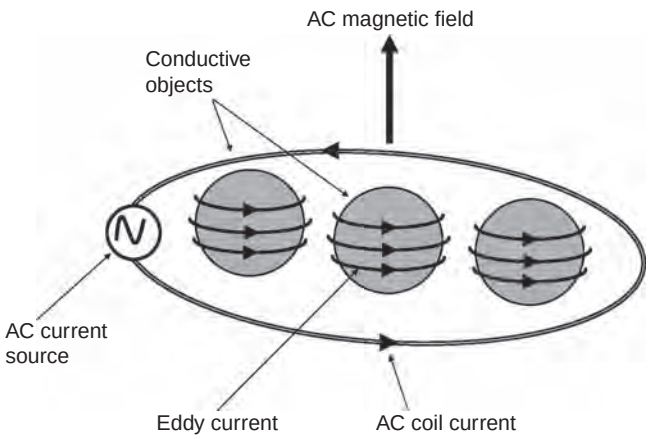

FIGURE 7.30

When multiple conductive objects are subject to an AC magnetic field, an eddy current on each object will form independently. This principle can be used to develop quasi-uniform induction heating over a packed bed of conductive "beads".

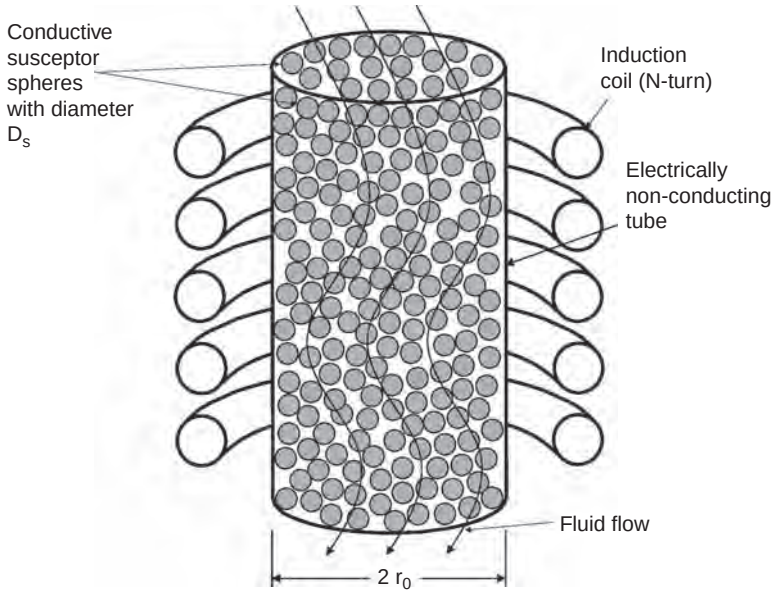

FIGURE 7.31
In a packed bed of conductive spheres or beads the bulk heating across the bed is uniform due to independent eddy current formation on each bead. This can be used for uniform or gentle heating of fluids.

solenoid then the equivalent resistance of this load per equivalent circuit of Figure 7.7a can be found as in Duquenne et al. [61] and modified to fit the nomenclature here as:

$$R_{\text{eq}} = (\ell - \psi)\frac{4\pi r_0^2 N^2}{\sqrt{2}\,\ell\, D_s\,\sigma\,\delta}\Im(x) \tag{7.64}$$

where ψ is the volume void ratio of the packed bed, σ and δ are the conductivity and skin depth associated with the sphere's material of construction, and $\Im(x)$ is defined by Eqs (7.38)–(7.40).

Another application that utilizes uniform heating of packed beds with induction heating is heterogeneous gas-phase catalysis [67,69]. Certain endothermic gas phase reactions require contacting of reactant gases with high-temperature metallic catalysts. For example, in the synthesis of hydrogen cyanide with ammonia and methane, the use of a platinum catalyst would allow the process to go forward at 1100°C. Heating of the catalyst to this temperature using conventional approaches creates problems with catalytic selectivity. This means that many side reactions will occur because locations other than the catalyst surface are heated as well. When the catalyst surface is induction heated, the process can be run with high selectivity because competing reactions, such as decomposition of ammonia, can be

minimized due to the lower temperatures in locations adjacent to the reaction area.

7.6.2 RF inductive effects in conductive liquids and medical applications

In the previous section the transfer of heat to fluids with induction heating through spherical susceptors in a packed bed was described. The eddy current effect can be applied to the liquid directly, however, if the liquid possesses adequate conductivity. Such an effect can be used effectively for heating or characterization/sensing of conductive liquids without any susceptor elements. In addition, biological bodies, because of their adequate ionic conductivity, can be heated directly by induction coils, which are also called helical applicators [70]. In this class of application, the limb is inductively heated for the purpose of hyperthermia treatment of deep-seated cancerous tissues.

One example is the direct induction heating of industrial conductive liquids. Many conductive liquids, such as acids, are corrosive. Heating these liquids with conventional heat exchangers is difficult from a maintenance standpoint because they corrode the metallic heat exchanges quickly. Delivery of heat to this class of conductive liquids on an industrial scale using induction heating has been demonstrated [71].

The most critical requirement for practical and efficient eddy current induction into liquids is adequate conductivity. In order to create numerical sense of how inductive probes interact with ionic fluids, the following example is instructive.

Example

A salt solution with conductivity of 170 mS/cm (17 S/m) when put in a test tube with an ID of 22.5 mm and placed in a seven-turn solenoid with ID 30 mm and height 41 mm will reduce the quality factor of the solenoid from 334 to 151. This yields an applicator efficiency of 55%.

The second application of eddy current effects in liquids is in industrial detection and sensing [72]. The amplitude of eddy current, which can be measured from the inductive probe, is an indicator of the liquid's conductivity. This information can be used to detect process upsets or in the case of decanters it can tell what liquid is at the location of the probe. Figure 7.32 shows a conceptual diagram.

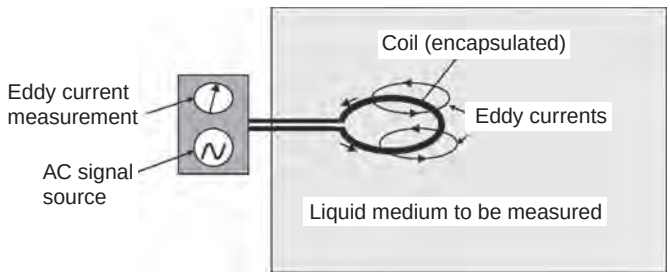

FIGURE 7.32 *General concept of eddy current detector for noncontact detection of a liquid's conductivity.*

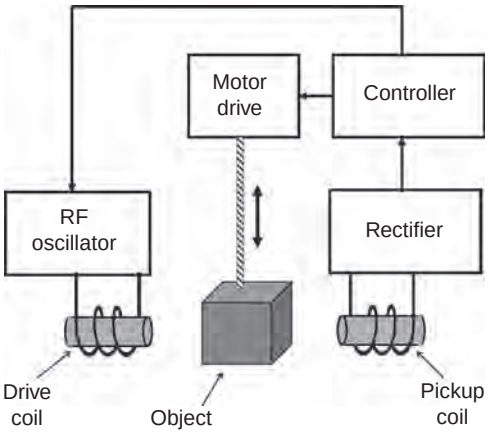

FIGURE 7.33 *Schematic diagram of a dual-coil inductive tomography system.*

7.6.3 Inductive probes in non-destructive evaluation/sensing/tomography

Inductive methods, in addition to liquid conductivity detection as described above, can be used for nondestructive evaluation (NDE) and tomography [73]. Figure 7.33 shows a simplified diagram of a two-coil experimental biomedical tomography system [74]. The object to be imaged is moved via a motor drive that can be moved along the line of symmetry between the two coils. This is used for excitation purposes at 2 MHz, and pickup coil is used for receiving the signal through the object to be examined. Both coils are covered with grounded electrostatic screens to ensure the coupling mechanism between the coils is predominantly inductive as opposed to capacitive. The excitation coil is driven from a sinusoidal supply at 2 MHz and the detection coil forms a resonant circuit with the capacitance of the connecting cables and detection circuitry that is tuned to the excitation frequency. The object is scanned between the coils at typically a few centimeters per second. The recorded data were fed into an image reconstruction computer and images were reconstructed.

REFERENCES

[1] L.C. Shen, J.A. Kong, Applied Electromagnetism, PWS Engineering, Boston, 1987, pp. 483–485.

[2] www.inductionsystems.com

[3] M.E. Van Valkenburg (Ed.), SAMS Reference Data for Engineers: Radio, Electronics, Computer, and Communications, eighth ed., Prentice Hall, Carmel, IN, 1993, pp. 4–24.

[4] J.H. Rose, Scaling relation for the inductance of a coil on ferromagnetic half space, J. Appl. Phys. 82 (9) (November 1997).

[5] P.R. Stauffer, et al., Practrical induction heating coil designs for clinical hyperthermia with ferromagnetic implants, IEEE Trans. Biomed. Eng. 41 (1) (January 1994).

[6] X.K. Zhang, et al., Theoretical and experimental analysis of magnetic inductive heating in ferrite materials, J. Appl. Phys. 93 (10) (2003).

[7] P.A. Bottomley, NMR imaging techniques and applications: a review, Rev. Sci. Instrum. 53 (9) (September 1982).

[8] M. Mehdizadeh, RF Coils for magnetic resonance imaging, RF Design. (October 1991) 29–38.

[9] J.R. Roth, Industrial Plasma Engineering, vol. 1, Principles, Institute of Physics Publishing, Bristol, 1995.

[10] www.comsol.com

[11] C.V. Dodd, Analytical solutions to eddy-current probe-coil problems, J. Appl. Phys. 39 (4) (May 1968).

[12] S. Ramo, J.R. Whinnery, T. Van Duzer, Fields and Waves in Communication Electronics, third ed., Wiley, Hoboken, NJ, 1994.

[13] J. Mispelter, et al., NMR Probeheads for Biophysical and Biomedical Experiments, Imperial College Press, London, 2006.

[14] S. Ramo, J.R. Whinnery, T. Van Duzer, Fields and Waves in Communication Electronics, third ed., Wiley, Hoboken, NJ, 1994, pp. 75–76.

[15] R.G. Carter, et al., Coil-System design for production of uniform magnetic fields, Proc. IEEE. 123 (11) (1976).

[16] M. Mehdizadeh, A design technique for producing desired field pattern in generalized RF coils, Soc. Magn. Reson. Med. Book Abstr. (1989) 936.

[17] S. Zinn, S.L. Semiatin, Elements of induction heating, EPRI/ASM (1988) 244–246.

[18] V.I. Rudnev, D. Loveless, R. Cook, M. Black, Handbook of Induction Heating, Manufacturing Engineering and Materials Processing, CRC Press, 2002.

[19] K.J. Coakley, et al., Estimation of Q-factors and resonant frequencies, IEEE Trans. Microw. Theory Tech. 51 (3) (2003) 862–868.

[20] R.J. Riegert, Private communication.

[21] S. Kashyap, et al., New inductive applicators for electromagnetic hyperthermia, J. Microw. Power (1988) 13–18.

[22] P.N. Murgatroyd, et al., Frequency-dependent inductance and resistance of foil conductor loops, Proc. IEEE. 124 (5) (1977).

[23] D.W. Adleman, D.M. Grant, An efficient decoupler coil design, J. Magn. Reson. 36 (1979) 451–477.

[24] J.S. Hyde, W. Froncisz, A. Kusumi, Dispersion electron spin resonance with the loop-gap resonator, Rev. Sci. Instrum. 53 (1982) 1934–1937.

[25] W.N. Hardy, L.A. Whitehead, Split-ring resonator for use in magnetic resonance for 200 to 2000 MHz, Rev. Sci. Instrum. 52 (1982) 213–216.

[26] M. Mehdizadeh, T.K. Ishii, J.S. Hyde, W. Froncisz, Loop–gap resonator: a lumped-mode microwave resonant structure, IEEE Trans. Microw. Theory Tech. (December 1983) 1059–1064.

[27] M. Mehdizadeh, T.K. Ishii, Electromagnetic field analysis and calculation of the resonance characteristics of the loop–gap resonator, IEEE Trans. Microw. Theory. Tech. (July 1989) 1113–1118.

[28] J. Cheng, et al., Radically different effects on materials by separated microwave electric and magnetic fields, Mater. Res. Innov. 5 (2002) 170–177.

[29] K.I. Rybakov, et al., Microwave heating of conductive powder materials, J.Appl. Phys. 99 (2006) article 023506.

[30] E.R. Davies, et al., A Ligand-Endor spectrometer, J. Phys. E: Sci. Instrum. 1 (1968) 847–850.

[31] J.S. Hyde, US Patent 3,250,985, 1975.

[32] A. Carrington, Microwave Spectroscopy of Free Radicals, Academic Press, New York, 1974, pp. 50–53.

[33] T.K. Ishii, Microwave Engineering, second ed., Harcourt Brace Jovanovich, San Diego, 1989, p. 92.

[34] D. Agrawal, et al., Effect of microwave electric and magnetic fields in single mode cavity on material processing, Proceedings of International Symposium on Microwave Science and its Application to Related Fields, 2002.

[35] R. Roy, D. Agrawal, J. Cheng, S. Gedevanishvilli, Full sintering of powdered-metal bodies in a microwave field, Nature 399 (1999) 668–670.

[36] J. Luo, et al., Theory and experiments of electromagnetic loss mechanism for microwave heating of powdered metals, Appl. Phys. Lett. 84 (25) (2004) 5076.

[37] J. Mispelter, et al., NMR Probeheads for Biophysical and Biomedical Experiments, Imperial College Press, London, 2006, p. 336.

[38] A. Leroy-Willig, The slotted cylinder, an efficient probe for NMR imaging, Magn. Reson. Med. 2 (1985) 20–28.

[39] C.E. Hayes, et al., An efficient, highly homogeneous radiofrequency coil for whole-body NMR imaging at 1.5 T, J. Magn. Reson. 63 (1985) 622–628.

[40] J. Mispelter, et al., NMR Probeheads for Biophysical and Biomedical Experiments, Imperial College Press, London, 2006, p. 317.

[41] F. Grover, Inductance Calculations, Dover Phoenix ed., Dover Publications, New York, 2004 (originally published 1947).

[42] University of Missouri University of Science and Technology, Electromagnetic Compatibility Lab website. <http://emclab.mst.edu/inductance/>.

[43] H.A. Wheeler, Inductance formulas for circular and square coils, Proc. IEEE 70 (12) (December 1982).

[44] S. Ramo, J.R. Whinnery, T. Van Duzer, Fields and Waves in Communication Electronics, third ed., Wiley, Hoboken, NJ, 1994, pp. 194–195.

[45] M.E. Van Valkenburg (Ed.), SAMS Reference Data for Engineers: Radio, Electronics, Computer, and Communications, eighth ed., Prentice Hall, Carmel, IN, 1993, pp. 3–6.

[46] R.J. Riegert, Private communication.

[47] A.D. Podoltsev, Analysis of effective resistance and eddy-current losses in multiturn winding of high-frequency magnetic components, IEEE Trans. Magn. 39 (1) (January 2003) 539–548.

[48] M.E. Van Valkenburg (Ed.), SAMS Reference Data for Engineers: Radio, Electronics, Computer, and Communications, eighth ed., Prentice Hall, Carmel, IN, 1993, pp. 4–6.

[49] R.J. Riegert, Private communication.

[50] M.T. Thompson, Available at: <http://members.aol.com/marctt/Technical/Inductance_References.htm/>.

[51] D. Schieber, On the inductance of printed spiral coils, Arch. Elktrotech. 68 (1985) 155–159.

[52] B.A. Ancion, et al., Circuit properties of coils, IEEE Proc. Sci. Meas. Technol. 44 (5) (1997).

[53] J. Mispelter, et al., NMR Probeheads for Biophysical and Biomedical Experiments, Imperial College Press, London, 2006, p. 103.

[54] E.J. Davies, Conduction and Induction Heating, Peter Peregrinus, 1990.

[55] P.N. Paraskevopoulos, et al., Handbook of Induction Heating, Marcel Dekker, 2003.

[56] V. Pilic, Selective heat treating, Adv. Mater. Processes 149 (2) (1996) 37–39.

[57] P.M. Slangen, et al., Induction heating: a novel tool for zeolite synthesis, Zeolites 18 (1996) 63–66.

[58] A.D. Savia, Induction heating of samples in vacuum system, Proceedings of COMSOL User's Conference, Grenoble, 2007. Available at: <http://cds.comsol.com/dl/papers/2595/della_savia.pdf/>.

[59] N.R. Stansel, Induction Heating, McGraw-Hill, New York, 1949.

[60] D. Delage, R. Ernst, Modelisation Electrique d'un systeme de fusion par induction en creuset froid, Rev. Gen. Electrotherm. 4 (1983) 262–272.

[61] P. Duquenne, A. Deltour, G. Lacoste, Application of inductive heating to granular media medelling of electrical phenomena, Can. J. Chem. Eng. 72 (1994) 975–981.

[62] K. Thompson, Y.B. Gianchandani, J.B. Booske, Direct silicon–silicon bonding by electromagnetic induction heating, J. Microelectromech. Syst. 11 (4) (2002) 285–292.

[63] K. Thompson, J. Booske, Y. Gianchandani, R. Cooper, RF and microwave rapid magnetic induction heating of silicon wafers, in: M. Willert-Porada (Ed.), Advances in Microwave and Radio Frequency Processing, Springer, Berlin, 2006.

[64] K.J. Coakley, et al., Estimation of Q-factors and resonant frequencies, IEEE Trans. Microw. Theory Tech. 51 (3) (2003) 862–868.

[65] Advanced Design System, <http://eesof.tm.agilent.com/products/ads_main.html/>.

[66] E.B. Baumeister, C.O. Bennett, Fluid-particle heat transfer in packed beds, A.I.Ch.E. J. 4 (1) (1958) 69–74.

[67] M. Mehdizadeh, T.A. Koch, K.R. Krause, S.K. Sengupta, B.E. Blackwell, US Patent 6,315,972, November 2001.

[68] P. Duquenne, A. Deltour, G. Lacoste, Application of inductive heating to granular media: temperature distribution in a granular bed, Int. J. Heat Mass Transfer 36 (9) (1993) 2473–2478.

[69] T.A. Koch, K.R. Krause, M. Mehdizadeh, Improved safety through distributed manufacturing of hazardous chemicals, 5th World Congress of Chemical Engineering, July 1996, Paper 52a, American Institute of Chemical Engineers, New York, 1996.

[70] P.S. Ruggera, et al., Development of a family of RF helical coil applicators which produce transversely uniform axially distributed heating in cylindrical fat–muscle phantoms, IEEE Trans. Biomed. Eng. BME 31 (1) (January 1984).

[71] UIE, Electromagnetic Induction and Electric Conduction in Industry, Center Français de L'Electricité, 1997, pp. 567–573.

[72] http://content.honeywell.com/sensing/pressreleases/2000/5000tc.stm

[73] A.J. Peytony, et al., An overview of electromagnetic inductance tomography: description of three different systems, Meas. Sci. Technol. 7 (1996) 261–271.

[74] S. Al-Zeibak, et al., A feasibility study of in vivo electromagnetic imaging, Phys. Med. Biol. 38 (1993) 151–160.

CHAPTER 8

RF/Microwave Applicators and Systems for Joining and Bonding of Materials

CHAPTER CONTENTS

INTRODUCTION

Joining of dielectrics is perhaps the second most widespread application of RF and microwave heating after domestic microwave heating of food. The reason for this success is that volumetric heating with electromagnetic fields directly deposits energy to the joining surfaces where the increase in temperature is needed most. On the other hand, poor thermal conductivity in most dielectrics makes it difficult for conventional heat transfer methods to impart heat at the joining line efficiently.

While we use "joining" as the most general description, other terms such as welding, bonding, and sealing are used in the industry that reflect specifics of the method and the materials. In all these methods volumetric heating is used for fusion welding, adhesive curing, or implant joining of dielectrics. At the end of the process, the workpieces remain mechanically

Microwave/RF Applicators and Probes for Material Heating, Sensing, and Plasma Generation

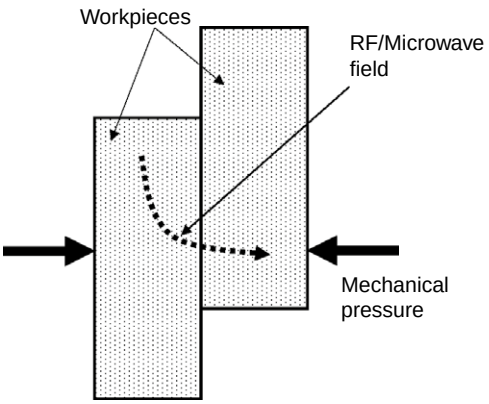

FIGURE 8.1 *General arrangement of a high-frequency/electromagnetic bonding/joining operation. Three elements are needed: intense field, presence of material that are susceptible to high-frequency heating, and mechanical pressure.*

joined upon return to room temperature. These methods include radio-frequency (RF) welding, induction implant welding, and microwave welding.

In electromagnetic welding three main elements are typically needed for the process to be completed, as shown in Figure 8.1: first, an intense field (depending on the situation it is either an electric or magnetic field) at sufficiently high frequency generated by an appropriate applicator; second, the presence of materials that are susceptible to heat in the field; third, a sufficient amount of mechanical pressure.

Most review literature in this area [1–10] is geared towards process and operational issues. In this chapter, however, in keeping with the scope of the book, the emphasis is on applicator and system design, as well as a review of the latest development in these areas. We will first discuss the general attribute and categorize the various methods in Section 8.1. In Section 8.2 we will cover the subject of RF welding of thermoplastics, which has been in commercial existence for decades and is widespread. In the subsequent sections we will cover induction implant welding and a newer technique of microwave welding.

8.1 PHYSICAL CONFIGURATIONS IN HIGH-FREQUENCY JOINING

There are four general physical configurations for electromagnetic joining of dielectrics, as shown in Figure 8.2. In each configuration the presence of a properly applied RF/microwave electromagnetic field at a frequency appropriate for the situation is assumed. In this section these major categories are defined and discussed in some detail.

8.1.1 Electromagnetic fusion welding

The first and most common configuration (Figure 8.2a) is fusion welding, where two workpieces that are typically the same polymeric material are softened and fused together with the combined application of electromagnetic volumetric heating and mechanical pressure. In fusion welding both dielectrics need to be heated via an E field to their melting or softening point. As such, the heating is governed by the general E-field heating equation (Eq. (1.18)). This process is effective as long as a combination of the

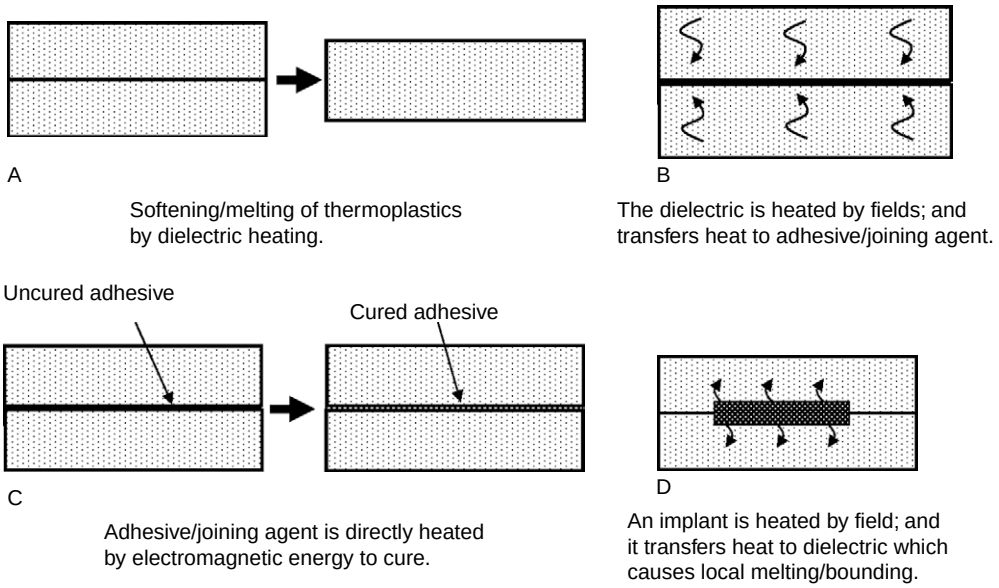

FIGURE 8.2 *Various physical forms of electromagnetic welding with RF/microwave fields.*

E field, the frequency of operation, and the dielectric loss are high enough to generate sufficient heat for proper softening or melting. In this modality the electric field direction can be either vertical or horizontal to the joining surface but, as we will see later, vertical is more common. The most widely used dielectric fusion welding method in the industry today is RF fusion welding, also known as dielectric welding, which is covered in detail in Section 8.2. RF welding has serious material compatibility limitations, and can only be implemented on a few (though highly common) thermoplastics such as polyvinyl chloride (PVC) with very high dielectric loss. For lower-loss thermoplastics microwave welding, which uses a radically different applicator configuration, is covered in Section 8.4.

8.1.2 Electromagnetic joining with curable adhesives or joining agents

Radio-frequency or microwave curing of adhesives is a commercially important process that is used in a number of practical settings. It is used in the fixation of prosthetic joints in some fields of medicine, the acceleration of adhesive setting in the woodworking industry [11], and the bonding of automobile parts in the automotive industry [12].

In the first category of adhesive electromagnetic joining, as shown in Figure 8.2b, the two workpieces are heated with electromagnetic fields, and

transfer the heat to a thermally cured adhesive placed at the joining surfaces [13]. In this modality the temperature of the joint is raised to the curing temperature of the adhesive, but stays below the melting point of the main workpieces. The adhesive is not necessarily heated with electromagnetic fields, therefore it does not need to have high dielectric loss, nor is it necessary for the direction of the fields to promote heating of the adhesive. Volumetric electromagnetic heating is useful here because the main material has typically low thermal conductivity, and transferring the heat to the adhesive would be slow with conventional hotplate methods. This modality is often used in joining of thick bulk items such as wood [1], even though plastics and other dielectrics have also been subject to this type of joining. Since softening or melting is not required, the need for high fields or high voltages is limited, which makes this modality less challenging to implement.

The other adhesive joining modality is shown in Figure 8.2c, where the adhesive or a joining agent receives the energy directly from the electromagnetic fields. This method is useful when the main workpieces to be joined do not have sufficient dielectric loss, and curing the adhesive by direct electromagnetic heating is needed. Low-loss thermoplastics such as high-density polyethylene (HDPE) [14] are good candidates for this method, but the adhesive must be high in dielectric loss for proper curing. In addition, since the adhesive layer is usually thin compared with other dimensions in the system, the direction of E fields must be parallel to the adhesive surface to deposit significant amounts of energy into the adhesive or joining agent. An example of an effective field configuration for the adhesive RF joining process [7] is shown in Figure 8.3. A parallel-plate set of electrodes is used to edge-join a number of rods with square cross-section. The electric field is in parallel with the plane of the adhesive, which is the most efficient way to interact the fields with the adhesive plane.

In another example of this modality, an applicator configuration for adhesive stray-field bonding of layers of a continuous ribbon is described [14], shown in Figure 8.4. A stray-field electrode system applies an E field, which has a strong component parallel to the ribbon/adhesive stack. The two ribbons to be joined can be of any dielectic materials, even those with low loss factor such as HDPE. The adhesive or joining agent between them needs to have a high dielectric loss. Experiments [14] have shown that a liquid polymer such as acrylic is very effective. The RF frequency in such an arrangement is one of the ISM bands of 13.6, 27.12, or 40.68 MHz. The RF power level in this process is dependent upon the required production speed, the time required for the specific adhesive to heat-cure, and the width of the ribbon.

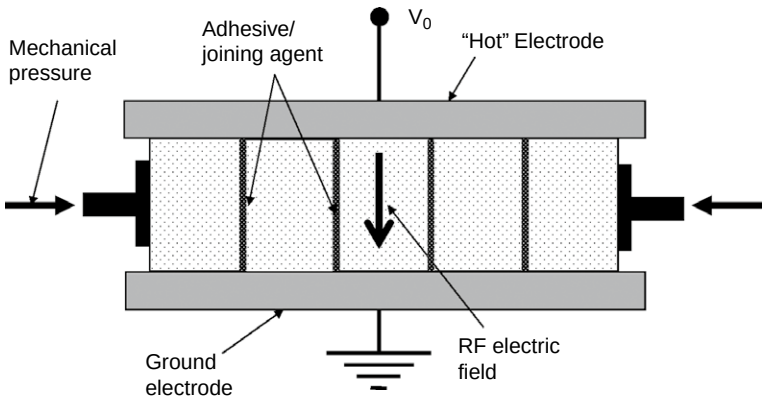

FIGURE 8.3
RF edge-joining with the direction of E-field matching the adhesive plane.

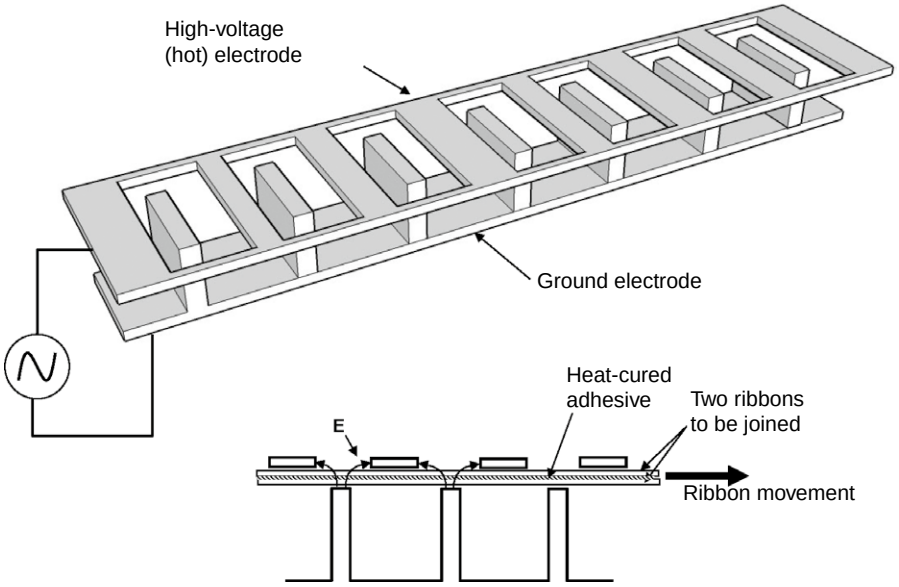

FIGURE 8.4
A stray-field ribbon bonding applicator (After Ref. [4]). This arrangement is effective because of the heavy presence of E-field longitudinal components.

8.1.3 Electromagnetic joining with susceptive implants

Figure 8.2d shows the last electromagnetic joining modality where an implant, which is typically an electromagnetically heated solid or semi-solid, is placed between the two workpieces. Heating of the implant produces local melting of the main workpieces, and upon subsequent cooling the pieces are joined. Here the main joined materials need not be electromagnetically heated. An advantage of this method is that the joint can be undone if the heating process is repeated. The main difference between this

modality and those with curing adhesive shown in Figure 8.2b and c is that the bond line is fused together instead of adhesive being the joining agent. One advantage of susceptive implant systems is the capability to undo the bond by subjecting the workpiece to the electromagnetic fields again.

Most joining performed with this method in the industry is induction implant welding, which is covered in Section 8.5, while microwave welding, which is covered in Section 8.4, is also used.

8.2 RF FUSION WELDING OF THERMOPLASTICS: APPLICATOR AND SYSTEM CONSIDERATIONS

Of all the configurations of electromagnetic welding, RF fusion welding is easily the most common. In addition to traditional applications in the assembly of common plastic parts, there have been recent, less common applications such as bonding of capsules in pharmaceuticals [15], and in manufacturing containers for high-pressure gases for medical applications [16,17].

The most common form of fusion welding applicator is shown in Figure 8.5, where the dielectric workpieces to be welded are between two metal electrodes (usually aluminum); a strong E field in RF frequencies is applied together with mechanical pressure. RF heating would soften or melt the workpieces and the mechanical pressure fuses them together. In this configuration the electrodes play three roles: first, they provide the E field by a high RF voltage connected to one of the electrodes; second, they provide the mechanical pressure; and third, the electrodes play the part of the die, where they set the lateral size and pattern of the weld. Due to the prevalence of RF

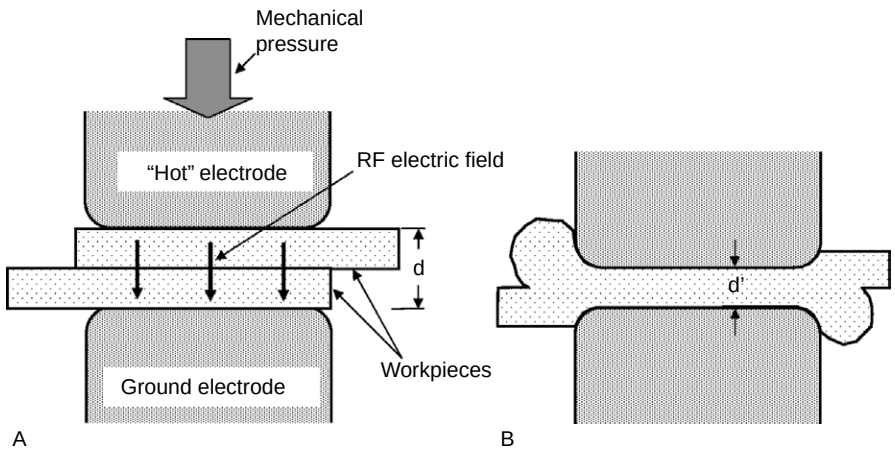

FIGURE 8.5
RF fusion welding of thermoplastics. (A) Before the application of RF energy. (B) Conclusion of welding process.

fusion welding (also known as dielectric welding), several aspects of applicator design and practice are covered in some detail in this section.

8.2.1 System and process for RF fusion welding

To understand the attractiveness of RF welding compared to its traditional rival, hot plate welding, Figure 8.6 shows a comparison of thermal profiles between hotplate welding (*a*) and RF welding (*b*). In hotplate welding the heat from the hotplate surface must be transferred to the joining surface through the material which typically has poor thermal conductivity. Therefore a thermal profile is established where the joining is the coolest point. In electromagnetic welding, however, the electrodes are cold and the heat is deposited into the workpieces uniformly, but some heat is transferred to the electrodes, which create the heating profile shown in Figure 8.5b, where the joining surface is at the highest temperature. In many industrial cases hotplate welding is slow and costly since the die must be heated and cooled each time a weld is made.

The process steps for RF fusion welding are depicted in the chart of Figure 8.7[12]. The *E* field and the pressure start together at the beginning of the process. After a few seconds, which depends on several process factors, the workpiece becomes melted and the electrodes are brought closer to a predetermined "stop" point. At this point the RF field stops, but the pressure remains in place, and the "soaking" period starts, where the newly formed joint solidifies before the pressure is taken off and the welding process ends.

Figure 8.8 shows a schematic 3-D view of a modern RF welding system. The electrode system is composed of the "hot" and ground electrodes,

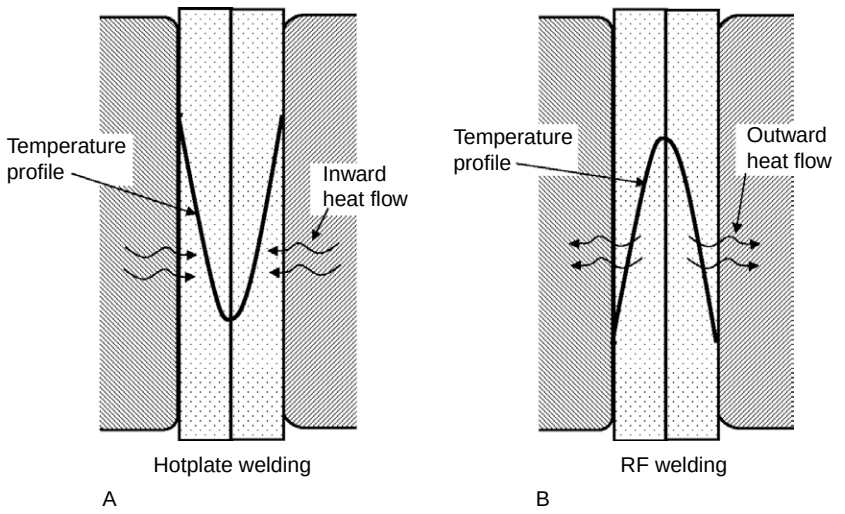

FIGURE 8.6
Thermal profile comparison between hotplate welding and electromagnetic welding.

FIGURE 8.7
Temperature history of glue (After Ref. [12]).

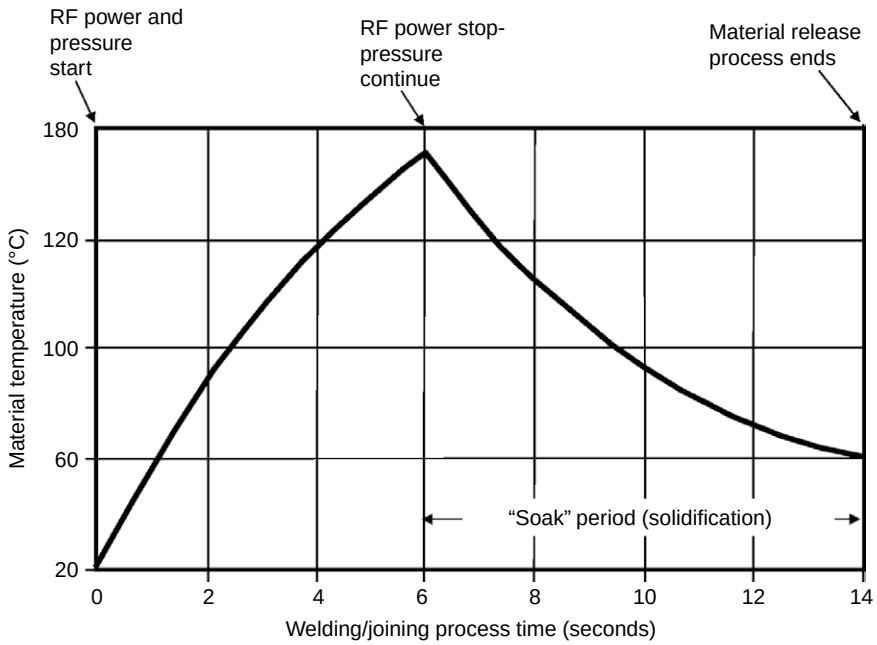

FIGURE 8.8
Essential parts of a modern RF welding system.

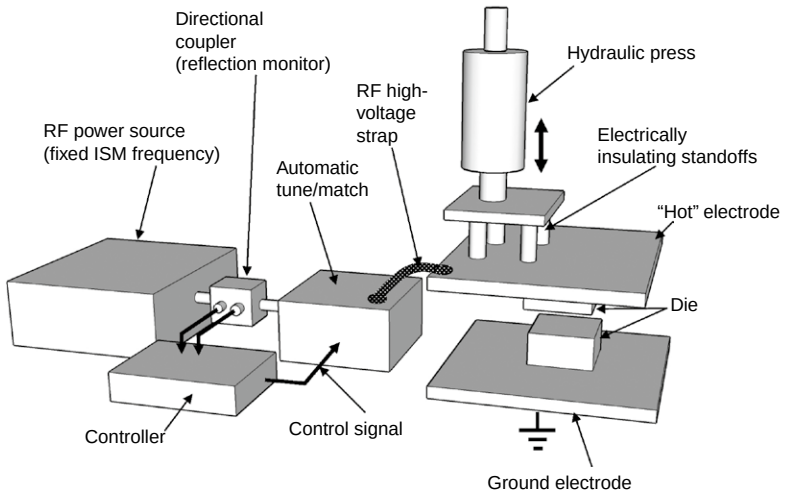

which hold the high-voltage difference needed to produce the electric field in the workpiece. The die, which is the part in intimate contact with the workpiece, is made of an easily machinable metal, and holds the shape of the weld line. Separated from the hot electrode is a hydraulic press system that produces the mechanical pressure needed to join the workpieces in conjunction with the RF heating.

8.2.2 Parallel-plate welding applicator: RF power requirements considering heat losses

In industrial applications of RF fusion welding the cost of manufacturing is heavily dependent upon the time allowed for each weld. Therefore optimizing the weld time is a necessity, which makes it useful to know the power needed for the allotted time for each weld. In this section we will cover a method to calculate the power requirements versus other parameters. Because of the intimate contact between the dielectic workpiece and the electrodes, the heat losses are significant in the computation of power requirements; therefore the heat losses to the electrodes are computed.

Consider a planar dielectric load, which could be a stack of one or more layers of dielectrics sandwiched between two parallel electrodes. Upon the start of the weld process all parts are assumed at room temperature, and it is further assumed that the mass of the metal is large enough so that all the heat transferred to it by the dielectric is taken away to the interior of the metal mass.

The computations for heat losses have been worked out by Brown et al. [11] from the first principles of thermodynamics and are given in the form of equations and nomograms, which were common prior to the digital computing age. An alternative modern method is to use finite element analysis with multi-physics capabilities [18] to solve this problem. However, in cases where employing these methods is expensive or unavailable, Brown et al.'s results have been modernized here by converting the work into the SI system and using curve-fitting methods to replace nomograms, so that the computation can be done with a calculator or programmed into a simple code for one of the currently available computing systems.

Referring to the configuration shown in Figure 8.5, the power requirement per unit volume (in watts per cubic meter) of the workpiece material is given [11] as:

$$P_v = \frac{\pi^3 k\,\Delta T}{4d^2 f\left(\dfrac{\pi^2 k t}{c\rho d^2}\right)} \tag{8.1}$$

where k is the dielectric's thermal conductivity in W/m-°C, ΔT is the necessary dielectric temperature rise, d is the total thickness of the dielectric workpieces while being pressed by the electrodes, at the beginning of the joining for welding process, t is the time required to complete the welding job in seconds, c is the specific weight of the dielectric in kg/m^3, and

ρ is the specific heat of the dielectric in J/kg-°C. Function f is a third-degree polynomial:

$$f(x) = 0.59 + 0.73x - 0.07x^2 - 0.29x^3 \tag{8.2}$$

where variable x is defined as:

$$x = \log_{10}\left(\frac{\pi^2 k t}{c \rho d^2}\right) \tag{8.3}$$

which is valid when the argument is over the range of $0.1 \leq x \leq 10$.

Example 8.1

Two sheets of PVC, each 2 mm thick with the weld dimensions of 3 cm × 20 cm, are being RF welded together using aluminum electrodes. A temperature rise to softening of 130°C within 5 seconds is required. Calculate the RF power needed, knowing that part of the heat will transfer to the electrodes. Compare this result with the same case, but with no heat losses.

Solution

For PVC, the thermal conductivity, specific weight, and specific heat are listed as $k = 0.167$ W/m-°C, $c = 1400\,\text{kg/m}^3$, and $\rho = 1672$ J/kg-°C respectively. Using $d = 4$ mm as the thickness of both PVC layers, then $x = -0.686$ and is inserted into Eqs (8.2) and (8.3). Inserting in Eq. (8.1), $P_v = 7.05 \times 10^7\,\text{W/m}^3$. Multiplying this by the volume of the welded area $v = 2.4 \times 10^{-5}\,\text{m}^3$, the power required is calculated to be $P = 1697$ W (with heat losses).

For comparison purposes we calculate the power required if the heat losses are ignored:

$$P\ (\text{no losses}) = v\ (\text{m}^3) \times c\ (\text{kg/m}^3) \times \rho\ (\text{J/kg-°C}) \times \Delta T\ (\text{°C})/t\ (\text{seconds})$$

$$P = 2.4 \times 10^{-5} \times 1400\ \text{kg/m}^3 \times 1672 \times 130/5 = 1460\ \text{W}$$

Comparing the two figures, this means that 237 W is lost to the electrodes.

Most RF welding and joining jobs are done on small parts and need only up to a few kilowatts of power. The smallest systems, which are tube sealers used in medical applications [19], are around 100 W. However, for applications such as automotive trim panels [12], heal pads for automotive carpets,

and other automotive applications, the power requirements are quite high and 100 kW is sometimes used.

8.2.3 Parallel-plate welding applicator fields, power, and voltage for fusion welding

In the radio-frequency welding parallel-plate applicator of Figure 8.5, two layers of thermoplastic with dielectric loss factor ε_r'' are to be fusion welded at frequency f such that the distance between the two electrodes is d (double the thickness of each layer), and the welding area is A. Using Eq. (1.18), the power imparted per cubic meter of material from the RF field is:

$$P_v = 2\pi \varepsilon_0 \varepsilon_r'' f E^2 \tag{8.4}$$

where E is the electric field in volts/meter and $\varepsilon_0 = 8.85 \times 10^{-12}$ is the permittivity of free space.

Considering the volume of the workpiece Ad, the power dissipated is then:

$$P = P_v A d \tag{8.5}$$

Using the relationship $E = V/d$ the voltage V needed to perform the welding is:

$$V = \sqrt{\frac{P d}{2\pi \varepsilon_0 \varepsilon_r'' f A}} \tag{8.6}$$

The level of voltage applied is very important in determining the success of a welding job. Because of close spacing between the electrodes, too high a voltage may cause arcing, overheating, or burning at the edges of the workpiece. For example, if the dielectric loss is too low, according to Eq. (8.6) the voltage needs to be increased up to the point where arcing may occur before the power level needed to soften the thermoplastic is reached.

Equation (8.6) calculates the needed voltage needed only at the beginning of the welding process. After the thermoplastic starts heating the dielectric loss increases, and after it softens, in the case of fusion welding, the distance between electrodes decreases. Both these changes tend to reduce the voltage needed as the welding continues [20]. Therefore this equation computes the worst case for voltage requirements.

Example 8.2

In Example 8.1, suppose that the dielectric loss factor of a certain grade of PVC is $\varepsilon_r'' = 0.15$ and the frequency of operation is 27.12 MHz. Assume that the power efficiency of the electrode system is 70%. What is the electrode voltage at the beginning of the welding cycle?

Solution

The minimum power needed was calculated in Example 8.1 to be 1697 W. On the basis of 70% efficiency, the actual power dissipated $P = 1697/0.7 = 2424$ W. Inserting these values in Eq. (8.6) we obtain:

$$V = \sqrt{\frac{2424 \text{ W} \times 0.004 \text{ m}}{2\pi\, 8.85 \times 10^{-12} \times 0.15 \times 27.12 \times 10^{6} \times 0.03 \text{ m} \times 0.2 \text{ m}}} = 2680 \text{ V}$$

To demonstrate the impact of the material on the system design, if instead of PVC the workpiece was polystyrene with a dielectric loss of 0.005, the minimum voltage requirement would jump to 14.7 kV. With such a large voltage there is a high risk of arcing, particularly at the edges of the electrodes where the *E*-field gradients are higher. This example shows the limitations of RF fusion welding when the material does not have a sufficient loss factor. In the next section we will discuss arcing as a failure mechanism in more detail.

8.2.4 Failure mechanisms in RF welding

Because of the close proximity and high voltage in RF welding electrodes, arcing is the most common failure mechanism. When arcing occurs, in addition to the process upset and loss of the part, the die itself is damaged, where the replacement is expensive and time-consuming. Following an arcing event, if the die is not replaced, the location of the arc becomes a weak point for future arcs [20]. Because of the above factors prevention of arcing is an important consideration for an RF welding system.

The starting point of an arcing failure is either through corona discharges at the edges of the die or by punch-through breakdown. Heating of polymer usually raises its dielectric loss, which in turn reduces its voltage breakdown capability. The heating of the dielectric and reduction of the electrode gap happen towards the end of the welding operation, which leads to most breakdowns happening in this period.

The electric fields, which are more intense at the electrode edges, heat the polymer earlier than the bulk (the middle of electrode). Therefore most arcs and damage occur at the edges. Corona at the edges is another mechanism for overheating, polymer damage, and arcing.

A simple way around arcing is to have smooth electrodes and rounded electrodes, but this may cause undesired shape effects. Therefore making very round edges for the die, while it reduces the chances of arcing, is not always a possibility.

One way to reduce the chances of arcing is to increase the loss factor of the material per Eq. (8.6). For some dielectrics such as PVC, adding plasticizers [4] will lead to a higher loss factor. Another way to decrease the chance of arcing is to allow more time for welding to take place at a lower electrode voltage. In a high production rate environment this is a tradeoff that needs to be considered carefully.

In the next two sections we will discuss two system and electrode modification methods to prevent arcing. In Section 8.2.7, we will describe a tripping circuit used to prevent arcing.

8.2.5 Dielectric buffer layer in RF fusion welding

The buffer layer is an additional layer of a low-loss dielectric between the electrodes in addition to the workpieces [21], as shown in Figure 8.9. The use of a buffer layer, which has several advantages in certain types of dielectric welding, is particularly helpful in welding of thin sheets, where the electrodes come very close towards the end of the welding due to softening of the material, when the possibility of arcing is the highest. In asymmetrical electrode systems, as shown in Figure 8.9, the edges of the top electrode tend to provide

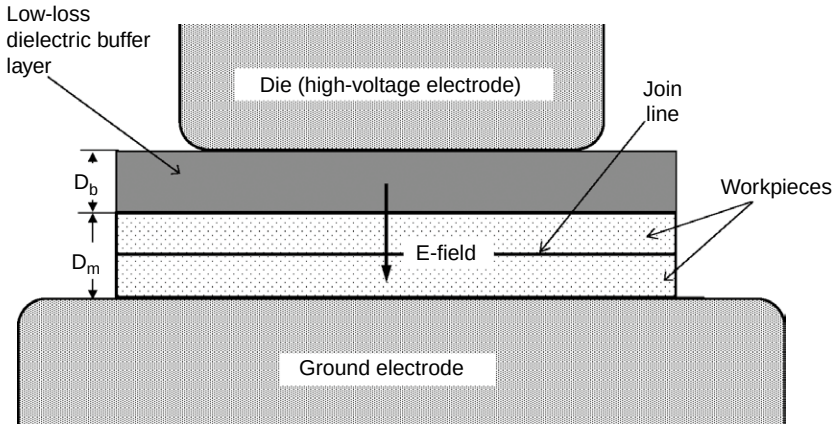

FIGURE 8.9 *RF welding with a buffer layer to prevent arcing.*

additional heating, which may damage the material. The buffer layer, when it is placed near the high-voltage electrode, will also prevent this damage.

The buffer layer, since it has a far smaller thermal conductivity than the metal electrodes, tends to reduce the heat loss, which in turn reduces the need for higher power, hence higher voltage. Another advantage of the buffer layer is that it reduces the change in the electrode distance, which will lead to a less pronounced change in the value of the electrode capacitance, which in turn reduces the effort needed to retune the circuit.

The material chosen for the buffer layer is a dielectric such as PTFE, polypropylene, silicone, or polyamide. These materials all have low dielectric loss in common, which prevents them from heating in the RF field. These dielectrics also tend to have high breakdown voltage limits as well. This is particularly important since the main workpieces tend to have a lower dielectric breakdown in melted condition. The buffer layer keeps the electrodes from arcing under this condition. The buffer layer is deemed useful [22] in situations where the workpiece has metal parts. Without a buffer layer separating the metal, parts would arc with the closest electrode.

The buffer layers we have discussed so far are separate bodies from either the electrode or the workpiece. In another recent work by Smith et al. [23], the electrodes are coated with a low-loss dielectic such as PTFE, the thickness of which is several times the skin depth. At 27 MHz that is about 250 μm.

While adding the buffer layer helps in reducing the possibility of arcing, the workpiece still needs the same electric field for the welding to take place because of added electrode distance. Therefore the voltage between the electrodes must be increased when the buffer is present. Increasing the voltage requirements could be costly and may cause other problems such as local corona damage. Therefore it is important to know the amount of added electrode voltage when the buffer is added. Figure 8.9 shows an RF welding electrode set where two thermoplastic sheets with dielectric constant ε_r' and dielectric loss factor ε_r'' and a total thickness D_m are to be welded. A buffer layer with dielectric constant ε_{rb}' and negligible dielectric loss has a thickness D_b. Referring to Eq. (A3.1) in Appendix A3.1, for two-layer parallel plates, inserting the parameters in Figure 8.9, the absolute value of the electric field in the thermoplastic layers is:

$$E_m = \frac{\varepsilon_{rb}' V_{0b}}{\sqrt{D_b^2(\varepsilon_r'^2 + \varepsilon_r''^2) + 2\varepsilon_r'\varepsilon_{rb}' D_b D_m + D_m^2 \varepsilon_{rb}'^2}} \tag{8.7}$$

where V_{0b} is the voltage across the electrodes. Let us equate this electric field with the field in the case of no buffer layer, V_0/D_m, where V_0 is the voltage level when no buffer is used. Following simplifications in view of the fact that in thermoplastics $\varepsilon_r'^2 >> \varepsilon_r''^2$, the following equation shows the required electrode voltage when a buffer is used V_{0b} versus the electrode voltage without a buffer layer:

$$V_{0b} = V_0\left(1 + \frac{\varepsilon_r' D_b}{\varepsilon_{rb}' D_m}\right) \tag{8.8}$$

According to Eq. (8.8), to keep the required voltage at a minimum, the second term in the parentheses should be kept as small as possible, which means keeping the buffer layer thin and using a buffer layer with a high dielectric constant. Silicone rubber is usually a good choice for a buffer layer due to its very low dielectric loss factor, high dielectric constant, good mechanical properties, high dielectric strength, and durability after many welds. The thin coating of electrodes described by Smith et al. [23] fits this criterion.

8.2.6 Electrode edge overheating/arcing and the use of a conjugate (symmetrical) electrode to reduce it

The economy of the RF welding process calls for welding at the fastest rate, which would increase the need to use as high an electric field through the material as possible. This in turn requires higher voltages between the electrodes. The downside of this trend is the fact that the electric fields are stronger at the edges of electrodes, which often results in overheating or air discharges (corona or arcing) at the edges of the workpiece.

This situation of edge overheating and arcing is particularly observed in RF bonding of wear-resistant heal pads for automotive interior carpeting, where a sheet of vinyl is bonded to the shag side of the carpet, which is typically made of nylon. Nylon's dielectric loss increases with temperature, which gives it thermal runaway properties. During the RF welding process of the heal pad to the carpet, severe discoloration is observed. Therefore it is important to find ways of reducing the overheating at the edges of the electrodes.

Francisco and Riegert [24] have devised an electrode configuration that significantly reduces the edge effect overheating for automotive heal pads using a conjugate set of electrodes, as shown in Figure 8.10. In a conjugate electrode system the edge fields are significantly reduced in comparison

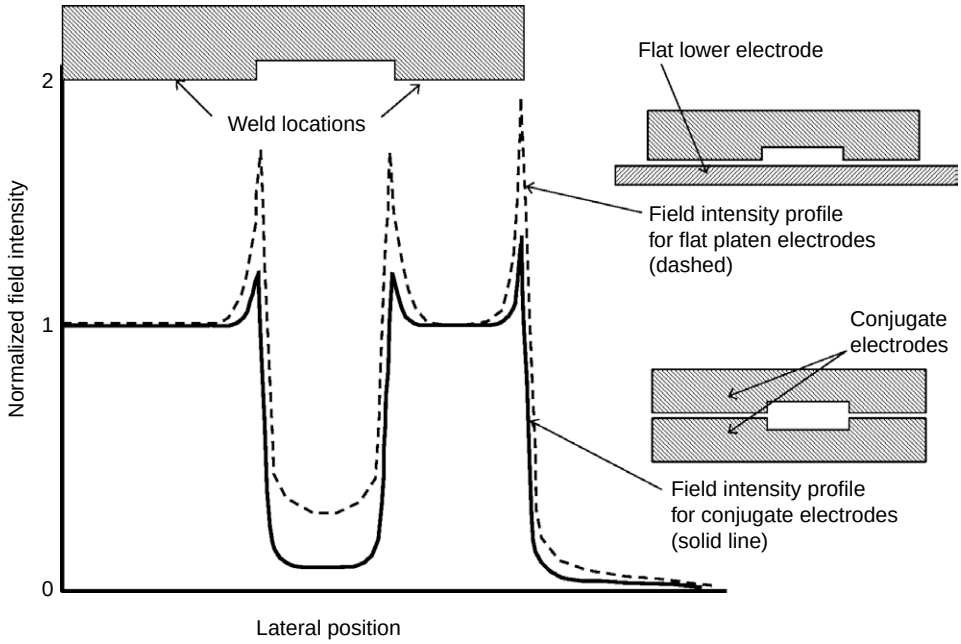

FIGURE 8.10 *The use of conjugate electrodes will reduce the intensity of the fields at the edges. (After Francisco and Riegert [24].)*

with a conventional electrode system where the pattern needed for the heal pad is only placed on the upper (or "hot") electrode. The symmetrical nature of conjugate electrodes reduces the high electric fields at the edges as proven by a modeling study.

A comparison of field intensity profile from a modeling study [24] for conventional asymmetrical electrodes with flat platen on one hand and the conjugate electrode set on the other hand is shown in Figure 8.10. The field intensity is significantly lower at the electrode edges for the case of conjugate electrodes.

8.2.7 Parameters and tradeoffs, and limitations in RF fusion welding

Even though RF fusion welding appears to be a simple process, a welding cycle is quite dynamic with a number of parameters that need to be considered. There are issues related to the material to be welded, hardware considerations, and finally timing/process order concerns.

The primary limitation of RF welding is the limited range of materials that can be welded. At the regulatory allowed bands of RF frequencies (13.56, 27.12, and 40.68 MHz) only a narrow range of dielectrics have a combination of properties required to be considered for RF fusion welding. The material parameters of interest are the dielectric loss, melting/softening point, dielectric breakdown, and changes to these parameters as the temperature of the material is raised. A few thermoplastics, particularly PVC, are known to be suitable materials for RF welding due to their high dielectric loss and low softening point. The dielectric loss of PVC can be increased markedly by making it plasticized. Unplasticized PVC has a relative dielectric loss of 0.01 and, depending on the level of plasticization, can be increased to a value up to 0.4, which means a 40-fold increase in heat generation with the same electric field.

There are, however, serious environmental issues with PVC due to the presence of halogens that release dioxins and other pollutants when PVC is land filled. Burning of PVC releases hydrogen chloride gas and dioxins, which are toxic. Because of these concerns, there has been an intense effort to find PVC replacement materials. One of the challenges is RF weldability of PVC replacements.

In order to make PVC replacement materials, several methods are utilized to increase the dielectric loss. These include addition of carbon, metal powders, or high dielectric loss minerals [10], or the use of multi-layers, some of the layers being high loss due to addition of CO to ethylene copolymers [25].

Another method is the addition of inherently conductive polymers such as polyaniline (PANI) to halogen-free PVC replacements. Figure 8.11 shows a comparison of addition of two different levels of PANI on the heating capability of HDPE [26].

All of the methods being tried for replacing PVC for RF weldability have various disadvantages such as cost, loss of mechanical properties, loss of optical clarity, or problems with appearance. Intense research into resolving all these issues is ongoing.

On the hardware and process timing front, we treated the voltage/electric field versus the failure mechanisms in Section 8.2.4. Another issue is the maximum lateral size of the workpiece in consideration of wavelength effects [11]. Due to standing waves, there is a gradual variation of voltage away from the feed point of the electrodes, which may cause non-uniformity of heating of the workpiece. Feeding the electrode at multiple points with the distance between the feed point at one-eighth wavelength is suggested [11].

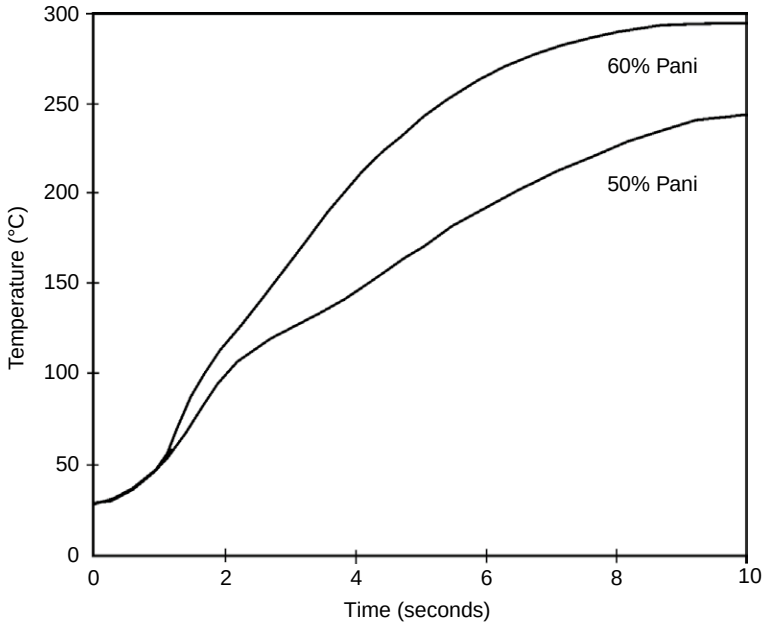

FIGURE 8.11
Addition of PANI increases RF heating capability of HDPE for welding purposes (After Ref. [26]).

8.3 SYSTEMS AND CIRCUIT ISSUES IN RF WELDING

In addition to system issues involved in all RF power systems, RF fusion welding offers a set of specific challenges that will be discussed in this section. Part of these involve the failure mechanism in RF welding that was discussed in the last section. The others involve the dynamic nature of RF welding where a welding cycle goes through several phases with simultaneous changes in material properties and electrode position.

8.3.1 System/circuit schemes in RF welding

RF welding differs from most other RF heating applications in that there is a substantial change in the impedance of the electrode system during a single welding cycle. The change comes mostly from the distance between the electrodes changing due to closing of the jaw to press the softened workpiece. A secondary change in the impedance of the electrode occurs due to a change in the dielectric properties of the workpiece as its temperature increases during the welding process. The change in the electrode's impedance is complicated by the fact that the electrode has to be resonated due to

the need for a high electric field. This all means there is a need for dynamic tuning and impedance matching during the welding cycle.

In traditional RF welding systems, the circuit scheme was one of the triode feedback oscillator methods, where the operating frequency varies as a result of the change in the electrode impedance. This style of control is no longer favored due to a tightening of the regulations on ISM bands, which do not tolerate deviation of the frequency beyond a very narrow band.

The new control approach [27], as shown in Figure 8.8, calls for a fixed frequency power source at the ISM frequency (usually 27.12 MHz). The power output of the power source goes through a directional coupler that monitors the forward and reflected power and feeds the information to a controller, which in turn sends a control signal to an automatic tune/match circuit, which also includes the inductive element that resonates the capacitive electrode system. The automatic tune/match system would change its circuit elements dynamically so that the reflected power measured by the directional couple is kept at a minimum.

8.3.2 Arc detection circuit for the applicator in RF welding

Because of the presence of high voltages, arcing during the process is always a possibility. Arcing may render an expensive die unusable because of physical damage, and also because the location where the arc occurred is likely to arc again. Therefore it is necessary to protect the welder for the occurrence of arcing.

An arc suppressor system applies a moderate DC voltage (a few hundred volts) across the electrodes. When the workpiece is squeezed between the two electrodes, a very small DC current flows through it. As the material becomes heated, the DC resistivity of the material decreases as the dielectric loss increases, therefore the DC current increases slightly. The arc suppressor is adjusted to react with a preset level of DC current and trip the system, or lower the electrode voltage prior to an arc.

A typical arrangement of an arc suppressor system for RF welders is shown in Figure 8.12.

The sensitivity of the arc suppressor can be adjusted for a given job by setting the minimum DC current where the suppressor activates. Usually, the most sensitive settings are for situations where there is a higher DC resistivity, such as in a thick material, small weld area, or where a buffer dielectric layer is used. Conversely, for thin material, large area, or no buffer layer, a higher threshold current setting is used. Otherwise too many nuisance activations of arc suppression will result.

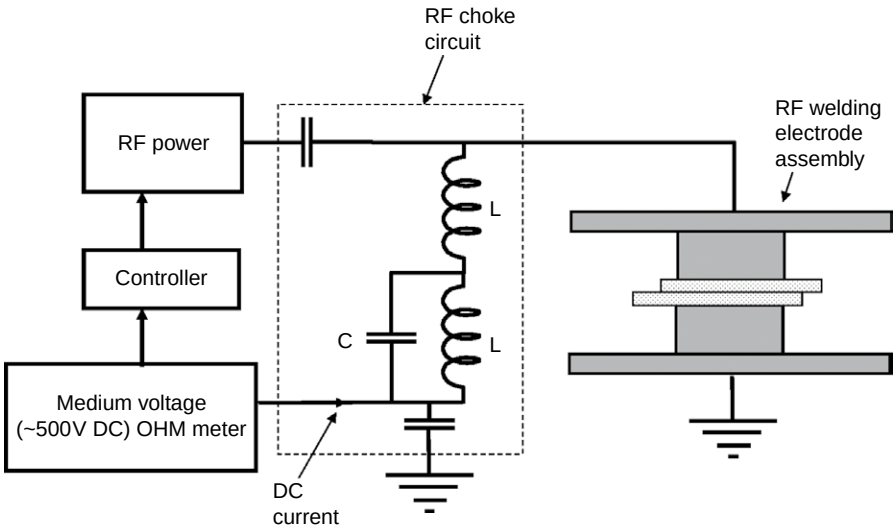

FIGURE 8.12
Arc suppression system for RF welding.

8.4 APPLICATORS AND SYSTEMS FOR MICROWAVE WELDING AND JOINING

Microwave welding/joining uses one of the ISM frequency bands above 300 MHz, particularly 2450 MHz, for joining of dielectrics. Unlike RF fusion welding, with a huge installed base in the industry, microwave welding is restricted to a few specialty applications and is mostly in the research phase. A body of literature has appeared in this area [10,28–36] in recent times. There has been particular attention paid to microwave welding of HDPE due to the need for an industrially efficient method for welding of this polymer. This shows that continued research in this area could bring huge rewards in terms of the possibilities of creating a successful set of industrial applications. The process offers considerable promise as a means for continuous processing of manufactured parts. A major concern is the heating uniformity, which needs to be addressed by innovations in applicator design.

8.4.1 Applicator configurations in microwave welding

The mechanical configuration in most microwave welding work is similar to Figure 8.2c, where the microwave energy heats a joining agent that is designed to absorb microwaves readily. Microwaves, due to their far higher frequency, are effective [37–39] in heating the join according to Eq. (8.4). The joining agent can be either a thermally cured adhesive or a susceptor material that brings the workpieces to a local melting or softening at the joint line.

Microwave welding is particularly useful for bonding of materials like HDPE, where the dielectric loss is very low, and RF fusion welding is not possible since the material cannot be heated efficiently with fields. One of the advantages of microwave implant bonding is that parts can be disassembled by microwave reheating [32].

In the joining configuration of Figure 8.2c, when the workpiece material is low loss, the only lossy material in the system would be the joining agent; therefore the fill factor of the applicator would be very low, which would lead to low power efficiency. Microwaves would be particularly useful in such applications because the high frequency would raise the power deposition markedly. Another factor that would be helpful in increasing power efficiency is making the joining agent have as high a dielectric loss as possible. In addition to these criteria, having the electric field parallel to the plane of the joint would be necessary to obtain good efficiency.

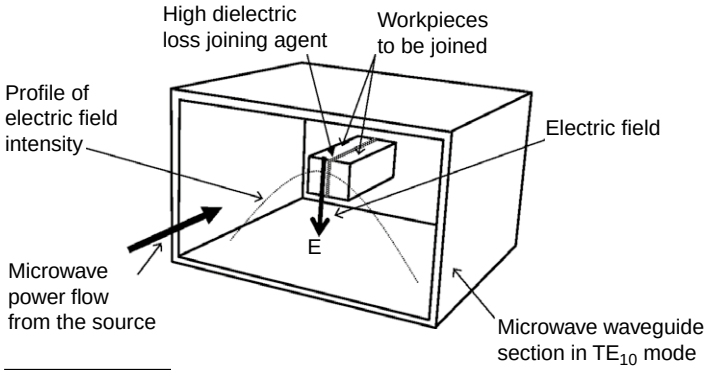

FIGURE 8.13 *A general arrangement for microwave welding where the joining surface is together with the joining agent with high dielectric loss is placed in parallel with the electric field. A TE_{10} waveguide can accommodate that.*

An applicator configuration that demonstrates the idea of the microwave welding process is shown in Figure 8.13 [32], where the workpieces are placed in a microwave waveguide at the TE_{10} propagation mode. The joining surface, containing the joining agent, is placed in parallel with the maximum of the principal electric field, which in the case of the TE_{10} mode is parallel to the shorter wall of the waveguide. The waveguide, as a transmission line, is connected at one end to the microwave power source and a dummy load is connected to the other end, where the residual power not absorbed by the joining agent is absorbed.

A practical configuration for microwave welding of parts [28] is shown in Figure 8.14, where the plastic workpieces that have a low dielectric loss are placed in a multimode microwave cavity. The parts are pressed together via an external dielectric pressure member, and a microwave choke prevents microwave leakage. Joining agents or implants are heated in the microwave field and weld the workpieces together.

Another configuration of microwave welding is butt-joining of parts using a microwave open-ended waveguide held close to the joining surface, as shown in Figure 8.15. More details on the operation of open-ended waveguides are given in Chapter 6. This configuration can also use a horn applicator.

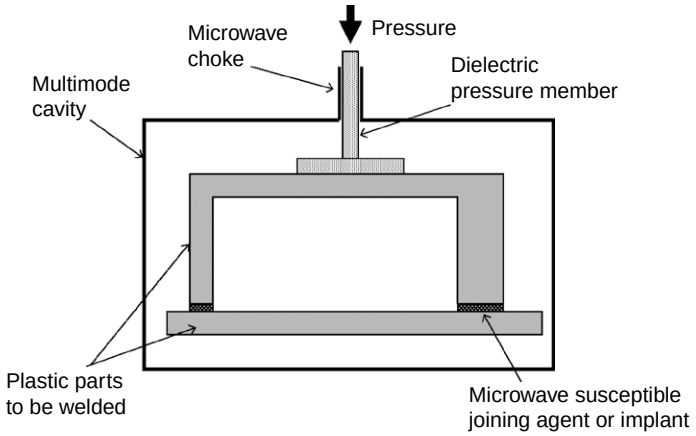

FIGURE 8.14
A microwave welding arrangement using a multimode microwave cavity. (After Wise and Froment [28].)

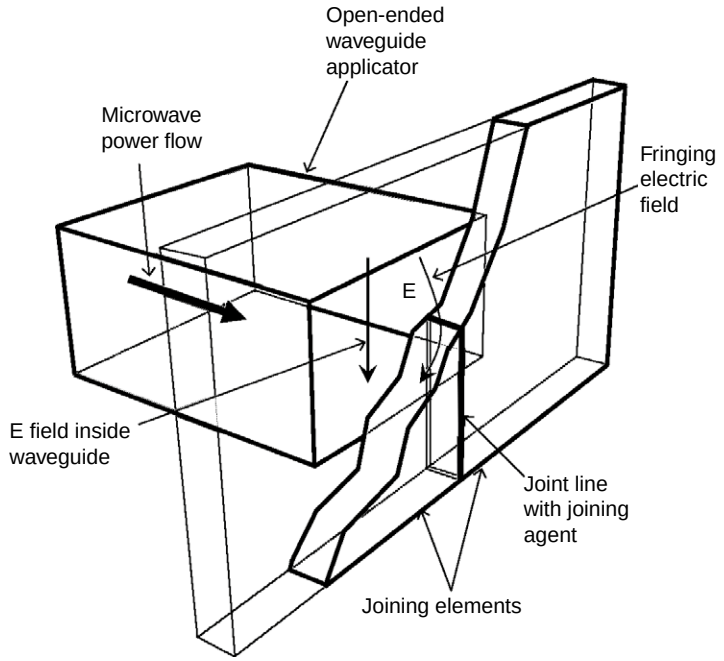

FIGURE 8.15
Microwave welding with an open-ended waveguide operating at TE_{10} mode. It is important that the short wall of the waveguide is parallel to the join line in order to couple the fringing E-field efficiently.

A continuous version of this welding method can be envisioned [40] as shown schematically in Figure 8.16. The applicator in this case is an open-ended waveguide where the open end is placed as close as is practical to the weld point. Depending on the scale of the operation and local regulatory issues, one of the ISM bands of 434, 896, 915 MHz, or 2.45 GHz can be used. The lower frequencies in this list provide for higher power and possibly deeper field penetration and thereby the opportunity for welding thicker workpieces and higher throughput.

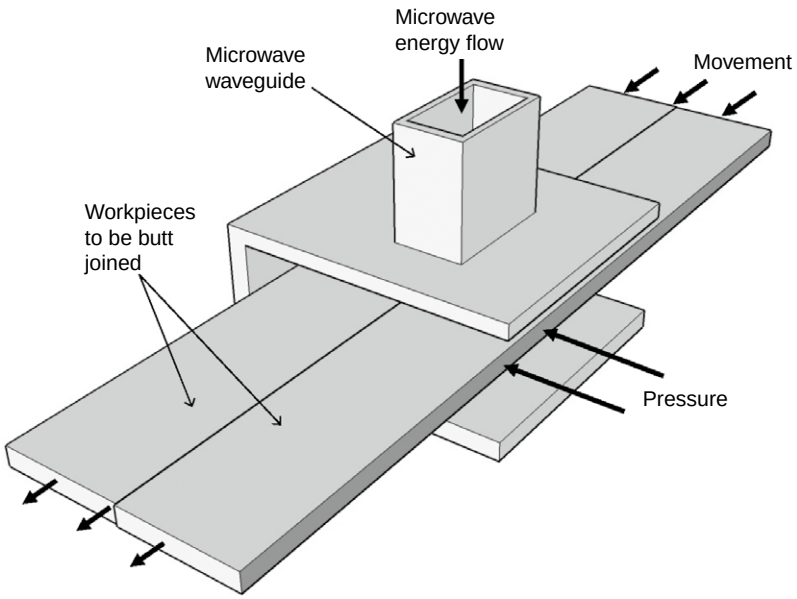

FIGURE 8.16
Continuous butt welding using an open-ended microwave waveguide. (After Siores and Rego [40].)

8.4.2 Joining agents or implant materials for microwave welding

A joining agent is a material placed at the bonding surface of the joining elements for the purpose of absorbing the microwave energy and generating heat. One of the advantages of using microwaves is that because of the high frequency, the dielectric loss requirement for the joining agent is modest, which gives the designer access to a wide range of materials. It is important for the joining agent not to have thermal runaway properties, otherwise damage to the joining surface and a weak joint can result. Polar polymers that melt will absorb more strongly when molten, and absorption increases as viscosity decreases, so they go into thermal runaway.

While non-polar polymers do not exhibit thermal runaway, adhesives such as epoxies can be heated by microwaves because they have polar groups in the hardener component. As the adhesive cures and the chemical bonds become less mobile, the ability to absorb microwave energy decreases as well, so the process is self-limiting. This is quite a desirable effect for industrial robustness of the process because this limiting temperature is well below the melting point of the joining elements.

A note should be made here that the possibility of welding without a joining agent exists; Tran et al. [41] devised a new technique for welding thermoplastic materials using microwave energy without any addition of absorbing materials. The technique involves creating a micro-plasma between

polymer parts to achieve good welding. The technique is demonstrated by joining two polypropylene rods having a diameter of 20 mm without any conducive polymer such as polyaniline.

Addition of carbon black particles to the base polymer of the parts to be joined is another method of creating sufficient loss factor for use as joining agent [42]. A carrier strip is created with addition of carbon black to the thermoplastic and strong bonds are obtained.

8.4.3 Miniature microwave welding via a special applicator configuration

A novel microwave welding technique, which combines microwave measurements with heating, has been developed [32] for bonding of polymeric microfluidic devices. The bonding is achieved by patterning the polyaniline, which is a conductive polymer, at the polymer–joint interface. The polyaniline fills the milled microchannels. The absorbed electromagnetic energy is then converted into heat, facilitating the localized microwave bonding of two polymethylmethacrylate (PMMA) substrates. A coaxial open-ended probe (microwave microscopy, Chapter 6) was utilized to study the dielectric properties of the PMMA and polyaniline at a range of temperatures up to 120°C at 2.45 GHz. The measurements confirm a difference in the dielectric loss factor of the PMMA substrate and the polyaniline, which proves that differential heating using microwaves is possible. Microfluidic channels of 200 and 400 μm widths were sealed using a microwave power of 300 W for a welding period of 15 seconds. The results of the interface evaluations and leak test show that strong bonding is formed at the polymer interface, and there is no fluid leak up to a pressure of 1.18 MPa.The temperature field of microwave heating was found by using direct measurement techniques. A numerical simulation with the finite element method confirmed and validated the experimental results. No global deformation of the PMMA substrate occurred during the welding.

8.5 MAGNETIC FIELD/INDUCTIVE APPLICATORS FOR JOINING OF MATERIALS

Induction welding of thermoplastic materials has been in commercial use for about two decades due to the unique operational and performance advantages it provides [43–48]. The principles and design methods of induction heating were discussed in detail in Chapter 7. For induction welding, in particular, the frequency range of 2–15 MHz is most common. This frequency is somewhat higher than most industrial induction heating installations.

This high frequency is needed to compensate for the low fill factor of induction welding.

Referring to Figure 8.2, which shows various formats of electromagnetic joining, in induction welding the mechanical arrangement is the option shown in Figure 8.2d. In this configuration an implant, which is susceptible to heating by high-frequency magnetic fields, is volumetrically heated and transfers the heat to the joining parts.

8.5.1 Inductive implant welding of thermoplastics

Figure 8.17 shows the basic arrangement, where a joining agent, under mechanical pressure from the joining parts, is subjected to high-frequency magnetic fields using a high-frequency magnetic field applicator, which is represented by a solenoid-type coil.

In induction welding there are two separate types of heating mechanism that can occur depending on the type of joining agent, both of which result in the transfer of heat from the joining agent to the bulk of the polymeric parts, which will cause melting and fusion upon cooling.

The first heating mechanism is through eddy currents, which typically requires a high-conductivity solid joining agent such as a sheet metal, a metal mesh, or perforated metal. For eddy current heating to be effective, materials with lower bulk conductivities than metals can possibly be used, but that requires an increase in frequency or fill factor, or both. The governing theories for such tradeoffs are detailed in Chapter 7.

The second heating mechanism is through hysteresis heating, which requires magnetically lossy materials such as ferrites. A description of conditions for this modality to work was given in Chapter 7. The composition of the joining agent in this case is a mixture of a ferromagnetic powder with either the same thermoplastic as the parts to be joined or a compatible material.

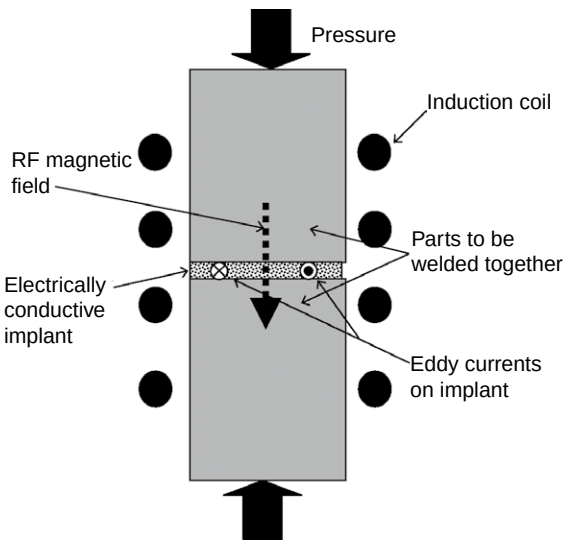

FIGURE 8.17 *Basic arrangement of an induction welding operation when the implant is heated with eddy currents. In cases where the implant is made of magnetically lossy materials, such as ferrites, the mechanism for heating is magnetic hysteresis.*

8.5.2 Applicator types used for inductive welding

A planar applicator for induction welding is shown in Figure 8.18, in which a single loop or

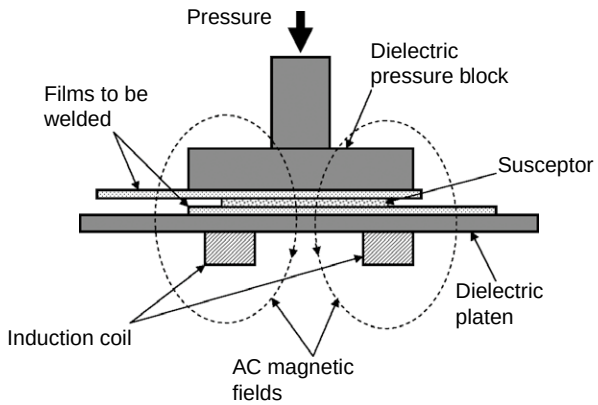

FIGURE 8.18 *Induction welding of two insulating film/sheets using a conductive or magnetically lossy susceptor. The applicator in this case is a planar loop or a spiral (pancake) coil.*

a spiral (pancake) coil can be used. This arrangement can be used for induction welding of two sheet-like materials. The susceptors in this case can be either eddy current type or hysteresis ferromagnetic type. If the area or the length of the susceptors is large, care must be taken to ensure uniformity of heating.

Figure 8.19 shows the arrangement of an inductive welding system used for a relatively complex structure [44] involving joining of two dome-like parts. The induction coil is located at the circumference of the part. In this case, due to a low fill factor, a flux concentrator, which is a ferrite device, is used in order to concentrate the energy into the susceptor implant.

One of the most widespread and successful applications of induction welding is cap sealing used in pharmaceuticals and other bottle packaging where a secure seal is needed. The arrangement of such a process is shown in Figure 8.20. The susceptor in this case is typically an aluminum sheet with a thickness of around 200 μm. The induction field heats the aluminum disk mostly on the exterior edge, which requires the most heat to adhere to the rim of the plastic bottle.

8.5.3 System issues in induction welding

Induction welding systems are different from most other applications of induction heating in that the active induction load, which is the implant material placed between the joining pieces, has a very small volume. This means that the induction coil has typically a low fill factor, which is one of the issues contributing to low applicator efficiencies. As we mentioned in Chapter 7, the disadvantages of having a low applicator efficiency go well

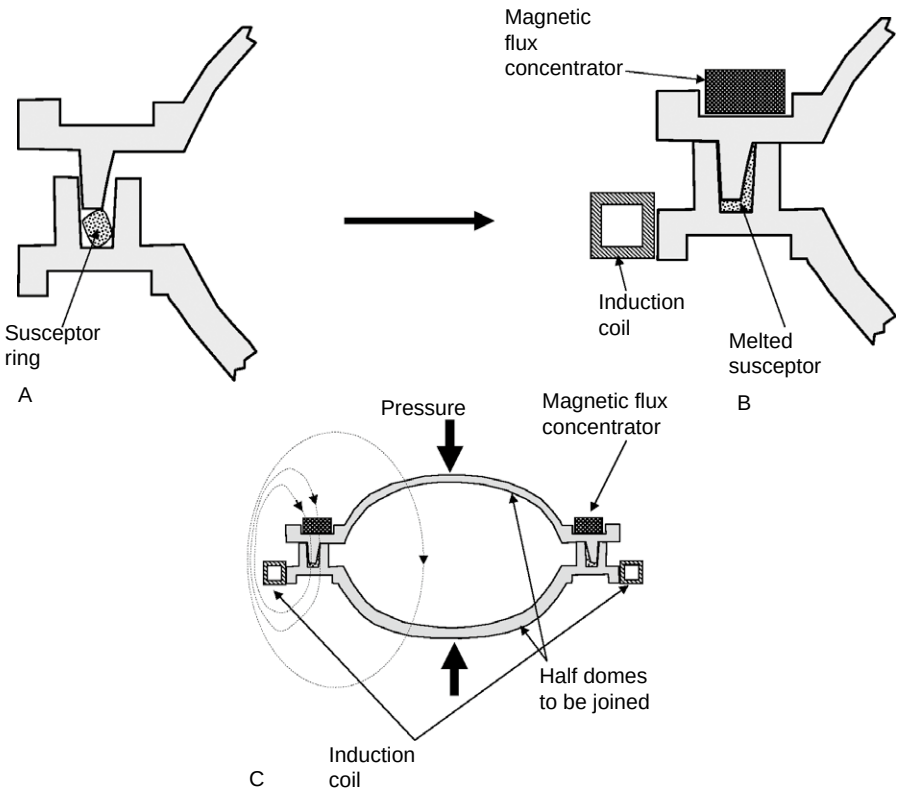

FIGURE 8.19
Tongue and groove induction welding arrangement of two plastic half shells with the aid of a magnetic flux concentrator. (A) Joining members and susceptor prior to welding. (B) After welding. (C) Field configuration.

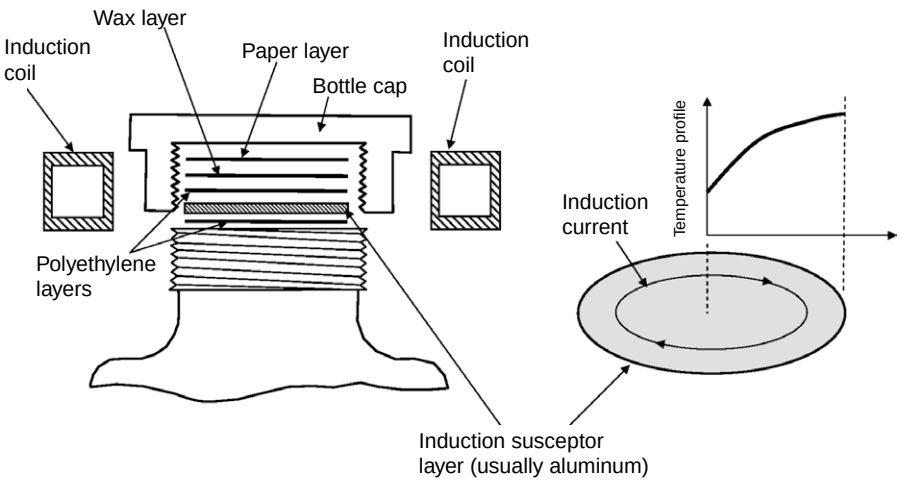

FIGURE 8.20
Layers of cap sealing from Codaco patent.

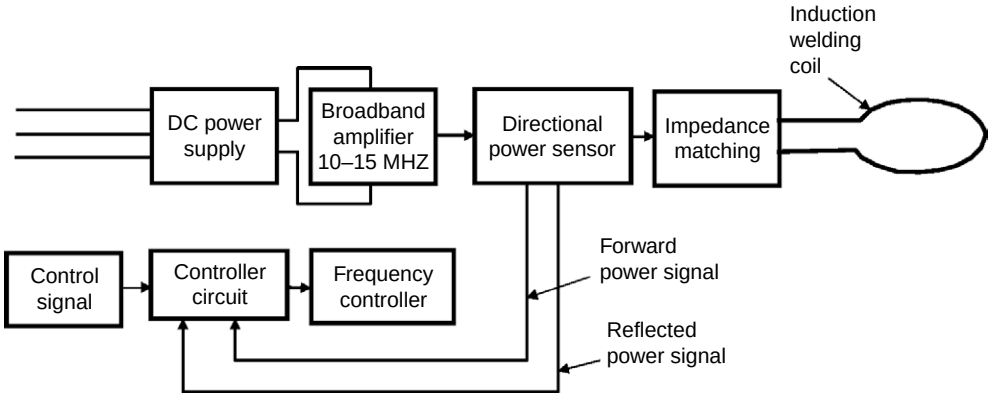

FIGURE 8.21 *Block diagram of an induction welding system. (After Ref. [49].)*

beyond energy waste. In such systems, the delivery of sufficient energy to the implant load requires very high voltages and currents that are beyond the capability of most available components. To resolve these issues, higher induction welding systems use a frequency range of 2–15 MHz as compared to ranges below 450 kHz that are used in most industrial induction systems.

Because of the high frequency, induction welding systems, instead of inverter–converter technology, which is used in lower frequency systems, employ RF amplifiers. A block diagram of an induction welding system using RF amplifier technology is shown in Figure 8.21 [49]. This type of system, which uses the 50 Ω method of power transmission [12], is equipped with directional power sensing for keeping the reflected power to a minimum.

REFERENCES

[1] A. Benatar, D.A. Grewell (Eds.), Plastic and Composite Welding Handbook, Hanser, Munich, 2003.

[2] A. Yousefpour, et al., Fusion bonding/welding of thermoplastic comosites, J. Thermoplast. Compos. Mater. 17 (2004) 303–341.

[3] J. Rotheiser, Joining of Plastics, Handbook for Designers and Engineers, second ed., Hanser, Munich, 2004.

[4] T.L. Wilson, Radio frequency dielectric heating in industry, Electric Power Research Institute, Final Report EM-4949, Research Project, 1987, 2416-21.

[5] D. Bialod (Ed.), Electromagnetic Induction and Electric Conduction in Industry, Centre Français d'Electricité, 1987, pp. 530–541.

[6] V.K. Stokes, Joining methods for plastic and plastic composites: an overview, Polym. Eng. Sci. 29 (19) (1989) 1310–1324.

[7] M. Rothstein, Encyclopedia of Polymer Science and Technology: Dielectric Heating, Wiley, New York, 1966 Vol. 5, 1–23.

[8] S. Ebnesajjad, Fluoroplastics – Melt Processible Fluoroplastics, Users Guide and Databook, William Andrew, 2002, pp. 279–283.

[9] C.A. Harper, et al., Plastic Materials and Processes: A Concise Encyclopedia, Wiley, New York, 2003, p. 135.

[10] C.A. Harper, Handbook of Plastics, Elastomers and Composites, McGraw-Hill, New York, 2002, p. 528.

[11] G.H. Brown, et al., Theory and Application of Radio-Frequency Heating, D. Van Nostrand, 1947.

[12] C. Marchand, T. Meunier, Recent developments in industrial radio-frequency technology, J. Microw. Power 25 (1) (1990) 39–46.

[13] H.W. Denny, W.B. Warren, RF bonding impedance study, Georgia Institute of Technology Interim Report, 1967. Available at NITS, www.ntis.gov

[14] T.D. Gorbold, Electrode Apparatus for Stray Field Radio Frequency Heating, US Patent 6,995,345 B2, assigned to Codaco Inc., 2006.

[15] Draisey et al., Capsules, US Patent 6,923,980, 2005.

[16] J.I. Isuchukwu, et al., Polymeric Pressure Chambers and Method for Making the Same, US Patent 6,345,730, 2002.

[17] J.I. Isuchukwu, et al., Ambulatory Storage System for Pressurized Gases, US Patent 6,651,659, 2003.

[18] COMSOL website: www.comsol.com

[19] Sebra Inc. website: http://www.sebra.com/rf.htm

[20] K.D. Raughley, Private communication.

[21] R.C. Metaxas, Foundations of Electroheat, A Unified Approach, Wiley, 1996, pp. 98–99.

[22] Fletcher et al., US Patent Application 2005/0252896A1, Nov. 2005.

[23] Smith et al., US Patent Application 2007/0045240A1, 2007.

[24] H.B. Francisco, R.J. Riegert, Apparatus for Radio-Frequency Boding of Thermoplastic Members, US Patent Number 6,030,490, February 2000.

[25] Kelch, et al., US Patent 6,558,809, 2003.

[26] C.Y. Wu, A. Benatar, Microwave welding of high density polyethylene using intrinsically conductive polyaniline (joining of plastics and plastic composites), Polym. Eng. Sci. 37 (4) (1997) 738–744.

[27] Gruenspecht et al., RF Welding Device, US Patent 7,012,232 B1, March 2006.

[28] R.J. Wise, I.D. Froment, Microwave welding of thermoplastics, J. Mat. Sci. 36 (2001) 5935–5954.

[29] H.W. So, A. Taube, Numerical investigation of the influence of material properties and adhesive layer thickness on the heating efficiency of microwave curing of an adhesive-bonded joint, Polym. Eng. Sci. 44 (8) (2004) 1414–1418.

[30] J.F. Harper, D.M. Price, Microwave forming and welding of polymers, 10th International Conference on Microwave and RF Heating, Loughborough University, Loughborough, UK, 2005.

[31] P. Chandrasekhar, Conducting Polymers, Fundamentals and Applications: A Practical Approach, Springer, 1999.

[32] A.A. Yussuf, et al., Rapid microwave welding of two polymethylmethacrylate (PMMA) substrates, ANTEC Conf. Proc. 1 (2004) 1256–1260.

[33] S. Staicovici, C.Y. Wu, A. Benatar, Welding and disassembly of microwave welded HDPE bars, J. Reinf. Plast. Compos. 18 (35) (1999) Also at: http://jrp.sagepub.com.

[34] H.-s. Noh, et al., Wafer bonding using microwave heating of parylene intermediate layers, J. Micromech. Microeng. 14 (2004) 625–631.

[35] K.F. Lei, et al., Microwave bonding of polymer-based substrates for micro/nano fluidic applications, Conference on Solid State Sensors, Actuators and Microsystems, 2003.

[36] Y.C. Lin, et al., Single mode microwave welding of HDPE using conductive polyaniline/HDPE composites: in "Fusion Bonding of Polymer Composites: From Basic Mechanisms to Process Optimisation," Proceedings of the 53rd Annual Technical Conference, ANTEC, 2002, p. 63.

[37] G.W. Maaczynski, Adhesive processing by electromagnetic irradiation, Polym. Eng. Sci. 28 (1988) 1270–1274.

[38] V.K. Varadan, et al., Microwave joining and repair of composite materials, Polym. Eng. Sci. 31 (7) (1991) 470–486.

[39] H.S. Ku, E. Siores, J.A.R. Ball, Microwave facilites for welding thermoplastic composites and preliminary results, J. Microw. Power Electromagn. Energy 34 (4) (1999) 195–205.

[40] E. Siores, D.D. Rego, Joining of materials with microwave energy, Aust. Weld. J. 18 (21) (1994).

[41] N. Tran, W.K. Tam, M. Malcmann, Microwave welding of thermoplastic rods without any conductive material, Proceedings of the Fourth World Congress on Microwave and Radio Frequency Applications, Microwave Working Group, Inc., pp. 232–240, 2005.

[42] H.J. Lause, et al., Method of welding thermoplastic substrates with microwave frequencies, US Patent 5,338,611, 1994.

[43] V.K. Stokes, Experiments on the induction welding of thermoplastics, Polym. Eng. Sci. 43 (9) (2003) 1523–1541.

[44] V.A. Kagan, et al., Benefits of induction welding of reinforced thermoplastics in high performance applications, J. Reinf. Plast. Compos. 24 (2005) 1345. DOI: 10.1177/0731684405048846, http://jrp.sagepub.com/cgi/content/abstract/24/13/1345.

[45] D.A. Grewell, et al., Plastics and Composites Welding Handbook, Hanser, Munich, 2003, p. 407.

[46] Handbook of Plastics Joining – A Practical Guide, Plastic Design Library (PDL), Norwich, NY, 1999, p. 586.

[47] R. Messer, Trends in key joining technologies for the twenty-first century, Assembly Autom. 20 (2) (2000) 118–128.

[48] R.J. Nichols, Advances in the emabond™ induction welding process for high-performance assembly of demanding thermoplastics, Assembly Technol. Expo (2003) 10.

[49] W.J. Ryan, et al., US Patent 6,600,142, Assignee: Codaco Inc., 2003.

FURTHER READING

Banks et al., 1998 H.T. Banks, S.R. Durso, M.A. Goodhart, M.L. Joyner, On the radio-frequency inputs in dipolar heating of adhesives, Tech Report CRSC-TR98-3, North Carolina State University, January 1998.

Banks, 2001 H.T. Banks, et al., Nonlinear exothermic contributions to radio-frequency bonding of adhesives, Anal. Real World Appl. 2 (3) (2001) 357–386.

Fastfuse et al., 2009 Fastfuse Radio Frequency Lamination: Ceralink, Inc. website: http://www.ceralink.com/products/rf-lamination.htm, 2009.

Jauss, 1997 M. Jauss, et al., Joining of thermoplastic composites by bolt and microwave welding, Proceedings of ICCM-11, Gold Coast, Australia, 1997.

Malaczynski, 1996 G.W. Malaczynski, et al., Selection of adhesive system for radio frequency heating of structured sheet molding compound components, Polym. Eng. Sci. 36 (1996) 106–116.

Yousefpour, 1999 A. Yousefpour, et al., Fusion bonding of thermoplastic composite materials, J. Thermoplast. Compos. Mater. (1999) Available online at: http://jtc.sagepub.com.

Zhou et al., S. (Shuangjie (Shirley)) Zhou, et al., Status of Microwave Adhesive Bonding Research, Available at: Website of the Automotive Division of the Society of Plastics Engineers International (SPE), http://www.speautomotive.com/SPEA_CD/SPEA2001/pdf/d/D4.pdf

CHAPTER 9

Design Considerations for Applicators in Continuous-flow Microwave/RF Processing

CHAPTER CONTENTS

INTRODUCTION

Continuous-flow processes, as opposed to batch processes, provide better economy in most cases where high throughput and low labor costs are required. Batch processes are used in special cases where specific process ambient conditions such as a vacuum are necessary in high value-in-use products with limited production volume. The principles of microwave/RF applicator design and material interactions, as discussed in previous chapters, still apply to continuous-flow processes. There are, however, specific issues related to continuous processes that are dealt with in this chapter.

Microwave/RF Applicators and Probes for Material Heating, Sensing, and Plasma Generation

Figure 9.1 shows a simplified schematic of a microwave/RF continuous process, where a product bed of any cross-sectional shape (shown here as rectangular) flows with a constant velocity v over all of its cross-section through a microwave or RF processing zone with length L. The mode of product transport could be a conveyor belt in the case of flowable solids to self-supporting webs and sheets. In actual industrial cases there are varieties of product type and flows that fall outside of these assumptions. Examples are products that are distinct units arranged on a conveyor belt, or fluids that have plug or turbulent flow. While the emphasis in this chapter is on flowable solids and webs, many of the topics are also applicable to liquids and other continuous configurations.

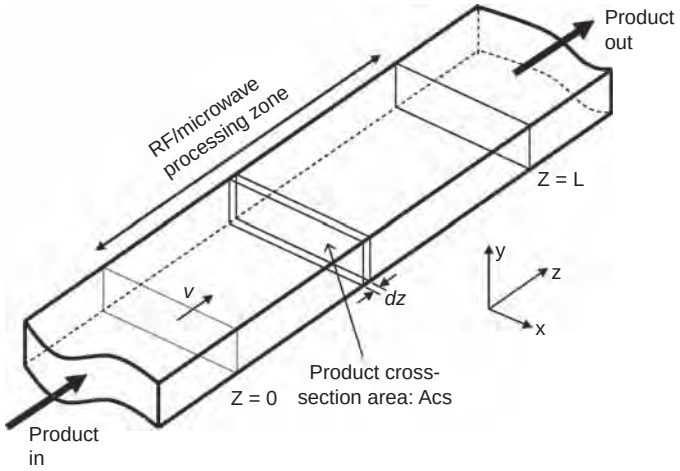

FIGURE 9.1 *A general view of a continuous-flow process.*

Following some general considerations and design guidelines in Sections 9.1 and 9.2, we will discuss RF and microwave continuous systems separately in Sections 9.3 and 9.4 respectively. Finally, in Section 9.5 the important issue of reducing RF/microwave emissions from entry and exit ports to comply with safety and communication regulations will be covered.

9.1 GENERAL CONSIDERATIONS FOR CONTINUOUS RF/MICROWAVE MATERIAL PROCESSING SYSTEMS

9.1.1 Power requirements for a continuous system

In the simplest case of a continuous processing system, the power required from all sources P (in kilowatts) is:

$$P = R_{pr}C_p\Delta T + h_{fg}R_{sol} \tag{9.1}$$

where R_{pr} is the product throughput in kg/second, C_p the material specific heat in kJ/kg-°C, ΔT the temperature rise in °C, h_{fg} the heat of evaporation for the solvent being removed in kJ/kg, and R_{sol} the rate of moisture removal in kg/second. In most common drying applications, the heat of evaporation for water at 100°C is 2257 kJ/kg.

As an example, let us find the power required for a process in which a peak production rate of 1000 kg/h of a solid material with 9% moisture by weight is to be dried. The specific heat for the material is 0.15 kcal/kg-°C.

The rate of moisture removal is $0.09 \times 1000\,\text{kg/h} = 90\,\text{kg/h}$ of water.

$$P = 1000\ \text{kg/h} \times 1/3600\ \text{h/s} \times 0.15\ \text{kcal/kg-°C} \times 4.18\ \text{kJ/kcal} \times (100 - 20)\text{°C} + 2257\,\text{kJ/kg} \times 90\ \text{kg/h} \times 1/3600\ \text{h/s}) = 70\ \text{kW}$$

The power level calculated by Eq. (9.1) does not include energy requirements due to heat losses and any process reaction energy in an endothermic reaction taking place in the material. These factors must be added to Eq. (9.1). Also, in some processes other energy sources such as hot gas may be employed that may reduce power requirements from the RF or microwave source.

Manufacturers of RF/microwave conveyor systems most often rate their equipment using calorimetry by measuring the energy dissipation into a flowing water load. Therefore some power losses into the system are taken into account when the system is rated. It is good practice, however, to leave a safety margin of 20–30%. In the example above a system rated at 90–100 kW is preferred.

In Eq. (9.1), an implicit assumption is made that the material specific heat and the solvent's heat of evaporation do not change through the process. In most practical cases, for the purpose of computing the process power required, these assumptions are valid.

9.1.2 Relationship between the product flow rate and process geometry

In the design of a microwave/RF continuous-flow process, there are a number of geometrical limitations that have to be considered at the outset. For example, the penetration depth of energy into the material in a microwave process, as described in Section 1.2.6 and Eq. (1.32), may impose a limit on the maximum depth of the product bed. There may also be limits as to the width and length of the process flow based on various commercial and technical factors. A clear example is how wide an RF process can be before wavelength effects impose non-uniformity of fields across the width. The basic data may impose a required minimum residence time for the process to complete. For example, drying of a temperature-sensitive product may need a longer time to make up for a low process temperature. To fulfill these considerations, a relationship between the main geometrical and timing parameters will be described below.

In continuous processes involving flowing or conveyed materials, where all parts of the cross-section travel at the same speed, the following relationship holds between the product and geometrical parameters:

$$T_r R_{pr} = A_{cs} \rho L \tag{9.2}$$

where T_r is the product residence time (in seconds), R_{pr} is the product rate (kg/s), A_{cs} is the cross-sectional area of the product in a plane vertical to the flow (in m^2), ρ is the specific weight of the product (in kg/m^3), and L is the length of the active part of the process where the heating occurs (in meters).

In the same example as in Section 9.1.1 above, suppose the basic data are supplemented by the residence time being 10 minutes for the drying process to complete and the longitudinal length of the applicator system is 3 meters. The specific weight of the product is $500\,kg/m^3$. Using Eq. (9.2) we have:

$$10 \text{ min} \times 60 \text{ min/s} \times 1000 \text{ kg/h} \times 1/3600 \text{ h/s} = A_{cs} \times 500 \text{ kg/m}^3 \times 3 \text{ m}$$

From the above, the cross-sectional area of the product flow is calculated to be $A_{cs} = 0.11\,m^2$. Assuming a product bed with a rectangular cross-section, if width of the the product bed w is 1.0 meter, then the height of the product bed h would be 11 cm.

In cases where the product is a granular or pellet-like material on a flat conveyor belt, the cross-section will have a trapezoidal shape due the angle of repose at the edges. In such cases, the relationship between the cross-sectional area and the width and height of the bed is:

$$A_{cs} = h\left(w_b - \frac{h}{\tan\alpha}\right) \tag{9.3}$$

where w_b is the base width of the bed and α is the angle of repose (the angle that the edge of the product bed makes with the conveyor belt). In the above example, where the product bed's cross-section was calculated to be $0.11\,m^2$, if w_b is 1 meter and the angle of repose is 45°, then from Eq. (9.3), the bed height $h = 0.1\,m$.

9.1.3 Heating uniformity issues in RF/microwave conveyor systems

As we have described in Chapters 3–5, heating uniformity is one of the most critical challenges in RF/microwave processing. The uniformity concerns are somewhat mitigated in continuous or conveyor heating by the fact that the

forward movement of the product would even out non-uniformities in the product movement (z) direction. In addition, in many cases, the product bed height is short compared to the non-uniformity caused by wavelength effects; this would mitigate uniformity concerns in the y direction. An example is heating or drying of webs, or granular materials beds at RF frequencies. Because of these factors, in most cases, the uniformity is an issue in one (usually the x) direction.

To illustrate this issue, let us use the example in Section 9.1.2, where the depth of the product bed was calculated to be 11 cm. Suppose that the product is a powder with bulk complex permittivity $5.47 + j\ 0.37$. The question to answer is whether the penetration depth of microwaves at 2450 MHz would produce adequate uniformity into the bed (in the y direction). Using Eq. (1.32) for penetration depth, we find the attenuation into the bed is such that the power is attenuated at a rate of 5.5% for every centimeter of material depth. For our example at the middle of the product bed height (5 cm), the deposited power is attenuated by 27% from the surface. For most practical applications this is adequate uniformity.

In some cases a non-uniformity issue in one of the lateral directions can compound itself with the progression in the longitudinal (z) direction, and create a very large thermal for drying non-uniformity at the product exit. This situation can become particularly severe in cases where the product has temperature-dependent dielectric properties, such as materials with thermal runaway properties.

9.1.4 Temperature and control issues in continuous systems

We addressed the general issue of temperature rise in volumetric RF/microwave heating in Chapter 1. In industrial continuous-flow processes, there is a goal temperature at the exit of the process, within a specified error window. In order to reach this goal, an automatic feedback control system is often used [1]. The goal of this section is to address the temperature rise issues that are specific to microwave and RF continuous processing of materials.

The automatic feedback control of RF/microwave continuous processes provides unique opportunities and challenges as compared with conventional processes. One advantage of the use of RF/microwave equipment is control agility because of the volumetric and instantaneous nature of energy deposition into the product without the delay associated with conventional heat transfer. Since the material's bulk temperature reacts quickly with any changes in the power input, the feedback delay is greatly reduced.

One challenge, however, is the incompatibility of thermocouples, which are the most widely used form of thermometry, with the intense fields.

Because of this, several other methods of thermometry, such as RTDs, fluoro-optic or fiber-optic thermometry, or infrared thermometry are used [2,3]. Shielded thermocouples can sometimes be used.

Because of the potential for non-uniformity of temperature in RF/microwave continuous processing, there may be a need for more than one thermometry point at the product outlet in certain processes. This is particularly true in heating of materials with thermal runaway properties. In such cases, if the measurement point is at a particularly low- or high-temperature spot, the other points may remain too cold or become too hot.

9.1.5 General theory of continuous RF/microwave processing

In Figure 9.1 a generic continuous process is shown, where a product is subject to RF or microwave fields in a "process zone" with length L. The reference starting point where $z = 0$ is where the product enters this zone, and $z = L$ is the product exit point. It is assumed that all parts of the product cross-section are traveling at the fixed velocity v.

The RF or microwave power P (in watts) dissipated into a volume V of the product is found by replacing some constants and a slight modification to Eq. (1.18):

$$P = Kf\varepsilon_r'' E^2 V \tag{9.4}$$

where $K = 5.56 \times 10^{-11}$, E is the RMS value of the electric field in the product (in V/m), f is the frequency of operation (Hz), and ε_r'' is the material's bulk loss factor. Using Eqs (9.4) and (1.41), the following differential equation for temperature can be found using a derivation given by Boldor et al. [4]:

$$K f E(t)^2 \varepsilon_r'' = -\lambda \rho_0 \frac{dA}{dt} + C_p(t)\rho_0 [1 + A(t)]\frac{dT}{dt} \tag{9.5}$$

where t is the time variable in seconds, $E(t)$ is the RMS value of the electric field in V/m, ρ_0 is the specific weight of the bulk product in kg/m^3, $C_p(t)$ is the specific heat of the bulk product in kJ/kg-°C as a function of time, $A(t)$ is the moisture fraction of the product as a function of time, and $T(t)$ is the temperature of the product as a function of time.

In the most general case, the solution of Eq. (9.5) would require highly rigorous methods [5]. There are, however, simplifying factors for most practical cases that yield simpler solutions. For example, in cases where a large amount of moisture needs to be removed, the sensible heat can be

neglected in favor of a much larger heat of evaporation. Therefore the second term on the right-hand side will disappear. In the exact opposite case, where little or no moisture may need to be removed, the first term on the right-hand side can be dropped. A practical example to show how Eq. (9.5) can be used will be shown in Section 9.3.2.

9.2 PREPARATION FOR CONTINUOUS PROCESS DESIGN AND COLLECTION OF BASIC DATA

The design of a continuous process should begin with generation of basic data, which may include gathering or collecting material data such as specific heat, specific weight, dielectric properties at the frequencies of interest, etc. The next step involves a series of small-scale RF or microwave heating experiments to observe and measure the desired effect, such as drying or completion of a reaction. The small-scale experiment may be done in two stages. The first is a laboratory experiment where the only interest is observing the effect in a laboratory. This is necessary only if the process is novel. In most cases, however, by the time a decision is made to use a continuous process, this type of preliminary experiments have already been done.

In the second stage a larger-scale batch experiment is performed where as many of the industrial process's attributes as possible are kept intact. The reason a batch experiment is preferred at this stage is that it is much easier to connect instruments and collect data from a batch experiment compared to a continuous one. Another reason is that the amount of material needed for the batch experiment can be limited. But it is important that this amount is large enough so that an accurate assessment of thermal issues can be made. If the quantity is too small, the problem of high surface-to-volume ratio would give inaccurate basic data, because experiments with too high a surface area tend to lose heat to the material boundaries too quickly. If the product is in granule or pellet form, it is best to have a batch container that has the same product height as the envisioned continuous process.

Figure 9.2 shows a representation of a batch experiment for collecting basic data for an RF drying process involving granular or pelleted material [6,7]. The vessel is wholly made of polytetrafluoroethylene (PTFE), which has very low RF loss, and has a capacity of 650 cm^3. Since there is a need for dry purge gas to carry the released moisture away, the container is equipped with a plenum at the bottom with a perforated PTFE plate. By maintaining a positive pressure in the plenum the purge gas will be distributed evenly through the material bed. Since thermocouples are not compatible with high electric fields, a fluoro-optic thermometer [2] was used.

The vessel is placed between the electrodes of a 3 kW variable power RF batch oven at a frequency of 27 MHz. The electrode voltage is recorded and by dividing the voltage by the electrode distance the electric field is also recorded. An important figure that is very useful in the design of a continuous process is the time it takes to achieve the results in the basic data experiments. For example, in a drying process it is important to note how long it takes to achieve the desired drying level at the recorded electric field levels.

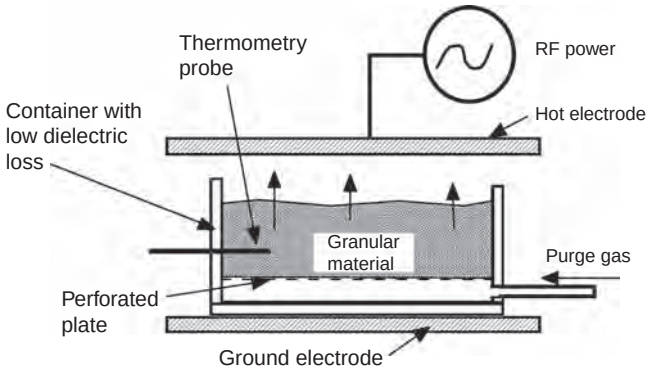

FIGURE 9.2 *A parallel-plate RF system used for collecting basic data for developing a conveyor RF process.*

An example of type of data collected in this type of experiment is described by Thuery [8]. The desired process involves drying of temperature-sensitive crop protection pesticides [7] that are in granular form. We will describe the process in detail in Section 9.3.2.

9.3 RADIO-FREQUENCY PARALLEL-PLATE CONTINUOUS PROCESSES FOR GRANULAR MEDIA

9.3.1 RF parallel-plate continuous system

Conveyor systems for solid materials, either in granular or pelleted form, or in discrete object form (such as fiber bobbins), are one of the most commonly used RF heating systems. Figure 9.3 shows a process [7] where a granular or pellet-like material is dried [9,10]. The RF power circuit and electrode system analysis for parallel-plate RF systems were described in Chapter 3. In the system shown in Figure 9.3 a purge air system through the product insures efficient removal of the released moisture. The active "hot" electrodes as well as the bottom electrodes are perforated aluminum, and are a part of hollow aluminum air plenums. The perforated non-metal conveyor belt carries the product over the ground electrode, and the purge air that has gone through the materials is sucked by the air-handling system connected to the hot electrode plenums.

As we discussed in Chapter 3, in RF systems of this type the electric field under each of the two electrodes (and therefore the power deposition into the material) is set by the electrode height. An advantage of a dual-electrode system is the ability to have the two electrodes at different heights, thereby depositing different amounts of power into the product. This is often necessary because the product properties change along the process, and therefore the need for power deposition changes as well.

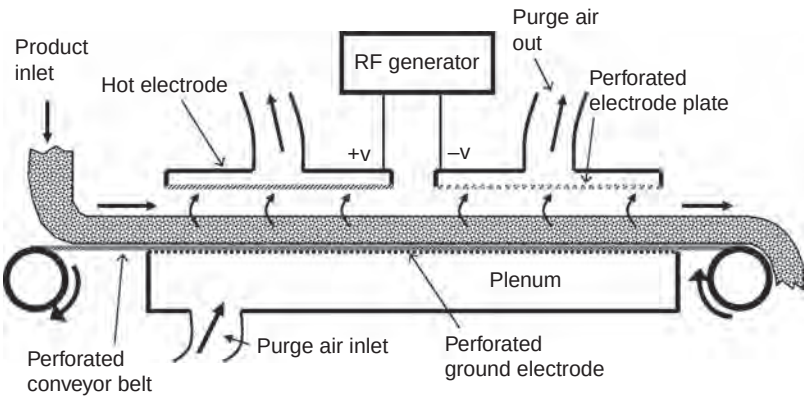

FIGURE 9.3 *A dual-electrode RF electrode system where a granular or pellet-like material is dried.*

9.3.2 Continuous process example: RF drying of temperature-sensitive herbicide granules

Agricultural pesticide and herbicide products are often sold to the farmer as dry, water-dispersible granules [7]. The chemical compounds having the pesticidal or herbicidal activity contained in these products, however, are typically not water soluble. These products must be formulated with additives to produce water-dispersible granules for use by the end-user. The active ingredients and the additives that comprise the product formulation are typically manufactured as one or more fine powders. To agglomerate the formulation into larger particles or granules suitable for end-user application, water and sometimes other solvents are added. This moisture or solvent must be driven out after the granules are formed without damaging or degrading the product, which is often quite temperature sensitive, and could degrade at temperatures above 70°C. In the drying step the moisture level must be typically reduced from a range of 5–30% to below 1% to prevent the product from caking before it reaches the end-user.

A conventional method of drying this type of products is the vibrating fluidized bed [11]. In this process a high flow rate of warm air, at a velocity typically exceeding 50 meters (about 150 feet) per minute, is applied to a bed of the wet product. This high-velocity air flow delivers the heat of evaporation to the product, mechanically fluidizes the product bed, and removes the vaporized moisture from the process. Vibration of the whole vessel is used to aid the fluidization of the product bed. The humid and typically dusty exhausted process air is then passed through a dust collector, filtered, refrigerated to remove the moisture, reheated to the specified process temperature, and then fed back into the process. The disadvantage of the vibrating

fluidized bed process is the large volume of air required per unit volume of product. The air-handling system for such a process is quite large in physical dimensions, represents a large investment of capital, and, due to its energy consumption, is expensive to operate. The agitation of the product inherent in such a drying process partially breaks up the granules and creates large volumes of fines or dust, which reduces the first-pass process yield. These fines must be removed from the air cycle and returned for re-granulation.

An RF drying system [7], as described in Section 9.3.1 (Figure 9.3), reduces the amount of purge air needed by an order of magnitude. It also eliminates agitation that significantly improves the product yield.

In the design of this process a series of batch experiment in an RF system as described in Section 9.2 (Figure 9.2) was used. The following are the batch test specifications:

- **Vessel** – PTFE vessel (10 cm W × 15 cm L × 10 cm H) with a perforated fiberglass mesh bottom mesh size of 0.5 mm.
- **Vessel capacity** – 650 grams.
- **Bed height** – 7 cm.
- **Purge air flow** – 60 liters/minute at a temperature of 60°C.
- **Air velocity through the product** – 5 m/min.
- **Maximum RF power level** – 3 kW.
- **Frequency** – 27 MHz
- **Electrode size** – 30 cm × 30 cm.
- **Thermometry** – fluoro-optic probe inside the material bed [2].

The control method for the experiment was to set the power level at all times so that the bed temperature remains at 60°C. Using this methodology, the 10% moist product dried to less than 1% moisture in 15 minutes. To separate the effect of RF energy from that of the warm air, Figure 9.4 shows a comparison between the drying versus time with the RF power on and off. As is evident, the RF almost does all the drying. The purge air removes the moisture and the product is kept below the temperature of degradation by the removal of the heat of evaporation.

The batch experiment proved that the process is potentially viable; therefore a continuous pilot process similar in configuration to Figure 9.3 was developed and tested.

We will now explain how the maximum temperature of the process remains low, which prevents degradation of the product. The left-hand side of Eq. (9.5) shows total RF energy, while the right-hand side has two terms: the first one represents the evaporation energy and the second term relates to the temperature increase. The uniform flow of purge air increases the

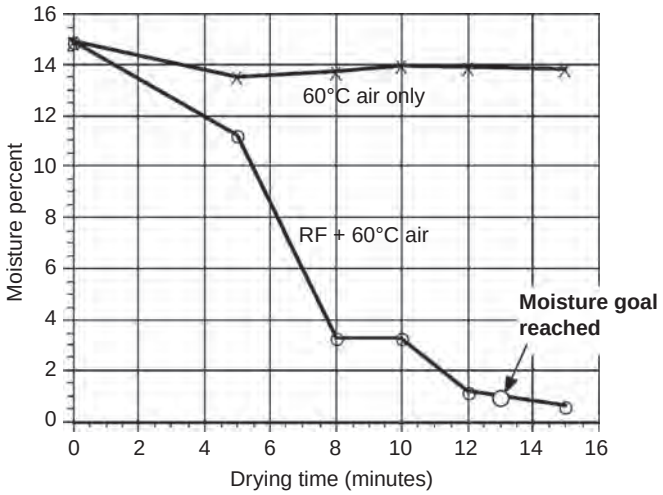

FIGURE 9.4 *A comparison of drying versus time with the RF power on and off. Almost all the drying is done with the RF energy.*

evaporation energy and reduces the temperature increase term. Therefore the faster the material dries (large dA/dt), the lower the temperature increase will be. By proper control of the RF power application and air flow, the temperature increase term can be decreased essentially to zero (dT/dt = 0).

Given the above, Eq. (9.5) can be simplified by setting the first term on the right-hand side of the equation to zero, and the equation reduces to:

$$K f E(t)^2 \varepsilon'' = -\lambda \rho_0 \frac{\mathrm{d}A}{\mathrm{d}t} \tag{9.6}$$

If we assume that the moisture removal is done linearly, then the term dA/dt is a negative constant, which means the electric field along the process length is related to the dielectric loss by:

$$E = \frac{K'}{\sqrt{\varepsilon_r''}} \tag{9.7}$$

where K' is a constant. Figure 9.5 shows the measured bulk dielectric properties of a particular granular herbicide versus moisture level. The dielectric loss decreases as the process moves forward and the product becomes drier; therefore, according to Eq. (9.7) the electric field must increase with the square root of the dielectric loss function as the process goes on. This fact was used in the continuous process design in Ref. [7] in designing the gaps between the hot and ground electrodes.

In the continuous process the goal was to dry a granular herbicide with a flow rate of 180 kg/h with an initial moisture level of 9.5% and a goal moisture level of below 1%. The product has a specific weight of 620 kg/m^3, a heat capacity of 0.6 kJ/kg, and the basic data performed according to Section 9.2 yielded a residence time of 15 minutes for gentle drying so that the temperature does not exceed 60°C.

Using Eq. (9.1), the power required is calculated to be 11.8 kW. An RF dryer with a maximum power level of 25 kW, operating at a frequency of 27.12 MHz manufactured by Strayfield Ltd [9] was used. There are two

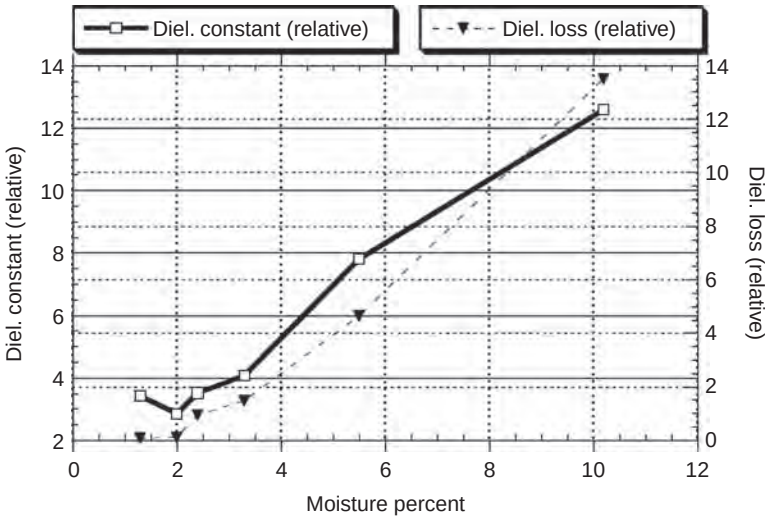

FIGURE 9.5 *The variations of the dielectric properties of the bulk product to be RF dried versus moisture percentage by weight.*

energized electrodes, each with length 130 cm (in the direction of product flow) and width 60 cm. A conveyor belt 61 cm in width, made of glass-reinforced polyester mesh with a mesh size of 0.5 mm, allows for the air to pass through the granular product as it is transported between the energized and grounded electrodes. The total length of the drying zone is 3.06 meters, which includes a 46 cm dead zone between the two electrodes. The conveyor speed is 6.8 m/h.

Using the above figures and Eq. (9.2), the product cross-sectional area was found to be 0.024 m^2. Using Eq. (9.3), a base product width of 48 cm, and an angle of repose of 45°, the bed height is calculated to be 5 cm. Using the above parameters, the actual drying yielded a moisture level of 0.5%, which is within the specification of below 1%.

9.3.3 Continuous process example: RF processing of polyamide pellets with thermal runaway

In the manufacturing of specialty thermoplastic parts the producer of the resin sells the raw product in the form of small pellets of the order of 2.5 mm (0.1 inch) in size. The parts manufacturer then places the pellets in an extruder, which melts them using a combination of pressure and high temperature. In some cases even a small amount of water in the pellets causes problems for the extrusion process. Therefore, some thermoplastic pellet products that have a residual amount of moisture of 2% or less need

to be reduced to 0.2% or less prior to the extrusion step. In this section the design of an RF continuous-drying continuous process is described that provides much improved performance over the conventional hot gas drying method for polyamide pellets.

Conventional dryers usually operate at low temperatures of less than 100°C in order to minimize yellowing of the product. A major delay factor in driving moisture out of a polymer is the slow rate of released water diffusion through the polymer matrix [12]. As a result a long residence time that can approach several hours is needed. This requires a large vessel, and therefore a large amount of floor space to hold the polymer. In addition, conventional dryers heat the polymer up to the drying temperature by means of a large volume of heated gas flowing through the polymer. Thus, a large flow of hot, dry gas is needed to flow through the vapor space around the polymer. Consequently, large systems to move the gas within the system, i.e. a blower, are needed as well.

Process control is another difficulty with conventional dryers. Due to the long residence time any process upset would require a change in the process conditions with a built-in delay in obtaining a response. This would make it difficult to control in such a way that the discharge moisture is maintained at a fixed value. Specifically, changes made to the dryers during the operation of a process take a long time to materialize due to the amount of time the polymer is in the dryer. For example, if a change is made in the processing system, the full effects of that change will not show up in some cases for up to 24 hours.

A patent by Lowe [6] describes a process where the use of a conveyor RF dryer reduces both the amount of time and amount of gas flow to a small fraction of the conventional process. It has been shown [13–15] that RF electric fields speed up the diffusion of water in polyamide resins by disrupting the hydrogen bonds between the water and the amide links. This allows the water to diffuse out of the polyamide resins very quickly, significantly reducing the residence time to 15 minutes, according to experiments [6]. In addition, minimizing the exposure of polyamide resin to oxygen during the drying process at the reduced residence time and low temperature eliminates or minimizes the increase in yellowness during drying. Moreover, due to the short residence times a much smaller vessel is used to hold the thermoplastic; thus, less space is required to house the process.

Due to the direct and non-contact nature of RF heating, an inert gas is used only to take the water away from the polyamide resin. Thus, there is less gas flow per unit volume of polymer, which improves the overall energy consumption per unit weight of the product.

Lowe showed that in a process with 2275 kg/h of throughput, the amount of energy used for gas heating is reduced from 130 kW to a mere 7.5 kW. Furthermore, it was shown that RF drying is easier to control than conventional drying to a fixed polymer discharge moisture due to the short residence time. Using an RF dryer with similar configuration as that shown in Section 9.2, a process for drying polyamide pellets was developed.

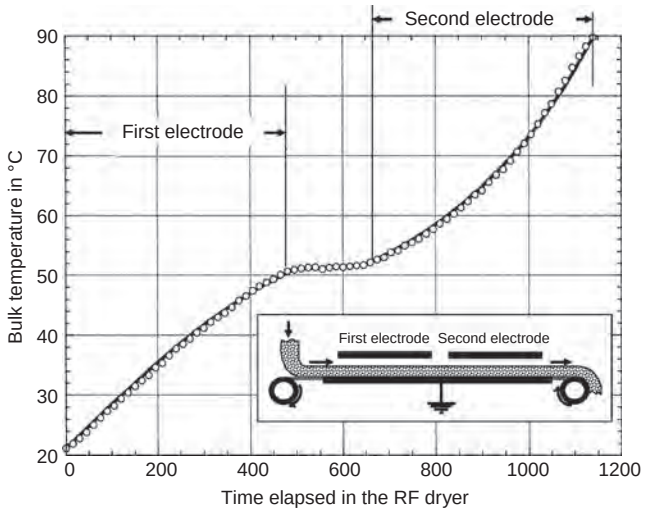

FIGURE 9.6 *The temperature variations of the bulk product under the dual-electrode RF system with flat electrodes.*

Following a batch test in a setup similar to Figure 9.2, a pilot scale conveyor RF drying test was conducted. For this test a 27 KHz, 50 kW RF system manufactured by Strayfield International [9] was used. By placing a thermometer in the pellet bed and measuring the temperature increase, the temperature profile shown in Figure 9.6 was produced. The curve shows good linearity of temperature rise when the product goes through the first electrode and is heated to about 52°C, but the temperature rise becomes nonlinear through the second electrode, where the product temperature is raised to 90°C. This nonlinearity causes temperature control instability, which means the product can exit the system hotter than is meant with even the slightest process upset. Such a situation would make an automated feedback control system difficult to operate.

There are two reasons for the accelerated temperature rise towards the end of the drying process: first, the polyamide's dielectric loss increases sharply with temperature as shown in Figure 9.7, where curve fitting yields the following function for relative dielectric loss versus temperature:

$$\varepsilon_r''(T) = 0.0566 + e^{(0.0427\,T - 5.66)} \tag{9.8}$$

The second reason for a nonlinear temperature profile is the voltage standing-wave (wavelength) effect on the electrode. Figure 9.8 shows the curve representing the variations of voltage along the electrodes. The length of the electrode is 1.22 m, which is 11% of the wavelength at 27 MHz. Using the transmission-line theory, the voltage along the electrode was calculated to follow the relationship:

$$V = V_{\max} \sin\left[\frac{\pi}{2}(0.43z + 0.47)\right] \tag{9.9}$$

FIGURE 9.7
The increase in dielectric loss factor of polyimide pellets with temperature.

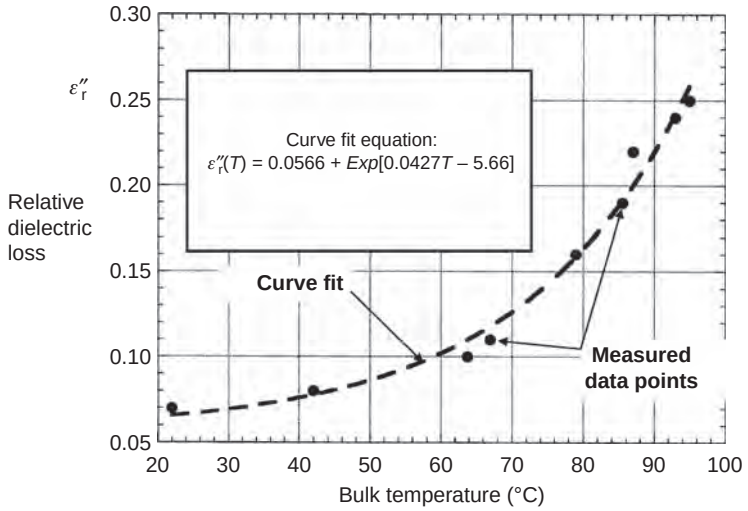

FIGURE 9.8
The variation of RF voltage along the electrodes due to the standing-wave (wavelength) effect.

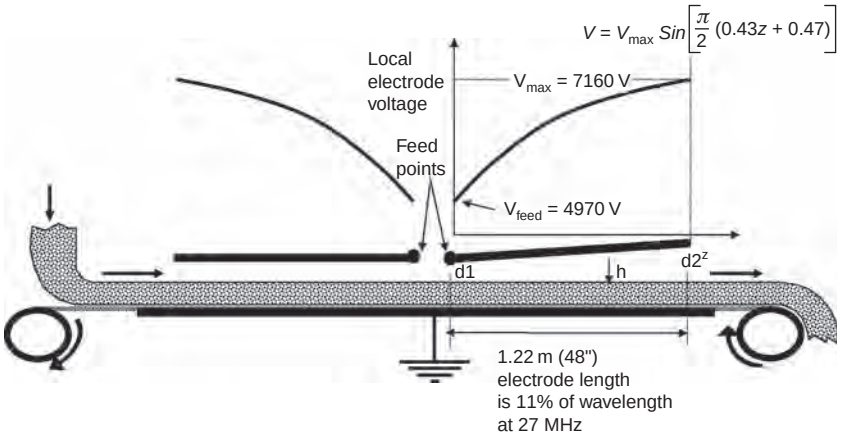

where V is the voltage at any longitudinal point z along the electrode, with the origin of z being the feed point of the second electrode, and V_{max} is the voltage at the exit point. For a particular case where the feed point voltage was 4970 V, the voltage at the exit point turned out to be close to 7160 V, which is quite a significant change.

Using Eq. (9.9), and applying the relation $E = V/d$ to the structure, the electric field as a function of distance along the process $E(z)$ is found to be:

$$E(z) = \frac{V_{max} \sin\left[\frac{\pi}{2}(0.43z + 0.47)\right]}{h + \varepsilon_r d_1 + \frac{\varepsilon_r (d_2 - d_1)}{l} z} \tag{9.10}$$

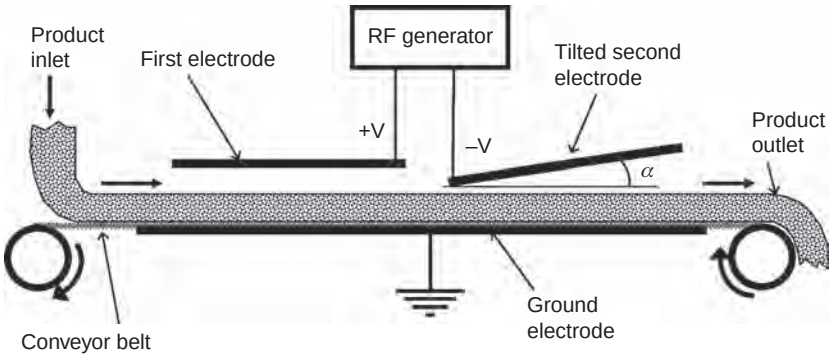

FIGURE 9.9 *The dual-electrode RF dryer with second (tilted upwards; exit) electrode.*

To solve the problem of nonlinear heating, the method shown in Figure 9.9 was utilized, where the electrode is tilted upwards so that the increased distance between the electrode and the ground plane leads to a lower electric field near the electrode exit to compensate for the two factors mentioned above. To find the geometrical parameters of this electrode structure, one may think of a trial-and-error approach, but the high expense of each test prohibits that option. An analytical method was used [16,17] as follows.

Using Eq. (9.5), in this problem the moisture is low enough so that the terms involving moisture level, A, can be neglected. Then the following differential equation is found:

$$K f E(z)^2 \varepsilon_r''(T) = C_p(T)\rho_0 \frac{dT}{dz} \tag{9.11}$$

Of the functions included in the above equation, we have already defined $E(z)$ in Eq. (9.10) and $\varepsilon_r''(T)$ in Eq. (9.9). The only remaining function is that of the specific heat versus temperature, $C_p(T)$, which is tabulated for the polyamide pellets in question as:

$$C_p(T) = 1261 + 8.5T \tag{9.12}$$

The differential equation (9.11) can now be solved by inserting Eqs (9.9), (9.10), and (9.12). As a result, an optimum angle of tilt for the second electrode of Figure 9.9 was found to be 9.4° from the horizon for the particular case of this process. Figure 9.10 shows a comparison of the temperature profile for flat electrode and tilted electrode cases. This shows that

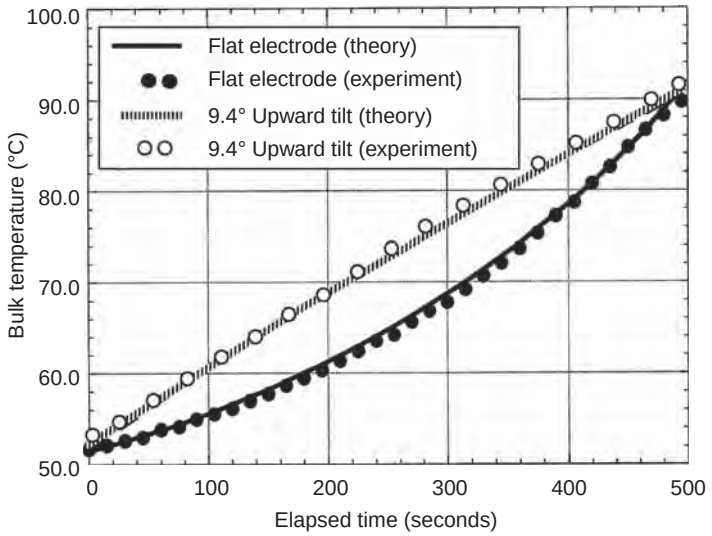

FIGURE 9.10
The variation of RF voltage along the electrodes due to the standing-wave (wavelength) effect.

the temperature profile along the length of the second electrode was made linear using this approach.

9.4 MICROWAVE CONTINUOUS PROCESSING OF SOLIDS

Continuous microwave processing of solid materials can be divided into three groups from an applicator design standpoint. They are single-mode cavity applicators, multimode ovens, and transmission-type applicators. Microwave continuous processing has been in use in the industry for the past few decades with variable levels of success. A review article [18] provides an overview and update of the state of this industry.

9.4.1 Resonant single-mode continuous processing of webs and multi-strand fibers

Single-mode microwave cavities, as discussed in detail in Chapter 4, have a highly defined electromagnetic field configuration that is perfectly uniform in at least one direction. Another advantage of single-mode cavities is the capability to apply very intense electric fields into material of low dielectric loss. It is often difficult to process low-loss materials with either multimode or transmission-type applicators because the electric field is not intense enough to deposit adequate heat per unit volume for the intended process.

An industrial example [19] of a continuous process using a single-mode cavity is shown in Figure 9.11, where a TM_{110} mode rectangular cavity that operates in the ISM frequency band of 915 MHz is used. The cavity is split along the direction parallel to the main electric field component. The web or multi-strand of the fiber is placed in the split and is positioned in such a way that it is parallel to the main electric field component. In web processing the width of the web is perpendicular to the direction of the electric field, which assures field uniformity at least across the width. In such a configuration the field along the web's direction of movement would be a sine function, but the movement of the web would average out such non-uniformity.

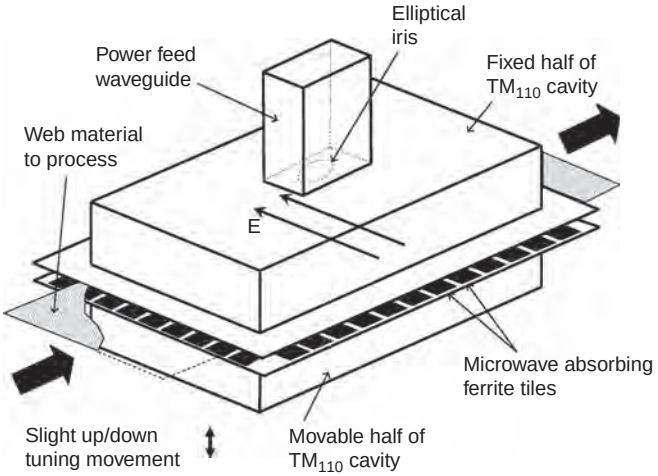

FIGURE 9.11 *A single-mode rectangular cavity used for continuous microwave processing of a sheet material.*

In processing very-low-loss materials the quality factor of the cavity is high, which would make the bandwidth narrow. In such cases there is a need for tuning of the cavity in case the process upsets changes. This tuning is done with a slight movement of one of the two cavity halves, thereby slightly changing the gap between them.

The cavity split is made along the direction that does not cut the surface currents along the walls of the cavity, therefore the microwave radiation to outside of the cavity is minimal. But a small amount of radiation is present that may go beyond the radiation safety limits. Therefore a series of ferrite tiles are placed along a lip in the split to absorb any stray radiation.

An example of the use of this single-mode applicator was in drying of a multi-filament of spun poly(*p*-phenylene terephthalamide) (PPD-T), with 20–200 weight percent moisture [19]. Several strands of this multi-filament were layered side by side in a slit of the cavity, with internal dimensions of 30.5 cm width and 68.6 cm length, where each cavity half was 8.13 cm deep. The coupling iris is designed such that the system runs in an overcoupled mode. In this mode of operation added load, i.e. moisture, increases the power coupling into the cavity for more drying.

The described applicator can dry such fibers using a residence times as short as 50 ms by heating to temperatures of several hundred degrees celsius. This is only possible when extremely high fields generated in a single-mode cavity are used.

9.4.2 Continuous microwave processes with multimode ovens

Continuous microwave processing using multimode ovens is perhaps the most successful and widespread industrial application of microwaves [20,21]. This success is due to the robustness of multimode cavity configurations as discussed in detail in Chapter 5. The basis of operation in continuous processing with multimode ovens is not very different from that of batch multimode ovens as covered in Chapter 5. Continuous processes involving multimode ovens give generally more uniform results due to forward movement of the product, which results in evening out of the field intensity variations due to the standing-wave effect described in detail in Chapter 5.

One of the widely used applications is tempering of frozen foods, which is raising the temperature of deep-frozen food to right below freezing prior to further processing. In this application microwaves are particularly attractive because deep frozen food has a very low loss factor, which increases the penetration depth of microwaves per Eq. (1.32). Therefore large blocks of frozen food can be tempered relatively uniformly. Therefore microwave tempering is far more efficient and rapid than any conventional approach. Another successful continuous microwave process is rubber vulcanization [22], which uses a combination of microwave and hot air for a faster process with higher quality [18].

A great challenge is microwave emissions from the product entry and exit ports. Methods to reduce the emissions are covered in Section 9.5. The problem becomes more severe when the dimensions of the product exit/entrance opening become much larger than the wavelength. Using lower microwave frequencies, such as the 915 MHz ISM band, would tend to ease this problem, but this frequency is not available as an allowed ISM band in many regions of the world, including Europe (Appendix A9.1). An alternate frequency, which is universally available, is 433 MHz. This allows larger processes with larger depth of penetration into materials and better heating uniformity for smaller width processes [23].

9.4.3 Meandering (serpentine) microwave waveguide applicators

Meandering or serpentine waveguide applicators are particularly useful in continuous industrial processing of planar or wide web-like materials such as textiles, films, and paper products [20,21,24–28]. They take advantage of favorable fields and surface current properties of TE_{10} mode waveguides as follows.

Figure 9.12 shows the *E*-field and wall current configuration of the TE_{10} mode waveguide. The microwave power enters the waveguide section and

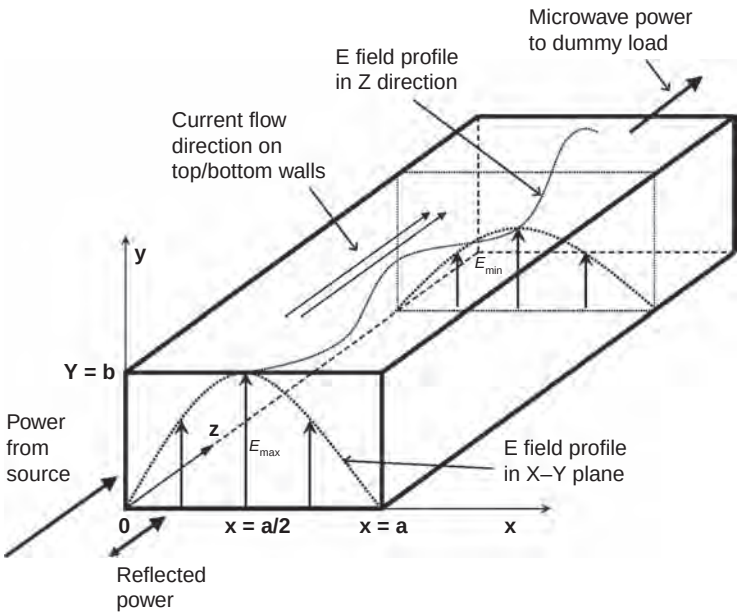

FIGURE 9.12
Electric fields and surface current directions in a TE10 waveguide.

exits toward a load at the other end of the section. The *E*-field intensity profile in the cross-section of the waveguide (in the *x*–*y* plane) has a sine function shape, which means the *E* field, is zero on the side walls and at a maximum intensity in the middle. If the load and source are impedance matched, which means there are no standing waves, the *E* field would be uniform in the longitudinal (*z*) direction. In cases where there is a mismatch, a standing-wave pattern will be formed where the maximum *E* field varies along the *z* direction, and the ratio of maximum to minimum field will depend on the mismatch level.

The surface currents on the opposing broad walls of the waveguide are in the longitudinal *z* direction. Therefore if two longitudinal narrow slots are made in these walls, the disturbance of the currents is minimal. Therefore the radiation from the slots and change in field configuration would also be minimal. The conditions explained above provide an opportunity to run a web-like material in the *x*–*y* plane through these slots in the *y*–*z* plane, as shown in Figure 9.13. If the slots are made in the middle of the top and bottom walls, then the product goes through the maximum *E* field.

Ideally, if the dummy load is matched and the material has a relatively low loss, the *E* fields are uniform over the width of the product, which is highly desired in an industrial system. In practice, however, there are two sources of non-uniformity over the width of the product. First, depending

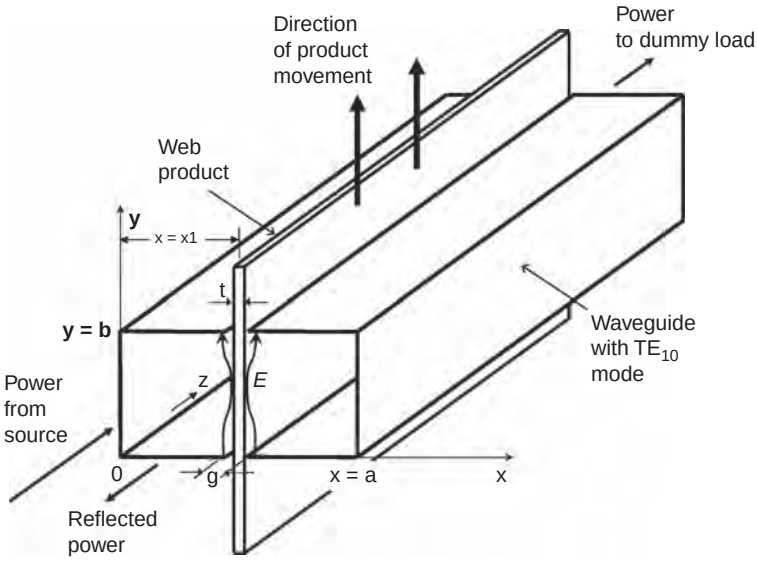

FIGURE 9.13 *A TE^{10} waveguide can be used for processing of a web/sheet material by making longitudinal slits along the broad wall.*

on the dielectric properties and the thickness of the material, as the energy imparted to the product at the edge is closer to the power source, the field would become weaker and the energy deposition would be reduced across the width of the web. A second source of non-uniformity is the impedance mismatch, which would contribute to a standing wave. This type of non-uniformity produces areas of high and low fields across the web.

The next challenge with this heating configuration, as with any transmission-line heating system, is that the *E* fields are relatively weak as compared to resonant applicators. Therefore the amount of energy transferred to the material for a product with reasonable width is quite small if only one pass is applied. This means that the product will receive only a fraction of the power, and most will be wasted into the dummy load. The meandering or serpentine applicator is designed to solve this problem by passing the same material through several successive sections similar to that shown in Figure 9.13. The simplest form of meandering or serpentine traveling wave applicator is shown in Figure 9.14, and uses waveguide bending between two adjacent segments.

To investigate the parameters involved in the design of a meandering or serpentine heating system, consider the geometry of Figure 9.13, where the distance of the dielectric sheet from the left side wall is x_1. The attenuation constant α (in nepers/meter) for a TE_{10} waveguide with a slab of lossy

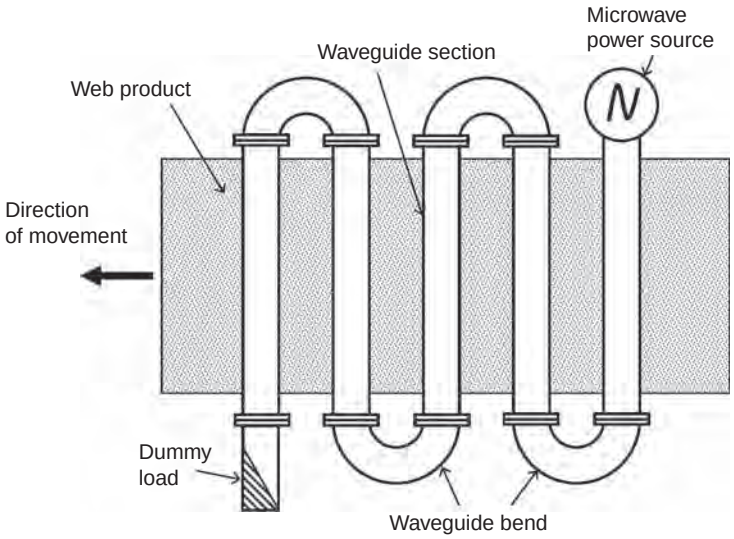

FIGURE 9.14
A basic meandering waveguide microwave applicator.

dielectric is found as follows [20], with some modification to reflect our specific geometry:

$$\alpha = \frac{2\pi f t \varepsilon_0 \varepsilon_r''}{a} \sqrt{\frac{\mu_0}{\varepsilon_0}} \frac{\lambda_g}{\lambda_0} \sin^2\left(\frac{\pi x_1}{a}\right) \tag{9.13}$$

where f is the frequency of operation, t is the thickness of the sheet product, ε_r'' is the loss factor of the product, λ_0 is the free space wavelength, λ_g is the wavelength within the unloaded waveguide, which can be shown in terms of cutoff wavelength λ_c as [29]:

$$\lambda_g = \frac{\lambda_0}{\sqrt{1 - \left(\frac{\lambda_0}{\lambda_c}\right)^2}} \tag{9.14}$$

The cutoff wavelength in the TE_{10} waveguide is defined as $\lambda_c = 2a$. For the highest E-field intensity $x_1 = a/2$. Given that 1 neper = 8.69 dB, then Eq. (9.13) becomes:

$$\alpha = \frac{0.18 f \varepsilon_r'' t}{a\sqrt{1 - \frac{2.25 \times 10^4}{f^2 a^2}}} \tag{9.15}$$

where α is the attenuation constant (in dB/m), f is the operating frequency (in MHz), and a is the waveguide width (in meters).

A numerical example is used here to clarify the relative importance of parameters in Eq. (9.15). For a polymer sheet material with the thickness of 2.5 mm and width of 2 m, and relative dielectric loss of $\varepsilon_r'' = 0.15$, a standard WR975 waveguide with inside dimensions of $a = 247.5$ mm by $b = 123.8$ mm at 915 MHz is used. Using Eq. (9.15), the attenuation constant is calculated to be $\alpha = 0.34$ dB/m. For a web product that is 2 m wide, the attenuation for one pass becomes 0.68 dB. This means that, in order to have 90% of the power dissipated in the product, there is a need for a serpentine waveguide system of about 15 passes. Using this many passes may be objectionable due to capital cost, complexity, and floor space.

One obvious way to reduce the number of passes is to increase the operating frequency to 2.45 GHz. Using a standard WR340 waveguide (86.4 mm × 43.2 mm) at 2.45 GHz, the attenuation per pass becomes 5.5 dB. So, at 2.45 GHz, there is only a need for two passes to achieve 90% power dissipation into the load.

In this particular example, however, moving to a higher frequency creates a few disadvantages. First, power sources with adequate power levels for the job may not be available at 2450 MHz. Second, by having such high dissipation per pass, the heating uniformity suffers because the power diminishes so quickly from the beginning to the end of each pass, that the product edge closest to the power source receives significantly more power than the edge farthest from the power source.

Because of the above concerns, the designer of this system may want to stay with 915 MHz and reduce the number of waveguide passes by using non-standard waveguides with shorter long wall, a. To explore this option, it needs to be said that the cutoff frequency of a standard WR975 waveguide is 606 MHz, which leaves a great deal of waveguide design flexibility for heating applications at 915 MHz. Equation (9.15) clearly shows that for smaller values of a (the broad wall of the waveguide) the attenuation constant increases significantly. The physical reason for this phenomenon is related to better fill factor in the case of a smaller waveguide. Let us apply this finding to our example. At 915 MHz, if the broad wall of the waveguide is reduced to 19 cm (cutoff frequency of 790 MHz), the attenuation per pass increases to 1.3 dB. This waveguide design change can reduce the number of passes needed to eight from the original 15, which is a great simplification of system size and expense.

In TE_{10} waveguides, the height of the short wall b is somewhat flexible, since there are no field variations in the y direction. Very small short wall sizes (smaller than half the broad wall) should be avoided so that the fringing fields due to the gap do not reduce the useful heating fields.

We have so far assumed that the dielectric loss of the product remains the same in all passes. In drying applications this is not the case, as the dielectric loss is reduced as the moisture is removed from one pass to the next. As a result, the amount of power needed in each pass may differ. The above method of designing the waveguide width based on the attenuation needed is a design flexibility that needs to be utilized.

As a result of several novel meandering configurations that have been devised [30], the concept has become commercialized [23] to address both the uniformity issue [31] and the stray radiation leakage problem in meandering applicators. Figure 9.15 shows one of the methods, where the waveguide sections are stacked together. Therefore the potential for radiation occurs only at the product inlet and outlet. Another advantage of such a design is compactness and saving of floor space.

9.4.4 Longitudinal-flow waveguide applicators (standing-wave applicators)

Figure 9.16 shows another configuration of continuous-flow microwave waveguide applicator [32], where the product flow is along a TE_{10} waveguide applicator. The product is placed in the maximum field in the middle of the long wall of the waveguide. While Figure 9.16 shows a conveyor belt below the product, this type of configuration is also used for heating of liquids where a non-metal tube is carrying the liquid. Figure 9.17

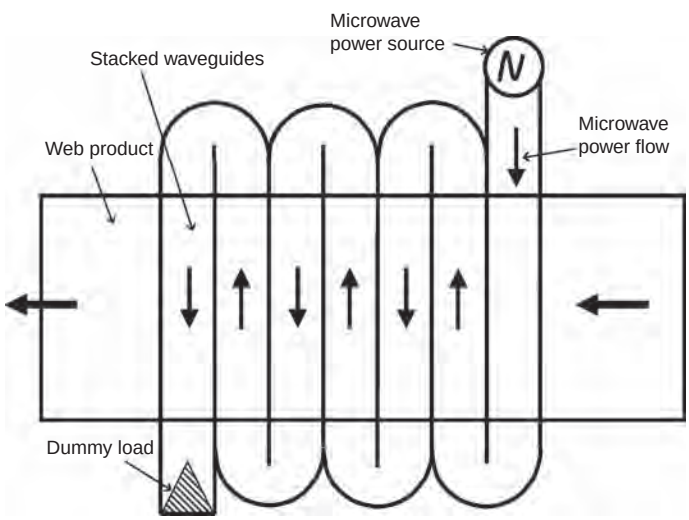

FIGURE 9.15
A stacked set of meandering waveguide applicator eliminates stray emissions from multiple openings. The whole system has only two openings for product entrance and exit.

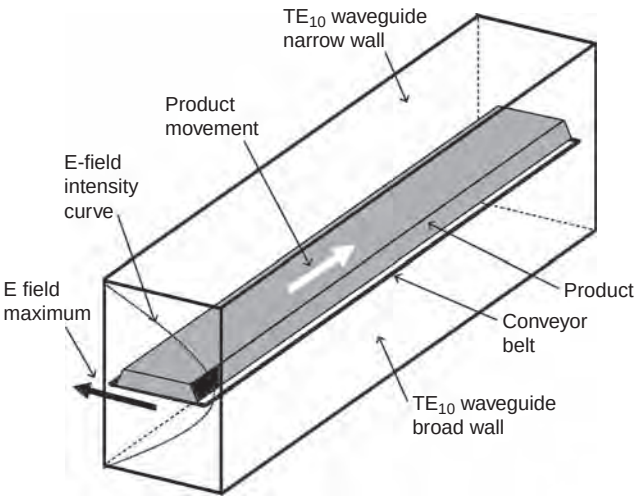

FIGURE 9.16 *General view of a longitudinal-flow waveguide applicator (also known as a standing-wave applicator). Moving product is typically placed at the center of the broad wall of a TE^{10} waveguide, which has the maximum E field.*

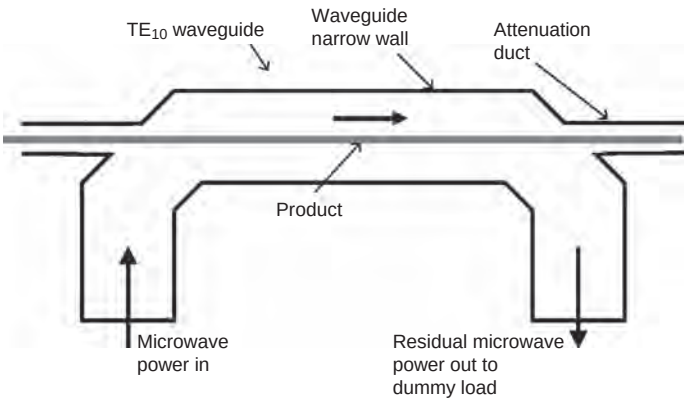

FIGURE 9.17 *A side view of the system, including the power source, the dummy load, and the product inlet–outlet with attenuation duct (choke) for reduction of microwave emissions.*

shows a side view of the system, including the power source, the dummy load, and the product inlet–outlet with attenuation tunnels for reduction of microwave emissions (Section 9.5).

When the objective is to dry a product, the dielectric loss at the beginning of the process is much higher than at the end. To keep the power deposition along the process even, the electric field at the beginning of the process must be smaller in exchange for higher electric fields at the end. For such cases an alternate configuration [33] similar to that in Figure 9.18 is devised, where the product is introduced to the waveguide in an off-center manner, so that according to Eq. (9.13) the field is less intense at the beginning of the process.

As for the application examples, a longitudinal-flow applicator has been used [34] for microwave-assisted continuous production of nanocrystalline metal powders using the polygol process. Another application involves processing discontinuous objects on a conveyor belt going through a longitudinal-flow applicator, as shown in Figure 9.19 [23].

9.5 EMISSIONS REDUCTION METHODS TO IMPROVE SAFETY OF MICROWAVE PROCESSES

9.5.1 Introduction

The need to reduce or eliminate stray RF/microwave emissions arises for three reasons. The first is regulatory issues due to occupational safety, the second is harmful interference with instruments that are invariably present in the immediate vicinity, and the third that the emissions are a waste of energy. All microwave/RF systems have a metallic enclosure, as well as

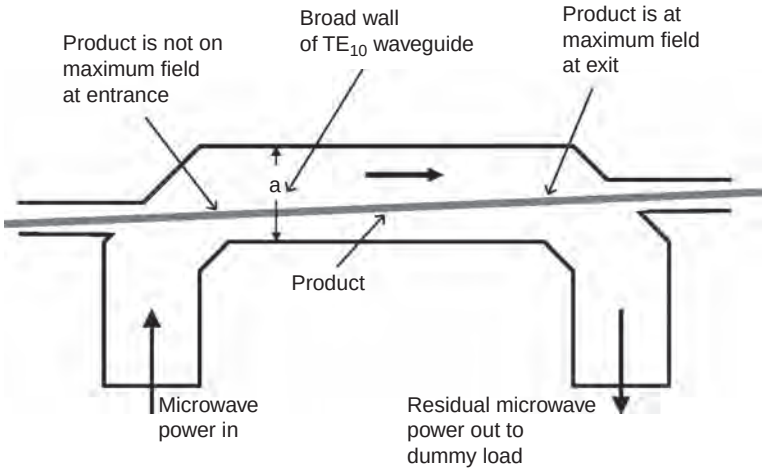

FIGURE 9.18 *An alternate configuration for a longitudinal-flow waveguide applicator where the product is introduced to the waveguide in an off-center manner; the field is less intense at the beginning of the process. After Ref. [33].*

FIGURE 9.19 *Photograph of a longitudinal waveguide continuous applicator. Courtesy of Industrial.*

EMI gaskets for seams and doors, which are very effective when properly designed.

Here we assume that the operating frequency is one of the Industrial, Scientific, and Medical (ISM) frequencies allowed [35–39] (Appendix A9.1). If the operating frequency falls outside of the ISM bands, meeting the regulations will become much more difficult, because interference with communication devices can occur at far lower emission levels than that of safety considerations.

Meeting emissions regulations is more critical for continuous processes, because they require product inlet and outlet ports that can readily cause leakage of RF/microwave radiation. In addition, many microwave/RF processes may require openings for various reasons. An example is infrared thermometers and imaging equipment that must have line-of-sight view of the material. Such open ports in practice cause the same concerns as those for product inlet and outlet ports. In this section we will discuss various methods to eliminate or reduce emissions from open ports to an acceptable minimum. Figure 9.20a shows a general view of a rectangular attenuation duct and Figure 9.20b shows a general view of a cylindrical attenuation tunnel.

Design considerations for an open port depend entirely on the minimum required size of the opening for the function it is supposed to serve. All openings must include a metallic tunnel, which is also called a vestibule, or an attenuation choke or attenuation tunnel. An opening without a

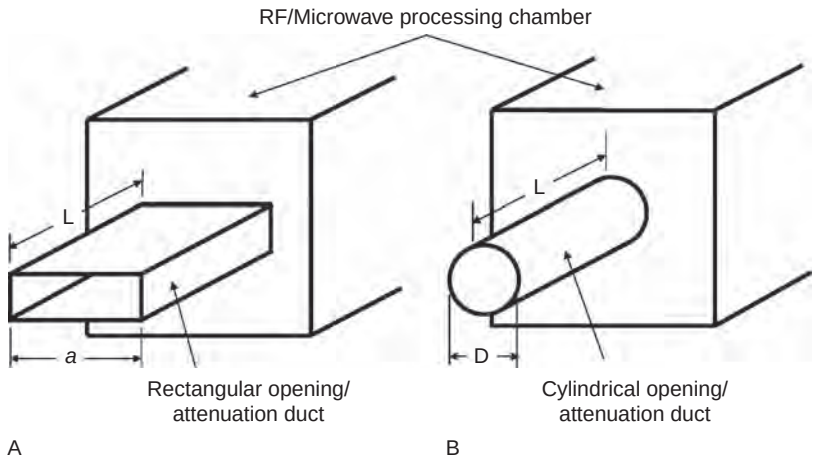

FIGURE 9.20 *Attenuation ducts (choke) for prevention of microwave emissions. (A) Rectangular duct. (B) Cylindrical duct.*

vestibule is bound to radiate energy, unless it is extremely small compared to the operating wavelength.

Open ports attached to a microwave or RF heating chamber can generally be categorized into two types from a size standpoint. An electrically small or below-cutoff opening is one where the waves do not propagate, but the wave amplitude diminishes quickly with distance (also called the evanescent mode). In above-cutoff openings the attenuation of a vestibule with metallic walls is minimal, and energy leaks out regardless of the vestibule's length, unless certain techniques (discussed in Section 9.5.4) are used.

Therefore the first consideration is to find out if the required opening is below or above cutoff for the operating frequency, which will be discussed in the next section.

9.5.2 Cutoff frequencies for cylindrical and rectangular waveguides

In a rectangular opening, the waveguide mode with the longest cutoff wavelength is TE_{10}. The cutoff wavelength for this mode in meters is given [7] as $\lambda_c = 2a$, where a is the longer dimension in meters. Therefore the cutoff frequency in MHz for a rectangular vestibule is:

$$f_c = 150/a \tag{9.16}$$

where a is the long dimension of the opening (in meters). This is the frequency above which the waves propagate along the attenuation tunnel.

In the case of a cylindrical vestibule, the mode with the longest cutoff wavelength is TE_{11}. The cutoff wavelength for this mode is given [7] as $\lambda_c = 1.7D$, where D is the inner diameter of the vestibule. Therefore the cutoff frequency (in MHz) for a cylindrical vestibule becomes:

$$f_c = 176/D \tag{9.17}$$

where D is the inner diameter of the vestibule (in meters).

Conversely, Eqs (9.16) and (9.17) could be used to determine cutoff dimensions of rectangular and cylindrical vestibules for several ISM frequencies, as shown in Table 9.1. For diameters larger than the cutoff diameter, substantial leakage occurs regardless of the vestibule length. For diameters smaller than cutoff, the amount of leakage depends on the length of the vestibule, as will be described later.

Generally, as the tunnel dimensions are widened to approach the above numbers, then the tunnel must be made longer to be effective. The following analysis is done to account for the length versus cross-sectional dimensions.

Table 9.1 Cutoff dimensions of rectangular and cylindrical vestibules for several ISM frequencies.

ISM Frequency	Cutoff Inside Diameter (*D*) for Cylindrical Attenuation Tunnel	Cutoff Large Dimension (*a*) for Rectangular Attenuation Tunnel
27.12 MHz	6.48 m	5.53 m
40.68 MHz	4.32 m	3.68 m
915 MHz	19.23 cm	16.3 cm
2.45 GHz	7.18 cm	6.12 cm
5.8 GHz	3.03 cm	2.58 cm

9.5.3 Below-cutoff attenuation ducts (chokes)

For below-cutoff vestibules of any geometry, the attenuation constant is given [21] as:

$$\alpha = \frac{2\pi}{\lambda}\sqrt{\left(\frac{\lambda}{\lambda_c}\right)^2 - 1} \tag{9.18}$$

where α is in nepers per meter, λ is the operating wavelength, and λ_c is the cutoff wavelength. For a rectangular below-cutoff vestibule, $\lambda_c = 2a$, and knowing that 1 neper/meter is 8.696 dB/meter, and after further simplification:

$$\alpha = 0.18\sqrt{\frac{22{,}500}{a^2} - f^2} \tag{9.19}$$

where α is the attenuation constant (in dB/m), a is the large cross-section of the rectangular vestibule (in meters), and f is the operating frequency (in MHz).

For a cylindrical vestibule, $\alpha = 1.7D$. After simplification, Eq. (9.18) becomes:

$$\alpha = 0.18\sqrt{\frac{31{,}100}{D^2} - f^2} \tag{9.20}$$

where D is the diameter of the vestibule and f is the operating frequency (in MHz).

In using Eqs (9.19) and (9.20) an attenuation level of 40 dB would be adequate for most practical situations where the radiation safety regulation is considered for ISM frequencies. When a non-ISM frequency is used, much more strict thresholds apply.

Example

In a 2450 MHz microwave process there is a need for an infrared imager viewing port that has a 5 cm diameter. What is the length of the attenuation duct for the viewing port so that the attenuation level is 40 dB?

Using Eq. (9.20) the attenuation constant becomes 457 dB/meter. To obtain 40 dB the length of the vestibule turns out to be 8.57 cm.

An examination of Eqs (9.18)–(9.20) reveals that for frequencies far below cutoff ($\lambda \gg \lambda_c$), the attenuation constant becomes frequency independent. For a cylindrical far-below-cutoff tunnel, Eq. (9.20) becomes:

$$\alpha = 32/D \tag{9.21}$$

and for a rectangular far-below-cutoff tunnel:

$$\alpha = 27.3/a \tag{9.22}$$

The above equations are particularly useful for quick calculation of attenuation in openings and vestibules in RF systems, because they are almost always far below cutoff. This fact may lead one to conclude that RF systems are relatively easy to keep within emissions regulations. In reality RF systems pose a particularly difficult challenge, which is the presence of harmonics of the ISM frequency, which obviously fall into a non-ISM band. In this case the emission standards are much tougher to meet. To solve this problem high-power RF systems utilizing a harmonic suppression system can be used.

9.5.4 Above-cutoff attenuation ducts for product entry/exit (vestibules)

In continuous processes, the size of the openings for product entrance and exit must comply with the product and process requirements, which sometimes set these dimensions to be larger than the cutoff. Therefore the vestibules at the exit and entrance can leak the microwave energy out, which leads to both safety problems and energy wastage.

Close examination of Table 9.1 reveals that in RF frequencies of 27 and 40 MHz, almost any industrial process can take advantage of below-cutoff attenuation. The reason is that the wavelength in RF systems is typically larger than the opening needed for product entry and exit. For microwave heating systems, however, due to the small wavelength, it is highly likely that the cross-sectional dimensions of the product are larger than the cutoff dimensions. Therefore techniques other than waveguide cutoff are necessary to maintain acceptable levels.

One useful technique is the use of an absorptive dielectric lining inside the attenuation tunnel. Theoretical data for using various thicknesses of lossy dielectric material with a dielectric loss factor of $\varepsilon_r'' = 1.5$ do exist [21]. In most practical cases, however, the attenuation tunnel must be very long for this method to be effective.

Another method is the use of lossy ferrite or ferrite-loaded materials. Most waveguide modes have strong magnetic fields parallel to the walls. A lossy ferrite material has a high magnetic loss (the imaginary part of the permeability). A particular type of ferrite-loaded material that contains ferrite particle sizes that are tuned to various microwave frequencies is Eccosorb SF, manufactured by Emerson Cumings Inc. [40]. A lining of 2.16-mm-thick (0.085 inch) Eccosorb SF 2.5 (which is tuned for maximum absorption at 2.5 GHz, lining a WG340 waveguide (86 mm × 43 mm) at 2.45 GHz yields an impressive attenuation of 260 dB/m.

A major challenge in the design of above-cutoff attenuation tunnels occurs when the required opening is large (multi-wavelength). In this case, many of the waveguide modes are close to the TEM mode, and travel through the waveguide as plane free-space waves, where the waveguide walls play a small role in setting the boundary conditions. In such cases, lining the walls with absorbing materials is only effective to a limited extent.

9.5.5 Resonant (reflective) choking methods of attenuation tunnels

In the previous section we discussed methods involving absorbing materials as lining for above-cutoff ports in microwave conveyor systems. A challenge with the absorptive approach is that in many high-power cases the absorptive material may become heated and lose its effectiveness. In this section we will describe another effective technique using resonance that in effect reflects, rather than absorbs, emissions from the microwave chamber.

Resonant methods of reduction of emissions from an above-cutoff opening take advantage of the fact that these systems have a narrow frequency band, and the operating frequency can be selectively removed by putting a band-stop filter between the microwave chamber and the outside. This filtering method, which in different publications has been given names such as waffle-iron filter or corrugated choke, involves repetitive metallic features that are tuned to resonate at the frequency of microwave operation. Figure 9.21 shows one such structure [41–43], where the filter elements have rectangular shapes. Referring to the geometry shown in Figure 9.21, an example given [41] involves a matrix of 3 × 5 blocks, each having a width $w = 86.36$ mm, $g = 14.88$ mm, $l = 28.79$ mm, $b = 974$ mm, and

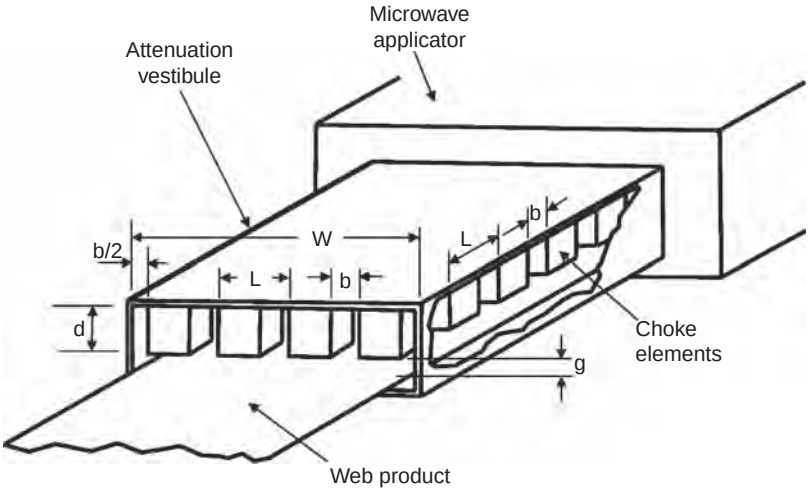

FIGURE 9.21 *Double corrugated choke system. After Ref. [41].*

$d = 28.3$ mm will provide a filtering of -90 dB at the frequency range of 2.4–2.5 GHz.

It is important to note that if one technique is inadequate for reducing emissions to an acceptable level, then both resonant and absorptive techniques should be used within the same attenuation tunnel. Since absorptive materials are subject to overheating they should be used farthest away from the heating chamber, and a resonant waffle-iron filter should be used in that position. Figure 9.22 shows this combination approach [43]. In this method, the resonant elements first reduce the emission to a relatively low level, so that no heating of the absorptive lining is possible.

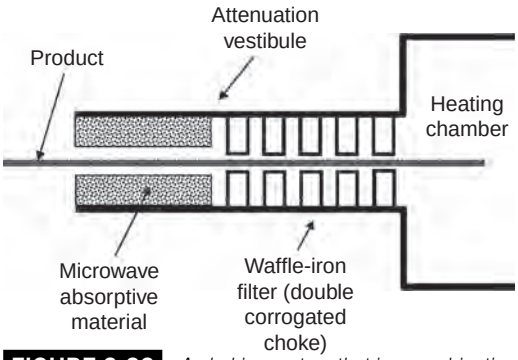

FIGURE 9.22 *A choking system that is a combination of corrugated choke (waffle-iron filter) and absorptive material lining.*

REFERENCES

[1] G. Roussy, J.A. Pearce, Foundations and Industrial Applications of Microwave and Radio Frequency Fields: Physical and Chemical Processes, Wiley, New York, 1995.

[2] LumaSense Technologies Inc. website URL: http://www.lumasenseinc.com/

[3] Neoptix Inc. URL: http://www.neoptix.com

[4] D. Boldor, et al., A model for temperature and moisture distribution during continuous microwave drying, J. Food Process Eng. 28 (2005) 68–87.

[5] J.C. Monzon, Electromagnetic paper drying, IEEE Trans. Microwave Theory Tech. 43 (2) (Febuary 1995).

[6] D.J. Lowe, US Patent 5,237,755.

[7] M. Mehdizadeh, R.Q. Freeman, W.L. Geigle, E.W. Williams, US Patent 5,950,325, 1999.

[8] J. Thuery, Microwaves: Industrial, Scientific, and Medical Applications, Artech House, Boston, 1992.

[9] Strayfield Ltd. URL: http://www.strayfield.co.uk

[10] T. Koral, Radio frequency and bulk heating, Biscuit World 7 (4) (Nov. 2004).

[11] C.M. Van't Land, Industrial Drying Equipment, Marcel Dekker, 1991, pp. 217–220.

[12] J.A. Barrie, Water in polymers, in: J. Crank, G.S. Park (Eds.), Diffusion in Polymers, Academic Press, London, 1968, pp. 259–314.

[13] C. Gibson, et al., Microwave enhanced diffusion in polymeric materials, J. Microw. Power Electromagn. Energy 23 (1) (1988).

[14] V.E. Semenov, K.I. Rybakov, Enhanced mass and charge transfer in solids exposed to microwave fields, in: M. Willert-Porada (Ed.), Advances in Microwave and Radio Frequency Processing, Springer, 2006, pp. 472–481.

[15] Y. Nakai, et al., Enhanced gas permeability of cellulose acetate membranes under microwave irradiation, J. Memb. Sci. 256 (1–2) (July 2005) 72–77.

[16] R.J. Riegert, Private communication.

[17] M. Mehdizadeh, New field modification methods for improved performance in continuous processing of thermally sensitive materials with RF/microwave, 40th Annual Microwave Symposium Proceedings, International Microwave Power Institute, August 2006.

[18] E. Kubel Jr., Special Focus: Advancements in microwave heating technology, Industrial Heating, Jan. 2005. Available online at: http://www.industrialheating.com/CDA/Archives/744efb4be5cb7010VgnVCM100000f932a8c0

[19] D.R. Herfindahl, H.F. Huang, R.W. Lewis, W.A. Wallace, Microwave Resonant Cavity Applicator for Heating Articles of Indefinite Length, US Patent 5,146,058, Sept. 1992.

[20] A.C. Metaxas, R.J. Meredith, Industrial Microwave Heating, Peter Peregrinus, 1983.

[21] R.J. Meredith, Engineers' Handbook of Industrial Microwave Heating (Power and Energy Series), IEE Press, Cambridge, UK, 1998.

[22] Cober Electronics Inc. URL: www.cober.com

[23] Industrial Microwave Systems, Inc., URL: www.industrialmicrowave.com

[24] F.W. Aherns, Application of a device for uniform web drying and preheating using microwave energy, Georgia Institute of Technology Report ID: DE-FC07-00ID13872, URL: http://www.osti.gov/bridge/servlets/purl/816299-HmEAk9/native/816299.pdf, 2003.

[25] S.G. Kashyap, J.G. Dunn, A waveguide applicator for sheet materials, IEEE Trans. Microwave Theory Tech. 24 (2) (Febuary 1976) 125–126.

[26] P.L. Jones, et al., Dielectric drying, Drying Technol. 14 (5) (1996) 1063–1098.

[27] J.M. Drozd, W.T. Joines, US Patent 5,958,275, 1999.

[28] V.N. Tran, et al., Improving the uniformity of the meander applicator for laminar chemical processing, Proceedings of the Annual Microwave Heating

Symposium, Conference, Vol. 37, pp. 35–38, 2002. Available online at: http://users.wpi.edu/~qwug/files/Tran-et-al_2002.pdf

[29] T.K. Ishii, Microwave Engineering, second ed., Oxford University Press, USA, 1995.

[30] J.M. Drozd, W.T. Joines, US Patent 5,958,275, 1999.

[31] F.W. Aherns, Use of new applicator design ideas to improve uniformity of paper drying via microwave energy, Drying Technol. 19 (10) (2001) 2531–2548.

[32] A.C. Metaxas, Foundations of Electroheat: A Unified Approach, Wiley, New York, 1996.

[33] J M. Drozd, W.T. Joines, US Patent 6,246,037, 2001.

[34] D. Lewis III, et al., US Patent Application 2004/0255721 A1, 2004.

[35] Federal Communications Commission Office of Engineering and Technology, Policy and Rules Division FCC Online, Section 5.150 Table of Frequency Allocations 47 C.F.R., §2.106 revised on 11 October 2006. Available online at: http://www.fcc.gov/oet/spectrum/table/fcctable.pdf

[36] OFCOM, United Kingdom Table of Radio Frequency Allocations 9 kHz–105 GHz, RA 365, 2000. Available online at URL: http://www.ofcom.org.uk/static/archive/ra/publication/ra_info/ra365.htm

[37] D. Hoolihan, Amendment 1 brings improvements to CISPR 11, Compliance Engineering, July/August 2000. Available online at: http://www.ce-mag.com/archive/2000/julyaugust/Hoolihan.html

[38] R. Kitchen, RF and Microwave Radiation Safety, second ed., Newnes, 2001.

[39] J.M. Osepchuk, et al., Safety and environmental issues, in: M.E. Golio (Ed.), The RF and Microwave Handbook, CRC Press, 2001, pp. 3-28–3-43.

[40] Emerson & Cuming Inc. URL: www.emersoncuming.com

[41] J.M. Catala-Civera, et al., Design parameters of multiple reactive chokes for open ports in microwave heating systems, Advances in Microwave and Radio Frequency Processing, Willert-Porada, M., Editor, 8th International Conference on Microwave and High-Frequency Heating, Springer-Verlag, Berlin, 2006.

[42] P. Soto, Analysis, design, and experimental verification of microwave filters for safety issues in open-ended waveguide systems, IEEE Trans. Microwave Theory Tech. 48 (11) (2000) 2133–2139.

[43] D. Tipton, US Patent 3,897,543.

Appendix A2.1

Mode Chart for Cylindrical Cavities

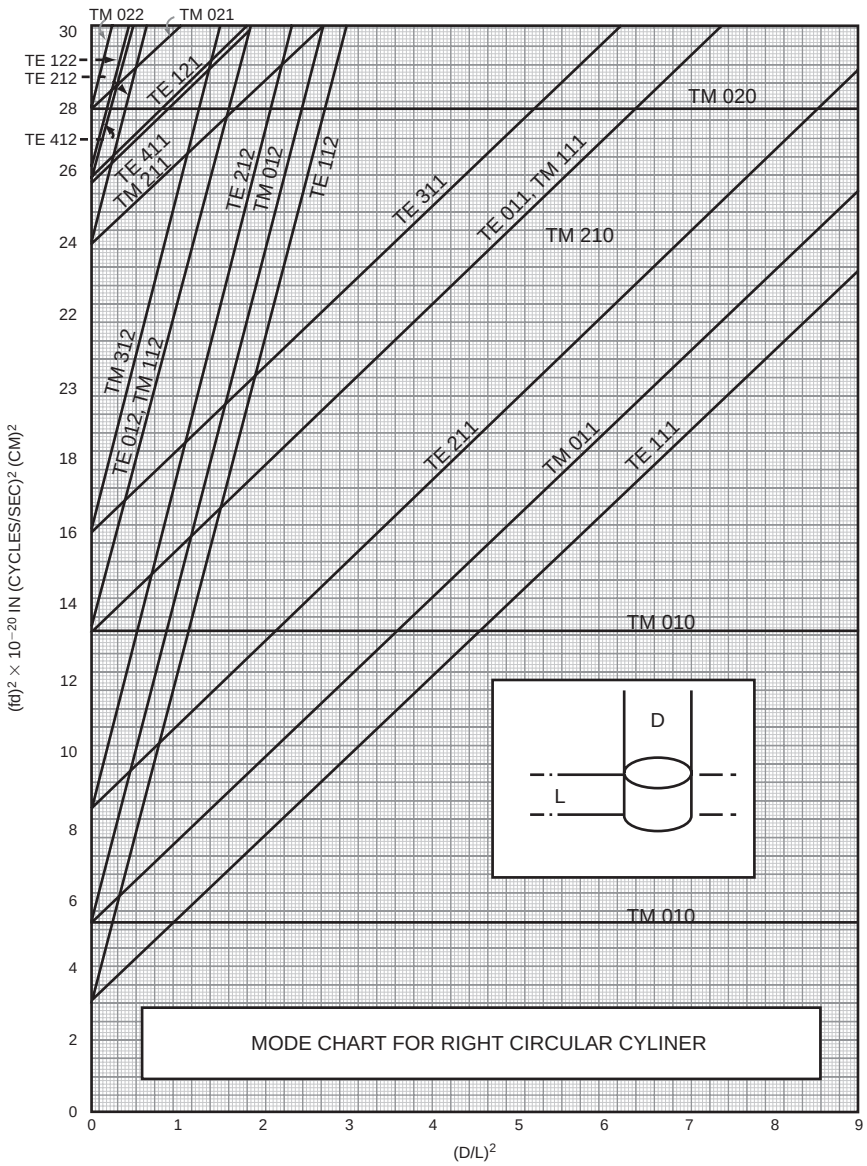

From: T.S. Saad et al. (Eds), Microwave Engineer's Handbook, vol. 1, Artech House, Dedham, MA, 1971.

Appendix A3.1

Impedance/Admittance and Electric Field Solutions for a Parallel-plate Applicator with Dual Layers of Real Dielectric Materials

Consider Figure 3.9, where a pair of parallel plates with area A have two layers of dielectric materials with complex permittivities of $\varepsilon_1 = \varepsilon_0(\varepsilon'_{r1} - j\varepsilon''_{r1})$ and $\varepsilon_2 = \varepsilon_0(\varepsilon'_{r2} - j\varepsilon''_{r2})$, with thicknesses of d_1 and d_2 respectively. Here $_0$ is the permittivity of a vacuum and terms with "r" subscripts are the relative dielectric properties of each material.

The solution to the Laplace equation in a single x dimension yields the following set of equations for the potential function in the two dielectric regions:

$$\phi_1 = c_1 x + c_2 \tag{A3.1}$$

$$\phi_2 = c_3 x + c_4 \tag{A3.2}$$

where c_1–c_4 are constants. The displacement current densities J_1 and J_2 in each dielectric can be written as:

$$J_1 = j\omega\varepsilon_1 \tag{A3.3}$$

$$J_2 = j\omega\varepsilon_2 \tag{A3.4}$$

where $\omega = 2\pi f$ in rad/s is the angular frequency, f being the operating frequency in Hz. We apply the following boundary conditions:

$$\begin{aligned} \phi_1 &= 0 \quad @ \quad x = 0 \\ \phi_1 &= \phi_2 \quad @ \quad x = d_1 \\ \phi_2 &= V_0 \quad @ \quad x = d_1 + d_2 \\ J_1 &= J_2 \quad @ \quad x = d_1 \end{aligned} \tag{A3.5}$$

Using the above boundary conditions and solving for the constants, the voltage functions become:

$$\phi_1 = \frac{\varepsilon_2 V_0}{d_2 \varepsilon_1 + d_1 \varepsilon_2} x \tag{A3.6}$$

and

$$\phi_2 = \frac{\varepsilon_1 V_0}{d_2 \varepsilon_1 + d_1 \varepsilon_2} x + \frac{(d_1 \varepsilon_2 - d_1 \varepsilon_1) V_0}{d_2 \varepsilon_1 + d_1 \varepsilon_2} \tag{A3.7}$$

Applying the gradient equation to Eqs (A3.6) and (A3.7), the electric field intensities inside the two dielectric layers are found as:

$$E_1 = -\nabla\varphi_1 = -\frac{\mathrm{d}\phi_1}{\mathrm{d}x} = -\frac{\varepsilon_2 V_0}{d_2\varepsilon_1 + d_1\varepsilon_2} \tag{A3.8}$$

$$E_2 = -\nabla\varphi_2 = -\frac{\mathrm{d}\phi_2}{\mathrm{d}x} = -\frac{\varepsilon_1 V_0}{d_2\varepsilon_1 + d_1\varepsilon_2} \tag{A3.9}$$

We then combine Eqs (A3.3) and (A3.9), and since the area of the parallel plates is A, then the total current is $I = JA$.

Furthermore, the total complex admittance $Y = I/V_0$ across the plates becomes:

$$Y = \frac{j\omega A}{\frac{d_1}{\varepsilon_1} + \frac{d_2}{\varepsilon_2}} \tag{A3.10}$$

Now, replacing ε_1 and ε_2 with complex dielectric properties, and $\varepsilon_2 = \varepsilon_0(\varepsilon'_{r2} - j\varepsilon''_{r2})$, then expanding the complex terms using the Mathematica™ command "ComplexExpand" as in Appendix A3.2 to obtain complex admittance, we obtain:

$$\begin{aligned} Y = {} & \omega\varepsilon_0 A \frac{d_2 \varepsilon''_{r2}\left(\varepsilon'^2_{r1} + \varepsilon''^2_{r1}\right) + d_1 \varepsilon''_{r1}\left(\varepsilon'^2_{r2} + \varepsilon''^2_{r2}\right)}{d_2^2\left(\varepsilon'^2_{r1} + \varepsilon''^2_{r1}\right) + d_1^2\left(\varepsilon'^2_{r2} + \varepsilon''^2_{r2}\right) + 2d_1d_2\left(\varepsilon'_{r1}\varepsilon'_{r2} + \varepsilon''_{r1}\varepsilon''_{r2}\right)} \\ & + j\,\omega\varepsilon_0 A \frac{d_2 \varepsilon'_{r2}\left(\varepsilon'^2_{r1} + \varepsilon''^2_{r1}\right) + d_1 \varepsilon'_{r1}\left(\varepsilon'^2_{r2} + \varepsilon''^2_{r2}\right)}{d_2^2\left(\varepsilon'^2_{r1} + \varepsilon''^2_{r1}\right) + d_1^2\left(\varepsilon'^2_{r2} + \varepsilon''^2_{r2}\right) + 2d_1d_2\left(\varepsilon'_{r1}\varepsilon'_{r2} + \varepsilon''_{r1}\varepsilon''_{r2}\right)} \end{aligned} \tag{A3.11}$$

The admittance expression above is often most convenient when circuit elements are analyzed. The admittance has two components, conductance G and susceptance B:

$$Y = G + jB$$

Referring to the equivalent circuit of Figure 3.9b, $R = 1/G$ and $C = B/\omega$. Therefore the resistance in the equivalent circuit of Figure 3.9b becomes:

$$R = \frac{1}{\omega\varepsilon_0 A}\frac{d_2^2\left(\varepsilon_{r1}'^2 + \varepsilon_{r1}''^2\right) + d_1^2\left(\varepsilon_{r2}'^2 + \varepsilon_{r2}''^2\right) + 2d_1d_2\left(\varepsilon_{r1}'\varepsilon_{r2}' + \varepsilon_{r1}''\varepsilon_{r2}''\right)}{d_2\,\varepsilon_{r2}''\left(\varepsilon_{r1}'^2 + \varepsilon_{r1}''^2\right) + d_1\,\varepsilon_{r1}''\left(\varepsilon_{r2}'^2 + \varepsilon_{r2}''^2\right)}$$

and the capacitance is:

$$C = \varepsilon_0 A\frac{d_2\,\varepsilon_{r2}'\left(\varepsilon_r'^2 + \varepsilon_{r1}''^2\right) + d_1\,\varepsilon_{r1}'\left(\varepsilon_{r2}' + \varepsilon_{r2}''^2\right)}{d_2^2\left(\varepsilon_{r1}'^2 + \varepsilon_{r1}''^2\right) + d_1^2\left(\varepsilon_{r2}'^2 + \varepsilon_{r2}''^2\right) + 2d_1d_2\left(\varepsilon_{r1}'\varepsilon_{r2}' + \varepsilon_{r1}''\varepsilon_{r2}''\right)}$$

If the impedance expression is desired, then $Z = 1/Y$, and:

$$Z = \frac{1}{\omega\varepsilon_0 A}\left(\frac{d_1\varepsilon_{r1}''}{\varepsilon_{r1}'^2 + \varepsilon_{r1}''^2} + \frac{d_2\varepsilon_{r2}''}{\varepsilon_{r2}'^2 + \varepsilon_{r2}''^2}\right) - j\frac{1}{\omega\varepsilon_0 A}\left(\frac{d_1\varepsilon_{r1}'}{\varepsilon_{r1}'^2 + \varepsilon_{r1}''^2} + \frac{d_2\varepsilon_{r2}'}{\varepsilon_{r2}'^2 + \varepsilon_{r2}''^2}\right) \quad \text{(A3.12)}$$

To find the amplitude of the electric field in each of the two dielectric layers, we will find the absolute values of Eqs (A3.8) and (A3.9) and insert $\varepsilon_1 = \varepsilon_0(\varepsilon_{r1}' - j\varepsilon_{r1}'')$ and $\varepsilon_2 = \varepsilon_0(\varepsilon_{r2}' - j\varepsilon_{r2}'')$, which yields:

$$E_1 = V_0\sqrt{\frac{\varepsilon_{r2}'^2 + \varepsilon_{r2}''^2}{d_1^2(\varepsilon_{r2}'^2 + \varepsilon_{r2}''^2) + d_2^2(\varepsilon_{r1}'^2 + \varepsilon_{r1}''^2) + 2d_1d_2(\varepsilon_{r1}'\varepsilon_{r2}' + \varepsilon_{r1}''\varepsilon_{r2}'')}} \quad \text{(A3.13)}$$

and

$$E_2 = V_0\sqrt{\frac{\varepsilon_{r1}'^2 + \varepsilon_{r1}''^2}{d_1^2(\varepsilon_{r2}'^2 + \varepsilon_{r2}''^2) + d_2^2(\varepsilon_{r1}'^2 + \varepsilon_{r1}''^2) + 2d_1d_2(\varepsilon_{r1}'\varepsilon_{r2}' + \varepsilon_{r1}''\varepsilon_{r2}'')}} \quad \text{(A3.14)}$$

Appendix A3.2

Mathematica™ Worksheet for Derivation of Dual-layer Parallel Plates with Real Dielectrics

```
In[1]:= (* Admittance of a composite double lossy
           dielectric layers between two parallel plates *)

In[2]:= (* In the expression below,
           e1 and e2 represent complex relative permittivities of the two layers (ε1 and ε2) *)

In[3]:= I w A / (d2 / e2 + d1 / e1)
```

$$\text{Out[3]}= \frac{i A w}{\frac{d1}{e1}+\frac{d2}{e2}}$$

```
In[4]:= % /. {e1 → ep1 - I epp1, e2 → ep2 - I epp2}
```

$$\text{Out[4]}= \frac{i A w}{\frac{d1}{ep1-i epp1}+\frac{d2}{ep2-i epp2}}$$

```
In[5]:= ComplexExpand[%, TargetFunctions → {Re, Im}]
```

$$\text{Out[5]}= \frac{A\,d1\,epp1\,w}{(ep1^2+epp1^2)\left(\left(\frac{d1\,ep1}{ep1^2+epp1^2}+\frac{d2\,ep2}{ep2^2+epp2^2}\right)^2+\left(\frac{d1\,epp1}{ep1^2+epp1^2}+\frac{d2\,epp2}{ep2^2+epp2^2}\right)^2\right)}+$$
$$\frac{A\,d2\,epp2\,w}{(ep2^2+epp2^2)\left(\left(\frac{d1\,ep1}{ep1^2+epp1^2}+\frac{d2\,ep2}{ep2^2+epp2^2}\right)^2+\left(\frac{d1\,epp1}{ep1^2+epp1^2}+\frac{d2\,epp2}{ep2^2+epp2^2}\right)^2\right)}+$$
$$i\left(\frac{A\,d1\,ep1\,w}{(ep1^2+epp1^2)\left(\left(\frac{d1\,ep1}{ep1^2+epp1^2}+\frac{d2\,ep2}{ep2^2+epp2^2}\right)^2+\left(\frac{d1\,epp1}{ep1^2+epp1^2}+\frac{d2\,epp2}{ep2^2+epp2^2}\right)^2\right)}+\right.$$
$$\left.\frac{A\,d2\,ep2\,w}{(ep2^2+epp2^2)\left(\left(\frac{d1\,ep1}{ep1^2+epp1^2}+\frac{d2\,ep2}{ep2^2+epp2^2}\right)^2+\left(\frac{d1\,epp1}{ep1^2+epp1^2}+\frac{d2\,epp2}{ep2^2+epp2^2}\right)^2\right)}\right)$$

```
In[6]:= (* The Real Part of the Admittance (cut and paste from above) *)
```

$$\text{In[7]:=}\quad \frac{A\,d1\,epp1\,w}{(ep1^2+epp1^2)\left(\left(\frac{d1\,ep1}{ep1^2+epp1^2}+\frac{d2\,ep2}{ep2^2+epp2^2}\right)^2+\left(\frac{d1\,epp1}{ep1^2+epp1^2}+\frac{d2\,epp2}{ep2^2+epp2^2}\right)^2\right)}+\frac{A\,d2\,epp2\,w}{(ep2^2+epp2^2)\left(\left(\frac{d1\,ep1}{ep1^2+epp1^2}+\frac{d2\,ep2}{ep2^2+epp2^2}\right)^2+\left(\frac{d1\,epp1}{ep1^2+epp1^2}+\frac{d2\,epp2}{ep2^2+epp2^2}\right)^2\right)}$$

$$\text{Out[7]=}\quad \frac{A\,d1\,epp1\,w}{(ep1^2+epp1^2)\left(\left(\frac{d1\,ep1}{ep1^2+epp1^2}+\frac{d2\,ep2}{ep2^2+epp2^2}\right)^2+\left(\frac{d1\,epp1}{ep1^2+epp1^2}+\frac{d2\,epp2}{ep2^2+epp2^2}\right)^2\right)}+\frac{A\,d2\,epp2\,w}{(ep2^2+epp2^2)\left(\left(\frac{d1\,ep1}{ep1^2+epp1^2}+\frac{d2\,ep2}{ep2^2+epp2^2}\right)^2+\left(\frac{d1\,epp1}{ep1^2+epp1^2}+\frac{d2\,epp2}{ep2^2+epp2^2}\right)^2\right)}$$

```
In[8]:= Simplify[%]
```

$$\text{Out[8]=}\quad \frac{A\,(d2\,(ep1^2+epp1^2)\,epp2+d1\,epp1\,(ep2^2+epp2^2))\,w}{(ep2^2+epp2^2)\,d1^2+2\,d2\,(ep1\,ep2+epp1\,epp2)\,d1+d2^2\,(ep1^2+epp1^2)}$$

```
In[9]:= (* The Imaginary Part of the Admittance (cut and paste) *)
```

$$\text{In[10]:=}\quad \left((A\,d1\,ep1\,w)\Big/\left((ep1^2+epp1^2)\left(\left(\frac{d1\,ep1}{ep1^2+epp1^2}+\frac{d2\,ep2}{ep2^2+epp2^2}\right)^2+\left(\frac{d1\,epp1}{ep1^2+epp1^2}+\frac{d2\,epp2}{ep2^2+epp2^2}\right)^2\right)\right)+(A\,d2\,ep2\,w)\Big/\left((ep2^2+epp2^2)\left(\left(\frac{d1\,ep1}{ep1^2+epp1^2}+\frac{d2\,ep2}{ep2^2+epp2^2}\right)^2+\left(\frac{d1\,epp1}{ep1^2+epp1^2}+\frac{d2\,epp2}{ep2^2+epp2^2}\right)^2\right)\right)\right)$$

$$\text{Out[10]=}\quad \frac{A\,d1\,ep1\,w}{(ep1^2+epp1^2)\left(\left(\frac{d1\,ep1}{ep1^2+epp1^2}+\frac{d2\,ep2}{ep2^2+epp2^2}\right)^2+\left(\frac{d1\,epp1}{ep1^2+epp1^2}+\frac{d2\,epp2}{ep2^2+epp2^2}\right)^2\right)}+\frac{A\,d2\,ep2\,w}{(ep2^2+epp2^2)\left(\left(\frac{d1\,ep1}{ep1^2+epp1^2}+\frac{d2\,ep2}{ep2^2+epp2^2}\right)^2+\left(\frac{d1\,epp1}{ep1^2+epp1^2}+\frac{d2\,epp2}{ep2^2+epp2^2}\right)^2\right)}$$

```
In[11]:= Simplify[%]
```

$$\text{Out[11]=}\quad \frac{A\,(d2\,ep2\,(ep1^2+epp1^2)+d1\,ep1\,(ep2^2+epp2^2))\,w}{(ep2^2+epp2^2)\,d1^2+2\,d2\,(ep1\,ep2+epp1\,epp2)\,d1+d2^2\,(ep1^2+epp1^2)}$$

Appendix A4.1

Field Analysis of TM_{0n0} Cylindrical Cavities with Two Concentric Layers of Real Dielectric at the Axis

Ronald J. Riegert

The wave equation in cylindrical coordinates, can be written in the following form for a general field component that varies only in radial direction, ψ (E or H field):

$$\frac{1}{r}\frac{\partial}{\partial r}\left(r\frac{\partial \psi}{\partial r}\right) + k^2\,\psi = 0 \tag{A4.1}$$

where:

$$k = k_0\sqrt{\varepsilon_i}$$

The parameter $\varepsilon_i = \varepsilon'_{ri} - \varepsilon''_{ri}$ is the complex relative permittivity of the region i and:

$$k_0 = 2\pi f^* \sqrt{\varepsilon_0 \mu_0} \tag{A4.2}$$

where f^* is the complex frequency, which is related to the operating frequency and cavity quality factor Q as:

$$f^* = f\left(1 + \frac{j}{2Q}\right) \tag{A4.3}$$

In an ideal TM_{0n0} cavity only E_z and H_ϕ components exist, and they are of the form:

$$E_z = K_1 J_0(k\,r) + K_2 N_0(k\,r) \tag{A4.4}$$

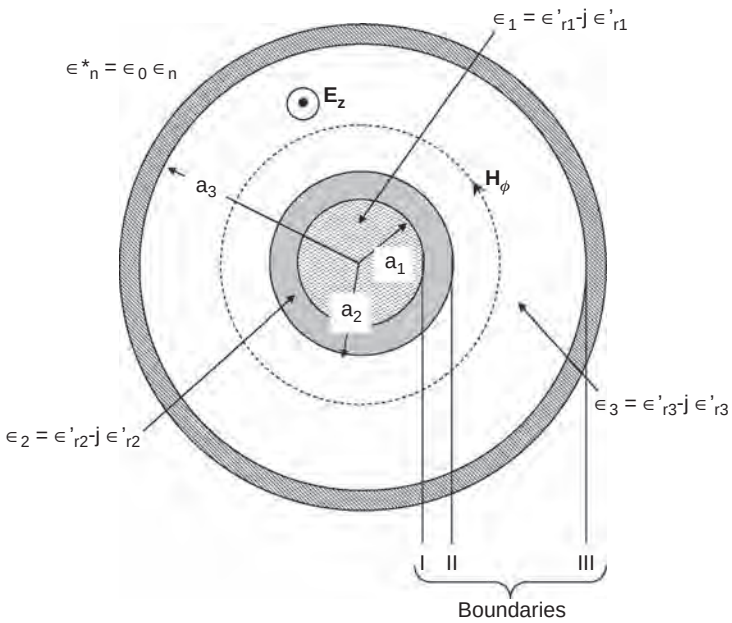

FIGURE A4.1 *Top view of TM_{010} loaded cavity structure.*

$$H_\phi = j\sqrt{\frac{\varepsilon_0}{\mu_0}}[K_3 J_1(k r) + K_4 N_1(k r)] \tag{A4.5}$$

where J_0 and N_0 are zero-order Bessel functions of the first and second type, J_1 and N_1 are first-order Bessel functions of the first and second type, and coefficients in the form of K_i are constants.

Applying the equality of E_z components at the boundaries I and II (Figure A4.1), we obtain the following two equations:

$$J_0\left(k_0\sqrt{\varepsilon_1}a_1\right) = A_1 J_0\left(k_0\sqrt{\varepsilon_2}a_1\right) + A_2 N_0\left(k_0\sqrt{\varepsilon_2}a_1\right) \tag{A4.6}$$

$$\begin{aligned} A_1 J_0\left(k_0\sqrt{\varepsilon_2}a_2\right) + A_2 N_0\left(k_0\sqrt{\varepsilon_2}a_2\right) = {} & A_3 J_0\left(k_0\sqrt{\varepsilon_3}a_2\right) \\ & + A_4 N_0\left(k_0\sqrt{\varepsilon_3}a_2\right) \end{aligned} \tag{A4.7}$$

Applying equality of the H_ϕ components from Eq. (A4.5) for boundary I gives:

$$\sqrt{\varepsilon_1} J_1\left(k_0\sqrt{\varepsilon_1}a_1\right) = A_1\sqrt{\varepsilon_2} J_1\left(k_0\sqrt{\varepsilon_2}a_1\right) + A_2\sqrt{\varepsilon_2} N_1\left(k_0\sqrt{\varepsilon_2}a_1\right) \tag{A4.8}$$

where all coefficients in the form of A_i are constants.

The metal–dielectric condition for boundary III is:

$$E_z = -Z_{\mathrm{m}} H_\phi \tag{A4.9}$$

where Z_{m} is the surface impedance:

$$Z_{\mathrm{m}} = (1 + j)\sqrt{\frac{\omega \mu_0}{2\sigma}} \tag{A4.10}$$

Applying this condition to Eqs (A4.6) and (A4.7), we obtain:

$$A_3 J_0\left(k_0 \sqrt{\varepsilon_3} a_3\right) + A_4 N_0\left(k_0 \sqrt{\varepsilon_3} a_3\right) = (1 - j)\sqrt{\frac{\omega \varepsilon_0 \varepsilon_3}{2\sigma}}\left[A_3 J_1\left(k_0 \sqrt{\varepsilon_3} a_3\right) + A_4 N_1\left(k_0 \sqrt{\varepsilon_3} a_3\right)\right] \tag{A4.11}$$

The following matrix can be formed from Eqs. A4.6-8 and A4.11:

$$\begin{bmatrix} 0 \\ 0 \\ 0 \\ 0 \\ 0 \end{bmatrix} = \begin{bmatrix} c_1 & c_2 & c_3 & 0 & 0 \\ c_4 & c_5 & c_6 & 0 & 0 \\ 0 & c_7 & c_8 & c_9 & c_{10} \\ 0 & c_{11} & c_{12} & c_{13} & c_{14} \\ 0 & 0 & 0 & c_{15} & c_{16} \end{bmatrix} \begin{bmatrix} 1 \\ A_1 \\ A_2 \\ A_3 \\ A_4 \end{bmatrix} \tag{A4.12}$$

where the coefficients c_1 to c_{16} are:

$$\begin{aligned}
c_1 &= -J_0\left[k_0 \sqrt{\varepsilon_1}\, a_1\right] & c_8 &= -N_0\left[k_0 \sqrt{\varepsilon_2}\, a_2\right] \\
c_2 &= J_0\left[k_0 \sqrt{\varepsilon_2}\, a_1\right] & c_9 &= J_0\left[k_0 \sqrt{\varepsilon_3}\, a_2\right] \\
c_3 &= N_0\left[k_0 \sqrt{\varepsilon_2}\, a_1\right] & c_{10} &= N_0\left[k_0 \sqrt{\varepsilon_3}\, a_2\right] \\
c_4 &= -\sqrt{\varepsilon_1} J_1\left[k_0 \sqrt{\varepsilon_1}\, a_1\right] & c_{11} &= -\sqrt{\varepsilon_2} J_1\left[k_0 \sqrt{\varepsilon_2}\, a_2\right] \\
c_5 &= \sqrt{\varepsilon_2} J_1\left[k_0 \sqrt{\varepsilon_2}\, a_1\right] & c_{12} &= -\sqrt{\varepsilon_2} N_1\left[k_0 \sqrt{\varepsilon_2}\, a_2\right] \\
c_6 &= \sqrt{\varepsilon_2} N_1\left[k_0 \sqrt{\varepsilon_2}\, a_1\right] & c_{13} &= \sqrt{\varepsilon_3} J_1\left[k_0 \sqrt{\varepsilon_3}\, a_2\right] \\
c_7 &= -J_0\left[k_0 \sqrt{\varepsilon_2}\, a_2\right] & c_{14} &= \sqrt{\varepsilon_3} N_1\left[k_0 \sqrt{\varepsilon_3}\, a_2\right] \\
c_{15} &= J_0\left(k_0 \sqrt{\varepsilon_3} a_3\right) - (1 - j)\sqrt{\frac{\omega \varepsilon_0 \varepsilon_3}{2\sigma}} J_1\left(k_0 \sqrt{\varepsilon_3} a_3\right) \\
c_{16} &= N_0\left(k_0 \sqrt{\varepsilon_3} a_3\right) - (1 - j)\sqrt{\frac{\omega \varepsilon_0 \varepsilon_3}{2\sigma}} N_1\left(k_0 \sqrt{\varepsilon_3} a_3\right)
\end{aligned} \tag{A4.13}$$

The determinant of the c-matrix shown in Eq. A4.12 must be set equal to zero. This is solved in Mathematica™ notebook shown in Appendix A4.2.

Appendix A4.2

Mathematica™ Notebook for Computation of Single-mode TM_{0n0} Cavities for Material Heating and Sensing Applications

```
In[1]:= (* Mathematica Program for
          Calculation of parameters of a TM0n0 Cylindrical
          Cavity with a concentric dielectric
          pipe carrying a lossy dielectric.

            Definition of dimensional and material property variables:
            Inner radius of the dielectric pipe: r1
             Outer radius of the dielectric pipe: r2
             Inner radius of the cavity: r3 (all in meters)
               Complex relative permittivity of the load, tube, and annular space:
            ε1,ε2,ε3 (all in form of a–I b)
          Conductivity of the Cavity walls: σ (3.9 10^7 S/m in case of aluminum

                Definition of electrical parameters:
                 Quality factor: Q
                   Resonant frequency: f (in Hz)
                     Note: Using complex f, in form of f(1+j/(2 Q)) is better.*)

In[2]:= (* Permeability and Permittivity of Free Space Values Defined: *)

In[3]:= μ0 = 4 π 10^ -7;

In[4]:= ε0 = 8.8510^ -12;

In[5]:= (* Define the C Matrix *)

In[6]:= cmat := {{c1, c2, c3, 0, 0}, {c4, c5, c6, 0, 0}, {0, c7, c8, c9, c10}, {0, c11, c12, c13, c14}, {0, 0, 0, c15, c16}}

In[7]:= (* Determinant of the C matrix (to be set equal to zero later) *)

In[8]:= solneqn := Det[cmat]

In[9]:= (* Set up the χ function to assign values for the C matrix *)
```

```
In[10]:= χ[r1_, r2_, r3_, ε1_, ε2_, ε3_, f_] := Block[{c1, c2, c3, c4, c5, c6, c7, c8, c9, c10,
           c11, c12, c13, c14, c15, c16, k},
         k = 2 π f Sqrt[ε0 μ0];
         c1 = -BesselJ[0, k ε1^0.5 r1];
         c2 = BesselJ[0, k ε2^0.5 r1];
         c3 = BesselY[0, k ε2^0.5 r1];
         c4 = -Sqrt[ε1] BesselJ[1, k ε1^0.5 r1];
         c5 = Sqrt[ε2] BesselJ[1, k ε2^0.5 r1];
         c6 = Sqrt[ε2] BesselY[1, k ε2^0.5 r1];
         c7 = -BesselJ[0, k ε2^0.5 r2];
         c8 = -BesselY[0, k ε3^0.5 r2];
         c9 = BesselJ[0, k ε3^0.5 r2];
         c10 = BesselY[0, k ε3^0.5 r2];
         c11 = -Sqrt[ε2] BesselJ[1, k ε2^0.5 r2];
         c12 = -Sqrt[ε2] BesselY[1, k ε2^0.5 r2];
         c13 = Sqrt[ε3] BesselJ[1, k ε3^0.5 r2];
         c14 = Sqrt[ε3] BesselY[1, k ε3^0.5 r2];
         c15 = BesselJ[0, k ε3^0.5 r3] - (1 - I) Sqrt[2 π f ε0 ε3 / (2 σ)] BesselJ[1, k ε3^0.5 r3];
         c16 = BesselY[0, k ε3^0.5 r3] - (1 - I) Sqrt[2 π f ε0 ε3 / (2 σ)] BesselY[1, k ε3^0.5 r3];
       solneqn]

In[11]:= (* At this point the known parameters need to be defined. For example, if the idea is to find the
         inner radius of the cavity (r3), all other physical and material properties need to be defined
         with the following line: *)

In[12]:= {r1 = .0125, r2 = .0165, ε1 = 4.52 - I 0.13, ε2 = 3.5 - I 0.002, ε3 = 1, σ = 3.9 10^7, f = 915 10^6}

Out[12]= {0.0125, 0.0165, 4.52 - 0.13 i, 3.5 - 0.002 i, 1, 3.9×10^7, 915000000}

In[13]:= (* Now, the root of function χ should be found for the unknown variable, which in
         in this case is r3. There is a need for setting a range for the variable in the expected
         range. *)

In[14]:= FindRoot[χ[r1, r2, r3, ε1, ε2, ε3, f] == 0, {r3, .01, .1}, MaxIterations → 30]

Out[14]= {r3 → 0.110588 + 0.00040269 i}

In[15]:= (* The above example shows the inner radius of the cavity is r3=
         11.05 cm to obtain the 915 MHz resonant frequency.
           But note that r3 for higher order modes can also be found by defining other expected ranges
         for those modes. To clarify, let us plot the real part of χ versus r3. The nth
         zero crossing point define r3 for TM0n0 modes. *)
```

```
In[16]:= Plot[Re[χ[r1, r2, r3, ε1, ε2, ε3, 915 10^6]], {r3, .01, .6}, PlotRange → All]
```

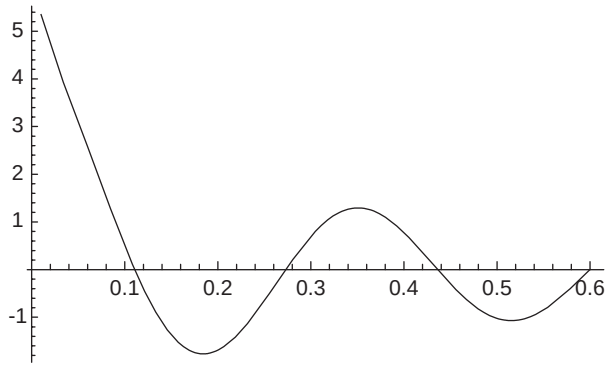


```
Out[16]= -Graphics-

In[17]:= (* ---------- *)

         (* In the following example, all the dimensional and material properties are known. The goal is to
            find the loaded resonant frequency and the quality factor: *)

In[18]:= {r1 = .0125, r2 = .0165, r3 = .1105, ε1 = 4.52 - I 0.13, ε2 = 3.5 - I 0.002, ε3 = 1, σ = 3.9 10^7}

Out[18]= {0.0125, 0.0165, 0.1105, 4.52 - 0.13 i, 3.5 - 0.002 i, 1, 3.9 × 10^7}

In[19]:= FindRoot[χ[r1, r2, r3, ε1, ε2, ε3, f] == 0, {f, 800 10^6, 1000 10^6}, MaxIterations → 30]

Out[19]= {915000000 → 9.15551 × 10^8 + 2.59435 × 10^6 i}

In[20]:= (* This means that the resonant frequency is 918.54 MHz. The Q is half the real part divided by the
            imaginary part. *)

In[21]:= 0.5 * (9.1555*^8 / (2.59435*^6))

Out[21]= 176.451

In[22]:= (* The above number is the loaded quality factor for this example. In order to find the
            applicator efficiency we will find the unloaded quality factor by making all dielectric
            data to be equal to unity (relative dielectric constant of vacuum) as follows: *)

In[23]:= {r1 = .0125, r2 = .0165, r3 = .1105, ε1 = 1, ε2 = 1, ε3 = 1, σ = 3.9 10^7}

Out[23]= {0.0125, 0.0165, 0.1105, 1, 1, 1, 3.9 × 10^7}

In[24]:= FindRoot[χ[r1, r2, r3, ε1, ε2, ε3, f] == 0, {f, 800 10^6, 1000 10^6}, MaxIterations → 30]

Out[24]= {915000000 → 1.03863 × 10^9 - 11752.4 i}

In[25]:= {f → 1.0386278193954107`*^9 + 11752.438414409557` i}
```

```
Out[25]= {915000000 → 1.03863×10^9 - 11752.4 i}

In[26]:= (* The removal of the dielectrics has raised the resonant frequency to 1038.6 GHz from the
            loaded figure of 915 MHz.  The unloaded Q factor is 0.5*Real Part/Imaginary Part of
            the complex frequency: *)

In[27]:= 0.5*1.038610^9/11752.438

Out[27]= 44186.6

In[28]:= (* The above number is the unloaded Q factor.  The palliator efficiency is approximately
            equal to 1-Ql/Qu, which is (in percent): *)

In[29]:= 100(1 - 176.45/44186.6)

Out[29]= 99.6007
```

Appendix A5.1

Analysis of an Example of Rectangular Cavity Mode for Power Density

```
(* TEmnk Mode Energy Density in Rectangular Cavity
   (from Ishii, T.K., "Microwave Engineering, 2nd Edition,",
    Oxford University Press, 1995, pp 123) *)

(* Ex Component *)
E1 Cos[m Pi x/a] Sin[n Pi y/b] Sin[k Pi z/l]
```

$$\text{Out[1]=}\quad E1\,\cos\left[\frac{m\pi x}{a}\right]\sin\left[\frac{n\pi y}{b}\right]\sin\left[\frac{k\pi z}{l}\right]$$

```
In[2]:= (* Ey Component (Ez component is zero because we only have transverse, x-y E field components) *)

In[3]:= E2 Sin[m Pi x/a] Cos[n Pi y/b] Sin[k Pi z/l]
```

$$\text{Out[3]=}\quad E2\,\cos\left[\frac{n\pi y}{b}\right]\sin\left[\frac{m\pi x}{a}\right]\sin\left[\frac{k\pi z}{l}\right]$$

```
In[4]:= %1 /. E1 → (I w mu H3) (n Pi/b)/((m Pi/a)^2 + (n Pi/b)^2)
```

$$\text{Out[4]=}\quad \frac{i\,H3\,mu\,n\,\pi\,w\,\cos\left[\frac{m\pi x}{a}\right]\sin\left[\frac{n\pi y}{b}\right]\sin\left[\frac{k\pi z}{l}\right]}{b\left(\frac{m^2\pi^2}{a^2}+\frac{n^2\pi^2}{b^2}\right)}$$

```
In[5]:= (* Ex Component Complete *)

In[6]:= %3 /. E2 → -I (w mu H3/((m Pi/a)^2 + (n Pi/b)^2)) (m Pi/a)
```

$$\text{Out[6]=}\quad -\frac{i\,H3\,m\,mu\,\pi\,w\,\cos\left[\frac{n\pi y}{b}\right]\sin\left[\frac{m\pi x}{a}\right]\sin\left[\frac{k\pi z}{l}\right]}{a\left(\frac{m^2\pi^2}{a^2}+\frac{n^2\pi^2}{b^2}\right)}$$

```
In[7]:= (* Ey Component Complete *)

In[8]:= (* Total E^2 (proportional to power) *)

In[9]:= (%4^2 + %6^2) * -1
```

$$\text{Out[9]=}\quad \frac{H3^2\,m^2\,mu^2\,\pi^2\,w^2\,\cos\left[\frac{n\pi y}{b}\right]^2\sin\left[\frac{m\pi x}{a}\right]^2\sin\left[\frac{k\pi z}{l}\right]^2}{a^2\left(\frac{m^2\pi^2}{a^2}+\frac{n^2\pi^2}{b^2}\right)^2}+\frac{H3^2\,mu^2\,n^2\,\pi^2\,w^2\,\cos\left[\frac{m\pi x}{a}\right]^2\sin\left[\frac{n\pi y}{b}\right]^2\sin\left[\frac{k\pi z}{l}\right]^2}{b^2\left(\frac{m^2\pi^2}{a^2}+\frac{n^2\pi^2}{b^2}\right)^2}$$

```
In[10]:= Simplify[%]
```

$$\text{Out[10]}= \frac{a^2 b^2 H3^2 mu^2 w^2 \left(b^2 m^2 \text{Cos}\left[\frac{n\pi y}{b}\right]^2 \text{Sin}\left[\frac{m\pi x}{a}\right]^2 + a^2 n^2 \text{Cos}\left[\frac{m\pi x}{a}\right]^2 \text{Sin}\left[\frac{n\pi y}{b}\right]^2\right) \text{Sin}\left[\frac{k\pi z}{l}\right]^2}{\left(b^2 m^2 + a^2 n^2\right)^2 \pi^2}$$

```
In[11]:= (* Substitute values for TE314 mode at 2452.12 MHz,
           which was determined to be one of the operating modes *)

In[12]:= %10 /. {a → 0.35, b → 0.25, l → 0.30, m → 3, n → 1, k → 4, w → 2Pi2452.1210^6, mu → 4Pi10^-7, H3 → 1}

Out[12]= 619724. (0.5625 Cos[12.5664 y]^2 Sin[26.9279 x]^2 + 0.1225 Cos[26.9279 x]^2 Sin[12.5664 y]^2) Sin[41.8879 z]^2

In[13]:= % /. y → 0.11

Out[13]= 619724. (0.118199 Cos[26.9279 x]^2 + 0.0197504 Sin[26.9279 x]^2) Sin[41.8879 z]^2

In[14]:= Plot3D[% / 619724, {x, 0, .35}, {z, 0, .3}]
```

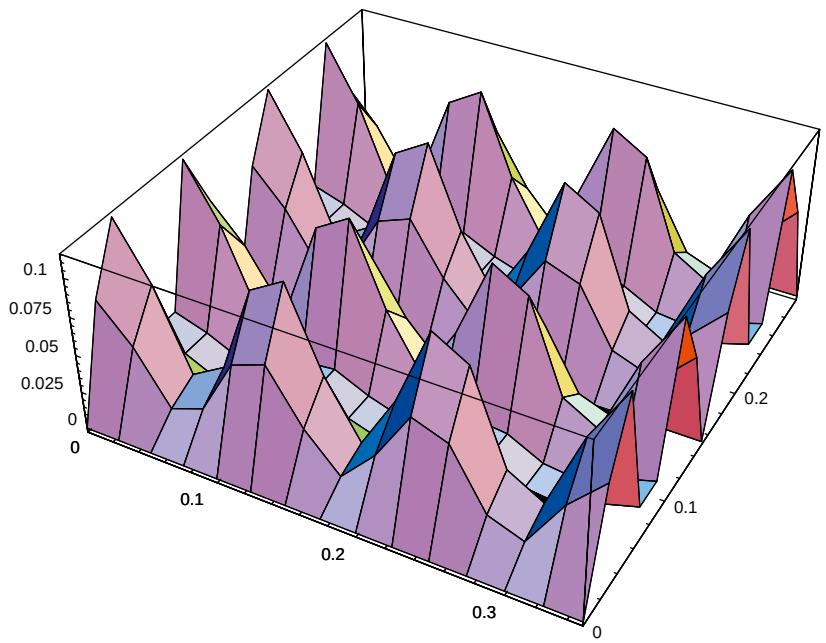


```
Out[14]= -SurfaceGraphics-
```

```
In[15]:= ContourPlot[%13/619724, {x, 0, .35}, {z, 0, .3}]
```

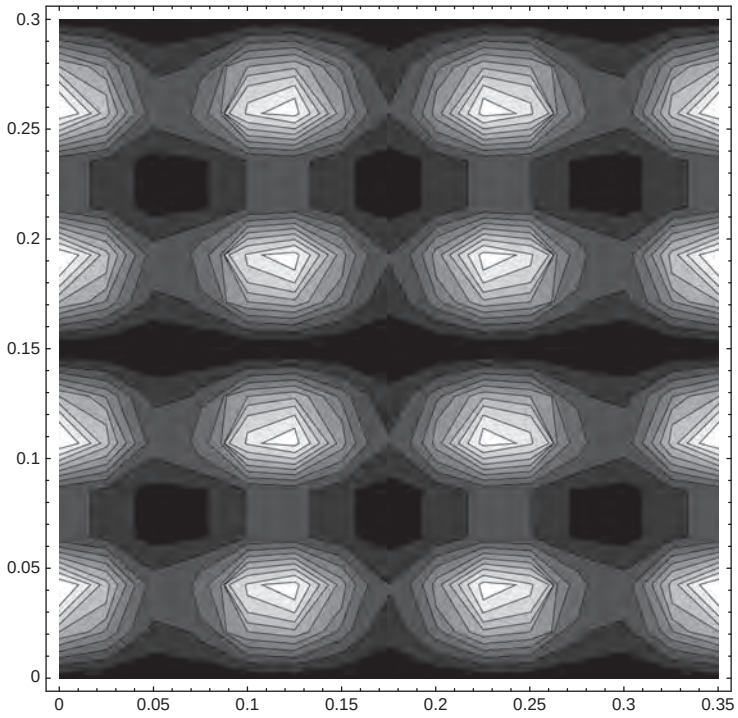


```
Out[15]= -ContourGraphics-
```

Appendix A5.2

Mathematica™ Notebook for Computation of Possible Modes Over a Given Bandwidth for a Rectangular Multimode Cavity

```
In[1]:= (* Mathematica Notebook to Compute the Possible
           Rectangular Cavity Modes over a Given Bandwidth

     The dimensions of the rectangular Cavity with their designations are:
      a (meters), at x direction, mode designation: m
    h (meters) at y direction, mode designation: n
    l (meters) at z direction, mode designation: k

    The frequency equation (in MHz) is: *)

In[2]:= (* The source bandwidth is defined by lower limit frequency is 2425 MHz,
      and the upper limit frequency is 2475 MHz. We will find the
       allowable modes and their resonant frequencies between these two limits *)

In[3]:= {f1 = 2425, f2 = 2475}

Out[3]= {2425, 2475}

In[4]:=
    3 10^8 Sqrt[(m / (2 a))^2 + (n / (2 h))^2 + (k / (2 l))^2] / 10^6

Out[4]= 300 Sqrt[k^2/(4 l^2) + m^2/(4 a^2) + n^2/(4 h^2)]

In[5]:= (* Let us consider a cavity with dimensions a=30 cm, h=25 cm, and l=35 cm. *)

In[6]:= 300 Sqrt[k^2/(4 l^2) + m^2/(4 a^2) + n^2/(4 h^2)] /. {a → 0.30, h → 0.25, l → 0.35}

Out[6]= 300 Sqrt[2.04082 k^2 + 2.77778 m^2 + 4. n^2]
```

```
In[7]:= Do[If[! (m + n == 0 || n + k == 0 || m + k == 0) && % > f1 && % < f2, Print[{m, n, k, %}]],
          {m, 0, 20}, {n, 0, 20}, {k, 0, 20}]

{0, 2, 5, 2455.98}

{0, 4, 1, 2437.97}

{1, 4, 0, 2451.53}

{2, 1, 5, 2439.64}

{2, 3, 3, 2427.56}

{4, 1, 3, 2452.15}

In[8]:= (* The goal of the above statement [1] is to find
            the possible modes within the frequency range of 2425 and 2475,
          which is a typical bandwidth for a magnetron power source. The
            first three numbers are the mode numbers,
          m,n,and k; and the last number is the resonant frequency for
            that mode. The statement will exclude mode
            numbers with two zeros, which are not possible., *)

In[9]:= (* [1] Riegert, R.J., Private Communication *)
```

Appendix A6.1

Mathematica™ Worksheet for Finding the Admittance and Equivalent Circuit Parameters of the Open-ended Coaxial Probe

```
(* The normalized admittance
   of an open ended coaxial probe.
     (From Xu, 1991, Chapter 5 references)
    The function y, once it is integrated over the variable ζ from zero to
   infinity, would be the ratio Y/Y0,
  where Y is the admittance and Y0 is the characteristic admittance of the coaxial
    Line. The function y is:

*)

In[2]:= y[a_, b_, k_, ε_, ζ_, εi_] :=
  (I k ε / ((Sqrt[εi] Log[b / a])))(BesselJ[0, ζ a] - BesselJ[0, ζ b])^2 / ζ / Sqrt[(ζ^2 - k^2 ε)]

In[3]:= (*

    And the Characteristic Impedance of the Coaxial Line is:

*)

In[4]:= Z0[a_, b_, εi_] := 138 Log[10, b / a] / Sqrt[εi]

In[5]:= (*

  Where a and b are the radii of the inner and outer conductors in meters,
  k=2π/λ is the wave number, ε=ε'-j ε'' is
          the complex permittivity, ζ is the integral
          variable, and εi is the dielectric constant of the coaxial line's
    dielectric filling between the center and outer conductors.
          *)
```

```
In[6]:= (* For Example: a=1 mm, b=4 mm,
          at 1 GHz (λ=0.3 m) in a media with permittivity of 3–j0.2 If we Integrate the variable ζ over zero to infinity,
          which is chosen to be 4000 here we get: *)

In[7]:= y = NIntegrate[y[1 10^-3, 4 10^-3, 2 Pi / 0.3, 3 - I 0.2, ζ, 2.1], {ζ, 0, 3000}]

Out[7]= 0.00364352 + 0.0542729 i

In[8]:= (*
          The Values of the Equivalent Capacitance (Ceq) in Farads,
          and the Equivalent Resistance (Req) in Ohms are found to be:
        *)

In[9]:= {Ceq = Im[y] / (Z0[a, b, εi] * 2 Pi f), Req = Z0[a, b, εi] / Re[y]} /. {a → 0.001, b → 0.004, εi → 2.1, f → 10^9}

Out[9]= {1.50659×10^-13, 15735.8}
```

Appendix A6.2

Mathematica™ Notebook for Impedance of the Extended Center Conductor Coaxial Line

```
In[1]:= (* Mathematica Code for Input Impedance
          of an extended coaxial monopole probe

  Geometrical parameters:  inner conductor radius a, outer conductor radius b, h is the
length of the extended center conductor (all in meters), εp and εpp are real
and imaginary components of the relative permittivity, and f is frequency in Hz.
    Functions Rheat, Rrad, and XD are resistance due to near field energy absorption,
resistance due to radiation, and reactive impedance, respectively (all in Ohms) *)
```

```
In[2]:= Rheat[a_, b_, h_, εp_, εpp_, f_] := Block[{x, k, α, β, Ka, Leq, A, B},
                                              x = εpp / εp;
                                              k = 2 π f / (3 × 10^8);
                                              α = k Sqrt[(Sqrt[1 + x^2] - 1) εp / 2];
                                              β = k Sqrt[(Sqrt[1 + x^2] + 1) εp / 2];
                                              Ka = 60 (Log[h / a] - 1);
                                              Leq = β h (1 + .19 / (Log[h / a] - .81));
                                              A = Tan[h (α / β) Leq];
                                              B = Tan[Leq];
                                    N[(k / β) (Ka / (1 + (α / β)^2)) ((A (1 + B^2) + (α / β) B (1 - A^2)) / (A^2 + B^2))]]
```

```
In[3]:= Rrad[a_, b_, h_, εp_, εpp_, f_] := Block[{x, k, α, β, Leq},
                                            x = εpp / εp;
                                            k = 2 π f / (3 × 10^8);
                                            α = k Sqrt[(Sqrt[1 + x^2] - 1) εp / 2];
                                            β = k Sqrt[(Sqrt[1 + x^2] + 1) εp / 2];
                                            Leq = β h (1 + .19 / (Log[h / a] - .81));
                                  N[10 * (k / β) * Leq^2 (1 + .133 (1 - (α / β)^2) Leq^2 +
                                      0.02 (1 - 6 (α / β)^2 + (α / β)^4) Leq^4)]]
```

```
In[4]:= XD[a_, b_, h_, εp_, εpp_, f_] := Block[{x, k, α, β, Ka, Leq, A, B},
                                          x = εpp / εp;
                                          k = 2 π f / (3 × 10^8);
                                          α = k Sqrt[(Sqrt[1 + x^2] - 1) εp / 2];
                                          β = k Sqrt[(Sqrt[1 + x^2] + 1) εp / 2];
                                          Ka = 60 (Log[h / a] - 1);
                                          Leq = β h (1 + .19 / (Log[h / a] - .81));
                                          A = Tan[h (α / β) Leq];
                                          B = Tan[Leq];
                                          N[(k / β) (Ka / (1 + (α / β)^2)) (1 / (A^2 + B^2)) ((α / β) A (1 + B^2) - B (1 - A^2))]]

In[5]:= RD[a_, b_, h_, εp_, εpp_, f_] := Rheat[a, b, h, εp, εpp, f] + Rrad[a, b, h, εp, εpp, f]

In[6]:= (* Example#1: If a=1 mm, b=5 mm, h=8 mm, εp=6.1 ,εpp=0.08 ,f=2.45 GHz, what are the equivalent circuit
           components of the monopole? *)

In[7]:= {Rheat[1 × 10^-3, 5 × 10^-3, 8 × 10^-3, 6.1, .08, 2450 × 10^6],
         Rrad[1 × 10^-3, 5 × 10^-3, 8 × 10^-3, 6.1, .08, 2450 × 10^6]
         , XD[1 × 10^-3, 5 × 10^-3, 8 × 10^-3, 6.1, .08, 2450 × 10^6]}

Out[7]= {0.0756401, 6.69824, -11.2461}

In[8]:= (* Above are the resistances Rheat, Rrad, and reactive impedance XD (all in Ohms) *)

In[9]:= (* Example#2: If a=1 mm, b=5 mm, εp=6.1 ,εpp=0.08 ,f=2.45 GHz, draw a plot of RD (sum of Rheat and
           Rrad) versus h. *)

        $DefaultFont = {"Arial", 16}

In[10]:= {"Arial", 20}

Out[10]= {Arial, 20}

In[11]:= Plot[RD[1 × 10^-3, 5 × 10^-3, h, 6.1, .08, 2450 × 10^6], {h, 3 × 10^-3, 15 × 10^-3},
          Frame → True, GridLines → Automatic, PlotStyle → Thickness[.005]]
```

Out[11]=

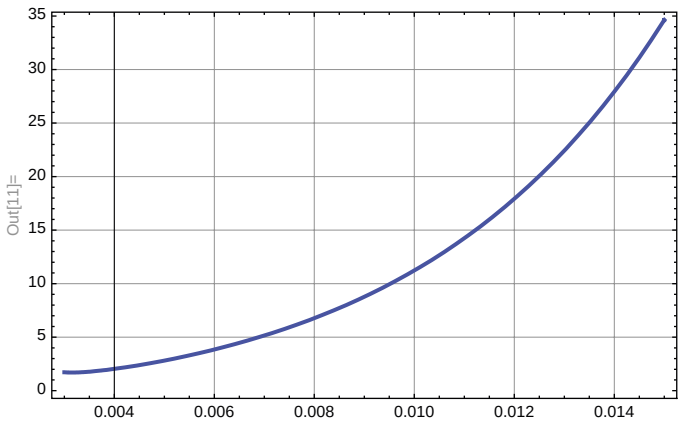

Appendix A6.3

Admittance of Open-ended Waveguide with Dielectric Material Loading

```
In[1]:= (* Calculation of input addmittance for an
           open ended waveguide in TE10 mode held
           against a real dielectric load

        Parameter definitions: The material has complex dielectric constant of εr at wavelength
          λ0. The long wall of the waveguide is a (in y direction) and short wall is b (in x
            direction. All units are SI. Variables k1, k0, K1,K2, Ge, and Kr are dependent
            on primary varaiables of function f[a,b,εr,λ0,x,y] *)

In[2]:= f[a_, b_, εr_, λ0_, x_, y_] := Block[{k1, k0, K1, K2, Ge, kr},
                                        k0 = 2 Pi / λ0;
                                        k1 = Sqrt[k0^2 - (Pi / a)^2];
                                        K1 = k0^2 εr + (Pi / a)^2;
                                        K2 = k0^2 εr - (Pi / a)^2;
                                        kr = k0 εr^0.5;
                                        r = Sqrt[x^2 + y^2];
                                        Ge = Exp[-I kr r] / r;
                  ((2 I) / (Pi a b k1)) (b - x) (K2 (a - y) Cos[Pi y / a] + (a / Pi) K1 Sin[Pi y / a]) Ge]

In[3]:= (* Below, the function Yoe (Y open ended) would calculate the normalized admittance. *)

In[4]:= Yoe[a_, b_, εr_, λ0_] := Integrate[f[a, b, εr, λ0, x, y], {x, .001 b, b}, {y, 0.001 a, a}]

In[5]:= (* For example, using an X-band WR-90 Waveguide with cross-sectional dimentions of
             22.86 mm X 10.1 mm at the frequency of 10 GHz (λ0=30 mm) radiating into a dielectric
             with complex dielectric constant εr=4.5-j0.5, the normalized complex admittance becomes: *)

In[6]:= N[Yoe[0.02286, 0.0101, 4.5 - 0.5 I, 0.035]]

Out[6]= 3.24346 + 0.338242 i

In[7]:= N[Yoe[.086, 0.043, 77 - I 12, .12]]

Out[7]= 11.288 - 2.18679 i
```

```
In[8]:= (* Below is the Normalized Admittance of the Open-Ended Waveguide. *)

In[9]:= N[Yoe[.086, 0.043, 3 - I 0.01, .12]]

Out[9]= 2.37127 + 0.399866 I

In[10]:= (* To find the actual Admittance, we use Characteristic Admittance of a TE10 Waveguide *)

In[11]:= N[(1 / 377) (a / b) Sqrt[1 - (0.5 λ / a)] * N[Yoe[.086, 0.043, 3 - I 0.01, .12]]] /. {a → .086, λ → 0.12, b → .043}

Out[11]= 0.00691684 + 0.00116638 I
```

Appendix A7.1

Field Analysis of Circular Loop Applicator

```
In[1]:= (*
        The magnetic field components
         Hr and Hz from a circular loop

          Parameters: The loop carries a current of 1 Amperes,
        with the diameter of R at an arbitrary point A with coordinates x,
        y,z when the origin is the center of the circle.  Here,
        r is the distance between the origin and point A. The geometry is shown in Fig. 7.6 *)

In[2]:= Hr[r_, z_, R_] := Block[{k},
          k = Sqrt[4 R r/((R + r)^2 + z^2)];
          (1/(2 π r)) (z/((R + r)^2 + z^2)^0.5) ((R^2 + r^2 + z^2) EllipticE[k]/((R - r)^2 + z^2) - EllipticK[k])]

In[3]:= Hz[r_, z_, R_] := Block[{k},
          k = Sqrt[4 R r/((R + r)^2 + z^2)];
          (1/(2 π)) (1/((R + r)^2 + z^2)^0.5) ((R^2 - r^2 - z^2) EllipticE[k]/((R - r)^2 + z^2) + EllipticK[k])]

In[4]:= (* For example, for R=1 m, at a plane 0.2 m above the circle,
          the magnetic field amplitude can be 3D plotted as: *)

In[5]:= Plot3D[Sqrt[Hz[Sqrt[x^2 + y^2 + .2^2], .2, 1]^2 + Hz[Sqrt[x^2 + y^2 + .2^2], .2, 1]^2],
          {x, -1.2, 1.2}, {y, -1.2, 1.2}]
```

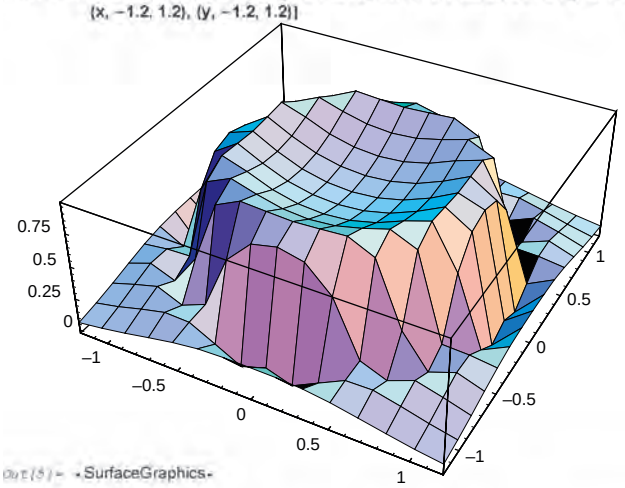


```
Out[5]= -SurfaceGraphics-

In[6]:=
        (* In the same condition as above, if the observation plane is raised to 0.5 meter,
          the 3D Plot of the magnetic field amplitude: *)
```

```
In[7]:= Plot3D[Sqrt[Hz[Sqrt[x^2 + y^2 + .5^2], .5, 1]^2 + Hz[Sqrt[x^2 + y^2 + .5^2], .5, 1]^2],
  {x, −1.2, 1.2}, {y, −1.2, 1.2}]
```

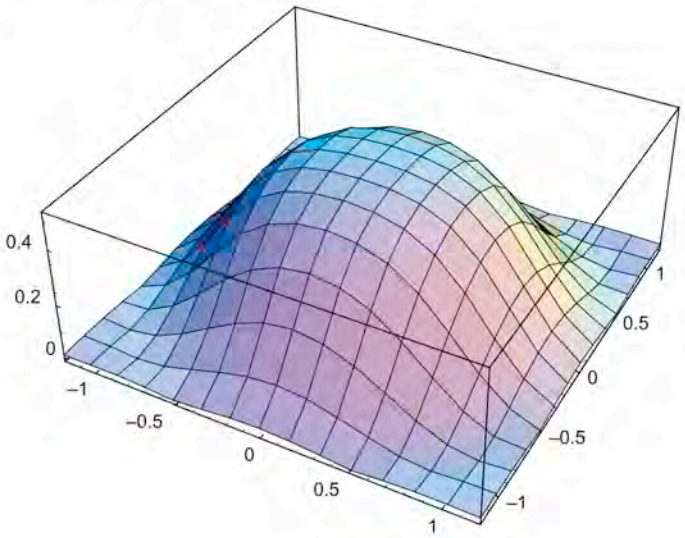


```
Out[7]= -SurfaceGraphics-

In[8]:= (* In the above two plot the field intensities between the elevations
    of 20% and 50% of the diameter are compared. At the lower elevation the
    local extra intensity at the vicinity of the loop itself is demonstrated. *)

In[9]:= (* Another way of showing the field intensity at 50% elevation is contour plot as shown below: *)
```

```
In[10]:= ContourPlot[Sqrt[Hz[Sqrt[x^2 + y^2 + 0.5^2], 1, 1]^2 + Hz[Sqrt[x^2 + y^2 + 0.5^2], 0.5, 1]^2],
          {x, −1.2, 1.2}, {y, −1.2, 1.2}]
```

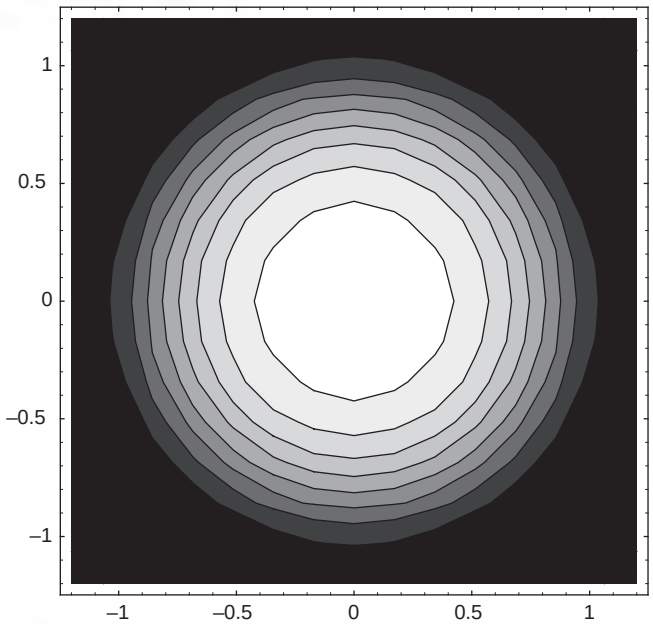


```
Out[10]= -ContourGraphics-
```

```
In[11]:= (* A side view (y–z) plot of the field components Hr
            and Hz at the elevation of 20% of radius can be drawn as follows: *)
```

```
In[12]:= Plot[{Hr[Sqrt[0^2 + y^2 + .2^2], 0.2, 1], Hz[Sqrt[0^2 + y^2 + 0.2^2], .2, 1]}, {y, −1.2, 1.2}]
```

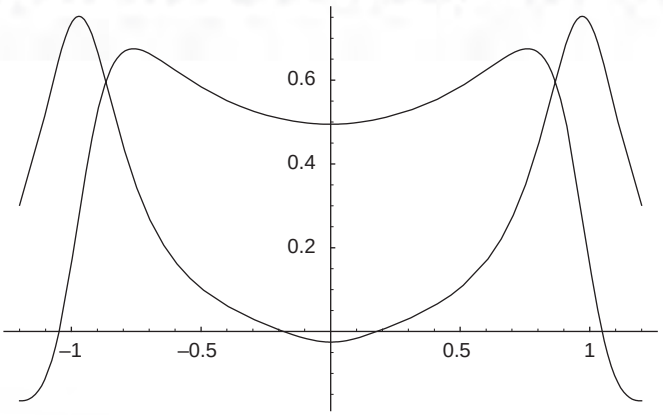


```
Out[12]= -Graphics-
```

Appendix A7.2

Mathematica™ Program for Eddy Current Induction into a Conductive Cylinder

```
(* Eddy–current Heating of a Solid Core in a Long Cylindrical Solenoid

   Code written by  Ronald J. Riegert *)

In[2]:= (* Definitions:,
   ℒ = length of solenoid and core,
   ℐ = peak current flowing in solenoid windings,
   η = solenoid number–of–turns per unit length,
   ω = 2π f = angular frequency of current in windings,
   μ0 = 4π 10^–7 H/m = magnetic permeability of vacuum,
   r0 = radius (diameter/2) of solenoid core,
   rc = radius (diameter/2) of solenoid coil,
   μ = magnetic permeability of core material,
   σ = conductivity of core material,
   δ = Sqrt[2/(ω μ σ)] = skin depth in core material,
   ρ = radial cooordinate,
   H[ρ] = magnetic field pointing in the z– (axial) direction,
   H0 = η ℐ = magnetic field between solenoid core and windings (r0 ≤ ρ ≤ rc),
   Efield[ρ] = H'[ρ]/σ = electric field pointing in the ϕ–direction,
   Rw = resistance of core windings (resisitance of empty/unloaded solenoid coil),
   W0 = peak magnetic energy stored in the empty (unloaded) coil,
   L0 = W0/ℐ^2 = inductance of the empty (unloaded) coil,
   Pcore = peak power dissipated in the core due to flow of induced eddy–currents,
   Wcore = peak magnetic energy stored in the core,
   Rload = Pcore/ℐ^2 = effective resistance seen by current ℐ due to eddy–currents in core,
   Lload = Wcore/ℐ^2 = inductance contributed by core, as seen by current ℐ,
   Wtot = total peak magnetic energy stored in the loaded coil,
   Rtot = Rload + Rw = total resistance of the loaded coil,
   Ltot = Wtot/ℐ^2 = total inductance of the loaded coil,
   Q = ω L/R = quality factor of an inductor with inductance L and resistance R,
   *)
```

```
In[3]:= (* Maxwell wave-equation for H[ρ] inside core(neglecting displacement current dD/dt): *)

In[4]:= D[H[ρ], {ρ, 2}] + D[H[ρ], ρ] / ρ + 2 I H[ρ] / δ^2 == 0
```

$$\text{Out[4]=}\quad \frac{2\,i\,H[\rho]}{\delta^2} + \frac{H'[\rho]}{\rho} + H''[\rho] == 0$$

```
In[5]:= FullSimplify[DSolve[%, H[ρ], ρ]][[1, 1]]
```

$$\text{Out[5]=}\quad H[\rho] \to \text{BesselJ}\left[0, \frac{(1+i)\,\rho}{\delta}\right] C[1] + \text{BesselY}\left[0, \frac{(1+i)\,\rho}{\delta}\right] C[2]$$

```
(* Check finiteness of magnetic field as ρ → 0: *)

In[6]:= Limit[H[ρ] /. %5, ρ → 0]

Out[6]= DirectedInfinity[-Sign[C[2]]]

(* Magnetic field must be finite at ρ = 0, so set integration constant C[2] = 0: *)

In[7]:= %% /. C[2] → 0
```

$$\text{Out[7]=}\quad H[\rho] \to \text{BesselJ}\left[0, \frac{(1+i)\,\rho}{\delta}\right] C[1]$$

```
(* Impose boundary condition that the magnetic field is continuous at the core surface: H[r0] = H0: *)

In[8]:= ((H[ρ] /. %) /. ρ → r0) == H0
```

$$\text{Out[8]=}\quad \text{BesselJ}\left[0, \frac{(1+i)\,r0}{\delta}\right] C[1] == H0$$

```
In[9]:= Solve[%, C[1]][[1, 1]]
```

$$\text{Out[9]=}\quad C[1] \to \frac{H0}{\text{BesselJ}\left[0, \frac{(1+i)\,r0}{\delta}\right]}$$

```
In[10]:= %%% /. %
```

$$\text{Out[10]=}\quad H[\rho] \to \frac{H0\,\text{BesselJ}\left[0, \frac{(1+i)\,\rho}{\delta}\right]}{\text{BesselJ}\left[0, \frac{(1+i)\,r0}{\delta}\right]}$$

```
(* Differentiate the magnetic field with respect to ρ: *)
```

```
In[11]:= D[%, ρ]
```

$$\text{Out[11]= } H'[\rho] \to -\frac{(1+i)\,H0\,\text{BesselJ}\left[1, \frac{(1+i)\rho}{\delta}\right]}{\delta\,\text{BesselJ}\left[0, \frac{(1+i)r0}{\delta}\right]}$$

```
(* Express the electric field in terms of the derivative of the magnetic field: *)

In[12]:= Efield[ρ] -> D[H[ρ], ρ] / σ
```

$$\text{Out[12]= } \text{Efield}[\rho] \to \frac{H'[\rho]}{\sigma}$$

```
In[13]:= % /. %%
```

$$\text{Out[13]= } \text{Efield}[\rho] \to -\frac{(1+i)\,H0\,\text{BesselJ}\left[1, \frac{(1+i)\rho}{\delta}\right]}{\delta\sigma\,\text{BesselJ}\left[0, \frac{(1+i)r0}{\delta}\right]}$$

```
In[14]:= %[[2]]
```

$$\text{Out[14]= } -\frac{(1+i)\,H0\,\text{BesselJ}\left[1, \frac{(1+i)\rho}{\delta}\right]}{\delta\sigma\,\text{BesselJ}\left[0, \frac{(1+i)r0}{\delta}\right]}$$

```
(* Form the complex-conjugate Efield*[ρ] of the electric field: *)

In[15]:= % /. Complex[a_, b_] :> Complex[a, -b]
```

$$\text{Out[15]= } -\frac{(1-i)\,H0\,\text{BesselJ}\left[1, \frac{(1-i)\rho}{\delta}\right]}{\delta\sigma\,\text{BesselJ}\left[0, \frac{(1-i)r0}{\delta}\right]}$$

```
(* Form the product Abs[Efield[ρ]]^2: *)

In[16]:= %% %
```

$$\text{Out[15]= } \frac{2\,H0^2\,\text{BesselJ}\left[1, \frac{(1-i)\rho}{\delta}\right]\text{BesselJ}\left[1, \frac{(1+i)\rho}{\delta}\right]}{\delta^2\sigma^2\,\text{BesselJ}\left[0, \frac{(1-i)r0}{\delta}\right]\text{BesselJ}\left[0, \frac{(1+i)r0}{\delta}\right]}$$

```
(* Peak power dissipated in core is Abs[J.E] = σ Abs[Efield[ρ]]^2 integrated over the volume of the core,
(differential volume element is 2π ℒ ρ dρ): *)

In[17]:= Pcore → 2 π ℒ Integrate[σ % ρ, {ρ, 0, r0}]
```

$$\text{Out[17]= } \text{Pcore} \to \frac{(1+i)\,H0^2\,\pi\,r0\,\mathcal{L}\left(\frac{i\,\text{BesselJ}\left[1, \frac{(1-i)r0}{\delta}\right]}{\text{BesselJ}\left[0, \frac{(1-i)r0}{\delta}\right]} - \frac{\text{BesselJ}\left[1, \frac{(1+i)r0}{\delta}\right]}{\text{BesselJ}\left[0, \frac{(1+i)r0}{\delta}\right]}\right)}{\delta\sigma}$$

```
(* (Note that, despite the explicit appearance of i = Sqrt[-1] in Pcore above, this expression is real!) *)

(* Verify result for Pcore using Poynting vector S[ρ] =
   E[ρ] x H*[ρ] integrated over surface of core.  First find E[r0]: *)
```

In[18]:=
$$\left(\text{Efield}[\rho] \to -\frac{(1+i)\,\text{H0}\,\text{BesselJ}\left[1,\frac{(1+i)\rho}{\delta}\right]}{\delta\,\sigma\,\text{BesselJ}\left[0,\frac{(1+i)\,\text{r0}}{\delta}\right]}\right) /.\ \rho \to \text{r0}$$

Out[18]=
$$\text{Efield}[\text{r0}] \to -\frac{(1+i)\,\text{H0}\,\text{BesselJ}\left[1,\frac{(1+i)\,\text{r0}}{\delta}\right]}{\delta\,\sigma\,\text{BesselJ}\left[0,\frac{(1+i)\,\text{r0}}{\delta}\right]}$$

```
(* On the core surface, S[r0] = E[r0] x H*[r0] = E[r0] H0: *)
```

In[19]:=
```
S[r0] → Efield[r0] H0 /. %
```

Out[19]=
$$\text{S[r0]} \to -\frac{(1+i)\,\text{H0}^2\,\text{BesselJ}\left[1,\frac{(1+i)\,\text{r0}}{\delta}\right]}{\delta\,\sigma\,\text{BesselJ}\left[0,\frac{(1+i)\,\text{r0}}{\delta}\right]}$$

```
(* Since the Poynting vector S[r0] is independent of ϕ and z,
the integral of S over the core surface is just the
 product of S[r0] and the core cylindrical surface area 2 π r0 ℒ: *)
```

In[20]:=
```
S[r0] 2 π r0 ℒ /. %
```

Out[20]=
$$-\frac{(2+2i)\,\text{H0}^2\,\pi\,\text{r0}\,\mathcal{L}\,\text{BesselJ}\left[1,\frac{(1+i)\,\text{r0}}{\delta}\right]}{\delta\,\sigma\,\text{BesselJ}\left[0,\frac{(1+i)\,\text{r0}}{\delta}\right]}$$

```
(* Peak power dissipated in core should be the real part of this expression: *)
```

In[21]:=
```
PcoreS -> Simplify[(% + (% /. Complex[a_, b_] :> Complex[a, -b]))/2]
```

Out[21]=
$$\text{PcoreS} \to \frac{(1+i)\,\text{H0}^2\,\pi\,\text{r0}\,\mathcal{L}\left(\frac{i\,\text{BesselJ}\left[1,\frac{(1-i)\,\text{r0}}{\delta}\right]}{\text{BesselJ}\left[0,\frac{(1-i)\,\text{r0}}{\delta}\right]}-\frac{\text{BesselJ}\left[1,\frac{(1+i)\,\text{r0}}{\delta}\right]}{\text{BesselJ}\left[0,\frac{(1+i)\,\text{r0}}{\delta}\right]}\right)}{\delta\,\sigma}$$

```
(* By Poynting's Theorem, PcoreS should be the same as the previously calculated Pcore: *)
```

In[22]:=
$$\text{Pcore} \to \frac{(1+i)\,\text{H0}^2\,\pi\,\text{r0}\,\mathcal{L}\left(\frac{i\,\text{BesselJ}\left[1,\frac{(1-i)\,\text{r0}}{\delta}\right]}{\text{BesselJ}\left[0,\frac{(1-i)\,\text{r0}}{\delta}\right]}-\frac{\text{BesselJ}\left[1,\frac{(1+i)\,\text{r0}}{\delta}\right]}{\text{BesselJ}\left[0,\frac{(1+i)\,\text{r0}}{\delta}\right]}\right)}{\delta\,\sigma}$$

Out[22]=
$$\text{Pcore} \to \frac{(1+i)\,\text{H0}^2\,\pi\,\text{r0}\,\mathcal{L}\left(\frac{i\,\text{BesselJ}\left[1,\frac{(1-i)\,\text{r0}}{\delta}\right]}{\text{BesselJ}\left[0,\frac{(1-i)\,\text{r0}}{\delta}\right]}-\frac{\text{BesselJ}\left[1,\frac{(1+i)\,\text{r0}}{\delta}\right]}{\text{BesselJ}\left[0,\frac{(1+i)\,\text{r0}}{\delta}\right]}\right)}{\delta\,\sigma}$$

```
(* Check: *)
```

In[23]:= **(PcoreS /. %%) == (Pcore /. %)**

Out[23]= True

In[24]:= **%% /. H0 → η I**

$$\text{Out[24]= Pcore} \to \frac{(1+i)\,\pi\,r0\,I^2\,\mathcal{L}\,\eta^2\left(\frac{i\,\text{BesselJ}\left[1,\frac{(1-i)\,r0}{\delta}\right]}{\text{BesselJ}\left[0,\frac{(1-i)\,r0}{\delta}\right]}-\frac{\text{BesselJ}\left[1,\frac{(1+i)\,r0}{\delta}\right]}{\text{BesselJ}\left[0,\frac{(1+i)\,r0}{\delta}\right]}\right)}{\delta\,\sigma}$$

In[25]:= **Rload → (Pcore /. %) / I^2**

$$\text{Out[25]= Rload} \to \frac{(1+i)\,\pi\,r0\,\mathcal{L}\,\eta^2\left(\frac{i\,\text{BesselJ}\left[1,\frac{(1-i)\,r0}{\delta}\right]}{\text{BesselJ}\left[0,\frac{(1-i)\,r0}{\delta}\right]}-\frac{\text{BesselJ}\left[1,\frac{(1+i)\,r0}{\delta}\right]}{\text{BesselJ}\left[0,\frac{(1+i)\,r0}{\delta}\right]}\right)}{\delta\,\sigma}$$

(* Introduce convenient dimensionless parameter x = r0/δ: *)

In[26]:= **% /. r0 → x δ**

$$\text{Out[26]= Rload} \to \frac{(1+i)\,\pi\,x\,\mathcal{L}\,\eta^2\left(\frac{i\,\text{BesselJ}\left[1,(1-i)\,x\right]}{\text{BesselJ}\left[0,(1-i)\,x\right]}-\frac{\text{BesselJ}\left[1,(1+i)\,x\right]}{\text{BesselJ}\left[0,(1+i)\,x\right]}\right)}{\sigma}$$

(* Introduce convenient dimensionless factor F[x] defined by: *)

In[27]:= $$\mathcal{F}[x] \to \frac{(1+i)\left(\frac{i\,\text{BesselJ}[1,(1-i)\,x]}{\text{BesselJ}[0,(1-i)\,x]}-\frac{\text{BesselJ}[1,(1+i)\,x]}{\text{BesselJ}[0,(1+i)\,x]}\right)}{2}$$

Out[27]= $$\mathcal{F}[x] \to \left(\frac{1}{2}+\frac{i}{2}\right)\left(\frac{i\,\text{BesselJ}[1,(1-i)\,x]}{\text{BesselJ}[0,(1-i)\,x]}-\frac{\text{BesselJ}[1,(1+i)\,x]}{\text{BesselJ}[0,(1+i)\,x]}\right)$$

(* Simplify Rload by substituting F[r0/δ]: *)

In[28]:= $$\left\{\left(\%\% /. (1+i)\left(\frac{i\,\text{BesselJ}[1,(1-i)\,x]}{\text{BesselJ}[0,(1-i)\,x]}-\frac{\text{BesselJ}[1,(1+i)\,x]}{\text{BesselJ}[0,(1+i)\,x]}\right)\to 2\,\mathcal{F}[x]\right),\ \%\right\} /. x \to r0/\delta$$

Out[28]= $$\left\{\text{Rload} \to \frac{2\,\pi\,r0\,\mathcal{L}\,\eta^2\,\mathcal{F}\left[\frac{r0}{\delta}\right]}{\delta\,\sigma},\ \mathcal{F}\left[\frac{r0}{\delta}\right]\to\left(\frac{1}{2}+\frac{i}{2}\right)\left(\frac{i\,\text{BesselJ}\left[1,\frac{(1-i)\,r0}{\delta}\right]}{\text{BesselJ}\left[0,\frac{(1-i)\,r0}{\delta}\right]}-\frac{\text{BesselJ}\left[1,\frac{(1+i)\,r0}{\delta}\right]}{\text{BesselJ}\left[0,\frac{(1+i)\,r0}{\delta}\right]}\right)\right\}$$

(* Examine behavior of F[x]: *)

In[29]:= **F[x] /. %%**

Out[29]= $$\left(\frac{1}{2}+\frac{i}{2}\right)\left(\frac{i\,\text{BesselJ}[1,(1-i)\,x]}{\text{BesselJ}[0,(1-i)\,x]}-\frac{\text{BesselJ}[1,(1+i)\,x]}{\text{BesselJ}[0,(1+i)\,x]}\right)$$

In[30]:= **F[∞] → Limit[%, x → Infinity]**

Out[30]= $\mathcal{F}[\infty] \to 1$

```
In[31]:= ℱ[0] -> Limit[%%, x → 0]
Out[31]= ℱ[0] → 0
In[32]:= Plot[{1, %%%}, {x, .001, 10}, AxesLabel → {r0/δ, ℱ[r0/δ]}, PlotStyle → {{Dashing[{.025, .015}]}, {Dashing[{}]}}]
```

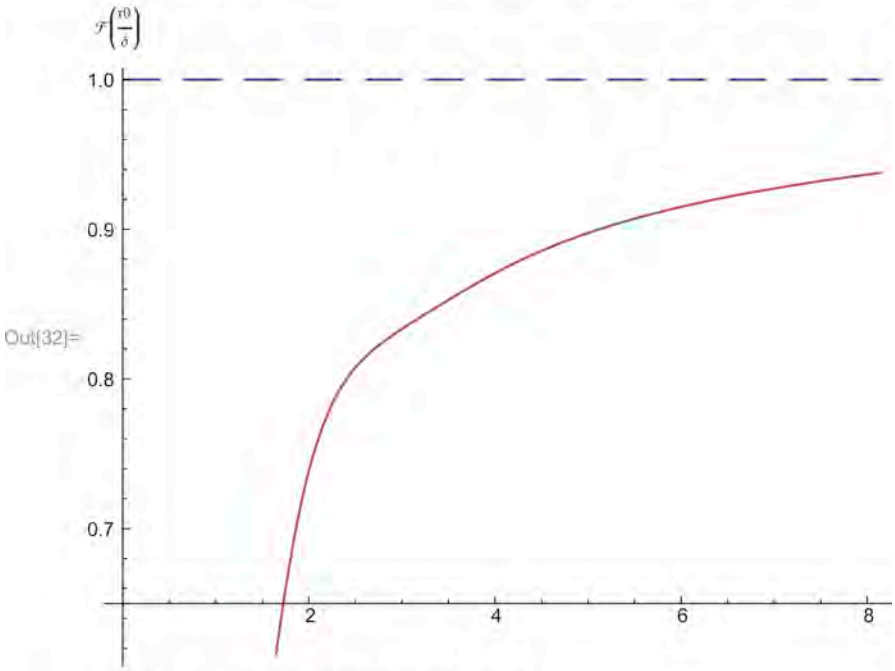

Out[32]=

```
(* Determine limiting form of Rload for δ >> r0: *)
In[33]:= Rload → (1 + i) π r0 ℒ η² (i BesselJ[1, (1-i)r0/δ] / BesselJ[0, (1-i)r0/δ] - BesselJ[1, (1+i)r0/δ] / BesselJ[0, (1+i)r0/δ]) / (δ σ)
Out[33]= Rload → (1 + i) π r0 ℒ η² (i BesselJ[1, (1-i)r0/δ] / BesselJ[0, (1-i)r0/δ] - BesselJ[1, (1+i)r0/δ] / BesselJ[0, (1+i)r0/δ]) / (δ σ)
In[34]:= Rload[δ / r0 -> ∞] → Normal[Series[%[[2]], {r0, 0, 4}]]
Out[34]= Rload[δ/r0 → ∞] → π r0⁴ ℒ η² / (2 δ⁴ σ)
(* Determine limiting form of Rload for δ << r0 (x >> 1): *)
In[35]:= Rload[δ / r0 -> 0] → 2 π r0 ℒ η² ℱ[r0/δ] / (δ σ) /. ℱ[r0/δ] → 1
Out[35]= Rload[δ/r0 → 0] → 2 π r0 ℒ η² / (δ σ)
(* Recall magnetic field in core: *)
```

```
In[36]:= H[ρ] → H0 BesselJ[0, (1+ί) ρ/δ] / BesselJ[0, (1+ί) r0/δ]

Out[36]= H[ρ] → H0 BesselJ[0, (1+ί) ρ/δ] / BesselJ[0, (1+ί) r0/δ]

In[37]:= %[[2]]

Out[37]= H0 BesselJ[0, (1+ί) ρ/δ] / BesselJ[0, (1+ί) r0/δ]

In[38]:= H0 BesselJ[0, (1+ί) ρ/δ] / BesselJ[0, (1+ί) r0/δ]

Out[38]= H0 BesselJ[0, (1+ί) ρ/δ] / BesselJ[0, (1+ί) r0/δ]

(* Form the complex-conjugate H*[ρ] of the magnetic field: *)

In[39]:= % /. Complex[a_, b_] :> Complex[a, -b]

Out[39]= H0 BesselJ[0, (1-ί) ρ/δ] / BesselJ[0, (1-ί) r0/δ]

(* Form the product Abs[H[ρ]]^2: *)

In[40]:= % %%

Out[40]= H0^2 BesselJ[0, (1-ί) ρ/δ] BesselJ[0, (1+ί) ρ/δ] / (BesselJ[0, (1-ί) r0/δ] BesselJ[0, (1+ί) r0/δ])

In[41]:= H0^2 BesselJ[0, (1-ί) ρ/δ] BesselJ[0, (1+ί) ρ/δ] / (BesselJ[0, (1-ί) r0/δ] BesselJ[0, (1+ί) r0/δ])

Out[41]= H0^2 BesselJ[0, (1-ί) ρ/δ] BesselJ[0, (1+ί) ρ/δ] / (BesselJ[0, (1-ί) r0/δ] BesselJ[0, (1+ί) r0/δ])

(* Peak magnetic energy stored in core is μ Abs[H[ρ]]^2 integrated over the volume of the core,
(differential volume element is 2π ℒ ρ dρ): *)

In[42]:= Wcore → 2 π ℒ Integrate[μ % ρ, {ρ, 0, r0}]

Out[42]= Wcore → (1/2 + ί/2) H0^2 π r0 ℒ δ μ (BesselJ[1, (1-ί) r0/δ] / BesselJ[0, (1-ί) r0/δ] - ί BesselJ[1, (1+ί) r0/δ] / BesselJ[0, (1+ί) r0/δ])
```

In[43]:= % /. H0 → η I

Out[43]= Wcore → $\left(\frac{1}{2}+\frac{i}{2}\right)\pi r0\, I^2 \mathcal{L}\delta\eta^2\mu\left(\frac{\text{BesselJ}\left[1,\frac{(1-i)r0}{\delta}\right]}{\text{BesselJ}\left[0,\frac{(1-i)r0}{\delta}\right]}-\frac{i\,\text{BesselJ}\left[1,\frac{(1+i)r0}{\delta}\right]}{\text{BesselJ}\left[0,\frac{(1+i)r0}{\delta}\right]}\right)$

In[44]:= Lload → (Wcore /. %) / I^2

Out[44]= Lload → $\left(\frac{1}{2}+\frac{i}{2}\right)\pi r0\,\mathcal{L}\delta\eta^2\mu\left(\frac{\text{BesselJ}\left[1,\frac{(1-i)r0}{\delta}\right]}{\text{BesselJ}\left[0,\frac{(1-i)r0}{\delta}\right]}-\frac{i\,\text{BesselJ}\left[1,\frac{(1+i)r0}{\delta}\right]}{\text{BesselJ}\left[0,\frac{(1+i)r0}{\delta}\right]}\right)$

(* Again introduce the dimensionless parameter x = r0/δ: *)

In[45]:= % /. r0 → x δ

Out[45]= Lload → $\left(\frac{1}{2}+\frac{i}{2}\right)\pi x\,\mathcal{L}\delta^2\eta^2\mu\left(\frac{\text{BesselJ}[1,(1-i)x]}{\text{BesselJ}[0,(1-i)x]}-\frac{i\,\text{BesselJ}[1,(1+i)x]}{\text{BesselJ}[0,(1+i)x]}\right)$

(* Introduce a second convenient dimensionless factor G[x] defined by: *)

In[46]:= G[x] -> $\left(\frac{1}{2}+\frac{i}{2}\right)\left(\frac{\text{BesselJ}[1,(1-i)x]}{\text{BesselJ}[0,(1-i)x]}-\frac{i\,\text{BesselJ}[1,(1+i)x]}{\text{BesselJ}[0,(1+i)x]}\right)$

Out[46]= G[x] → $\left(\frac{1}{2}+\frac{i}{2}\right)\left(\frac{\text{BesselJ}[1,(1-i)x]}{\text{BesselJ}[0,(1-i)x]}-\frac{i\,\text{BesselJ}[1,(1+i)x]}{\text{BesselJ}[0,(1+i)x]}\right)$

(* Simplify Lload by substituting G[r0/δ]: *)

In[47]:= $\left\{\%\% /. \left(\frac{1}{2}+\frac{i}{2}\right)\left(\frac{\text{BesselJ}[1,(1-i)x]}{\text{BesselJ}[0,(1-i)x]}-\frac{i\,\text{BesselJ}[1,(1+i)x]}{\text{BesselJ}[0,(1+i)x]}\right)\to G[x],\ \%\right\}$ /. x → r0/δ

Out[47]= $\left\{\text{Lload}\to\pi r0\,\mathcal{L}\delta\eta^2\mu\,G\left[\frac{r0}{\delta}\right],\ G\left[\frac{r0}{\delta}\right]\to\left(\frac{1}{2}+\frac{i}{2}\right)\left(\frac{\text{BesselJ}\left[1,\frac{(1-i)r0}{\delta}\right]}{\text{BesselJ}\left[0,\frac{(1-i)r0}{\delta}\right]}-\frac{i\,\text{BesselJ}\left[1,\frac{(1+i)r0}{\delta}\right]}{\text{BesselJ}\left[0,\frac{(1+i)r0}{\delta}\right]}\right)\right\}$

(* Examine behavior of G[x]: *)

In[48]:= G[x] /. %%

Out[48]= $\left(\frac{1}{2}+\frac{i}{2}\right)\left(\frac{\text{BesselJ}[1,(1-i)x]}{\text{BesselJ}[0,(1-i)x]}-\frac{i\,\text{BesselJ}[1,(1+i)x]}{\text{BesselJ}[0,(1+i)x]}\right)$

In[49]:= G[∞] → Limit[%, x → Infinity]

Out[49]= G[∞] → 1

In[50]:= G[0] → Limit[%%, x → 0]

Out[50]= G[0] → 0

```
In[51]:= Plot[{1, %%%}, {x, .001, 10}, AxesLabel → {r0/δ, 𝒢[r0/δ]},
  PlotStyle → {{Dashing[{.025, .015}]}, {Dashing[{}]}}, PlotRange → All]
```

$\mathcal{G}\left(\frac{r0}{\delta}\right)$

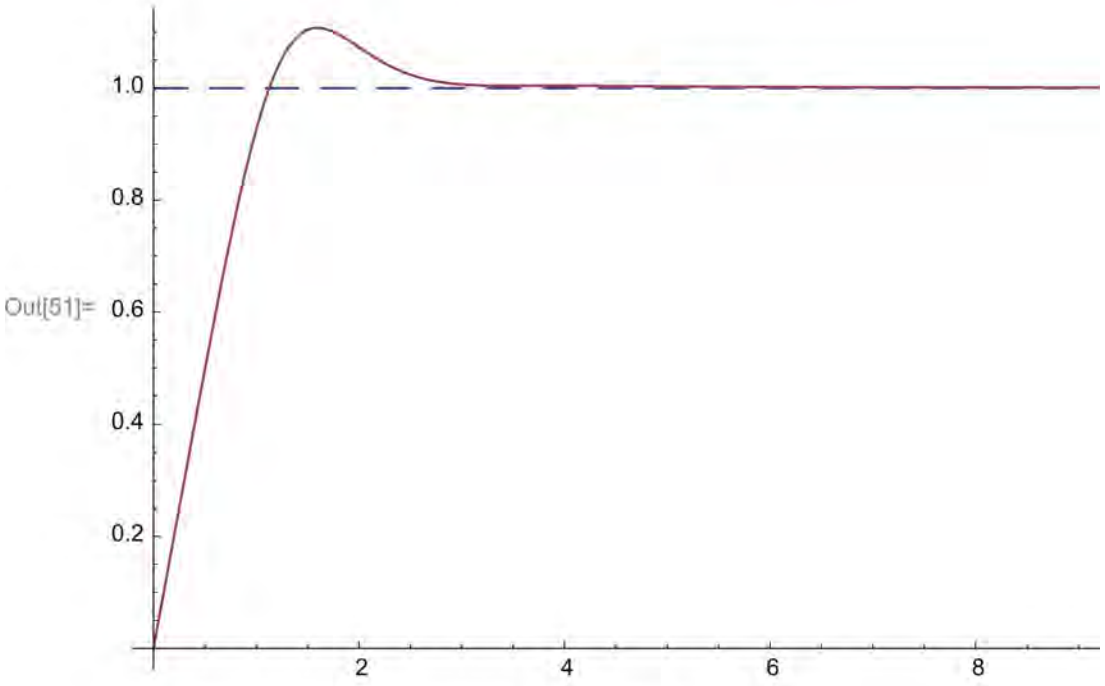


```
(* Determine limiting form of Lload for δ >> r0: *)
```

$$\text{In[52]:= Lload} \to \left(\frac{1}{2}+\frac{i}{2}\right)\pi\, r0\, \mathcal{L}\,\delta\,\eta^2\,\mu\left(\frac{\text{BesselJ}\left[1,\frac{(1-i)\,r0}{\delta}\right]}{\text{BesselJ}\left[0,\frac{(1-i)\,r0}{\delta}\right]}-\frac{i\,\text{BesselJ}\left[1,\frac{(1+i)\,r0}{\delta}\right]}{\text{BesselJ}\left[0,\frac{(1+i)\,r0}{\delta}\right]}\right)$$

$$\text{Out[52]= Lload} \to \left(\frac{1}{2}+\frac{i}{2}\right)\pi\, r0\, \mathcal{L}\,\delta\,\eta^2\,\mu\left(\frac{\text{BesselJ}\left[1,\frac{(1-i)\,r0}{\delta}\right]}{\text{BesselJ}\left[0,\frac{(1-i)\,r0}{\delta}\right]}-\frac{i\,\text{BesselJ}\left[1,\frac{(1+i)\,r0}{\delta}\right]}{\text{BesselJ}\left[0,\frac{(1+i)\,r0}{\delta}\right]}\right)$$

```
In[53]:= Lload[δ / r0 -> ∞] → Normal[Series[%[[2]], {r0, 0, 4}]]
```

$$\text{Out[53]= Lload}\left[\frac{\delta}{r0}\to\infty\right] \to \pi\, r0^2\, \mathcal{L}\,\eta^2\,\mu$$

```
(* Determine limiting form of Lload for δ << r0 (x >> 1): *)
```

$$\text{In[54]:= Lload}[\delta / r0 \to 0] \to \pi\, r0\, \mathcal{L}\,\delta\,\eta^2\,\mu\,\mathcal{G}\left[\frac{r0}{\delta}\right] /.\ \mathcal{G}\left[\frac{r0}{\delta}\right] \to 1$$

Out[64]= $\text{Lload}\left[\frac{\delta}{\text{r0}} \to 0\right] \to \pi\, \text{r0}\, \mathcal{L}\, \delta\, \eta^2\, \mu$

```
(* Recall Rload and Lload: *)
```

In[65]:= $\left\{\text{Rload} \to \frac{2\pi\, \text{r0}\, \mathcal{L}\, \eta^2\, \mathcal{F}[\text{x}]}{\delta\, \sigma},\ \text{Lload} \to \pi\, \text{r0}\, \mathcal{L}\, \delta\, \eta^2\, \mu\, \mathcal{G}[\text{x}]\right\}$

Out[65]= $\left\{\text{Rload} \to \frac{2\pi\, \text{r0}\, \mathcal{L}\, \eta^2\, \mathcal{F}[\text{x}]}{\delta\, \sigma},\ \text{Lload} \to \pi\, \text{r0}\, \mathcal{L}\, \delta\, \eta^2\, \mu\, \mathcal{G}[\text{x}]\right\}$

```
(* Compute the dimensionless load quality-factor Qload = ω Lload/Rload: *)
```

In[66]:= $\text{Qload} \to \omega\, \text{Lload} / \text{Rload}\ /.\ \%$

Out[66]= $\text{Qload} \to \frac{\delta^2\, \mu\, \sigma\, \omega\, \mathcal{G}[\text{x}]}{2\, \mathcal{F}[\text{x}]}$

```
(* Insert the definition of the skin depth δ: *)
```

In[67]:= $\%\ /.\ \delta \to \text{Sqrt}[2/(\omega\, \mu\, \sigma)]$

Out[67]= $\text{Qload} \to \frac{\mathcal{G}[\text{x}]}{\mathcal{F}[\text{x}]}$

In[68]:= $\text{Qload} \to \frac{\mathcal{G}[\text{x}]}{\mathcal{F}[\text{x}]}$

Out[68]= $\text{Qload} \to \frac{\mathcal{G}[\text{x}]}{\mathcal{F}[\text{x}]}$

```
(* Recall the definitions of F[x] and G[x]: *)
```

In[69]:= $\left\{\mathcal{F}[\text{x}] \to \left(\frac{1}{2} + \frac{i}{2}\right)\left(\frac{i\, \text{BesselJ}[1, (1-i)\,\text{x}]}{\text{BesselJ}[0, (1-i)\,\text{x}]} - \frac{\text{BesselJ}[1, (1+i)\,\text{x}]}{\text{BesselJ}[0, (1+i)\,\text{x}]}\right),\right.$

$\left.\mathcal{G}[\text{x}] \to \left(\frac{1}{2} + \frac{i}{2}\right)\left(\frac{\text{BesselJ}[1, (1-i)\,\text{x}]}{\text{BesselJ}[0, (1-i)\,\text{x}]} - \frac{i\, \text{BesselJ}[1, (1+i)\,\text{x}]}{\text{BesselJ}[0, (1+i)\,\text{x}]}\right)\right\}$

Out[69]= $\left\{\mathcal{F}[\text{x}] \to \left(\frac{1}{2} + \frac{i}{2}\right)\left(\frac{i\, \text{BesselJ}[1, (1-i)\,\text{x}]}{\text{BesselJ}[0, (1-i)\,\text{x}]} - \frac{\text{BesselJ}[1, (1+i)\,\text{x}]}{\text{BesselJ}[0, (1+i)\,\text{x}]}\right),\ \mathcal{G}[\text{x}] \to \left(\frac{1}{2} + \frac{i}{2}\right)\left(\frac{\text{BesselJ}[1, (1-i)\,\text{x}]}{\text{BesselJ}[0, (1-i)\,\text{x}]} - \frac{i\, \text{BesselJ}[1, (1+i)\,\text{x}]}{\text{BesselJ}[0, (1+i)\,\text{x}]}\right)\right\}$

In[60]:= $\text{Qload}[\text{x}] \to \text{Simplify}[\text{Together}[\%\%[[2]]\ /.\ \%]]$

Out[60]= $\text{Qload}[\text{x}] \to -\frac{i\, \text{BesselJ}[0, (1+i)\,\text{x}]\, \text{BesselJ}[1, (1-i)\,\text{x}] + \text{BesselJ}[0, (1-i)\,\text{x}]\, \text{BesselJ}[1, (1+i)\,\text{x}]}{\text{BesselJ}[0, (1+i)\,\text{x}]\, \text{BesselJ}[1, (1-i)\,\text{x}] + i\, \text{BesselJ}[0, (1-i)\,\text{x}]\, \text{BesselJ}[1, (1+i)\,\text{x}]}$

```
(* Examine behavior of Qload[x]: *)
```

```
In[61]:= Qload[δ/r0 → 0] -> Limit[%[[2]], x → 0]
```

```
Out[61]= Qload[δ/r0 → 0] → ∞
```

```
In[62]:= Qload[δ/r0 → ∞] -> Limit[%%[[2]], x → Infinity]
```

```
Out[62]= Qload[δ/r0 → ∞] → 1
```

```
Needs["BarCharts`"]; Needs["Histograms`"]; Needs["PieCharts`"]
```

```
(* Peak magnetic energy stored in the empty coil (core radius r0 = 0)
 is μ0 H0^2 times the internal volume π rc^2 ℒ of the coil: *)
```

```
In[63]:= W0 → μ0 H0^2 π rc^2 ℒ /. H0 → η ℐ
```

```
Out[63]= W0 → π rc^2 ℐ^2 ℒ η^2 μ0
```

```
In[64]:= L0 → (W0 /. %) / ℐ^2
```

```
Out[64]= L0 → π rc^2 ℒ η^2 μ0
```

```
(* Total peak magnetic energy Wtot stored in the loaded coil is Wload = Lcore ℐ^2,
plus μ0 H0^2 times the internal volume π (rc^2 - r0^2)
 ℒ between the core surface and the coil windings: *)
```

```
In[65]:= Wtot → Lload ℐ^2 + Simplify[μ0 H0^2 π (rc^2 - r0^2) ℒ /. {H0 → η ℐ, ℒ → L0/(π rc^2 η^2 μ0)}]
```

$$\text{Out[65]= } \text{Wtot} \to \text{Lload}\, \mathcal{I}^2 + \frac{\text{L0}\left(-\text{r0}^2 + \text{rc}^2\right)\mathcal{I}^2}{\text{rc}^2}$$

```
In[66]:= Ltot → %[[2, 1]] / ℐ^2 + Expand[%[[2, 2]] / ℐ^2]
```

$$\text{Out[66]= } \text{Ltot} \to \text{L0} + \text{Lload} - \frac{\text{L0}\,\text{r0}^2}{\text{rc}^2}$$

```
(* Total resistance of loaded coil is the load resistance plus the winding resistance: *)
```

```
In[67]:= Rtot → Rload + Rw
```

```
Out[67]= Rtot → Rload + Rw
```

```
(* Reexpress resistances in terms of inductances L and quality factors Q: *)
```

```
In[68]:= % /. {Rload → ω Lload / Qload, Rw → ω L0 / Q0}
```

$$\text{Out[68]= } \text{Rtot} \to \frac{\text{L0}\,\omega}{\text{Q0}} + \frac{\text{Lload}\,\omega}{\text{Qload}}$$

```
(* Introduce the total quality factor Qtot of the loaded coil: *)
```

In[69]:= $\text{Simplify}[\text{Qtot} \to \omega\, \text{Ltot} / \text{Rtot} /. \{\%, \%\%\%\}]$

Out[69]= $$\text{Qtot} \to \frac{\text{Q0 Qload}\left(\text{L0} + \text{Lload} - \frac{\text{L0 r0}^2}{\text{rc}^2}\right)}{\text{Lload Q0} + \text{L0 Qload}}$$

```
(* Summary of results for the inductance
 and quality factor of the loaded long solenoid coil: *)
```

In[70]:= $$\text{FullSimplify}\left[\left\{\text{Ltot} \to \text{L0} + \text{Lload} - \frac{\text{L0 r0}^2}{\text{rc}^2}, \text{Qtot} \to \frac{\text{Q0 Qload}\left(\text{L0} + \text{Lload} - \frac{\text{L0 r0}^2}{\text{rc}^2}\right)}{\text{Lload Q0} + \text{L0 Qload}}\right\} /.\right.$$
$$\left.\left\{\text{L0} \to \pi\, \text{rc}^2\, \mathcal{L}\, \eta^2\, \mu 0,\ \text{Lload} \to \pi\, \text{r0}\, \mathcal{L}\, \delta\, \eta^2\, \mu\, \mathcal{G}\left[\frac{\text{r0}}{\delta}\right],\ \text{Qload} \to \frac{\mathcal{G}\left[\frac{\text{r0}}{\delta}\right]}{\mathcal{F}\left[\frac{\text{r0}}{\delta}\right]}\right\}\right]$$

Out[70]= $$\left\{\text{Ltot} \to \pi\, \mathcal{L}\, \eta^2 \left(\left(-\text{r0}^2 + \text{rc}^2\right)\mu 0 + \text{r0}\, \delta\, \mu\, \mathcal{G}\left[\frac{\text{r0}}{\delta}\right]\right),\ \text{Qtot} \to \frac{\text{Q0}\left(\left(-\text{r0}^2 + \text{rc}^2\right)\mu 0 + \text{r0}\, \delta\, \mu\, \mathcal{G}\left[\frac{\text{r0}}{\delta}\right]\right)}{\text{rc}^2\, \mu 0 + \text{Q0 r0}\, \delta\, \mu\, \mathcal{F}\left[\frac{\text{r0}}{\delta}\right]}\right\}$$

Appendix A9.1

Selected Information on Frequency Allocations for ISM (Industrial, Scientific, and Medical) Applications

From: FCC Online Table of Frequency Allocations, 47 C.F.R. §2.106, revised on 23 September 2008. Full document (165 pages) is available online at URL: http://www.fcc.gov/oet/spectrum/table/fcctable.pdf

The following bands:

6765–6795 kHz (center frequency 6780 kHz)
433.05–434.79 MHz (center frequency 433.92 MHz) in Region 1 except in the countries mentioned in No. 5.280
61–61.5 GHz (center frequency 61.25 GHz)
122–123 GHz (center frequency 122.5 GHz), and
244–246 GHz (center frequency 245 GHz)

are designated for Industrial, Scientific, and Medical (ISM) applications. The use of these frequency bands for ISM applications shall be subject to special authorization by the administration concerned, in agreement with other administrations whose radiocommunication services might be affected. In applying this provision, administrations shall have due regard to the latest relevant ITU-R Recommendations.

5.150

The following bands:

13,553–13,567 kHz (center frequency 13,560 kHz)
26,957–27,283 kHz (center frequency 27,120 kHz)
40.66–40.70 MHz (center frequency 40.68 MHz)
902–928 MHz in Region 2 (center frequency 915 MHz)

2400–2500 MHz (center frequency 2450 MHz)
5725–5875 MHz (center frequency 5800 MHz), and
24–24.25 GHz (center frequency 24.125 GHz)

are also designated for Industrial, Scientific, and Medical (ISM) applications. Radiocommunication services operating within these bands must accept harmful interference which may be caused by these applications. ISM equipment operating in these bands is subject to the provisions of No. 15.13.

5.280

In Germany, Austria, Bosnia and Herzegovina, Croatia, the Former Yugoslav Republic of Macedonia, Liechtenstein, Portugal, Slovenia, Switzerland and Yugoslavia, the band 433.05–434.79 MHz (center frequency 433.92 MHz) is designated for Industrial, Scientific, and Medical (ISM) applications. Radiocommunication services of these countries operating within this band must accept harmful interference which may be caused by these applications. ISM equipment operating in this band is subject to the provisions of No. 15.13.

US218

The band 902–928 MHz is available for Location and Monitoring Service (LMS) systems subject to not causing harmful interference to the operation of all Federal stations authorized in this band. These systems must tolerate interference from the operation of Industrial, Scientific, and Medical (ISM) equipment and the operation of Federal stations authorized in this band.

US275

The band 902–928 MHz is allocated on a secondary basis to the amateur service subject to not causing harmful interference to the operations of Federal stations authorized in this band or to Location and Monitoring Service (LMS) systems. Stations in the amateur service must tolerate any interference from the operations of Industrial, Scientific, and Medical (ISM) devices, LMS systems, and the operations of Federal stations authorized in this band. Further, the amateur service is prohibited in those portions of Texas and New Mexico bounded on the south by latitude 31° 41′ North, on the east by longitude 104° 11′ West, and on the north by latitude 34° 30′ North, and on the west by longitude 107° 30′ West; in addition, outside this area but within 150 miles of these boundaries of White Sands Missile Range the service is restricted to a maximum transmitter peak envelope power output of 50 W.

Appendix A9.2

RF/Microwave Safety

Table A9.1 ACGIH Radio-frequency/Microwave Threshold Limit Values

Frequency	Power Density (mW/cm^2)	E^2 (V^2/m^2)	H^2 (A^2/m^2)
10 kHz–3 MHz	100	377,000	2.65
3–30 MHz	$900/f^2$	$3770 \times 900/f^2$	$900/37.7f^2$
30–100 MHz	1	3770	0.027
100–MHz	$f/100$	$3770 \times f/100$	$f/37.7 \times 100$
1–300 GHz	10	37,700	0.265

Source: http://niremf.ifac.cnr.it/docs/HANDBOOK/chp11.htm

Index

A

B

C

D

E

F

G

H

I

J

K

L

M

N

O

P

Q

R

S

T

V

W